ISOTHERMAL TRANSPORT OF SORBABLE GASES IN GRAPHITISED CARBON MEMBRANES : BLOCKAGE BY ADSORBED FILMS

by

ALAN DOUGLAS HAMILTON
B.Sc., A.R.C.S.

A thesis submitted
for the degree of
Doctor of Philosophy
in the
University of London

Department of Chemistry
Imperial College of Science and Technology
London SW7 2AY

February, 1980.

ISOTHERMAL TRANSPORT OF SORBABLE GASES IN GRAPHITISED CARBON MEMBRANES : BLOCKAGE BY ADSORBED FILMS - Alan D. Hamilton.

ABSTRACT

Isothermal flow of He, Ar, C_3H_8 and i-C_4H_{10} through Graphon and Black Pearls membranes has been investigated under 'simple adsorption' boundary conditions. The gases, as single species and as components of binary mixtures were studied over the temperature range 218 K to 473 K and steady-state integral permeabilities and diffusion coefficients determined. The permeabilities exhibited a marked dependence on both pressure and temperature and the existance of large 'extra flows' associated with an adsorbed film observed. The flow of i-C_4H_{10} and He/i-C_4H_{10} mixtures through the Graphon membrane was also examined under 'pressure-decay' conditions, resulting in the measurement of differential permeabilities and diffusion coefficients. These were compared and contrasted to those calculated from the integral results. Adsorption isotherms were also measured to aid the interpretation of the flow results. The effect of the adsorbed film of hydrocarbon upon the flow of a non-sorbed indicator gas, He, was examined for both membranes under different conditions. In each case a blockage curve 'universal' as regards hydrocarbon and temperature but specific to the membrane was obtained. It appeared that the blockage occurred primarily at one plane of the membrane due to different boundary conditions having little effect. The presence of 'key' adsorption sites, which have an initial marked effect on the gas flow was postulated, following the blockage effects observed even in the Henry Law region of adsorption. As the concentration of adsorbed gas was increased the blockage increased in a manner specific to each membrane until a condition of total blockage was attained. The compacted carbon was then acting as a semi-permeable membrane, permeable only to the hydrocarbon being transported by 'extra flow'.

DEDICATION

This thesis is dedicated with affection to my parents in recognition of the many personal sacrifices they willingly made for my school and university education.

ACKNOWLEDGEMENTS

I am indebted to my supervisor, Mr R. Ash, for his friendly advice and encouragement throughout the duration of this research project and to Professor R.M. Barrer F.R.S. for his helpful comments. I would also like to thank Mr D.E.G. Whiting and Dr A.V. Edge for their practical assistance and permission to include some of their experimental findings, (as yet unpublished). Finally I wish to express my gratitude to all those members of the Diffusion Research Group over the past three years for their personel contributions to a friendly working environment.

CONTENTS

LIST OF TABLES

LIST OF PLATES

LIST OF FIGURES

5.1. 'De Boers' (v - t) Plot for Different Carbons

5.2. Variation of 'q_{st}' with coverage

5.3. Concentration - Dependence of q_{st} : C_3H_8, i-C_4H_{10}/Graphon, Black Pearls

5.4. Typical ln (p/cm Hg) vs 1/T Plot for q_{st} Determination : i-C_4H_{10}/Graphon

5.5. Effect of Surface Heterogeneity on 'q_{st}'

5.6. The comparative Isotherm

5.7. Adsorption Isotherm in the form p/v vs v

5.8. Adsorption Isotherm : C_3H_8/Graphon Pellets : T/K = 393.2

5.9. Adsorption Isotherm : i-C_4H_{10}/Graphon Pellets : T/K = 453.2

5.10. Adsorption Isotherm : i-C_4H_{10}/Graphon Pellets : T/K = 423.2

5.11. Adsorption Isotherm : i-C_4H_{10}/Graphon Pellets : T/K = 393.2

5.12. Adsorption Isotherm : i-C_4H_{10}/Graphon Pellets : T/K = 358.2

5.13. Adsorption Isotherm : i-C_4H_{10}/Graphon Pellets : T/K = 343.2

5.14. Adsorption Isotherm : i-C_4H_{10}/Graphon Pellets : T/K = 308.2

5.15. Adsorption Isotherm : i-C_4H_{10}/Graphon Pellets : T/K = 273.2

5.16. Variation of $\tilde{K}_{He}T^{-\frac{1}{2}}$ with Temperature : Graphon, Black Pearls

5.17. Schematic Representation of Flux curve and Adsorption Isotherm

5.18. Permeability as a function of temperature and pressure

5.19. Variation of $\tilde{K}s/\tilde{K}g$ with temperature : Graphon, Black Pearls

5.20. Variation of $\tilde{K}s/A$ with pressure : C_3H_8, i-C_4H_{10}/Graphon, Black Pearls

5.21. Triple Plot : i-C_4H_{10}/Graphon : T/K = 453.2

5.22. Triple Plot : i-C_4H_{10}/Graphon : T/K = 423.2

5.23. Triple Plot : i-C_4H_{10}/Graphon : T/K = 393.2

5.24. Triple Plot : i-C_4H_{10}/Graphon : T/K = 358.2

5.25. Triple Plot : i-C_4H_{10}/Graphon : T/K = 343.2

5.26. Triple Plot : i-C_4H_{10}/Graphon : T/K = 308.2

5.27. Triple Plot : i-C_4H_{10}/Graphon : T/K = 273.2

5.28. Triple Plot : i-C_4H_{10}/Graphon : T/K = 268.2

5.29. Triple Plot : i-C_4H_{10}/Graphon : T/K = 258.2

5.30. Triple Plot : i-C_4H_{10}/Graphon : T/K = 248.2

5.31. Triple Plot : i-C_4H_{10}/Graphon : T/K = 233.2

5.32. Triple Plot : i-C_4H_{10}/Graphon : T/K = 218.2

5.33. Variation of $\tilde{K}_R$ with 'v' : He/i-C_4H_{10}/Graphon

5.34. Variation of $\tilde{K}_R$ with 'v' : He/i-C_4H_{10}/Graphon

5.35. Variation of $\tilde{K}_R$ with 'v_ℓ' : He/i-C_4H_{10}/Graphon

5.36. Variation of $\tilde{K}_R$ with p_1/p_0 : He/i-C_4H_{10}/Graphon

5.37. Variation of $\tilde{K}_R$ with p_1/p_0 : He/i-C_4H_{10}/Graphon

5.38. Triple Plot : C_3H_8/Graphon : T/K = 473.2

5.39. Triple Plot : C_3H_8/Graphon : T/K = 393.2

5.40. Triple Plot : C_3H_8/Graphon : T/K = 243.2

5.41. Triple Plot : C_3H_8/Graphon : T/K = 213.2

5.42. Variation of $\tilde{K}_R$ with p_1/p_0 : He/C_3H_8/Graphon

5.43. Variation of $\Delta\tilde{K}_R$ with p_1 (i-C_4H_{10}) : Graphon

5.44. Triple Plot : i-C_4H_{10}/Black Pearls : T/K = 343.2

5.45. Triple Plot : i-C_4H_{10}/Black Pearls : T/K = 308.2

5.46. Triple Plot : i-C_4H_{10}/Black Pearls : T/K = 273.2

5.47. Triple Plot : i-C_4H_{10}/Black Pearls : T/K = 233.2

5.48. Variation of $\tilde{K}_R$ with p_1/p_0 : He/i-C_4H_{10}/Black Pearls

5.49. Triple Plot : C_3H_8/Black Pearls : T/K = 273.2

5.50. Triple Plot : C_3H_8/Black Pearls : T/K = 213.2

5.51. Variation of $\tilde{K}_R$ with p_1/p_0 : He/C_3H_8/Black Pearls

5.52. Variation of $\tilde{K}_R$ with v : He/C_3H_8/Black Pearls

5.53. Variation of $\tilde{K}_R$ with p_1/p_0 : He/hydrocarbon/Carbolac, Black Pearls, Graphon

5.54. Concentration - Dependence of $\tilde{K}_R$: He/hydrocarbon/Carbolac

5.55. Blockage Curves for Carbolac : different mixtures

5.56. Concentration - Dependence of D : i-C_4H_{10}/Graphon

5.57. Concentration - Dependence of $\tilde{D}$: i-C_4H_{10}/Graphon

5.58. Concentration - Dependence of $\tilde{D}'_s$: i-C_4H_{10}/Graphon

5.59. Concentration - Dependence of D'_s : i-C_4H_{10}/Graphon

5.60. Concentration - Dependence of $\tilde{D}''_s$: i-C_4H_{10}/Graphon

5.61. Concentration - Dependence of D''_s : i-C_4H_{10}/Graphon

5.62. Concentration - Dependence of Diffusion coefficients : i-C_4H_{10}/Graphon : T/K = 453.2.

5.63. Concentration - Dependence of Diffusion coefficients : i-C_4H_{10}/Graphon : T/K = 423.2

5.64. Concentration - Dependence of Diffusion coefficients : i-C_4H_{10}/Graphon : T/K = 393.2

5.65. Concentration - Dependence of Diffusion coefficients : i-C_4H_{10}/Graphon : T/K = 358.2

5.66. Concentration - Dependence of Diffusion coefficients : i-C_4H_{10}/Graphon : T/K = 343.2

5.67. Concentration - Dependence of Diffusion coefficients : i-C_4H_{10}/Graphon : T/K = 308.2

5.68. Concentration - Dependence of Diffusion coefficients : i-C_4H_{10}/Graphon : T/K = 273.2

5.69. Concentration - Dependence of Diffusion coefficients : i-C_4H_{10}/Graphon : T/K = 268.2

5.70. Concentration - Dependence of Diffusion coefficients : i-C_4H_{10}/Graphon : T/K = 258.2

5.71. Concentration - Dependence of Diffusion coefficients : i-C_4H_{10}/Graphon : T/K = 248.2

5.72. Concentration - Dependence of D, $\tilde{D}$: i-C_4H_{10}/Graphon : T/K = 273.2

5.73. Concentration - Dependence of D, $\tilde{D}$: i-C_4H_{10}/Graphon : T/K = 308.2

5.74. Concentration - Dependence of $1/\sigma$ and D'_s : i-C_4H_{10}/Graphon : T/K = 453.2, 358.2

5.75. Concentration - Dependence of $1/\sigma$ and D'_s : i-C_4H_{10}/Graphon : T/K = 273.2, 233.2

5.76. Concentration - Dependence of D : C_3H_8/Graphon

5.77. Concentration - Dependence of $\tilde{D}$: C_3H_8/Graphon

5.78. Concentration - Dependence of D, $\tilde{D}$: C_3H_8/Graphon : T/K = 473.2

5.79. Concentration - Dependence of D, $\tilde{D}$: C_3H_8/Graphon : T/K = 393.2

5.80. Concentration - Dependence of D, $\tilde{D}$: C_3H_8/Graphon : T/K = 243.2

5.81. Concentration - Dependence of D, $\tilde{D}$: C_3H_8/Graphon : T/K = 213.2

5.82. Concentration - Dependence of D : C_3H_8/Black Pearls

5.83. Concentration - Dependence of $\tilde{D}$: C_3H_8/Black Pearls

5.84. Concentration - Dependence of D : i-C_4H_{10}/Black Pearls

5.85. Concentration - Dependence of $\tilde{D}$: i-C_4H_{10}/Black Pearls

5.86. Concentration - Dependence of D, $\tilde{D}$: C_3H_8/Black Pearls : T/K = 273.2

5.87. Concentration - Dependence of D, $\tilde{D}$: C_3H_8/Black Pearls : T/K = 213.2

5.88. Concentration - Dependence of D, $\tilde{D}$: i-C_4H_{10}/Black Pearls : T/K = 343.2

5.89. Concentration - Dependence of D, $\tilde{D}$: i-C_4H_{10}/Black Pearls : T/K = 308.2

5.90. Concentration -Dependence of D, $\tilde{D}$: i-C_4H_{10}/Black Pearls : T/K = 273.2.

5.91. Concentration - Dependence of D, $\tilde{D}$: i-C_4H_{10}/Black Pearls : T/K = 233.2

5.92. General form of the Concentration - Dependence of E.

CHAPTER 1

INTRODUCTION

The migration of fluids in porous media has been a subject which has attracted much attention over the years. Many of the properties of this flow can be considered under the following headings.

(i) The transport of non-sorbed gases.

(ii) The flow of a gas in equilibrium with an adsorbed film.

(iii) One-way or counter-flow of two or more gases in a mixture, each in equilibrium with a mixed adsorbed film on the surface.

(iv) The flow of capillary condensate of a single fluid.

(v) The flow of incompressible single fluids.

(vi) The flow of two immiscible fluids.

The transport of fluids such as petroleum, natural gas and water in porous strata, water in plants, reacting fluids in catalyst beds, air and water through packaging materials are a few real-life examples of the above categories.

This work has been primarily concerned with the first four types of fluid migration involved in the flow of sorbable gases through high surface area porous media.

The isothermal transport of gases was first quantitatively described by Graham (1846) who formulated the empirical law that 'the velocity of diffusion of a gas is inversely proportional to the square root of its density relative to air'. Knudsen (1909) later observed that this condition occurred only when the mean free path of the gas molecules was much greater than the dimensions of the pores through which they flowed. A theoretical equation was derived (later modified by Schmoluchowski, 1910) and gases diffusing according to it were described as undergoing 'Knudsen" flow or 'free molecular' flow. However Knudsen's equation was derived for gas flow through a single capillary and consequently the application of it to flow through a porous medium is somewhat misleading.

A 'dusty gas' model has been developed by Mason et al. (1961, 1962). This visualises the porous medium as a collection of spherical particles

which are very large in size as compared to a flowing gas molecule, and which are constrained to be fixed in space by experimental conditions. The D.G.M. was later refined by Breton and Massignon (1963) to include in the working equation physical parameters such as surface area, porosity and the mean pore radius.

These models were formulated for purely gas-phase flow but the work of Clausing (1930), Damköhler (1935) and Volmer (1921, 1925, 1926) provided evidence of an additional flow which contributes to the total flow. This has been attributed to the existence of mobile adsorbed films in the presence of a concentration gradient (Barrer and Gabor, 1960; Ash, Baker and Barrer, 1967). This 'extra' flow (earlier known as 'surface flow') has been the subject of interest to many with publications originating mainly from the research groups of Barrer, Carman, Flood and Kammermeyer.

The mechanism of extra flow has been greatly debated but it is now generally accepted (Barrer, 1963; Lallemand and Eyraud, 1973) that at sub-monolayer coverage a diffusive random walk mechanism is dominant (Aylmore and Barrer, 1966) whereas at coverages greater than monolayer hydrodynamic flow takes over, (Gilliland, 1958, 1962). This latter flow assumes that the adsorbed film acts as a two-dimensional fluid with properties analogous to those of three-dimensional fluids.

Considerable information concerning the flow of sorbed gases may be obtained directly from the experimental evidence and this does not require postulating a particular mechanism for extra flow. Fick's equation (1855) is used to treat the diffusion of matter in a similar way to Fouriers analysis of heat conduction, i.e. the flux is related to the concentration gradient by a quantity known as the diffusion coefficient, which may or may not be constant. The boundary conditions used must be carefully defined and those employed in this study are given in Chapter 2 along with the theoretical approach. This work follows the guidelines of studies previously emanating from the school of Barrer.

The adsorbed film can, under certain conditions, block the flow of a non-sorbed gas until the membrane becomes, in effect, semi-permeable. Ash, Barrer and Pope (1963) observed this for the Helium/SO_2/Carbolac system. A topical example of the use of the semi-permeable membrane is experimental work into the purification of sewer gas. Ammonia and

carbon dioxide are removed from the gas produced by anaerobic digestion processes. This produces 98% pure methane fit for home and industrial use (Financial Times, 1979, June 5, Technical Page).

Initially the diffusion rate is time dependent and a 'transient' state with related parameters is obtained. With increasing time the systems tends towards a steady-state. This study is concerned with isothermal transport in the steady-state and the derivable quantities for the hydrocarbon systems of propane and isobutane. These and those obtained for hydrocarbon/Helium mixtures are related to blockage behaviour and other characteristics specific to different graphitised carbon membranes.

CHAPTER 2 : THEORETICAL BACKGROUND

2.1. Introduction

This investigation is concerned with flow of sorbable gases and binary gas mixtures through a porous membrane. However many of the flow phenomena occurring in porous media are also observed for flow in a single capillary, this latter system being initially examined. The application of these basic principles of gas flow to the porous medium is then considered with attention being given to the 'extra' flow and 'blockage' effects which are present. A brief summary of the relevant background to adsorption is also included although the adsorption studies were made purely to aid the interpretation of the flow results.

2.2. Flow in a Single Capillary

If, under isothermal conditions, a pressure gradient is applied to a capillary, gas flow will occur. As the gradient increases the mode of flow changes through the regimes of molecular streaming (Knudsen flow), slip flow, streamline (viscous or Poiseuille) flow, turbulent flow to orifice flow. In the present work conditions are such that flow occurs predominantly by molecular streaming.

Knudsen (1909) derived an expression (from kinetic theory) for the mass flow of pure gas, which was converted to a volume flow/unit pressure gradient/unit time through a long single circular capillary. The expression was found experimentally to describe only the flow when molecule-wall collisions were dominant, i.e. the mean free path, λ of the molecules was much greater than the capillary radius, r. It was initially assumed that all the molecules striking the walls were randomly scattered but a later refinement by Schmoluckowski (1910) took into account the fact that only a fraction of the molecules, f, were randomly scattered. The volume flow may be expressed as a molar flow, J ($mol\,s^{-1}$) and a Knudsen permeability , K_K ($m^2 s^{-1}$) defined by :

$$K_K \equiv \frac{J\ell}{A_c\,\Delta C'_g} = \frac{4}{3}\,r\left(\frac{2RT}{\pi M}\right)^{\frac{1}{2}}\frac{(2-f)}{f} \qquad (2.1.)$$

in which M ($kg\ mol^{-1}$) is the molar mass of the flowing gas, ℓ (m) is the length and A_c (m^2) the cross-sectional area of the capillary, $\Delta C'_g$ ($mol\ m^{-3}$) is the concentration difference between the ends of the capillary.

If the expression proposed by Fick (1855), based on Fourier's work on heat conduction (given in equation (2.2) where the flow in the direction of x increasing is positive)

$$\frac{J}{Ac} \equiv - D \frac{\partial C}{\partial x} \qquad (2.2)$$

is applied to equation (2.1) the diffusion coefficient, D ($m^2 s^{-1}$) in (2.2) is given by :

$$D = \frac{4}{3} r \left(\frac{2RT}{\pi M}\right)^{\frac{1}{2}} \frac{(2-f)}{f} = K_K \qquad (2.3)$$

where $\Delta C'_g / \ell$ has been identified with $- \partial C / \partial x$.

Knudsen's proposed equation (2.1) was applicable only when molecule-wall collisions were dominant. In this region it would be expected that components in a mixture will flow independently of each other. The Knudsen permeability, K_K is constant for a given gas flowing through a given capillary at a certain temperature resulting in the relationship :

$$K_1 \left(\frac{M_1}{T_1}\right)^{\frac{1}{2}} = K_2 \left(\frac{M_2}{T_2}\right)^{\frac{1}{2}} \qquad (2.4)$$

when the subscripts 1 and 2 represent different gases and their associated properties.

If the mean free path of the molecules is much less than the capillary radius then molecule - molecule collisions become dominant and the flow then depends on the viscosity of the gas (Poiseuille flow). If the intermediate region ($\lambda \simeq r$) is considered, as $\lambda \Rightarrow r$ the molecular nature of the gas becomes more evident and a slip occurs at the walls. A good analysis of this region in terms of three components and their contribution to the total flow over a varying pressure gradient has been given by Weber (1954) and summarised by Barrer (1963). The three components consist of a Poiseuille term, a conduction term arising from slippage and a term due to diffusion in a pressure gradient and are schematically represented in Figure 2.1 and by the relationship

$$K = K_K \left\{ \frac{3\pi}{64} \frac{r}{\lambda} + \frac{\pi}{4} \left[\frac{2r/\lambda}{1 + (2r/\lambda)}\right] + \left[\frac{1}{1 + (2r/\lambda)}\right] \right\} \qquad (2.5)$$

where K is the resultant permeability. It may be seen that as

$r/\lambda \rightarrow \infty$: $K \rightarrow K_K \left(\frac{3\pi}{64} \cdot \frac{r}{\lambda}\right)$: streamline flow

$r/\lambda \rightarrow 0$: $K \rightarrow K_K$: Knudsen flow.

The expression (2.5) only applies when the pressure difference is very small compared to the mean pressure. Other equations exist for different conditions (Ash, Barrer and Nicholson, 1963; Ash, Barrer and Coughlan, 1972).

Figure 2.1. Schematic Representation of Webers (1954) Three Flow Components

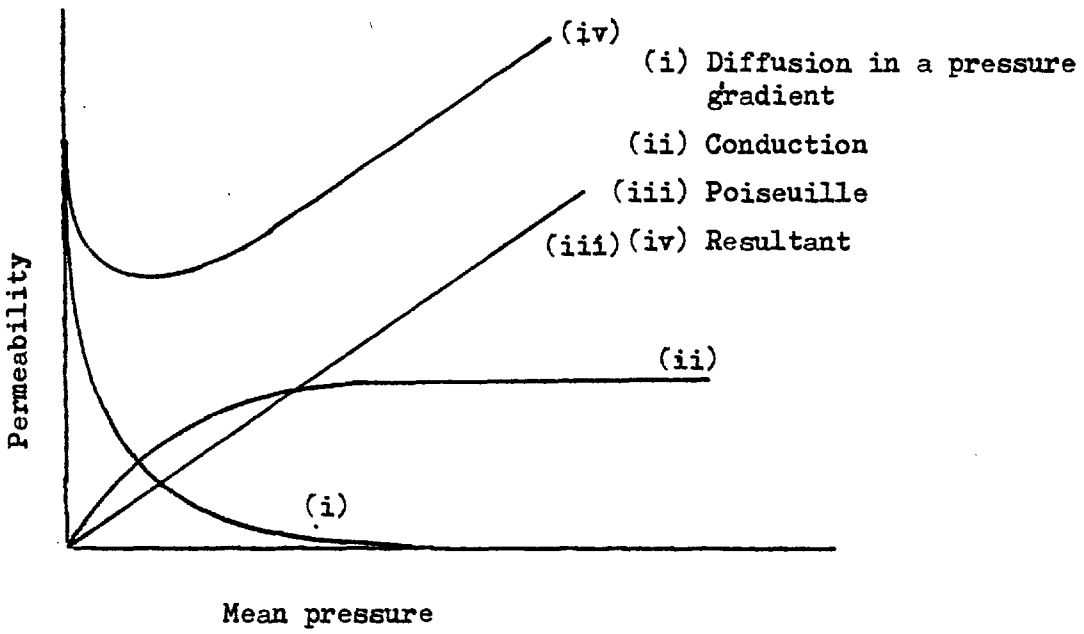

2.3. Flow in a Porous Medium

The porous media of this study consists of particles compressed to form a membrane containing channels, which may be tortuous, non-uniform or interconnecting with some exhibiting 'blind' pore character.

Many models have been used in the past to describe a porous medium. The simplest and probably the most misleading is that of a series of parallel uniform single capillaries. However valuable information can be obtained by utilizing semi-empirical relationships based on the Knudsen gas-flow through a single capillary. It is necessary to define the hydraulic radius, r_h of a bunch of capillaries :

$$r_h \equiv \frac{\text{area of cross-section of capillaries}}{\text{circumference of cross-section}} = \frac{\epsilon}{A} = \frac{r}{2} \qquad (2.6)$$

which can include the case of a porous medium where ϵ ($m^3 m^{-3}$) is the porosity or void volume per unit volume of porous media and A is the surface area ($m^2\ m^{-3}$). Other models of the porous medium have been proposed, such as the Dusty Gas Model (Mason et al. 1961) or representation as a bed of randomly dispersed spheres of variable diameters (Weissberg, 1963).

2.3.1. 'Conventional' Flow

The conventional flow technique (involved in the majority of work originating from the Barrer school) employed the following boundary conditions, known as 'simple adsorption' conditions:

$$c(x_1, t) = C_1 = \text{constant}, \quad t > 0 \qquad (2.7a)$$

$$c(x_2, t) = 0, \quad t > 0 \qquad (2.7b)$$

$$c(x, 0) = 0 \quad x_1 < x < x_2 \qquad (2.7c)$$

in which the membrane is bounded by the planes at $x = x_1$ and $x = x_2$ with ℓ ($\equiv x_2 - x_1$) being the thickness of the membrane, and C_1 the constant concentration at the ingoing face, $x = x_1$. In practice the condition (2.7b) is not exactly obeyed. It is experimentally arranged that the concentration at $x = x_2$, $C_2(t)$ does not exceed 1% of C_1 resulting in :

$$c(x_2 t) \equiv C_2(t) \ll C_1, \quad t > 0 \qquad (2.7b')$$

It is convenient to summarise the various concentrations employed and the relationships between them at this point; $\mathcal{C}$ is the total, C_s the Gibbs surface excess and C_g the gas-phase concentration all expressed in mol. (m^3 porous media)$^{-1}$, so that :

$$\mathcal{C} = C_s + C_g \qquad (2.8)$$

The quantities C_s and C_g are related to the more convenient, experimentally measurable concentrations, C'_g (mol (m^3 pore volume)$^{-1}$) and C'_s (mol (m^2 surface area)$^{-1}$) by :

$$C_g = \epsilon C'_g \qquad (2.9)$$

$$C_s = A C'_s \qquad (2.10)$$

The measured pressure is related to C'_g by the simple relationship :

$$C'_g = \frac{p}{RT} \tag{2.11}$$

where p is the pressure ($N\,m^{-2}$), R is the gas constant ($JK^{-1}\,mol^{-1}$) and T is the temperature of the porous membrane (K). C'_s is related to C'_g via the equilibrium adsorption isotherm.

Experimentally the steady state flow, J_{∞} ($mol.s^{-1}$) was determined by measuring the increase in the pressure, p_2, at $x = x_2$ as a function of time, t (s) in the calibrated outgoing volume, V (m^3). J_{∞} is then given by the relationship :

$$J_{\infty} = \frac{V}{RT_R} \cdot \frac{dp_2}{dt} \tag{2.12}$$

where T_R(K) is the ambient temperature. Barrer and Gabor (1960) suggest that the total steady state flux, J_{∞} may be split into two components, J_s and J_g. This division arises due to the existence of flows over and above those expected for pure gas phase flow, J_g, which are found for gases adsorbing in the membrane. This extra flow, J_s, associated with adsorption is related to the total flow by the relationship :

$$J_{\infty} = J_s + J_g \tag{2.13}$$

Employing Fick's equation (2.2) the differential overall, surface and gas phase diffusion coefficients are defined :-

$$J_{\infty}/A_c \equiv -D\, dC/dx \tag{2.14}$$

$$J_s/A_c \equiv -D_s\, dC_s/dx \tag{2.15}$$

$$J_g/A_c \equiv -D_g\, dC_g/dx \tag{2.16}$$

One may also define integral diffusion coefficients in the following manner :-

$$J_{\infty}/A_c \equiv \tilde{D}\,\frac{\Delta C}{\ell} \tag{2.17}$$

$$J_s/A_c \equiv \tilde{D}_s\,\frac{\Delta C_s}{\ell} \tag{2.18}$$

$$J_g/A_c \equiv \tilde{D}_g\,\frac{\Delta C_g}{\ell} \tag{2.19}$$

Assuming that both ϵ and A are independent of the distance into the membrane, x, then equations (2.15) and (2.16) defining the differential diffusion coefficients can be written as :

$$\frac{J_{\infty}}{A_c} = - D \frac{dC}{dx} \tag{2.14}$$

$$\frac{J_s}{A_c} = - AD_s \frac{dC'_s}{dx} \tag{2.20}$$

$$\frac{J_g}{A_c} = - \epsilon D_g \frac{dC'_g}{dx} \tag{2.21}$$

An equivalent form of equation (2.14) under the employed boundary conditions (2.7b') is :

$$\frac{J_{\infty}}{A_c} = \frac{1}{\ell} \int_o^{C_1} D \, dC \tag{2.22}$$

which yields upon differentiation :

$$D(C_1) = \frac{\ell}{A_c} \cdot \left(\frac{\partial J_{\infty}}{\partial C_1}\right) \tag{2.23}$$

and similarly:

$$D_s(C'_{s_1}) = \frac{\ell}{A_c} \cdot \frac{1}{A} \left(\frac{\partial J_s}{\partial C'_{s_1}}\right) \tag{2.24}$$

$$D_g(C'_{g_1}) = \frac{\ell}{A_c} \cdot \frac{1}{\epsilon} \left(\frac{\partial J_g}{\partial C'_{g_1}}\right) \tag{2.25}$$

Recalling the boundary condition (2.7b') the integral diffusion coefficients may be evaluated with the following modified forms of equations (2.17) to (2.19)

$$\frac{J_{\infty}}{A_c} = \tilde{D} \frac{C_1}{\ell} \tag{2.26}$$

$$\frac{J_s}{A_c} = A \tilde{D}_s \frac{C'_{s_1}}{\ell} \tag{2.27}$$

$$\frac{J_g}{A_c} = \epsilon \tilde{D}_g \frac{C'_{g_1}}{\ell} \tag{2.28}$$

The integral diffusion coefficient, $\tilde{D}$ of (2.26) is then related to the corresponding differential quantity (if the coefficients are functions of concentration only) by :

$$\tilde{D}(C_1) = \frac{1}{C_1} \int_0^{C_1} D(C)\, dC \qquad (2.29)$$

$$D = \tilde{D} + C_1 \left(\frac{\partial \tilde{D}}{\partial C_1}\right) \qquad (2.30)$$

It is convenient to define an integral permeability, $\tilde{K}$ ($m^2 s^{-1}$) as the flow through unit membrane cross-sectional area (normal to the direction of the flow), per unit gas-phase concentration gradient. $\tilde{K}$ is given by the relationship :

$$\tilde{K} \equiv \frac{J_{\infty}}{A_c} \cdot \frac{\ell}{\Delta C'_g} \qquad (2.31)$$

where $\Delta C'_g$ is the concentration drop in the gas-phase (mol. m^{-3}) between the faces of the membrane. In these experiments with the boundary condition (2.7b') $\Delta C'_g \simeq C'_{g_1}$ and recalling equation (2.11) the integral permeability may be written in the form :

$$\tilde{K} = \frac{J_{\infty} \ell}{A_c} \cdot \frac{RT_p}{p_1} \qquad (2.32)$$

Due to the above definition the permeability may also be divided in a similar way to the flux (equation 2.13) :

$$\tilde{K} = \tilde{K}_g + \tilde{K}_s \qquad (2.33)$$

It has been seen that for Knudsen flow in a single capillary the quantity $\tilde{K}(M/T)^{\frac{1}{2}}$ is a constant. This has also been observed to be the case in porous media for non-sorbed gases (Barrer and Grove, 1951; Ash and Grove, 1960). Helium is considered to be non-sorbed for the systems under study (this is further discussed in section 5.2.1) and thus the gaseous component, $\tilde{K}_g$ of the sorbed gas flow can be calculated by :

$$\tilde{K}_g = \tilde{K}^{He} \left(\frac{M^{He}}{M}\right)^{\frac{1}{2}} \qquad (2.34)$$

where M^{He}, M are molar masses and $\tilde{K}^{He}$ is the experimental helium permeability at the temperature of the $\tilde{K}$ determination. The permeability of flow can be divided in several ways (Ash, Barrer and Sharma, 1976).

(a) The flow of pure helium may serve to evaluate the flow of the sorbable gas which would have occurred in the gas phase in the absence of adsorption.

(b) Helium can be used as a non-sorbed internal indicator to evaluate the flow of the gas phase component of the sorbable gas, taking into account any blockage of the gas phase by the adsorbed film (Ash, Barrer and Pope, 1963b; Ash, Barrer, Lowson, 1973; Ash, Barrer and Sharma, 1976).

(c) A division of the total flow is made with one component (at any cross-section) wholly confined to the surface and the other wholly in the gas phase. Estimates of this have been made by Ash, Barrer and Pope (1963b) for specific conditions.

This study employs divisions of type (a) and (b) to calculate $\tilde{K}_g$.

A relationship between the integral permeability and the integral diffusion coefficient may be derived by combining the defining equations ((2.31) and (2.17)) to give :

$$\tilde{K} = \tilde{D} \frac{\Delta C}{\Delta C'_g} \tag{2.35}$$

Taking into account the boundary conditions and re-arranging it follows that :

$$\tilde{D} = \frac{\tilde{K} C'_{g_1}}{C_1} = \frac{\tilde{K} C'_{g_1}}{(AC'_{s_1} + \epsilon C'_{g_1})} = \frac{\tilde{K}}{[\epsilon + A(C'_{s_1}/C'_{g_1})]} \tag{2.36}$$

The relationship between the integral permeability and the differential diffusion coefficient is somewhat more complex. Recalling the definition of D_g, equation (2.2) and integrating over the range $x = x_1$ to $x = x_2$:

$$\frac{J_g}{A_c} = \frac{1}{\ell} \int_0^{C'_{g_1}} D_g \, dC'_g \tag{2.37}$$

Taking into consideration the boundary conditions and substituting equation (2.32), defining $\tilde{K}_g$ in terms of J_g, equation (2.37) becomes :

$$\tilde{K}_g = \frac{1}{C'_{g_1}} \int_0^{C'_{g_1}} \epsilon D_g \, dC'_g \tag{2.38}$$

It has been shown that $\tilde{K}_g$ is related to the pure helium permeability (equation (2.34)) which is independent of concentration. It follows

that $\tilde{K}_g$ and D_g must also be independent of concentration and equation (2.38) can be written in the useful form :

$$\tilde{K}_g = \epsilon D_g \tag{2.39}$$

Considering equation (2.20) relating J_s and D_s :

$$\frac{J_s}{A_c} = - A D_s \frac{dC'_s}{dx} \tag{2.20}$$

If $\sigma = \partial C'_s / \partial C'_g$ (the slope of the equilibrium adsorption isotherm) then equation (2.20) can be modified to:

$$\frac{J_s}{A_c} = - A D_s \sigma \frac{dC'_g}{dx} \tag{2.40}$$

which upon integration from $x = x_1$ to $x = x_2$ becomes :

$$\frac{J_s}{A_c} = \frac{1}{\ell} \int_o^{C'_{g_1}} A D_s \sigma \, dC'_g \tag{2.41}$$

Substitution for $\tilde{K}_s$ (given by equation (2.31) and J_s) and instituting boundary condition results in :

$$\tilde{K}_s C'_{g_1} = \int_o^{C'_{g_1}} A D_s \sigma \, dC'_g \tag{2.42}$$

which differentiates to give the following relationship between $\tilde{K}_s$ and D_s :

$$D_s = \frac{\tilde{K}_s + C'_{g_1} (\partial \tilde{K}_s / \partial C'_{g_1})}{A \sigma} \tag{2.43}$$

Having defined an integral permeability, equation (2.31) a differential permeability, K can also be defined by the relationship :-

$$\frac{J_{oo}}{A_c} \equiv - K \frac{dC'_g}{dx} \tag{2.44}$$

which in the integrated form and noting the boundary conditions gives:

$$\frac{J_{oo}}{A_c} = \frac{1}{\ell} \int_o^{C'_{g_1}} K \, dC'_g \tag{2.45}$$

leading to :

$$K = \frac{\ell}{A_c} \left(\frac{\partial J_{oo}}{\partial C'_{g_1}} \right) \tag{2.46}$$

Recalling the definition of the integral permeability and combining with equation (2.46) :

$$\tilde{K}\, C'_{g_1} = \int_0^{C'_{g_1}} K \, dC'_g \tag{2.47}$$

which with differentiation becomes :

$$\tilde{K} + C'_{g_1} \left(\frac{\partial \tilde{K}}{\partial C'_{g_1}}\right) = K \tag{2.48}$$

The relationship between the differential K and the differential diffusion coefficient may be considered by recalling equations (2.23) and (2.46)

$$\frac{D}{K} = \left(\frac{\partial J_\infty}{\partial C_1}\right)\left(\frac{\partial C'_{g_1}}{\partial J_\infty}\right)$$

$$= \left(\frac{\partial C'_{g_1}}{\partial C_1}\right) = \frac{1}{A \dfrac{\partial C'_s}{\partial C'_g} + \epsilon} \tag{2.49}$$

which results in :

$$D = \frac{K}{[A\,\sigma + \epsilon\,]} \tag{2.50}$$

where $\sigma \left(= \dfrac{\partial C'_s}{\partial C'_g} \right)$ is the slope of the isotherm at C'_{g_1} .

Recalling the definition of J_g (equation 2.21) and combining with the definition of K_g (equation (2.44) and substituting K_g and J_g) :

$$\frac{J_g}{A_c} \equiv - K_g \frac{dC'_g}{dx} = - \epsilon D_g \frac{dC'_g}{dx} \tag{2.51}$$

Equation (2.51) results in :

$$K_g = \epsilon D_g \tag{2.52}$$

This is equivalent to equation (2.39) involving the integral permeability, $\tilde{K}_g$ with the assumption that $\tilde{K}_g$ is independent of concentration. This agrees with the requirement of equation (2.48), relating integral and differential permeabilities that $K = \tilde{K}$ if the integral permeability is independent of concentration.

Similar to the definition of K and the resulting equation (2.46) an equation for K_s may be obtained :

$$K_s = \frac{\ell}{A_c} \left(\frac{\partial J_s}{\partial C'_{g_1}}\right) \tag{2.53}$$

Combining equation (2.53) with the differentiated form of (2.24) :

$$\frac{\ell}{A_c}\left(\frac{\partial J_s}{\partial C'_{g_1}}\right) = K_s = A\, D_s\, \sigma \qquad (2.54)$$

a relationship between K_s and D_s is apparent

$$D_s = \frac{K_s}{A\,\sigma} \qquad (2.55)$$

An expression relating the differential and integral diffusion coefficients can be derived by combining the defining equations (2.22) and (2.26).

$$\frac{J_\infty}{A_c} = \frac{1}{\ell}\int_0^{C_1} D\, dC = \tilde{D}\,\frac{C_1}{\ell} \qquad (2.56)$$

which, on differentiation yields equation (2.57) similar to equation (2.48) for permeabilities

$$D = \tilde{D} + C_1\,(\partial\tilde{D}/\partial C_1) \qquad (2.57)$$

It can be seen that there are many inter-relating expressions involving integral and differential permeabilities and diffusion coefficients. The evaluation of diffusion coefficients can employ, if necessary, different routes depending on the concentration dependences of the flux, the permeability and on the isotherm as differentiation of these quantities are required.

2.3.2. 'Pressure-Decay' Flow

This technique initially introduced by Rigden (1943) and Blaine (1943) involves the flow of gas through a membrane from one fixed volume into another fixed volume until equilibrium is attained. The flow must therefore be non-steady state by its nature. However a 'quasi'- steady state approach was developed by Ash, Barrer and Sharma (1976) and this is briefly outlined here.

At all times :

$$n_1 + n_p + n_2 = n_o \qquad (2.58)$$

where n_1 and n_2 are the amounts of gas (mol) contained in fixed volumes V_1 and V_2 (m^3) either side of the membrane (bounded by the planes $x = x_1$ and $x = x_2$) at pressures p_1 and p_2 (Nm^{-2}) respectively and at a temperature of T_R (K). The amount of gas in the membrane is given by

n_p (mol) which is at temperature, T (K) and the total amount of gas in the system is n_o (mol).

At any time :

$$- J_1 + J_2 + \frac{dn_p}{dt} = 0 \qquad (2.59)$$

where J_1 and J_2 are the fluxes given by :

$$J_1 = - \frac{dn_1}{dt} = - \left(\frac{V_1}{RT_R} \right) \frac{dp_1}{dt} \qquad (2.60)$$

$$J_2 = \frac{dn_2}{dt} = \left(\frac{V_2}{RT_R} \right) \frac{dp_2}{dt} \qquad (2.61)$$

If $\Delta p = p_1 - p_2$ and for the conditions when J_1 and J_2 approach the same value J i.e. $dn_p/dt \rightarrow 0$ then combining equations (2.60) and (2.61) produces :

$$\begin{aligned} \frac{d\Delta p}{dt} &= - RT_R \left[J \left(\frac{1}{V_1} + \frac{1}{V_2} \right) \right] \\ &= - k' \Delta p \\ &= - k' RT \Delta C'_g \end{aligned} \qquad (2.62)$$

where $\Delta C'_g$ (mol m^{-3}) is the gas-phase concentration difference between the two faces of the membrane.

Defining a permeability, K^* ($m^2 s^{-1}$) :

$$K^* \equiv \frac{J \ell}{A_c \Delta C'_g} \qquad (2.63)$$

Combining equations (2.60) and (2.61) results in :

$$K^* = k' \frac{V_1 V_2}{V_1 + V_2} \frac{\ell}{A_c} \cdot \frac{T}{T_R} \qquad (2.64)$$

On integration, equation (2.62) becomes :

$$\ell n (\Delta p) = - k't + \ell n (\Delta p)_o \qquad (2.65)$$

Implicit in this treatment is the assumption that the decay of Δp is first order, equation (2.62) and that $dn_p/dt \rightarrow 0$. The first order assumption was found to be experimentally acceptable by Ash, Barrer and Sharma (1976) for long times.

A more rigorous theoretical treatment developed by Mr R. Ash (personal communication) results in first-order decay being predicted at long times and derives a similar expression for K^* to that given in equation (2.64). A brief outline of the procedure is presented here for a similar system to that described by the 'quasi'-steady state procedure. Additional quantities required are the gas-phase concentrations in the volumes V_1 and V_2 which are denoted by ϕ_1 and ϕ_2 respectively with the distribution of gas between the membrane and the associated volume assumed to obey Henry's Law (Henry Law constant, k).

The boundary conditions may be summarised :-

$$\begin{aligned} C(x_1,t) &= C_1 = k\phi_1(t), \quad t > 0 \\ C(x_2,t) &= C_2 = k\phi_2(t), \quad t > 0 \\ C(x,0) &= f(x), \quad x_1 < x < x_2 \\ \lim_{t\to 0} \phi_i(t) &= \phi_i \end{aligned} \tag{2.66}$$

where $f(x)$ is an initial arbitrary distribution of gas in the membrane (thickness $\ell \equiv x_2 - x_1$). It is assumed initially that the whole system is at temperature T. If transport occurs in the direction of x increasing from V_1 to V_2 then:

$$\frac{J}{A_c}(x,t) = -D\frac{\partial C}{\partial x} \tag{2.67}$$

At $x = x_1$:

$$V_1\,\phi_1(t) = V_1\phi_1 - \int_0^t J(x_1,t)\,dt \tag{2.68}$$

similarly :

$$V_2\,\phi_2(t) = V_2\phi_2 + \int_0^t J(x_2,t)\,dt \tag{2.69}$$

Assuming conservation of gas :

$$\phi_1(t) + \frac{A_c}{V_1}\int_{x_1}^{x_2} C(x,t)\,dx + \frac{V_2}{V_1}\phi_2(t) = \phi_1 + \frac{A_c}{V_1}\int_{x_1}^{x_2} f(x)\,dx + \frac{V_2}{V_1}\phi_2 \tag{2.70}$$

Solutions for $\phi_1(t)$, $\phi_2(t)$ and $C(x,t)$ are derived via the method of variation of parameters and then Laplace transforms. The solutions for $\phi_1(t)$ and $\phi_2(t)$ are relatively complex equations containing the quantities ϕ_1 , ϕ_2 , α_i and θ_n where :

$$\alpha_i = \frac{k A_c \ell}{V_i} \qquad (i = 1,2) \tag{2.71}$$

and β_n are the positive (non-zero) roots of the equation :

$$\beta^2 - (\alpha_1 + \alpha_2)\, \beta \cot \beta - \alpha_1 \alpha_2 = 0. \tag{2.72}$$

The quantity $\Delta\emptyset$ is defined :

$$\Delta\emptyset \equiv \emptyset_1(t) - \emptyset_2(t) \tag{2.73}$$

which on substitution for $\emptyset_1(t)$ and $\emptyset_2(t)$, is found to reduce at large times to :

$$\Delta\emptyset = \gamma \exp\left(-\frac{\beta_1^2 D t}{\ell^2}\right) \tag{2.74}$$

where γ is an arbitrary constant involving α_i, β_1 the initial arbitrary concentration distribution in the membrane $f(x)$ and $\emptyset_1$, $\emptyset_2$.

Equation (2.74) can be written as :

$$\ell n\,(\Delta\emptyset) = -\frac{\beta_1^2 D}{\ell^2}\, t + \ln \gamma \tag{2.75}$$

Consider β_1 : this is the first non-zero positive root of equation (2.72) and must involve α_1 and α_2. Barnes (1934) showed that for the case when $\alpha_1 = \alpha_2 = \alpha$

$$\beta_1 = (2\alpha)^{\frac{1}{2}} \left\{1 - \frac{\alpha}{12} + \frac{11\alpha^2}{1440} + \ldots\right\}$$

$$\simeq (2\alpha)^{\frac{1}{2}} \text{ for sufficiently small } \alpha, \tag{2.76}$$

which gives :

$$\frac{\beta_1^2 D}{\ell^2} = \frac{2\alpha D}{\ell^2} \tag{2.77}$$

In our case $V_1 \neq V_2$ and consequently $\alpha_1 \neq \alpha_2$. However in equation (2.72) the sum $(\alpha_1 + \alpha_2)$ can be replaced, to a first approximation by 2α where α corresponds to the harmonic mean, V_h of V_1 and V_2 : The geometric mean squared may be used to replace the $(\alpha_1\, \alpha_2)$ term. Spacek and Kubin (1967) showed that even when $V_1 = 2V_2$, V_h only differed from the geometric mean by $\sim 6\%$. Thus V_h may be used to evaluate α, which in turn, utilizing the result of Barnes, gives k' defined in equation (2.78).

$$k' \equiv \frac{\beta_1^2 D}{\ell^2} = \frac{2k A_c \ell}{V_h} \cdot \frac{D}{\ell^2} = \frac{2k A_c}{V_h} \cdot \frac{D}{\ell} \qquad (2.78)$$

Considering the total concentration, C at the membrane :

$$C = C_s + C_g = \epsilon C'_g + AC'_s \qquad (2.79)$$

with Henry Law adsorption (constant $k_s = C'_s/C'_g$) :

$$C = (\epsilon + Ak_s) C'_g \qquad (2.80)$$

Now as $C'_g.RT = p = \emptyset.RT_R$ [where C'_g is the concentration at the membrane (temperature T) and $\emptyset$ is the concentration in the bulk of the volume (temperature T_R)] equation (2.80) becomes :

$$k = (\epsilon + Ak_s) \frac{T_R}{T} \qquad (2.81)$$

On substitution into equation (2.78) :

$$k' = \frac{\beta_1^2 D}{\ell^2} = 2 \frac{(\epsilon + Ak_s)}{V_h} \cdot \frac{T_R}{T} \cdot \frac{A_c}{\ell} \cdot D \qquad (2.82)$$

Recalling the flux J(mol s^{-1}), equation (2.26) :

$$\frac{J}{A_c} = - D \frac{dC}{dx} = \frac{1}{\ell} (\Delta C) D$$

$$= \frac{1}{\ell} \cdot D (\epsilon + Ak_s) \Delta C'_g \qquad (2.83)$$

and defining a differential permeability, K^* :

$$K^* = \frac{J_{\infty} \ell}{A_c \Delta C'_g} = D (\epsilon + Ak_s) \qquad (2.84)$$

Substituting into equation (2.82)

$$k' = \frac{2K^*}{V_h} \cdot \frac{T_R}{T} \cdot \frac{A_c}{\ell} \qquad (2.85)$$

Equation (2.85) can thus be used to calculate the differential permeability from the slope, k' of the ln ($\Delta\emptyset$) vs t plot (linear at long times and small α by the relationship :

$$K^* = \left(\frac{2}{V_h}\right) \cdot \frac{T}{T_R} \cdot \frac{\ell}{A_c} \cdot k' = \left(\frac{V_1 V_2}{V_1 + V_2}\right) \frac{T}{T_R} \cdot \frac{\ell}{A_c} \cdot k' \qquad (2.86)$$

As can be seen both the 'quasi'-steady state and the theoretical approach of Mr R. Ash result in an equivalent equation for the permeability, K^*, although in this treatment, D is assumed constant and Henry Law adsorption takes place.

From the experimentally obtained differential permeability, K^* an overall differential diffusion coefficient, D^* may be evaluated (Ash, Barrer and Sharma, 1976).

$$D^* = \frac{K^* \Delta C'_g}{\Delta C} \tag{2.87}$$

As the permeability is determined from long time data the values of $\Delta C'_g$ and ΔC will be small and :

$$\frac{\Delta C'_g}{\Delta C} \simeq \frac{dC'_g}{dC} \tag{2.88}$$

Recalling equations (2.8) to (2.10) and substituting dC'_s/dC'_g with σ

$$\frac{dC'_g}{dC} = \frac{d\,C'_g}{d(AC'_s + \epsilon C'_g)} = \frac{1}{A\sigma + \epsilon} \tag{2.89}$$

and the differential diffusion coefficient is given by the expression :

$$D^* = \frac{K^*}{[A\sigma + \epsilon]} \tag{2.90}$$

where C'_g (in equation (2.89)) is calculated from the equilibrium pressure of gas. The relationship (2.90) can be compared with equation (2.40) of the 'conventional' flow theory which relates the calculated differential permeability to the differential diffusion coefficient.

$$D = \frac{K}{[A\sigma + \epsilon]} \tag{2.50}$$

Both expressions are identical, if it is assumed that K and K^* are the same. However this assumption cannot be made unless experimentally verified, in which case the magnitude and concentration dependence of the differential diffusion coefficients, D and D^* should be identical.

Throughout this discussion on the theory of both 'conventional' and 'pressure-decay' techniques the membrane has been assumed to be homogeneous as regards its structure. Any x-dependence of the porosity, surface area and pore structure has been tacitly ignored. The measured overall porosity and surface area are assumed to be good estimates of the mean of the local values. Diffusion coefficients throughout are assumed to be functions of concentration only and not functions of x. For the case

of strongly adsorbed gases flowing through a Graphon membrane, such as that employed here the concentration dependence of the diffusion coefficient has been shown to dominate any x-dependence (Ash, Barrer, Chio and Edge; 1979), although strong evidence does exist showing that this may not be the case for weakly adsorbed gases (Tsimillis and Petropoulos, 1977).

2.4. Relevant Adsorption Background

As the flow of gases is modified by adsorption, gas transport through porous membranes must be studied in conjunction with adsorption phenomena. Adsorption is a consequence of the surface forces (physical or chemical) of a solid attracting molecules of a gas or vapour. This results in physical (Van der Waals) adsorption or chemisorption, the former being applicable to this study. The adsorption isotherm, and the derived quantities, such as Henry Law constants and heats of adsorption, are therefore required to enable full interpretation of the flow.

The adsorption isotherm is a plot of the amount adsorbed, $v(cm^3$ s.t.p. $g^{-1})$ as a function of the equilibrium gas-phase concentration, C'_g (mol. m^{-3}) or more normally equilibrium pressure of adsorbate, p (cm Hg) where p and C'_g are related by equation (2.11). The isotherm shape may vary but the majority can be grouped into five classes (Brunauer, Emmett and Teller, 1938). If the measured isotherm is linear, Henry Law adsorption is said to have taken place and the 'Henry Law constant', k_s (m) can be evaluated:

$$k_s = \frac{\text{Gibbs excess surface concentration}}{\text{gas phase concentration}} = \frac{C'_s}{C'_g} \qquad (2.91)$$

where C'_s (mol. m^{-2}) and C'_g (mol. m^{-3}) are evaluated from the experimentally measured quantities, equation (2.11). The Henry Law constant can then be used to evaluate an energy of adsorption, $\Delta E'$ (J. mol^{-1}) (cf equation (5.31)). The adsorption isotherm may be used to investigate changes in adsorption properties produced by, for example, compaction of a solid into a membrane.

It is possible to evaluate from the measured isotherm the monolayer capacity, v_m (cm^3 s.t.p. g^{-1}) of the adsorbent. This is the quantity of adsorbate which can be accommodated in a completely filled single layer of molecules and is generally calculated by applying the well-known B.E.T. equation (cf equation (4.3), Brunauer, Emmett and Teller, 1938)

to a low temperature nitrogen isotherm. The value of v_m for nitrogen adsorption can then be used to evaluate the surface area of the solid, S ($m^2 g^{-1}$) via equation (2.92) :

$$S = \frac{v_m}{22414} N \sigma 10^{-18} \qquad (2.92)$$

where N is the Avogadro constant (mol^{-1}) and σ the cross-sectional area of an adsorbed N_2 molecule (nm^2). Once the surface area is known, v_m may be calculated for gases of known cross-sectional area. If other adsorbates produce isotherms which fit the B.E.T. equation, the values of v_m so obtained and the known values of the surface area may be employed to evaluate the cross-sectional area of the adsorbate molecule. This type of consideration is given further attention in sections 4.1/2/3 and 5.1.1.

Another approach to evaluate v_m based on the isotherm is that of the 't' plot proposed initially by de Boer and Lippens (1965). It was shown that for non-porous samples of aluminium hydroxides and graphitised carbons a multi-molecular layer of adsorbed nitrogen could be freely formed on all parts of the surface. The statistical thickness, t (nm) of this layer was calculated and shown to be independent of the adsorbent resulting in a 'universal t plot' (t versus p/p_o). This latter point has been questioned by several workers and is discussed in greater detail in section 5.1.1. Different 't' plots to that of de Boer have been proposed by Shull (1948), Cranston and Inkley (1957), Pierce (1968) and are reviewed by Dollimore and Heal (1970). Utilising the "universal t curve" a t vs v plot is then constructed for the gas under consideration and a value of the surface area, S_t calculated from its slope (cf equation (5.1)).

It is useful to derive a quantity known as the isosteric heat of adsorption, q_{st} ($J\ mol^{-1}$) from isotherms measured over a range of temperatures. This is evaluated by a Clausius-Clapeyron relationship to the isotherm at constant coverage :

$$q_{st} = - R \left[\frac{\partial \ln p}{\partial\ 1/T}\right]_v \qquad (2.93)$$

The heat of adsorption is generally expected to alter significantly in the vicinity of monolayer coverage, decreasing to a value near that of

the enthalpy of vaporisation. Variations before this drop can be attributed to energetic heterogeneity of the surface and lateral interactions between the adsorbate molecules. It is also possible to evaluate an energy of adsorption, $\Delta E''$ (J mol^{-1}) from the limiting value of q_{st} as the coverage tends to zero (cf equation 5.4). Theoretically both $\Delta E''$ and $\Delta E'$ (obtained from k_s) should agree.

This study is primarily concerned with flow and consequently the limited discussion of the adsorption isotherm has been confined to the aforementioned topics.

CHAPTER 3 : EXPERIMENTAL

3.1. The Membrane

3.1.1. The Carbons

The two membranes used in this work were compacted from 'Graphon' and 'graphitised Black Pearls'. Graphon is a graphitised form of the pelletised regular colour channel black known as Spheron 6. Black Pearls is a high colour channel black. The carbons were manufactured and supplied by the Cabot Corporation, Boston, Mass., U.S.A. in powder form. Both were produced by the 'channel process' in which natural gas is burnt in an oxygen deficient atmosphere. The flame is directed on to steel channels and the deposited carbon scraped off. The parent black is then graphitised by heating in an induction furnace at temperatures between 2700°C and 3000°C. The properties of these carbons are summarised in Table 3.1.

There is now universal agreement on the general microstructure of carbon blacks. The carbon atoms are chemically bonded to form plane, hexagonal networks called layer planes, which are similar to the layer planes in graphite but smaller. Biscoe and Warren (1942) with X-ray diffraction techniques found that the layer planes are piled in stacks ($\sim$ 0.35 nm apart) some three to five layers deep, called crystallites ($\sim$ 1.5 nm thick and $\sim$ 2 nm diameter) in which the layer planes are arranged roughly parallel and equidistant. However they are randomly oriented with respect to the layer normal so that the regular A.B.A. stacking of graphite does not occur. Electron microscope studies showed that the crystallites in turn are aggregated into clusters. In the case of channel blacks spheroidal particles exist in small and medium sized aggregates with some discrete particles. Heckman and Harling (1966) utilized oxidative attack to formulate the 'concentric crystallite' model (Figure 3.1 (a)). The outer shell of the particle was much more resistant to oxidation, implying a less well ordered centre portion consisting of small crystallites and single layer planes. Earlier X-ray diffraction and dark field electron microscopy (Hall, 1948) had showed the shell to be made up of larger more perfect crystallites whose layer planes are generally orientated parallel to the particle surface. In hi-colour blacks there appears to be no distinction between the external and internal orientations.

During graphitisation changes in crystallite size and orientation occur (Hess et al., 1968). The dimensions of the parallel layer groups

Table 3.1. : Properties of Graphitised Carbon Blacks

	Graphitized Black Pearls 2 *	Graphon †	Units
Surface area (N_2)	211.6	89.7	$m^2 g^{-1}$
Surface area (e.m.)	295.0	117.0	$m^2 g^{-1}$
Helium density	1.71	1.97	$g\ cm^{-3}$
Ash	0.06	0.08	%
Volatile content	0.00	0.06	% weight
pH	10.0	10.6	-
Average layer plane diameter	5.8	8.7	nm
Average crystallite thickness	2.2	4.3	nm

* Code name BP-D4

† Code name S6-D4

Figure 3.1. The 'Concentric Crystallite' Model

(a) Before Graphitisation

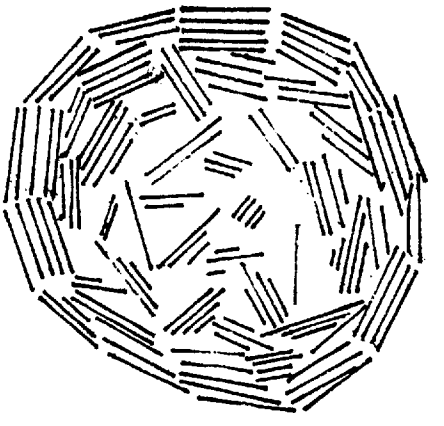

(b) After Graphitisation

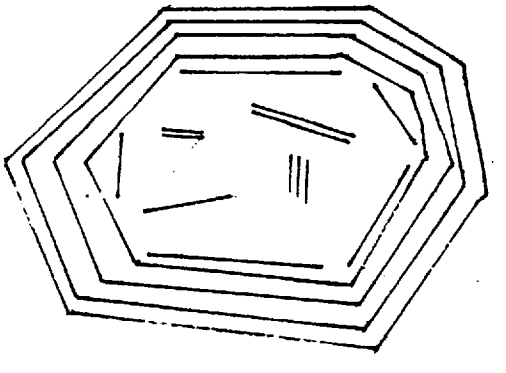

increase and the number of layers in the group increase, but initially the orientation remains random. Houska and Warren (1954) found that when the layer diameter increases to above 10 nm the layers begin to position themselves as in graphite. The layer planes at the surface grow to form an outer shell (Figure 3.1 (b)) whilst those in the more disordered interior grow and migrate to become parallel to the shell. This tends to leave a void in the interior which may be only partially occupied.

3.1.2. Membrane Construction and Characteristics

The Graphon membrane was constructed by Lowson (1968) and used by him in an investigation of helium flow (Ash, Barrer and Lowson, 1970). The Black Pearls membrane was of similar design (Figure 3.2). The method of fabrication of both membranes is briefly reproduced here.

The membrane holder consisted of a stainless steel tube of length ~ 9 cm and external diameter 1.5 cm which was manufactured in the departmental workshops. The internal diameter was accurately determined by adding weighed amounts of mercury and measuring the length of the mercury column. A side port was drilled out and a 0.24 cm internal diameter copper tube attached. The membrane was then fabricated using the technique of incremental compaction (Barrer and Gabor, 1959). Three accurately weighed amounts of carbon powder were added (Figure 3.3) and compressed between hardened steel plungers to the required porosity with the aid of a 1½ ton Dennison press. The length of each increment was determined by measuring the distance between the ends of the compression plungers with vernier calipers. The technique of incremental packing was employed to ensure, as far as possible, a relatively uniform homogeneous membrane.

A few layers of 100 mesh stainless steel gauze were then packed against each face of the membrane and fluted stainless steel retaining plungers screwed into place. A 5 cm wide, 0.3 cm internal diameter cooling coil of copper tubing was attached to the ingoing side and Kovar metal-glass seals silver soldered to the three outlets. To prevent excess heating and possible damage to the membrane during the soldering of a joint the remaining outlets were stoppered and as much of the assembly as possible was immersed in water. The membranes were designated 'Q' and 'R' after Ash, Baker and Barrer (1968); Ash, Barrer, Clint, Dolphin and Murray (1973); Ash, Barrer and Foley (1976) and their properties given in Table 3.2.

Figure 3.2. The Membrane Assembly

(a) Carbon Powder
(b) 100 Mesh Gauze
(c) Side Port
(d) Retaining Plunger
(e) Kovar Metal-Glass Seals
(f) Cooling Coil

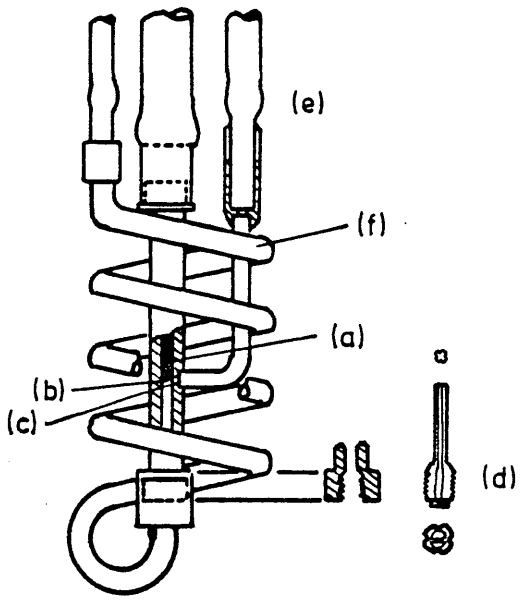

Figure 3.3. Incremental Compaction

(a) Carbon Powder Increments
(b) Side Port
(c) 100 Mesh Gauze
(d) Ingoing Side
(e) Outgoing Side

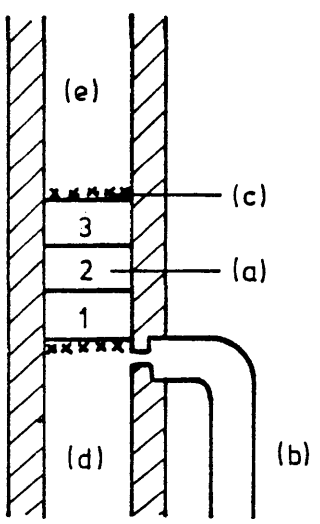

Table 3.2. : Properties of Compacted Membranes

(a) Compaction Details

Graphon Membrane 'Q'				
Increment	wt/g	ℓ/cm	Porosity	Gauge Press/ lb in^{-2}
1	0.0235	0.332	0.497	80
2	0.0265	0.340	0.503	100
3	0.0244	0.299	0.456	100
Graphitised Black Pearls Membrane 'R'				
Increment	wt/g	ℓ/cm	Porosity	Gauge Press/ lb in^{-2}
1	0.0286	0.413	0.497	200
2	0.0287	0.404	0.484	200
3.	0.0284	0.395	0.478	400

(b) Final Properties of the Membranes

	Graphon	Graphitised Black Pearls 2	Units
Cross-sectional area	7.146	8.050	10^{-6} m^2
Length	0.971	1.212	10^{-2} m
Wt of carbon	0.692	0.846	10^{-4} kg
Porosity	0.494	0.493	

Sorption Samples

The Graphon sample used for the adsorption studies was produced in pelletised form using the split plug technique of Barrer and Gabor (1960). The carbon being compressed to a porosity of 0.494 was comparable to the membrane. The graphitised Black Pearls 2 was used in the unconsolidated powder form. The samples weighed 3.2777 g and 4.1040 g for Graphon and Black Pearls respectively.

3.1.3. Outgassing Procedure

The membranes after exposure to the atmosphere or after a series of flow measurements required outgassing to give a reproducible surface. The Graphon and the graphitised Black Pearls membranes were heated under high vacuum to temperatures of 200°C and 250°C respectively. These temperatures were slowly developed to minimise the possibility of structural damage to the membrane. The outgassing time varied with contaminant. A minimum of 12 hours was employed but in some cases up to 60 hours was necessary before attaining a sticking vacuum.

3.2. General Features

3.2.1. Pumping System

The system of pumping was common to both flow and adsorption apparatus and is schematically shown in Figure 3.4. A rotary oil pump (Edwards, two stage) capable of creating a vacuum of 10^{-4} cm Hg backed a mercury diffusion pump to produce an ultimate 'sticking' vacuum of $\sim 10^{-6}$ to 10^{-7} cm Hg. The diffusion pump was connected to the high vacuum line by a liquid nitrogen cold trap. This prevented mercury contamination of the system and helped achieve a better vacuum by reducing the vapour pressure of condensible gases, such as water vapour which may be present. To maximise the pumping speed wide-bore Pyrex glass tubing ($\geq$ 12 mm internal bore) with 12 mm stopcocks was employed in the construction of the system.

A 5 dm^3 buffer volume branched off the connection between diffusion and rotary pumps, enabling the diffusion pump to function independently for a limited period. This allowed routine maintenance of the rotary pump to be carried out, such as belt and oil changes (at six monthly intervals).

A second rotary pump was connected to the low-vacuum line for the adjustment of mercury levels in McLeod gauges and manometers. It was also used for any preliminary evacuation of the apparatus (via a bypass connection). As a result a non-additive oil was used in the high-vacuum pump as it did not require protection from oxidation and contamination.

A built in safety feature was the inclusion of an oil trap and non-return valve above the rotary pump to prevent oil suck back into

Figure 3.4. The Pumping System

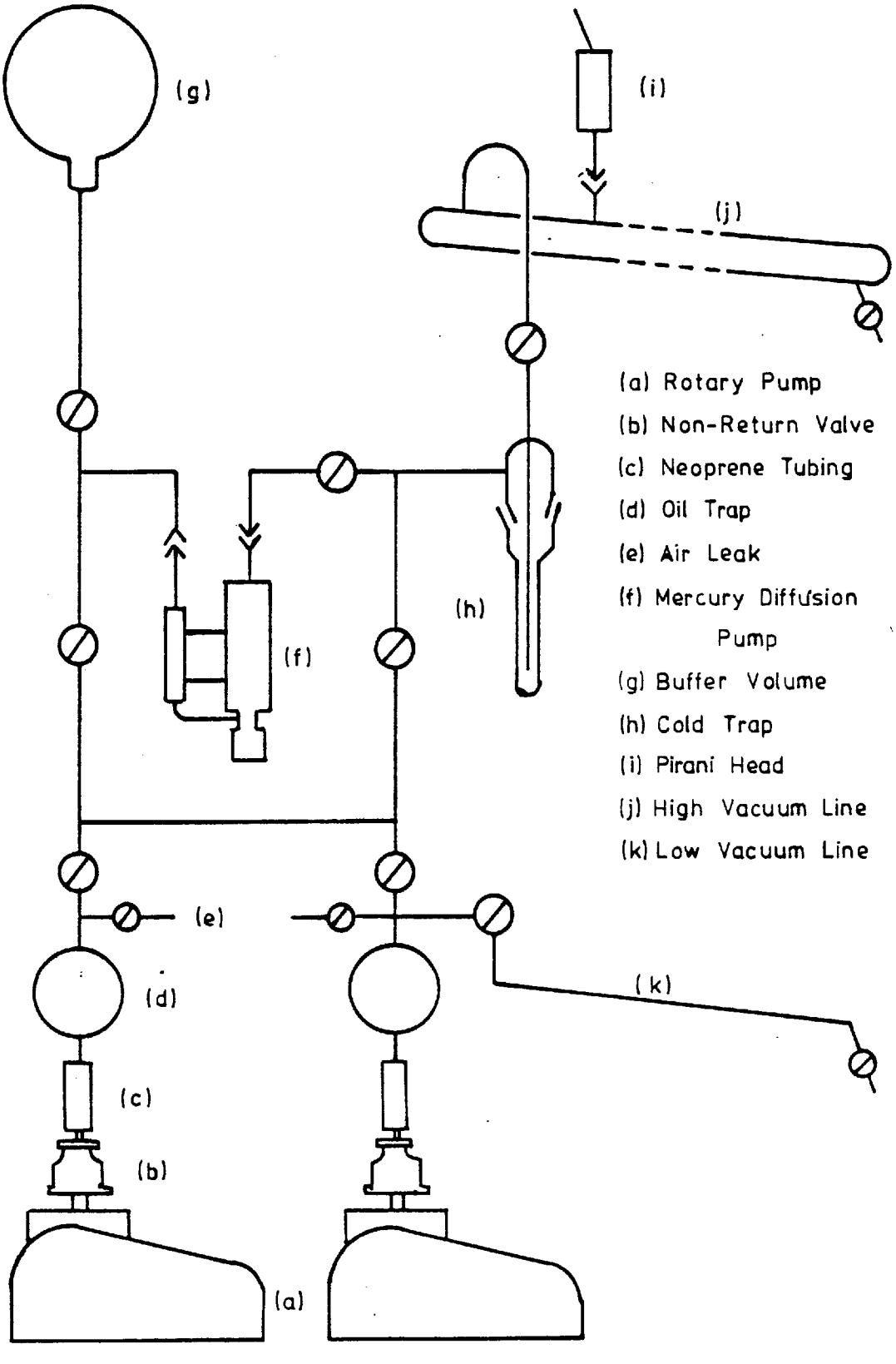

the apparatus in the event of a power failure. Each vacuum system contained a Pirani vacuum gauge (Edwards G5C-2) in the high vacuum line with a control unit (model 8-2) covering the range 1 - 10^{-5} cm Hg.

3.2.2. The Circulating Pump

In the flow experiments involving gas mixtures it was necessary to circulate the gases to ensure uniformity of composition. This was achieved using a reciprocating plunger pump similar in design to that of Barrer and Robins (1953) which streamed the gas mixture past the face of the membrane (Figure 3.5). The piston was a 2 cm diameter glass tube filled with lengths of soft iron packed with asbestos wool and vacuum sealed. It was surrounded by a copper wire coil and reciprocated under the action of an intermittent current supplied by a control unit. The valves were ground into their settings to be gas-tight and the whole assembly was constant volume in operation.

3.2.3. Thermostat Baths and Furnaces

(a) Outgassing Temperatures : The elevated temperatures were achieved using an electric furnace controlled by a Variac transformer. The furnace consisted of a fused silica casing with a winding of resistance wire and the exterior surrounded with asbestos rope.

(b) Adsorption and Flow Measurements : The constant temperature baths employed were as follows :

473 - 308 K : Silicone oil (Hopkin and Williams MS 550) in an insulated beaker of suitable size was heated by two 'Red-Rod' heaters connected to variable voltage transformers. One heater maintained the bath at ~ 5°C below the required temperature; the second, by means of a Gallenkamp relay and mercury contact thermostat, brought the temperature up to the constant experimental temperature. A uniform temperature control of ± 0.5 K was achieved with the utilization of a paddle stirrer.

273 K : Melting ice stirred in a dewar flask.

273 - 213 K : A 'leaky dewar' system was utilized for this range. Methylated spirits was employed as the thermostatting liquid and pelletised 'Card-ice' or liquid nitrogen as the refrigerant. The temperature was controlled to ± 1 K by means of a regulator/relay system and a 25 watt heating lamp.

77.4 K : Liquid nitrogen in a dewar flask.

Figure 3.5. The Circulating Pump

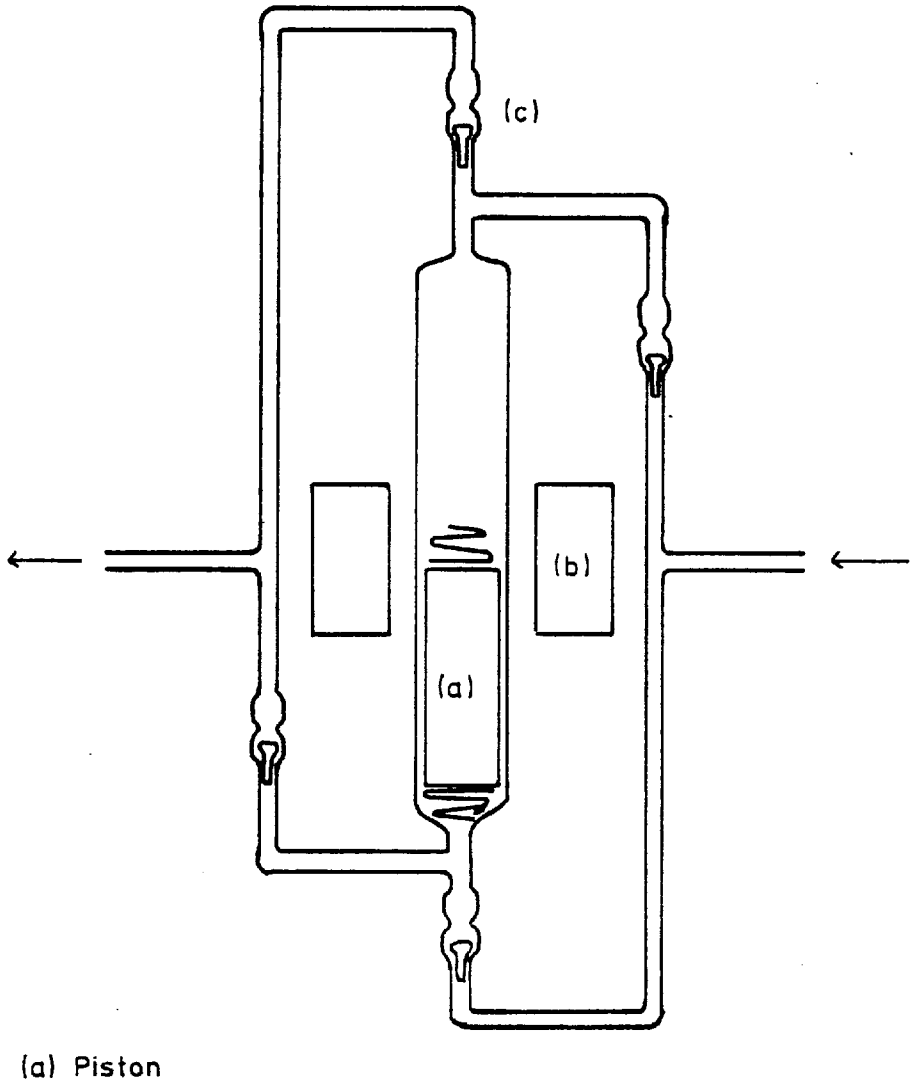

(a) Piston

(b) Coil

(c) Valves

3.2.4. Thermometers

A series of mercury in glass (0 to 50°C, 50° to 150°C, 150 to 200°C) with 0.1°C divisions were furnished by Sugden Powell Ltd. Each was supplied with a works certificate having been calibrated against N.P.L. thermometers. For the temperature range -50 to 0°C a mercury/thallium thermometer was employed. Also utilized for the low temperatures was an ammonia vapour pressure thermometer (range: -80 to -40°C). The vapour pressure data was taken from the 'Handbook of Chemistry and Physics'.

3.2.5. Gases Used

The gases He and Ar were B.O.C. research grade of specified purity (> 99.99%) supplied in one litre pyrex glass bulbs and filled to ~ atmospheric pressure. The hydrocarbons (C_3H_8 and $i\text{-}C_4H_{10}$) were stated to be 99.9% pure and were supplied in 500 cm^3 bulbs by the National Physical Laboratory. No further purification of the gases was undertaken.

3.2.6. McLeod Gauges

McLeod gauges were used for accurate pressure measurement in the range 10^{-3} cm Hg - 10^{-1} cm Hg. They could also be used to monitor the vacuum in the system when open to pumping.

The volume of the gauge was calculated from a number of determinations of the weight of distilled water required to fill the bulb. The cross-sectional area of the Veridia precision bore capillary limbs was calculated from the length of an accurately weighed mercury slug in several places.

Two gauges were used in this study on the 'conventional' apparatus (designated Gauge 1 and Gauge 2) and their characteristics are given in Table 3.3.

Table 3.3. McLeod Gauge Characteristics

McLeod Gauge	Capillary cross-sectional area / 10^{-6} m^2	Bulb volume / 10^{-3} dm^3
1	3.144	302.9
2	3.236	367.7

3.2.7. Mercury

The mercury used in McLeod gauges and manometers was cleaned by the following method to reduce 'sticking problems'. Any large particular impurities were first removed by filtration through a pin-holed filter paper. The mercury was then placed in a 1 dm^3 filter flask and covered with water to a depth of a few centimeters. Sodium peroxide was added and the mixture agitated overnight, resulting in acid-free mercury. The aqueous layer was removed and the mercury washed free of alkali with distilled water. Metal impurities were removed by overnight agitation with acidified potassium permanganate solution leaving an oxide scum on the surface. It was then rewashed with distilled water and passed dropwise into dilute nitric acid to dissolve the oxide. The mercury was again washed with distilled water and dried initially with a filter paper and then by heating to $\sim 120^{\circ}C$ in a fume cupboard. It was finally filtered into dry, clean storage bottles.

3.2.8. Miscellaneous

Differences in mercury levels in McLeod gauges and manometers were measured to $\pm 10^{-5}$ m with cathetometers (Precision Tool and Instrument Company) placed on cast-iron tables for stability.

Apiezon-N grease was used to lubricate all high vacuum ground glass taps; cone and sockets were sealed with Picein wax.

The measurement of time made use of a Rone stopwatch.

3.3. The Adsorption Isotherm Apparatus

A standard volumetric adsorption apparatus (Young and Crowell, 1962, p.284) was employed in the measurement of the adsorption isotherms and is shown in Figure 3.6. The apparatus was that used in the sorption kinetics studies of Craven (1976) with slight modifications to the gas supply line. The manometer was constructed from 10 mm precision bore Veridia glass tubing and all other connecting glassware from 3 mm bore capillary tubing to minimise the dead volume. The burette bulb volumes were calibrated by mercury weighings and the dead space by helium expansion. At each isotherm temperature the volume from the sample bulb to the tap

Figure 3.6. The Volumetric Adsorption Isotherm Apparatus

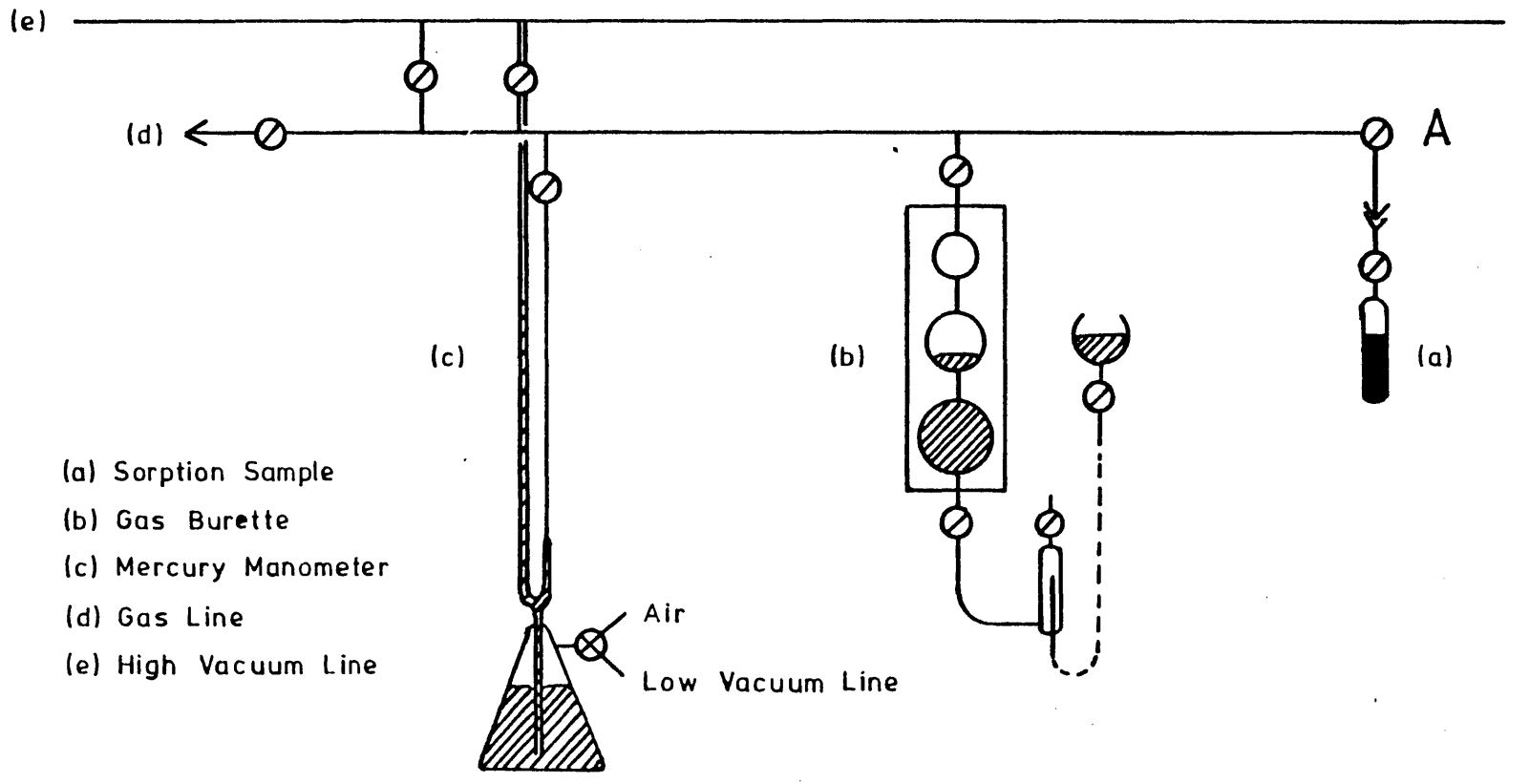

(Tap A) admitting gas to it was calibrated with helium. This resulted in a temperature dependent volume (in $cm^3\ K^{-1}$) for each sample and each temperature. This is referred to as $\emptyset_T$ in equation (4.2). It was due to the temperature gradient existing between the temperature of the room and that of the sample bulb. The remainder of the known volumes were considered to be at room temperature.

The volumetric technique of isotherm determination is common knowledge and is not discussed here. Equilibration times ranged from 1 hour to 3 hours depending on the sample. Isotherms of isobutane and propane were determined on both carbons at those temperatures where flow phenomena had been investigated. Some measurements were also undertaken on the actual membranes for comparison purposes. Low temperature nitrogen isotherms were measured for the purpose of B.E.T. analysis. The actual results obtained are presented in section 4.1. and the data in appendix A.

3.4. Isothermal Flow Apparatus

3.4.1. Introduction to Flow Apparatus

Two types of flow apparatus were employed in this study. Both were designed for isothermal work, but they differed in their boundary conditions. They were designated the 'conventional' and the 'pressure decay' apparatus and are discussed in greater detail in sections 3.4.2. and 3.4.3. respectively.

(a) The 'Conventional' Flow Apparatus : This essentially maintained a constant pressure difference across the membrane. The build up of pressure on the outgoing side was kept so as to be negligible in comparison to the constant ingoing pressure by means of large buffer volumes. The majority of previous work originating from these laboratories has employed this type of system.

(b) The 'Pressure-Decay' Flow Apparatus : A variable pressure head existed, with an initially large pressure head decaying to an equilibrium pressure on both sides of the membrane. These conditions have been used by Sharma (1970) in a study of hydrocarbon flow through Carbolac.

3.4.2. 'Conventional' Flow Apparatus

(a) Description The apparatus (Plate 3.1., Figure 3.7) consisted of a gas line, an ingoing side, a membrane and an outgoing side. The ingoing

Figure 3.7. The 'Conventional' Flow Apparatus

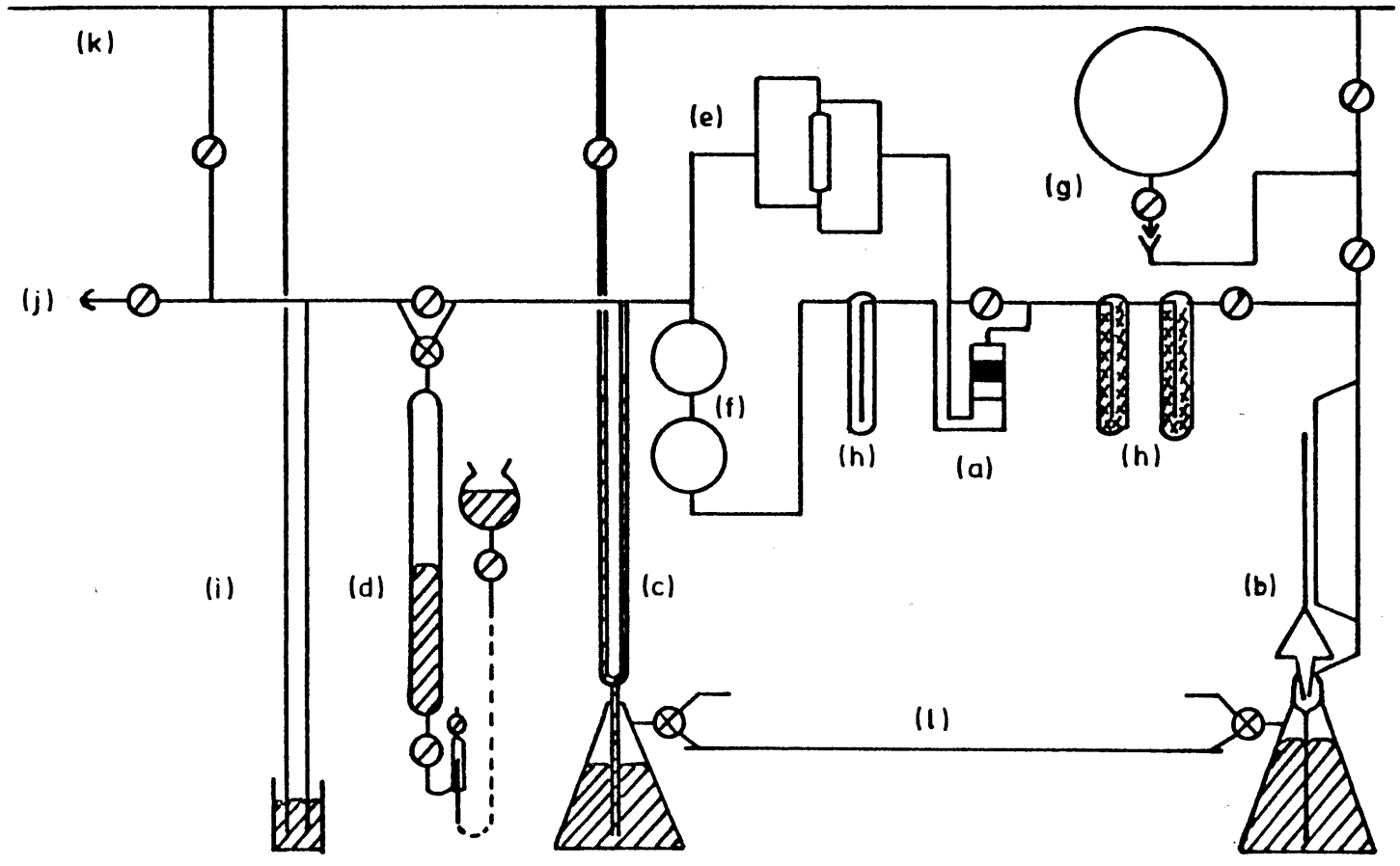

(a) Plug Assembley
(b) McLeod Gauge
(c) Ingoing Manometer
(d) Toepler Gauge
(e) Circulation Pump
(f) Ingoing Buffer Volumes
(g) Outgoing Buffer Volumes
(h) Cold Traps
(i) Safety Manometer
(j) Gas Line
(k) High Vacuum Line
(l) Low Vacuum Line

Plate 3.1.

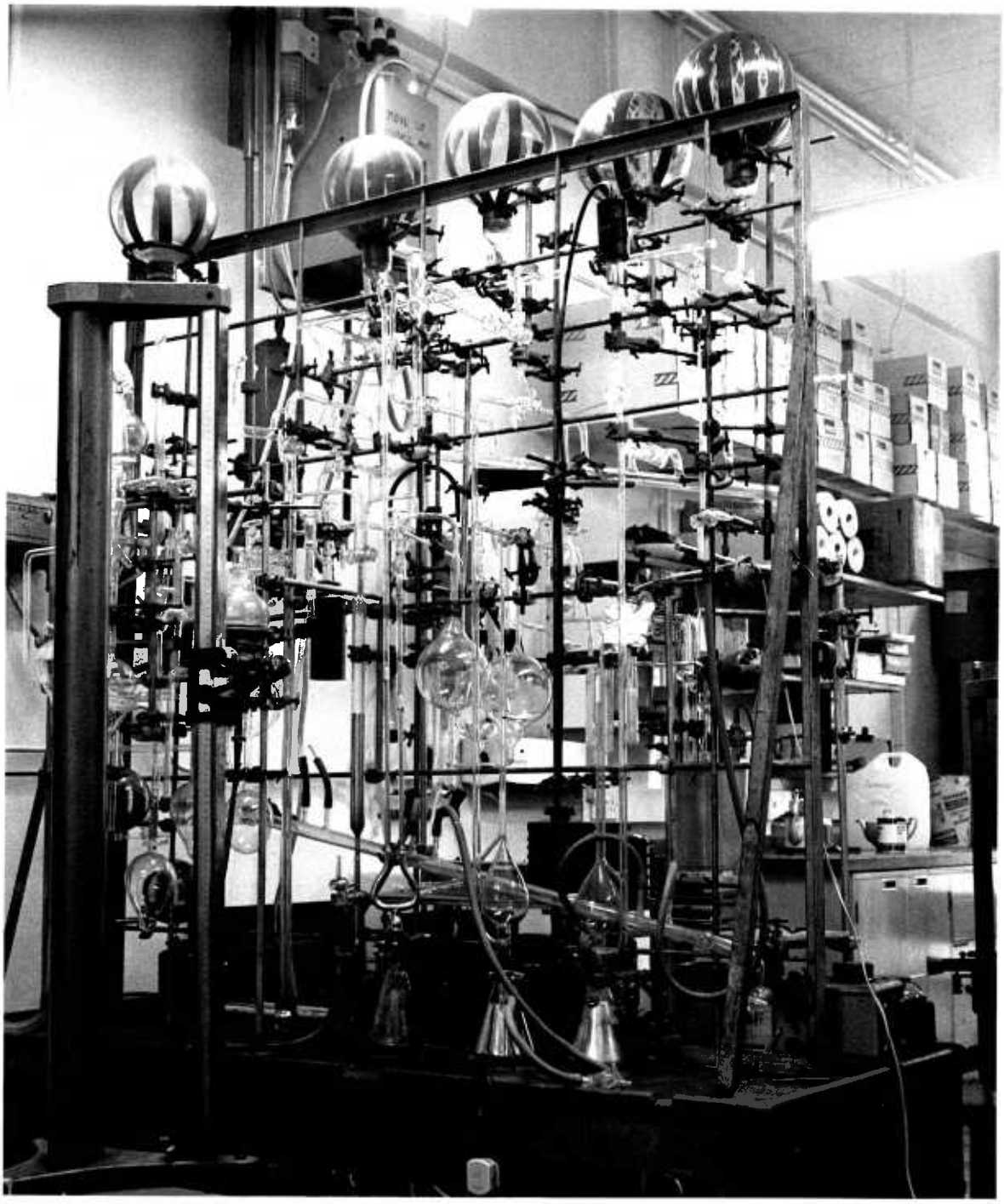

'Conventional' Flow Apparatus

side comprised a Toepler pump and two 1 dm^3 buffer volumes to maintain a constant ingoing pressure measured on the mercury manometer (10 mm bore Veridia tubing). The circulating pump (previously described, section 3.2.2) allowed the gas mixtures to be streamed past the ingoing face of the membrane ensuring evenly mixed gases. Care was taken to ensure that any 'stagnant' volumes were minimised.

The outgoing side consisted of two cold traps filled with glass beads to allow efficient freezing out of the condensible gases in mixture runs. The outgoing gas pressure was measured on a McLeod gauge as a function of time and four 5 dm^3 buffer volumes enabled maximum use of the gauge. The buffer volumes were calibrated by the repeated additions of distilled water and weighings. The dead space volume was calculated by helium expansion from the McLeod gauge bulb. These volumes, including the total outgoing volume as each of the buffers is opened are given in Table 3.4. The membrane assembly has previously been discussed (§3.1.2).

Table 3.4. 'Conventional' Flow Apparatus : Outgoing Volume

Component Buffer volume	Volume dm^3	Σ (outgoing volume)/dm^3	
		McLeod 1	McLeod 2
Dead space	0.462	0.764	0.829
α	5.437	6.216	6.277
β	5.523	11.745	11.810
γ	5.412	17.164	17.229
δ	5.346	22.528	22.593

(b) Technique

The outgassed membrane was initially thermostatted at the required temperature. Gas was admitted to the ingoing side from the gas line. The pressure, p_1 measured by means of the mercury manometer, was held constant by raising the level of mercury in the Toepler pump. The outgoing pressure, p_2 was measured as a function of time, t with the McLeod gauge, until a substantial linear section of the p_2 vs t plot developed (Figure 4.28). The time elapsed varied from 90 minutes to three or four hours

depending on the temperature of the run and the gas under consideration. The outgoing volume could be varied (Table 3.4) from one experiment to another maintaining p_2 in the McLeod gauge range.

In the case of gas mixture experiments, the sorbable component was allowed to achieve the steady-state flow. At the outgoing side of the membrane it was frozen out with the two liquid nitrogen cold traps. The initial pressure, p_1 was noted with the Toepler pump fully raised. The mercury in the pump was then lowered to accept a dose of helium or argon from the gas line. This was then pumped into the ingoing side via the two-way tap by raising the Toepler pump mercury level. The process was repeated until a partial pressure of ~ 4 cm Hg of helium or argon had been admitted. The total pressure was noted and the Toepler pump lowered to a level which would enable the ingoing pressure to be held constant over the course of a run. Due to the freezing out technique, only the outgoing pressure of the helium or argon was measured as a function of time. Subsequent calculations were thus made for varying ingoing pressures of hydrocarbon.

3.4.3. 'Pressure' Decay Apparatus

(a) Description

The high-vacuum rig (Plate 3.2, Figure 3.8) was made up of four units, a gas line, a calibration section, ingoing and outgoing sides and the membrane assembly. Pressures on the two sides of the membrane were measured with transducers (Bell and Howell : Type 4-326-L101 : range 0-15 p.s.i.A) and a capacitance manometer (discussed later in 3.4.3 (b)). The transducers were driven by a 10 volt stabilised power supply (Kingshill TR 215). The outputs were fed into a potentiometer, (H. Tinsley) supplied by a 2 volt power source (Fannell 0-30 volt L30-1), or into potentiometric chart recorders (Bryans Southern Instruments, Type 28000).

Both sides contained circulating pumps (cf §3.2.2) to stream the gas mixtures past the membrane faces. Originally the apparatus was designed for a membrane which allowed circulation of gas past each face. This assembly unfortunately was rendered unusable, and it was decided that an investigation on the 'conventional' membrane under 'pressure-decay'

Figure 3.8. The 'Pressure-Decay' Flow Apparatus

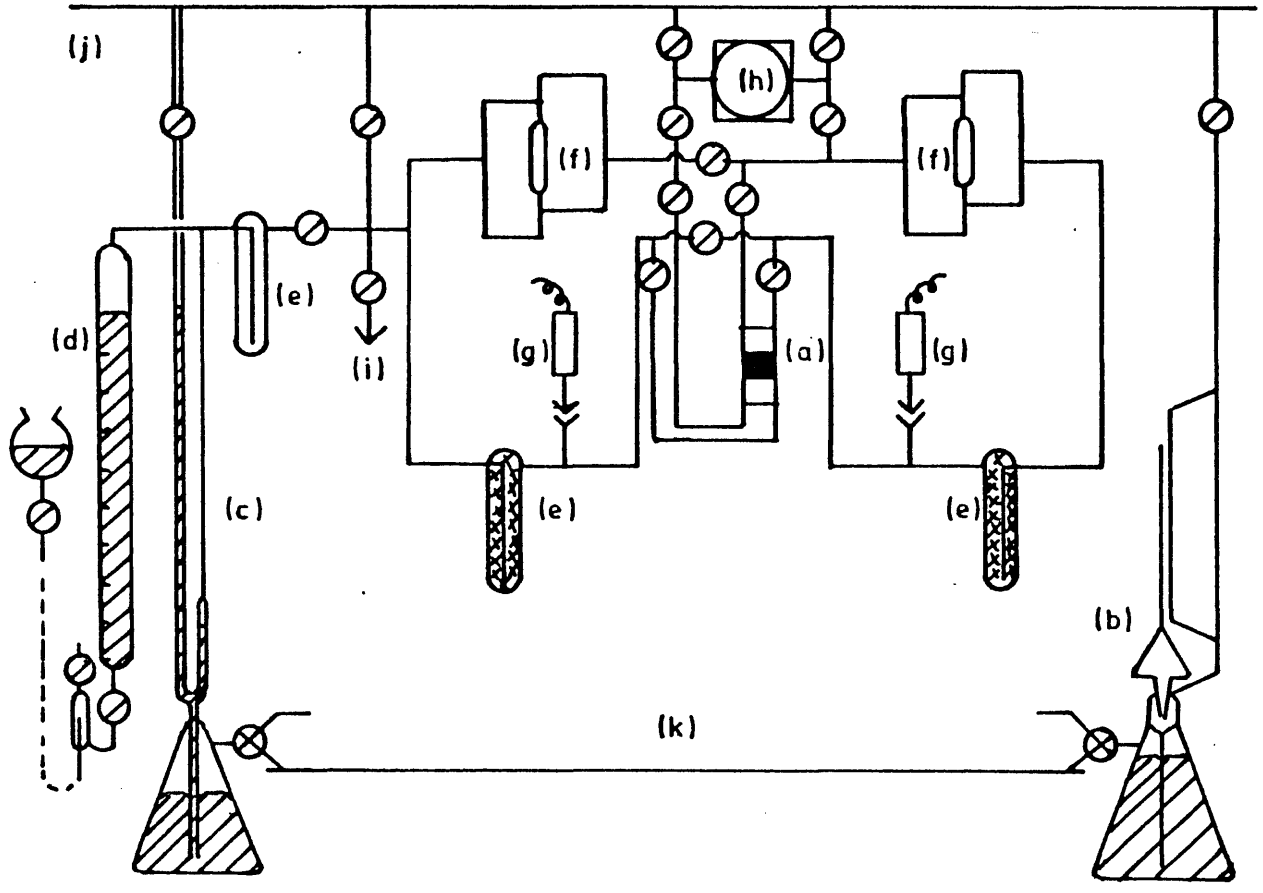

(a) Plug Assembley
(b) Monitor McLeod Gauge
(c) Calibration Manometer
(d) Gas Burette
(e) Cold Traps
(f) Circulation Pumps
(g) Pressure Transducers
(h) Capacitance Manometer
(i) Gas Line
(j) High Vacuum Line
(k) Low Vacuum Line

Plate 3.2.

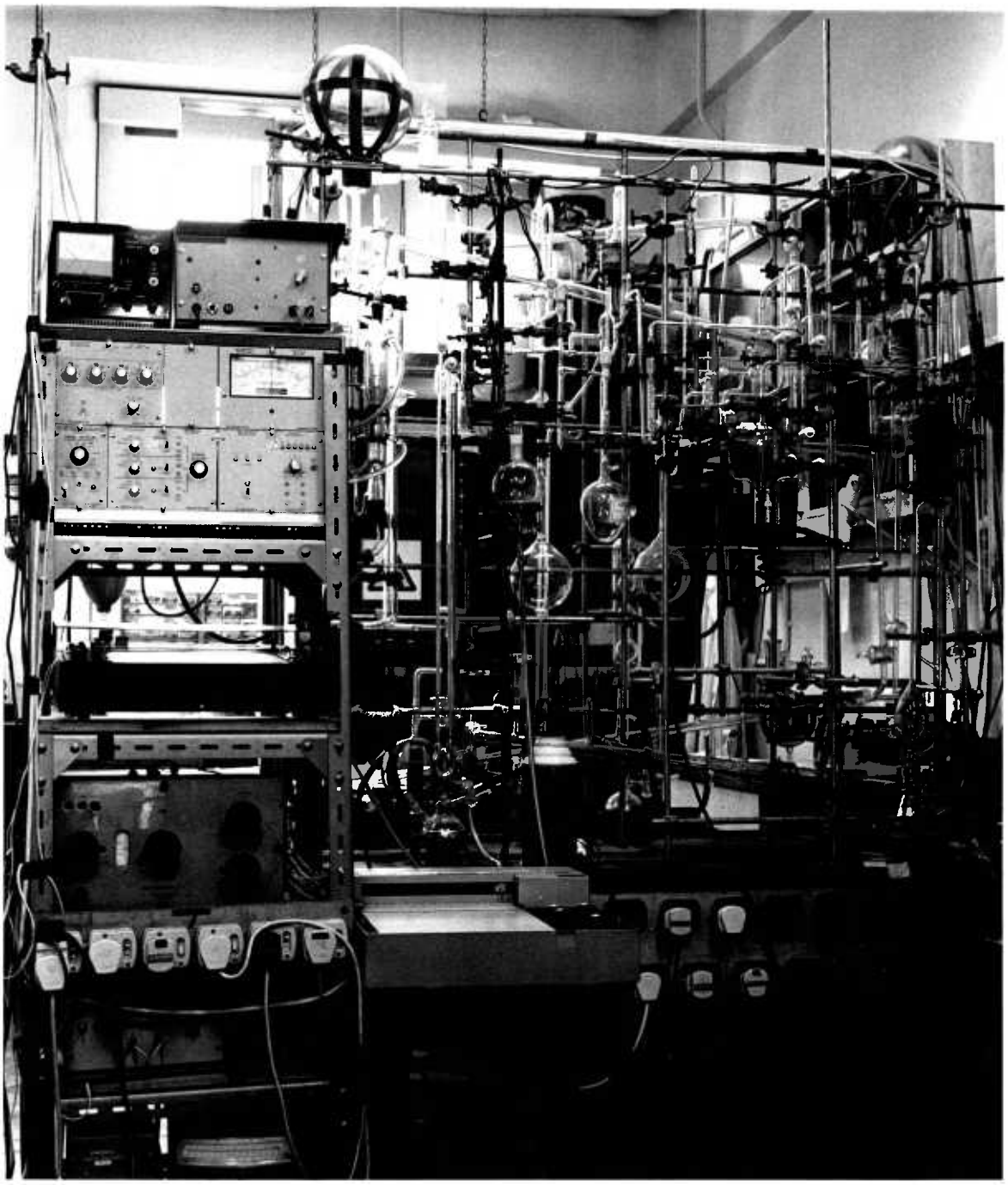

'Pressure-Decay' Flow Apparatus

conditions would be undertaken. This did mean however that mixing was not possible up to the face of the membrane due to the restriction of Kovar seals and the restraining plunger. An attempt was made to maximise mixing by a narrow glass tube connected to the circulation system. This was taken inside the outgoing Kovar seal down to the head of the retaining plunger.

Cold traps containing glass beads were incorporated on both sides in order that mixtures could be made up. Four taps at the membrane ensured that any sorption equilibrium previously established was not affected by the freezing out techniques.

A calibration unit was incorporated to allow calibration of all volumes by helium expansion, and transducers against known gas pressures (the transducers were periodically checked for drifting). It consisted of a gas burette (0 - 100 cm^3) and a precision bore mercury manometer. This unit was separated from the main system by a cold trap to ensure that no mercury contamination of the capacitance manometer could occur. The calibrated volumes are given in Table 3.5.

Table 3.5. Pressure-Decay Apparatus : Calibrated Volumes

	Volume / $10^{-3} dm^3$
Dead Space	127.4
Ingoing volume	132.9
Outgoing volume	151.8

(b) The Capacitance Manometer

The instrument used in this work was the 'Baratron' pressure meter type 170 manufactured by M.K.S. Instruments Inc. of Burlington, Mass., U.S.A. The capacitance manometer measures pressure as defined and therefore does not depend on the nature of the gas or composition. The pressure head (Figure 3.9) consists of a tensioned metal diaphragm positioned between two electrodes. As pressure deflects the diaphragm a change in capacitance between the diaphragm and each electrode occurs.

These capacitances are part of a bridge circuit which is balanced by a decade unit and the calibration is such that this reading is given in (cm Hg). The head used (Type 145- AH) was of differential design and could be used to measure a pressure difference or if one side was connected to high vacuum an absolute pressure in the range 1 - 100 cm Hg.

The Baratron system is modular in design and the following modules were incorporated into the system (schematically represented in Figure 3.10).

(a) 170M-7 : Electronics Unit This provided the basic power supply to the head and converted the head signal into two 0-10 V DC outputs per range. It also allowed different sensitivities, x 1, x 0.1, x 0.01, x 0.001 of the full scale range by the use of a precision voltage divider.

(b) 170M-26 : Analog Meter This meter utilized one of the D.C. outputs from the head and corresponded to the out-of-balance signal. The second D.C. output was fed into a potentiometric chart recorder.

(c) 170M-29 : Digital Offset Unit The unit consisted of three decade switches plus a vernier potentiometer and was used to adjust the D.C. output to zero. In this condition the dial readings gave the pressure directly in cm Hg.

(d) 170M-34 : Head Selector Unit This provided the option of three leads being powered continuously. It contained zero and quadrature adjustment controls for each head.

(e) Type 145AH : Head Sensor The head used was of all welded metal construction to minimise outgassing and leaks. It contained internal heaters to minimise temperature change effects on the sensor which were regulated to maintain the temperature at $50^{\circ}C \pm 0.1^{\circ}C$. Cajon VCR couplings were used to connect the head to the vacuum system via Kovar metal-glass seals.

A built in safety feature protects the diaphragm against over pressure with the fixed electrodes acting as stops against which the diaphragm can rest.

(c) Technique

The outgassed membrane was placed in the constant temperature bath and was allowed to achieve thermal equilibrium. The gas under study

Figure 3.9. Capacitance Manometer Pressure Head

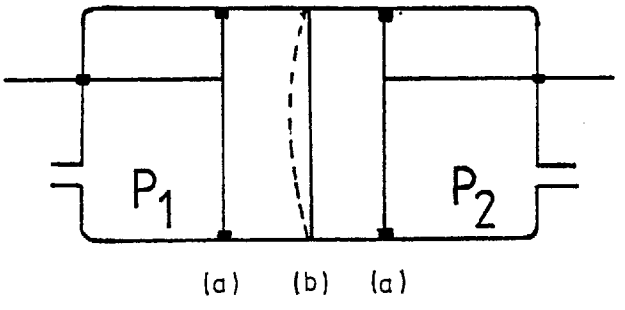

(a) Fixed electrodes : nickel deposited on ceramic
(b) Tensioned metal diaphragm

was admitted to the ingoing side at a known pressure, p_1 measured with the pressure transducer and/or the Baratron. At time, $t = 0$, the taps to the membrane were opened and the pressure difference, Δp between either side of the membrane was followed as a function of time. The outputs from the Baratron and both transducers were fed into potentiometric chart recorders (previously calibrated against known voltages) and continuously monitored.

After the completion of a run ($\sim$ 5 - 6 hours) the two sides were connected together and the final equilibrium pressure, p_∞ determined by accurately measuring the transducer outputs on the potentiometer.

For mixtures the basic procedure is as above apart from the formulation of the mixture. Sorption equilibrium was set up with both sides open to the membrane and an equilibrium pressure of sorbable gas in the system. The two sides (and hence also the membrane) were then isolated and the ingoing side frozen out. A pressure of $\sim$ 10 cm Hg of helium was then admitted to the ingoing side and the cold trap removed. Once thermal

Figure 3.10. Schematic Representation of the Baratron Modular System

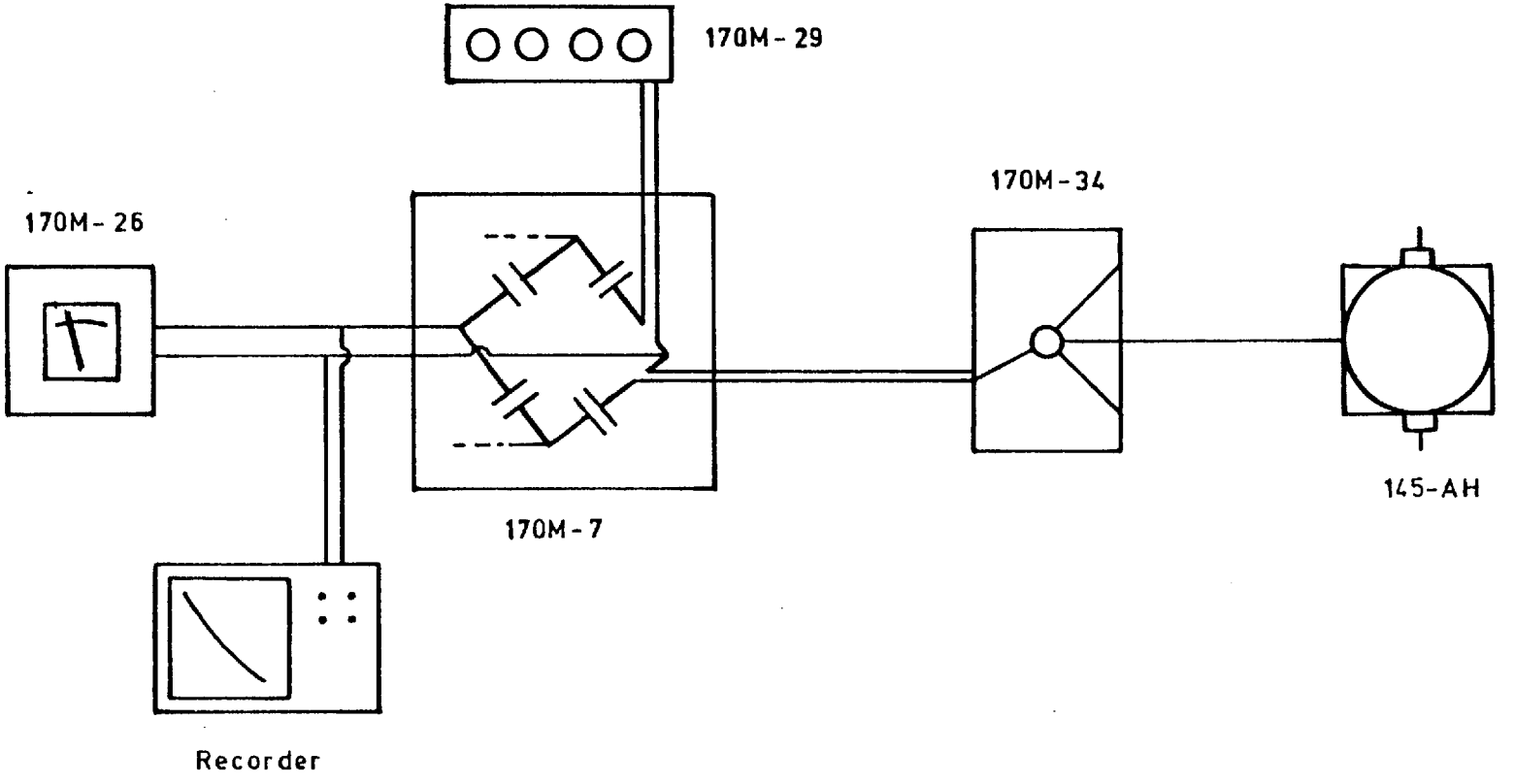

equilibrium had been established the circulation pumps were switched on, the taps to the membrane opened and the run was started. At completion, the equilibrium pressure of helium was measured with the two sides connected together. Mixing (as far as possible) was employed on the outgoing side to ensure that the gaseous component, having passed through the membrane was removed to other parts of the side. This was limited however for reasons already discussed (§3.4.3 (a)).

CHAPTER 4 : RESULTS

4.1. Adsorption Isotherms

4.1.1. Introduction

Adsorption measurements were made to allow the maximum interpretation of the flow data. However valuable information about the surfaces can also be obtained from the isotherms themselves.

The hydrocarbon isotherms were measured at temperatures for which flow experiments had been performed on the Graphon and graphitised Black Pearls samples. The Graphon sample was in the pelletised form (cf §3.2.2). However due to limited quantities of the Black Pearls carbon pelletisation was not undertaken and the isotherms were measured on the unconsolidated powder.

A comparison between isotherms measured on the pellets and the compacted membrane was undertaken for Graphon. This was only possible at low temperatures due to the small amount of carbon present in the membrane and the corresponding low uptakes of adsorbate.

Low temperature nitrogen isotherms were also measured at 77.4 K on both samples for surface area analysis.

Generally isotherms are of the form amount adsorbed, v (cm^3 stp g^{-1}) against equilibrium pressure, p (cm Hg). A gas at a known pressure, p_1 is admitted to a known volume, V_1 and the temperature, T_1 measured. The sample holder is then opened and the resulting equilibrium pressure, p_2 and the temperature, T_2 measured. Hence the amounts of gas before, n_1 (cm Hg cm^3 K^{-1}) and after, n_2 (cm Hg cm^3 K^{-1}) admission to the sample are given by the expressions :

$$n_1 = \frac{p_1 V_1}{T_1} \qquad (4.1)$$

$$n_2 = \frac{p_2 V_1}{T_2} + \phi_T p_2 \qquad (4.2)$$

where ϕ_T (cm^3 K^{-1}) is the temperature dependent volume of the adsorption sample holder. This accounts for the variation in temperature between the holder and the fixed volume V_1 and is evaluated by previous helium expansions for each isotherm temperature.

Thus the value of $(n_1 - n_2)$ gives the amount of gas adsorbed at the equilibrium pressure. This value is converted to cm^3 stp g^{-1} by

multiplying by the factor :

$$\frac{1}{\text{mass adsorbent}} \cdot \frac{273.2}{76}$$

4.1.2. Nitrogen Isotherms

Adsorption isotherms (Figures 4.1 and 4.2) were measured at liquid nitrogen temperature (77.4 K), the experimental data being given in Appendix A1 and 2. B.E.T. plots (Figures 4.3, 4.4) were constructed according to :

$$\frac{p}{(p_o - p)v} = \frac{1}{v_m C} + \frac{C - 1}{v_m C} \frac{p}{p_o} \qquad (4.3)$$

where p is pressure (cm Hg), p_o the saturated vapour pressure, v the amount adsorbed (cm^3 stp g^{-1}), v_m the monolayer capacity (cm^3 stp g^{-1}) and C a constant. These showed linearity in the regions p/p_o = 0.01 - 0.23 for Graphon and 0.1 - 0.4 for the graphitised Black Pearls. From the values of the slope and intercept the monolayer capacity is calculated giving 18.4 and 51.1 cm^3 stp g^{-1} for Graphon and Black Pearls respectively. The surface areas are given in Table 4.1 (based upon a value of 0.162 nm^2 for the cross-sectional area of the adsorbed nitrogen molecule, cf §5.1.1). To calculate the monolayer capacities of other adsorbed molecules values of 89.7 and 211.6 m^2 g^{-1} (figures quoted by the manufacturers, Cabot Corporation) were employed.

Literature values of surface area are given in Table 4.1 and cover the range 80.3 to 89.7 m^2 g^{-1} for Graphon.

'De Boer' 't' plots are shown in Figure 4.5 for Graphon and Black Pearls and these are discussed further in Section 5.1.1. The surface areas resulting from 'de Boer's' treatment are also given in Table 4.1.

A slight hump is observed for the Black Pearls Isotherm between v values of ~ 75 and 95 cm^3 stp g^{-1} centred at v = 87 cm^3 stp g^{-1} and $p/p_o \simeq 0.4$. This has been observed previously for Graphon (Joyner and Emett (1948)) and is repeated here with the hump between v values of 27 and 37 cm^3 stp g^{-1} and centred at v = 34 cm^3 stp g^{-1} and $p/p_o \simeq 0.4$

Figure 4.1. Nitrogen/Graphon Pellets Adsorption Isotherm : T/K = 77.4

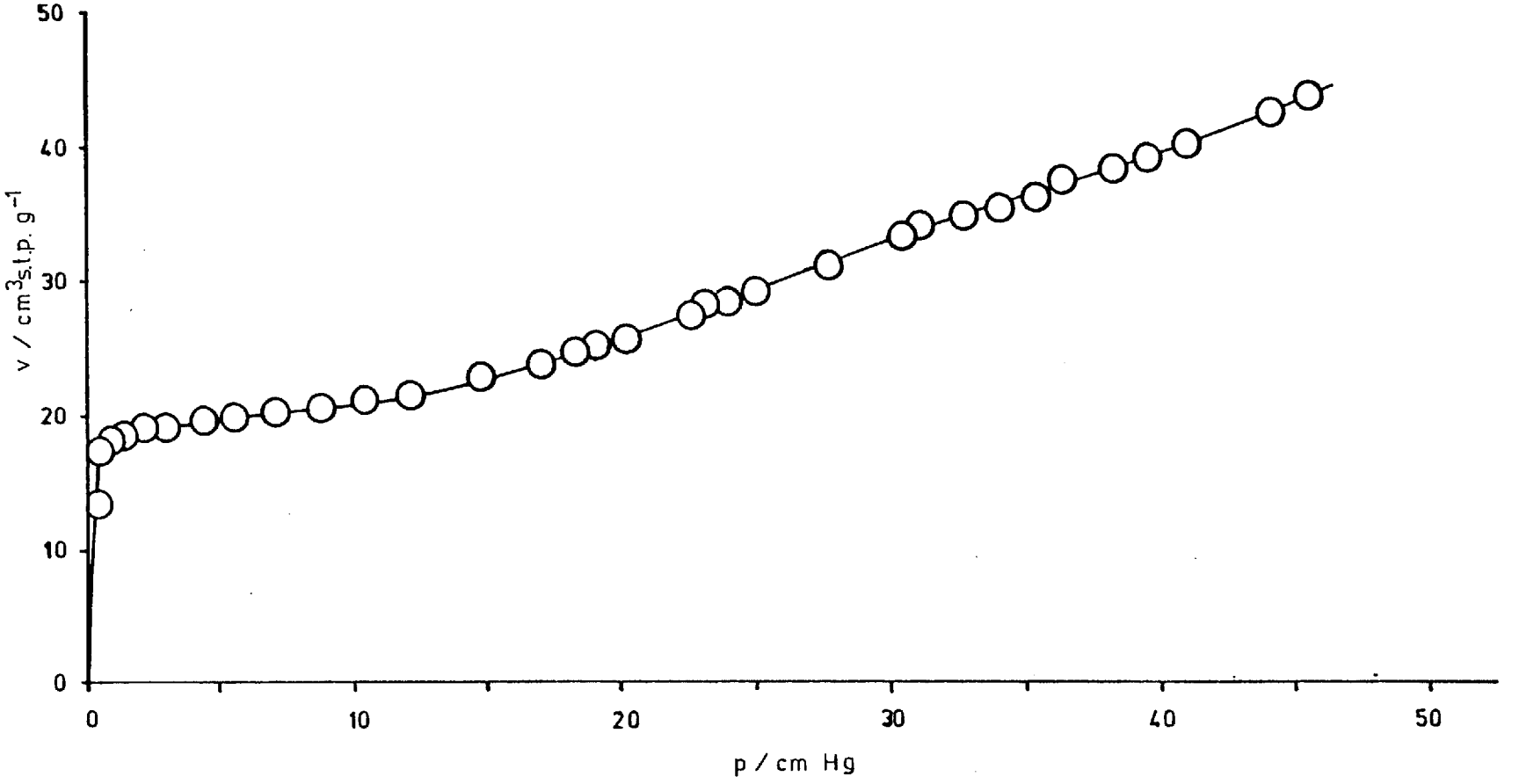

Figure 4.2. Nitrogen/Black Pearls Powder Adsorption Isotherm : T/K = 77.4

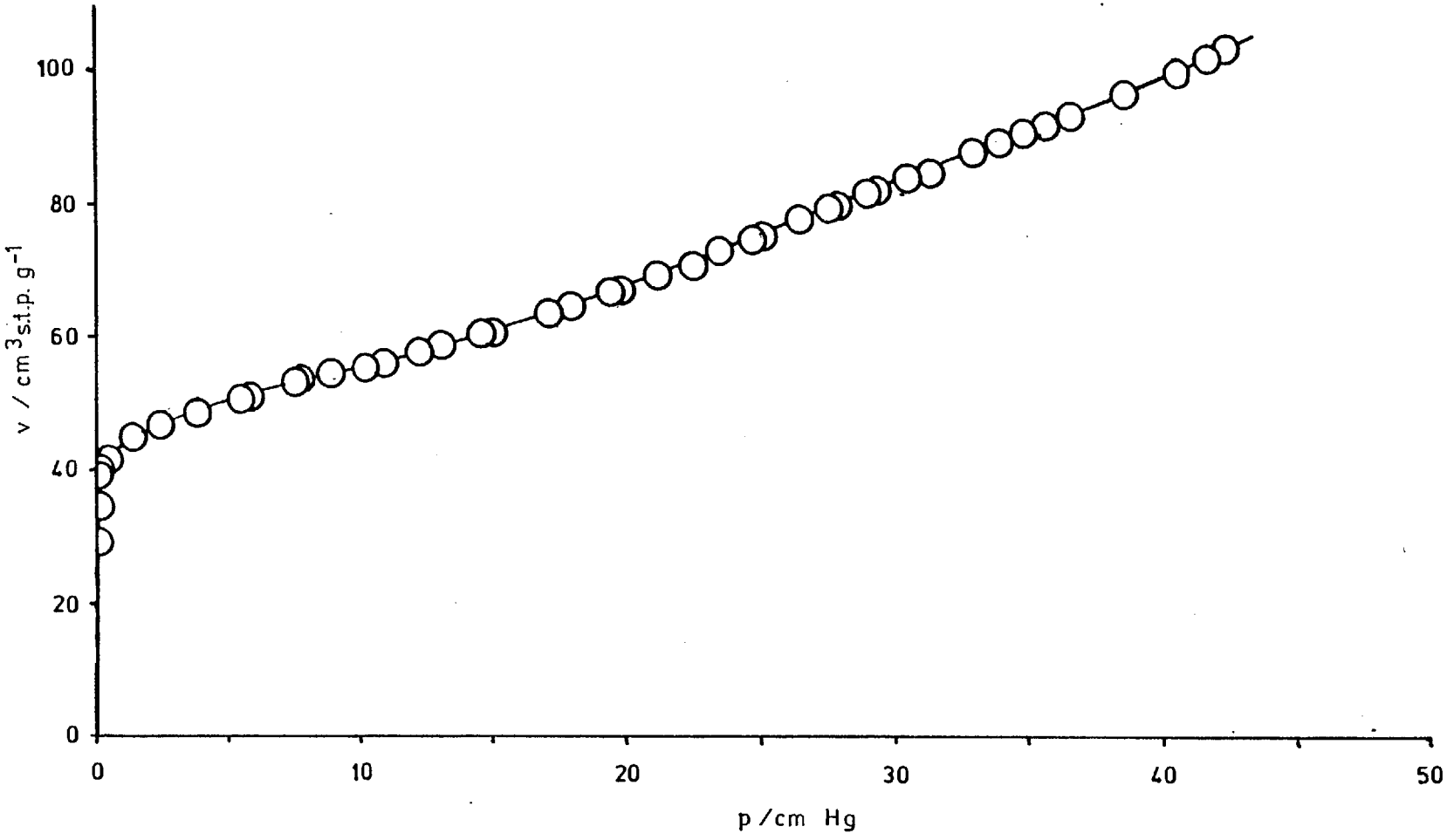

Figure 4.3. Nitrogen/Graphon Pellets : B.E.T. Plot

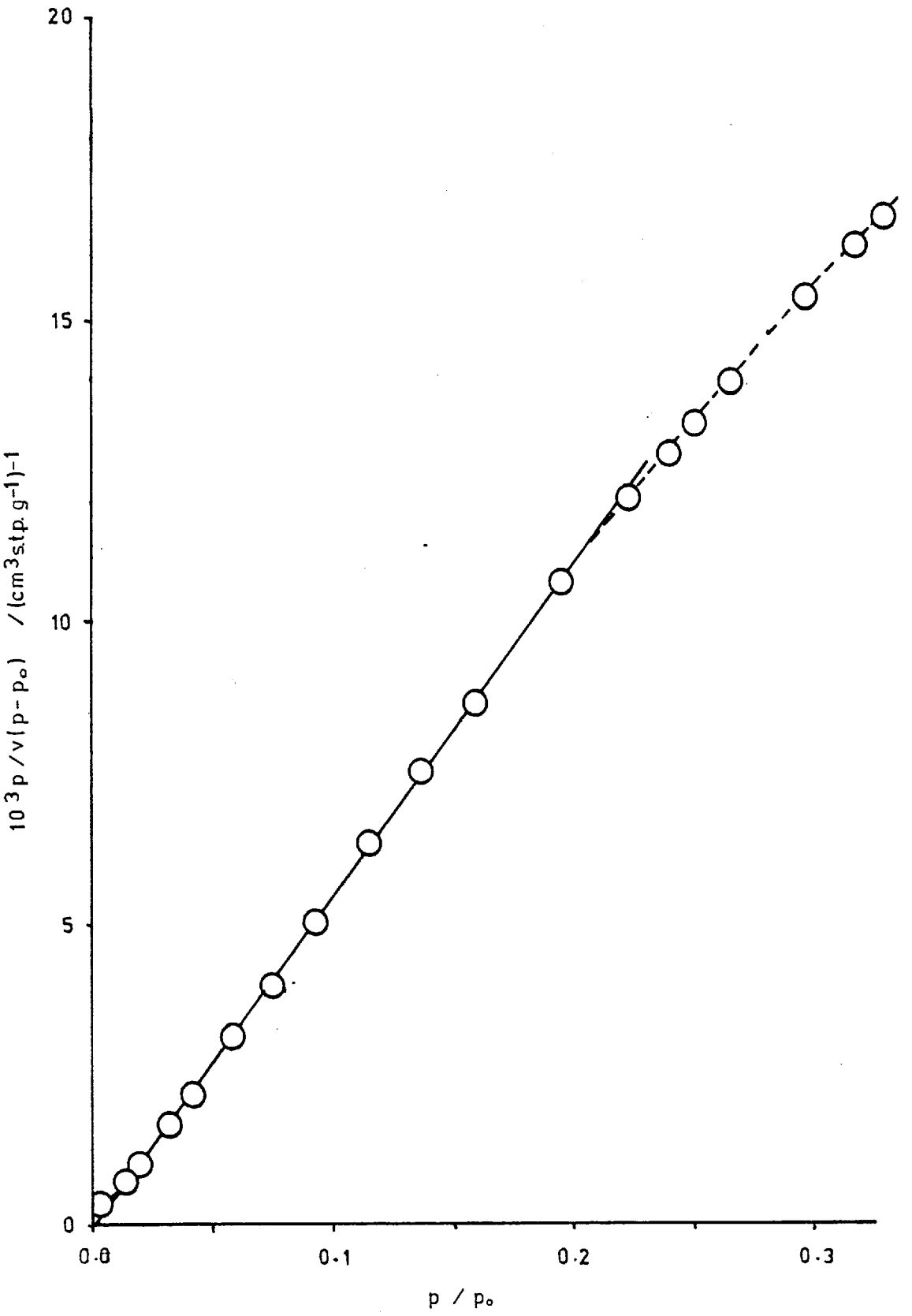

Figure 4.4. Nitrogen/Black Pearls Powder : B.E.T. Plot

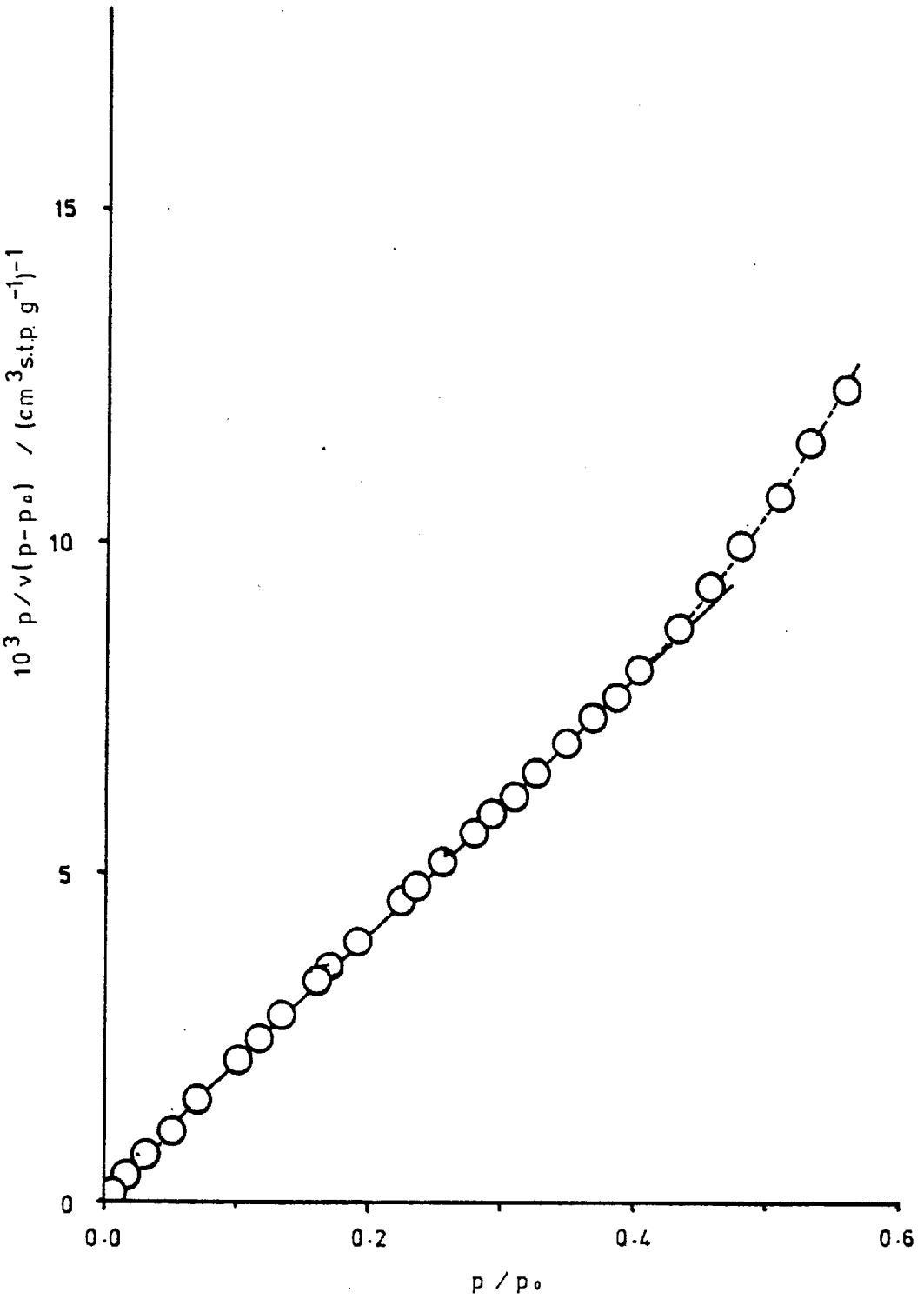

Figure 4.5. 'De Boers' (v - t) Plot for Graphon and Black Pearls

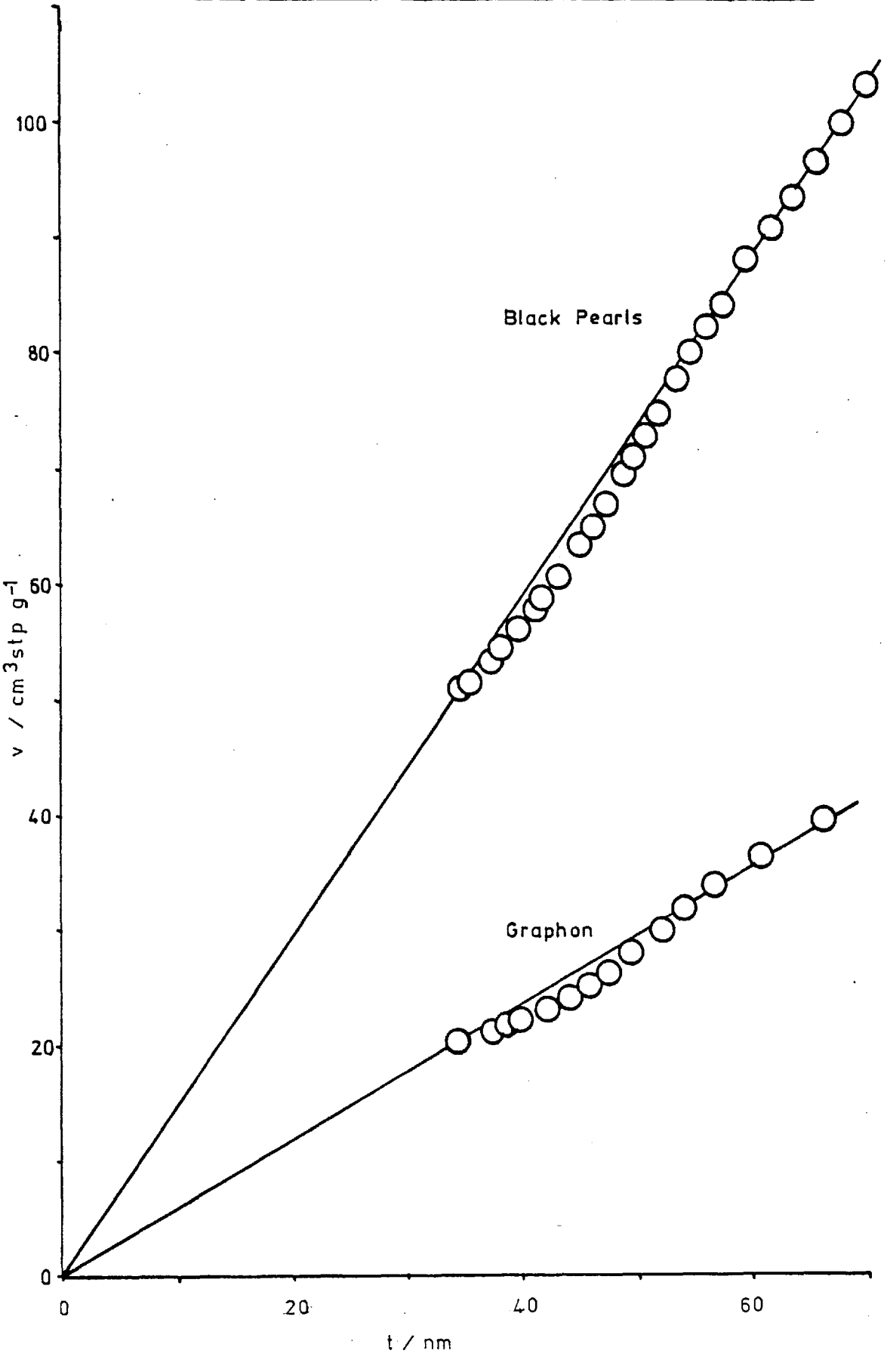

Table 4.1. Surface Areas from B.E.T. N_2 Isotherms

Adsorbent	Surface Area $m^2 g^{-1}$	Reference
Graphon (S6D4)	80.0	B.E.T. Plot } This work
	94.4	de Boer 't' Plot } This work
	89.7	Cabot technical data sheet (S6D4)
	89.0	Pope (1967)
	86.2	Murray (1976)
	80.3	Joyner and Emett (1948)
	85.0	Beebe, Biscoe, Smith and Wendell (1947)
	84.1	Ross and Good (1956)
	89.4	Chirnside and Pope (1964)
	84.1	Polley, Schaeffer and Smith (1953)
Black Pearls (BPD4)	220	B.E.T. Plot } This work
	228	de Boer 't' Plot } This work
	211.6	Cabot Technical data sheet
	210	Ash, Baker, Barrer (1967) (Argon)

4.1.3. Hydrocarbon Isotherms

The various adsorption systems which were studied are summarised below with the experimental data tabulated in Appendix A.3 to A.8 and graphically presented in Figures 4.6 to 4.12.

Graphon Pellets/C_3H_8 : T/K = 473, 393, 308, 273, 243 and 213.

Graphon Pellets/i-C_4H_{10} : T/K = 453, 423, 393, 358, 343, 308, 273, 268, 258, 248, 233 and 218.

Graphon Membrane/C_3H_8 : T/K = 243 and 213.

Graphon Membrane/i-C_4H_{10} : T/K = 248, 233 and 218.

Black Pearls powder/C_3H_8 : T/K = 273, 248 and 213.

Black Pearls powder/i-C_4H_{10} : T/K = 343, 308, 273, 248 and 233.

The effect of compaction upon the carbons and their uptake is shown in the comparative isotherms (Figures 4.13 to 4.17). An attempt was made to measure the isotherms at higher temperatures on the membrane. However due to the very small uptakes of gas spurious results were obtained which are not reported here.

Figure 4.6. Propane/Graphon Pellets Adsorption Isotherms

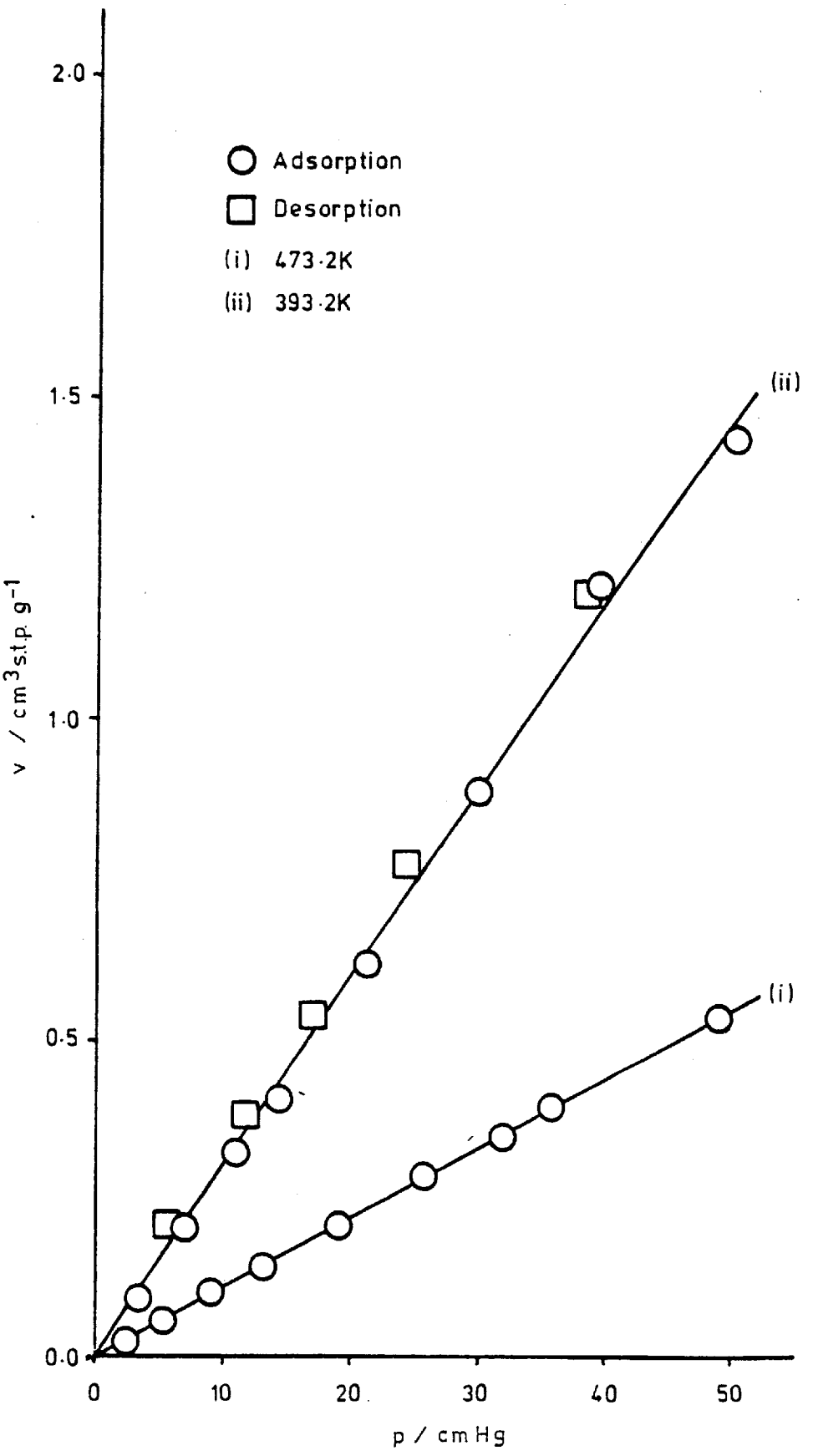

Figure 4.7. Propane/Graphon Pellets Adsorption Isotherms

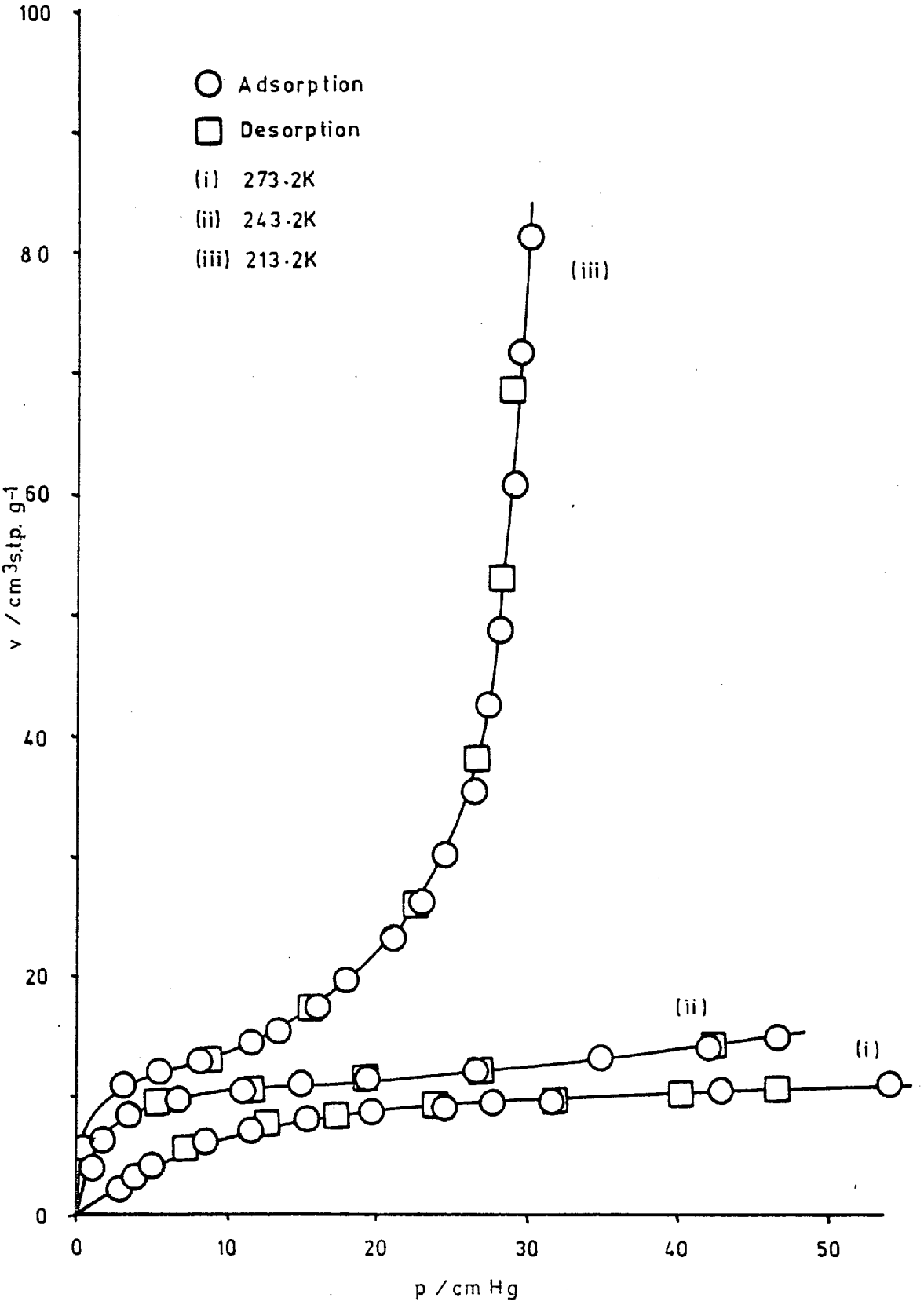

Figure 4.8. Propane/Graphon Membrane Adsorption Isotherms

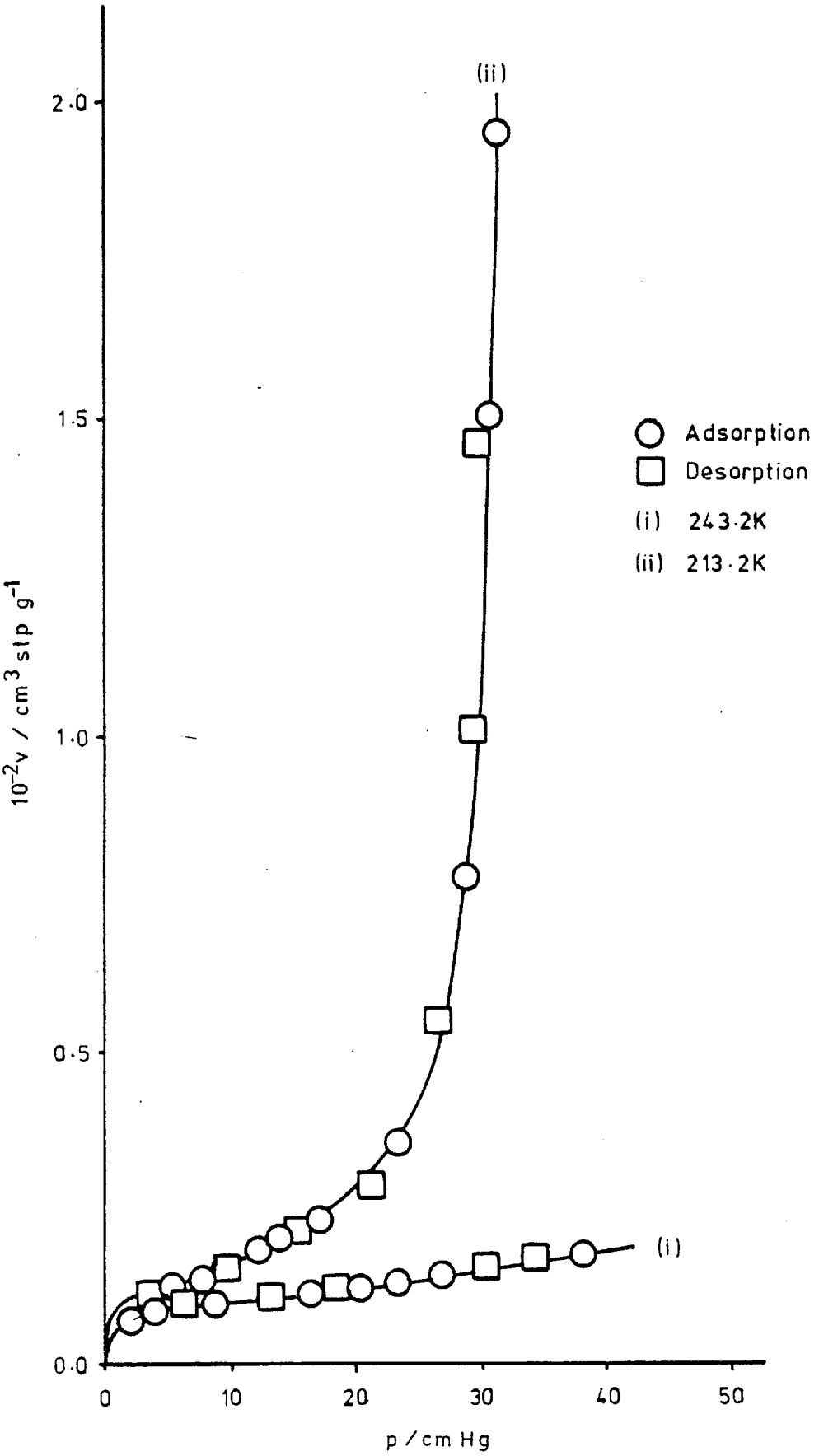

Figure 4.9. Isobutane/Graphon Pellets Adsorption Isotherms

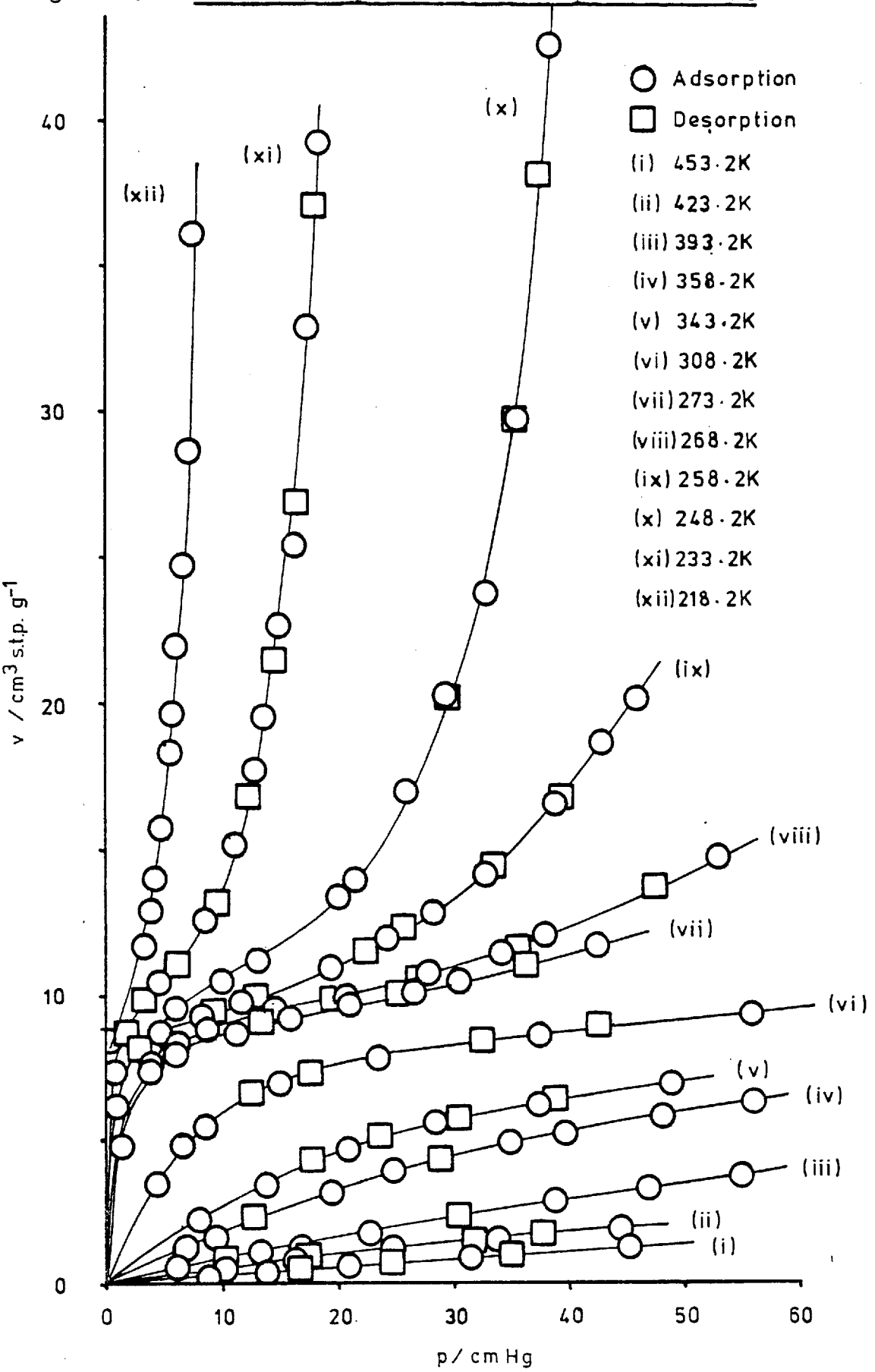

Figure 4.10. Isobutane/Graphon Membrane Adsorption Isotherms

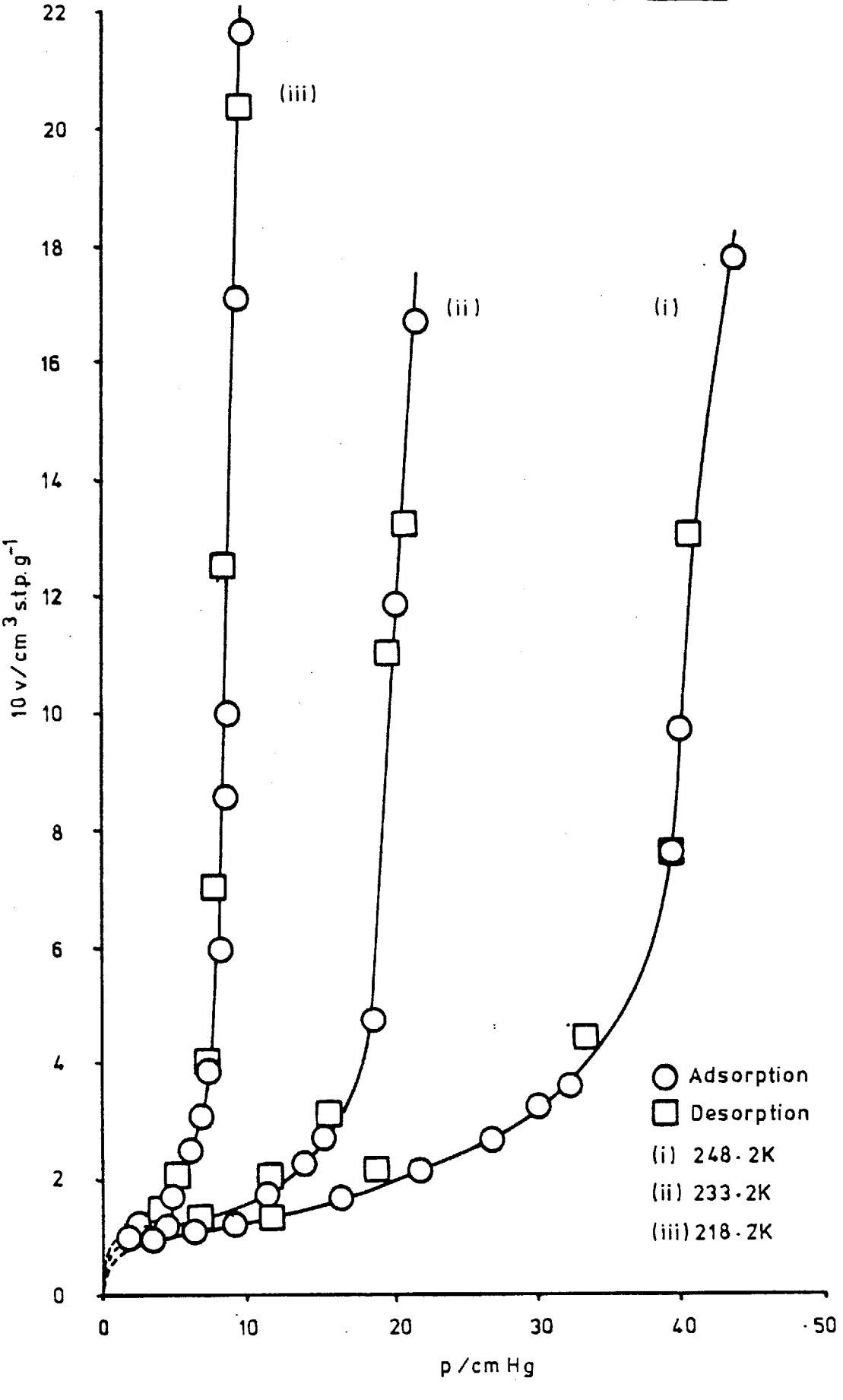

Figure 4.11. Propane/Black Pearls Powder Adsorption Isotherms

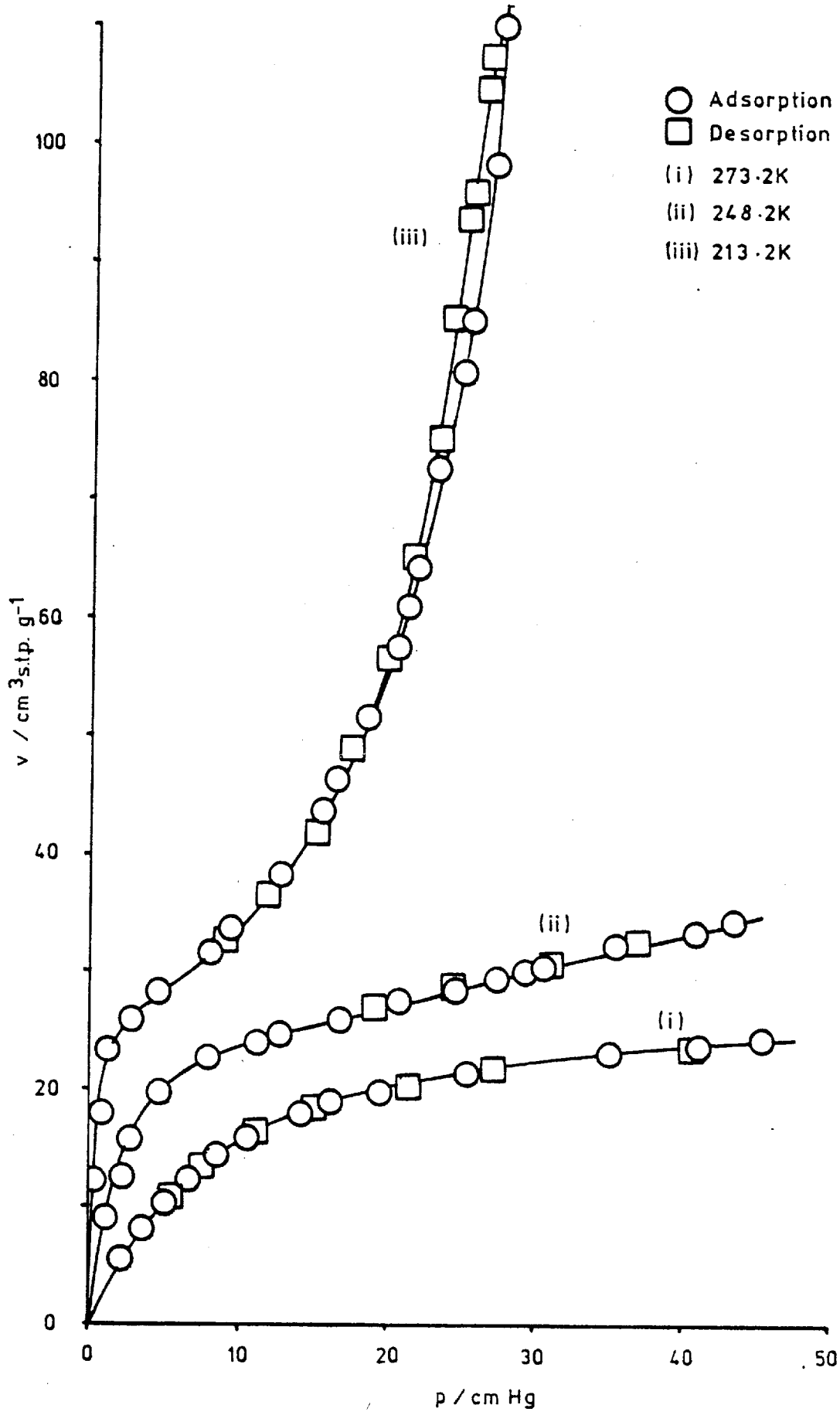

Figure 4.12. Isobutane/Black Pearls Powder Adsorption Isotherms

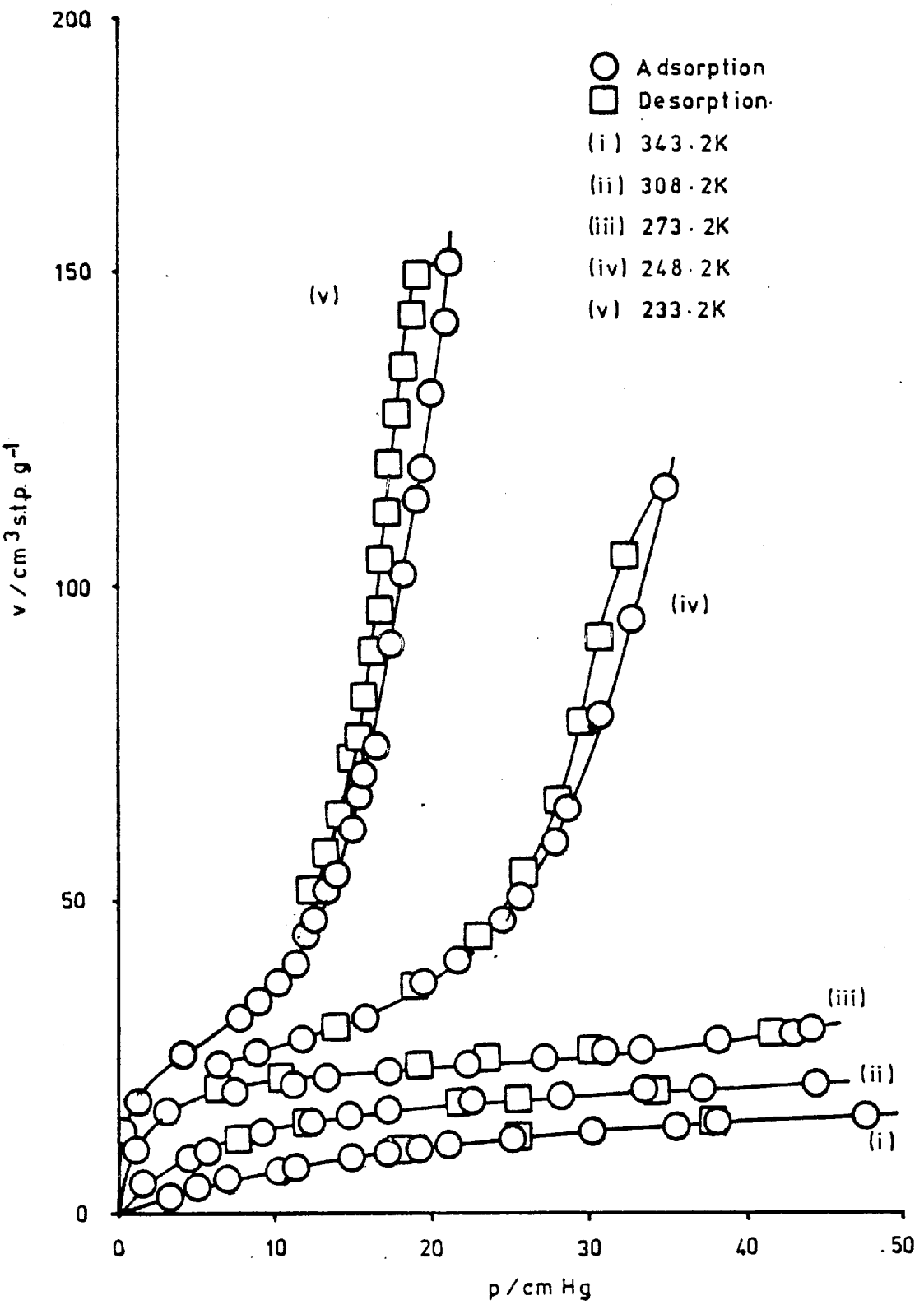

Figure 4.13. Propane/Graphon (Pellets - Membrane) Adsorption Isotherm

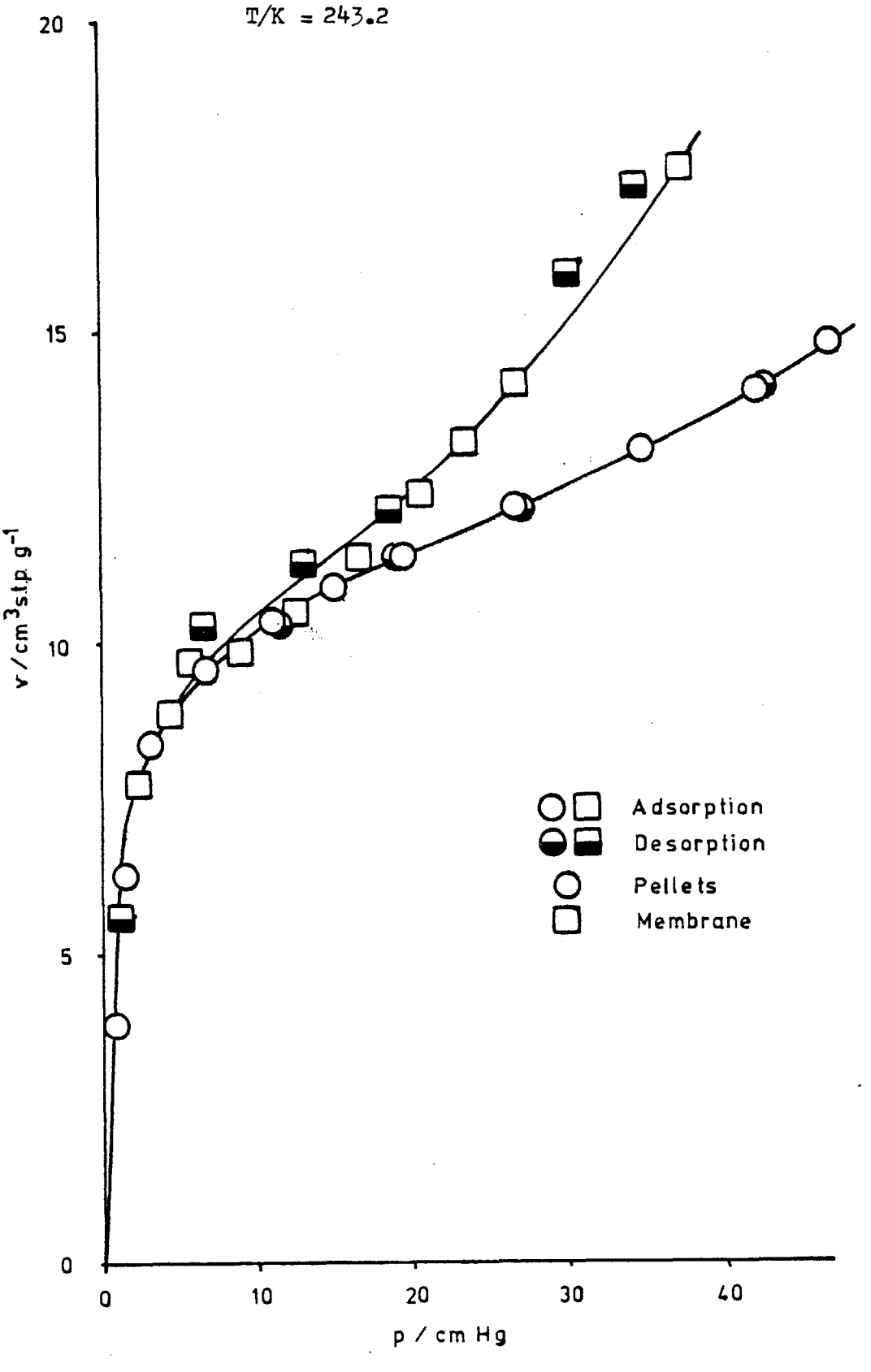

Figure 4.14. Propane/Graphon (Pellets - Membrane) Adsorption Isotherm

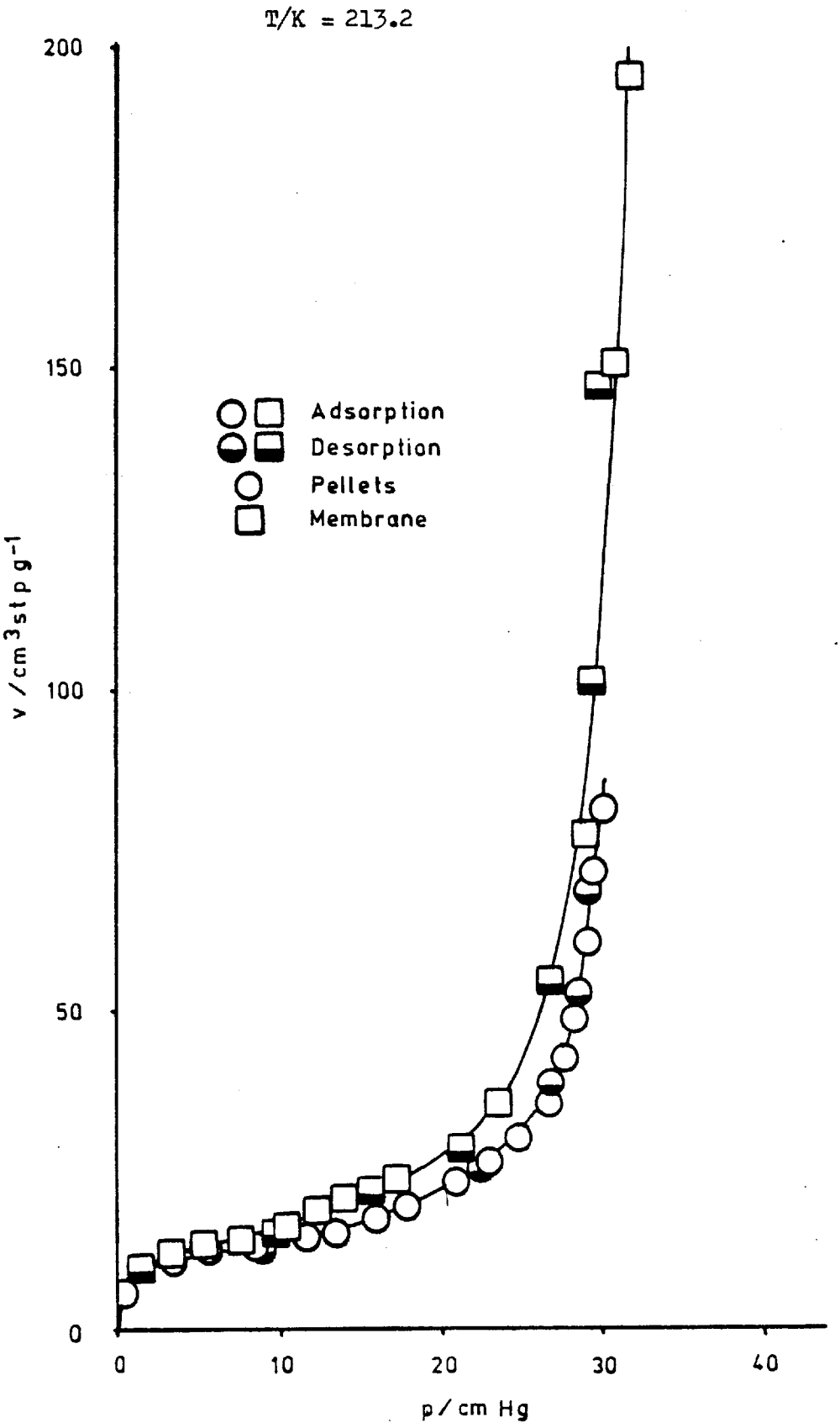

Figure 4.15. Isobutane/Graphon (Pellets - Membrane) Adsorption Isotherm

T/K = 248.2

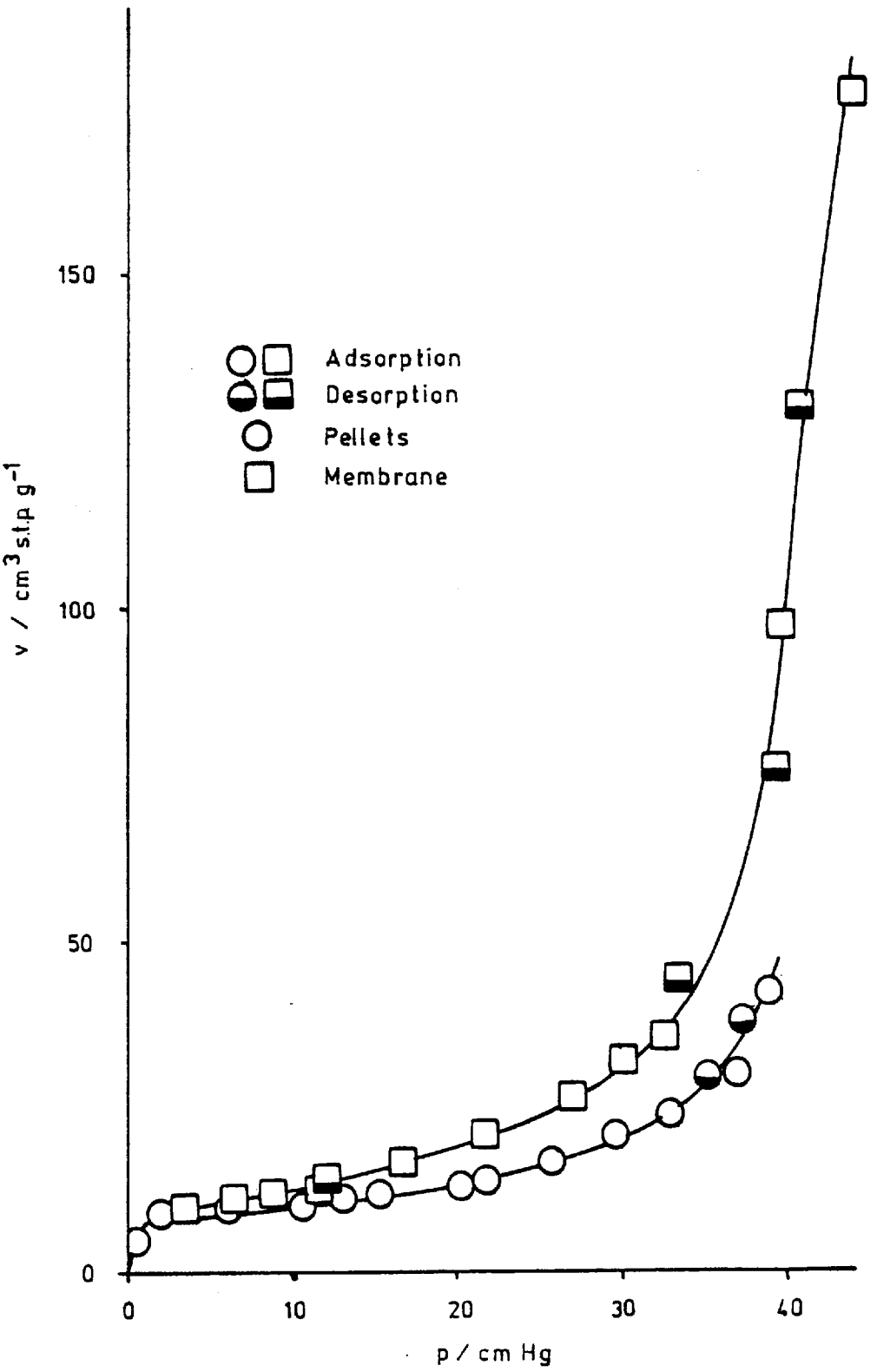

Figure 4.16. Isobutane/Graphon (Pellets - Membrane) Adsorption Isotherm

T/K = 233.2

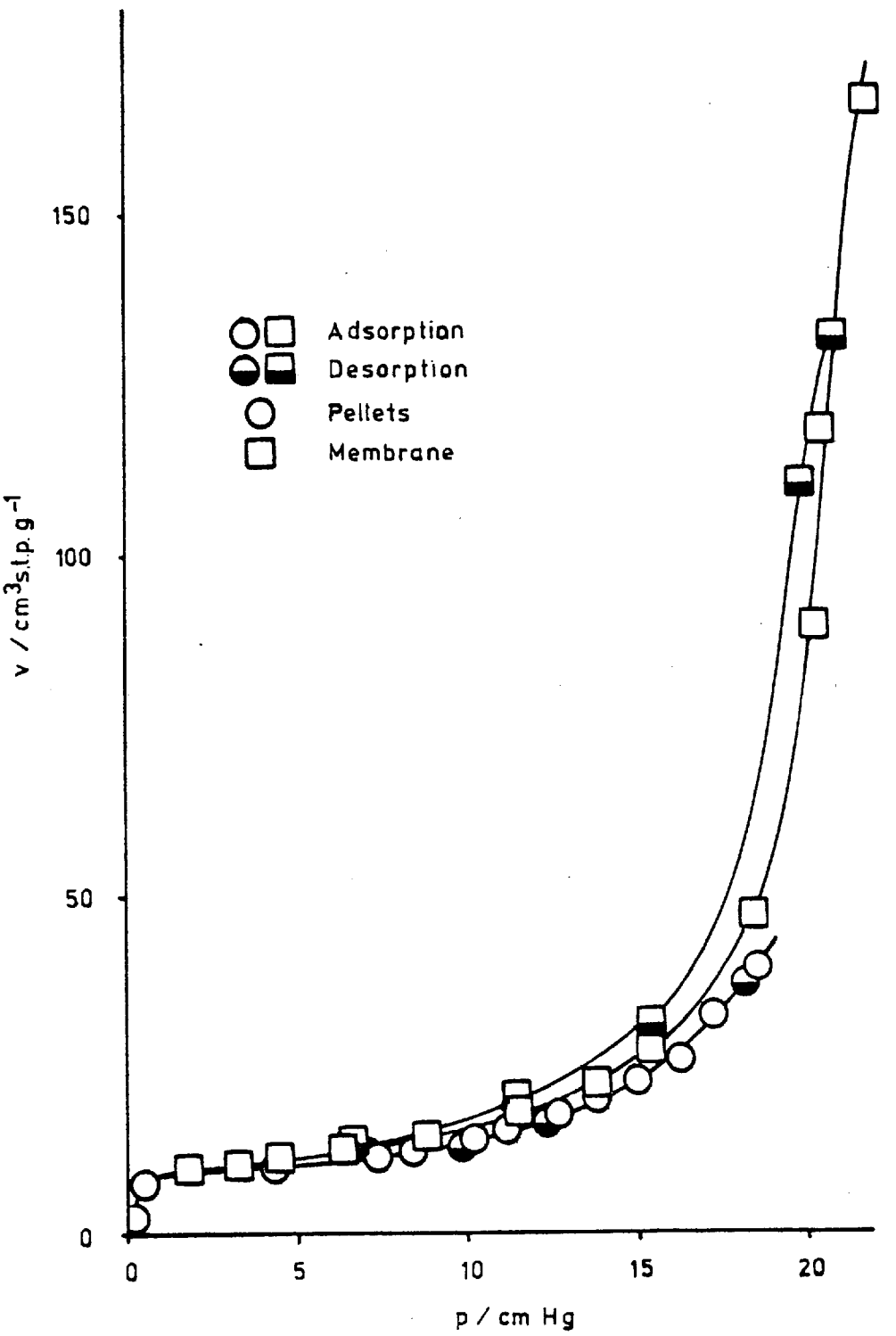

Figure 4.17. Isobutane/Graphon (Pellets - Membrane) Adsorption Isotherm

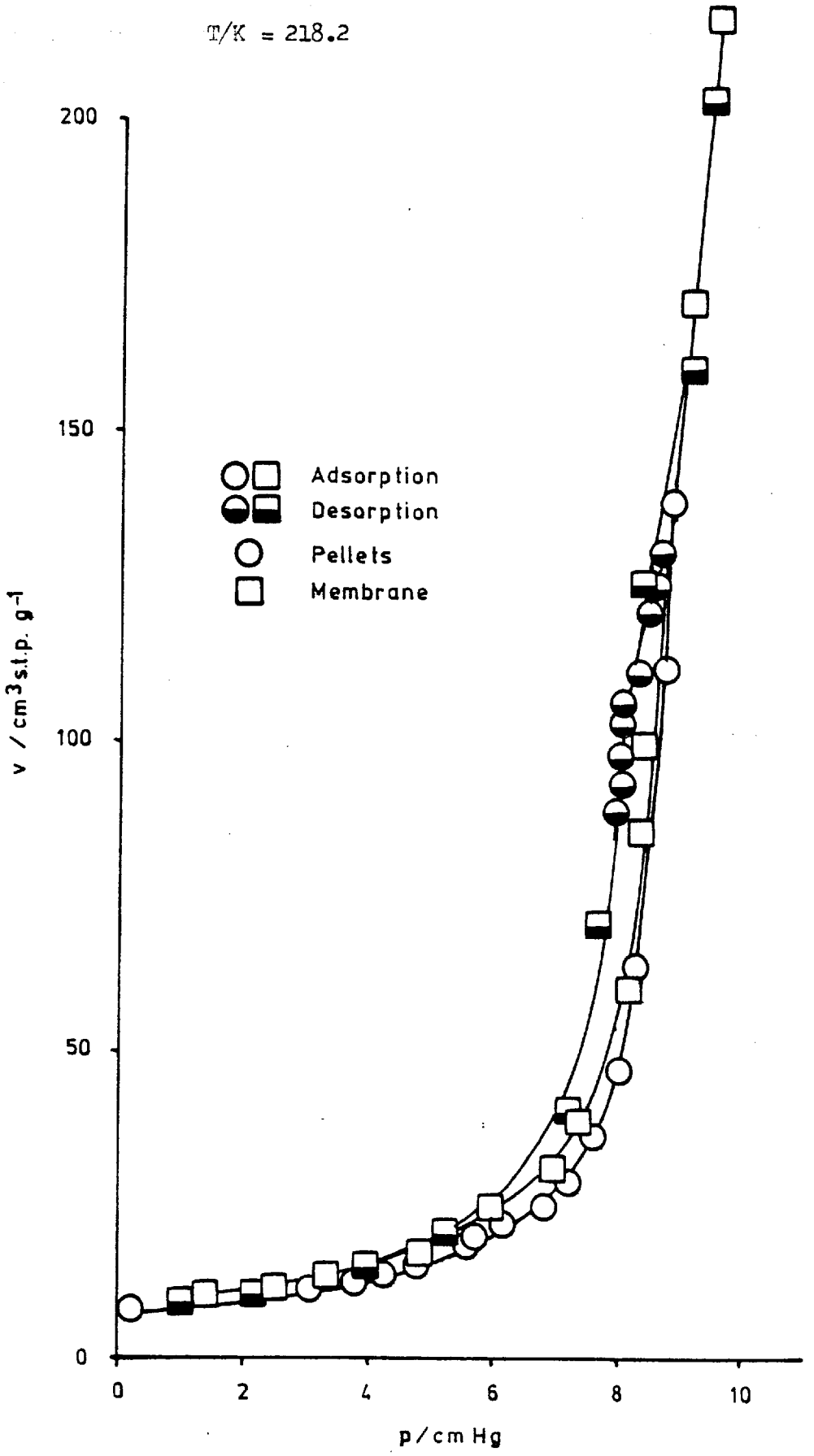

At several of the higher temperatures the isotherms exhibited Henry Law adsorption and the corresponding Henry Law coefficients, $k_s(m)$ were determined (Table 5.1) from the relationship :

$$k_s \equiv \frac{C'_s}{C'_g} \qquad (4.4)$$

in which C'_s is the Gibbs excess surface concentration (mol m^{-2}) and C'_g is the gas phase concentration (mol m^{-3}). However the majority of the isotherms were curved and of Type II in the Brunauer classification with very narrow hysteresis loops near the saturated vapour pressure.

It was possible to apply the B.E.T. equation to the experimental data at certain temperatures (Figures 4.18 and 4.23). Linear plots were obtained which resulted in the monolayer capacities given in Table 4.2. These values are utilised in a later discussion of the cross-sectional areas of adsorbed molecules and the surface areas determined by different molecules (cf §5.1.1).

Table 4.2. Monolayer Capacities of Hydrocarbons

Adsorbent	C_3H_8		$i\text{-}C_4H_{10}$	
	$\frac{v_m}{cm^3\ stp\ g^{-1}}$	C	$\frac{v_m}{cm^3\ stp\ g^{-1}}$	C
Graphon : pellets	9.9	176	8.0	354
Graphon : membrane	11.0	168	9.8	145
Black Pearls : powder	25.6	77	19.4	250

Isosteric Heats of Adsorption

The isosteric heats of adsorption, q_{st} (kJ mol^{-1}) were obtained by application of the Clausius-Clapeyron expression :

$$\ln p = -\frac{q_{st}}{RT} + \text{const.} \qquad (4.5)$$

where p is the pressure (Nm^{-2}), R the gas constant (J $mol^{-1}K^{-1}$) and T the temperature (K).

Figure 4.18. Propane/Graphon Pellets : B.E.T. Plot

T/K = 243.2

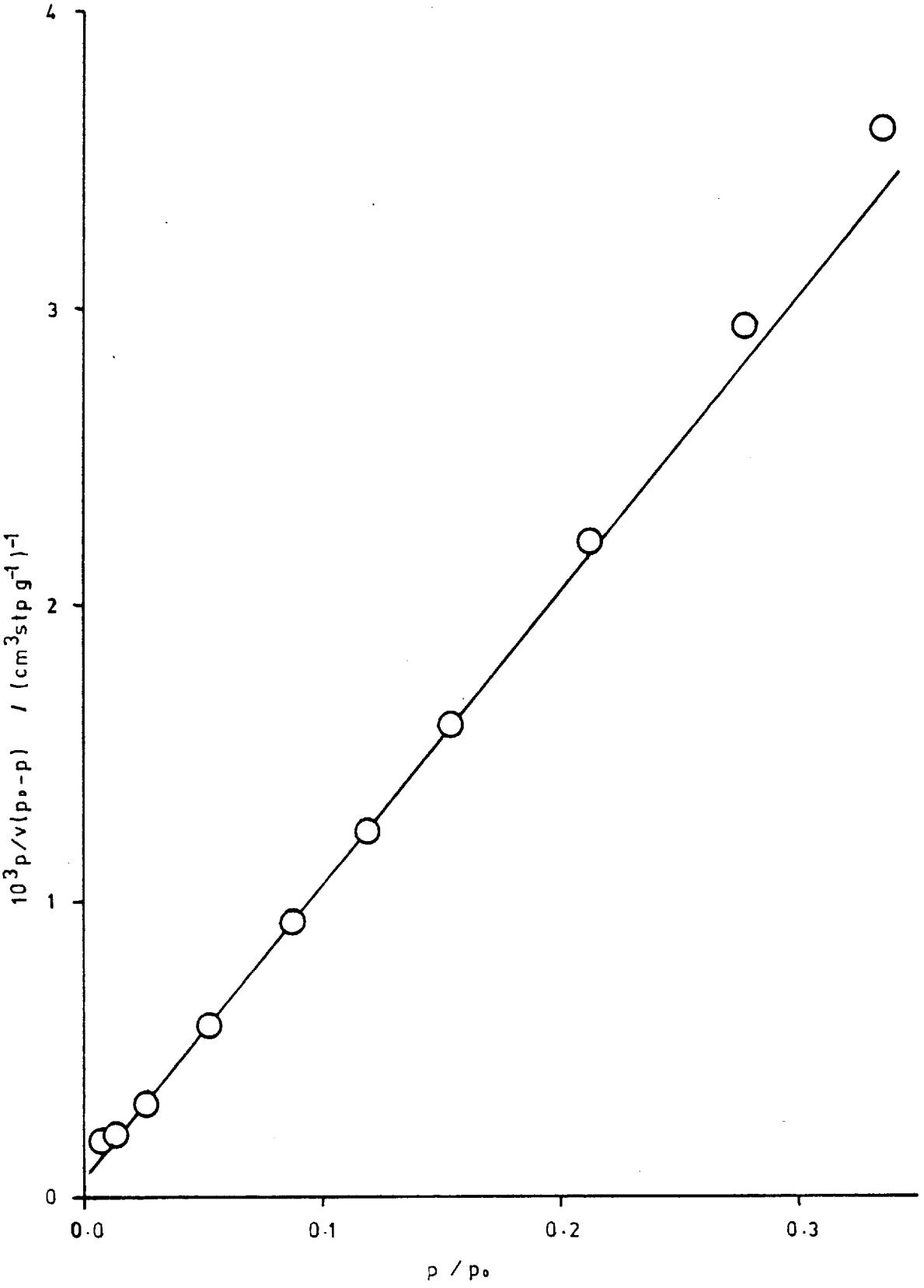

Figure 4.19. Propane/Graphon Membrane : B.E.T. Plot

T/K = 213.2

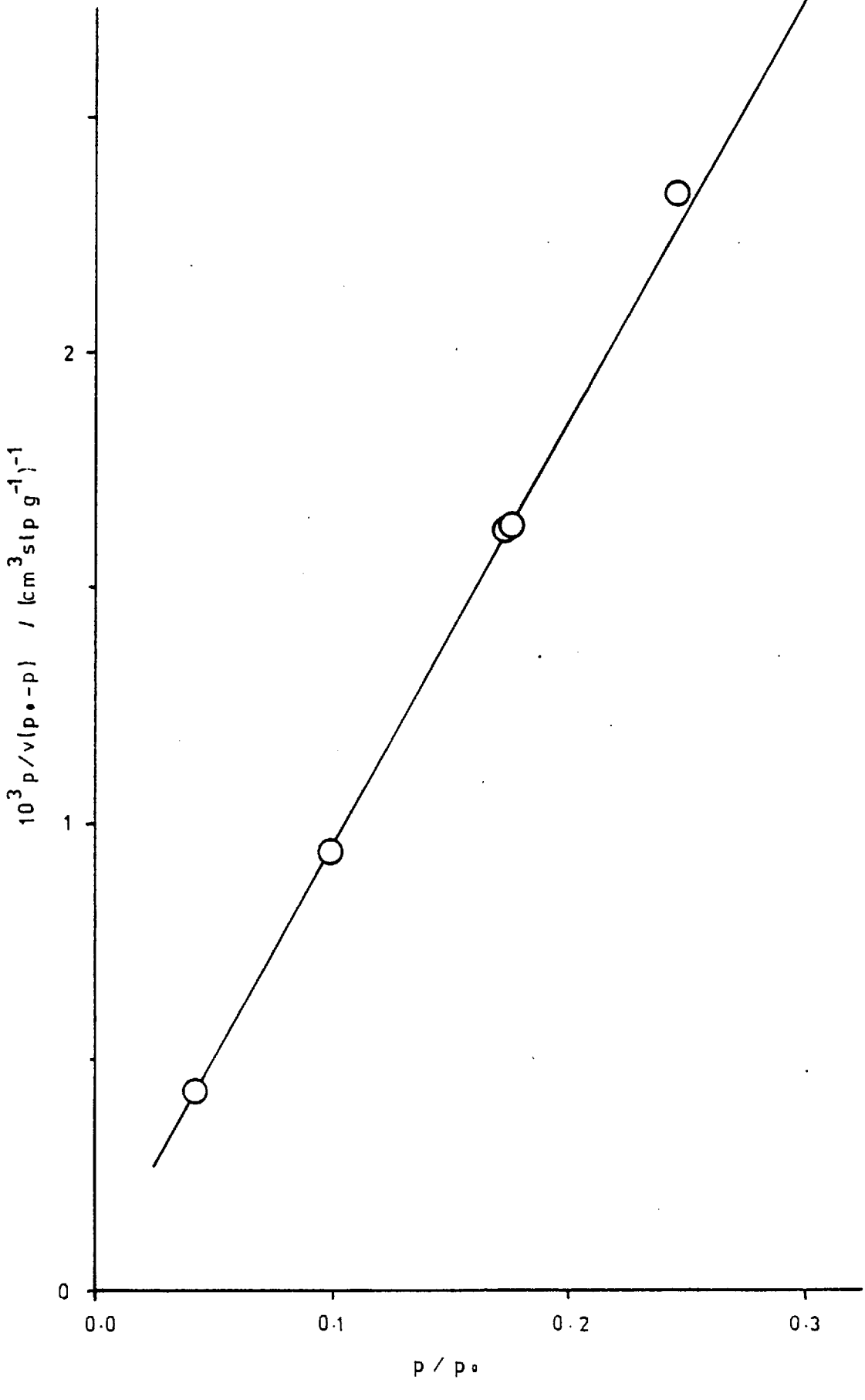

Figure 4.20. Isobutane/Graphon Pellets : B.E.T. Plot

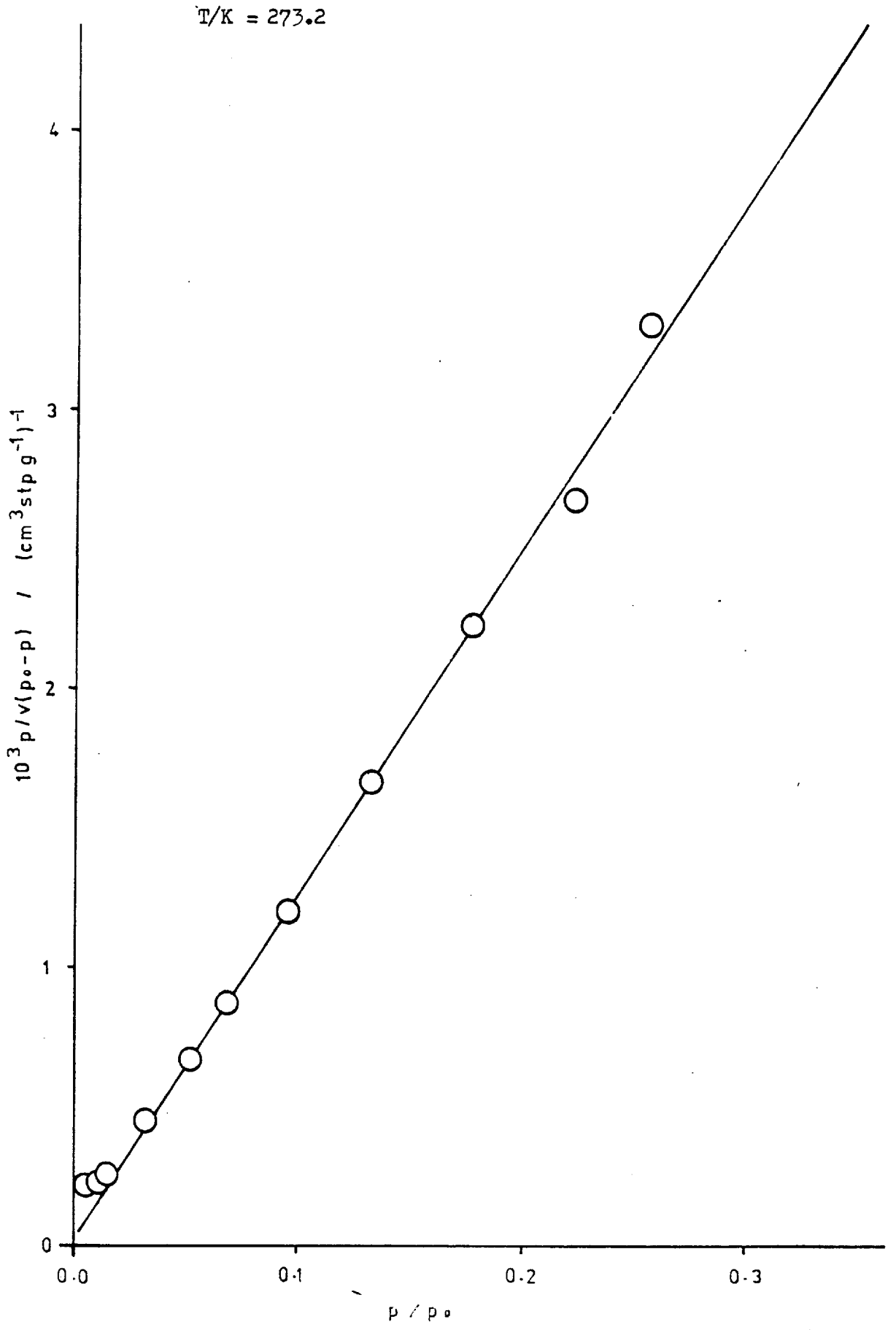

Figure 4.21. Isobutane/Graphon Membrane : B.E.T. Plot

T/K = 248.2

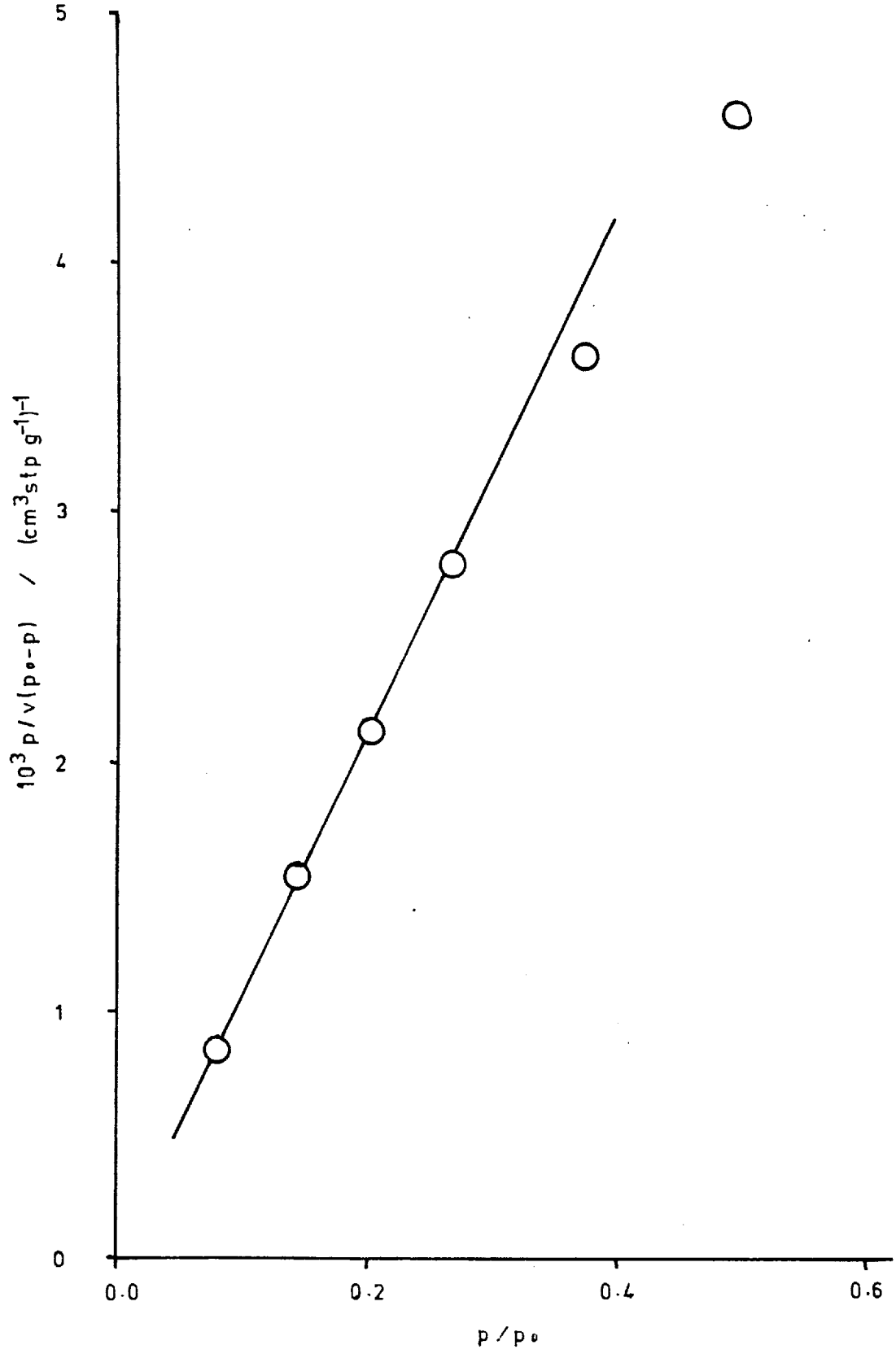

Figure 4.22. Propane/Black Pearls Powder : B.E.T. Plot

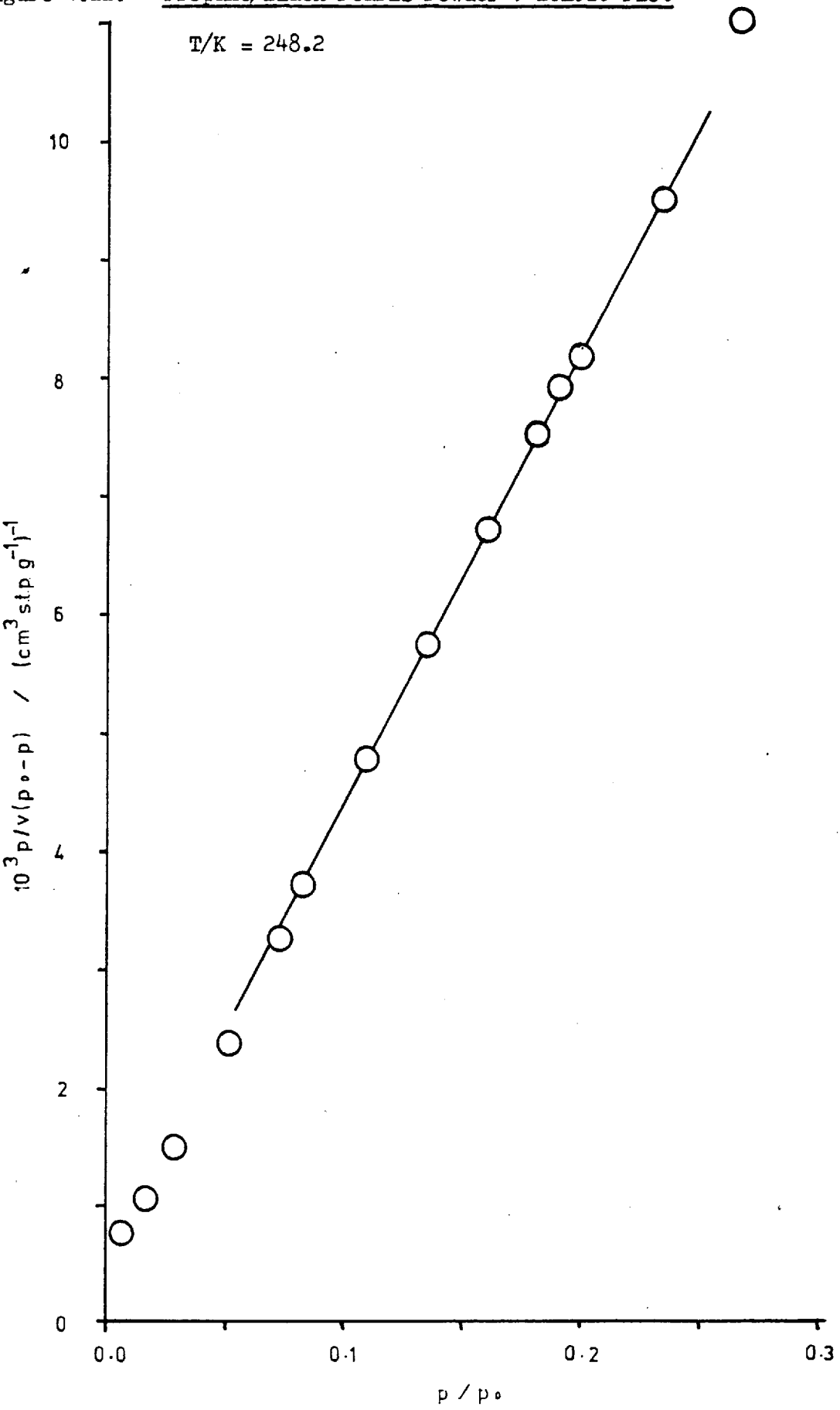

Figure 4.23. Isobutane/Black Pearls Powder : B.E.T. Plot

T/K = 273.2

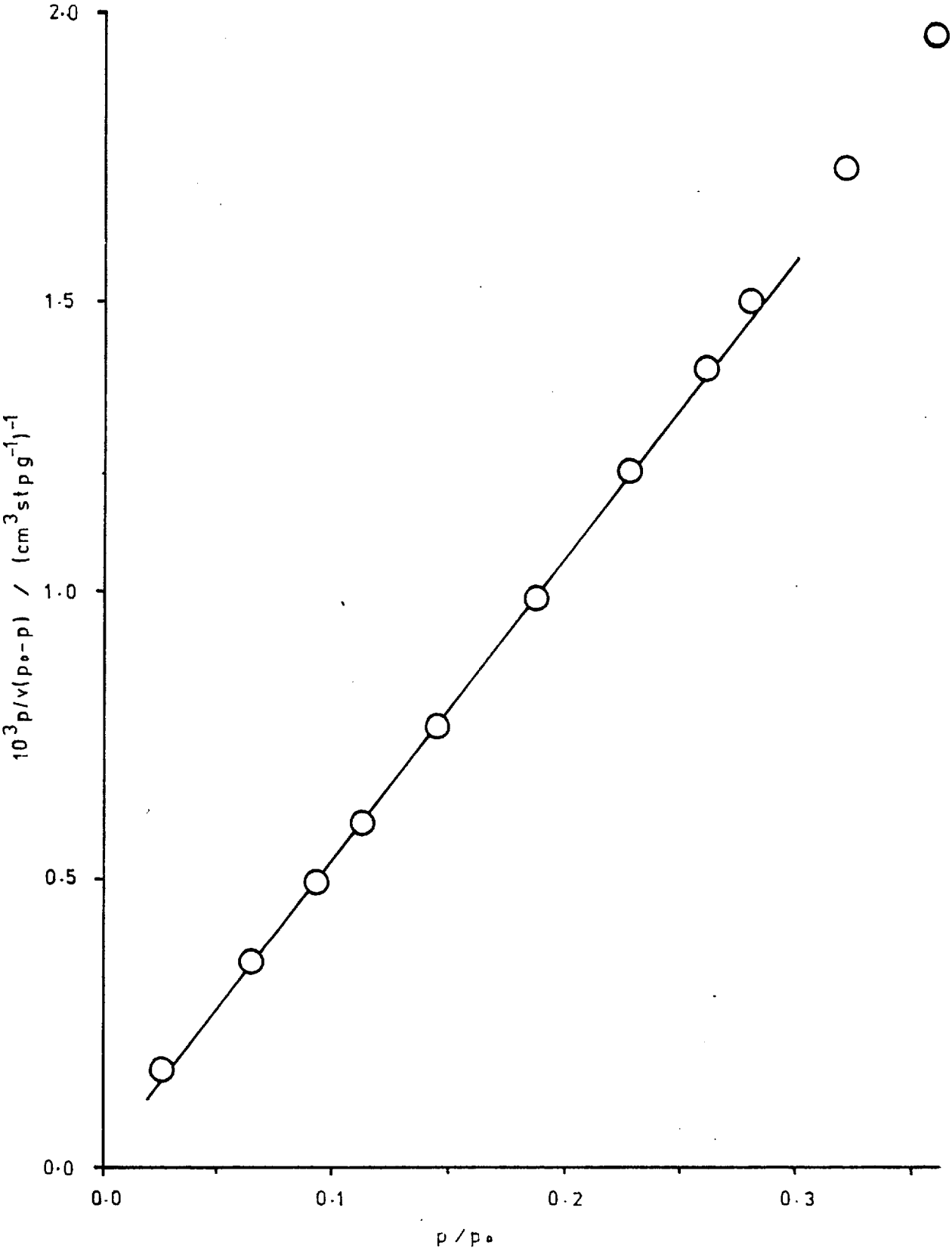

The variations of the heat of adsorption with coverage are shown in Figures 4.24 to 4.27 with a maximum occurring at $v/v_m = 1$.

4.2. 'Conventional' Flow Results

4.2.1. Introduction

Isothermal flow measurements under conditions of a constant Δp were made on Graphon and graphitised Black Pearls membranes. The flow of He, Ar, C_3H_8 and i-C_4H_{10} as single species and as components of binary mixtures was studied over the temperature range 213 to 473 K. The effect of varying the ingoing pressure, p_1 was also examined.

The experimental technique, described in Section 3.4.2 recorded the outgoing pressure, p_2 as a function of time, t in a fixed known volume, V. Typical plots of p_2 versus t are shown in Figure 4.28 for isobutane at 308.2 K with different values of p_1.

From the steady-state value of dp_2/dt the integral permeability, $\tilde{K}$ is obtained using equations (2.12) and (2.31) where J_∞ is the total molar flux ($mol.s^{-1}$).

$$J_\infty = \frac{1}{RT_R} \cdot \frac{d(pV)}{dt} = \frac{V}{RT_R} \cdot \frac{dp_2}{dt} \quad \text{for const. V} \qquad (2.12)$$

$$\tilde{K} = \frac{J_\infty \ell}{A_c \Delta C'_g} \qquad (2.31)$$

However for all practical purposes p_2 and C'_{g_2} can be considered negligible compared to p_1 and C'_{g_1}, so $\Delta C'_g \simeq C'_{g_1}$.

Hence equation (2.31) with substitution for J and $\Delta C'_g$ becomes :

$$\tilde{K} = V \cdot \frac{\ell}{A_c} \cdot \frac{T}{T_R} \cdot \frac{1}{p_1} \frac{dp_2}{dt} \qquad (4.6)$$

where C'_{g_1} has been expressed in terms of ingoing pressure, p_1 and the plug temperature, T by :

$$C'_{g_1} = \frac{p_1}{RT} \qquad (2.11)$$

It was a matter of experimental convenience to measure p in cm Hg, t in minutes and relevant lengths, areas and volumes in cm, cm^2, cm^3

Figure 4.24. Concentration - Dependence of 'q_{st}' : Propane/Graphon Pellets

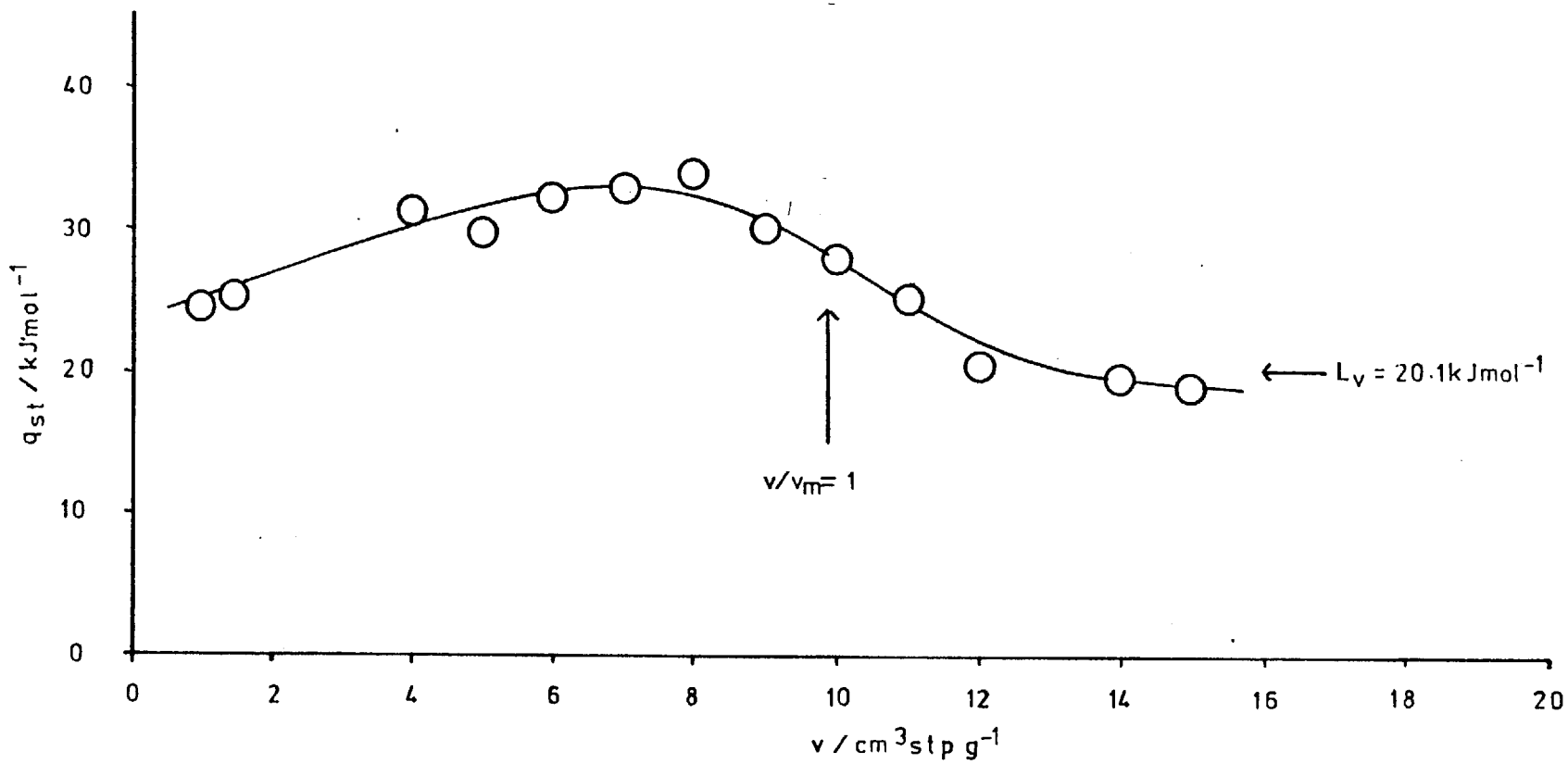

Figure 4.25. Concentration - Dependence of 'q_{st}' : Isobutane/Graphon Pellets

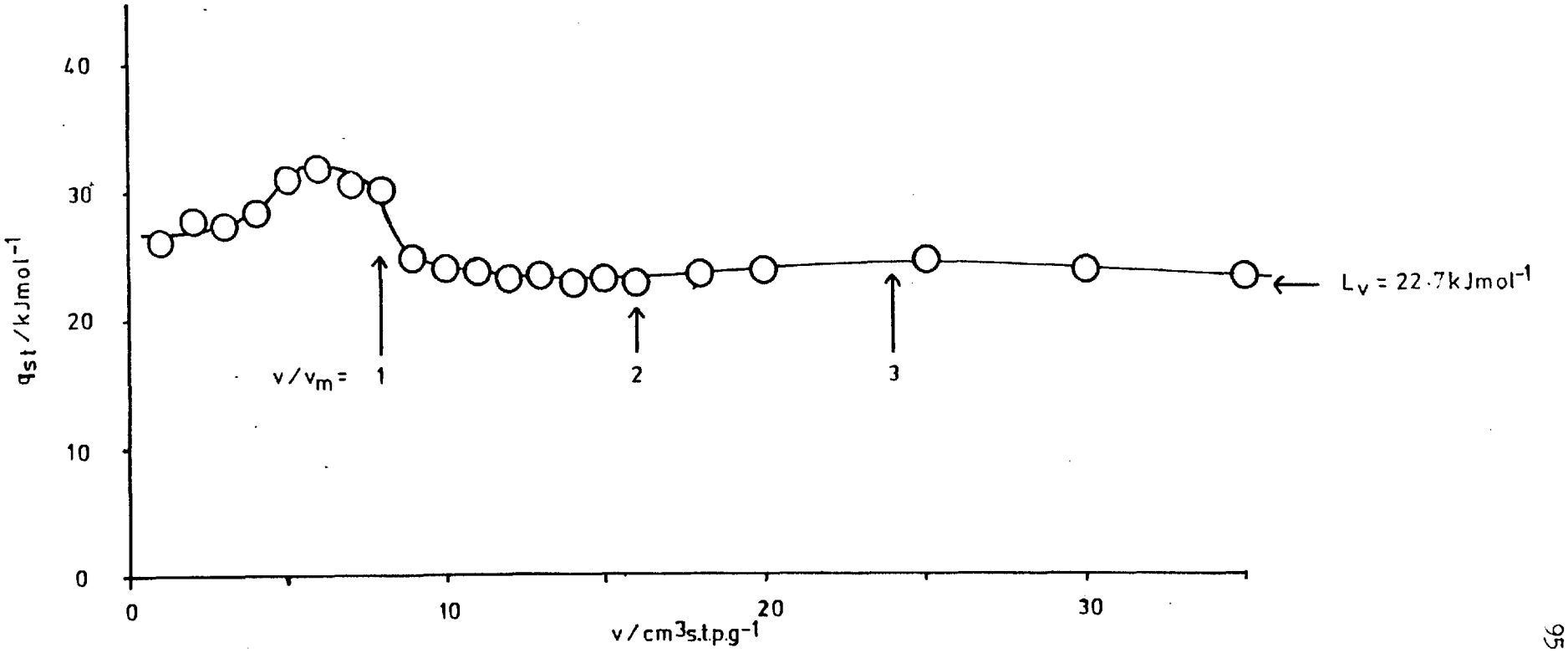

Figure 4.26. Concentration - Dependence of 'q_{st}' : Propane/Black Pearls

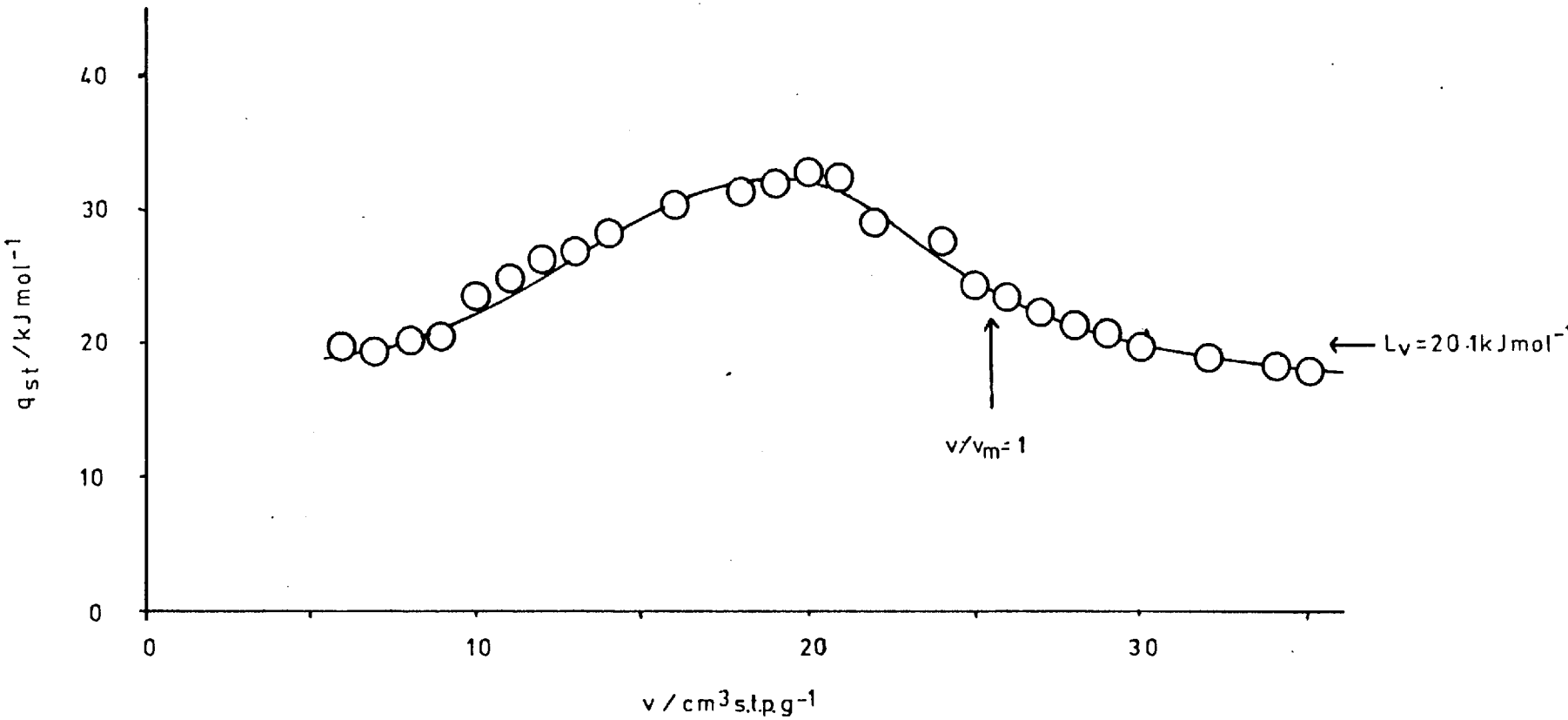

Figure 4.27. Concentration - Dependence of 'q_{st}' : Isobutane/Black Pearls

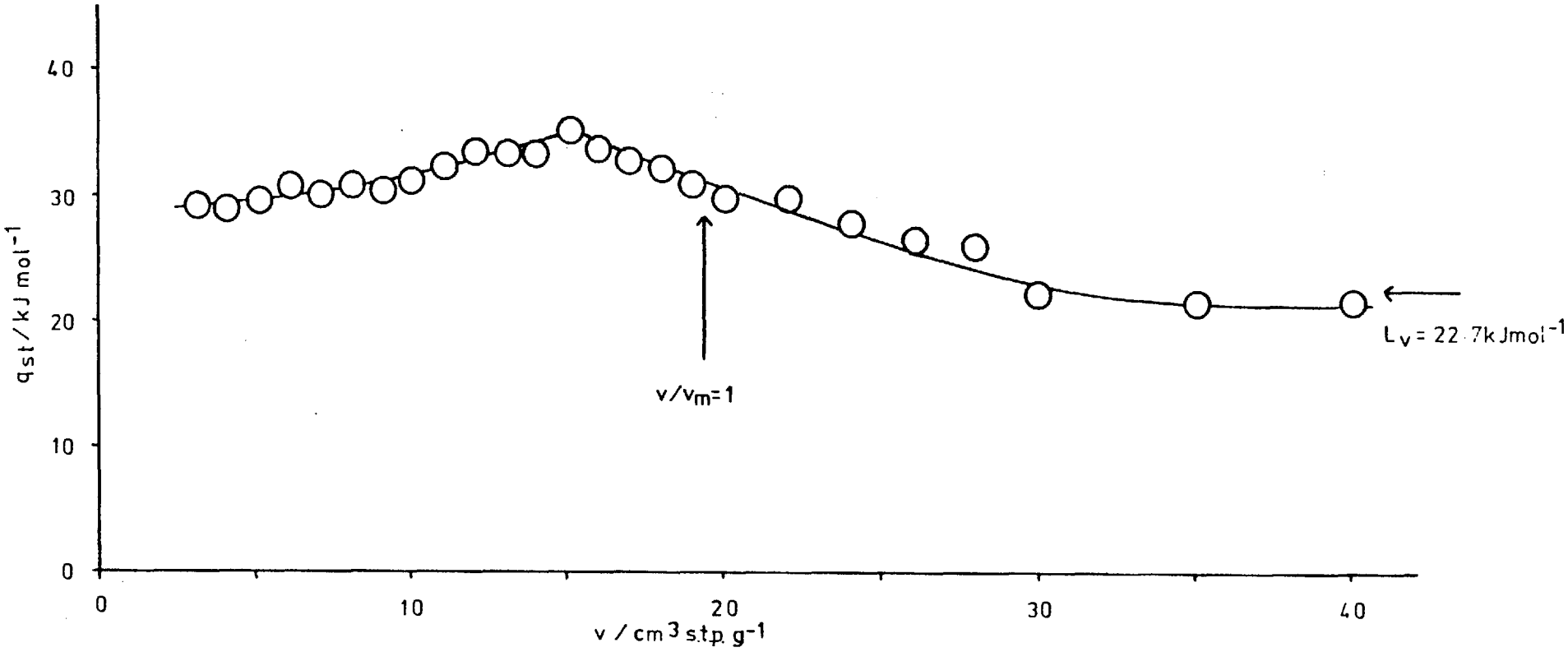

Figure 4.28. Typical Plots of p_2 vs t : Isobutane/Graphon : T/K = 308.2

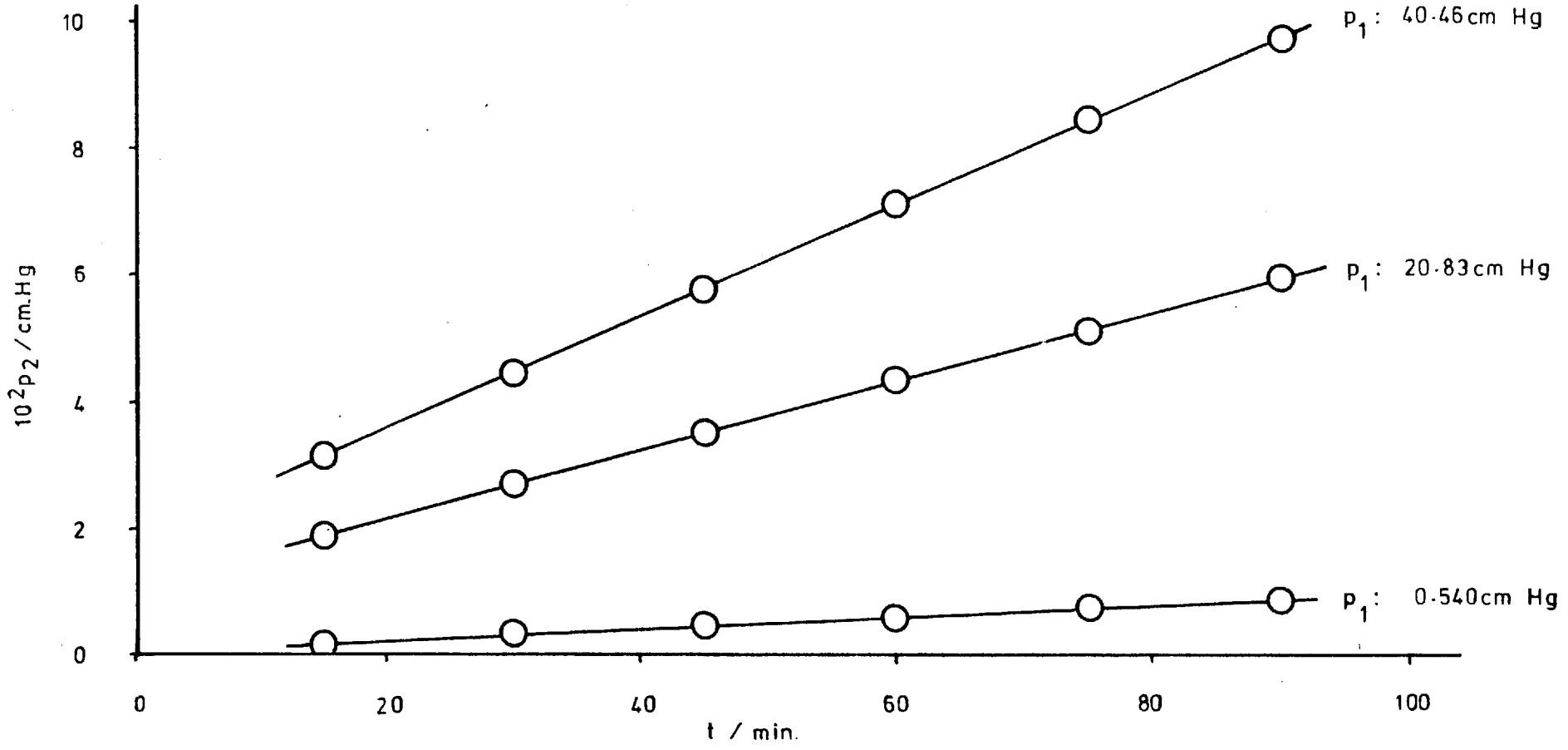

respectively. Thus the working equation for the permeability $\tilde{K}$ ($m^2 s^{-1}$) is given by equation (4.7) :

$$\tilde{K} = V \cdot \frac{\ell}{A_c} \cdot \frac{T}{T_R} \cdot \frac{1}{p_1} \cdot \frac{10^{-4}}{60} \cdot \frac{dp_2}{dt} \qquad (4.7)$$

The molar flux, J (mol s^{-1}) was back calculated from $\tilde{K}$ using equation (2.31).

In the case of mixtures the permeability of the non-sorbed component was measured and related back to the pure gas permeability in terms of a quantity known as the relative permeability, $\tilde{K}_R$, where

$$\tilde{K}_R = \frac{\tilde{K} \text{ component in mixture}}{\tilde{K} \text{ pure gas}} \qquad (4.8)$$

4.2.2. Single Species Flow

(a) Helium

The flow of helium was studied at various temperatures over ranges of p_1 values. The object of the exercise was to investigate any long term changes to the membrane's flow characteristics and to check that purely gas phase transport occurs. The values of $\tilde{K}$ as functions of temperature and pressure are tabulated in Appendix B.1 and B.2. Both of these were examined by investigating any variation in the quantity $\tilde{K}.T^{-\frac{1}{2}}$ over a pressure range and after a series of flow measurements. The plots of molar flux, J ($mol.s^{-1}$) as a function of ingoing pressure were linear and passed through the origin (Figure 4.29). Also there was no pressure dependence of the permeability indicating the absence of a viscous flow component and the applicability of the Knudsen relationship to the system (cf Figure 4.30). The variation over time is shown in Figures 4.31 and 4.32 for Graphon and Black Pearls respectively. As can be seen there was no appreciable variation and consequently it was assumed that no irreversible ageing of the membranes had occurred during the measurements made over a period of three years, such as that found for Carbolac membranes (Ash, Barrer and Lowson, 1973; Ash, Barrer and Sharma, 1976).

The values of $\tilde{K}_{He}$ used in further calculations of the quantity $\tilde{K}_g$ are given in Table 4.3. These are the smoothed values obtained

Figure 4.29. Pressure - Dependence of J_{He} : Graphon and Black Pearls

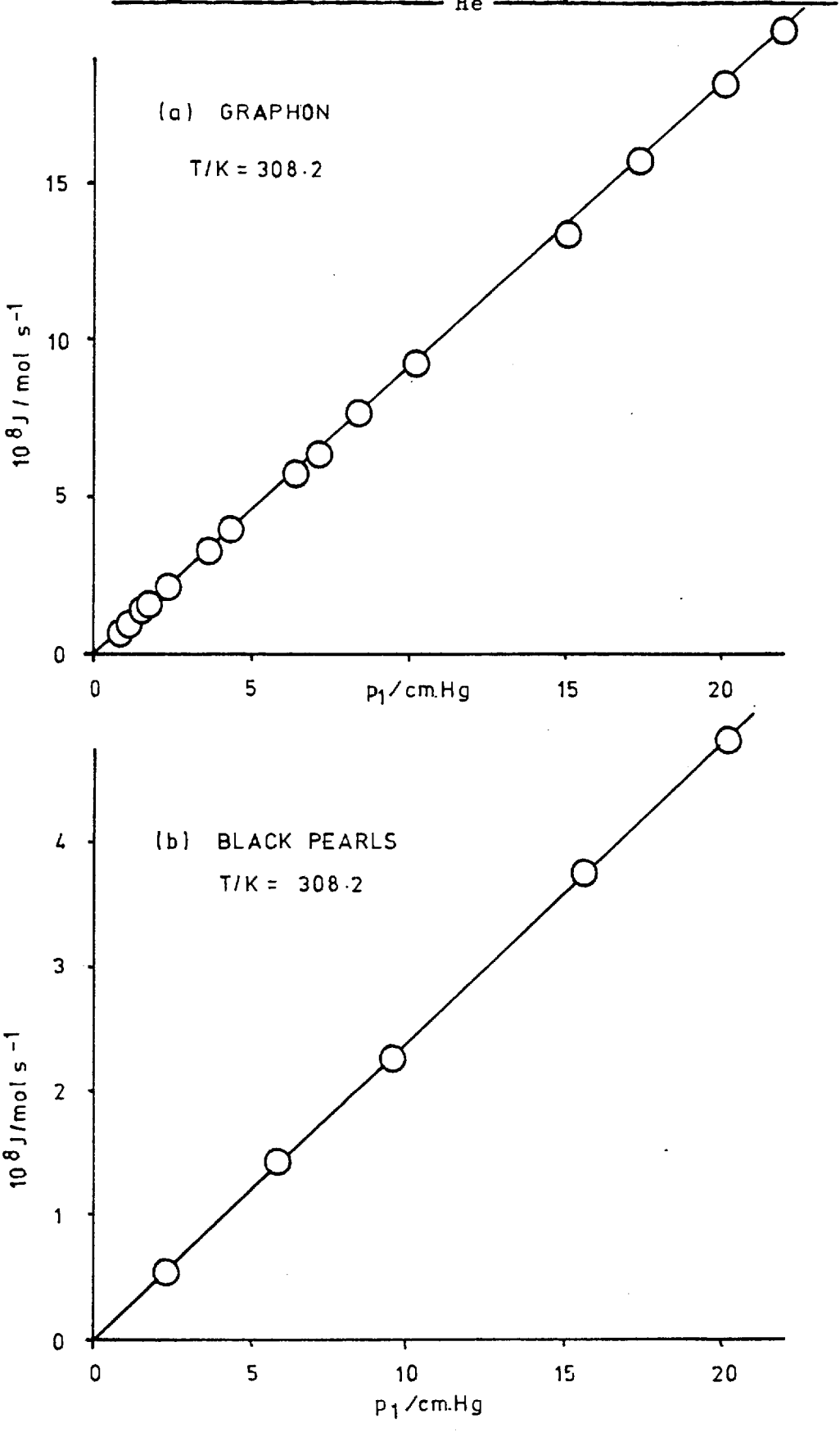

Figure 4.30. Pressure - Dependence of $\tilde{K}_{He}$: Graphon and Black Pearls

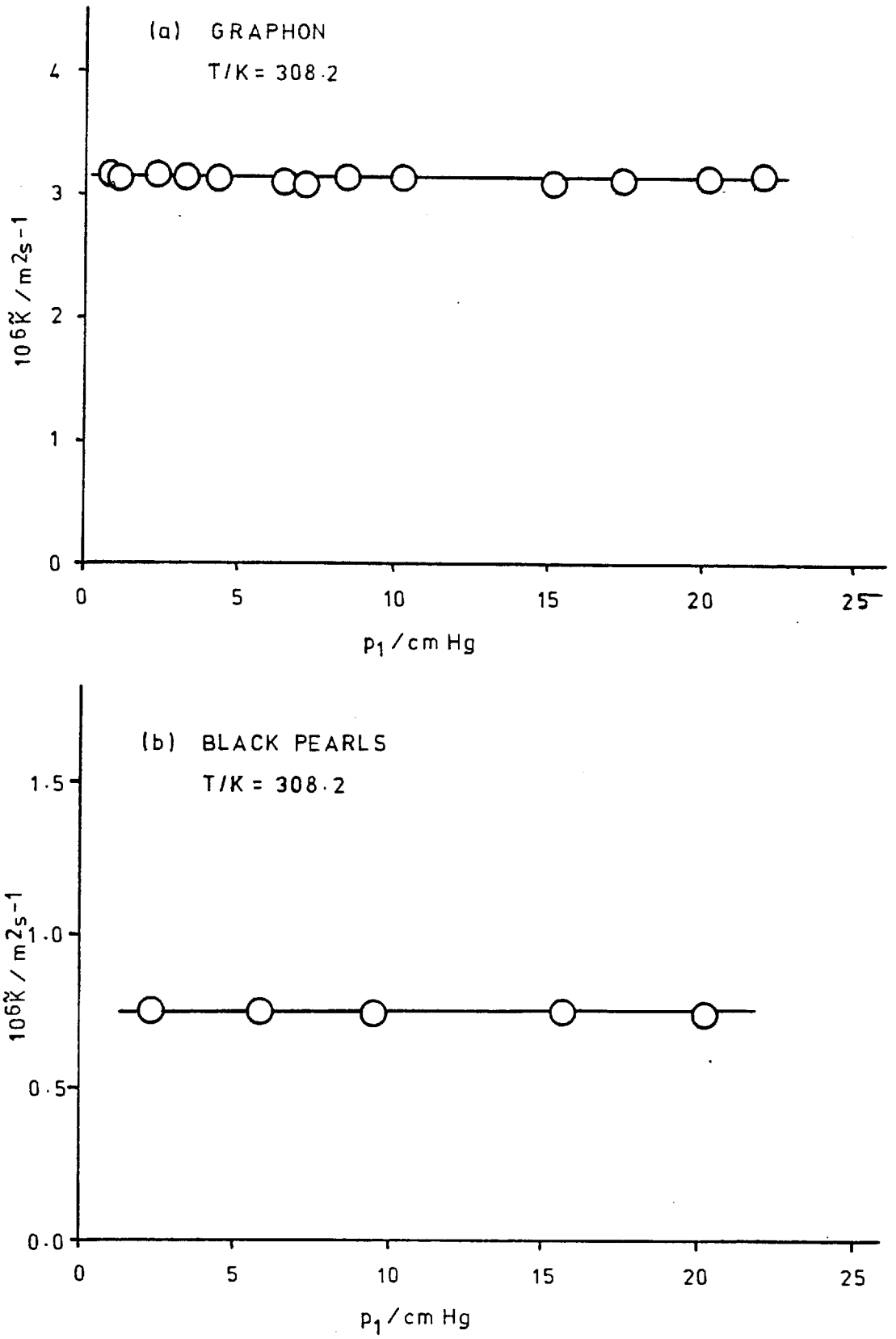

Figure 4.31. Variation of $\tilde{K}_{He}\,T^{-\frac{1}{2}}$ with experiment : Graphon

Figure 4.32. Variation of $\tilde{K}_{He} T^{-\frac{1}{2}}$ with experiment : Black Pearls

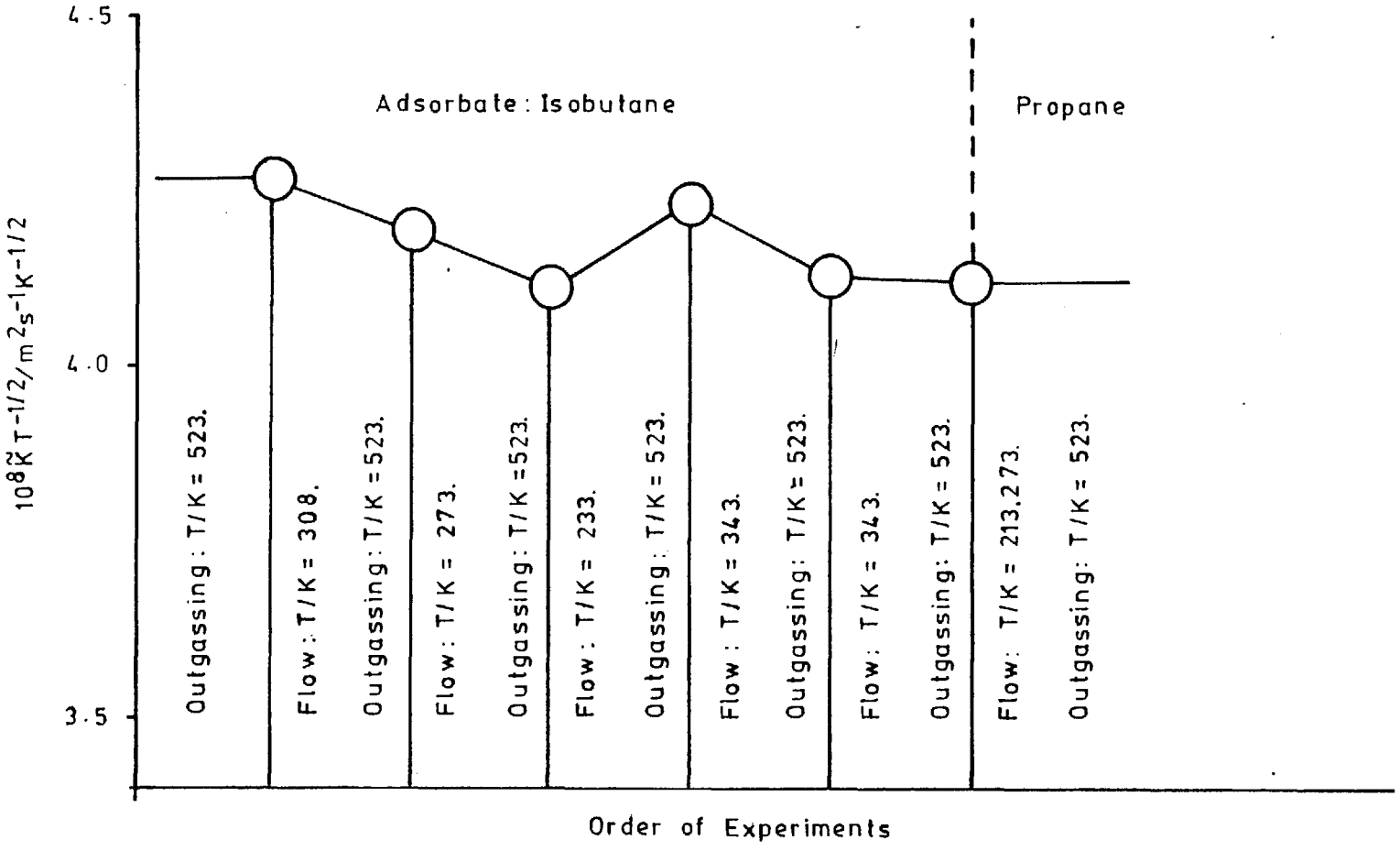

at various temperatures by the application of Knudsen's relationship :

$$\tilde{K}(M/T)^{\frac{1}{2}} = \text{constant} \qquad (2.4)$$

Literature values of the constant, $\tilde{K}T^{-\frac{1}{2}}$ are given in Table 4.4 for other membranes constructed from Graphon and graphitised Black Pearls.

Table 4.3. Permeability of Helium : $\tilde{K}_{He}$

Graphon

$\frac{T}{K}$	$\frac{10^6 \tilde{K}_{He}}{m^2 s^{-1}}$
218.2	2.63
233.2	2.72
248.2	2.81
258.2	2.87
268.2	2.92
273.2	2.95
308.2	3.13
343.2	3.30
358.2	3.38
393.2	3.54
423.2	3.67
453.2	3.80
213.2	2.60
243.2	2.78
473.2	3.88

Black Pearls

$\frac{T}{K}$	$\frac{10^7 \tilde{K}_{He}}{m^2 s^{-1}}$
213.2	6.23
233.2	6.52
273.2	7.05
308.2	7.49
343.2	7.90

Table 4.4. Comparison of the constant $\tilde{K}_{He}T^{-\frac{1}{2}}$ for Different Membranes

	$10^6 \tilde{K}T^{-\frac{1}{2}}/m^2 s^{-1} K^{-\frac{1}{2}}$	Source
Graphon	0.178	This work
	0.087	Ash, Baker, Barrer (1967)
	0.185	Murray (1976)
Black Pearls	0.042	This work
	0.032	Ash, Baker, Barrer (1967)

(b) Hydrocarbon/Graphon

Flow measurements were made using propane at T/K = 473.2, 393.2, 243.2 and 213.2, and isobutane at T/K = 453.2, 423.2, 393.2, 358.2, 343.2, 308.2, 273.2, 268.2, 258.2, 248.2, 233.2 and 218.2. (The data at T/K = 218.2 was measured by Mr D.E.G. Whiting in this laboratory and is included to complete the flow picture). The experimental data is tabulated in Appendix B2 to B4.

The variation of the molar flux, J ($mols^{-1}$) with temperature and pressure is shown in Figures 4.33 to 4.34. The integral permeability, $\tilde{K}$ ($m^2 s^{-1}$) at various temperatures is shown as a function of ingoing pressure, p_1 (cm Hg) in Figures 4.35 and 4.36, and as a function of relative pressure, p_1/p_0 (where p_0 is the saturated vapour pressure given at different temperatures in Table 4.5) in Figures 4.37 and 4.38.

Table 4.5. Saturated Vapour Pressures of Hydrocarbons as a f(T)

Adsorbate	T/K	p_0/cm Hg	Adsorbate	T/K	p_0/cm Hg
C_3H_8	213.2	31.98	$i\text{-}C_4H_{10}$	258.2	67.30
	243.2	125.6	(contd)	268.2	99.08
	273.2	354.8		273.2	118.9
	393.2	4102		308.2	350.8
	473.2	-		343.2	814.7
$i\text{-}C_4H_{10}$	218.2	9.780		358.2	1117
	233.2	21.95		393.2	2118
	248.2	44.16		423.2	3396
				453.2	5248

Source : Am. Petrol. Inst. Research Proj. 44.

(c) Hydrocarbon/Black Pearls

Isothermal flow measurements were made using C_3H_8 at T/K = 273.2 and 213.2 and $i\text{-}C_4H_{10}$ at T/K = 343.2, 308.2, 273.2 and 233.2. The experimental values of molar flux, J and integral permeability, $\tilde{K}$ are contained in Appendix B5 to 6 over a range of temperature and ingoing pressure, p_1. The variation of J with p_1 at different

Figure 4.33. Pressure - Dependence of J : C_3H_8/Graphon

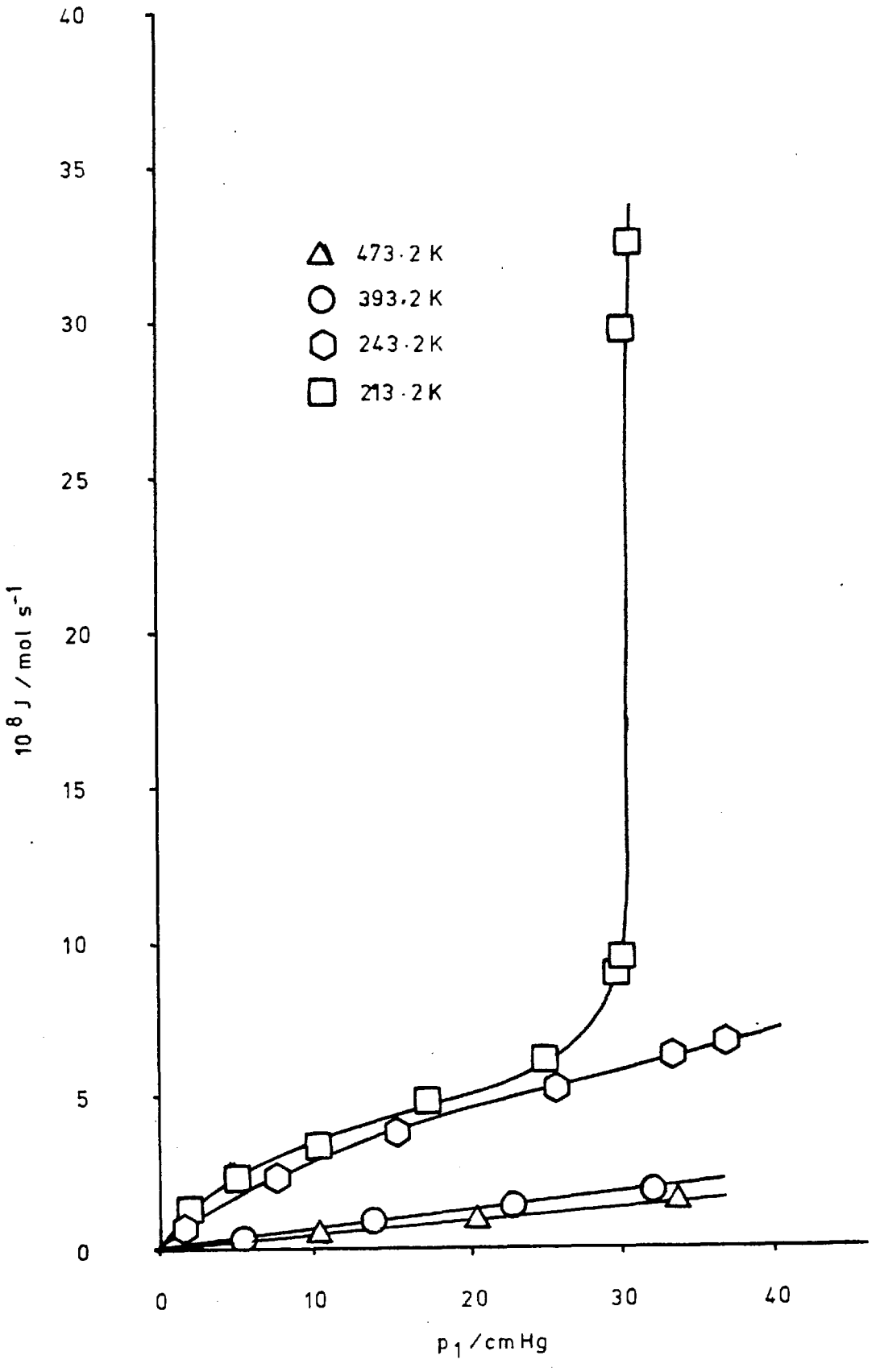

Figure 4.34. Pressure - Dependence of J : i-C_4H_{10}/Graphon

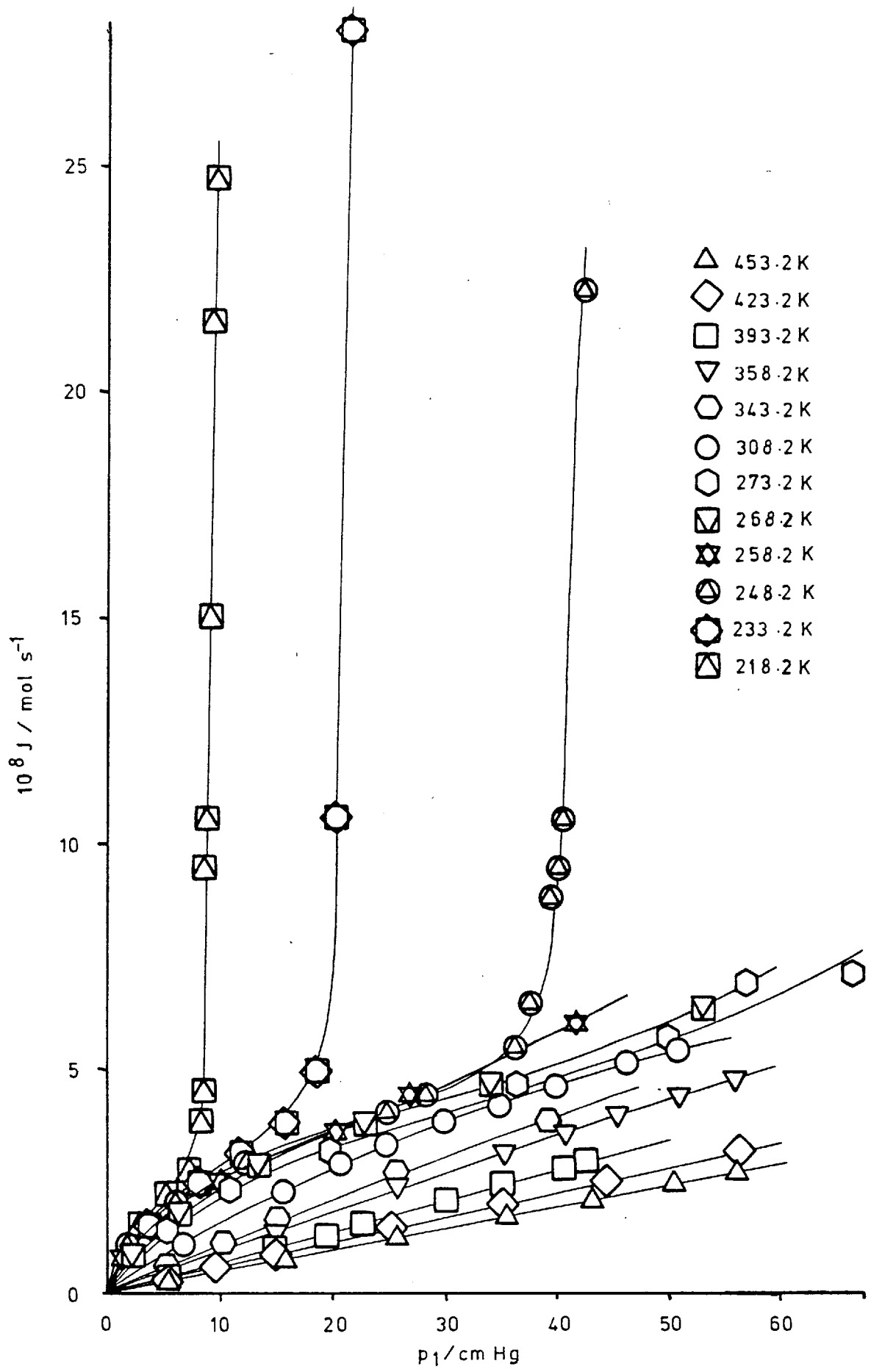

Figure 4.35. Pressure - Dependence of $\tilde{K}$: C_3H_8/Graphon

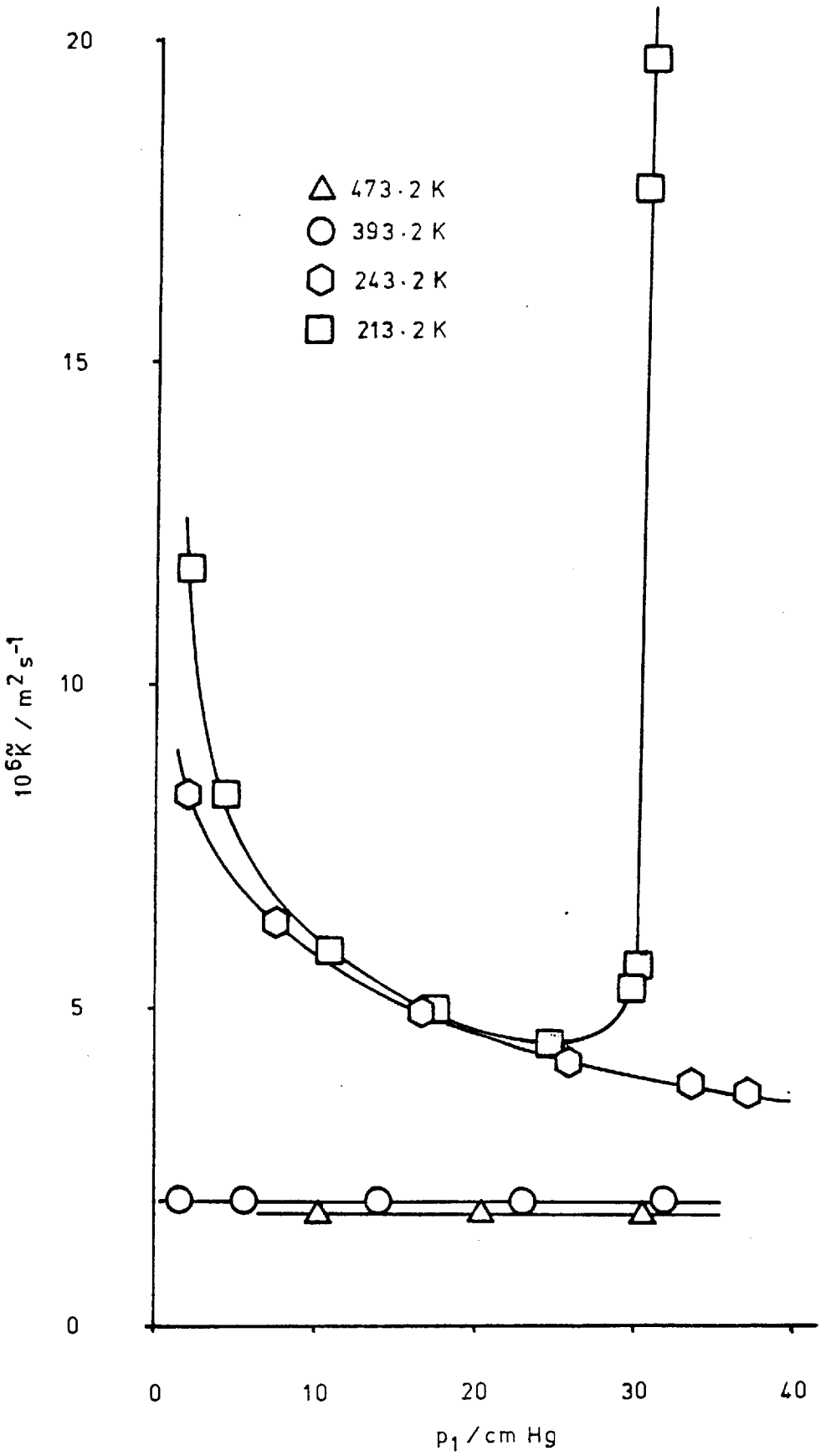

Figure 4.36. Pressure - Dependence of $\tilde{K}$: i-C_4H_{10}/Graphon

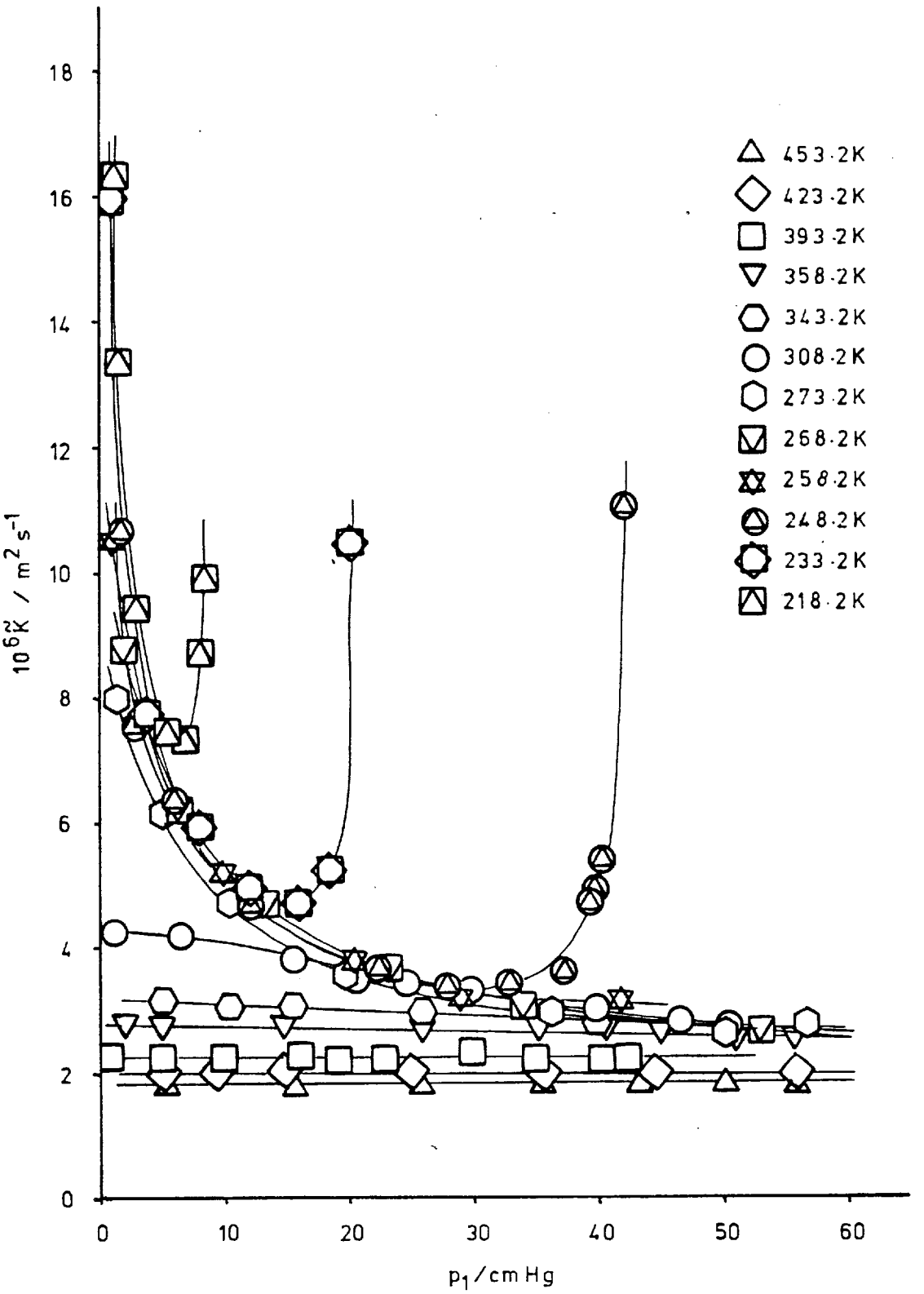

Figure 4.37. Variation of $\tilde{K}$ with p_1/p_o : C_3H_8/Graphon

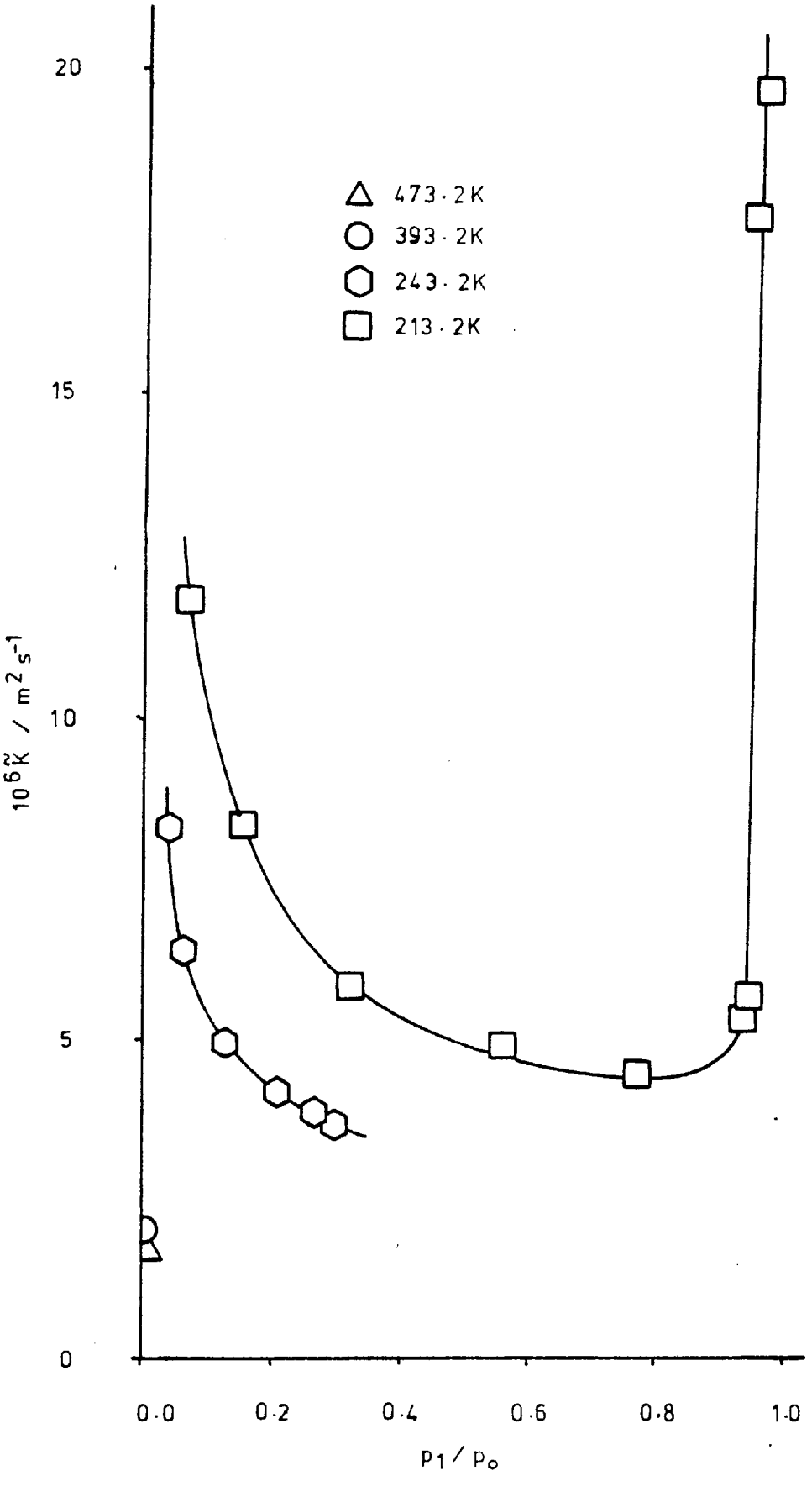

Figure 4.38. Variation of $\tilde{K}$ with p_1/p_o : i-C_4H_{10}/Graphon

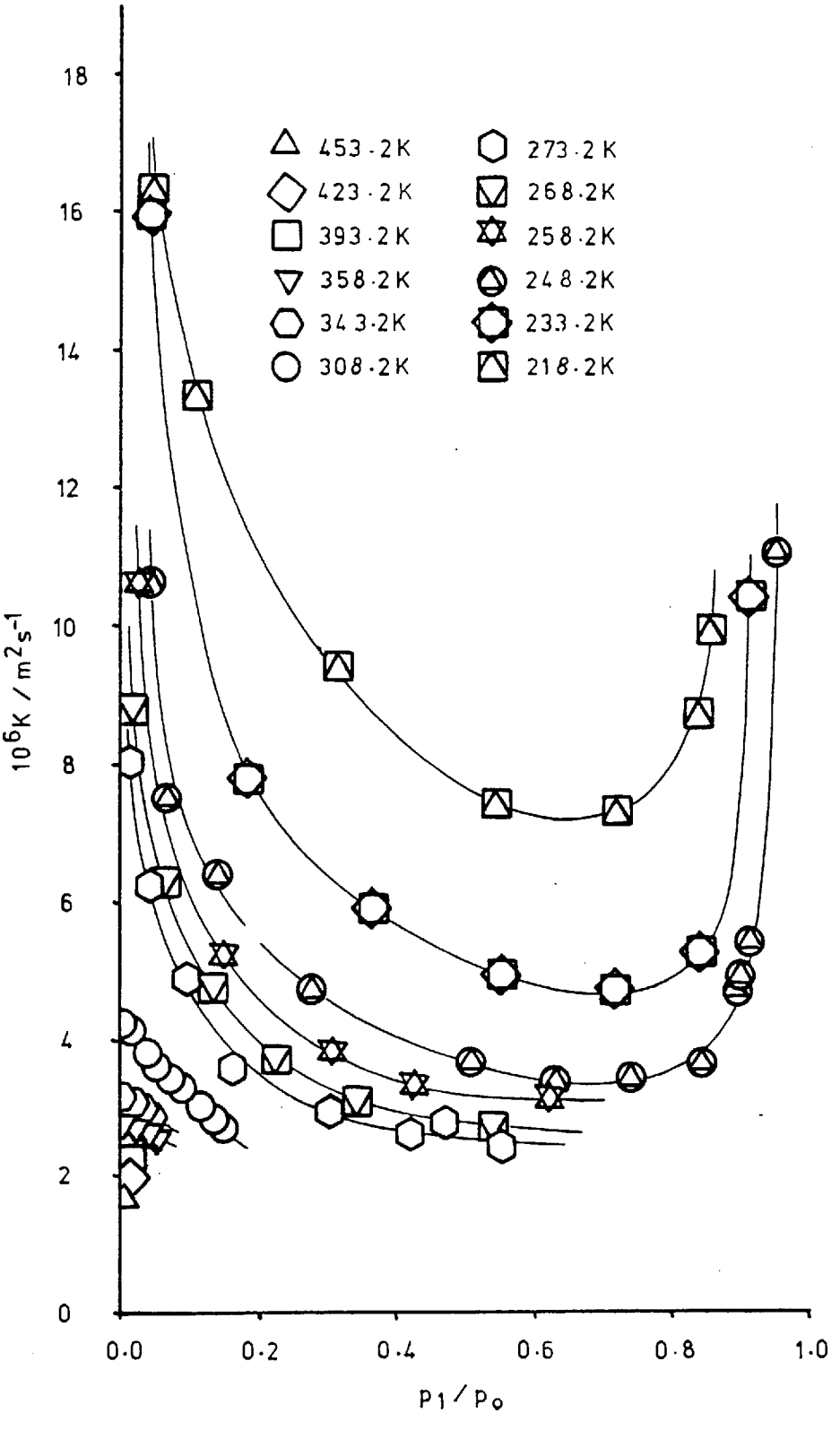

Figure 4.39. Pressure - Dependence of J : C_3H_8/Black Pearls

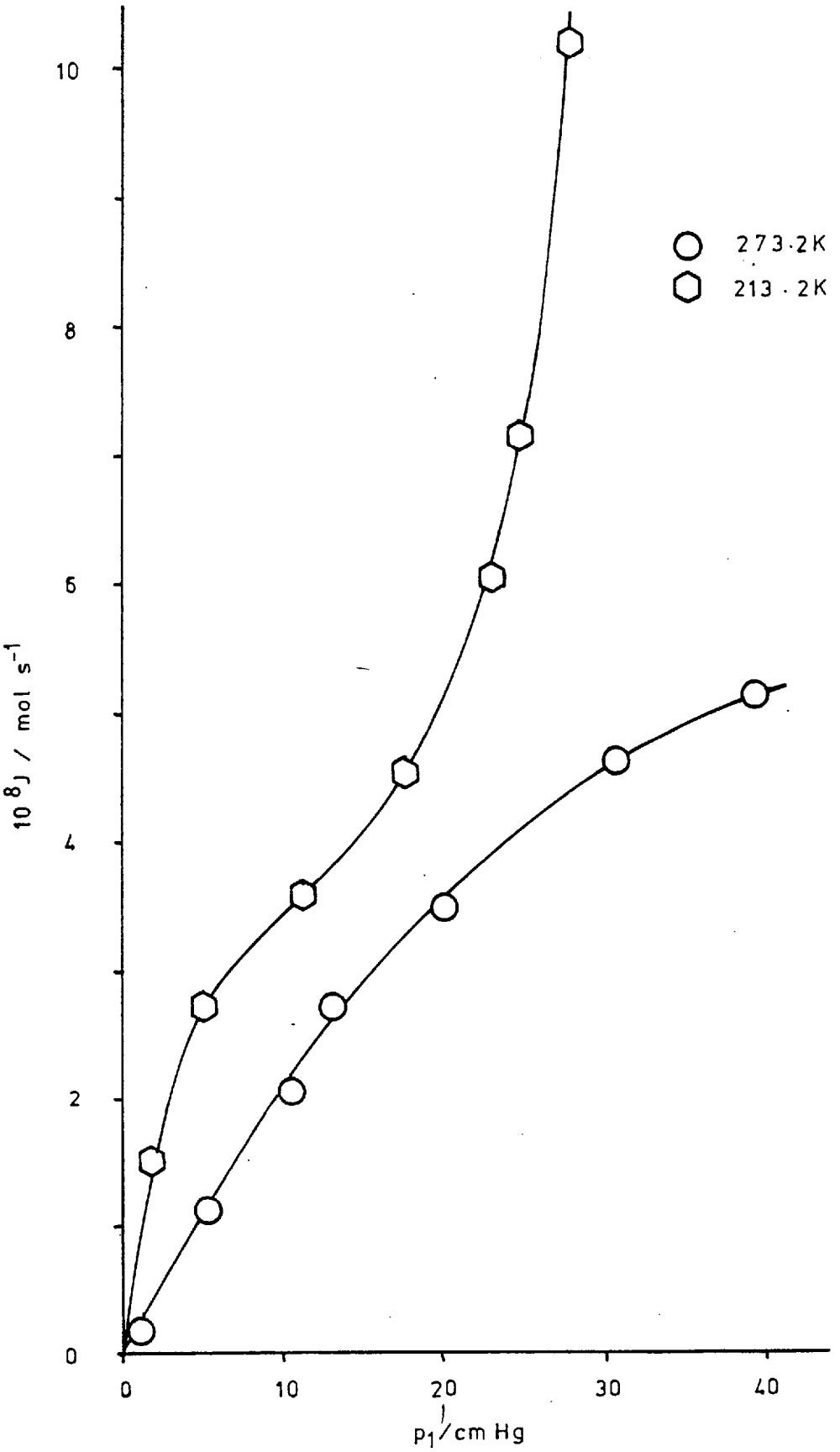

Figure 4.40. Pressure - Dependence of J : $i\text{-}C_4H_{10}$/Black Pearls

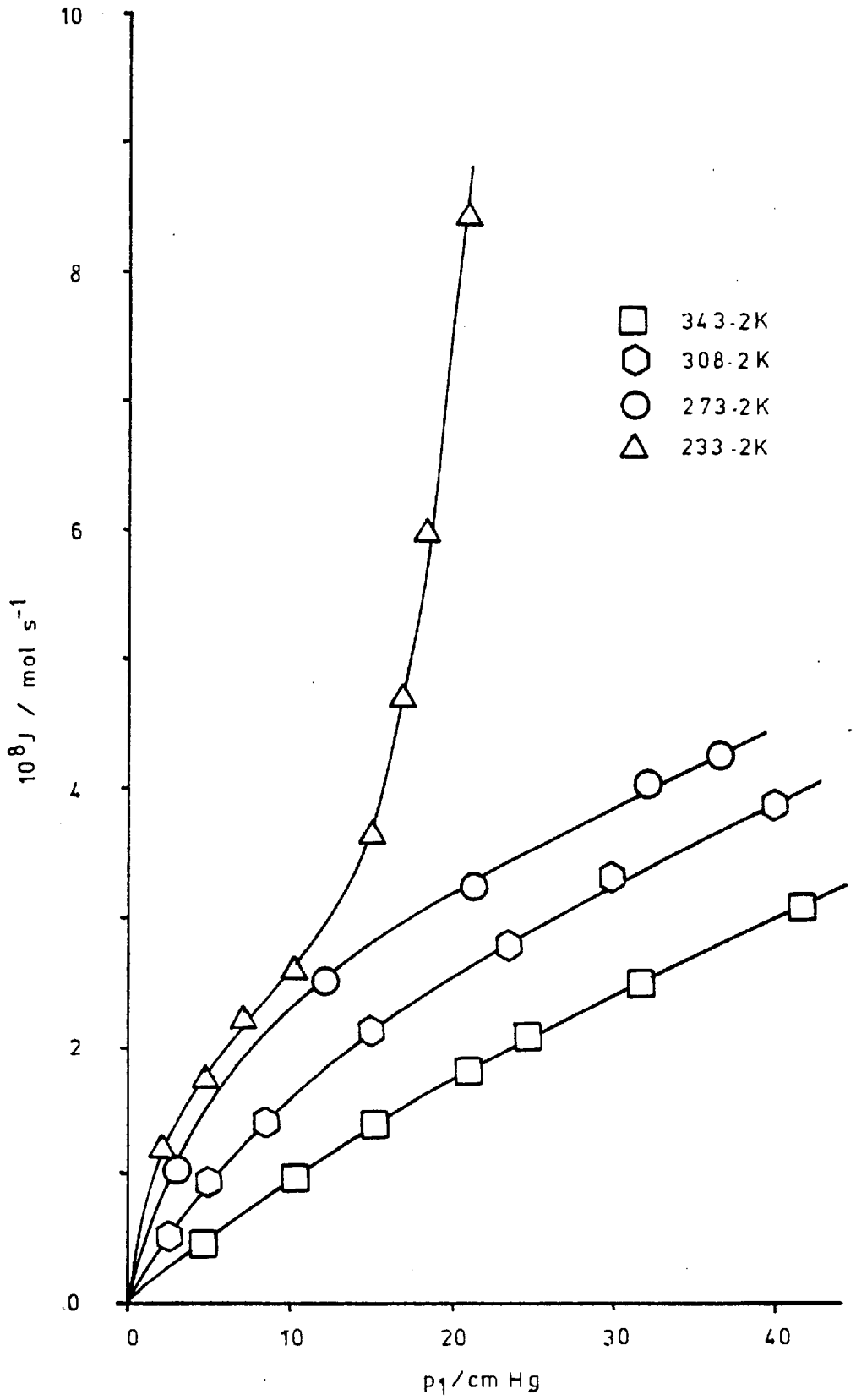

Figure 4.41. Pressure - Dependence of $\tilde{K}$: C_3H_8/Black Pearls

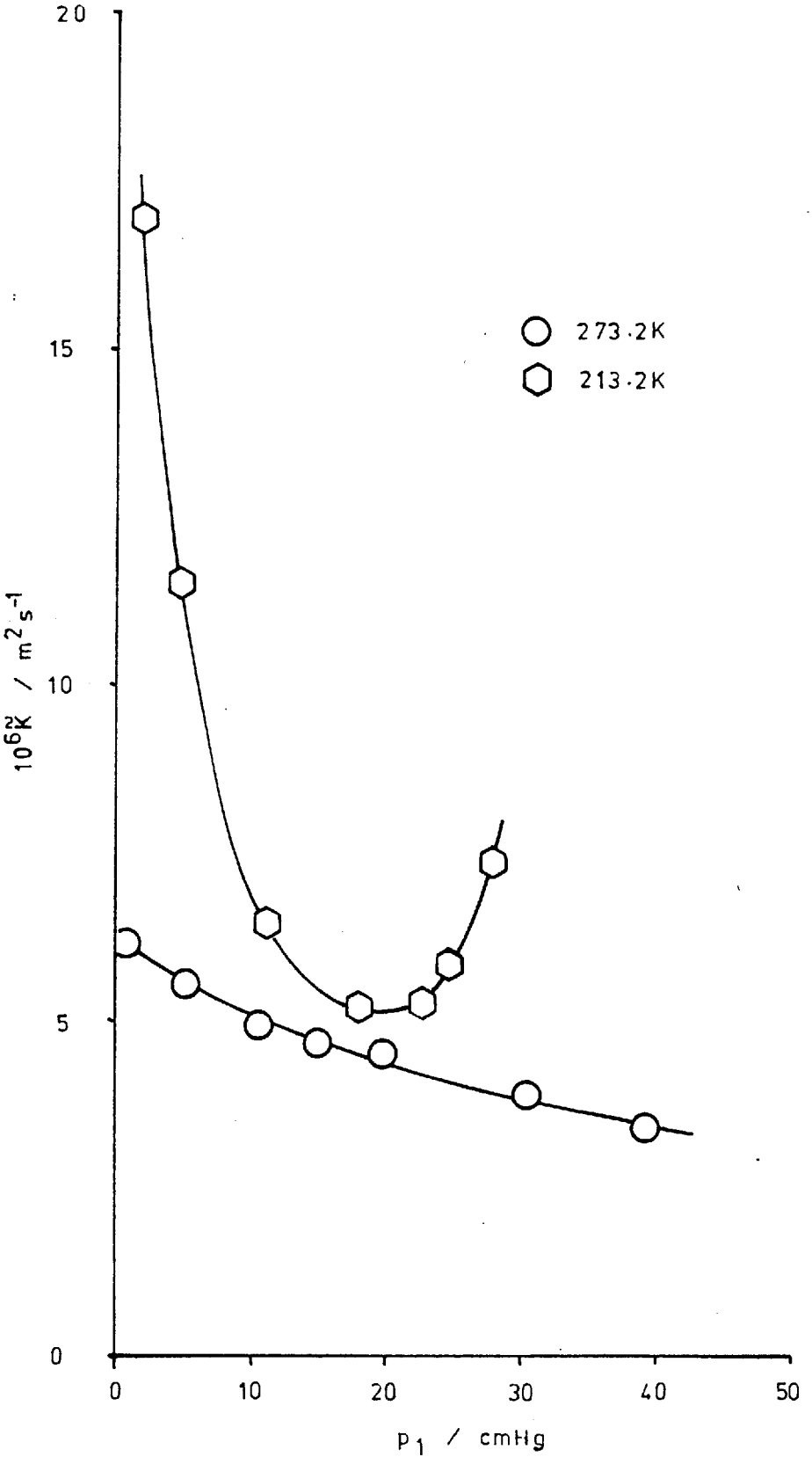

Figure 4.42. Pressure - Dependence of $\tilde{K}$: i-C_4H_{10}/Black Pearls

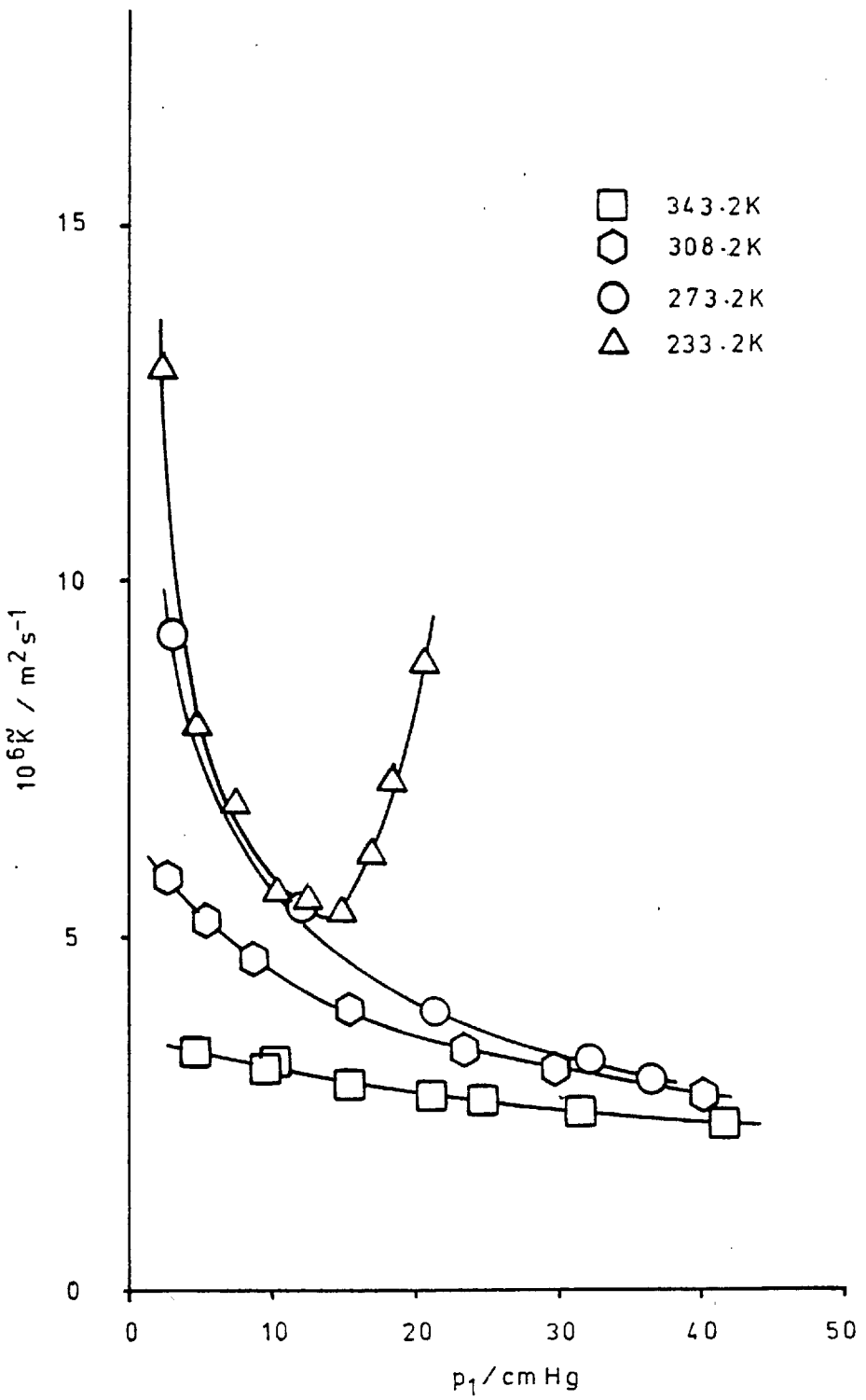

Figure 4.43. Variation of $\tilde{K}$ with p_1/p_o : C_3H_8/Black Pearls

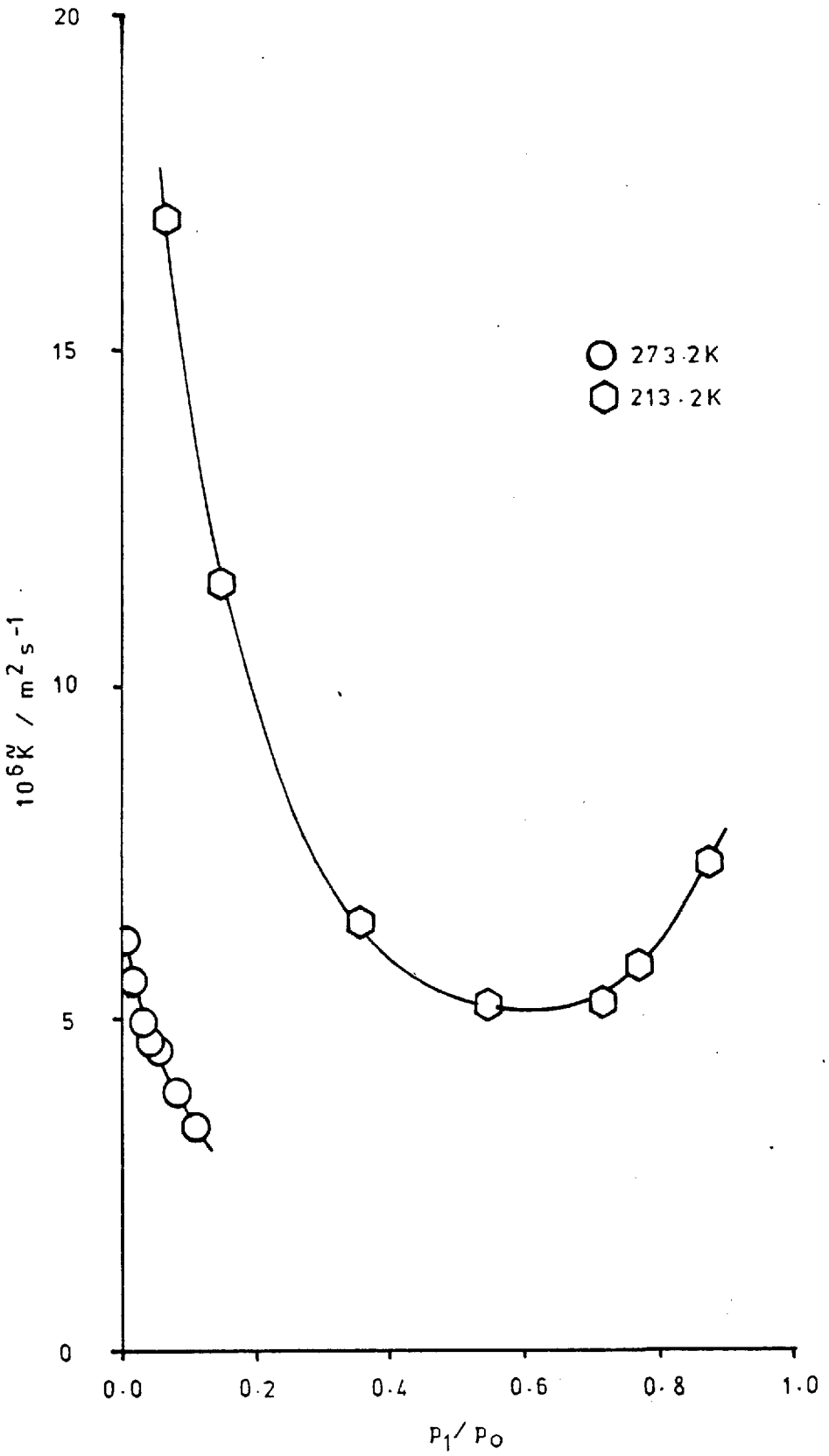

Figure 4.44. Variation of $\tilde{K}$ with p_1/p_o : i-C_4H_{10}/Black Pearls

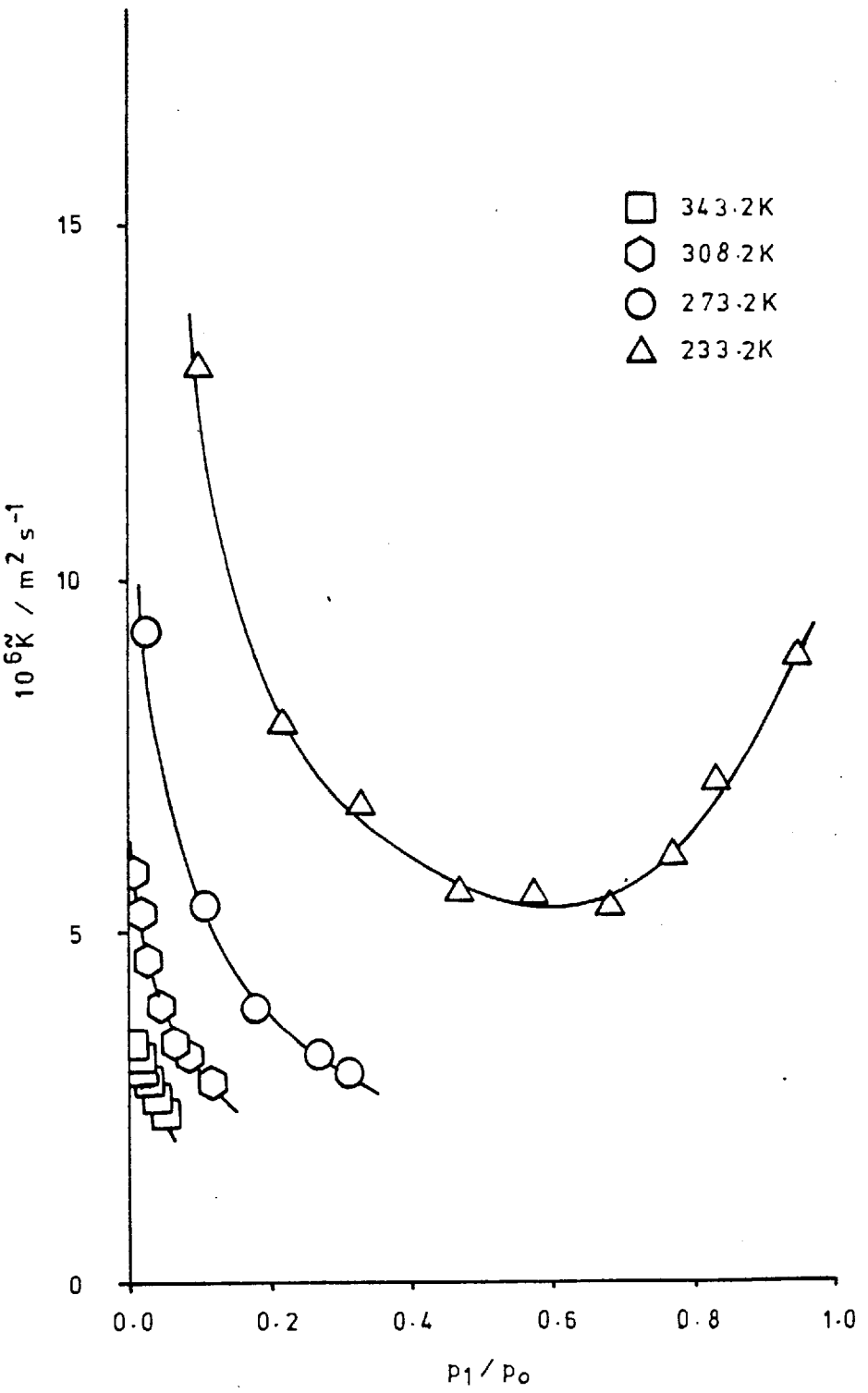

temperatures is shown in Figures 4.39 and 4.40. The corresponding pressure dependences of $\tilde{K}$ are presented in Figures (4.41, 4.42) and (4.43, 4.44) as a function of p_1 and p_1/p_0 respectively.

The shapes of the curves and further interpretation will be discussed in Section 5.2.

4.2.3. Binary Mixtures

Flow experiments involving binary gas mixtures were undertaken on both carbons. The majority were mixtures consisting of helium (non-sorbed component) and either propane or isobutane (sorbable component). Some measurements were made using mixtures of argon and a hydrocarbon on Graphon. (These will be discussed later). As previously mentioned (cf §4.2.1) the quantity determined was the permeability of the non-sorbed helium component, $\tilde{K}$ which was then used to present the measured data in the form $\tilde{K}_R$ versus ingoing pressure, p_1 of hydrocarbon. Values of $\tilde{K}$, $\tilde{K}_R$ at various temperatures and pressures are tabulated in Appendix B, 7 to 11 for both carbons. Figures 4.45 to 4.48 show the pressure dependence of $\tilde{K}_R$ for the hydrocarbon/helium mixtures at various temperatures on Graphon and Black Pearls respectively.

The argon/hydrocarbon results are plotted somewhat differently as described in greater detail in Section 5.2.3(d). Briefly the measured argon permeability is converted to an equivalent helium permeability, assuming only gas phase transport of Ar by the relationship :-

$$\frac{\tilde{K}\, M^{\frac{1}{2}}}{T^{\frac{1}{2}}} = \text{constant} \qquad (2.4)$$

This in turn is converted to a relative permeability and compared to that obtained from the helium mixtures for a given temperature (Figures 4.49 to 4.53). The tabulated data is given in Appendix B.11.

Maintenance of Boundary Conditions in Mixture Experiments

The experimental procedure assumes that the initial mixture composition remains constant throughout the course of an experiment. However at the low temperatures there is negligible flow of the non-sorbed component and rapid sorbed gas flow. It was considered necessary to make some calculations to gauge the magnitude of this effect.

Figure 4.45. Pressure - Dependence of $\tilde{K}_R$: He/C_3H_8/Graphon

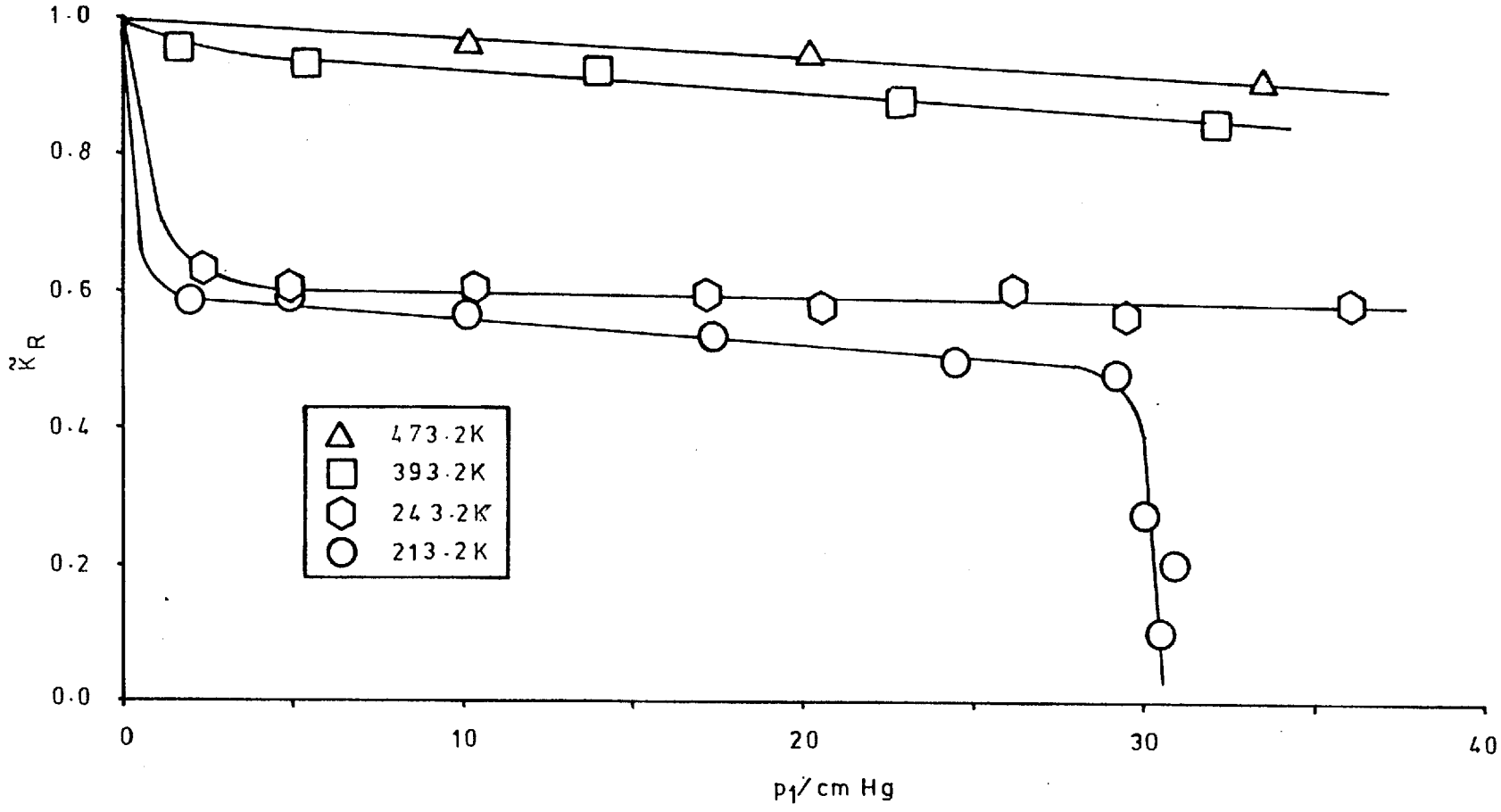

Figure 4.46. Pressure - Dependence of $\tilde{K}_R$: He/i-C_4H_{10}/Graphon

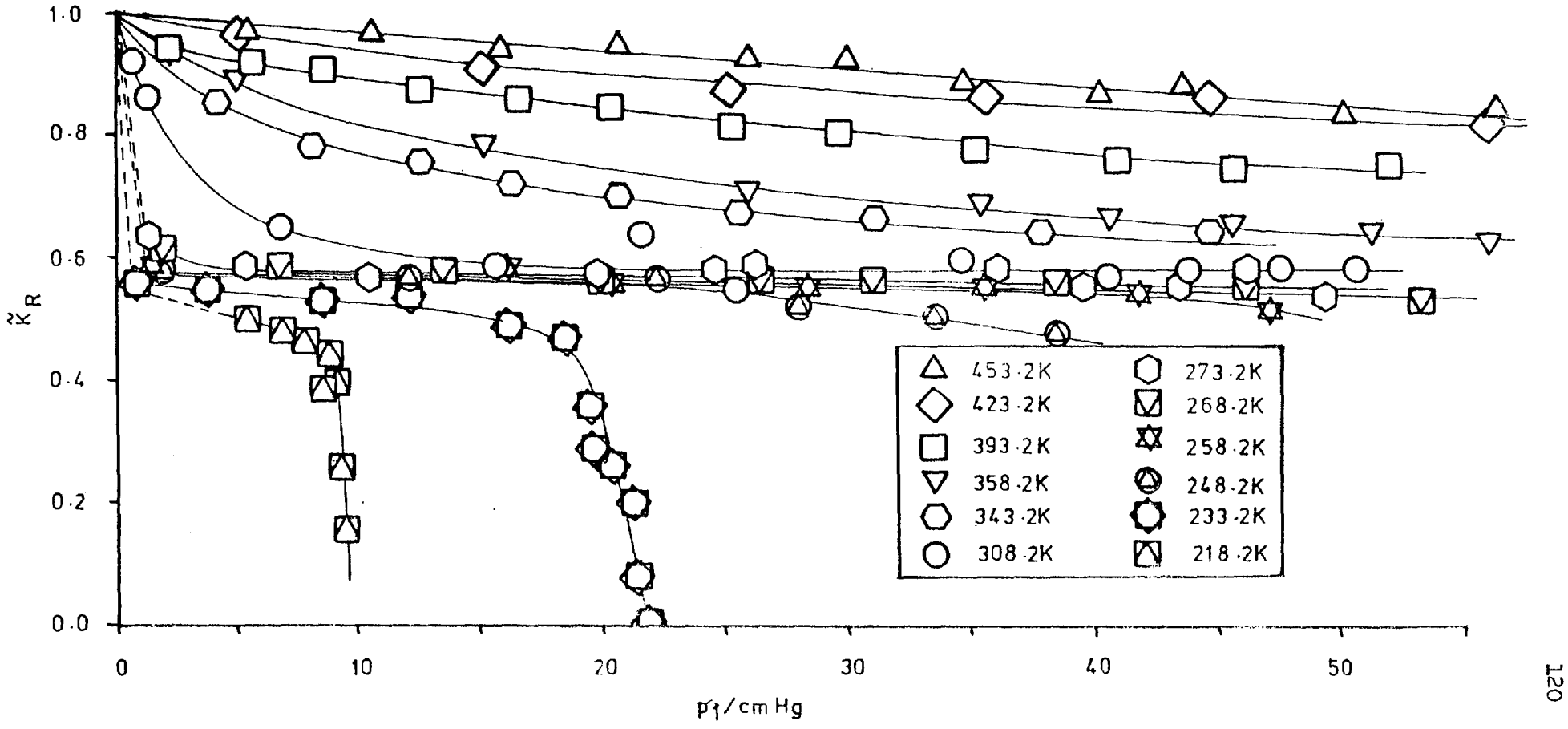

Figure 4.47. Pressure - Dependence of $\tilde{K}_R$: He/C_3H_8/Black Pearls

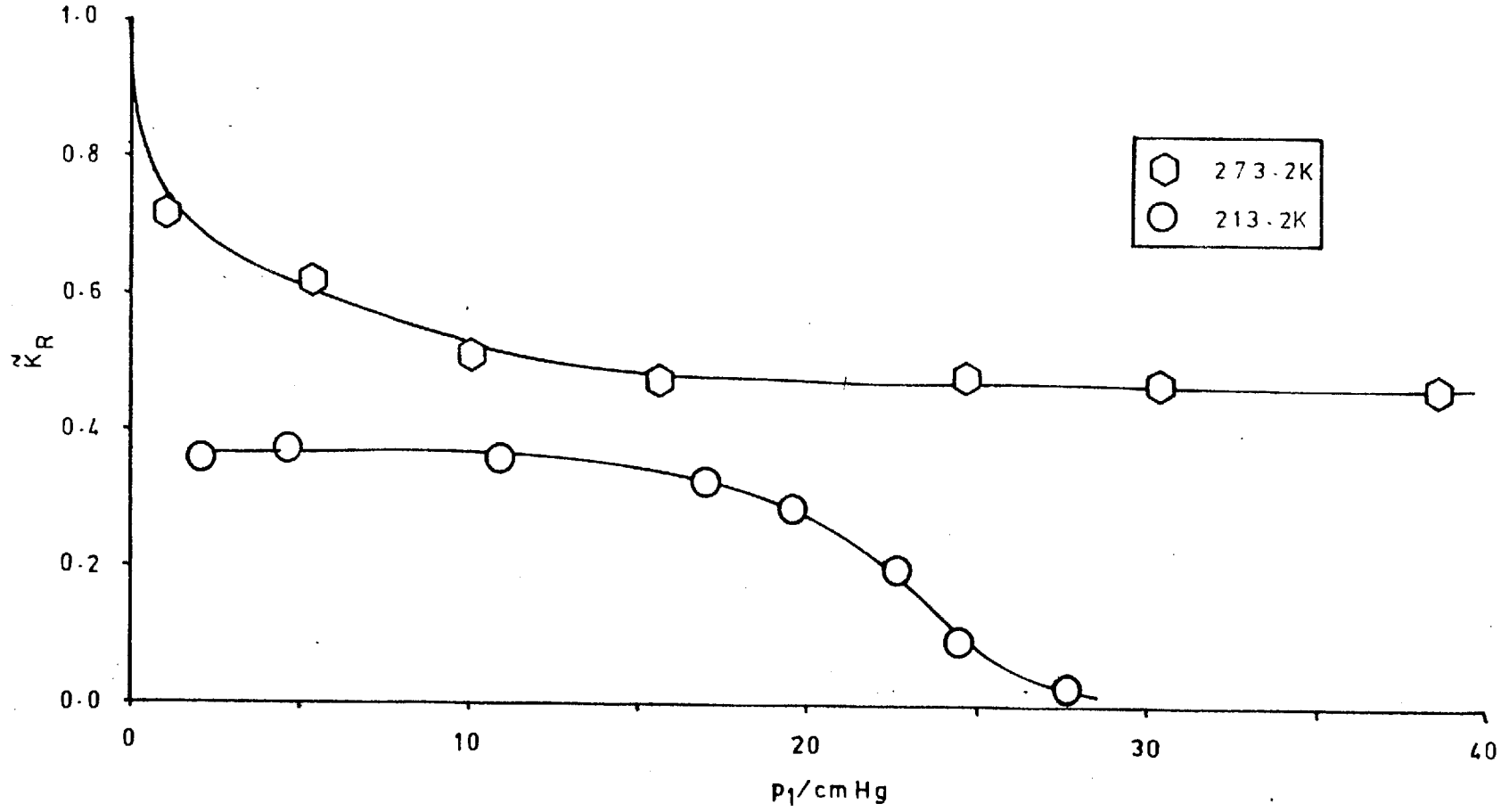

Figure 4.48. Pressure - Dependence of $\tilde{K}_R$: He/i-C_4H_{10}/Black Pearls

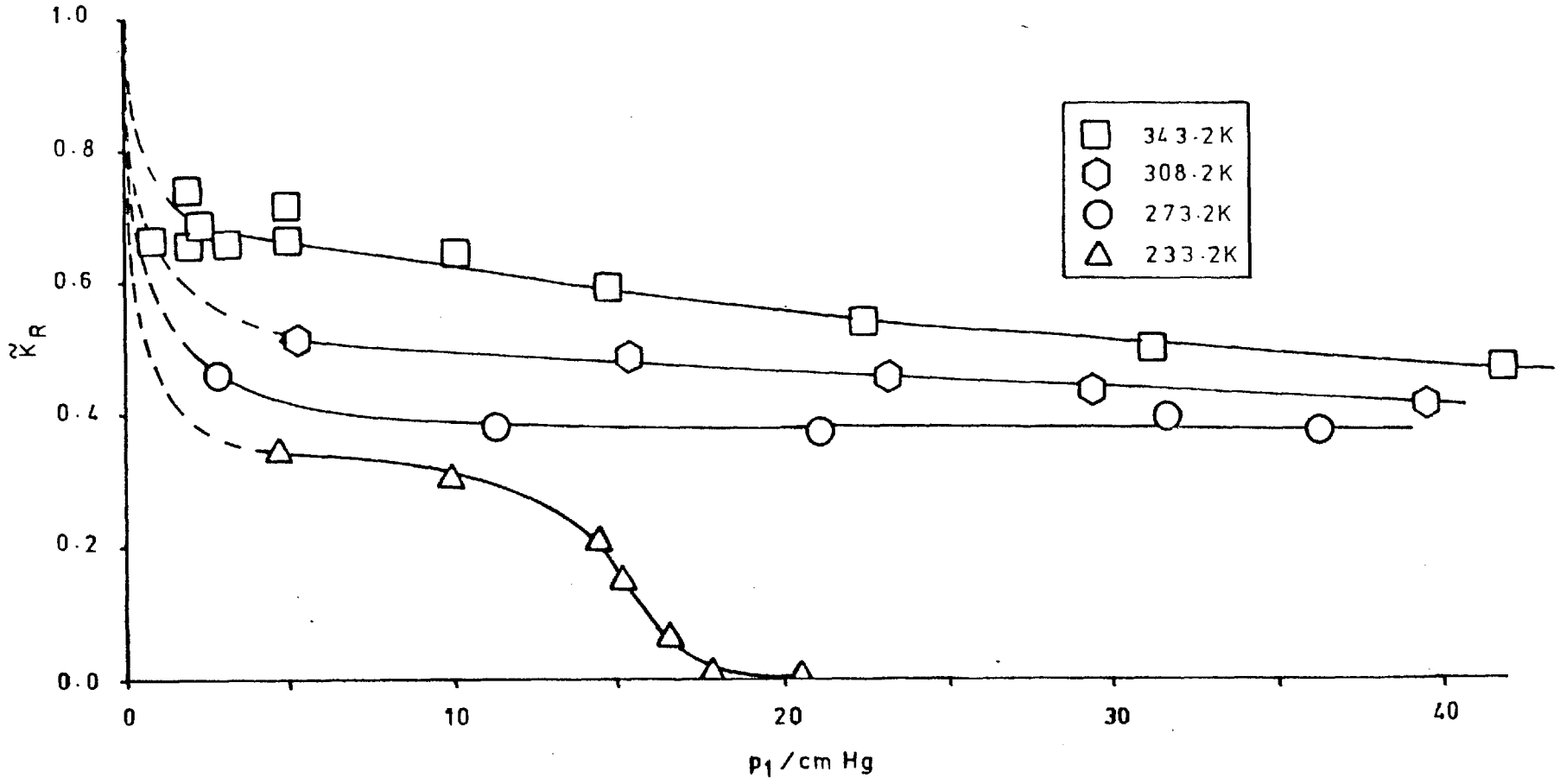

Figure 4.49. Pressure - Dependence of $\tilde{K}_R$: Ar/i-C_4H_{10}/Graphon : T/K = 453.2

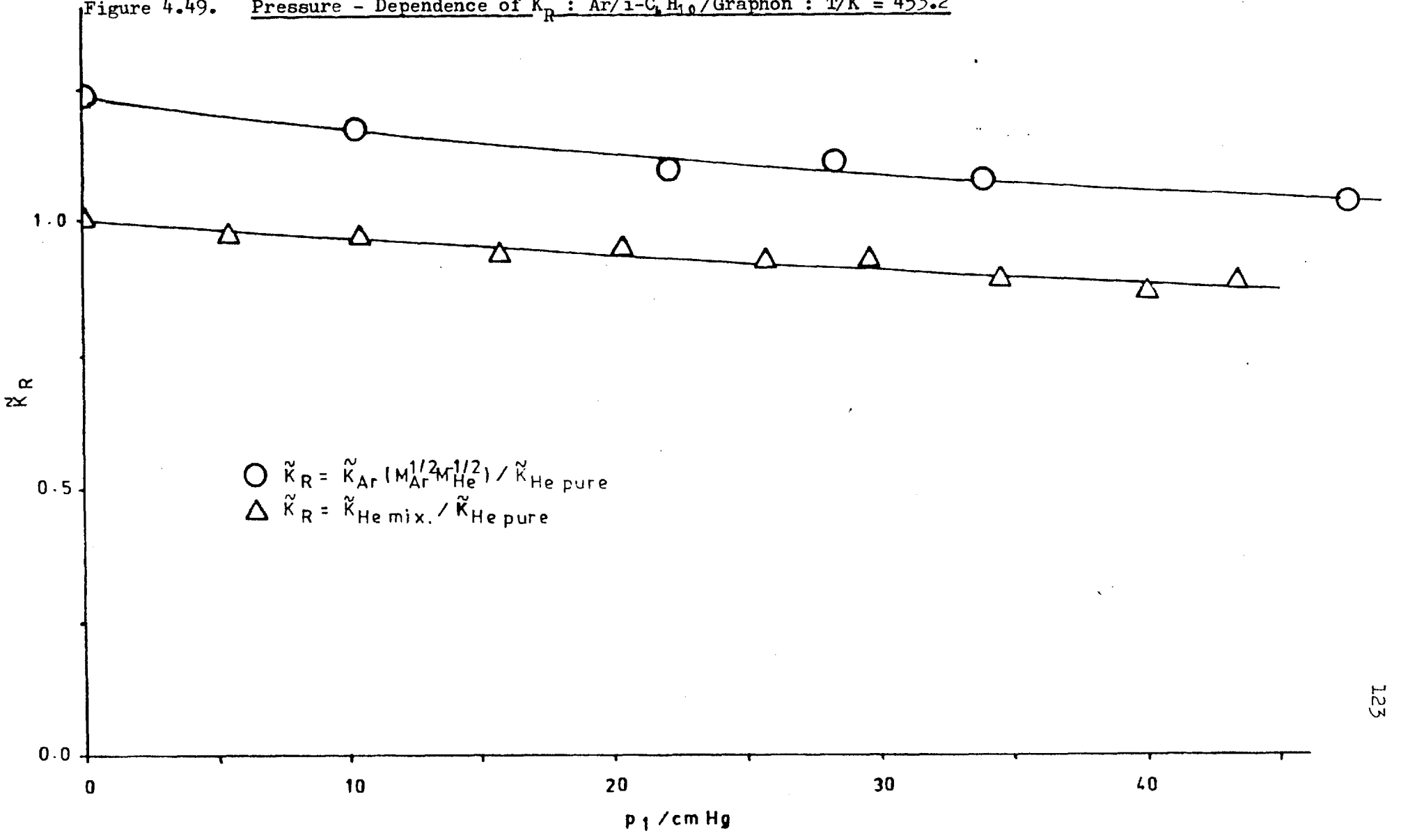

Figure 4.50. Pressure - Dependence of $\tilde{K}_R$: Ar/i-C_4H_{10}/Graphon : T/K = 393.2

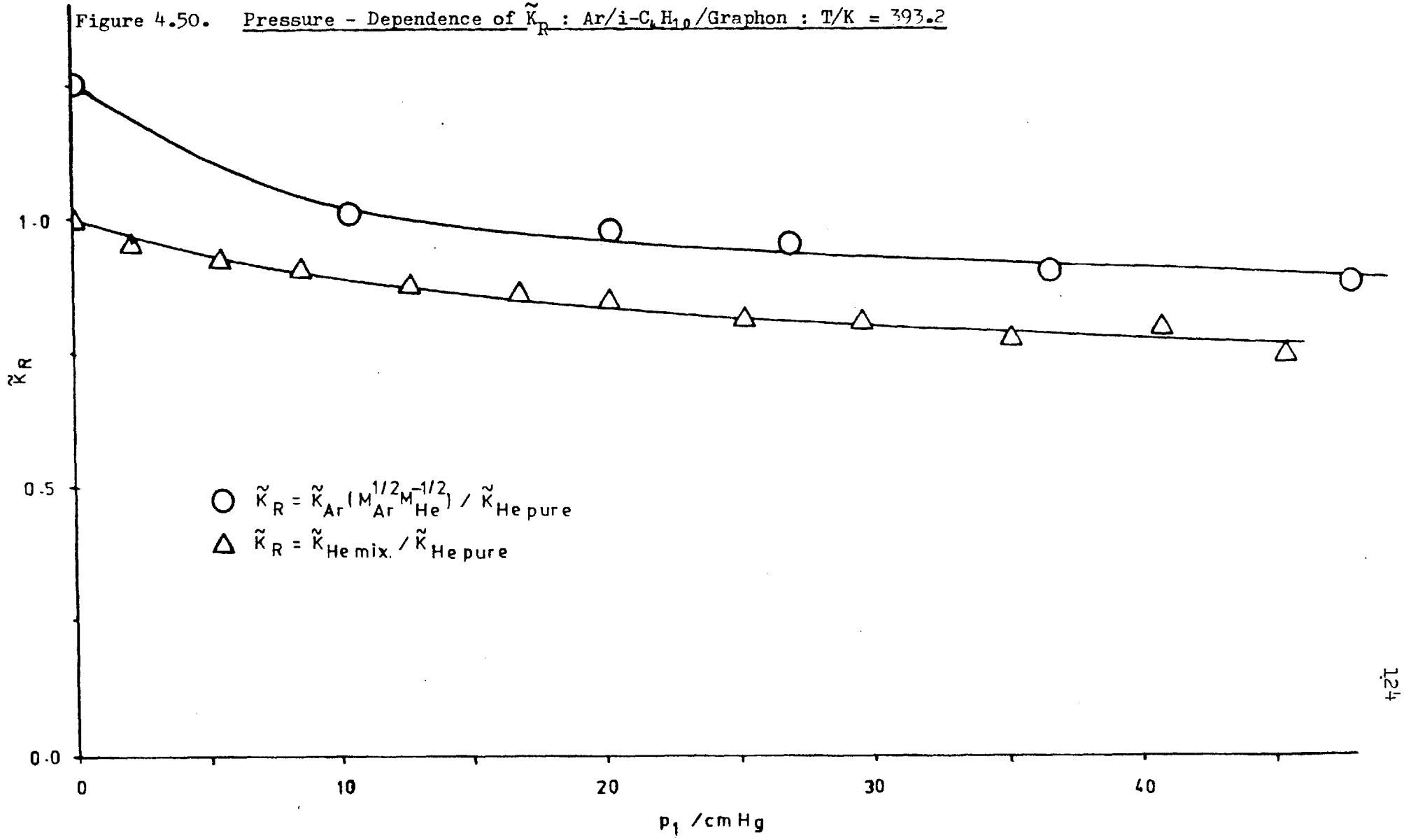

Figure 4.51. Pressure - Dependence of $\tilde{K}_R$: Ar/i-C_4H_{10}/Graphon : T/K = 308.2

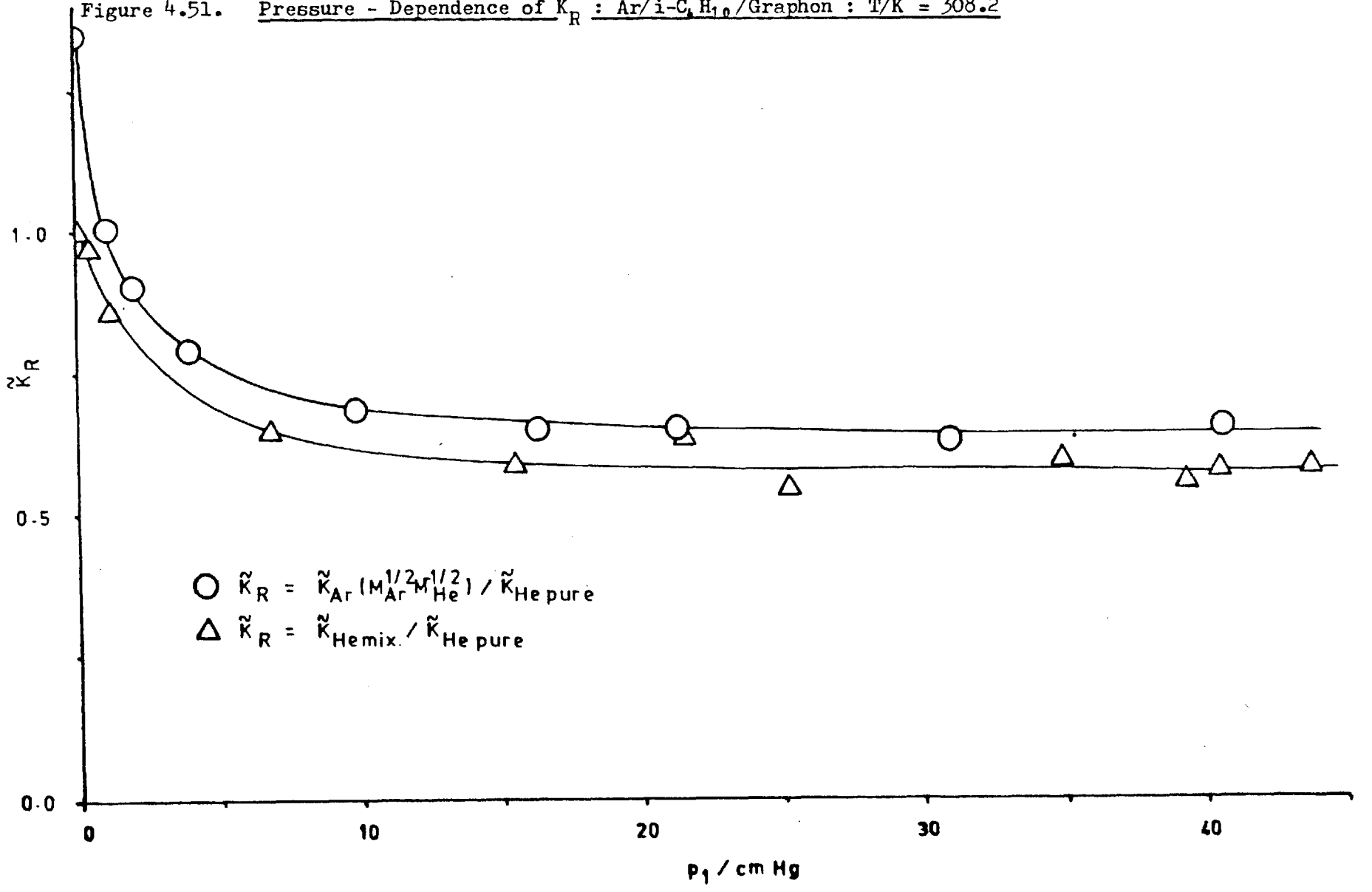

Figure 4.52. Pressure - Dependence of $\tilde{K}_R$: Ar/i-C_4H_{10}/Graphon : T/K = 273.2

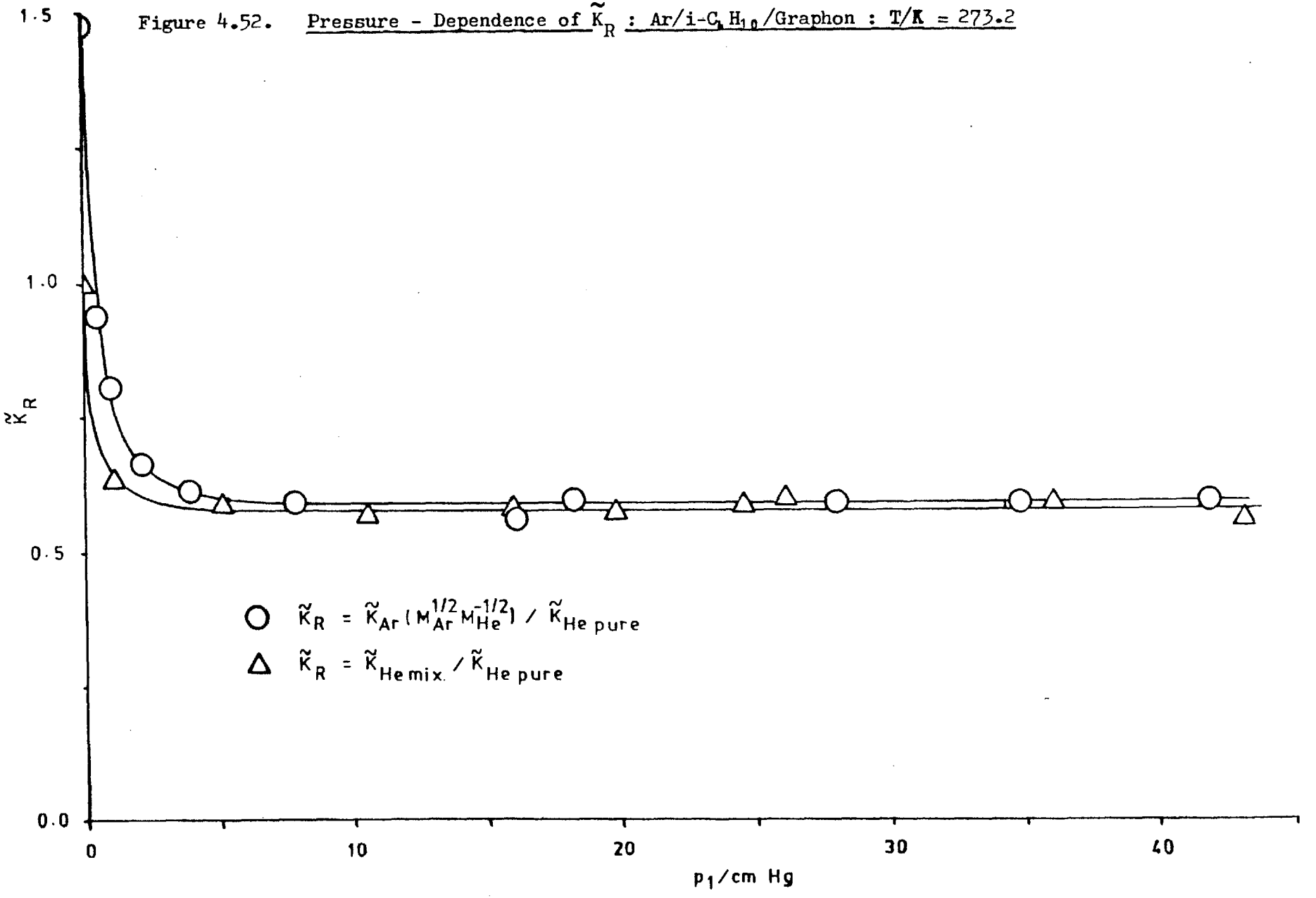

Figure 4.53. Pressure - Dependence of $\tilde{K}_R$: Ar/i-C_4H_{10}/Graphon : T/K = 233.2

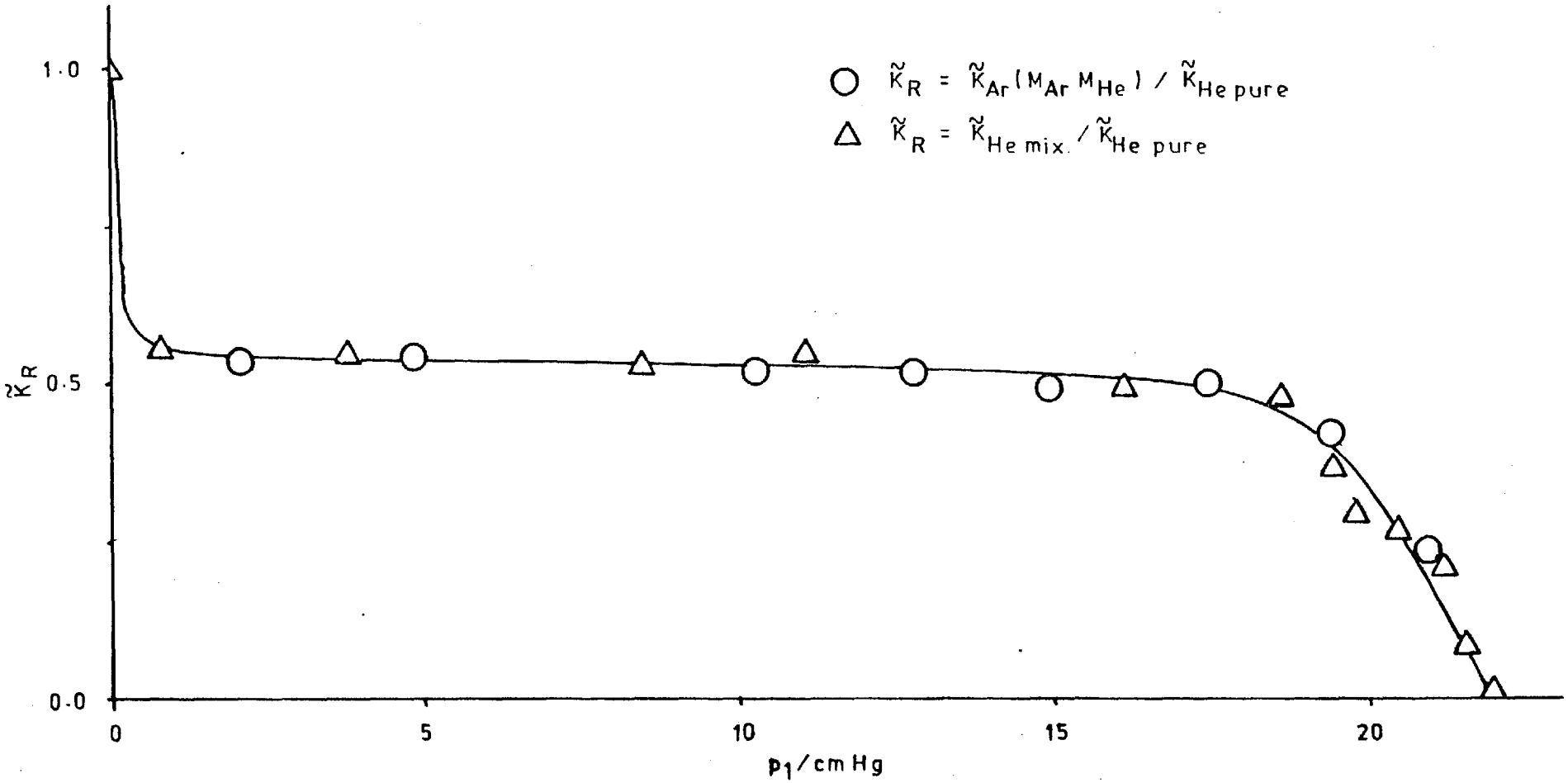

Throughout the course of an experiment the total ingoing pressure, p was maintained constant by the adjustment of the mercury level in the Toepler gauge. Assuming ideal behaviour the total pressure equals the sum of the partial pressures of the helium, p^{He} and hydrocarbon, p^{H}.

Thus :

$$p = p_o^{He} + p_o^{H} \quad : \text{initially}$$
$$= p_t^{He} + p_t^{H} \quad : \text{at time t} \qquad (4.9)$$

If the initial ingoing volume is V_1 and the volume at time t required to maintain a constant value of p_o is V_t, then :

$$\Delta V \equiv V_1 - V_t > 0 \qquad (4.10)$$

At time t the amount of gas remaining in the ingoing side, n_t must be related to the amount that has passed through the membrane, $J_{oo}t$ and the amount originally in the ingoing side by the relationship :

$$n_1 - J_{\infty} t = n_2 \qquad (4.11)$$

Thus for the indicator gas flow :

$$\frac{p_o^{He} V_1}{RT_R} - J_{\infty}^{He} t = p_t^{He} \frac{V_t}{RT_R} \qquad (4.12)$$

which re-arranges to :

$$p_o^{He} \frac{V_1}{V_t} - J_{\infty}^{He} t \frac{R T_R}{V_t} = p_t^{He} \qquad (4.13)$$

Equation (4.13) may also be written for the sorbed gas component :

$$p_o^{He} \frac{V_1}{V_t} - J_{\infty}^{H} t \frac{RT_R}{V_t} = p_t^{H} \qquad (4.14)$$

Adding (4.13) and (4.14) results in :

$$p_o \frac{V_1}{V_t} = J_{\infty} t \frac{RT_R}{V_t} + p_o \qquad (4.15)$$

(where $p_o = p_o^{H} + p_o^{He}$ and $J_{\infty} = J_{\infty}^{H} + J_{\infty}^{He}$)

Equation (4.15) may be re-arranged to give :

$$\Delta V = \frac{J_{\infty} t RT_R}{p_o} \qquad (4.16)$$

which gives the amount that the ingoing volume must be reduced to

maintain the ingoing pressure constant. Once ΔV is calculated for a given system values of p_t^H and p_t^{He} may be evaluated from equations (4.13) and (4.14). As regards maintaining the ingoing composition constant, it was considered experimentally necessary that the partial pressure of each component should not vary by more than 1% during the course of a run.

In the calculations made, an experimental run of 2 hrs was considered and the initial partial pressure of helium, p_o^{He} was taken as 4.0 cm Hg in each case. A value of 295.2 K was considered a fair estimate for the room temperature. The results are tabulated in Table 4.6 for the various systems in this study. The temperatures and pressures were chosen specifically to cover the whole range of partial pressures which existed. It can be seen that the sum of $\Delta p^H + \Delta p^{He}$ is zero (in the majority of cases) as expected. Considering the isobutane/Graphon system at high temperatures the helium component flows more rapidly than the isobutane as shown by a decrease in the partial pressure.

However as the temperature is decreased blockage effects restrict the flow and an increase in the partial pressure results. This increase remains less than 1% of the initial helium partial pressure until high coverages are approached. It can be seen from the blockage curves (Figures 4.45 to 4.48) that those pressures of hydrocarbon where an increase greater than 1% occurs correspond to the latter section of the curve, i.e. the region at the end of the flat plateau. It is accepted that the condition of constant ingoing composition must break down when almost total blockage of one component occurs, but for the majority of cases the assumption is valid.

Table 4.6. Percentage Change in Partial Pressures of Each Component during a Run

	$\frac{T}{K}$	$\frac{p_o^H}{cm\ Hg}$	$\frac{\Delta V}{cm^3}$	$\frac{\Delta p^H=(p_t-p_o)}{cm\ Hg}$	$\frac{\Delta p^{He}=(p_t-p_o)}{cm\ Hg}$	$\left\lvert\frac{\Delta p^H}{p_o^H}\right\rvert$ x100	$\left\lvert\frac{\Delta p^{He}}{p_o^{He}}\right\rvert$ x100
i-C_4H_{10}/Graphon	453.2	5.326	9.08	+ 0.006	- 0.006	0.11	0.16
		25.72	7.211	+ 0.006	- 0.008	0.02	0.21
		50.20	6.826	+ 0.011	- 0.007	0.02	0.17
	273.2	19.73	18.650	+ 0.012	- 0.016	0.06	0.40
		66.19	13.58	- 0.002	+ 0.008	0.00$_3$	0.20
	218.2	5.354	35.84	- 0.040	+ 0.041	0.75	1.02
		8.382	50.66	- 0.075	+ 0.077	0.89	1.93
		9.587	240.9	- 0.463	+ 0.463	4.83	11.59
C_3H_8/Graphon	213.2	24.71	29.44	- 0.034	+ 0.035	0.14	0.87
		29.90	35.02	- 0.053	+ 0.052	0.18	1.30
i-C_4H_{10}/Black Pearls	233.2	10.24	24.51	- 0.041	+ 0.041	0.40	1.02
		18.25	35.69	- 0.060	+ 0.063	0.33	1.57
C_3H_8/Black Pearls	213.2	17.45	28.28	- 0.047	+ 0.047	0.27	1.17
		27.85	42.47	- 0.074	+ 0.075	0.27	1.87

4.3. "Pressure Decay" Flow Results

4.3.1. Introduction

Isothermal flow measurements under 'pressure decay' conditions (cf §2.3.2) were made only on the Graphon membrane. Helium and isobutane were studied over the temperature range 233 to 393 K, as single species and also as a binary mixture. The pressure-decay technique was instituted specifically to examine the blockage behaviour.

The pressure decay technique involves the monitoring of the pressure difference, Δp between two fixed volumes, V_1 and V_2 separated by the membrane as a function of time, t(s). The calculation of the differential permeability, K requires the assumption that the pressure decay occurs by a first order process and that :

$$\ln (\Delta p/\text{cm Hg}) = - k't + \text{const.} \qquad (2.65)$$

where $k'(s^{-1})$ is the slope of the plot ln (Δp) vs t. The differential permeability, K^* $(m^2 s^{-1})$ defined by equation (2.63) arises from the 'quasi' steady-state flow (cf §2.3.2).

$$K^* \equiv \frac{J\,\ell}{A_c\,\Delta C'_g} = \frac{V_1\,V_2}{V_1+V_2}\,\frac{k'\ell}{Ac}\,\frac{T}{T_R} \qquad (2.64)\ (2.86)$$

where V_1 and V_2 (m^3) are the fixed ingoing and outgoing volumes respectively and T (K) is the membrane temperature.

The value of Δp as a f(t) was given indirectly from the outputs of pressure transducers on both sides and directly from the output of the 'Baratron' unit (cf §3.4.3(b)). These three outputs were fed into potentiometric chart recorders and a schematic representation of the traces is given in Figure 4.54 for a typical experiment reaching equilibrium as t tends to infinity.

From these traces a plot of ln $(\Delta p)/$cm Hg vs t was constructed and a value of the slope, k' obtained from the linear portion. The helium measurements resulted in a ln (Δp) vs t plot which was linear over the whole range; however in some cases for the mixture the plot exhibited an initial curved portion which will be discussed later in §5.3.1. A typical plot of this form is shown in Figure 4.55. The mixture results were again presented using the quantity K_R^* where :

Figure 4.54. Typical 'Pressure - Decay' Recorder Output

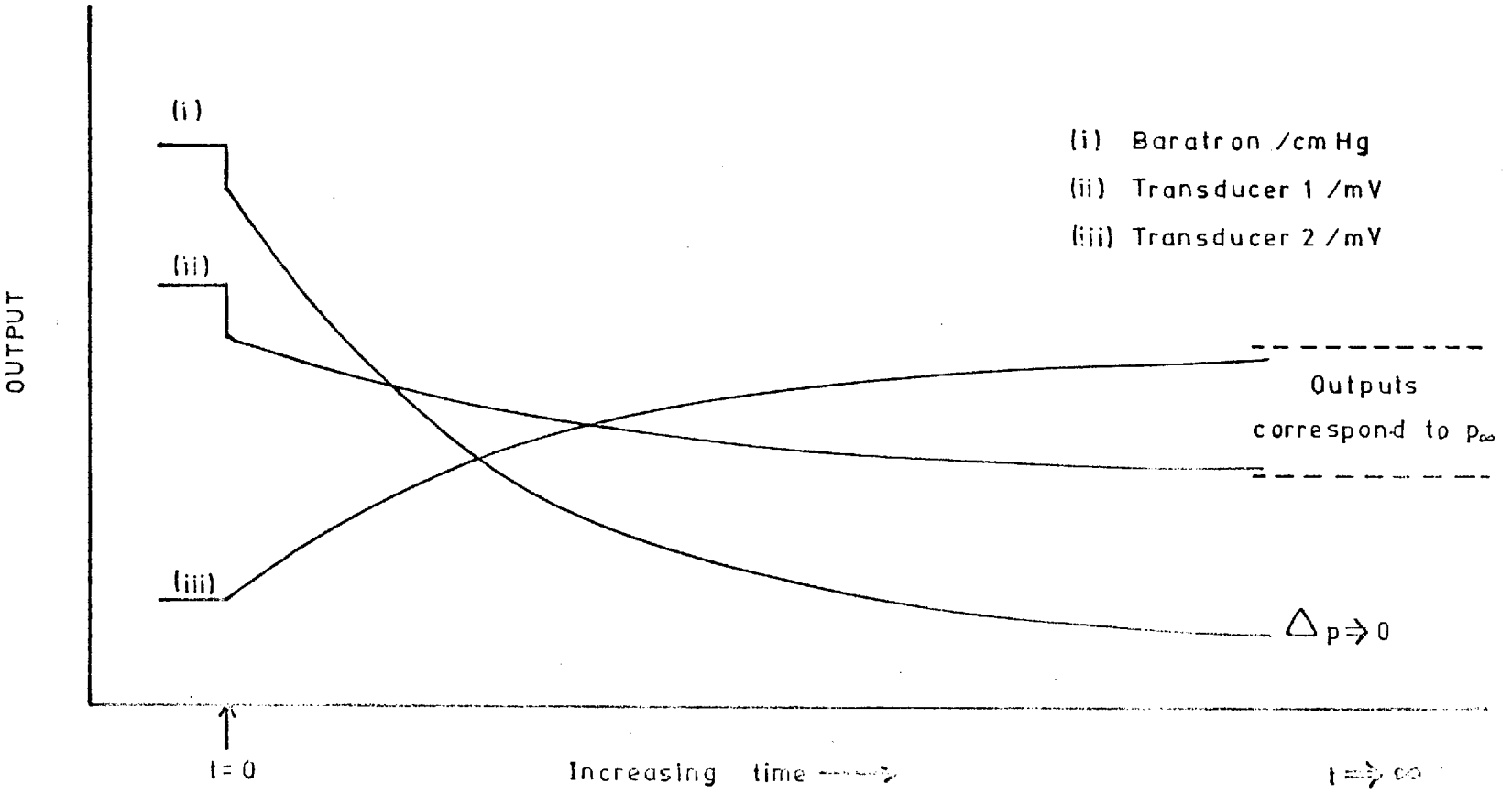

Figure 4.55. Typical ln (Δp/cm Hg) vs t plot : He/i-C_4H_{10}/Graphon

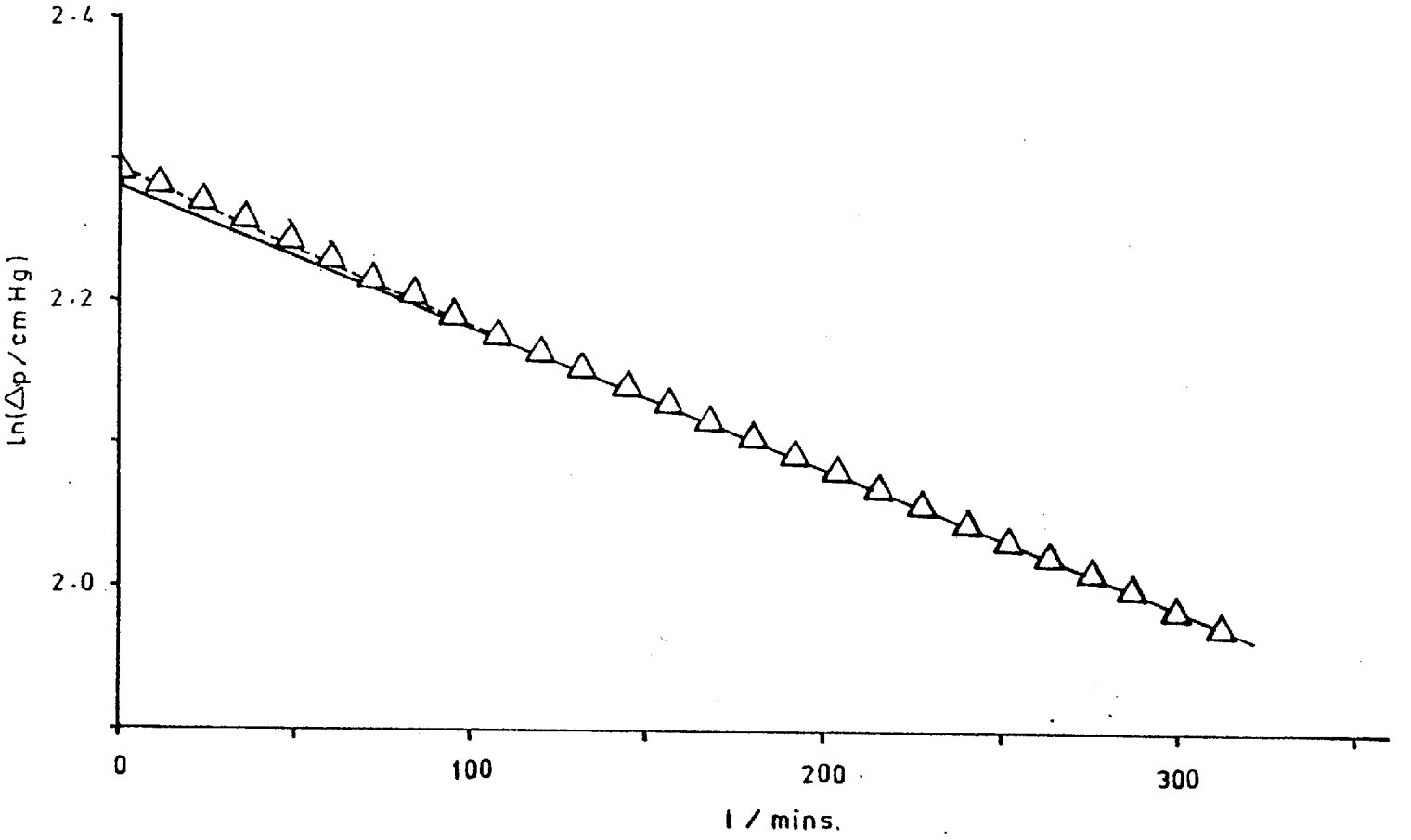

$$K_R^* = \frac{K_{He}^* \text{ mixture}}{K_{He}^* \text{ pure gas}} \qquad (4.17)$$

The advantages of the 'pressure decay' technique over the 'conventional' one lie in the fact that at long times the pressure difference between the two sides is very small and differential permeabilities are obtained directly instead of integral quantities. The differences and relationship between the differential and integral permeabilities is discussed in Section 5.3.2. It is also possible to examine the effect of a uniformly laid down layer of adsorbed material upon the flow of a non-sorbed indicator gas. In the 'conventional' apparatus a concentration gradient of adsorbed material exists in the membrane. As a result the blockage characteristics obtained from the two techniques could differ.

4.3.2. Single Species Flow

(a) Helium

The transport of helium was studied as a function of both temperature and equilibrium pressure, p_∞. The values of the helium permeability, K_{He}^* are given in Appendix C.1. Figure 4.56 shows the variation of K_{He}^* with equilibrium pressure at 308.2 K, and Figure 4.57 that of the product $K_{He}^* T^{-\frac{1}{2}}$ with the order of experiments. The absence of a pressure dependence of K_{He}^* indicated that the Knudsen relationship may be applied to the system as it contained no viscous flow component. The constancy of the product $K_{He}^* T^{-\frac{1}{2}}$ as different experiments were performed (Figure 4.57) showed that the Graphon membrane did not irreversibly age throughout the course of the investigation. The helium permeabilities given in Table 4.7 are calculated from a mean value of the constant $K_{He}^* T^{-\frac{1}{2}}$ (equal to 1.657×10^{-7} $m^2 s^{-1} K^{-\frac{1}{2}}$) obtained from the experimental data given in Appendix C.1.

Table 4.7 The Permeability of Helium

Graphon

$\frac{T}{K}$	$\frac{10^6 K_{He}^*}{m^2 s^{-1}}$
393.2	3.29
308.2	2.91
273.2	2.74
233.2	2.53

Figure 4.56. Pressure - Dependence of K^*_{He} : Graphon

T/K = 308.2

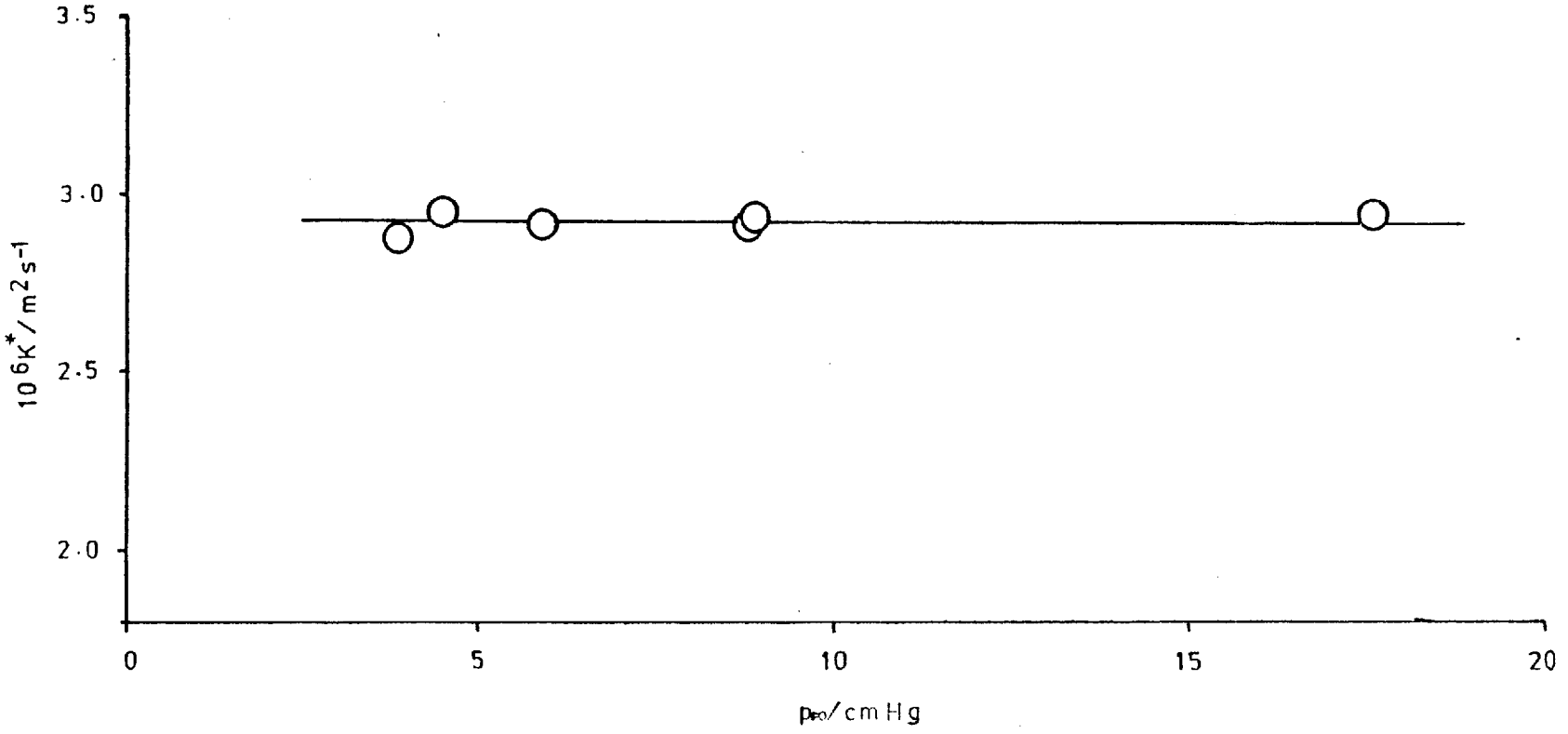

Figure 4.57. Variation of $K^{*}_{He} T^{-\frac{1}{2}}$ with experiment : Graphon

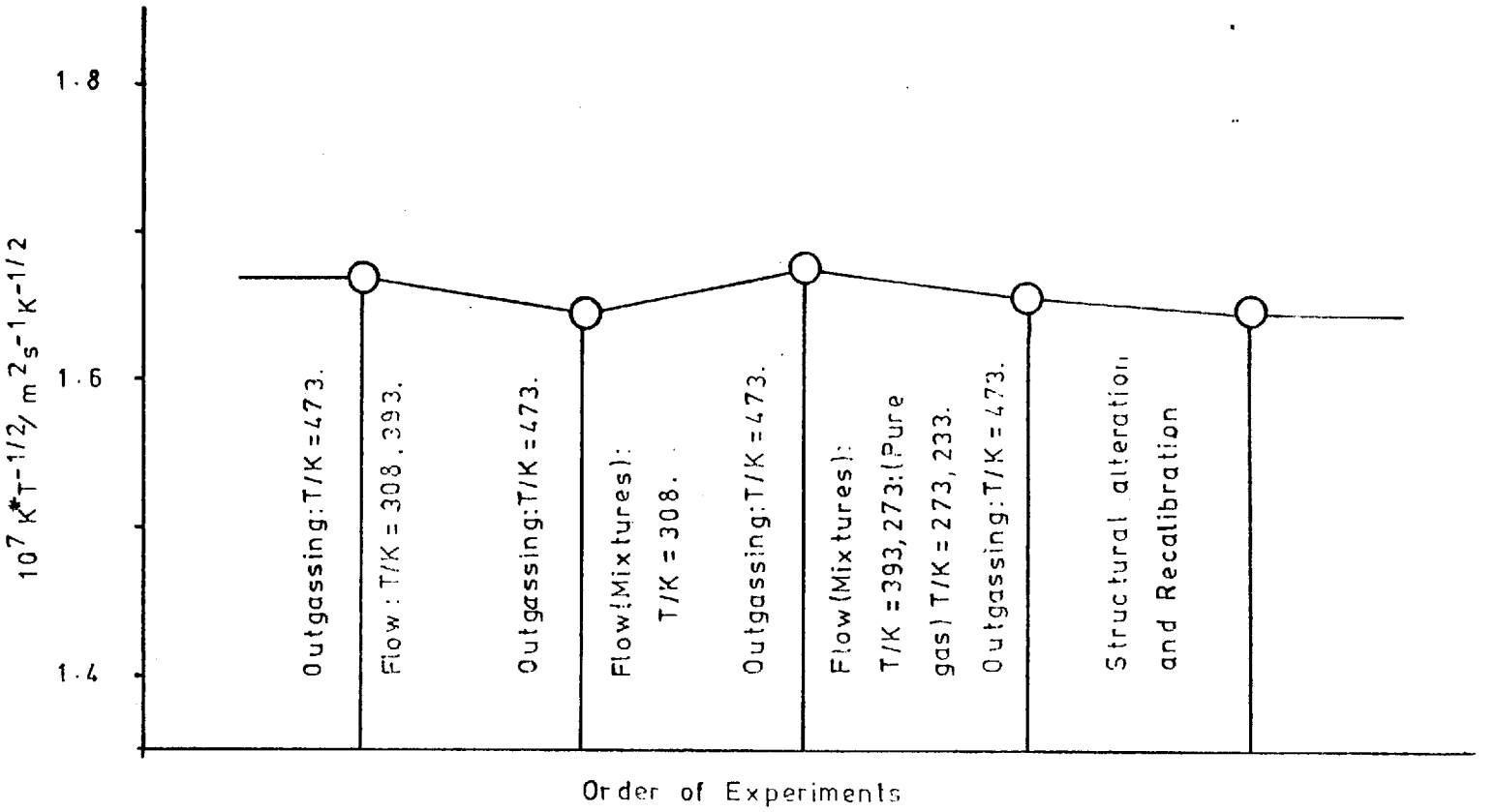

(b) Isobutane

Flow measurements were made at T/K = 393.2, 308.2, 273.2 and 233.2. The differential permeability, K^* (m^2 s^{-1}) data being tabulated in Appendix C.2 and presented graphically in Figure 4.58 as a function of the equilibrium pressure, p_{∞} (cm Hg) and as a function of relative pressure, p_{∞}/p_o in Figure 4.59. In order to attain equilibrium pressures in the region of the saturated vapour pressure it was necessary to adapt a method of interval additions. This involved raising the pressure of the ingoing side by a small amount ($\sim$ 5 cm Hg) whilst retaining the equilibrium pressure of gas from the previous run in the outgoing side. The saturated vapour pressure of isobutane as a function of temperature has been previously given in Table 4.5.

4.3.3. Helium/Isobutane Mixture Flow

Measurements were made for this mixture at T/K = 393.2, 308.2, 273.2 and 233.2. The results are tabulated in Appendix C.3 and presented graphically as the variation of K_R^* (cf §4.3.1) with equilibrium pressure, p_{∞} and relative pressure, p_{∞}/p_o in Figures 4.60, 4.61. Also included in Figure 4.61 is the superimposed blockage curve obtained from the helium/isobutane/Graphon system and the conventional flow apparatus. This is to enable further discussion in Section 5.3.3. A practical advantage of the pressure decay apparatus specific to the mixture experiments is that there are few, if any difficulties in maintenance of the boundary conditions. This was found to be a problem in the 'conventional' arrangement (cf §4.2.3 and Table 4.6).

4.4. Error Analysis

There are two types of error present in an experimental study such as this; random and systematic. The systematic error arises from any assumptions in the theory and deviation from the required boundary conditions, i.e. errors of method.

In the pressure-decay technique the boundary conditions were easily maintained. The 'simple adsorption' conditions of the conventional technique could not be rigorously maintained in the case of the very high coverage mixture experiments (discussed §4.2.3) but for the majority of the remaining cases systematic errors were considered to be negligible.

Figure 4.58. Pressure - Dependence of K^* : $i\text{-}C_4H_{10}$/Graphon

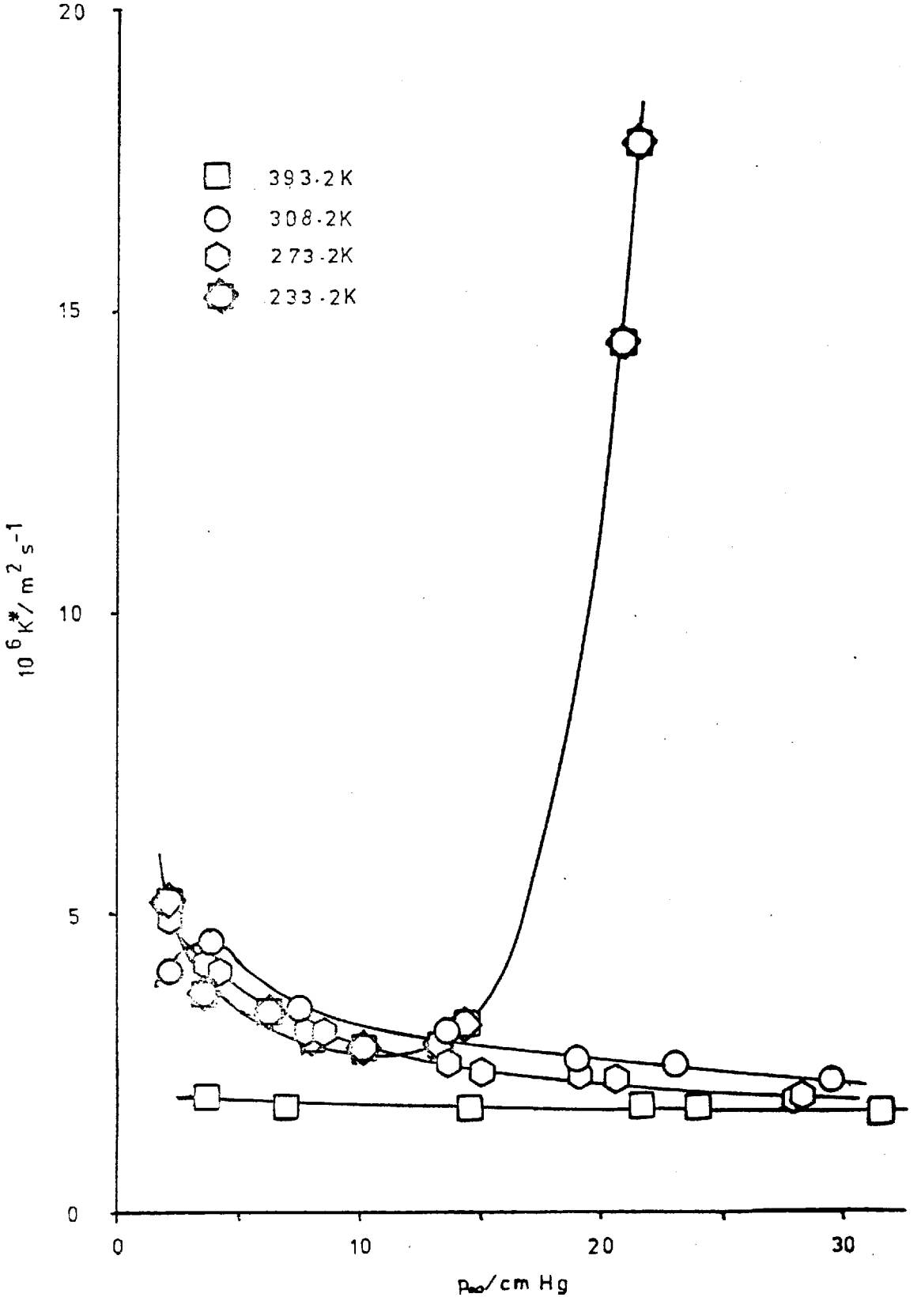

Figure 4.59. Variation of K^* with p_∞/p_o : i-C_4H_{10}/Graphon

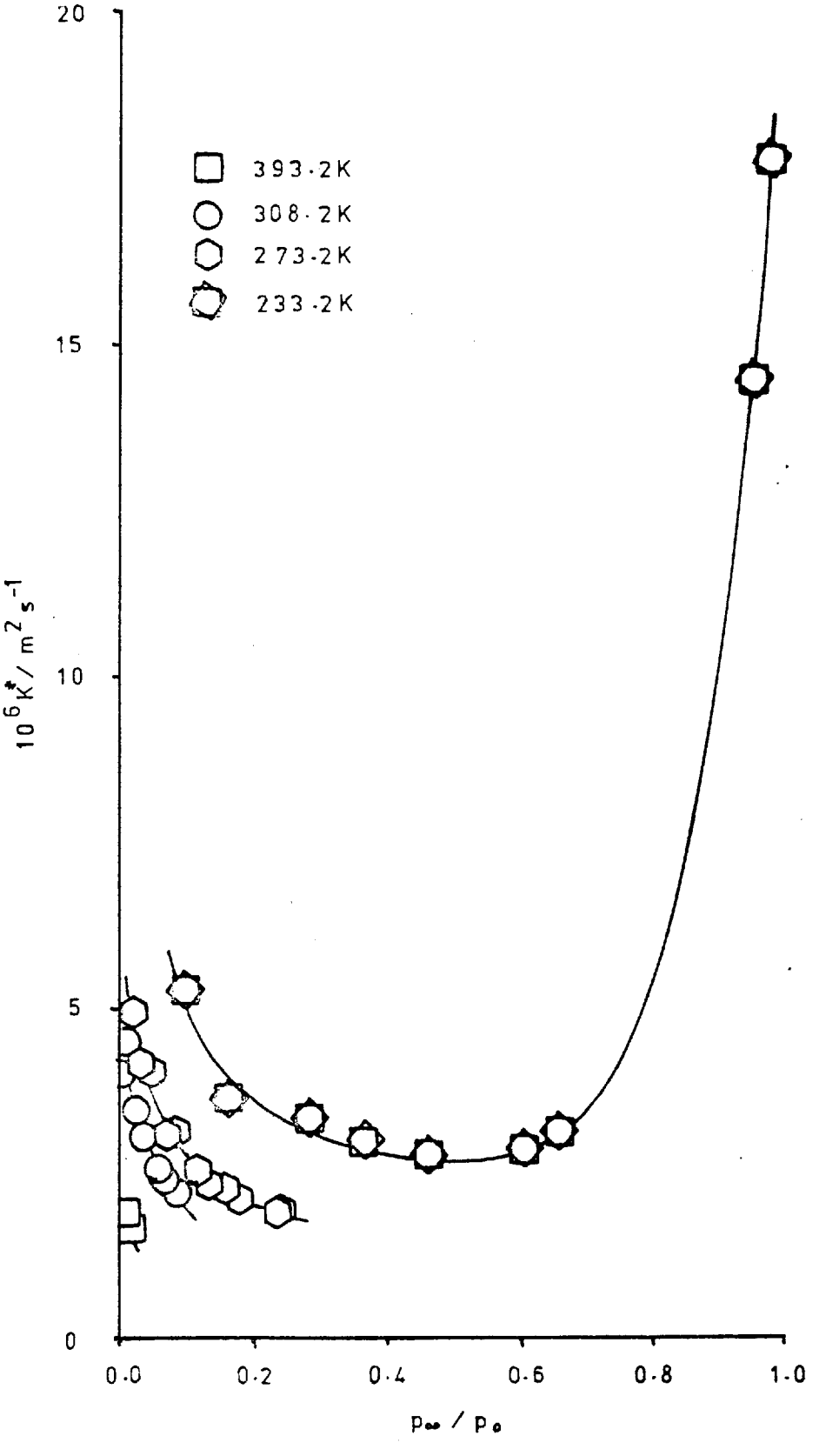

Figure 4.60. Pressure - Dependence of K_R^* : He/i-C_4H_{10}/Graphon

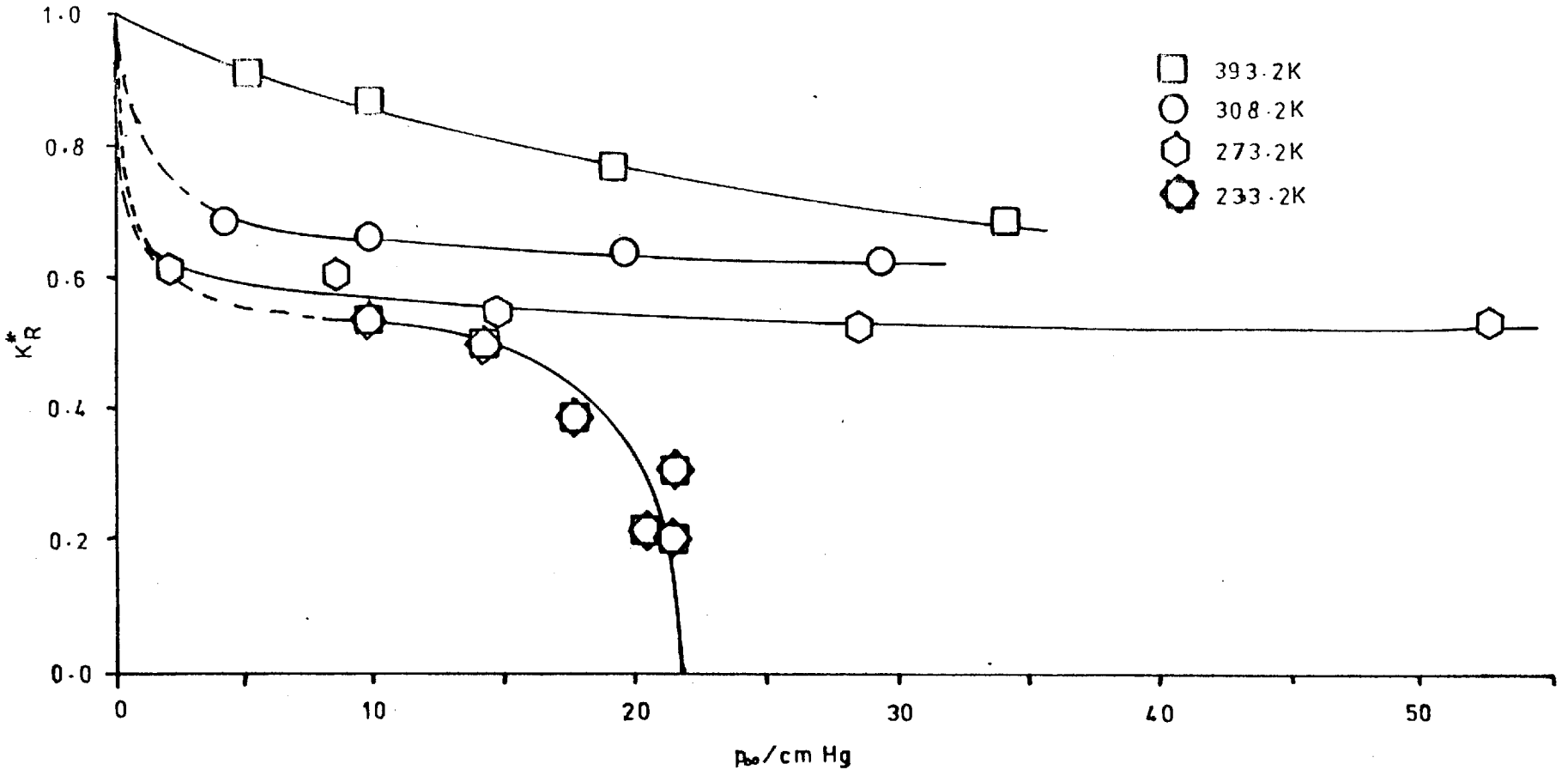

Figure 4.61. Variation of K_R^* with p_{oo}/p_o : He/i-C_4H_{10}/Graphon

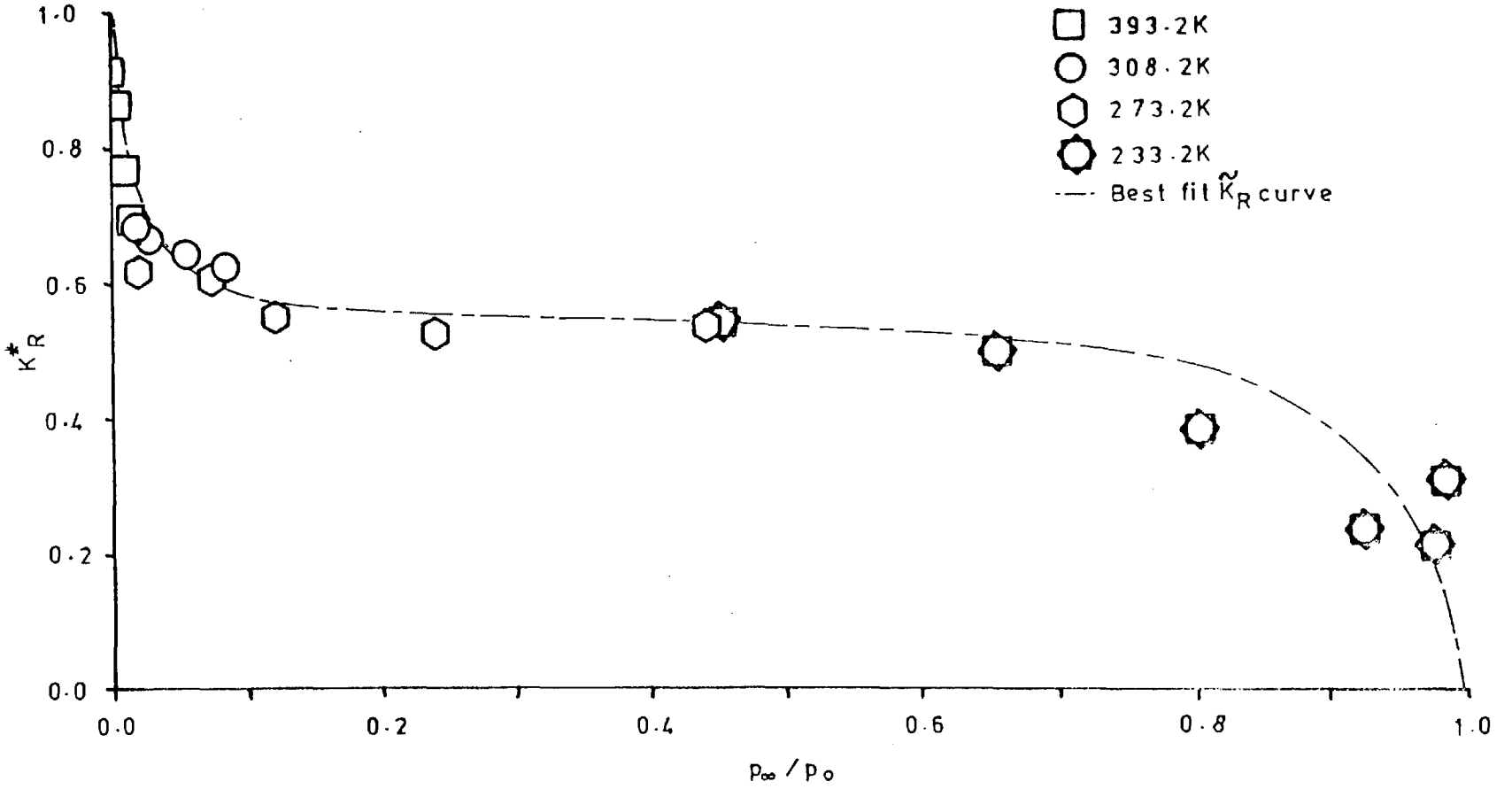

The random error in the permeabilities and other derived quantities must involve uncertainties in the membranes dimensions, volume calibrations, pressure and temperature measurements.

Membrane Dimensions : Cross-sectional area, A_c, ± 1.5%; length, ℓ, ± 1.0%; weight, ±0.1%; resulting porosity, ϵ, ±1.9%.

Volume Calibrations : Those measured by, filling with water, ±0.1%; those by helium expansion ±1.0%.

Temperature Measurement : The worst temperature control of thermostat baths was ±1.0 K (±0.5%). Room temperature could drift by up to ± 2.5 K, (i.e. ~ ±1.0%).

The conventional technique required the maintenance of a constant ingoing pressure (read on a manometer by means of a cathetometer to $\pm 10^{-5}$ m) by the adjustment of the mercury level in the Toepler gauge. This was generally achieved to better than ±1.0%. The outgoing pressure measurement involved the use of the McLeod gauge which can possess a substantial error due to sticking of the mercury. This was minimised by the cleaning procedure employed (§3.2.7) to bring measurement of the outgoing pressure within an uncertainty of ±1.0%. The error in the permeability measurement involves the error in the slope measurement. This quantity will include errors in room and membrane temperature, outgoing volumes and ingoing pressures. However if the slope is considered as a primary experimental quantity it can include the aforementioned errors and the overall uncertainty can be easily calculated for a particular experiment via the least squares method. Considering random experiments this gave an estimated error of ±0.5% in the slope. The combined uncertainties in the flux and permeability are given in Table 4.8.

The pressure decay technique involved the measurement of a pressure difference between the two sides of the membrane as a function of time. This would involve variations in room temperature, thermostat temperature and the absolute accuracy of the pressure monitoring devices. However again due to the evaluation of the slope of the ln (Δp/cm Hg) vs t plot, the least mean squares method can be employed to give an estimated error of ± 0.2%. Again combining the errors accumulated by the working

equation (2.64/2.86) an overall error of 3.0% is obtained.

The maximum absolute errors given in Table 4.8 appear fairly large but it was found that the reproducibility of results lay well within these limits. The worst example is a variation of ± 4% about the mean value of $\tilde{K}$ for the isobutane/Graphon system at T/K = 393.2.

It is well nigh impossible to extend an error analysis to include those derived quantities such as diffusion coefficients as the graphical differentiation of either the flux curves or the isotherm is required and the accuracy depends upon the degree of curvature and the ability to draw good tangents. It was found difficult to fit a polynomial expression to the curves due to their sigmoid shape.

Table 4.8. Estimated Maximum Errors

Quantity	Estimated Error
Integral Permeability, $\tilde{K}$	± 4.0%
Molar Flux, J	± 1.3%
Differential Permeability, K^*	± 3.0%

CHAPTER 5 : DISCUSSION OF RESULTS

5.1. Adsorption Results

5.1.1. Nitrogen Isotherms

The isotherms (Figures 4.1, 4.2) were of Type II in the Brunauer classification with a sharp knee and were thus well suited to B.E.T. analysis. Neither sample exhibited hysteresis indicating the non-porosity of the adsorbents.

The surface areas of 80 m^2g^{-1} and 220 m^2g^{-1} for Graphon and graphitised Black Pearls, as calculated from the B.E.T. plots (Figures 4.3, 4.4) compared favourably with the literature values (Table 4.1). The Graphon results were a little low but this may be attributed to the pelletised form. The surface area depends on the value taken for the cross-sectional area of the adsorbed nitrogen molecule. Generally 0.16 nm^2 has been used in the majority of quoted surface areas. Pierce and Ewing (1964) suggest a value of 0.20 nm^2 to be more appropriate for graphites. It is postulated that localized adsorption occurs with the nitrogen molecules being strongly attracted at all sites on the surface, but with a slightly stronger attraction at the graphite ring centres. Thus the close packing arrangement giving the value of 0.16 nm^2 is not applicable. Instead each molecule occupies four hexagonal units resulting in a theoretical value of 0.21 nm^2. Localized adsorption on graphite lattice sites has also been suggested for nitrogen adsorption by Isirikyan and Kiselev (1961, 1962) Pierce does accept that the value 0.16 nm^2, although not absolute is useful as regards a standard for surface area determinations.

'de Boer's' treatment of the low temperature nitrogen isotherm results in the v - t plots shown in Figure 4.5. The results of Lowson (1968) for adsorption on Carbolac are included in Figure 5.1 to allow a fuller discussion. The B.E.T. 'C' values were ~ 2000 and ~ 100 for Graphon and Black Pearls respectively and subsequently the 't' curve of de Boer was applied to the nitrogen isotherms. At 'C' values > 100 it is generally accepted (Lecloux and Pirard, 1979) that de Boer's 't' curve may be used in preference to other curves quoted in the literature (Pierce, 1968; Voet et al., 1968; Dollimore and Heal, 1970; Terman, 1973).

Figure 5.1. 'De Boers' (v - t) Plot for Different Carbons

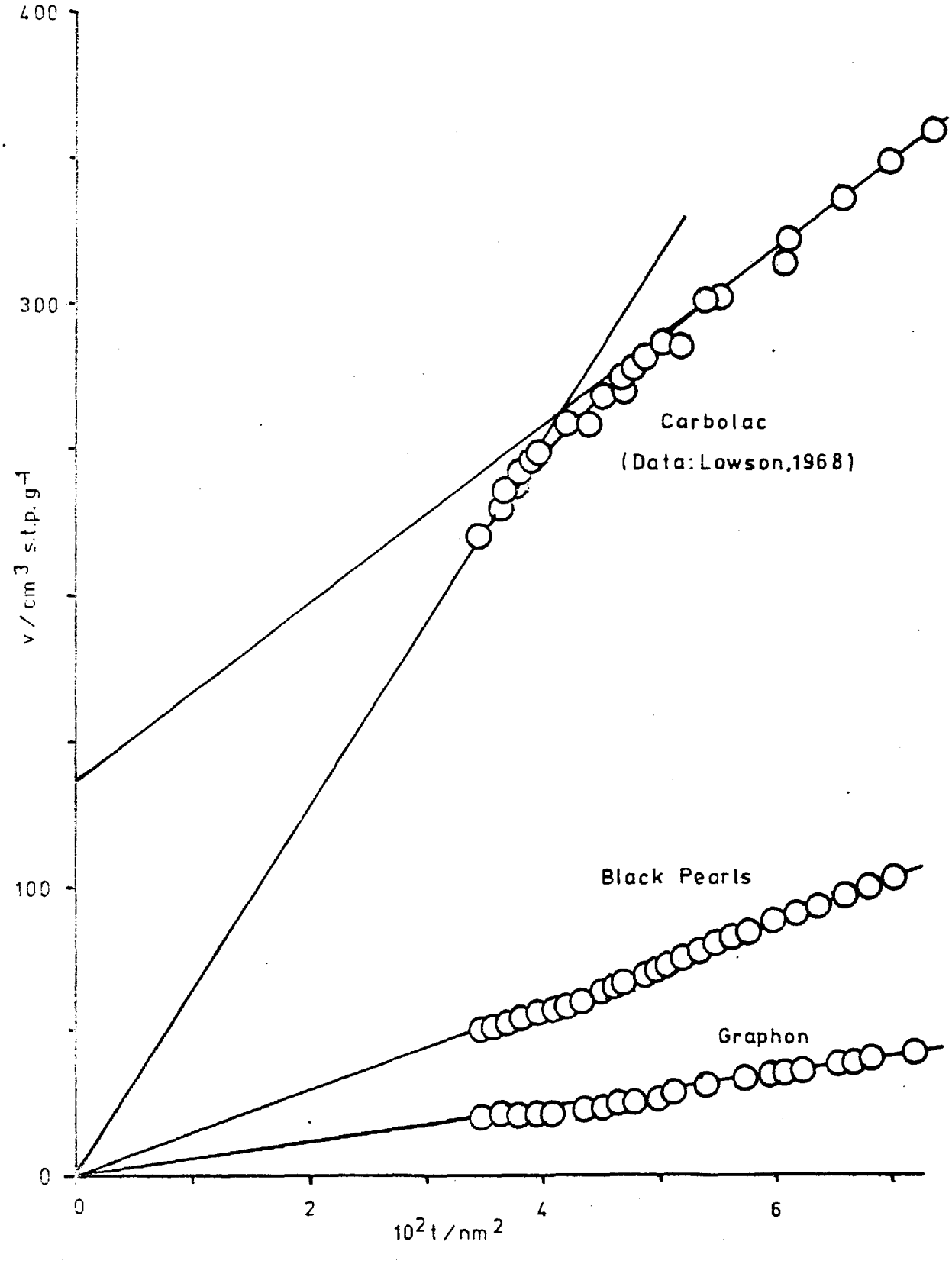

As can be seen for both Graphon and Black Pearls the v - t plot gives a straight line through the origin but that points corresponding to lower pressures deviate from this straight line. In the case of Carbolac, two straight parts occur which are connected in a curve. These plots are in agreement with de Boer's work on Graphon and Carbolac (de Boer, Linsen and Osinga, 1965; de Boer, Linsen, van der Plas and Zondervan, 1965). From the slopes of the linear portions the surface area, S_t ($m^2 g^{-1}$) may be calculated by equation (5.1), although in the case of Carbolac a distribution of surface areas is observed, attributable to variable pore dimensions.

$$S_t = 1.547\left(\frac{v}{t}\right) \qquad (5.1)$$

where v (cm^3 stp g^{-1}) is the amount adsorbed, t (nm) is the statistical thickness of the adsorbed layer and 1.547 is a numerical factor arising from the definition of 't'.

The values of S_{BET} (this work) and S_t are given in Table 5.1 and it can be seen that for both Graphon and Black Pearls the value obtained from the 't' curve is greater than that obtained from the B.E.T. method. de Boer, Linsen and Osinga (1965) found the ratio of S_t/S_{BET} to be 1.10 for three graphitised carbon blacks. In this work a mean ratio of 1.11 was observed for the two carbons.

Table 5.1. Comparison of Surface Areas Determined by B.E.T. and 't' plot methods

	$S_{BET}/m^2 g^{-1}$	$S_t/m^2 g^{-1}$	S_t/S_{BET}
Graphon	80.0	94.4	1.18
Black Pearls	220	227.8	1.03

Three possible explanations were put forward:

(a) Adsorption is localized in the first layer and a value of 0.20 nm^2 for the area of an adsorbed N_2 molecule (after Pierce and Ewing (1964)) must be used.

(b) The adsorbed N_2 molecules lose one degree of freedom of rotation, in which case the surface area is not determined by a mean diameter

but by the diameter along the axis of the molecule. de Boer, Linsen and Osinga (1965) suggests that the surface area resulting from a molecule rotating in a flat lying position is greater by a factor of 1.10.

(c) A smooth homogeneous surface results in a step-wise isotherm and it cannot be expected that the B.E.T. equation will give the real surface area. The steps will cause a too low value of v in the regions used for B.E.T. analysis. Abram and Morris (1971) obtained a value of 1.03 for the ratio of S_t/S_{BET} for samples of Sterling MT, Sterling FT and Graphon. Lowson's (1968) work on Carbolac yields a value of 1.02. It was concluded that this value lay within experimental error and that either method could be used to measure the surface areas of graphitised carbons. This view is reinforced by the work of Allen and Burevski (1977) on active carbons who found exact agreement between the values of S_{BET} and S_t if the appropriate 't' curve (depending on the BET 'C' value) was used. In the past few years the use of a 't' curve for specific 'C' values (Mikhail, Brunauer and Bodar, 1968) (Lecloux, 1970; Mikhail and Akkad, 1975) has been challenged. It has been suggested (Parfitt, Sing and Unwin, 1975; Nicholson and Sing, 1979) that a 't' curve measured on a non-porous substance which is chemically similar (rather than of similar C value) is more appropriate.

The value of the 't' plot analysis can be seen when the Carbolac plot is considered. In a porous solid multilayer adsorption can occur in the narrow pores and render a part of the surface unavailable for adsorption. The v - t plot then starts to deviate downwards from the straight line until another straight line is formed when only wide pores remain, The curve in between the two straight portions for Carbolac (cf Figure 5.1) means that a range of pore sizes exists. This forms the basis of the micropore method of pore size analysis developed by Mikhail et al. (1968). A pore shape is assumed and by taking tangents to the curve at various film thicknesses, the contributions to the total area of various sized pores can be calculated.

The monolayer capacities calculated from the hydrocarbon B.E.T. plots (Table 4.3) are used to provide values of the surface area. However a value must be assigned to the cross-sectional area of the adsorbed molecule, σ (m^2). Brunauer and Emett (1937) used a value for σ which was based on the liquid density of the adsorbate and given by equation (5.2) :

$$\sigma = f\left(\frac{M}{N\rho}\right)^{\frac{2}{3}} \qquad (5.2)$$

where M (kg mol^{-1}) is the molar mass, N (mol^{-1}) is the Avogadro constant, ρ (kg m^{-3}) is the density of the adsorbate in the ordinary liquid form and f is a packing factor, the value of which depends on the number of nearest neighbours. Livingston (1948) considered different values for 'f' but for the most common arrangement, i.e. twelve nearest neighbours in the liquid and six on the plane surface, f = 1.091. It can be seen in Table 5.2 that the values of surface areas, resulting from the cross-sectional area calculated in this way are lower than those determined by N_2 adsorption, i.e. it is incorrect to assume normal liquid packing. Maclellan (1967) reviews reported values of σ for a great many adsorbates on different adsorbents and proposes mean values (denoted σ_1) resulting in the surface areas also given in Table 5.2. Again it can be seen that there is a discrepancy between these values and those from the N_2 determination.

It is also possible to obtain values for σ using the nitrogen determined surface area and the monolayer capacities from the hydrocarbon data, σ_3. These are compared with those mean values of Maclellan (1967) and also with his literature values for C_3H_8 and $i\text{-}C_4H_{10}$ on specifically carbon black adsorbents, σ_2.

It is obvious that discrepancies will occur in calculations of surface areas by the B.E.T. method, if workers use different adsorbates and differing values of the cross-sectional areas. However as Pierce and Ewing (1964) state, nitrogen with a cross-sectional area of 0.162 nm^2 although not absolute is as good a reference adsorbate as any for surface area determination.

The calculation of surface areas and the shortcomings of the B.E.T. analysis of gas adsorption are summarised well in an article by Dollimore, Spooner and Turner (1976).

As can be seen from Figures 4.1 and 4.2, the nitrogen isotherms exhibit a 'hump' centred at $p/p_o \simeq 0.4$. Hill (1947) in his elementary treatment of localized and mobile monolayers predicted a step-like adsorption for homogeneous surfaces, such as are present in graphitised carbon blacks. These 'humps' or steps have been observed by a number of experimentalists and initially by Joyner and Emmett (1948) for the

Table 5.2. Comparison of Surface Areas and Cross-sectional Areas of Adsorbates.

	Graphon Pellets		Graphon Membrane		Black Pearls Powder	
	C_3H_8	$i\text{-}C_4H_{10}$	C_3H_8	$i\text{-}C_4H_{10}$	C_3H_8	$i\text{-}C_4H_{10}$
T/K	243.2	258.2	213.2	248.2	248.2	273.2
v_m/cm^3 stp g^{-1}	10.0	8.4	11.0	9.8	25.6	19.4
σ liq.dens/nm^2	0.278	0.323	0.267	0.319	0.280	0.329
σ_1/nm^2	0.364	0.507	0.364	0.507	0.364	0.507
σ_2/nm^2	0.320	0.470	0.320	0.470	0.320	0.470
σ_3/nm^2	0.298	0.354	0.271	0.304	0.320	0.422
*S_{BET}/m^2g^{-1} (N_2 adsorption)	80.0		-		220	
S_{BET}/m^2g^{-1} (σ liq.dens)	74.4	73.3	78.8	83.8	192.6	171.5
S_{BET}/m^2g^{-1} (σ_1)	97.4	115.1	107.5	133.2	250.0	264.3

* This work.

adsorption of nitrogen on Graphon. Polley, Schaeffer and Smith (1953) studied the effect of graphitisation on the adsorption of N_2, Ar and O_2. It was found that as many as three steps could occur at relative pressures of 0.35, 0.63 and 0.86. The size of the step increased as a direct consequence of the degree of graphitisation and subsequent surface homogeneity. Pierce and Ewing (1964) explain the 'Joyner-Emett' step as being due to an additional adsorption into the first layer along

with the start of second layer adsorption. At the completion of the step it is assumed that normal first layer packing applies.

It is seen that the heat of adsorption also exhibits certain characteristics corresponding to the steps. Several investigators publish heat of adsorption versus coverage plots of the form shown in Figure 5.2 notably Beebe et al. (1953) and Sams et al. (1962) for nitrogen adsorption.

Figure 5.2. Variation of q_{st} with coverage

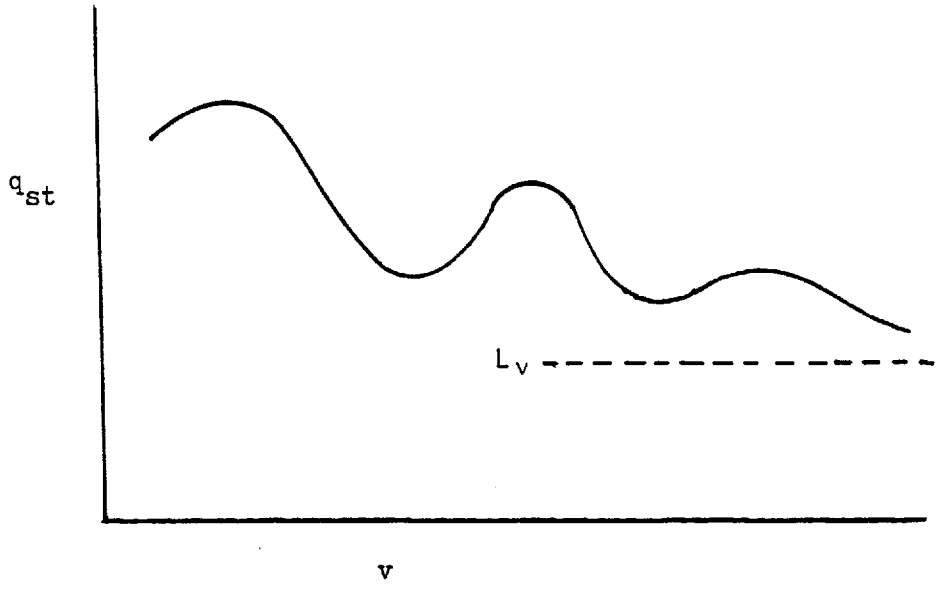

Each maxima in the heat curve correspond to a 'hump' in the isotherm but the initial hump is disguised by the large uptakes of adsorbent at low pressures. A fuller discussion of the heats of adsorption is given in §5.1.2(a).

5.1.2. Hydrocarbon Isotherms

(a) Henry Law constants and Heats of Adsorption

Henry Law constants, $k_s(m)$ were determined from the high temperature linear isotherms and are given in Table 5.3. When Henry Law adsorption occurs an energy of adsorption, $\Delta E'$ (kJ mol^{-1}) as defined by equation (5.3) can be calculated.

$$\ln\left(\frac{k_s(T_1)}{k_s(T_2)}\right) = \frac{\Delta E'}{R}\left(\frac{1}{T_2} - \frac{1}{T_1}\right) \qquad (5.3)$$

The integrated equation was used as only two isotherms exhibited linearity, and subsequently the values of $\Delta E'$ (Table 5.3) must be treated with caution.

As the isotherms became more curved it was possible to evaluate the isosteric heat of adsorption, q_{st} (kJ mol^{-1}) as defined by equation (2.93).

$$q_{st} = -R\left(\frac{\partial \ln p}{\partial\, 1/T}\right)_v \qquad (2.93)$$

A limiting value of q_{st} as $v \Rightarrow 0$ can be used to evaluate the energy of adsorption, $\Delta E''$ (kJ mol^{-1}) by means of equation (5.4) (Clint, 1966).

$$\Delta E'' = RT - (q_{st})_{v=o} \qquad (5.4)$$

The mean of the isotherm temperatures used in the heat of adsorption evaluation at low coverage was taken for T.

The values of q_{st} and the resulting $\Delta E''$ are given in Table 5.3 and it can be seen that fair agreement does exist between the two methods of ΔE determination for adsorption on Graphon.

Table 5.3. Henry Law Constants, Heats and Energies of Adsorption

		$\frac{T}{K}$	$\frac{10^8 k_s}{m}$	$\frac{-\Delta E'}{kJ\ mol^{-1}}$	$\frac{q_{st}}{kJ\ mol^{-1}}$	$\frac{-\Delta E''}{kJ\ mol^{-1}}$
Graphon	C_3H_8	473.2 393.2	1.62 3.70	16.0	23.0	19.4
	i-C_4H_{10}	453.2 423.2	3.72 5.84	24.0	26.7	23.1
Black Pearls	C_3H_8	-	-	-	19.5	17.6
	i-C_4H_{10}	-	-	-	28.5	26.5

An increase in the energy of adsorption of ~ 6 kJ mol^{-1} (mean from 2 carbons) takes place on increasing the number of carbons contained in the hydrocarbon. Lal and Spencer (1974) in a theoretical treatment of the interaction between hydrocarbons and the surface of a graphite lattice found a linear relationship with a 7.3 kJ mol^{-1} increase per carbon atom.

Other (cf Table 5.5) experimental measurements have shown the value to lie between 4 and 8 kJ mol^{-1} for various graphitised carbons. Literature values of q_{st} and the increase in ΔE are given in Tables 5.4 and 5.5 respectively along with the range of hydrocarbons that were covered.

Table 5.4. Limiting values of q_{st} at zero coverage

		q_{st}/kJ mol^{-1}	Reference
Graphon	C_3H_8	23.0	This work
		27.4	Lal and Spencer (1974)
		35.1	Di Corcia and Samperia (1973)
		24.7	Di Corcia and Samperia (1973) [H_2-treated Graphon]
		25.0	Murray (1976)
	$i\text{-}C_4H_{10}$	26.7	This work
		45.2	Di Corcia and Samperia (1973)
		28.4	Di Corcia and Samperia (1973) [H_2-treated Graphon]
Black Pearls	C_3H_8	19.5	This work
		27.4	Lal and Spencer (1974)
	$i\text{-}C_4H_{10}$	28.5	This work

Table 5.5. Literature values of $(-\Delta E)$ increase with Hydrocarbon

	Increase in $(-\Delta E)$ per carbon atom	Range of alkanes	Reference
Graphon	4.0	C_3 - C_4 (iso)	This work
Black Pearls	8.9	C_3 - C_4 (iso)	
Sterling MT D4	4.6	C_5 - C_9	Elkington and Cuthreys (1969)
Spheron 6 (1700°C)	7.9	C_5 - C_8	Kiselev (1957)
Sterling MT	6.0	C_2 - C_6	Ross, Olivier and Saelens (1962)
Graphon	5.4	C_1 - C_4	Murray (1976)
Graphon	6.0	C_5 - C_{12}	Clint (1972)
Theoretical	7.3	C_1 - C_6	Lal and Spencer (1974)

It must be noted that in this work a comparison between a n-alkane and an iso-alkane is being made. One would expect the value of q_{st} for isobutane to be lower than that for n-butane in accordance with the increase in the distance of some atoms from the adsorbent surface. Literature values of q_{st} for n-butane on Graphon range from 31 - 36 kJ mol^{-1} (Beebe, Biscoe and Warren, 1947; Murray, 1976) and the observed value for isobutane is 27 kJ mol^{-1}. Consequently the $(-\Delta E)$ increase per carbon atom would be less for the change from C_3 to C_4 (iso) than for the C_3 to C_4 (n) change. This is supported by the data in Table 5.5 for Graphon.

(b) Variation of q_{st} with coverage

The variations of the heat of adsorption with coverage are shown in detail in Figures 4.24 to 4.27 and summarised in Figure 5.3. As can be seen the basic form of each curve is an increase in q_{st} up to a maximum followed by a decrease to a value in the vicinity of the latent heat of vaporisation of the hydrocarbon. In some cases the value of q_{st} at high coverages is below that of the heat of vaporisation. This could be due to the fact that only two isotherms were available for the heat determination.

The isobutane-graphon system was studied in greater detail enabling, in some cases, the use of six isotherms in the heat determination. It is worth noting that in such cases the ln p vs 1/T plot did not deviate from linearity, even over a temperature range of 150 K. Typical plots are given in Figure 5.4. Two factors contribute towards the heat of adsorption: the heterogeneity of the surface and the lateral interactions between adsorbed molecules. The former causes a decrease in the heat, the latter an increase. The two carbons under study are both considered to be homogeneous as regards the surface. This is substantiated by the fact that there is no observed decrease in the heats before monolayer coverage. The heat curves schematically would appear as in Figure 5.5 for a carbon before and after graphitisation, i.e. heterogeneous and homogeneous surfaces. The work of Joyner and Emett (1948) into nitrogen adsorption on Spheron 6 and its graphitised form (Graphon) is a prime example resulting in these types of curves.

Figure 5.3. Concentration - Dependence of q_{st} : C_3H_8, i-C_4H_{10}/Graphon, Black Pearls

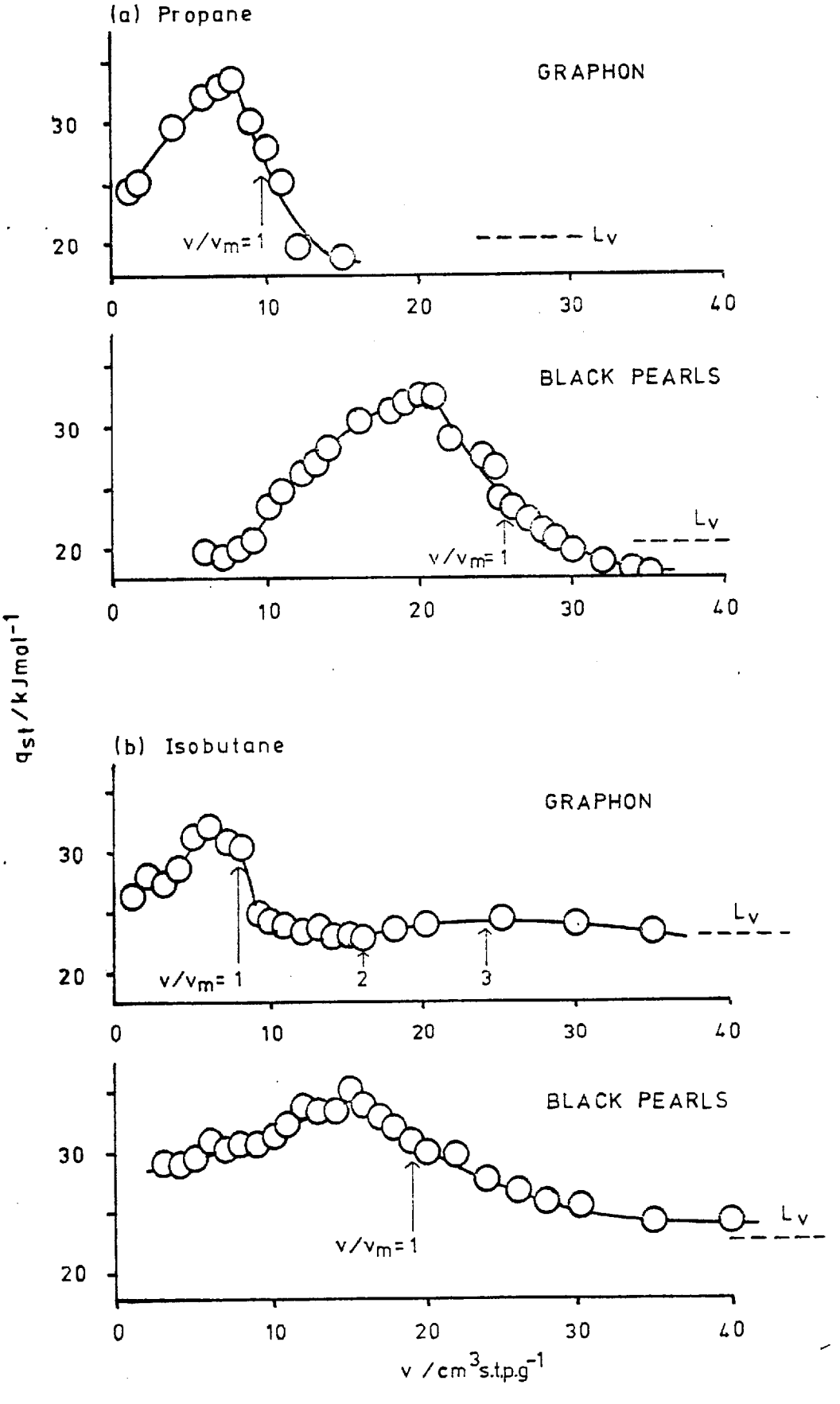

Figure 5.4. Typical ln (p/cm Hg) vs 1/T Plot of q_{st} Determination : i-C_4H_{10}/Graphon

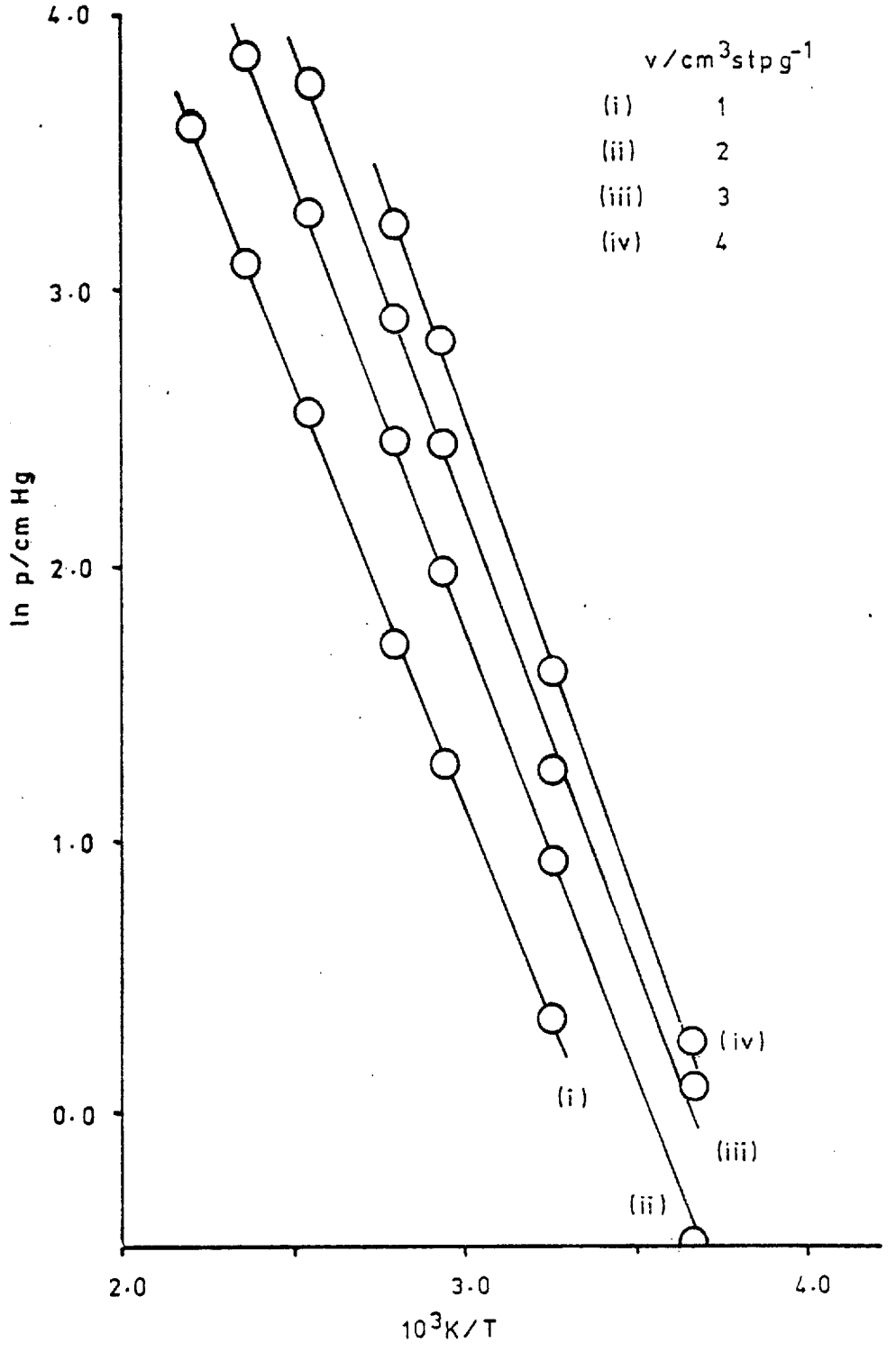

Figure 5.5. The Effect of Surface Heterogeneity on q_{st}

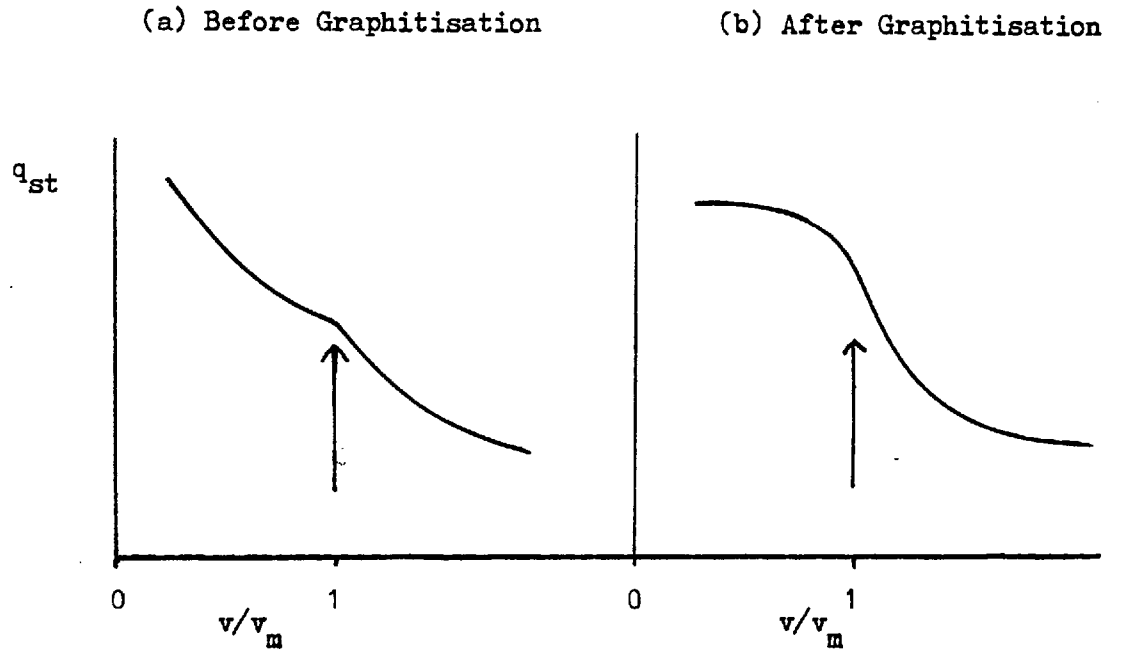

Comparing Graphon and Black Pearls one observes that lateral interactions between adsorbed molecules do occur in both cases for both hydrocarbons as indicated by the increase in q_{st} up to monolayer coverage. The magnitude of the increase being approximately the same for each gas on both carbons, Ash, Baker and Barrer (1967) in a flow study of SF_6 and argon measured heats of adsorption on both Graphon and Black Pearls. The increase in q_{st} up to the maximum value was again similar for both carbons in the case of SF_6. However for argon much smaller increases occurred indicating small and different argon-argon interactions for each carbon.

For the Graphon-isobutane heat curve a slight second maximum occurs at $v/v_m \simeq 3$. This may be due to experimental error but maxima are expected as each adsorbed layer reaches completion. A second maximum at $v/v_m = 2$ should be apparent but there is no evidence of this in Figures 4.25 and 5.3. The work of Beebe et al. (1953) and Sams et al. (1962) on Nitrogen adsorption provides evidence for the second maxima and indeed for a third. The reduction in the size of the maximum is due to adsorption into the second and third layers being not as well defined as the first layer. It has already been stated that the maximum in the heat curve correspond to 'steps' or 'humps' in the isotherm (cf 5.1.1).

However in the case of the hydrocarbon isotherms no steps are observed. A second maxima has been obtained for the ethylchloride/Graphon system (Moori, Pierce and Nelson-Smith, 1953) in which no detectable hump was observed in the isotherm.

The non-appearance of a hump in the isotherm may be due to the large molecules packing on the surface in such a way that the formation of the second layer is much less distinct than for the case of nitrogen adsorption.

(c) Comparison of Isotherms measured on Graphon pellets and compacted Membrane

The isotherms shown in Figures 4.8 and 4.10 are all of the sigmoid shape (Type II) normally observed for adsorption on free surfaces, such as the surface of non-porous particles. The section convex to the pressure axis arises from the formation of multilayers related to condensation to the bulk liquid.

Adsorption isotherms were determined on the pelletised Graphon sample and also on the compacted membrane. Comparative isotherms are shown in Figures 4.13 to 4.17 and differences observed.

Carman and Raal (1951) in a study of CF_2Cl_2 adsorption on Linde silica powder initially considered the effect of compaction. It was observed that up to monolayer coverage there was very little difference between isotherms measured on the compacted and uncompacted samples indicating similar adsorption processes. However as multilayer formation commences a transition from Type II to Type IV occurred with greater amounts being adsorbed on the membrane. At pressures near the saturated vapour pressure the membrane then reached a limiting amount adsorbed. The greater amount adsorbed by the membrane is due to the compaction process diminishing the pores between particles to such an extent that capillary condensation takes place at moderate values of p/p_o.

This transfer from Type II to Type IV upon compaction has subsequently been observed for many systems; hexane adsorption on P-33 carbon black (Kiselev, 1958), nitrogen adsorption on silica (Zwietering, 1956), water adsorption on alumina (Wade, 1965). In this work the differences between the uncompacted and compacted samples are probably diminished due to the uncompacted sample being in the pelletised form. Despite this the comparative isotherms show similar behaviour to previously

studied systems, i.e. similar adsorption up to monolayer coverage followed by multilayer adsorption in which the compacted membrane adsorbs more. A typical comparative isotherm is of the form shown in Figure 5.6.

It was observed in certain cases, for example the adsorption of argon on Carbolac (Barrer and Strachan, 1955) that the compacted isotherm was depressed in the monolayer region. Carbolac has a large surface area which is probably diminished on compaction by the adhesion of neighbouring particles. It was also observed that as the degree of compaction increased the depression of the isotherm increased and the hysteresis loop disappeared.

Figure 5.6. The Comparative Isotherm

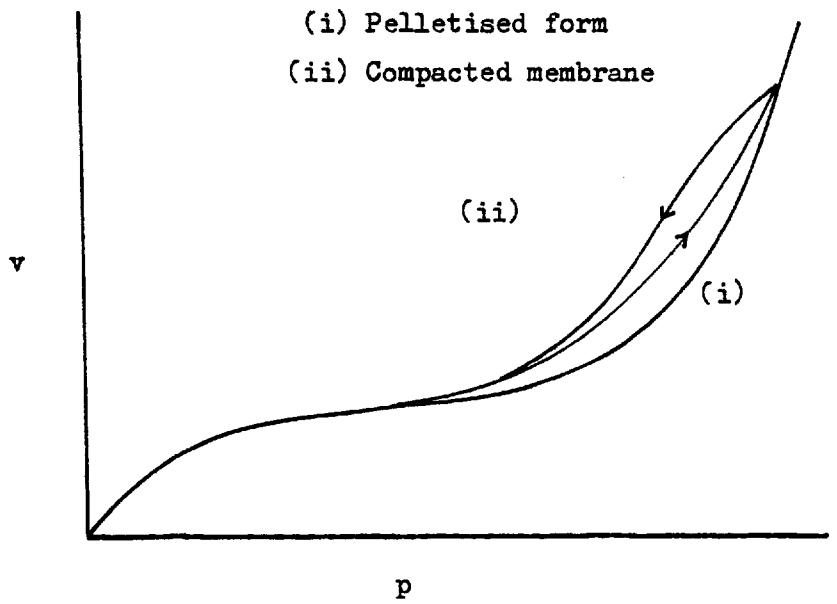

The hysteresis loops in the Type IV isotherm are a result of capillary condensation in open-ended pores of suitable dimensions, presumably produced on compaction. The various theories covering capillary condensation and hysteresis will not be considered here but a general summary is given by Gregg and Sing (1967).

(d) 'Low Coverage Adsorption Hysteresis'

As can be seen from Figures 4.6 to 4.12 the adsorption isotherms do not exhibit hysteresis at low coverages. However if they are

presented in the form p/v versus v an interesting anomaly appears. The adsorption on Graphon is shown in Figures 5.8 to 5.15 in this form. It can be seen that the desorption curve deviates downwards from the adsorption curve at low coverages.

If presented in this way the isotherm would be expected to be of the form shown in Figure 5.7 (a). The linear portion at low coverages corresponding to Henry Law adsorption. However as can be seen in reality (Figures 5.8 to 5.15) the isotherm is of the general form given in Figure 5.7 (b).

Figure 5.7. Adsorption Isotherm in the form p/v vs v

(a) : Expected form (b) : Experimentally observed form

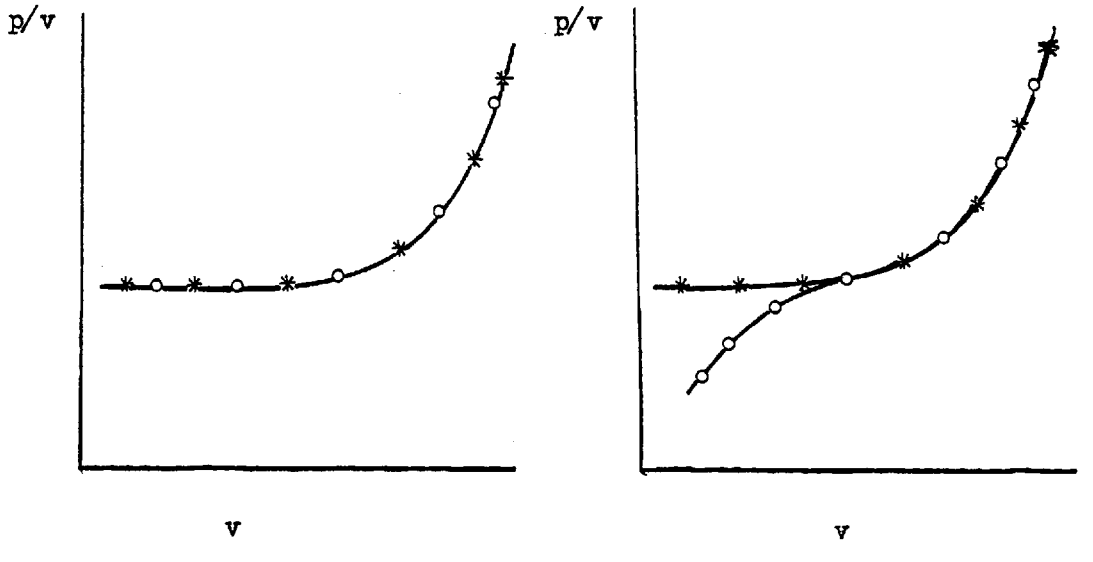

* Adsorption o Desorption

The data for propane at 393 K and for isobutane at 453, 423, 393, 358 and 343 K on Graphon all exhibited this 'hysteresis' effect. It is interesting to note that for the less strongly sorbed propane the 'hysteresis' closed at a much lower value of coverage than for isobutane. The source of the adsorption data apparently does not affect the isotherm format. Those isobutane isotherms at 393 K and 358 K were measured by Dr A.V.J. Edge in these laboratories using a different volumetric adsorption apparatus (also constructed of greased stopcocks). The length

Figure 5.8. Adsorption Isotherm : C_3H_8/Graphon Pellets

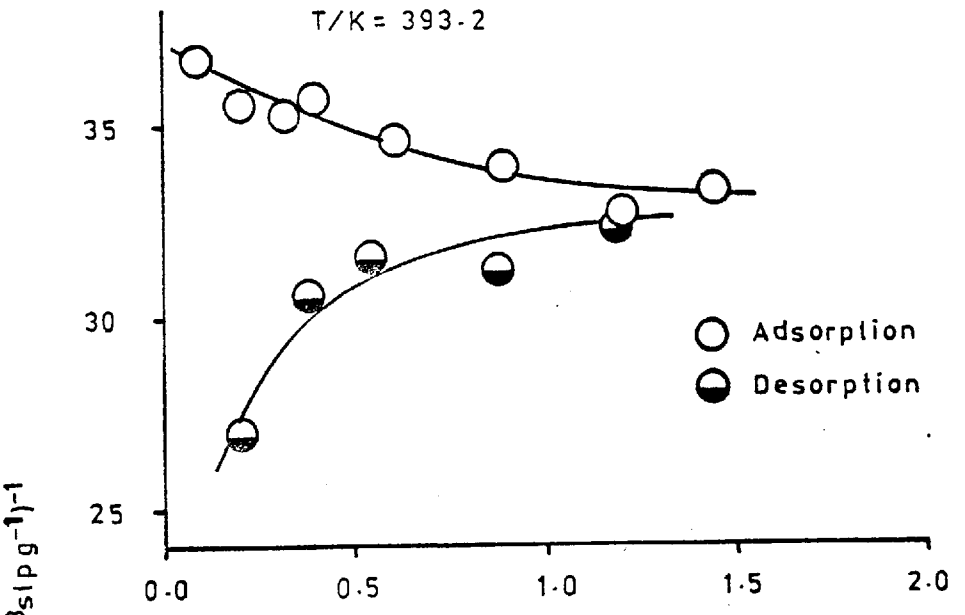

Figure 5.9. Adsorption Isotherm : i-C_4H_{10}/Graphon Pellets

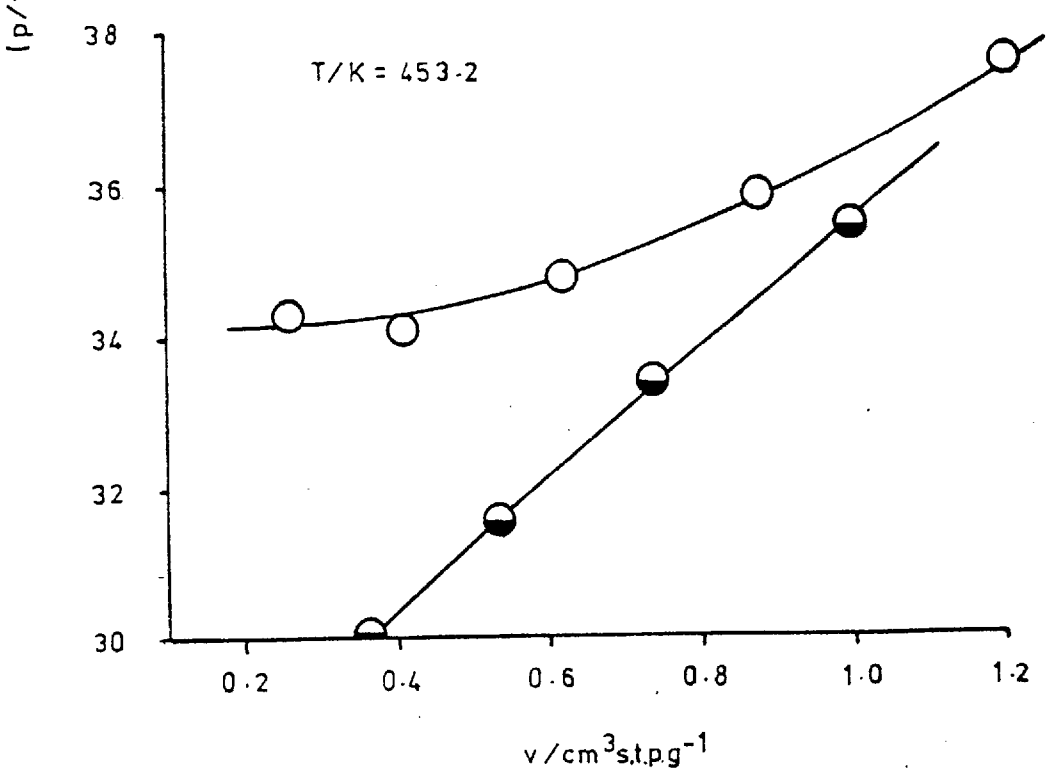

Figure 5.10. Adsorption Isotherm : i-C_4H_{10}/Graphon Pellets

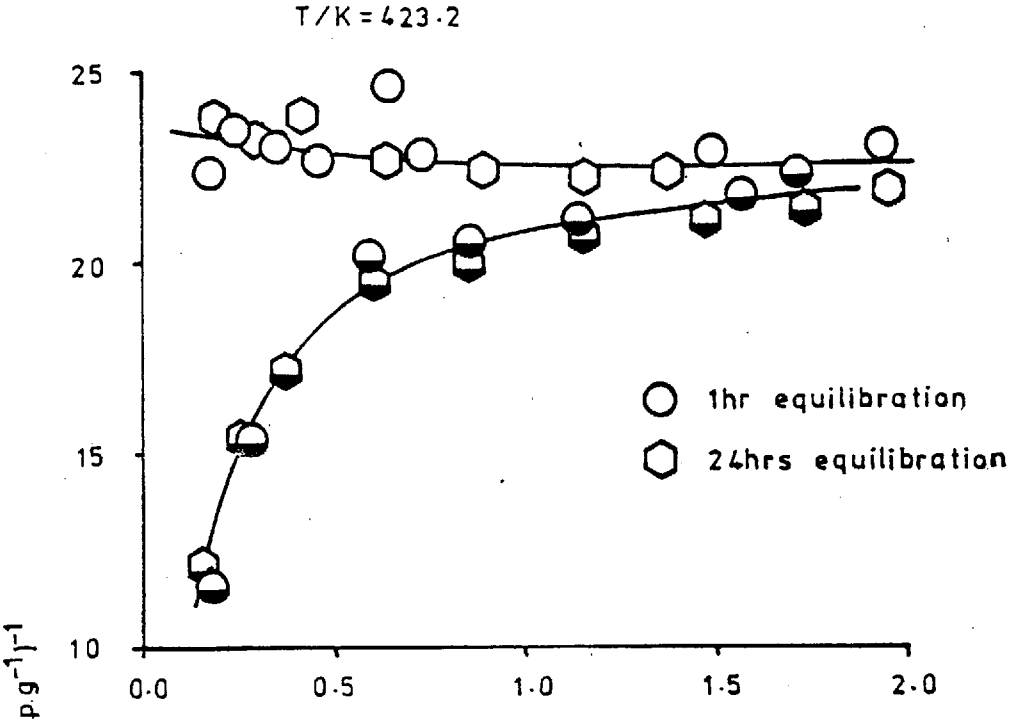

Figure 5.11. Adsorption Isotherm : i-C_4H_{10}/Graphon Pellets

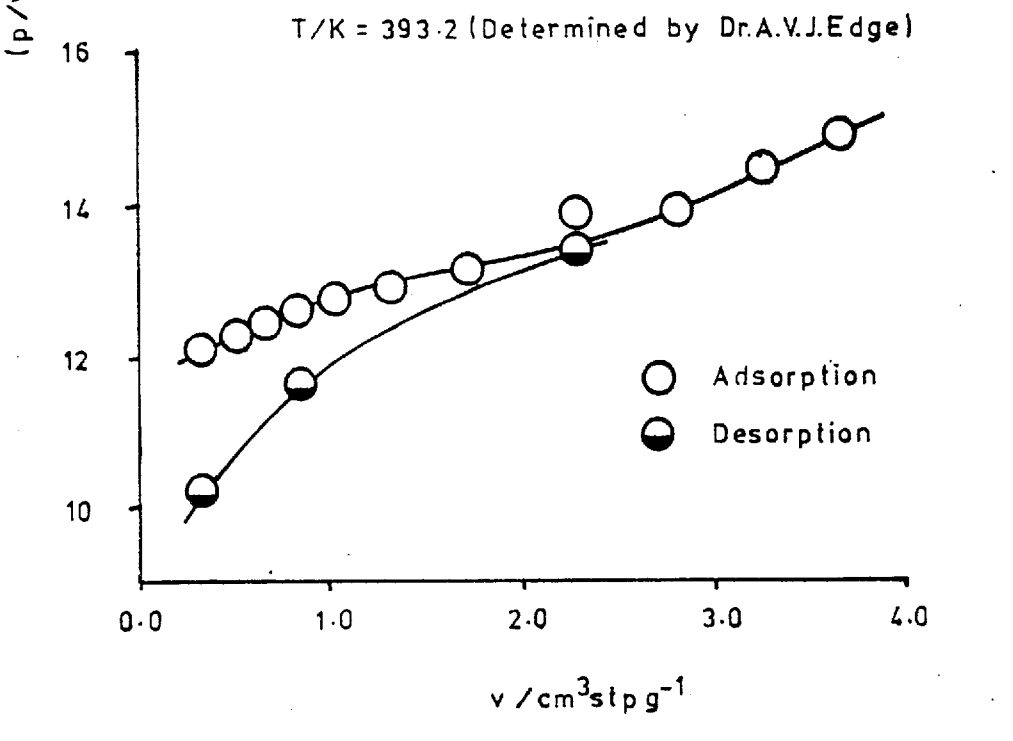

Figure 5.12. Adsorption Isotherm : i-C_4H_{10}/Graphon Pellets

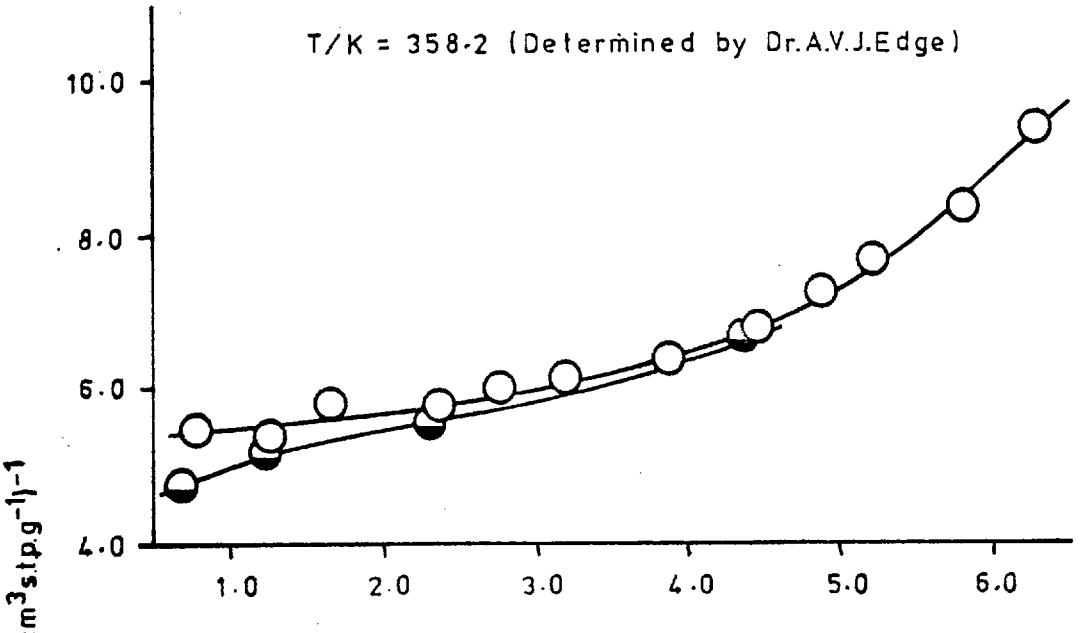

Figure 5.13. Adsorption Isotherm : i-C_4H_{10}/Graphon Pellets

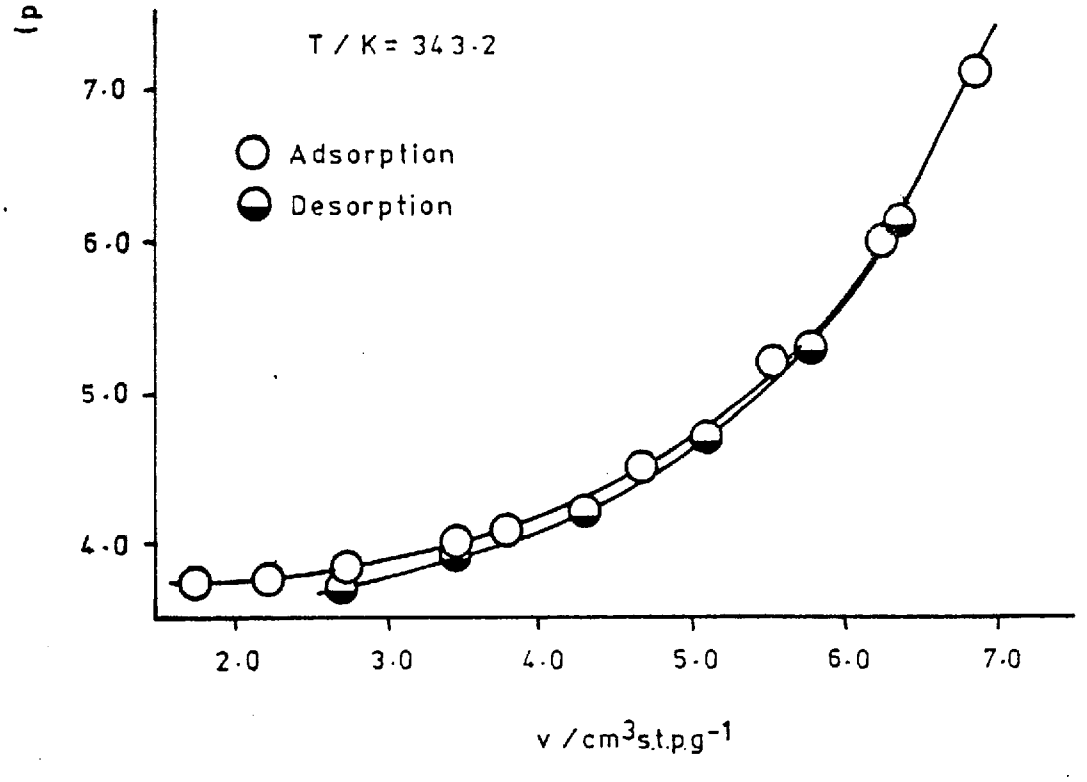

Figure 5.14. Adsorption Isotherm : i-C_4H_{10}/Graphon Pellets

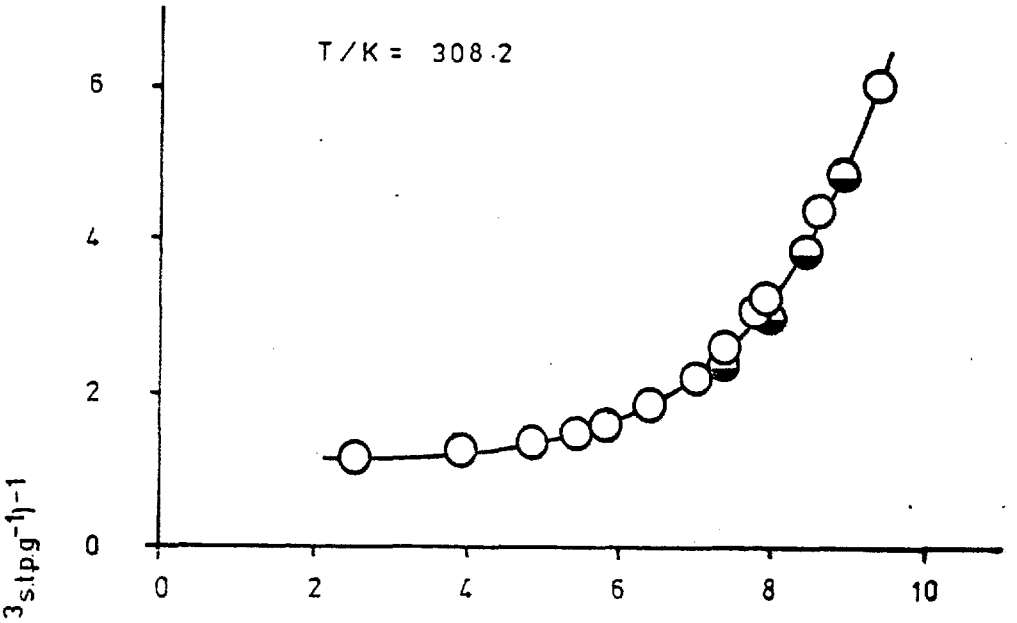

Figure 5.15. Adsorption Isotherm : i-C_4H_{10}/Graphon Pellets

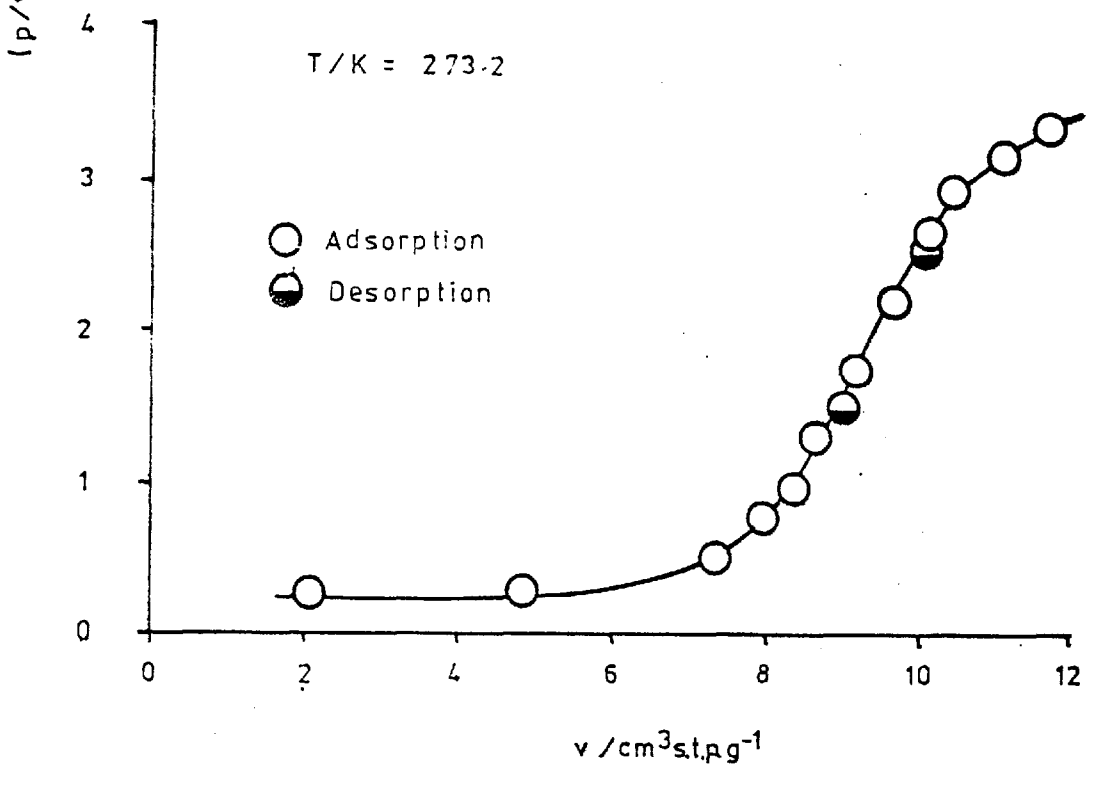

of equilibration time had no effect as can be seen from Figure 5.10 where both 1 hr and 24 hr equilibration times were examined.

It was unfortunate that none of the measured Black Pearls data was at low enough coverages to exhibit this effect, if it indeed existed. Therefore the 'hysteresis' may be due to some specific property of Graphon but lack of comparative data makes further discussion of this point impossible.

However the above observations may be attributed to a slow adsorption process into the tap grease. Throughout the course of an isotherm determination a substantial build up of adsorbate in the grease may occur (more so for the strongly sorbed gases). This gas will desorb as the equilibrium pressure is reduced for desorption measurements and will become detectable at lower coverages. It would appear that some arbitrary equilibrium amount exists for the grease as the equilibration time had no effect. The propane and isobutane behaviour at similar temperatures is in agreement with their relative strengths of sorbability.

A comprehensive study of isotherms measured on both 'greaseless' and 'greased' apparatus for different adsorbates and adsorbents would be of interest in assessing any benefits of this more sensitive presentation.

5.2. 'Conventional' Flow Results

5.2.1. Helium Flow

Helium has been widely used as a calibrating gas assumed non-sorbed. A test of the absence of extra flow is that when no viscous flow component exists :

$$\tilde{K}\,(M/T)^{\frac{1}{2}} = \text{constant} \qquad (2.4)$$

for a given membrane system, i.e. Knudsen's relationship for purely gas-phase flow holds. However Hwang and Kammermeyer (1966) observed a minimum in the variation of $\tilde{K}\,(M/T)^{\frac{1}{2}}$ with temperature for helium and nitrogen through a porous glass of characteristic pore diameter ($4\epsilon/A$) 4 nm. Ash, Barrer and Lowson (1970) in a critical study of helium flow through a Graphon membrane (characteristic diameter 22 nm) found no more than a 3% variation in the product. $\tilde{K}.T^{\frac{1}{2}}$ over the temperature range 573 K to 78 K, in contrast to the 10% increase observed by Hwang and

Kammermeyer. It is accepted that at very low temperatures extra flow of helium will exist as exemplified by the work on Vycor glass at liquid hydrogen temperatures (Hwang and Kammermeyer, 1967) and on Graphon and Black Pearls at liquid oxygen and nitrogen temperatures (Ash, Baker and Barrer, 1967).

In this work it is evident that no viscous flow component exists due to J being directly proportional to p_1 (Figure 4.29) and $\tilde{K}$ being independent of p_1 (Figure 4.30). Also the plots of $\tilde{K} T^{-\frac{1}{2}}$ appear to be relatively independent of temperature (Figure 5.16) and certainly do not exhibit the definite minimum observed by Hwang and Kammermeyer.

These two apparently conflicting sets of experimental data have been the subject of many theoretical investigations. Sandler (1972) used kinetic theory relationships to describe the behaviour found by Hwang and Kammermeyer. However Nicholson and Petropoulos have developed a theory which caters for both types of behaviour.

Initially Nicholson and Petropoulos (1973) used a narrow slit as a pore model and calculated the 'gas phase' flux making use of specific functional forms of the adsorption potential energy. This treatment qualitatively predicted the appearance of a temperature minimum for weakly adsorbed gases, the size of which decreased as the mean pore size increased. Further developments have recently been made (Nicholson and Petropoulos, 1975; Nicholson and Petropoulos, in press) using both slits and cylinders as pore models. The variations in the product $\tilde{K} T^{-\frac{1}{2}}$ with values falling below the classical Knudsen value are explained. Increasing the pore size is shown to broaden the minimum continuously, but it also tends to deepen before becoming shallower and eventually disappearing.

Thus in the particular systems under study here the use of helium as a calibrating gas does not appear to be invalidated. The value of $\tilde{K} T^{-\frac{1}{2}}$ also did not vary appreciably with the order of experiments (cf Figures 4.31, 4.32) indicating that the membranes had not 'aged' throughout the period of the investigation. Membranes compacted from Carbolac powder have been observed to age significantly with time (Ash, Barrer and Pope, 1963a; Ash, Barrer and Sharma, 1976).

Figure 5.16. Variation of $\tilde{K}_{He} T^{-\frac{1}{2}}$ with Temperature

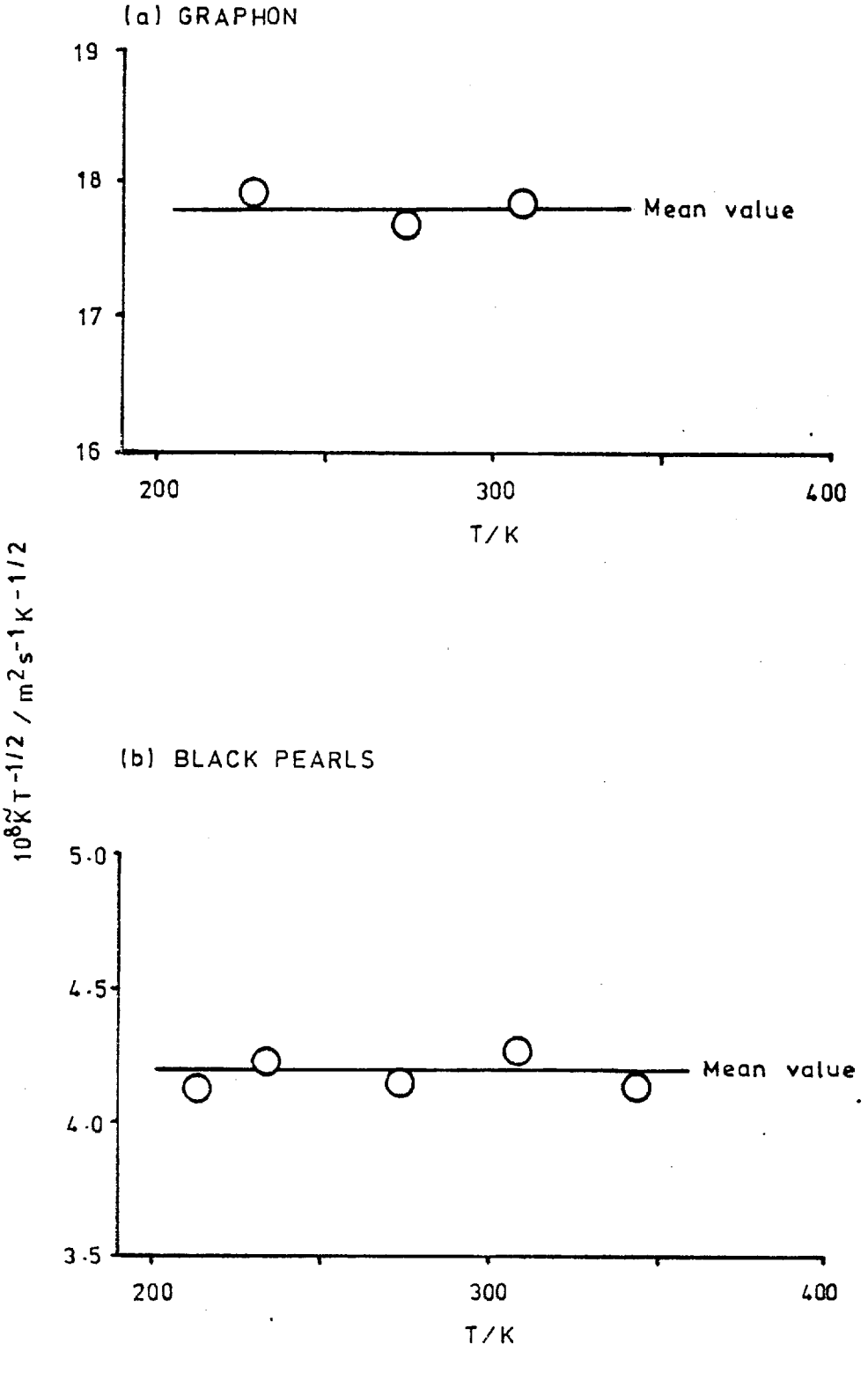

The structure factor as initially defined by Barrer and Gabor (1959) may be calculated for both membranes. These are < 1 when constrictions and tortuosity effects are dominant and > 1 when through channels of larger-than-average dimensions govern the flow. If the gas phase permeability, $\tilde{K}_g$ is independent of concentration the relationship :

$$\tilde{K}_g = \epsilon D_g \qquad (2.39)$$

is true where $\tilde{K}_g$ may be calculated from the helium permeability (also concentration independent). Hence a steady state gas phase diffusion coefficient, D_g ($m^2 s^{-1}$) may be calculated for helium at various temperatures.

A reference medium consisting of identical parallel cylindrical capillaries (of radius, $r = \frac{2\epsilon}{A}$) provides a value of D_g^{cyl} ($m^2 s^{-1}$) as calculated from the relationship :

$$D_g^{cyl} = \frac{4}{3} r \sqrt{\frac{2RT}{\pi M}} = \frac{8}{3} \frac{\epsilon}{A} \sqrt{\frac{2RT}{\pi M}} \qquad (5.5)$$

Hence the structure factor (χ_g) for the steady state flow of helium can be calculated from

$$\chi_g = \frac{D_g}{D_g^{cyl}} \qquad (5.6)$$

The values of D_g, D_g^{cyl} and χ_g are given for T/K = 308.2 for each membrane in Table 5.6.

Table 5.6. Diffusion coefficients for Helium Flow and Structure Factors

Membrane	$\frac{T}{K}$	$\frac{10^6 D_g^{cyl}}{m^2 s^{-1}}$	$\frac{10^6 D_g}{m^2 s^{-1}}$	χ_g
Graphon	308.2	9.40	1.66	0.18
Black Pearls	308.2	4.57	1.52	0.33

As can be seen the structure factors are much less than unity indicating that constrictions to the channel system are important to the flow but more so in the case of the Graphon membrane. Other work on different membranes has shown χ_g = 0.47 for the Graphon N membrane (Ash, Barrer, Clint, Dolphin and Murray, 1973) and χ_g = 0.15 for Black Pearls (as calculated from the results of Baker, 1966).

Figure 5.17. Schematic Representation of Flux curve and Adsorption Isotherm

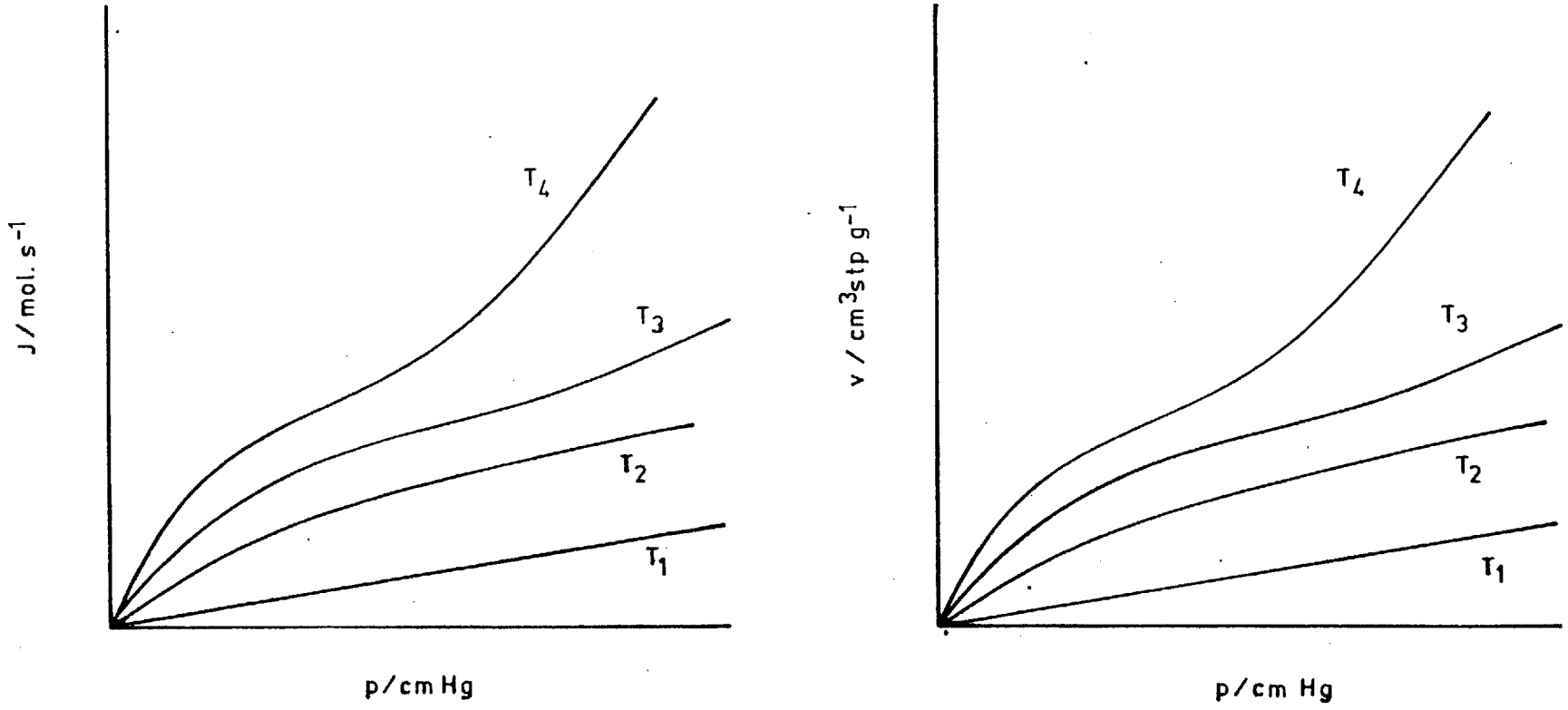

5.2.2. Single Hydrocarbon Flow

Variation of J

The variation of the molar flux, J ($mols^{-1}$) with temperature and pressure was shown in Figures 4.33, 4.34 and 4.39, 4.40. As the temperature increases both contributions to the total flux (gas phase flow and the extra flow associated with an adsorbed film) decrease. At higher temperatures when adsorption is almost in the Henry Law region the total flux tends to be proportional to the ingoing pressure. A similarity exists between the shape of the J curve and that of the isotherm. This is schematically shown in Figure 5.17 with the actual plots given in Chapter 4. At lower temperatures both curves have an initial portion concave to the pressure axis followed by a convex section as the saturated vapour pressure is approached.

The rapid upturn in the molar flux is related to the large uptakes of gas near the saturation vapour pressure and the associated rapid increase in extra flow. The relative magnitudes of the 'extra' and 'gas phase' flow are dealt with later when the permeabilities are considered.

The Variation of $\tilde{K}$

The temperature and pressure dependence of the integral permeability, $\tilde{K}$ is shown in Figures 4.35 to 4.38 and 4.41 to 4.44. The permeability versus pressure plot is of the general form schematically given in Figure 5.18.

Fig.5.18. The Permeability as a function of Temperature and Pressure

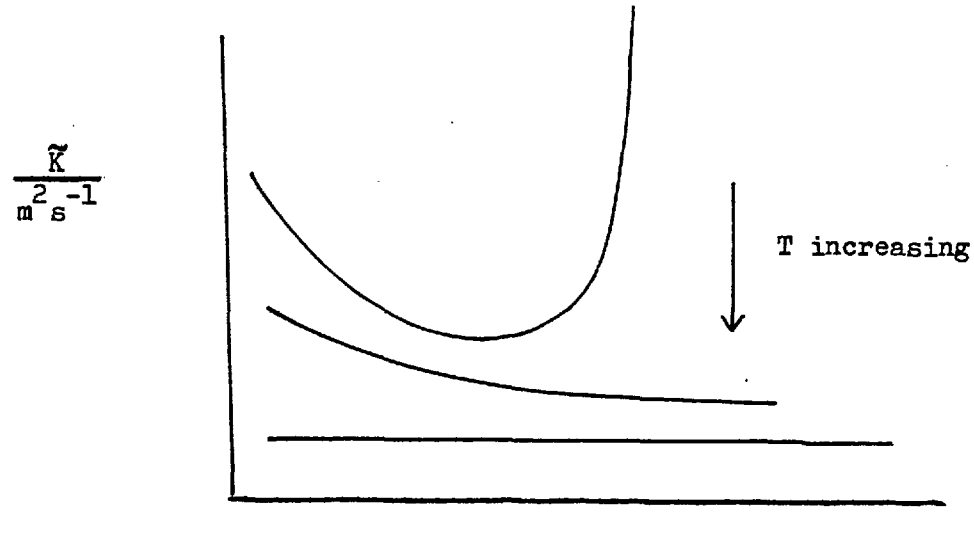

At high temperatures the permeability, $\tilde{K}$ is independent of the ingoing pressure of hydrocarbon as required by a linear J vs p_1 plot. Then as the temperature is lowered a marked increase in $\tilde{K}$ occurs at lower pressures. The increase in the pressure dependence of $\tilde{K}$ (due to the sigmoid shape of the J vs p_1 curve) as the temperature is lowered has been previously observed, Ar and SF_6 on Graphon and Black Pearls (Ash, Baker and Barrer, 1967), CO_2 through Vycor glass (Rhim and Hwang, 1974). It has been suggested that the decrease (i.e. $d\tilde{K}/dp$ is negative) is due to the blockage of some of the through channels by adsorbed molecules (Nicholson and Sing, 1979). However evidence presented in Section 5.2.3 indicates that for this membrane blockage effects also exist when there is no pressure dependence of $\tilde{K}$. In the case of isobutane flow through Graphon at T/K = 308.2 a flat maximum was observed at very low pressures. Other work on the Graphon-isobutane system (different membrane) in these laboratories has confirmed this finding (Ash, Barrer and Edge, to be published). Also work on the propylene-Graphon system at T/K = 273.2 and 298.2 exhibited this format (Horiguchi, Hudgins and Silveston, 1971) which was attributed, by the authors to a rapid increase in adsorption with increasing pressure. However this effect is not commonly observed.

As the temperature is decreased the permeability curve goes through a broad minimum. Carman (1951) supported by Weisz (1975) attributes the rapid upsurge at high values of p_1/p_o to multilayer formation and capillary condensation taking place. The effect of surface tension lowers the vapour pressure of the adsorbed gas and the driving force is not the measured gas pressure but a much larger capillary pressure difference. The appearance of a minimum in the $\tilde{K}$ vs p_1 curves has been observed at low temperatures for several systems, SO_2 through Carbolac (Pope, 1961), n-butane through Vycor glass (Gilliland, Baddour and Russel, 1958), Ar, N_2 and O_2 through ceramics (Lallemand and Eyraud, 1973). The dramatic increase in $\tilde{K}$ at high p_1/p_o was found for CF_2Cl_2 flow through Linde Silica (Carman and Malherbe, 1950) and also for the flow of water vapour through parallel sided glass channels (Roberts, 1973). Nicholson and Sing (1979) point out that capillary condensation in parallel sided channels is debatable and that the rapid flow rates exhibited are more likely to be due to multilayer effects.

Several workers report, in addition to the increase in permeability near $p_1/p_o = 1$, the appearance of a maximum at or near the saturated vapour pressure, due to bulk liquid condensing and leading to lower flow rates found with liquids, [NH_3 through Vycor glass (Brubaker, 1953), CF_2Cl_2 through a fine-pores graphite (Field, Watts and Weller, 1963)]. Rhim and Hwang (1974) also observe this maximum but at values of $p_1/p_o \simeq 0.5$ for the gases C_2H_6, CO_2 and n-C_4H_{10} through Vycor glass. However their experimental conditions employed a small pressure difference between the two sides and the mean pressure was used to calculate values of p_1/p_o.

A contrasting behaviour was found with ammonia flow through a Carbolac membrane (Ash, Barrer and Lowson, 1973). The permeability was independent of pressure at high temperatures as expected. However as the temperature decreased $d\tilde{K}/dp$ became positive and almost constant for a given temperature. No minimum existed and in fact at the lowest temperatures a sharp maximum was observed. This was attributed to ammonia adsorption in the Carbolac micropores, swelling the particles sufficiently to block a number of flow paths. Another example of this increase in $\tilde{K}$ with p_1 as the temperature is decreased is work on hydrocarbon flow through a cracking catalyst (Ash, Barrer and Logan, to be published).

This study was concerned with adsorption conditions, i.e. the permeability was always measured with increasing values of ingoing pressure. However Carman (1952) observed hysteresis effects in the $\tilde{K}$ vs p_1 curve and also in the corresponding adsorption isotherm. Similar effects were observed for n-butane flow through Vycor glass (Gilliland, Baddour and Russel, 1958). Further work, using the Graphon membrane of this study undertaken in these laboratories by Mr D.E.G. Whiting has indicated hysteresis in the plot of $\tilde{K}$ vs p_1 in the region of the saturated vapour pressure. Both earlier works showed that the value of the permeability was the same at both adsorption and desorption for a given amount adsorbed.

The total permeability may be split into two components (cf §2.3.1), a purely gas phase component, $\tilde{K}_g$ and a component, $\tilde{K}_s$ related to the extra flow generated by the adsorbed film where :

$$\tilde{K} = \tilde{K}_g + \tilde{K}_s \qquad (2.33)$$

Assuming non-sorbed Knudsen flow for helium the gaseous component of a sorbed gas may be calculated from the measured helium permeability. The value of $\tilde{K}_{He}$ may be taken from the single gas measurements or the mixture experiments and the difference is discussed later (§5.2.4). For the present discussion on the magnitude of the extra flow, the value of $\tilde{K}_{He}$ from the single gas measurements is used. Values of the ratio of $\tilde{K}_s/\tilde{K}_g$ have been calculated for the hydrocarbons at a fixed value of p_1 and the variation with temperature and gas is shown in Figure 5.19. As can be seen the 'extra flow' becomes increasingly important as the temperature decreases. In the case of Black Pearls/propane $\tilde{K}_s$ may be greater than sixty times the value of $\tilde{K}_g$. The data of Murray (1976) for n-butane on Graphon membrane 'N' (Figure 5.19 (a)) supplements the observation that the more strongly sorbed the gas the greater the extra flow contribution. This view is also supported by the work of Ash, Barrer and Sharma (1976) who found that the extra flows associated with adsorbed films became more and more dominant the larger the carbon number for the hydrocarbons $CH_4 \rightarrow C_5H_{12}$ through Carbolac.

If the quantity $\tilde{K}_s/A$ is considered, a comparison between the carbon is provided for their effectiveness in promoting extra flow (Ash, Baker and Barrer, 1976). The variation of $\tilde{K}_s/A$ with pressure is given in Figure 5.20 for a constant temperature on both carbons. It can be seen that for both gases the Graphon surface is more effective but the two carbons do have $\tilde{K}_s/A$ values of the same magnitude. The order of Graphon > Black Pearls is substantiated by work on argon flow (Ash, Baker and Barrer, 1967) which included the carbon Carbolac. The $\tilde{K}_s/A$ values for Carbolac fell two orders of magnitude below those for Graphon and Black Pearls indicating a very broken surface, consisting of blind pores and micropores. The greater the degree of surface roughness the less effective the surface in promoting extra flow.

It has been assumed, due to the constancy of the product $\tilde{K}.T^{-\frac{1}{2}}$ for helium that purely molecular streaming occurs in the gas phase. It is generally accepted that for this to be the case the mean free path of the gas molecule, λ (m) should be very much greater than the pore dimensions, d ($4\epsilon/A$,m). As the product $\tilde{K}.T^{-\frac{1}{2}}$ for the adsorbed gas flow cannot be directly measured for pure gas phase flow a consideration of the λ

Figure 5.19. Variation of $\tilde{K}s/\tilde{K}g$ with temperature

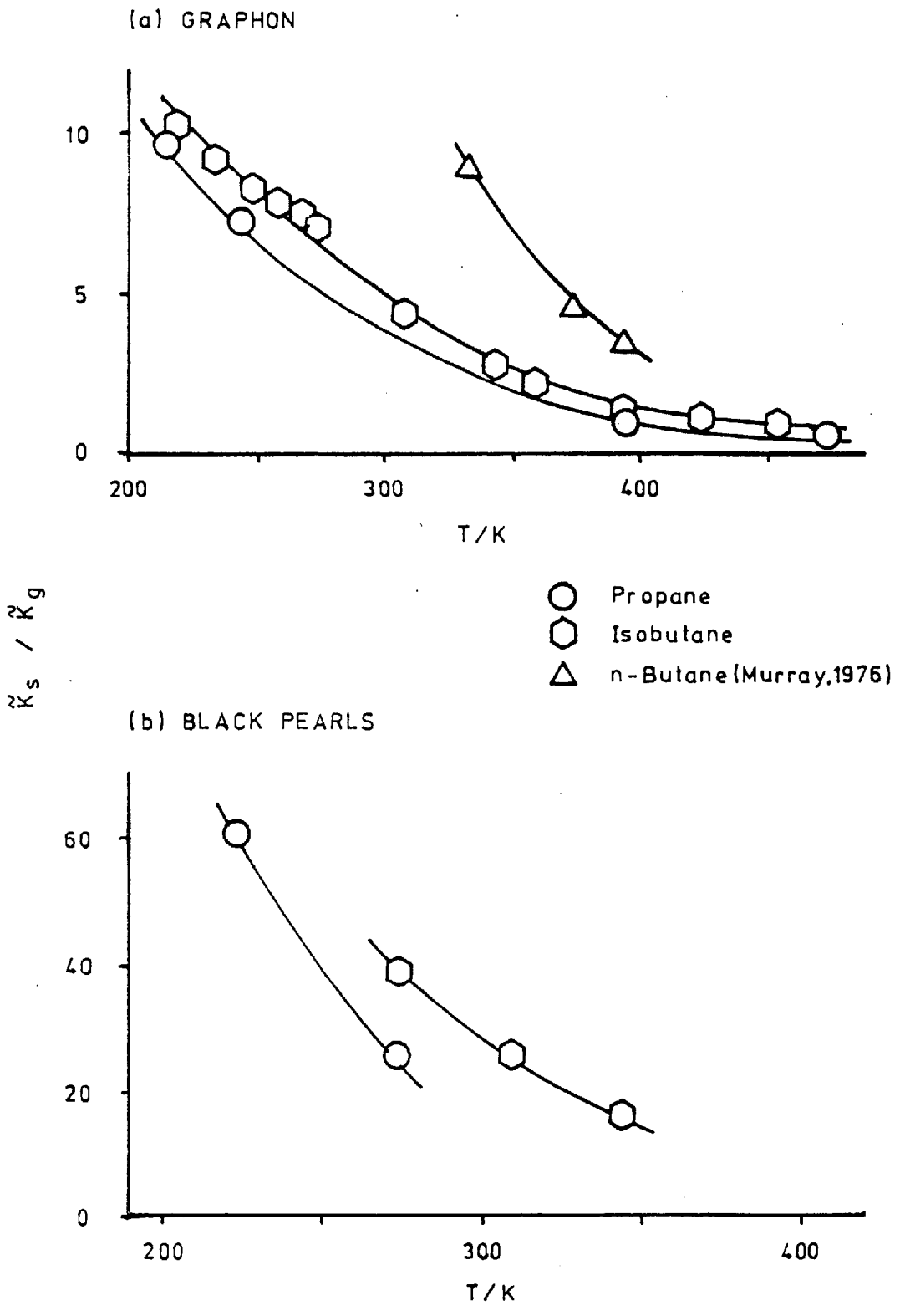

Figure 5.20. Variation of $\tilde{K}s/A$ with pressure

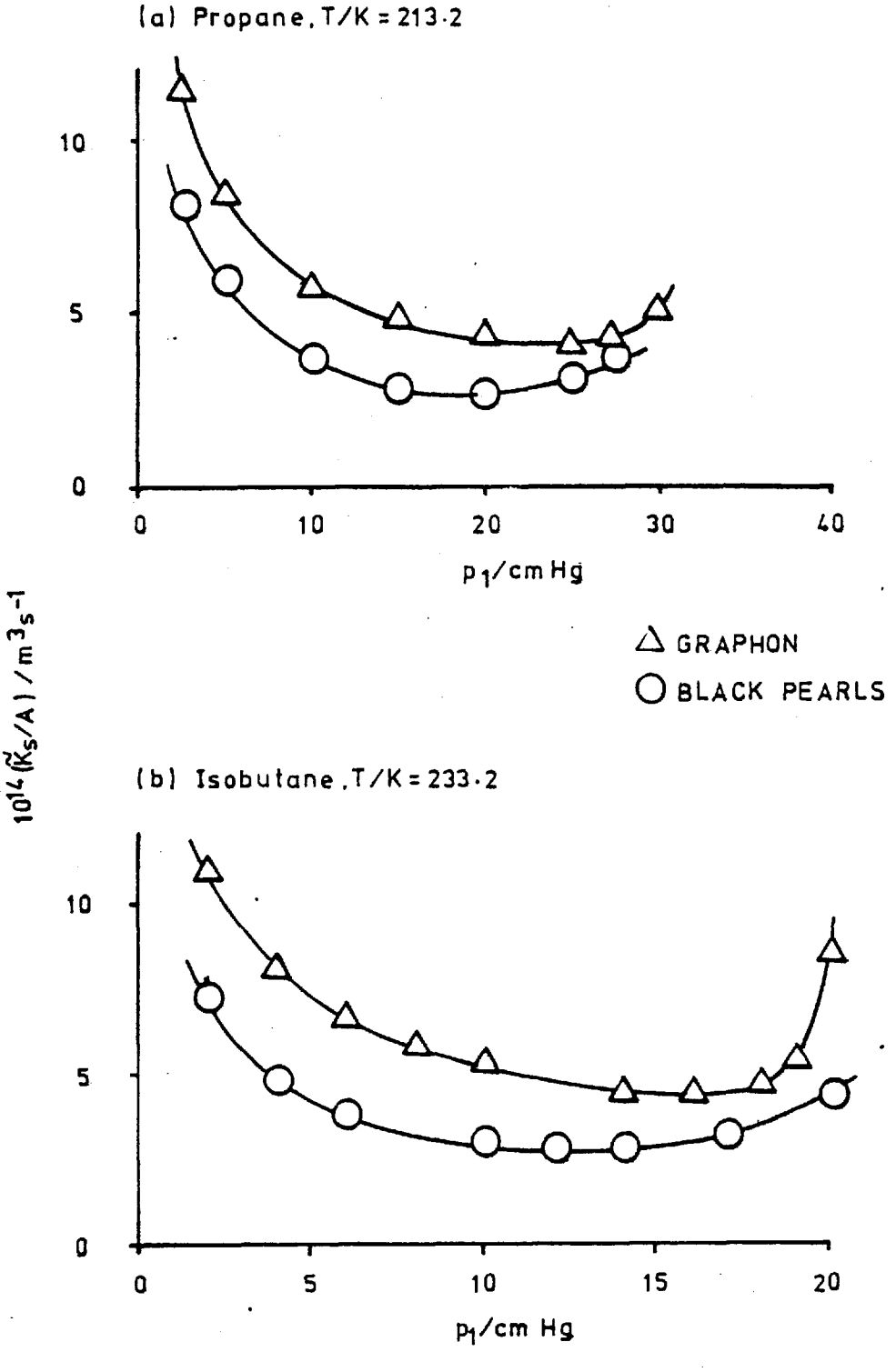

and d values is given. The worst cases will be at low temperatures and high pressures. The mean free path is calculated from the relationship :

$$\lambda = \frac{k.T}{\sqrt{2}.\pi.\delta^2 p} \qquad (5.7)$$

(Hirschfelder, Curtiss and Birch, 1954)

where k is the Boltzmann constant (JK^{-1}), T the temperature (K), p the pressure (Nm^{-2}) and δ the molecular diameter (m). The values of δ (obtained from viscosity data) are given by Hirschfelder, Curtiss and Birch (1954). These and the values of λ are tabulated in Table 5.7 along with the pore dimensions, d ($= 4\frac{\epsilon}{A}$). It can be seen that under some of the more adverse conditions λ has decreased to only a factor of three and five (for Graphon and Black Pearls respectively) greater than d. From the treatment of Webber (1954), discussed in Section 2.2 other modes of gas phase flow came into existence as $\lambda \Rightarrow d$. These tend to form a minimum in the permeability curve and may contribute to the observed minima of this study. This effect is of minor significance as the extra flow component, $\tilde{K}_s$ makes the major contribution to the total flow especially at low temperatures (Figure 5.19).

Table 5.7. Mean Free Path of Gas Molecules at Specific Temperatures and Pressures

	$\frac{\delta}{nm}$	$\frac{T}{K}$	$\frac{p}{cm\ Hg}$	$\frac{\lambda}{nm}$	$\frac{d}{nm}$	
C_3H_8	0.506	213	30	64.6	22	Graphon
i-C_4H_{10}	0.534	248	40	50.7	11	Black Pearls

5.2.3. Binary Mixture Flow

(a) Introduction

The mixture experiments were designed to examine the effect of an adsorbed film upon the transport of a non-sorbed indicator gas. The majority of the measurements were made with helium/hydrocarbon mixtures. The helium, being non-sorbed exhibits no extra flow and is transported

purely in the gas phase. The sorbable component, however, is also transported by an 'extra flow' which may be very much greater than the gas phase flow (cf §5.2.2). A limited amount of data was obtained for the argon/hydrocarbon system where both components can exhibit 'extra flow' under suitable conditions.

In a system exhibiting Knudsen flow both components of a mixture will flow independently of each other if transport is purely in the gas phase. It has also been assumed (Kammermeyer, 1958) that the extra flow and gaseous flow act in parallel with, and independent of each other for dilute adsorbed films. Aylmore and Barrer (1965) observed that under conditions at or near Henry Law adsorption, two components exhibiting extra flow would also be transported independently of each other. However as stronger adsorption takes place the independence of the 'gas phase' and 'extra' flows should deteriorate as increasing sorption will reduce the effective pore size and subsequently gas phase flow. Membranes formed from a high surface area carbon, Carbolac, have been studied in great detail for various gas mixtures (Ash, Barrer and Pope, 1963b; Ash, Barrer and Lowson, 1973; Ash, Barrer and Sharma, 1976). It was found that at relative pressures less than unity the adsorbed film was capable of totally blocking the flow of the non-sorbed indicator gas. However at the same time the enhanced extra flow component (cf §5.2.2) transported the sorbable gas rapidly through the membrane, i.e. the membrane was effectively acting in a semi-permeable capacity.

(b) Helium/isobutane/Graphon

Initially the flow of mixtures containing i-C_4H_{10} and helium through the Graphon membrane was considered. The pressure dependence of the relative permeability, $\tilde{K}_R$ at various temperatures is given in Figure 4.46. In order to assist the discussion triple plots were constructed (Figures 5.21 to 5.32). These present the pure hydrocarbon permeability, the adsorption isotherm and the relative helium permeability as a function of ingoing hydrocarbon pressure at a specific temperature.

The effect of the adsorbed film of isobutane upon the non-sorbed helium is shown by variations in $\tilde{K}_R$. If $\tilde{K}_R$ equals unity, there is no effect and if $\tilde{K}_R$ equals zero the helium flow is totally inhibited. It was assumed throughout this study that the presence of helium did not affect the hydrocarbon permeability. It can be seen (Figures 4.46, 5.21)

Figure 5.21. Triple Plot : i-C_4H_{10}/Graphon : T/K = 453.2

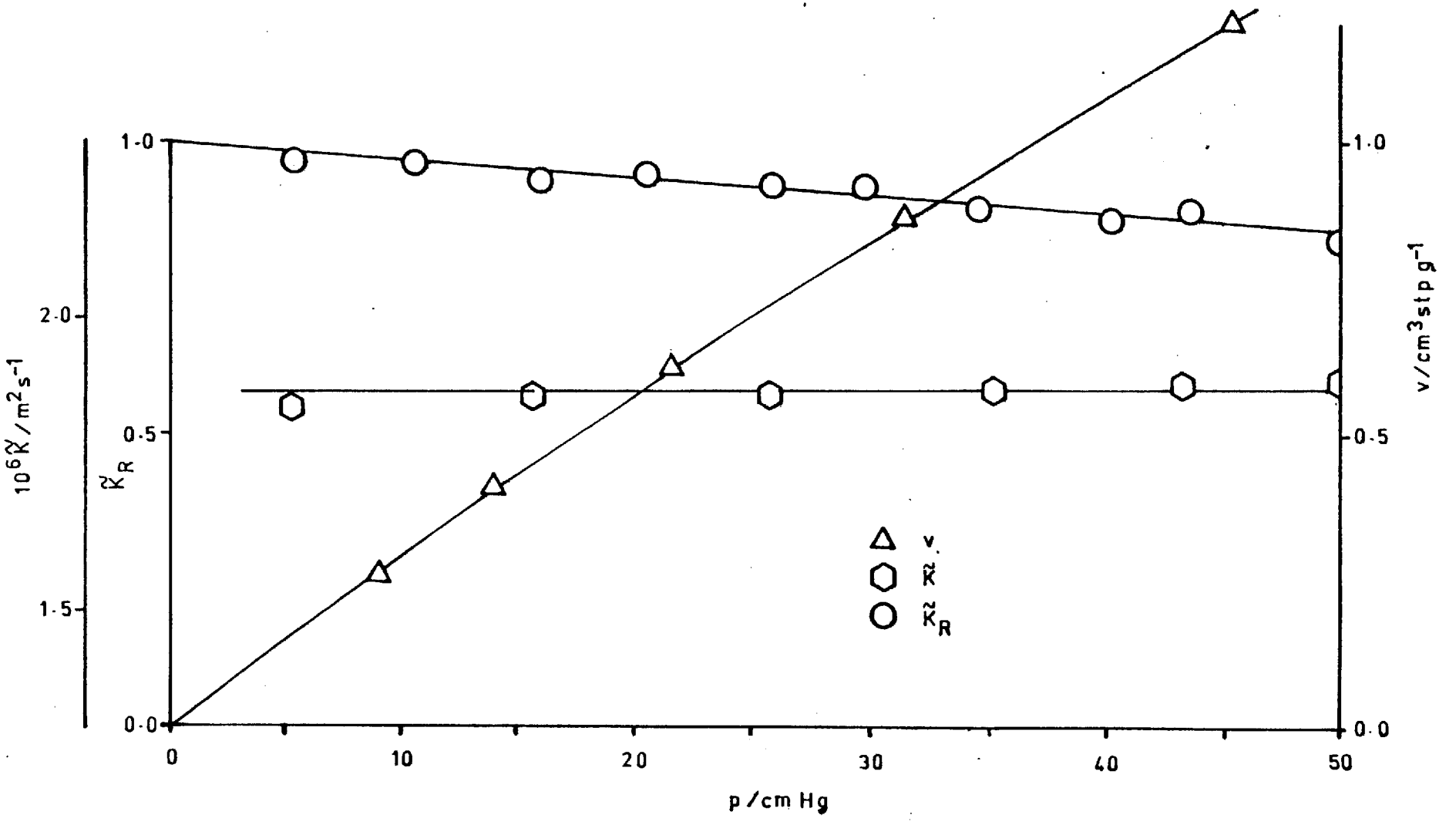

Figure 5.22. Triple Plot : i-C_4H_{10}/Graphon : T/K = 423.2

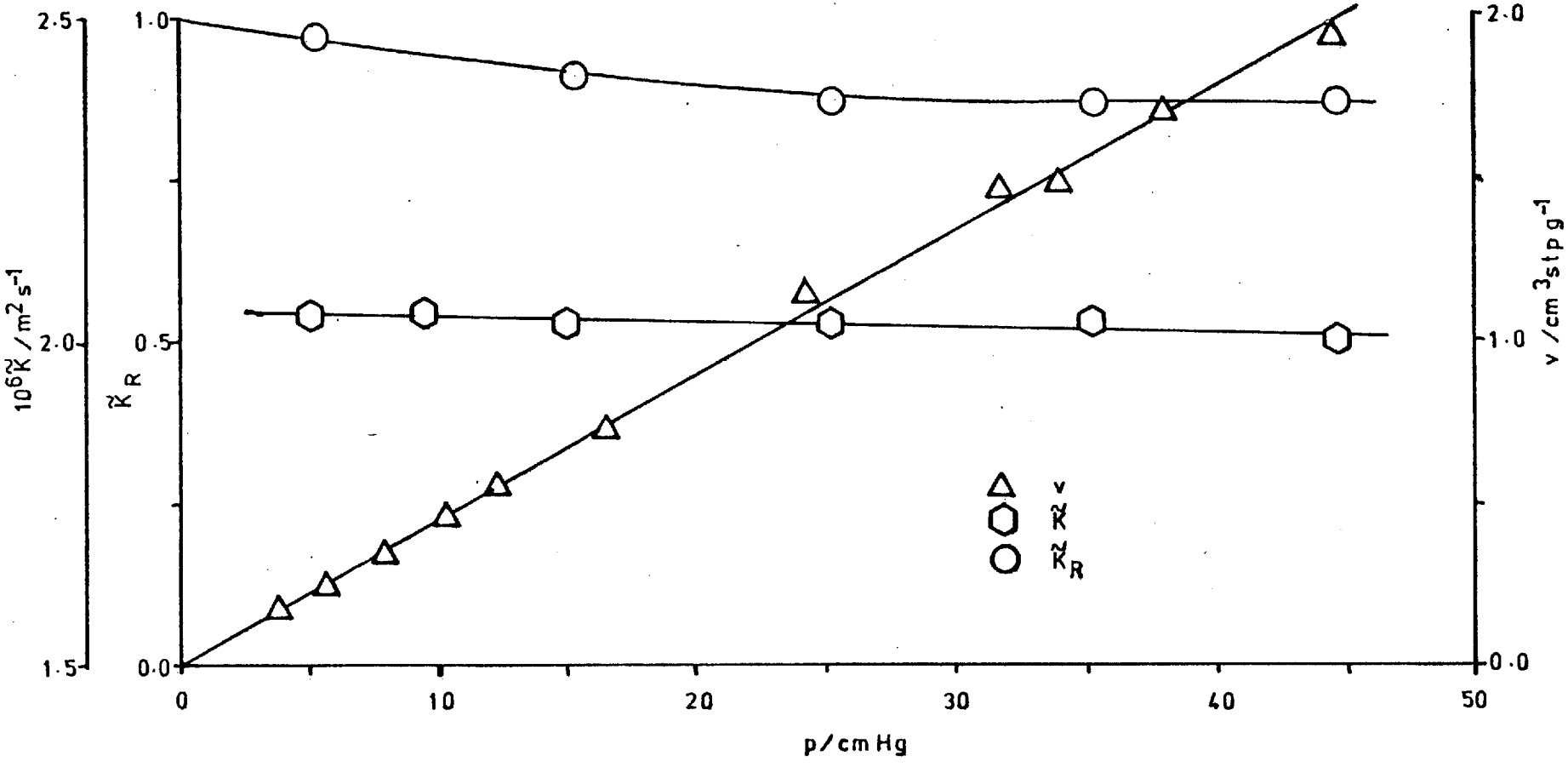

Figure 5.23. Triple Plot : i-C_4H_{10}/Graphon : T/K = 393.2

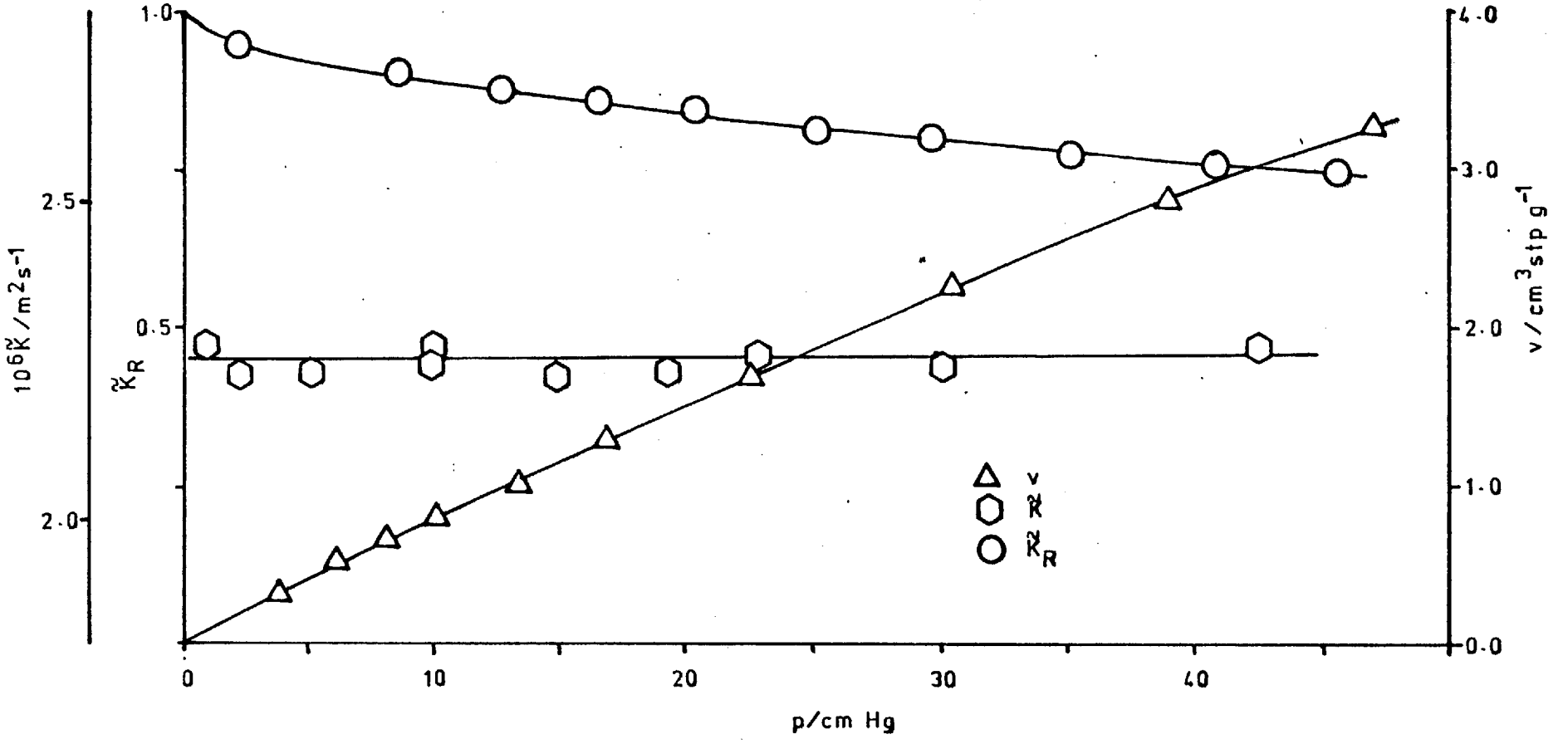

Figure 5.24. Triple Plot : i-C_4H_{10}/Graphon : T/K = 358.2

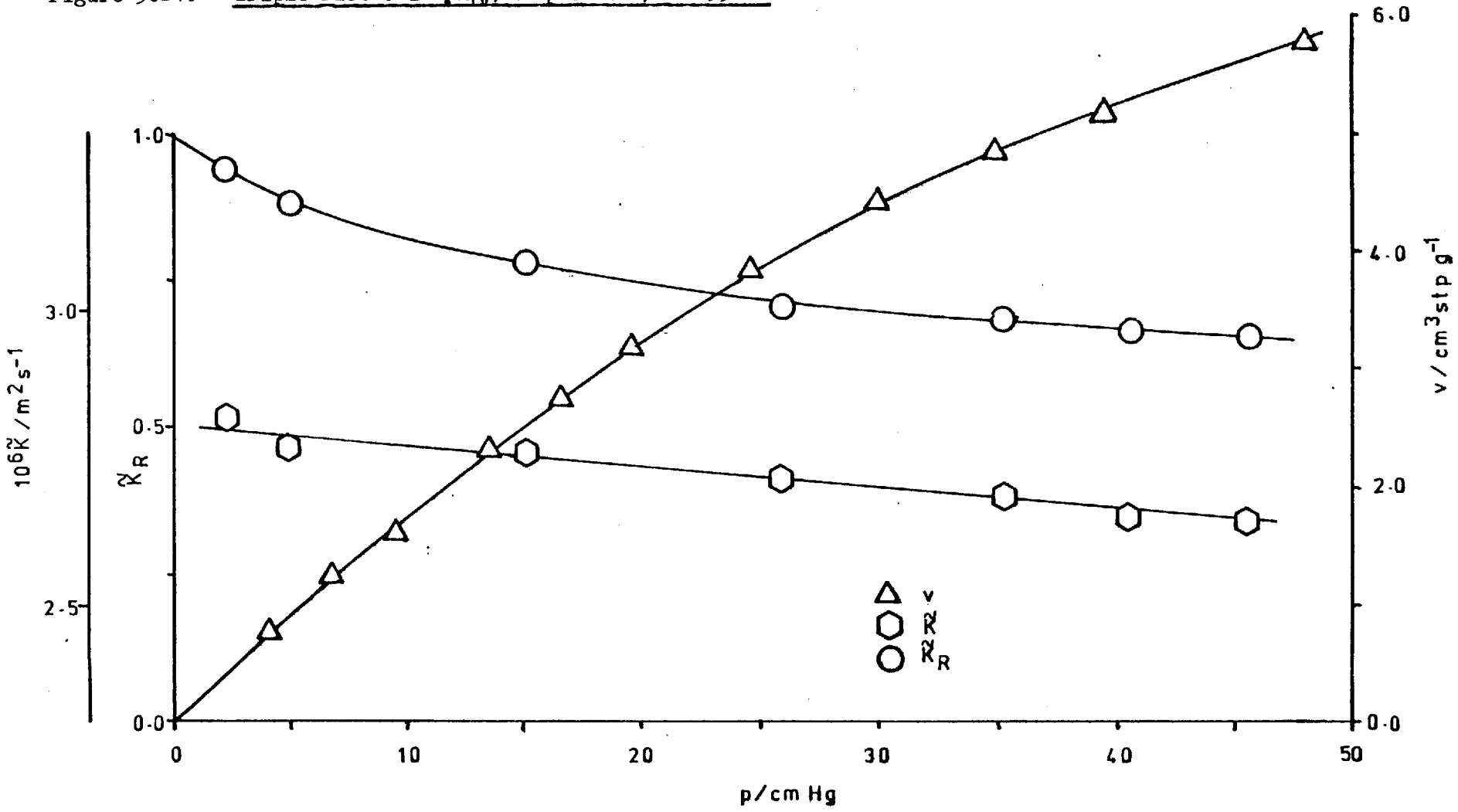

Figure 5.25. Triple Plot : i-C_4H_{10}/Graphon : T/K = 343.2

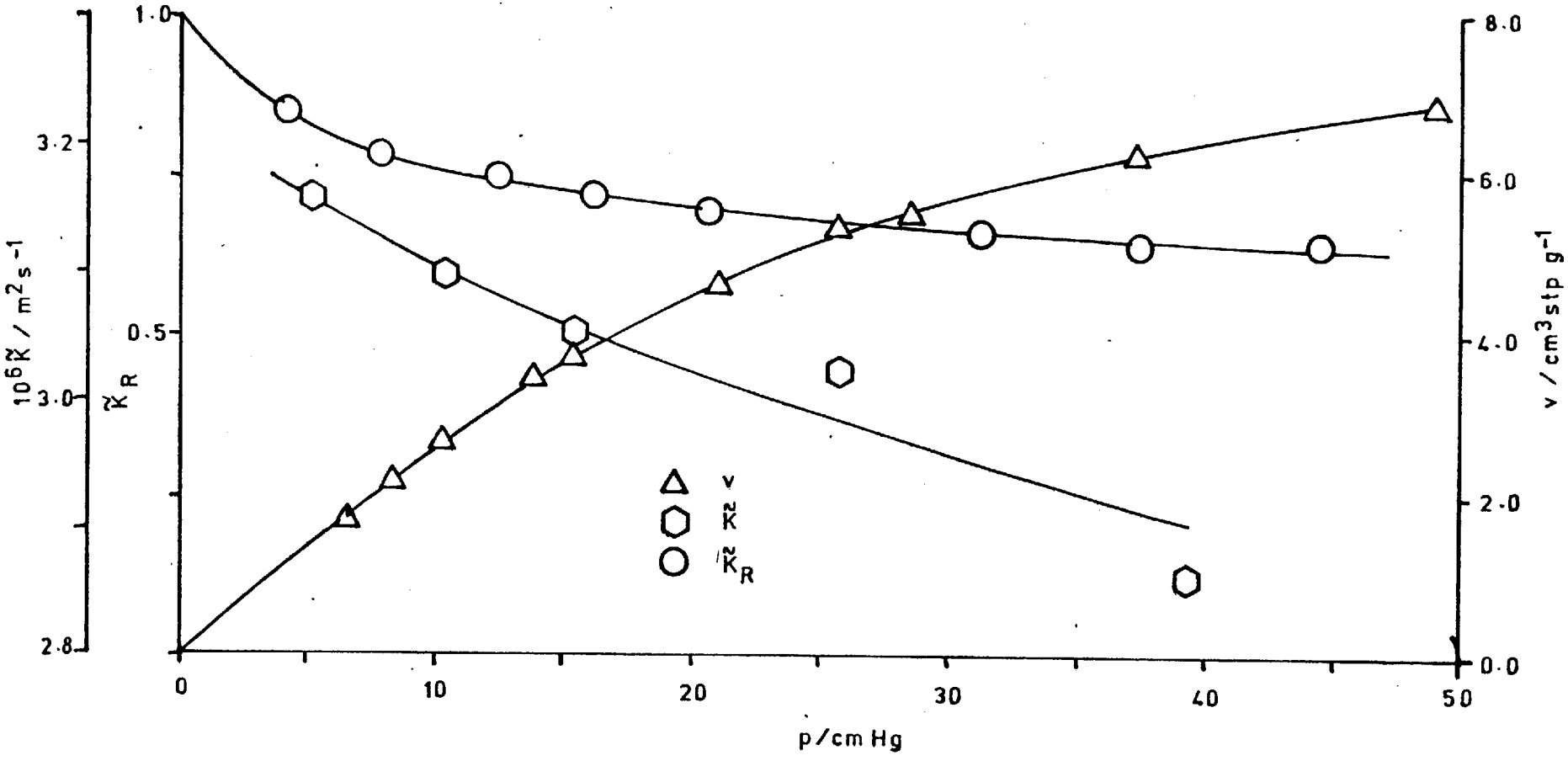

Figure 5.26. Triple Plot : i-C_4H_{10}/Graphon : T/K = 308.2

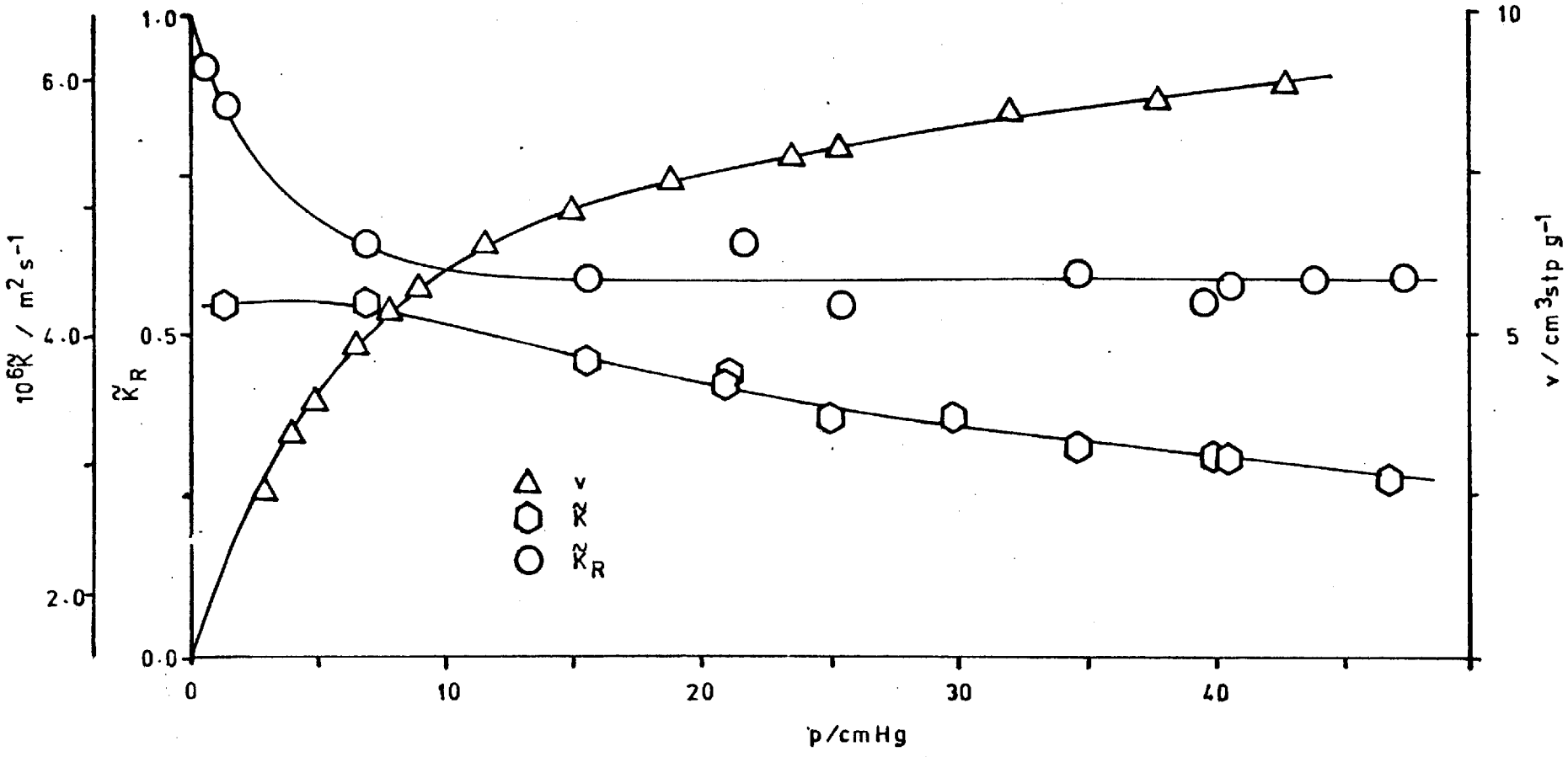

Figure 5.27. Triple Plot : i-C_4H_{10}/Graphon : T/K = 273.2

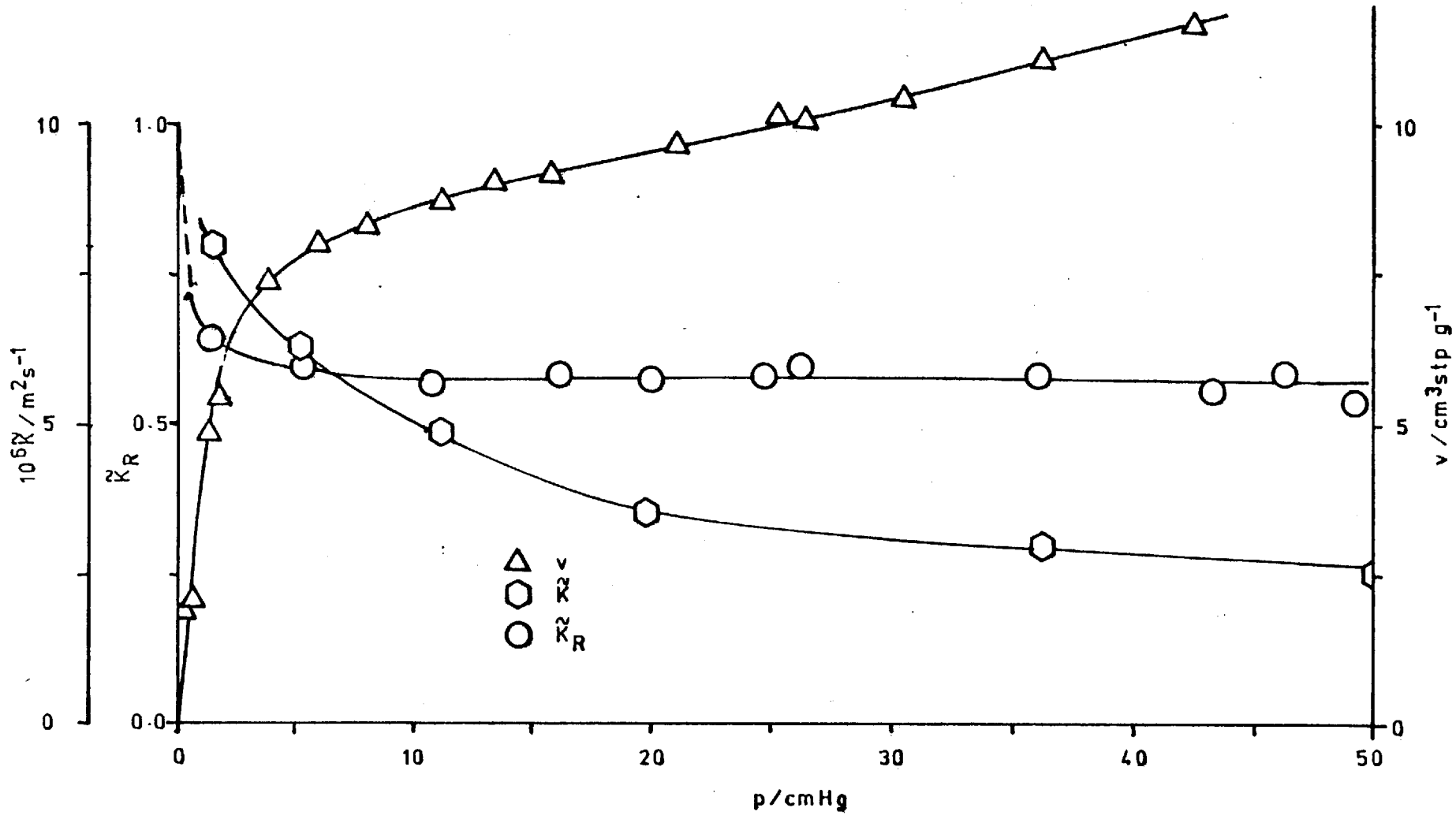

Figure 5.28. Triple Plot : i-C_4H_{10}/Graphon : T/K = 268.2

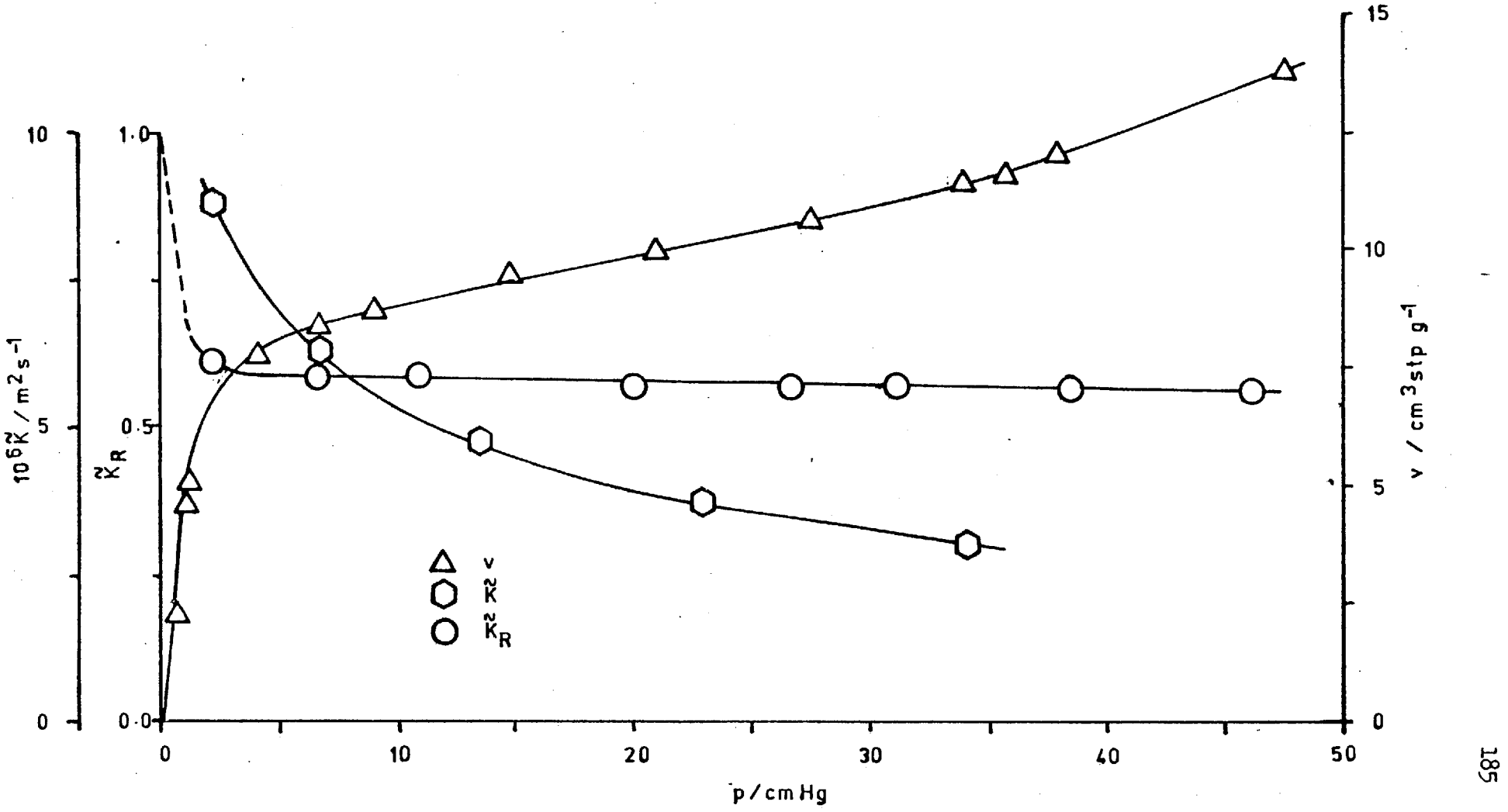

Figure 5.29. Triple Plot : i-C_4H_{10}/Graphon : T/K = 258.2

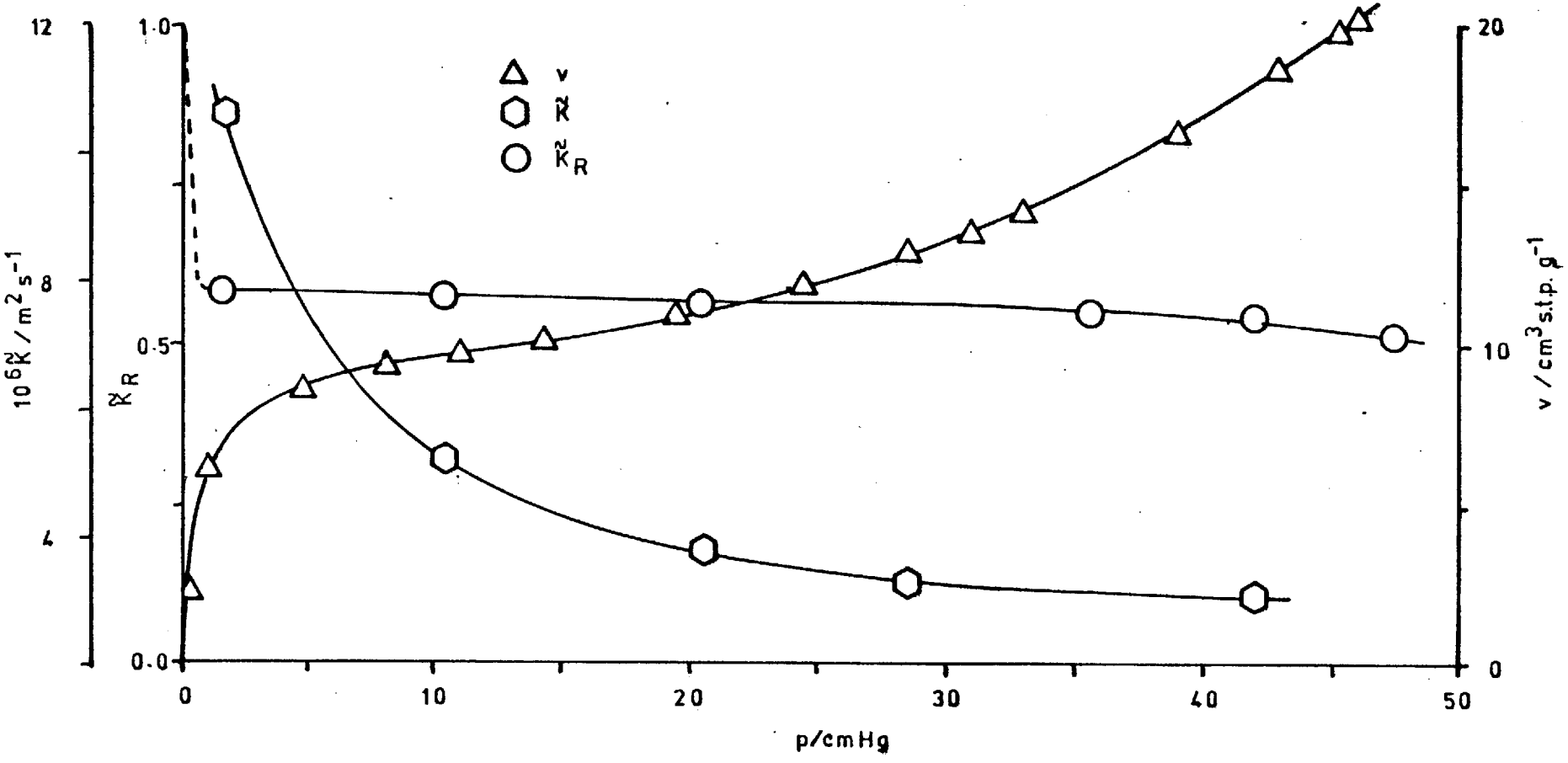

Figure 5.30. Triple Plot : i-C_4H_{10}/Graphon : T/K = 248.2

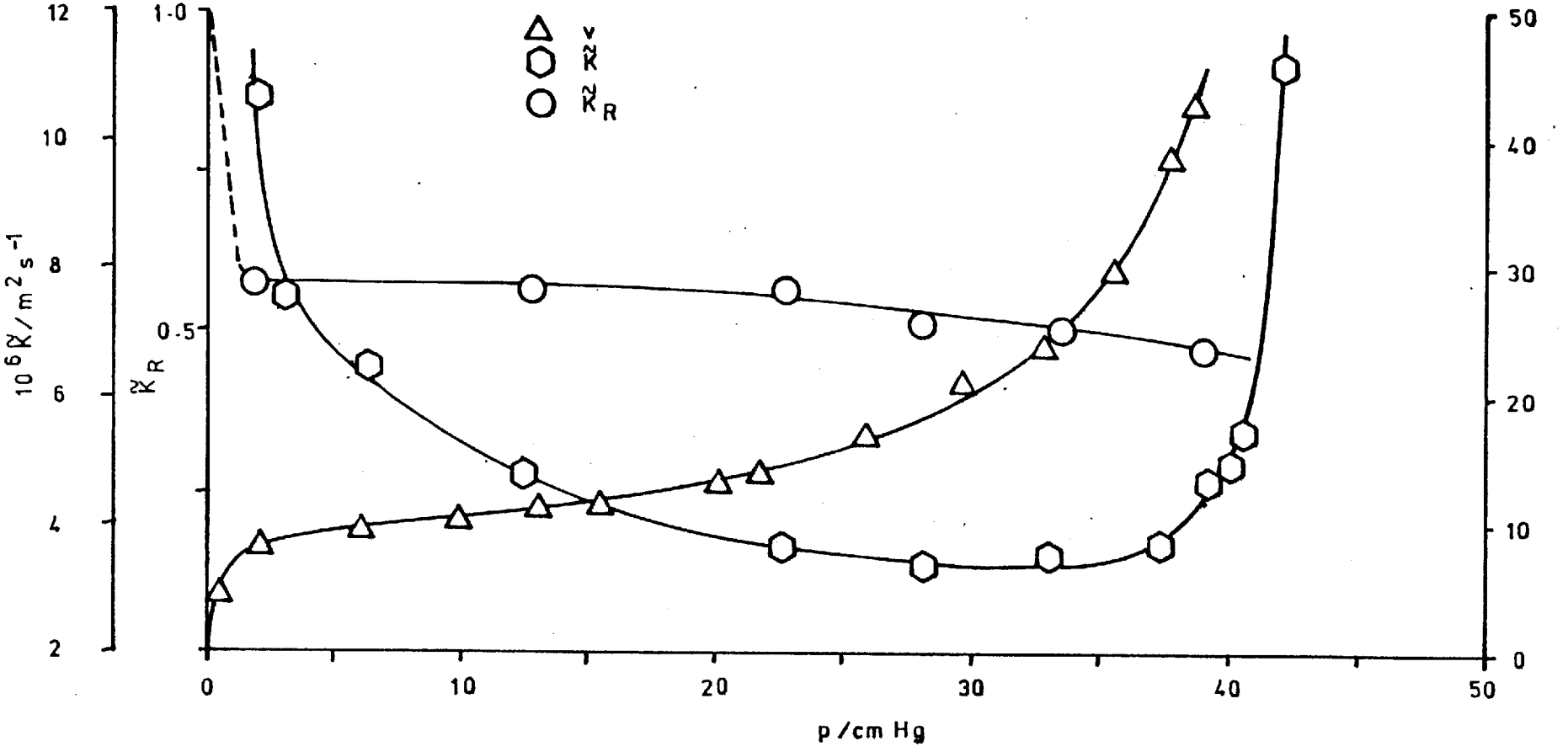

Figure 5.31. Triple Plot : i-C_4H_{10}/Graphon : T/K = 233.2

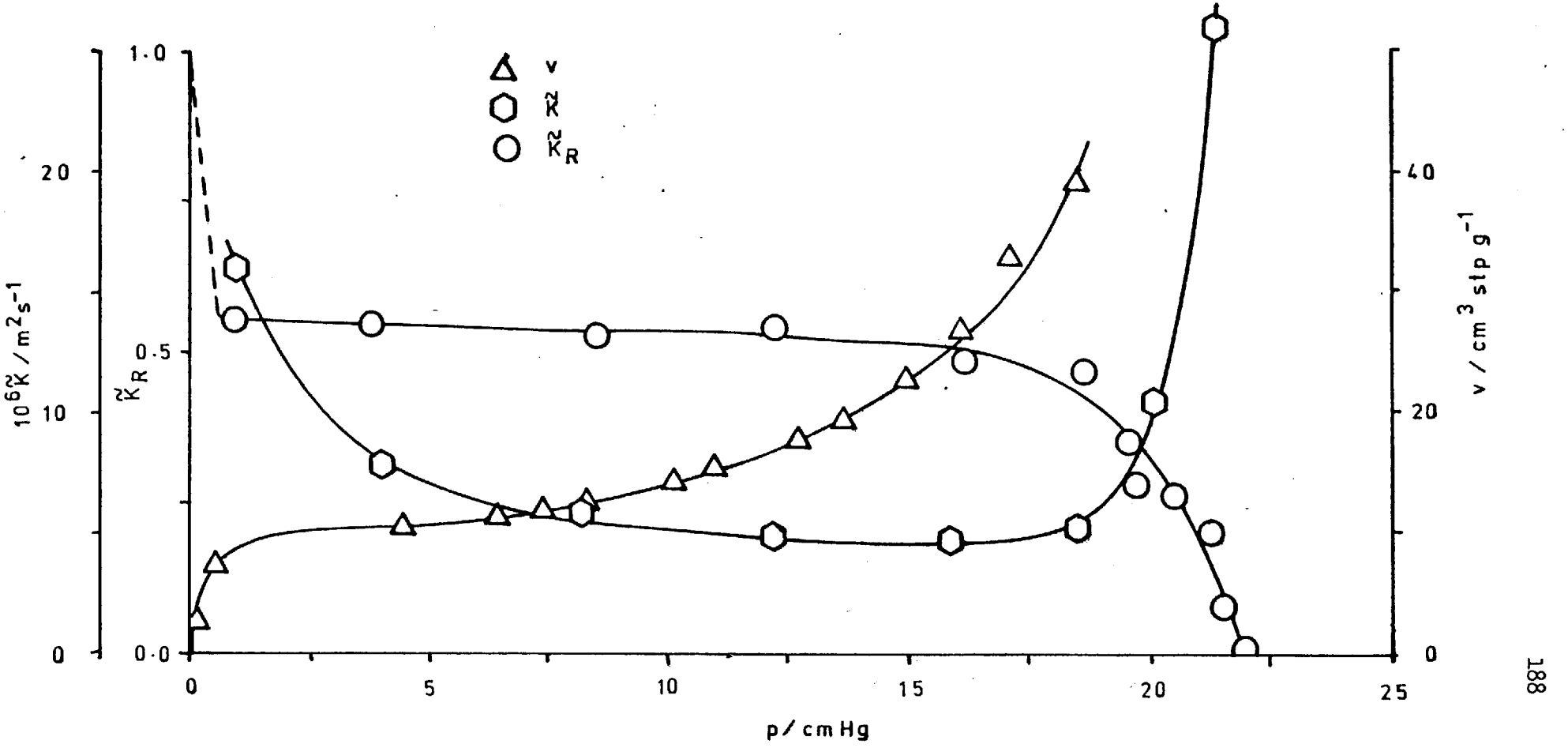

Figure 5.32. Triple Plot : i-C_4H_{10}/Graphon : T/K = 218.2

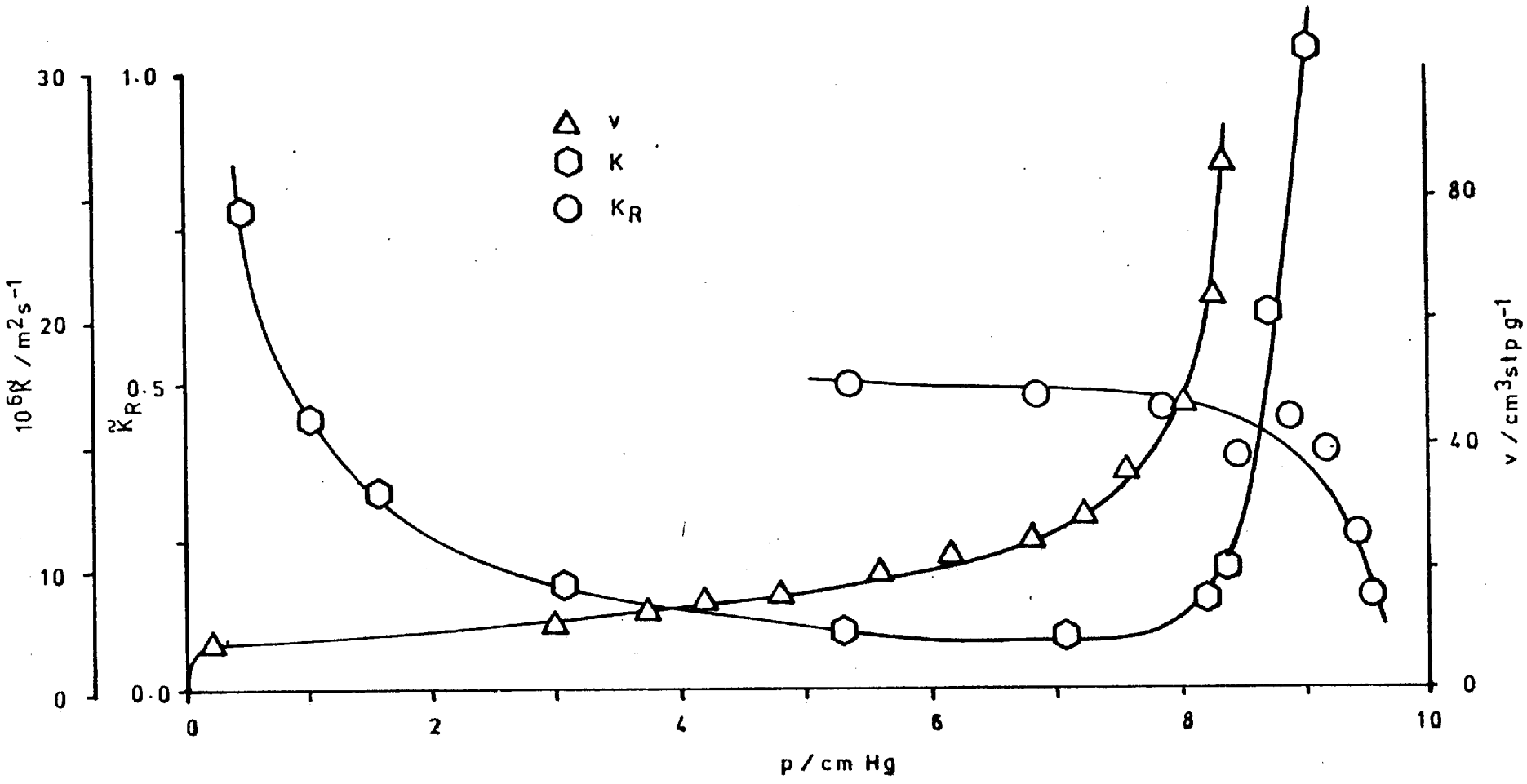

that at high temperatures near Henry Law adsorption where the pure isobutane permeability is independent of pressure there is blockage of the non-sorbed component. This was not expected as previous work on Carbolac (Aylmore and Barrer, 1966; Ash, Barrer and Lowson, 1973) had shown that at Henry Law adsorption two weakly adsorbed components flow independently of each other. It has been assumed up to present that at or near the Henry Law range "cross-effects between individual flows should be minimal", (Ash, Barrer and Foley, 1976). For the isobutane/helium system with Henry Law adsorption of the isobutane, a region of no blockage is expected, i.e. $\tilde{K}_R = 1$ over a pressure range of hydrocarbon. This is not the case indicating that there must be adsorption at some key sites, which are instrumental in governing the gas phase flow, for example constrictions in a channel. The presence of constrictions is also strongly indicated by the value of the structure factor, $\mathcal{K}_g$ as previously discussed (cf §5.2.1). It has been mentioned (cf §5.2.2) that previously (Nicholson and Sing, 1979) the decrease in the pure hydrocarbon permeability with ingoing pressure was attributed to the blockage of channels by the adsorbed film. However it can now be seen that blockage of channels can occur whilst the hydrocarbon permeability remains constant (refer to the triple plots at T/K = 453.2, 423.2 and 393.2, Figures 5.21 to 5.23).

At lower temperatures with greater surface populations a plateau appears in the blockage curve. From the triple plots it can be seen that this plateau exists even though substantial increases in the surface concentration are occurring. Also when the vicinity of the saturated vapour pressure of hydrocarbon is reached the blockage curve rapidly descends to a condition of total blockage. As illustrated in the triple plots at T/K = 233.2 and 218.2 (Figures 5.31 and 5.32) this region corresponds to the rapid increase in the pure hydrocarbon permeability which has been attributed to the transport of capillary condensate. These two effects together create a membrane semi-permeable to the non-sorbed component.

The values of $\tilde{K}_R$ were plotted as a function of the amount adsorbed, v (cm^3 stp g^{-1}) to remove the temperature dependence. It can be seen (Figure 5.33) that the results lie close to a universal curve in the low coverage region, $0 < \frac{v}{cm^3 \text{ stp } g^{-1}} < 10$ but that at higher coverages

Figure 5.33. Variation of $\tilde{K}_R$ with 'v' : He/i-C_4H_{10}/Graphon

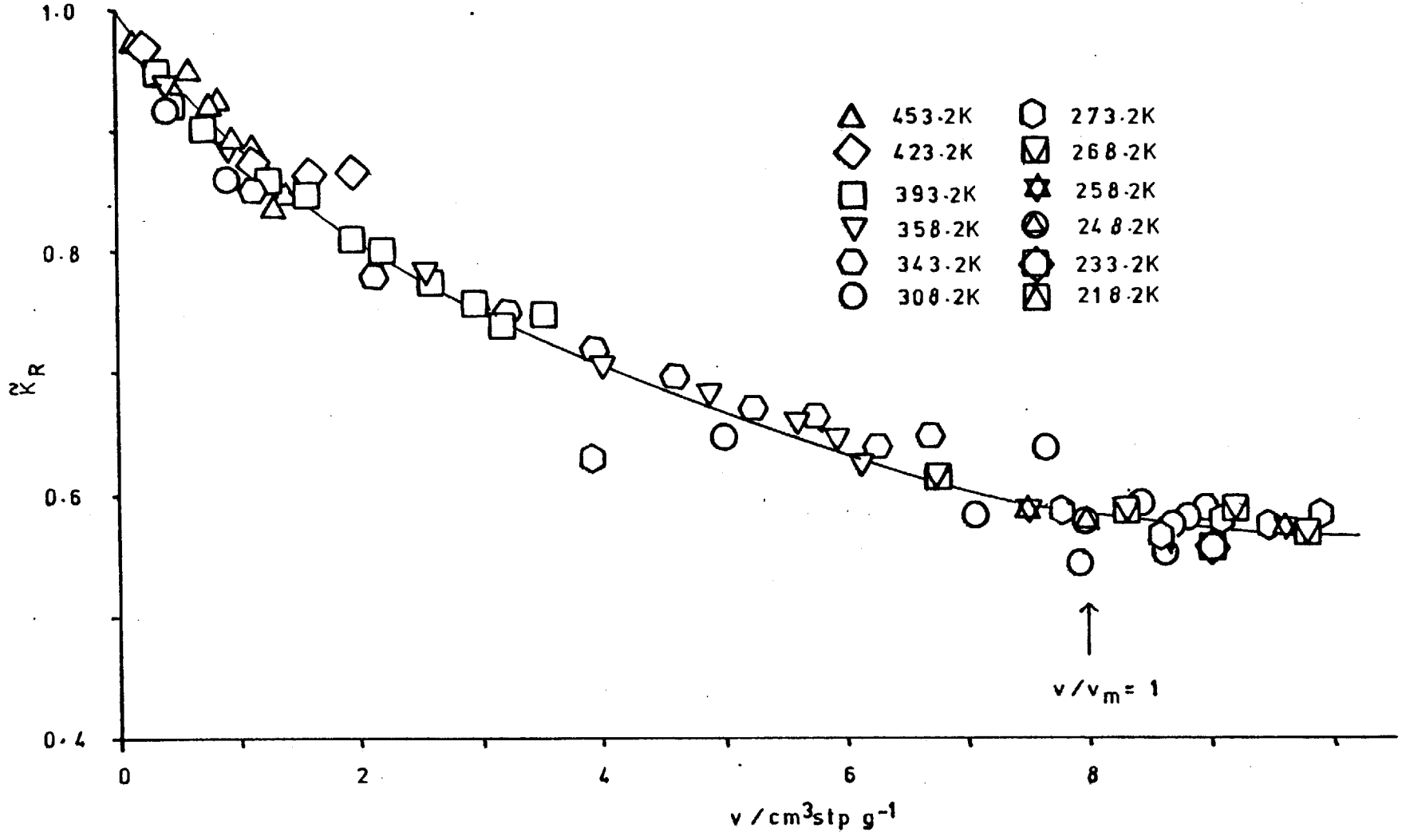

Figure 5.34. Variation of $\tilde{K}_R$ with 'v' : He/i-C_4H_{10}/Graphon

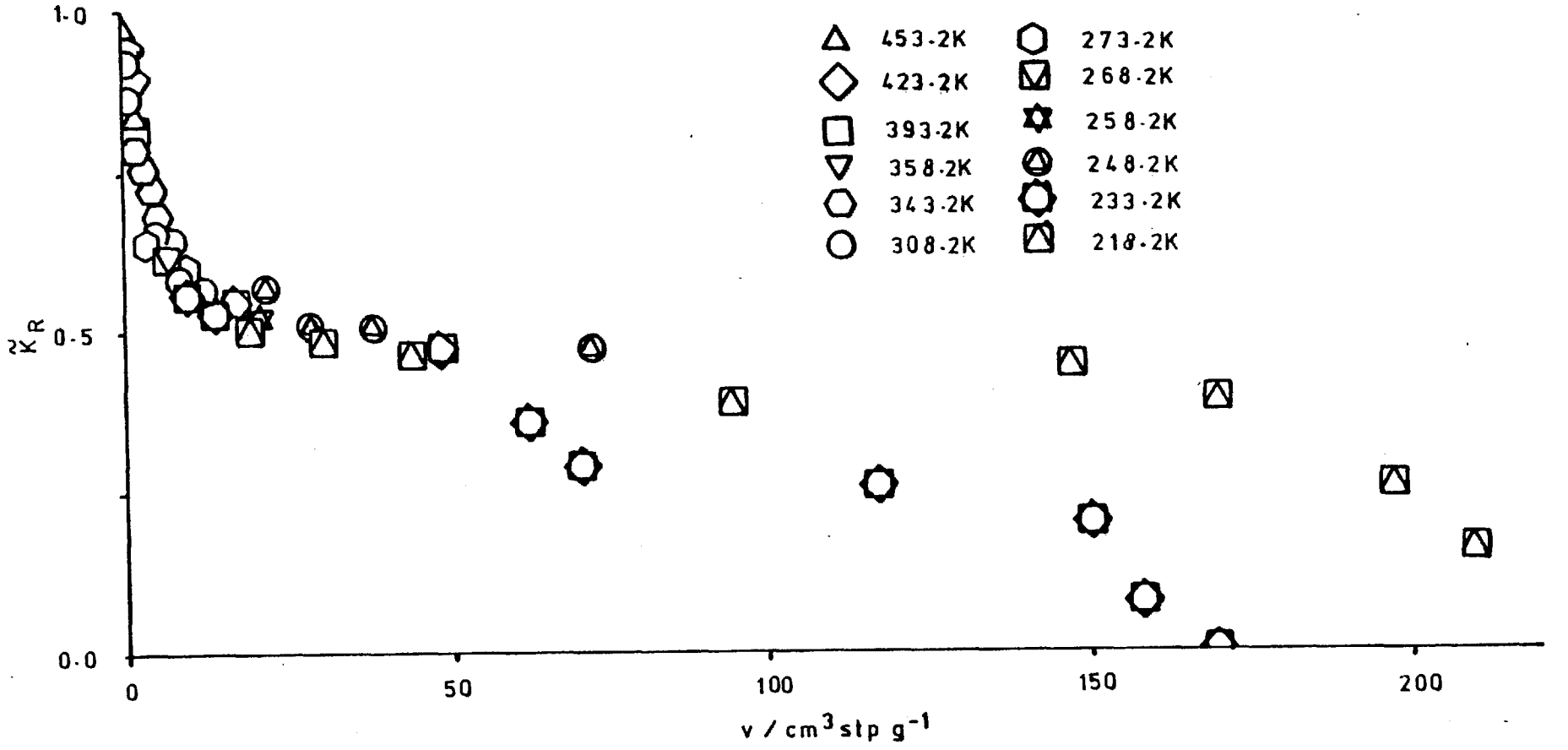

(Figure 5.34) the curve breaks up. The evidence again indicates the presence of key blockage sites in that the helium flow is effectively reduced by 50% when only a monolayer of isobutane has been adsorbed at the ingoing face.

In an effort to improve the universality of the curve at higher coverages the amount adsorbed was converted to a volume of liquid adsorbed, v_ℓ. This includes another temperature dependent variable, the liquid density. Ash, Barrer and Sharma (1976) in a study of helium/hydrocarbon mixture flow through a Carbolac membrane obtained a good universal curve of $\tilde{K}_R$ vs v_ℓ. This removed not only the temperature dependence but also different hydrocarbon results all fell on the same curve. The results for the helium/isobutane/Graphon system are presented in this way in Figure 5.35. It can again be seen that in the region $0.5 < \tilde{K}_R < 1.0$ a good common curve exists, but in the region of high coverages where the idea of the adsorbate as a volume of liquid is most valid the common curve breaks up. In Figure 5.35 the curve decreases immediately from a value of $\tilde{K}_R$ equal to unity. The results of Ash, Barrer and Sharma (1976) do not extrapolate directly back to $\tilde{K}_R = 1$ but the curve contains a turning point. This fits in with the idea of non-blocking with very dilute films. If, however, their results are plotted in the form $\tilde{K}_R$ vs p_1/p_o this turning point disappears (cf §5.2.3(c) and Figure 5.54). An explanation of the poor correlation in both Figure 5.34 and 5.35 at high coverages may be found by recalling the calculations of the change in ingoing composition which occurs throughout the course of an experiment (cf §4.2.3). At high coverages substantial changes of the order of 10% could occur (Table 4.6) which indicate that the apparatus was being employed outside its limits.

A much better correlation was obtained if only the primary data was used and not related to the isotherm data. Figures 5.36 and 5.37 show the variation of $\tilde{K}_R$ for the helium/isobutane/Graphon system with the relative pressure (of isobutane), p_1/p_o. It can be seen that the plateau observed in the initial measurements is no longer eliminated as in the case of the $\tilde{K}_R$ vs v and v_ℓ plots. The initial blockage characteristics are again present at very low relative pressures. This type of plot emphasises the feature that there is relatively minor blockage over the pressure region $0.05 < p_1/p_o < 0.85$ despite the amount

Figure 5.35. Variation of $\tilde{K}_R$ with 'v_ℓ' : He/i-C_4H_{10}/Graphon

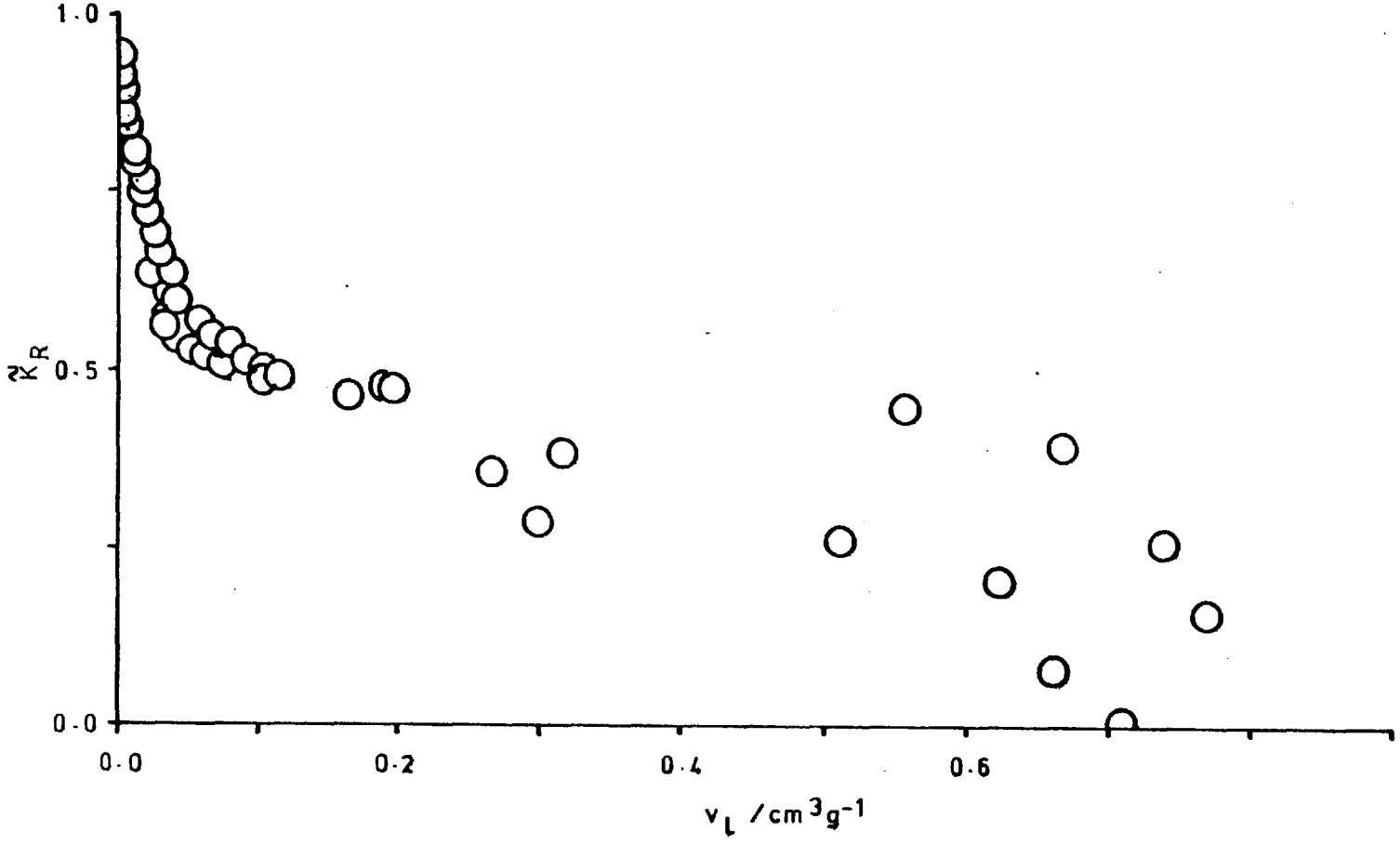

Figure 5.36. Variation of $\tilde{K}_R$ with p_1/p_o : He/i-C_4H_{10}/Graphon

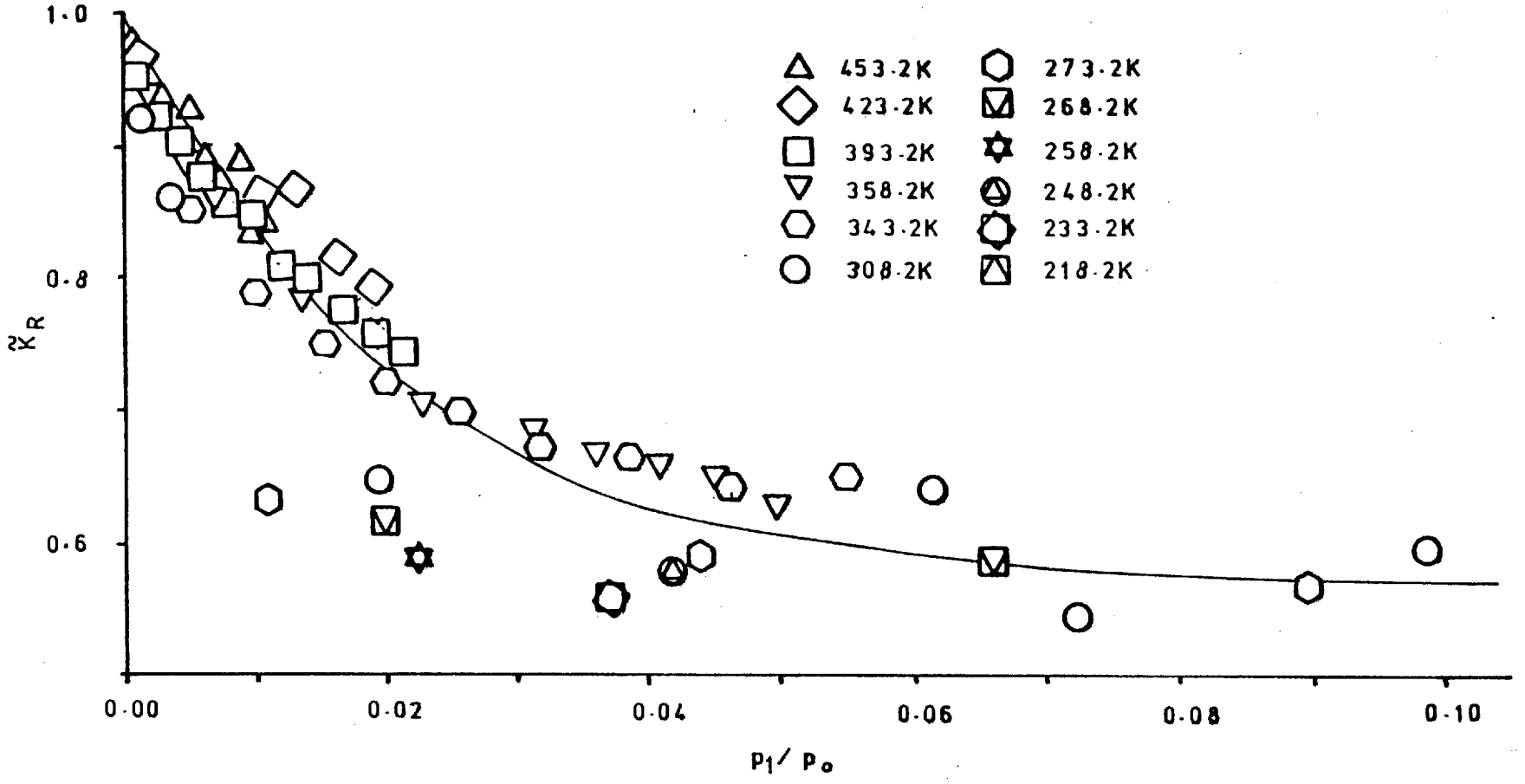

Figure 5.37. Variation of $\tilde{K}_R$ with p_1/p_o : He/i-C_4H_{10}/Graphon

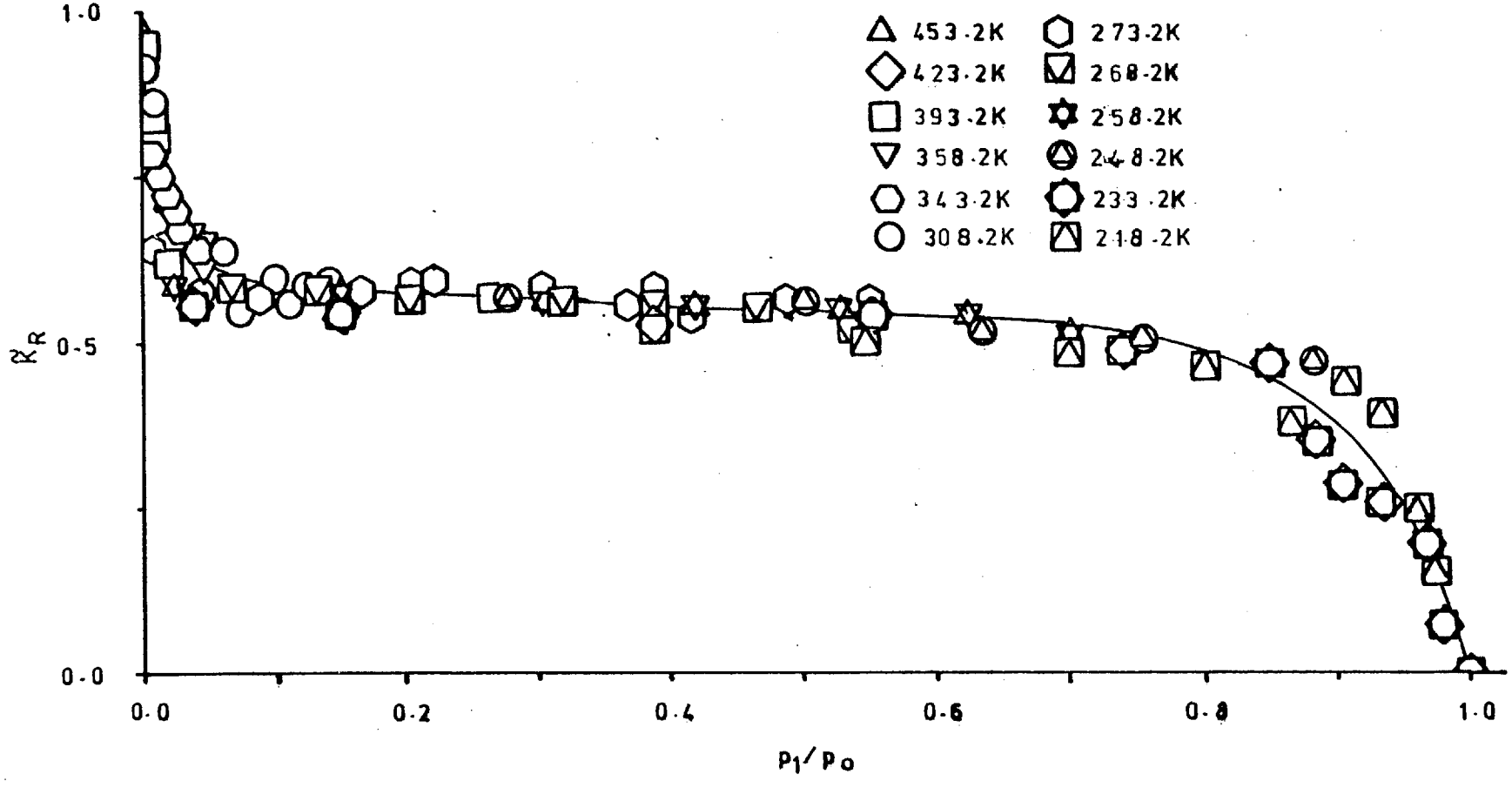

adsorbed for the initial blockage being multiplied by a factor of ~ 3 (cf Figures 5.27 to 5.31). It also emphasises the fact that for this Graphon membrane total blockage only occurs at the saturated vapour pressure of isobutane where presumably bulk condensation takes place.

(c) Helium/propane/Graphon

An interesting feature of the work on Carbolac (Ash, Barrer and Sharma, 1976) was that different hydrocarbons (C_2H_6, C_3H_8, n-C_4H_{10}, neo-C_5H_{12}) all resulted in the same $\tilde{K}_R$ vs v_ℓ blockage curve. To this end measurements were made on the helium/propane/Graphone system and the results are given in Figure 4.45 and the triple plots, Figures 5.38 to 5.41. Figure 5.42 shows the superimposition of the propane mixture measurements on the 'universal' $\tilde{K}_R$ vs p_1/p_o plot resulting from the isobutane mixtures. Several interesting features emerge from the results, the first (and most obvious) being that the propane results do indeed lie upon the $\tilde{K}_R$ vs p_1/p_o plot obtained from the isobutane mixtures (indicating at least a certain degree of universality between hydrocarbons). Secondly, at the higher temperatures (473.2 K and 393.2 K) there is definite Henry Law adsorption, definite blockage and definitely no pressure dependence of the pure propane permeability. This reinforces and indeed improves the idea (implied by the isobutane results) that key blockage sites are present in this Graphon membrane but are not (from the observations of Aylmore and Barrer, 1966; Ash, Barrer and Lowson, 1973) in compacted Carbolac membranes.

(d) Argon/isobutane/Graphon

The argon/isobutane/Graphon system was also studied. Argon flow through Graphon has previously been examined (Ash, Baker and Barrer, 1967) and the presence of an extra flow associated with the adsorbed film detected (over the temperature range 153 K to 323 K the ratio $\tilde{K}_s/\tilde{K}_g$ varied from 12.1 to 1.5). It was of interest to consider the effect of an adsorbed film on the total flow of the argon. The argon permeability in the presence of an adsorbed layer of isobutane was converted to an equivalent helium permeability by the relationship :

$$\tilde{K}_{He} = \tilde{K}_{Ar}\sqrt{\frac{M_{Ar}}{M_{He}}} \quad \text{at constant } T \qquad (5.8)$$

Figure 5.38. Triple Plot : C_3H_8/Graphon : T/K = 473.2

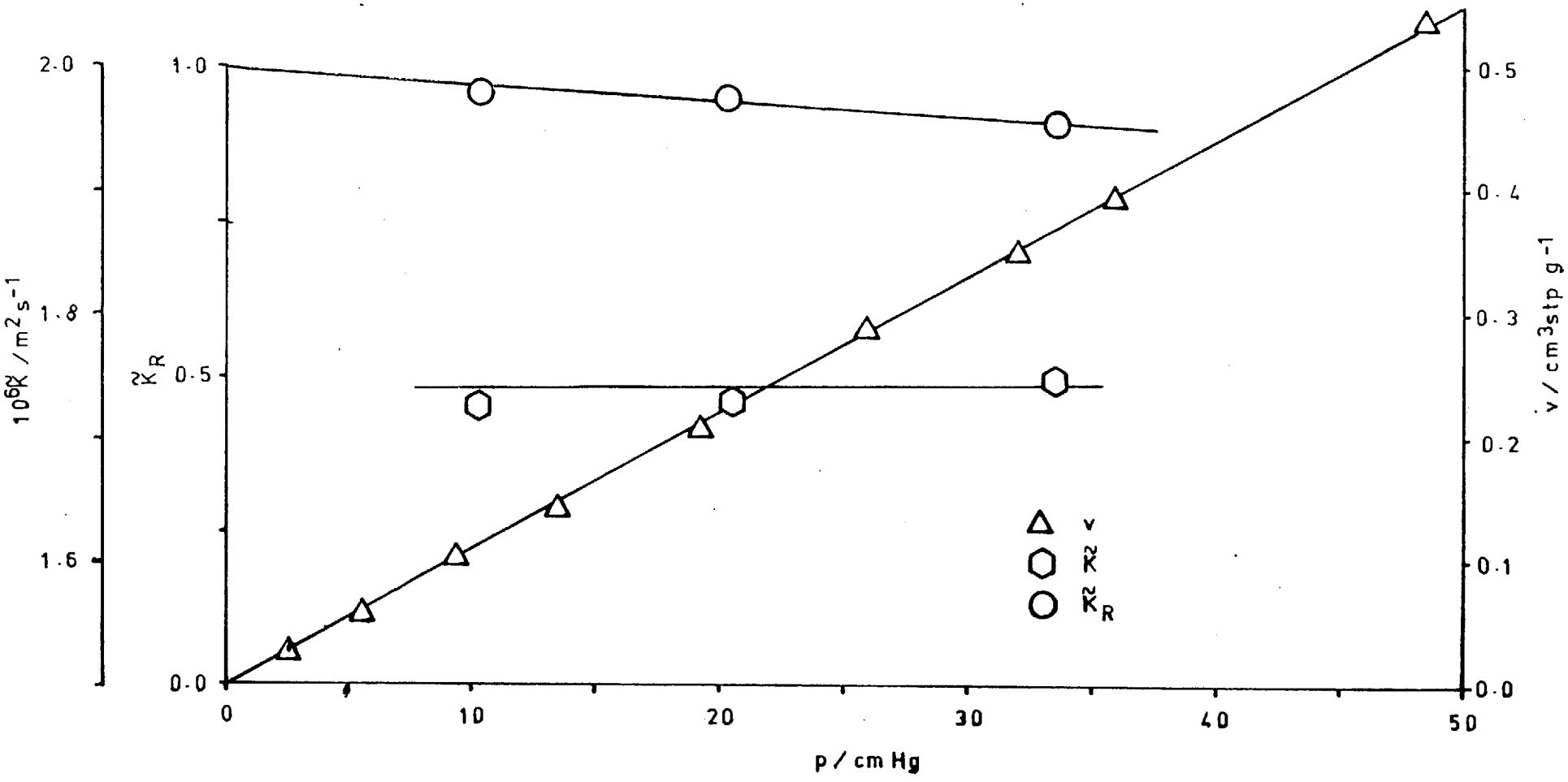

Figure 5.39. Triple Plot : C_3H_8/Graphon : T/K = 393.2

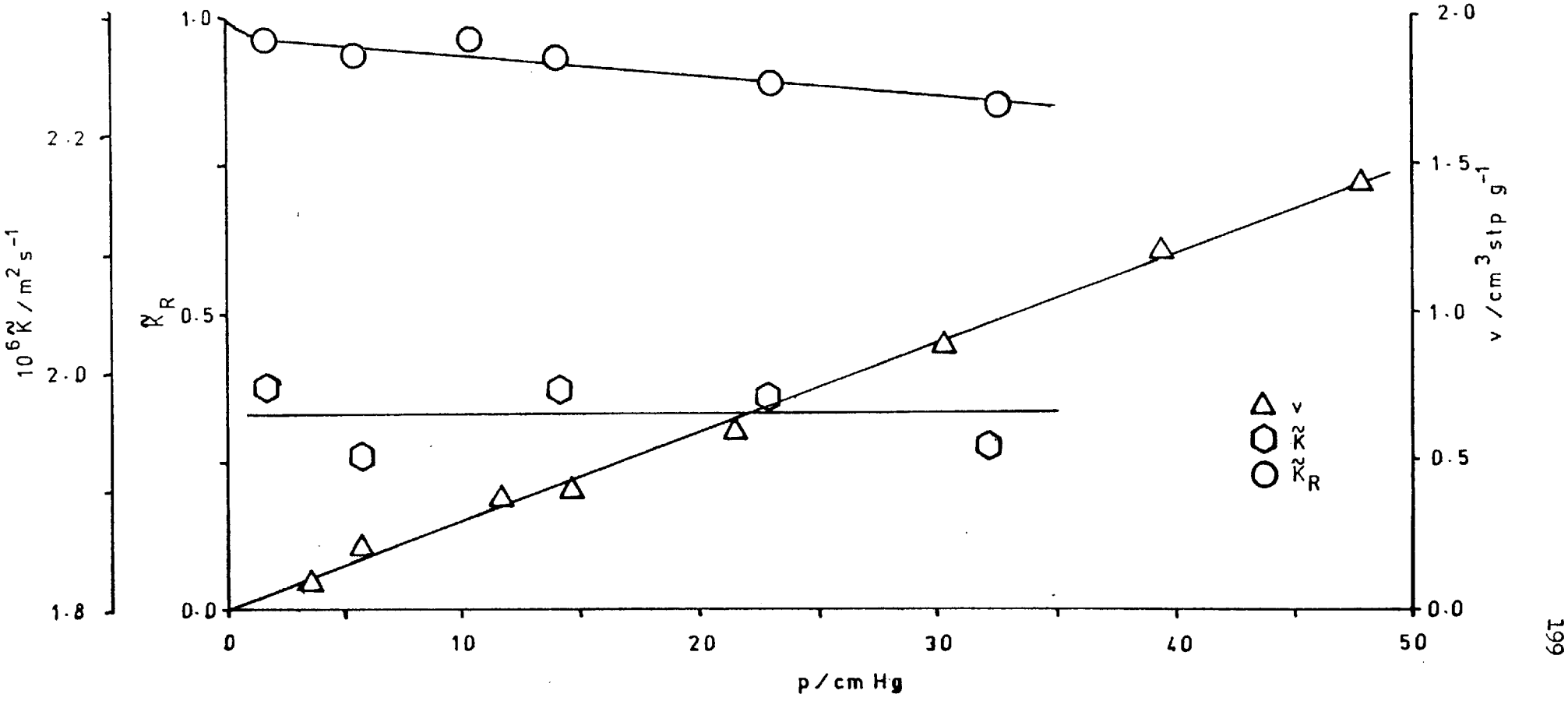

Figure 5.40. Triple Plot : C_3H_8/Graphon : T/K = 243.2

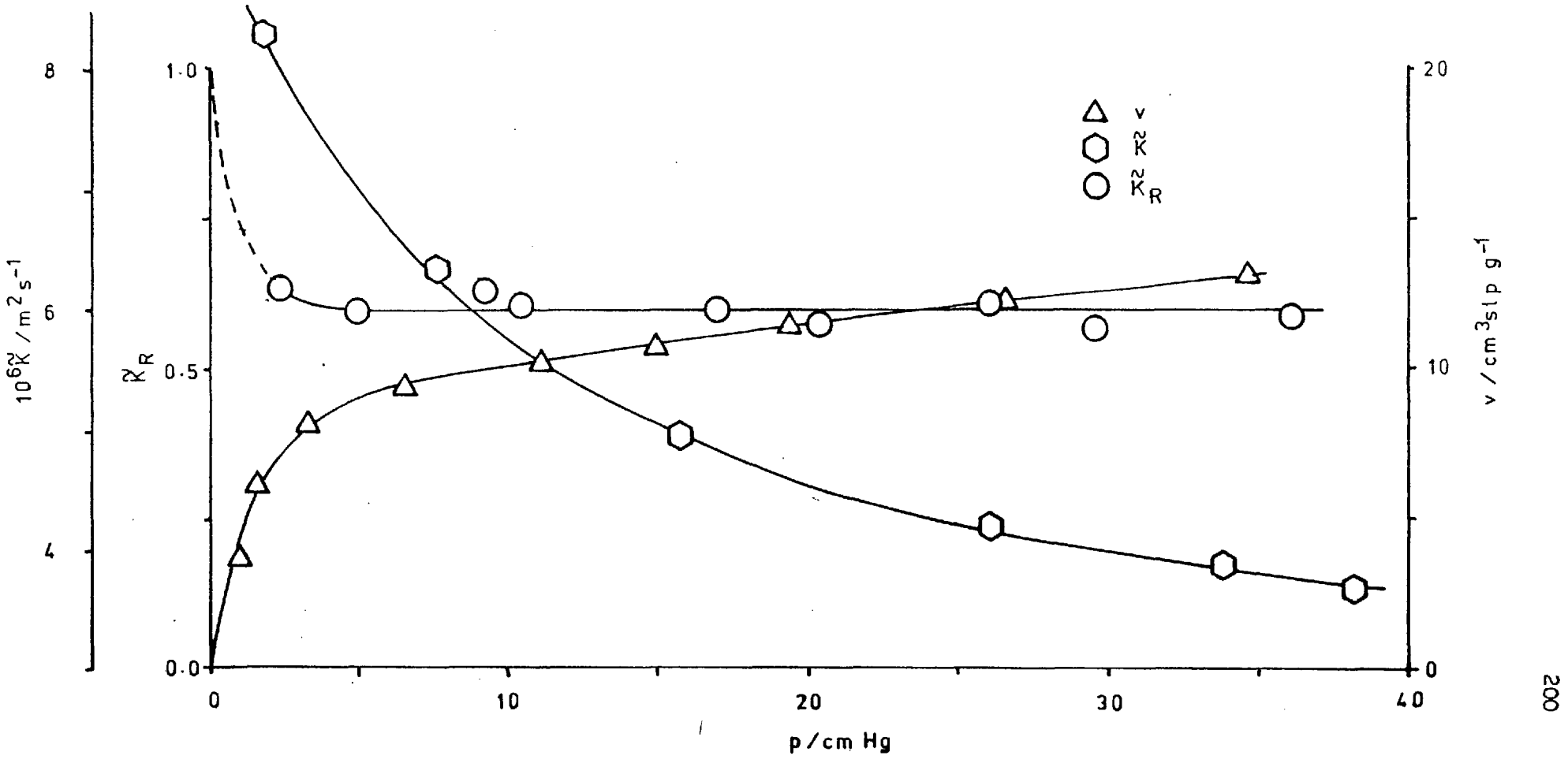

Figure 5.41. Triple Plot : C_3H_8/Graphon : T/K = 213.2

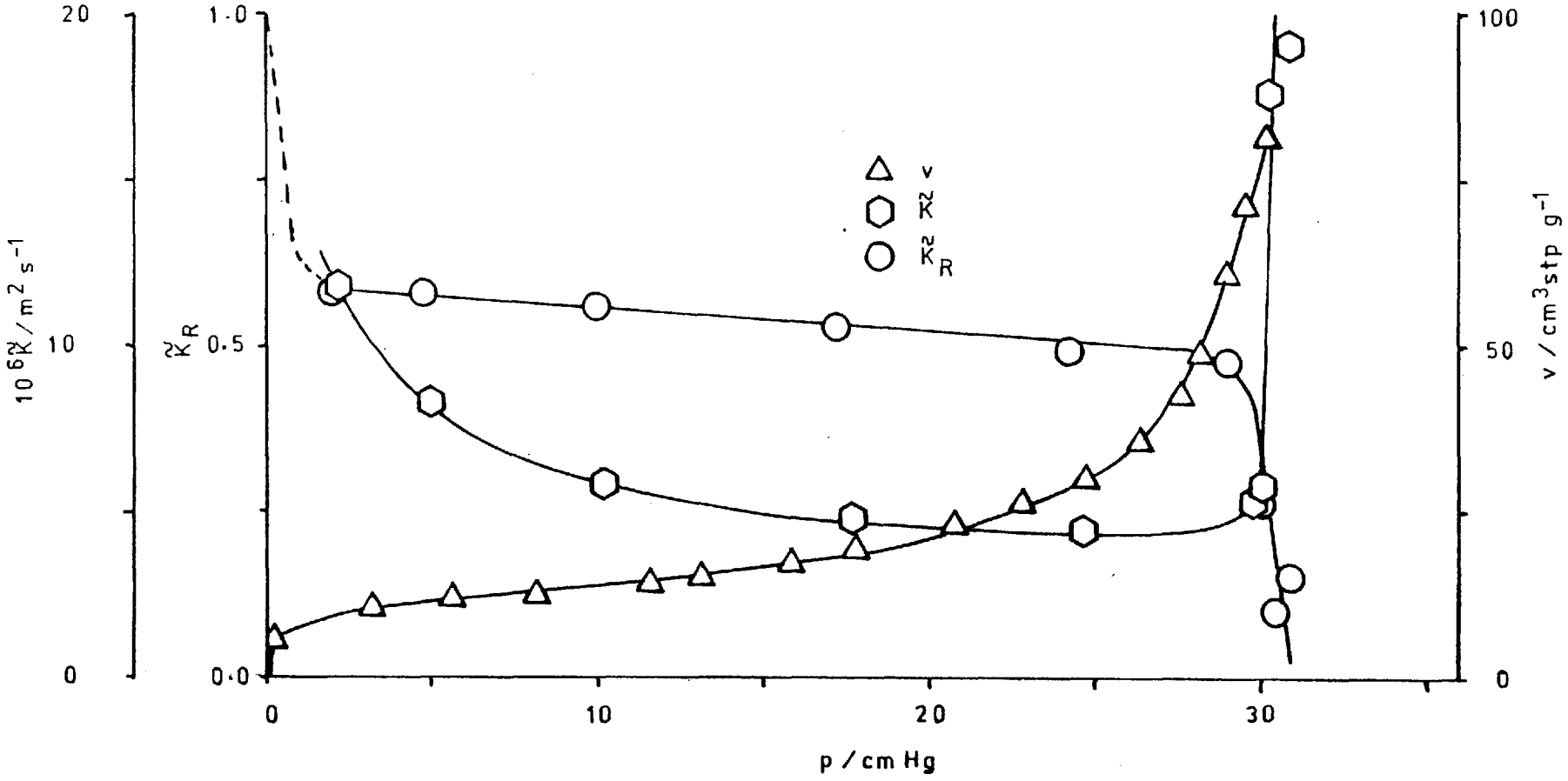

Figure 5.42. Variation of $\tilde{K}_R$ with p_1/p_o : He/C_3H_8/Graphon

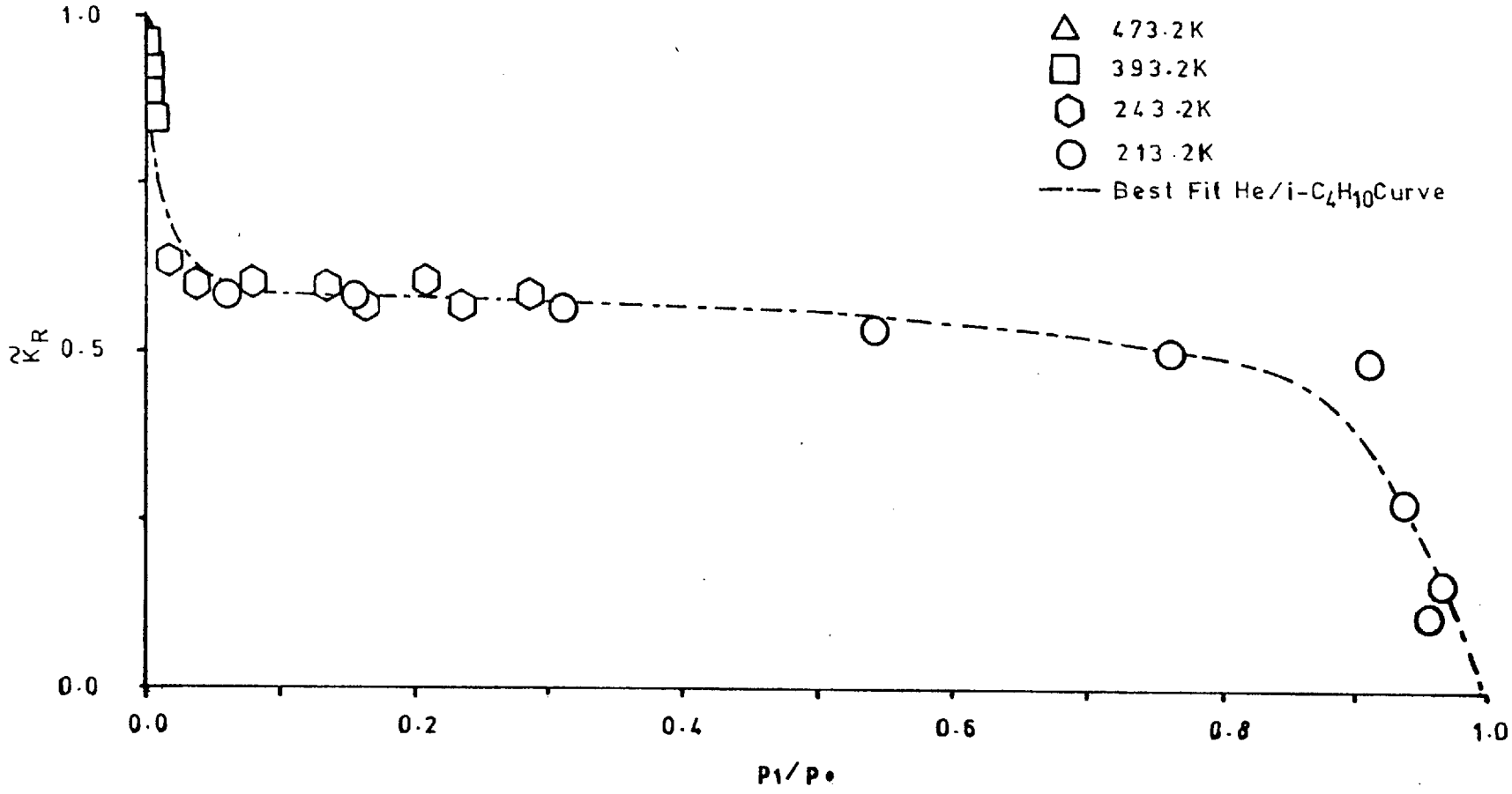

This assumes that the argon flow is purely in the gas phase. The converted argon permeability is then expressed as a relative helium permeability, $\tilde{K}_R$ and the comparative blockage curves are given in Figures 4.49 to 4.53. It can be seen that the blockage curves resulting from the argon measurements lie above those for the helium mixtures. This is due to the extra flow component of the argon raising the curve above that for purely gas phase flow. One would expect this contribution to increase as the temperature decreases due to increased argon adsorption, but in fact it is most evident at the higher temperatures (cf Figure 5.43). This behaviour can be easily understood due to competitive adsorption of isobutane which should increasingly restrict the argon adsorption as the temperature decreases. Eventually the extra flow component due to argon adsorption should become neglgible and the blockage curve assume the normal slope for pure gas flow, as indicated by the helium results. This is in fact observed for the argon/isobutane mixture at 233.2 K (Figure 4.53).

As the steady-state ingoing pressure of isobutane tends to zero at a given temperature an equilibrium amount of argon will be adsorbed and a certain total flow exist; the magnitude of which should increase as the temperature decreases. [The permeability of argon through Graphon has been found to be independent of pressure in the temperature range 195 K < T < 323 K (Ash, Baker and Barrer, 1967)]. This may also be seen from the blockage curves, as $p_1 \Rightarrow 0$ the value of $\tilde{K}_R$ increases as the temperature decreases. The rate at which this value of $\tilde{K}_R$ decays also increases as the temperature decreases and the isobutane adsorption increases. This may be seen in Figure 5.43 where $\Delta\tilde{K}_R$ ($= \tilde{K}_R^{Ar} - \tilde{K}_R^{He}$) is given as a function of temperature and pressure of isobutane.

The pure hydrocarbon isotherms, and in some cases the argon isotherms to the nearest temperature are included in the figures. [The argon isotherms were obtained by Baker (1966)]. It can be seen that at the higher temperatures in the vicinity of Henry Law adsorption for isobutane and definite Henry Law adsorption of argon the argon permeability is affected (Figure 4.49). This again affords evidence contrary to that of Aylmore and Barrer (1966), Ash, Barrer and Lowson (1973) for weakly adsorbed mixtures flowing through Carbolac, where the permeability is "characteristic for each gas; independent of the

Figure 5.43. Variation of $\Delta\tilde{K}_R$ ($= K_R^{Ar} - K_R^{He}$) with p_1 ($i\text{-}C_4H_{10}$) : Graphon

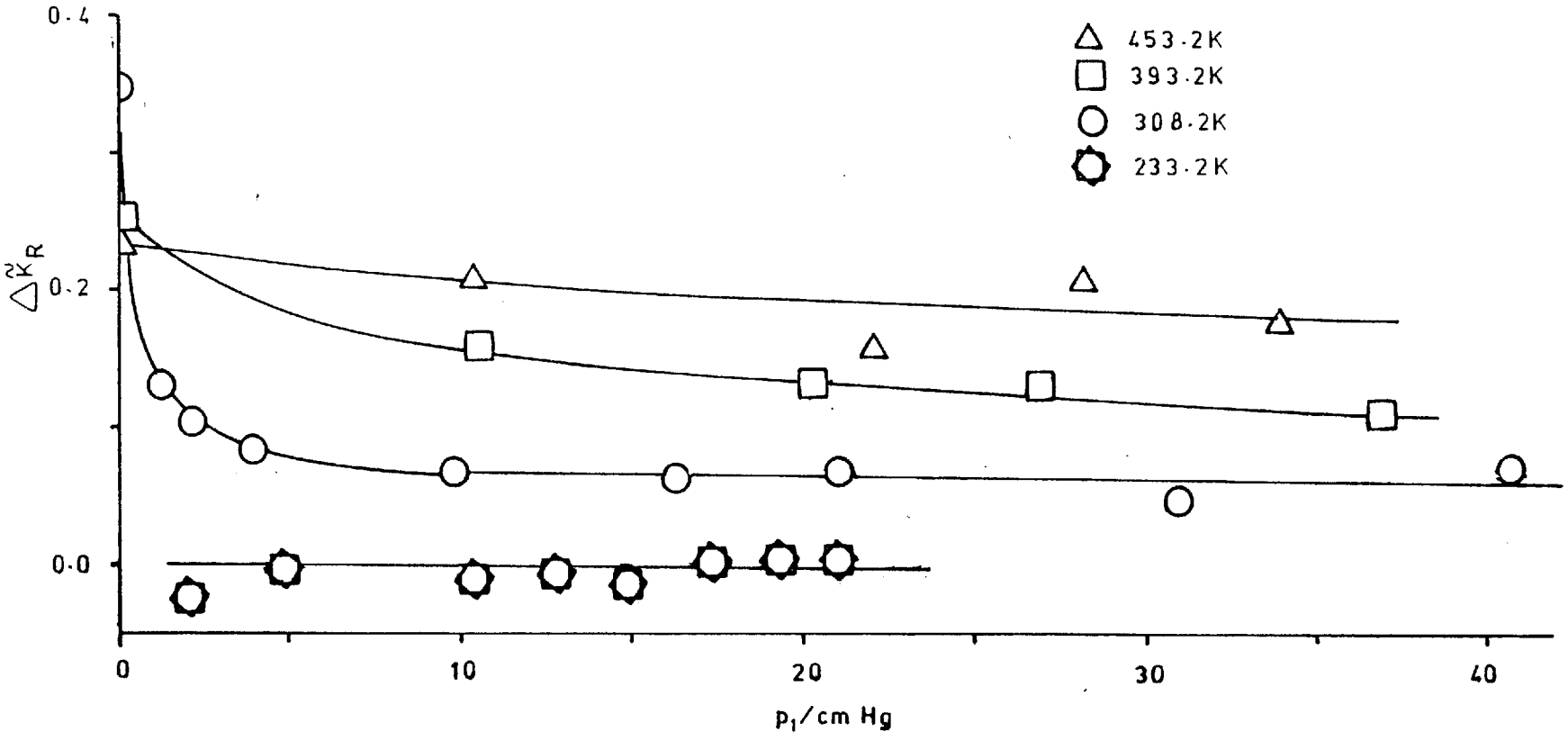

amount adsorbed and therefore of whether the isotherm obeys Henry's Law or is curved; and unaltered when there is a second flowing, adsorbed species competing for the same surface".

The extra flow component of the argon (indicated by the distance between the two blockage curves at a given pressure) at a given temperature can be seen to diminish to a constant value which, as the temperature decreases tends to zero (cf. Figure 5.43). A possible explanation is as follows. In the membrane there will exist a concentration gradient of hydrocarbon occupying key adsorption sites at the ingoing face. Further into the membrane these sites may become vacant and available for argon adsorption which in turn will promote a certain degree of extra flow. This certain degree will be a constant for the equilibrium concentration profiles of both hydrocarbon and argon in the membrane, i.e. constant for a given temperature. In other words, flux interconversion of the argon occurs with increasing distance into the membrane as J_{oo} ($= J_s + J_g$) must be constant for steady-state flow.

A study of weakly adsorbed gas mixtures of similar sorbabilities, such as that of Aylmore and Barrer (1966) for Carbolac should be undertaken for Graphon. This study, although under certain conditions both components are Henry Law adsorbed is still concerned with one strongly and one weakly adsorbed component, (cf. Figures 4.49 to 4.53 and the absolute adsorption values). Evidence has been provided for a reduction in both components of argon flow by an adsorbed layer of hydrocarbon (assuming that the gas phase flow is that described by the converted helium permeability). This appears to contrast strongly with earlier observations using a Carbolac membrane.

(e) Helium/isobutane/Black Pearls

As the results obtained for the Graphon membrane appeared quite different to those previously measured on Carbolac membranes, the study was extended to include the carbon 'graphitised Black Pearls' with an intermediate surface area. The results are again presented in the form $\tilde{K}_R$ vs p_1 (Figure 4.48) and in the triple plots (Figures 5.44 to 5.47) for the temperatures T/K = 343.2, 308.2, 273.2 and 233.2.

Although Henry Law adsorption is not occurring at 343.2 K it is still obvious that blockage of the gas phase does occur as soon as

Figure 5.44. Triple Plot : i-C_4H_{10}/Black Pearls : T/K = 343.2

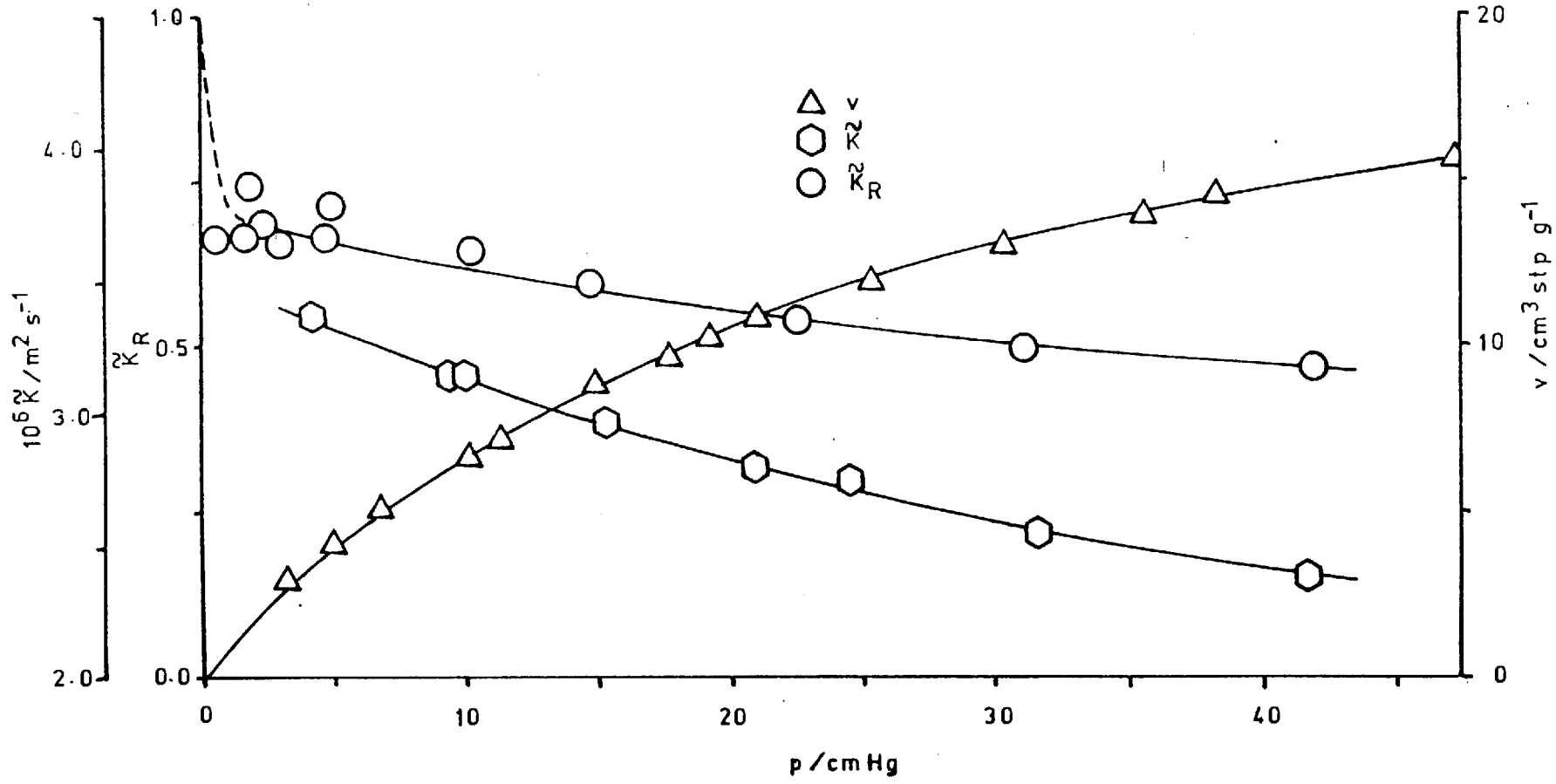

Figure 5.45. Triple Plot : i-C_4H_{10}/Black Pearls : T/K = 308.2

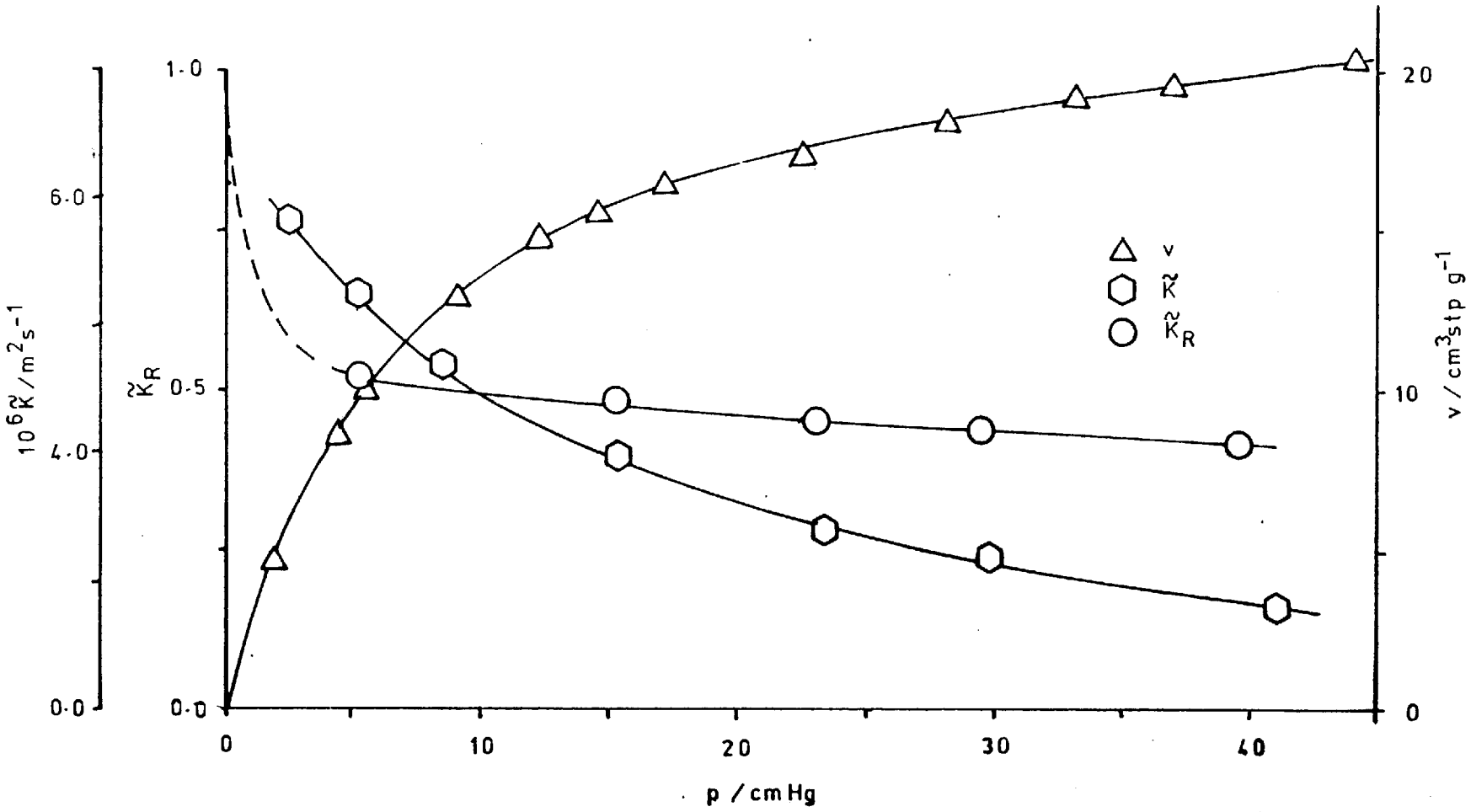

Figure 5.46. Triple Plot : i-C_4H_{10}/Black Pearls : T/K = 273.2

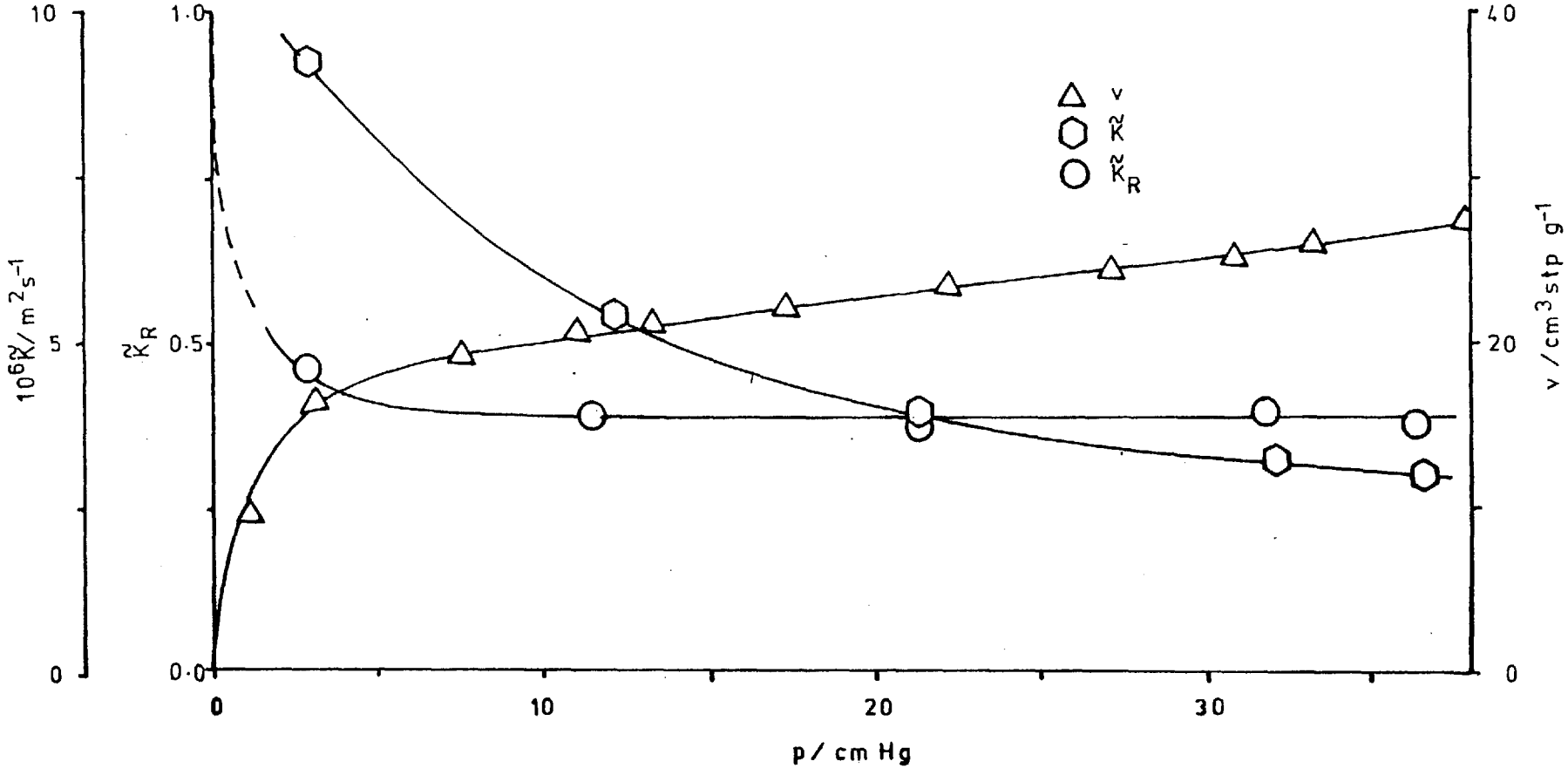

Figure 5.47. Triple Plot : i-C_4H_{10}/Black Pearls : T/K = 233.2

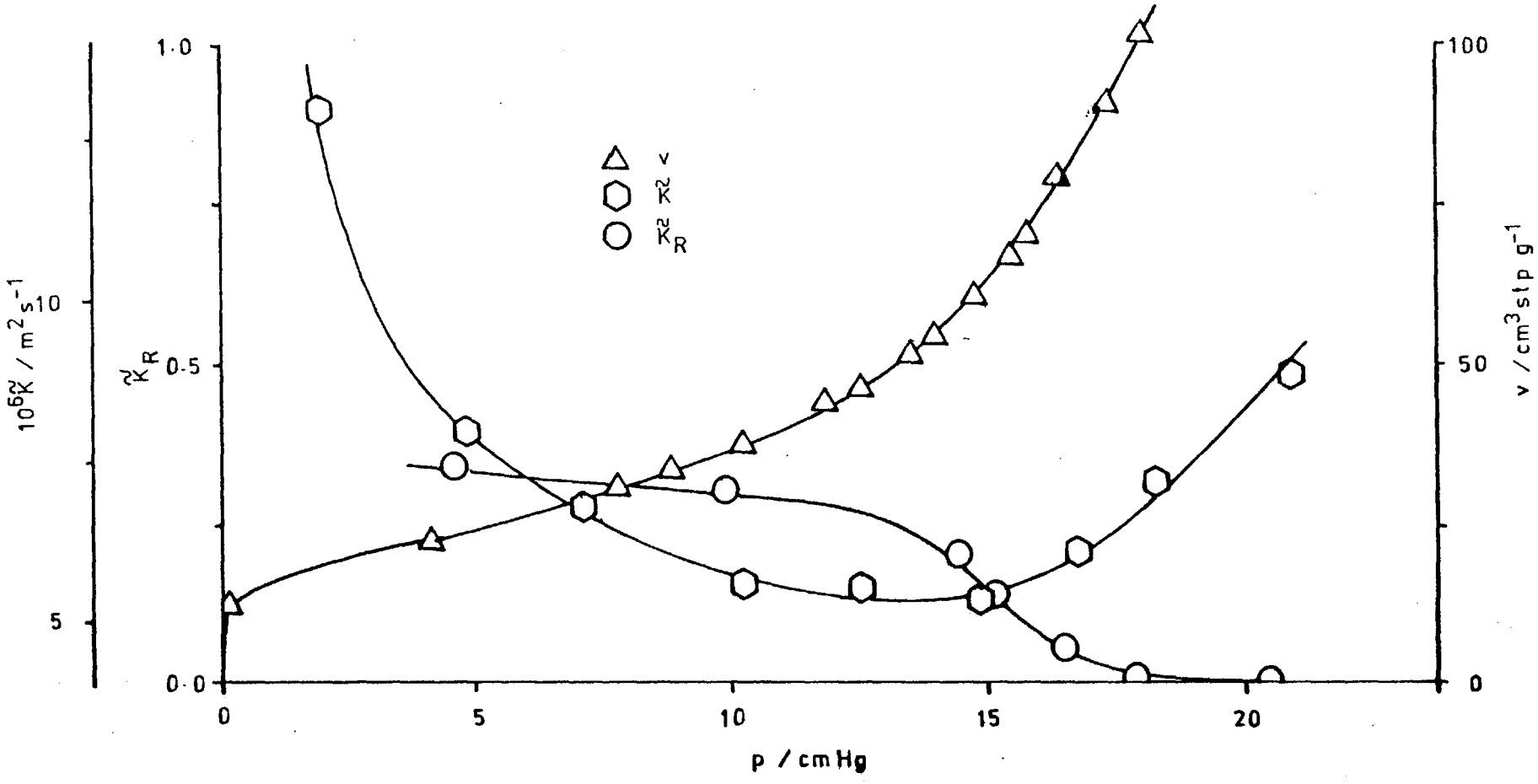

Figure 5.48. Variation of $\tilde{K}_R$ with p_1/p_o : He/i-C_4H_{10}/Black Pearls

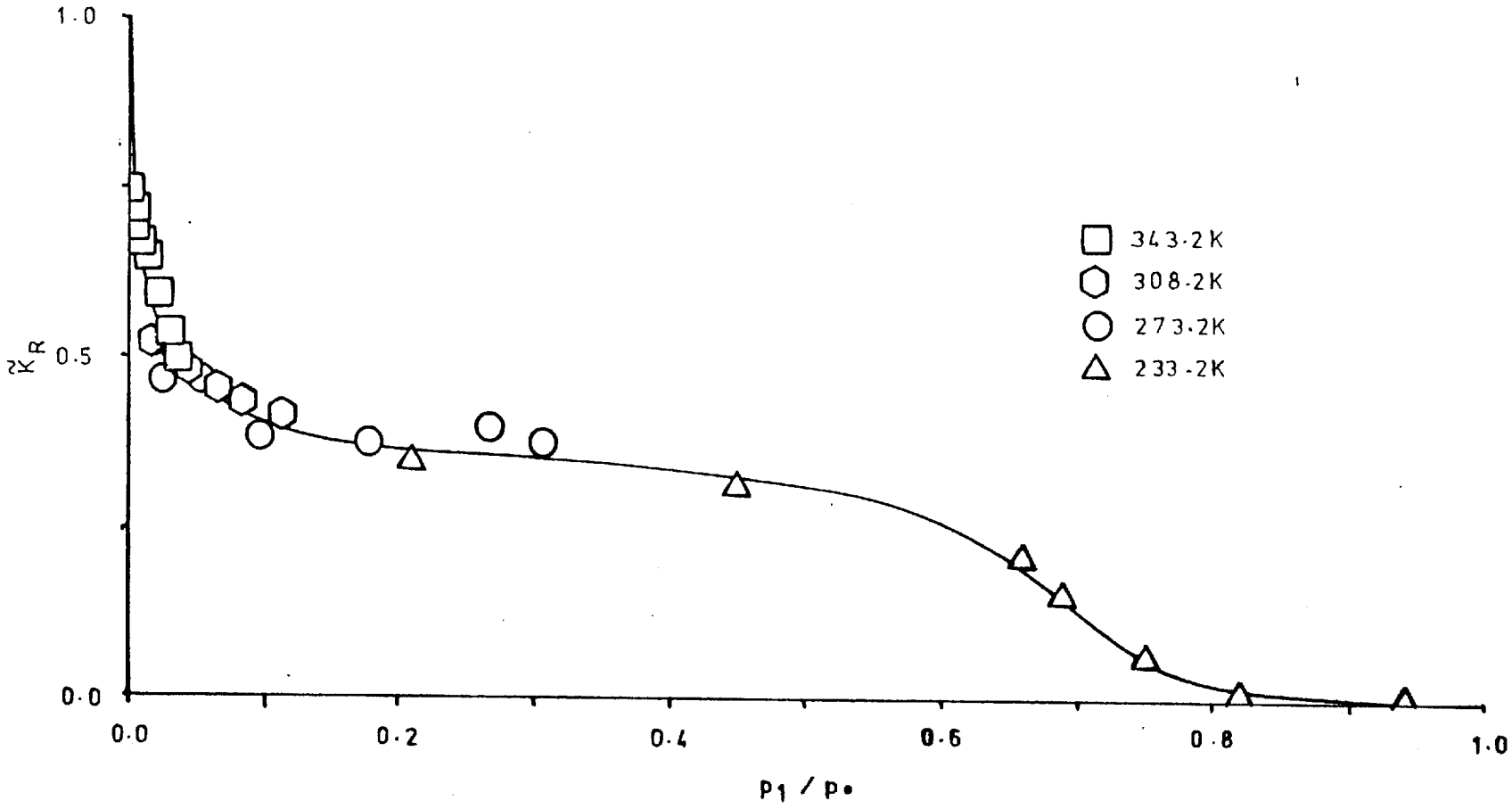

adsorption takes place. This is further substantiated by the correlating $\tilde{K}_R$ vs p_1/p_o plot (Figure 5.48) where the curve can be seen to extrapolate, without a turning point back to the value of $\tilde{K}_R = 1.0$ at $p_1/p_o = 0$. This type of behaviour, similar to that of Graphon is again contrasting those results on Carbolac.

As in the Graphon results there is a plateau (at $\tilde{K}_R \simeq 0.4$) after an initial sharp drop in the relative permeability over a relatively small p_1/p_o range. However in contrast to Graphon the plateau does not extend up to the vicinity of the saturated vapour pressure but instead a condition of total blockage occurs at p_1/p_o values of ~ 0.8.

(f) Helium/propane/Black Pearls

The blockage results are shown in Figures 4.47 and 5.49, 5.50. It can be seen that similar behaviour to the isobutane mixtures is obtained and in fact the propane mixture results are again correlated by the $\tilde{K}_R$ vs p_1/p_o plot (Figure 5.51). A plot of $\tilde{K}_R$ vs v is given in Figure 5.52 for both the isobutane and propane measurements. Similar to the work on Graphon the initial sharp drop is evident followed by a slow decrease to $\tilde{K}_R = 0$ at high coverages. After the initial rapid blockage, which is attributed to key site adsorption a plateau arises in both Graphon and Black Pearls. The plateau corresponds to a period of adsorption during which minimal further blockage arises. This is indicative of a system of fairly wide channels with a number of narrow constrictions which can greatly affect the non-sorbed gas flow if blocked. After initial adsorption at the key constrictions adsorption can occur in channels without affecting the gas flow. Eventually multilayer adsorption and capillary condensation commences in channels of suitable dimensions and blockage affects again arise.

(g) Blockage Behaviour of Different Membranes

The flow of gas mixtures through porous membranes has only received minor attention in the past and studies (utilizing the extra flow component) into separations of components are even more limited. Porous glass has been used to separate the components of a propane/carbon dioxide mixture (Kammermeyer and Wyrick, 1958) and previous work in these laboratories has considered several gas mixtures with Carbolac membranes (Ash, Barrer and Pope, 1963(b); Aylmore and Barrer, 1966; Ash, Barrer and Lowson, 1973; Ash, Barrer and Sharma, 1976).

Figure 5.49. Triple Plot : C_3H_8/Black Pearls : T/K = 273.2

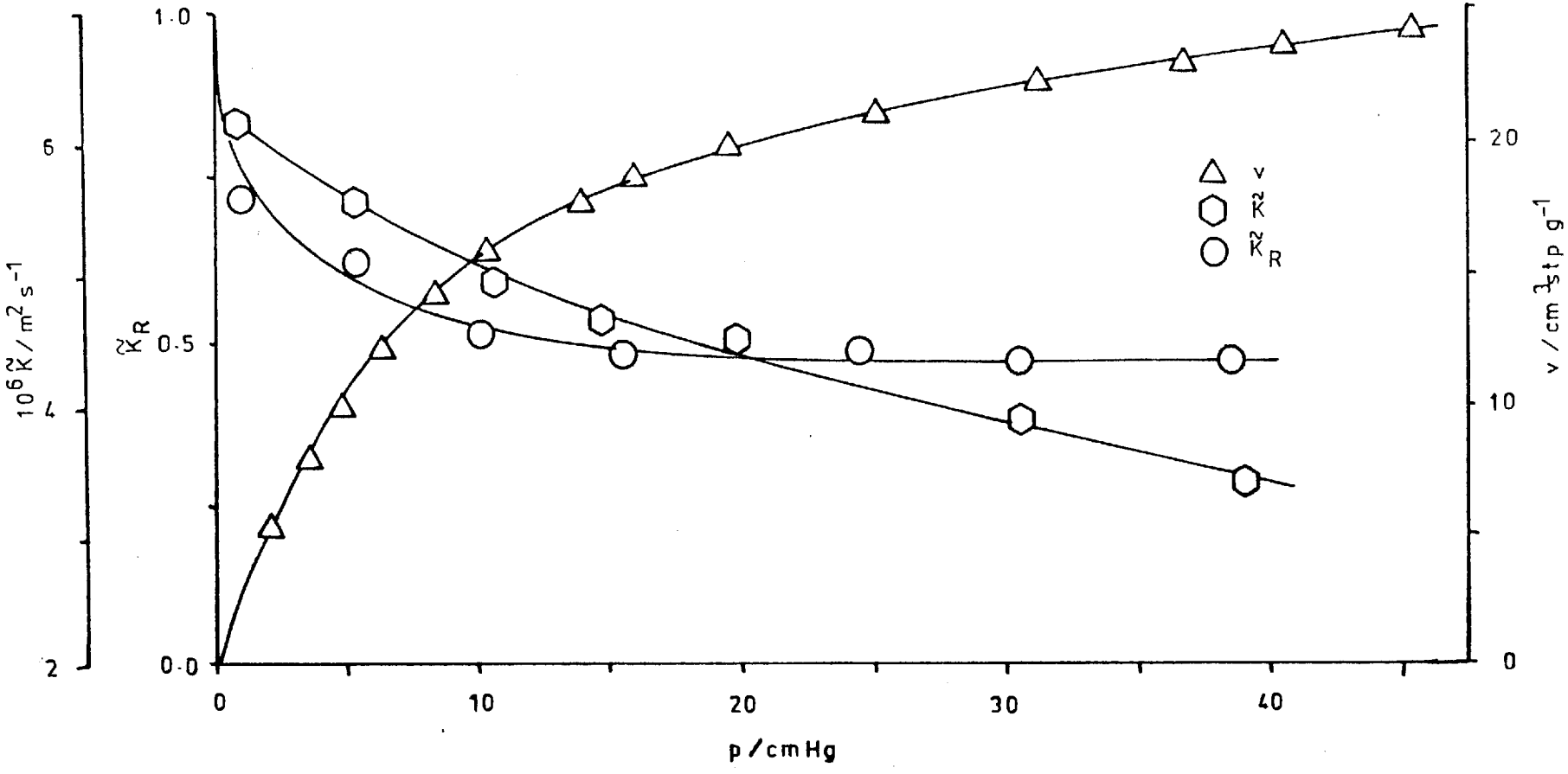

Figure 5.50. Triple Plot : C_3H_8/Black Pearls : T/K = 213.2

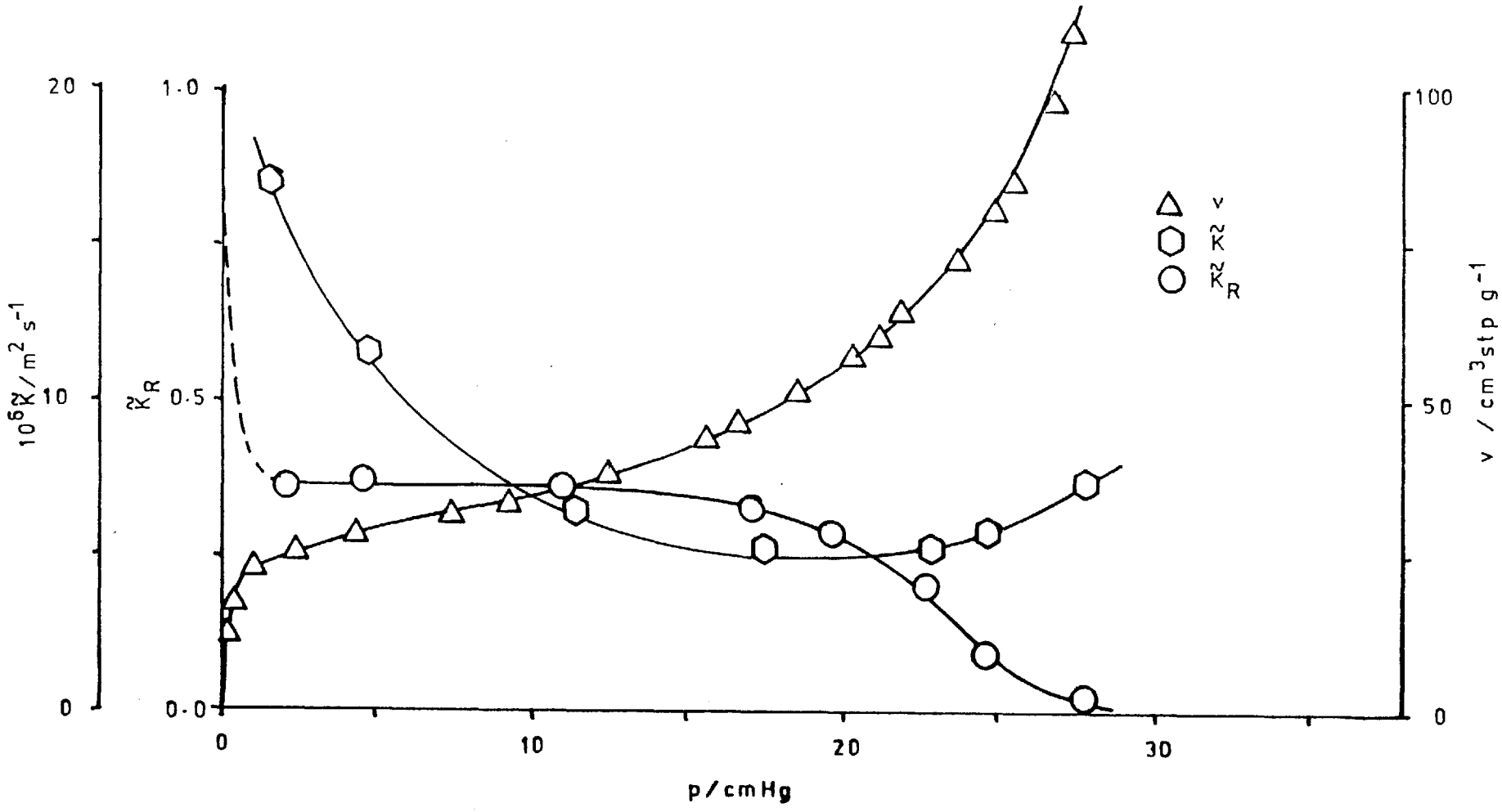

Figure 5.51. Variation of $\tilde{K}_R$ with p_1/p_o : He/C_3H_8/Black Pearls

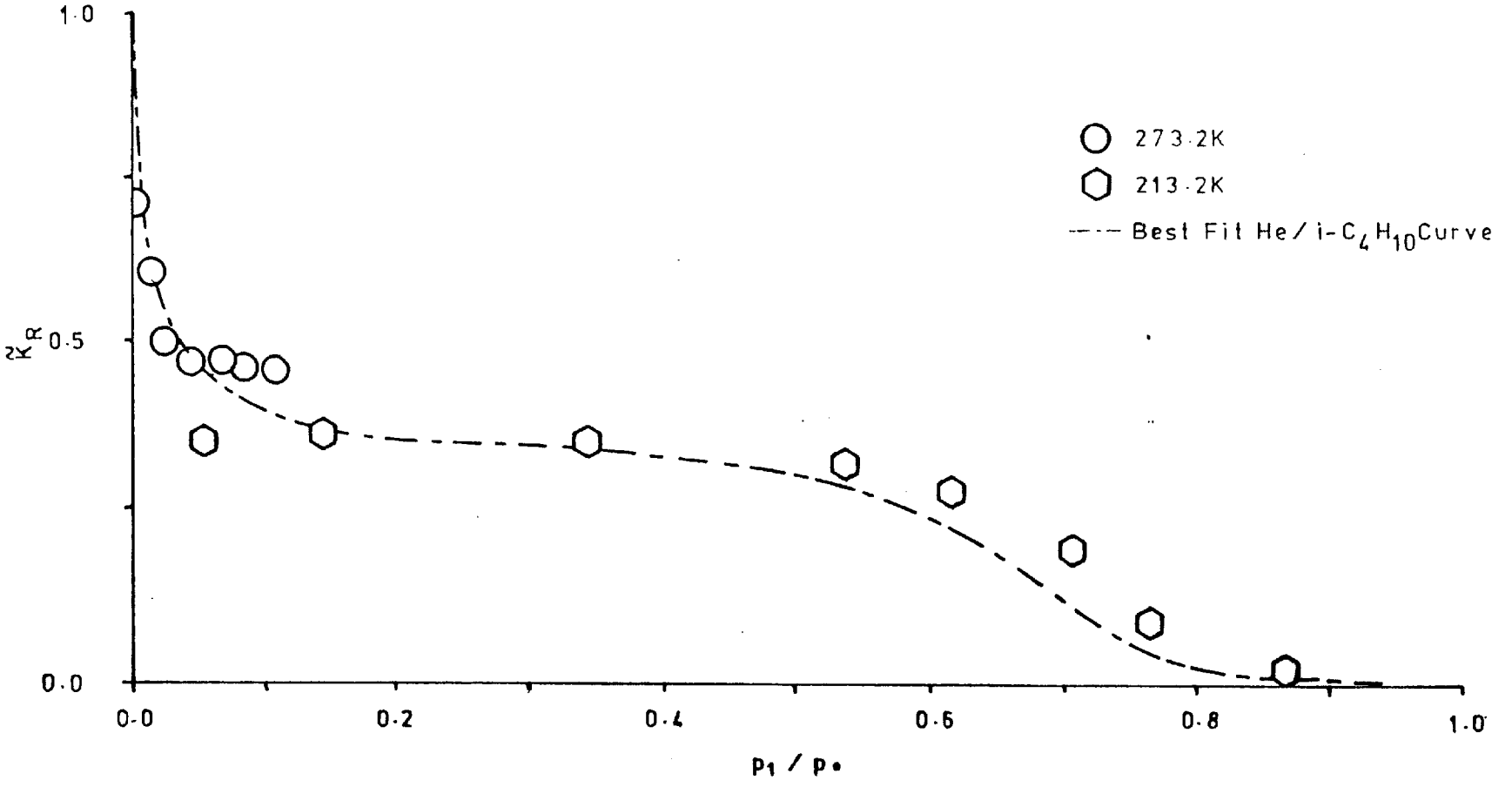

Figure 5.52. Variation of $\tilde{K}_R$ with v : He/C_3H_8/Black Pearls

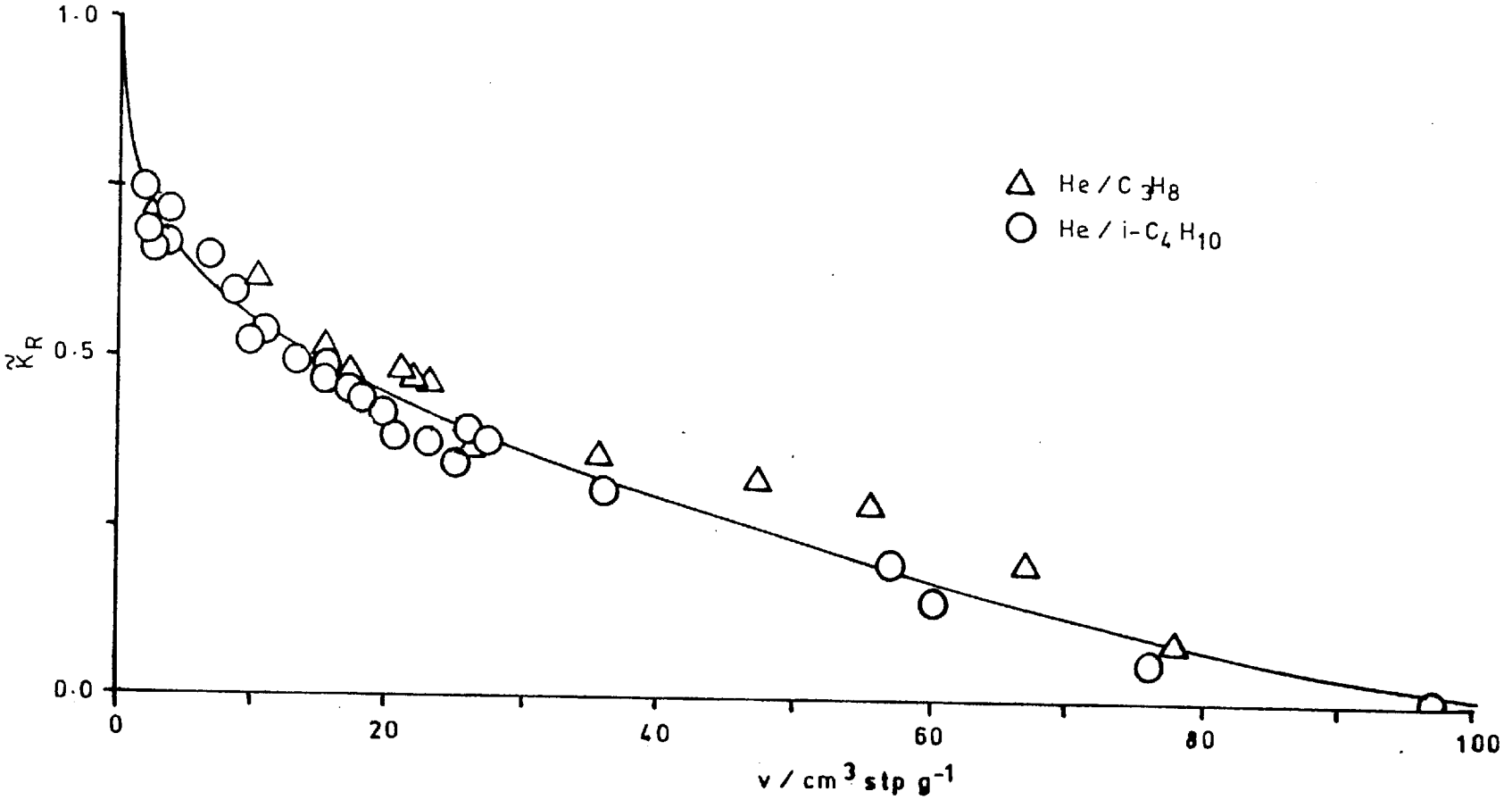

In this work the effect of an adsorbed film of hydrocarbon upon the flow of a non-sorbed indicator gas through Graphon and Black Pearls membranes has been studied. The previous study most comparable is that of Ash, Barrer and Sharma (1976) with the flow of hydrocarbon/helium mixtures through Carbolac. It must be noted that 'pressure decay' techniques were used, but as is shown later (§5.3.3) this does not appear to significantly alter the blockage curves.

In Figure 5.53 a comparison is made between the $\tilde{K}_R$ vs p_1/p_o plots for the different carbons with their respective hydraulic radii (ϵ/A) given. The results for Carbolac are those calculated and replotted from the work of Sharma (1970). If plotted in the p_1/p_o form the curve does not exhibit the turning point found in the $\tilde{K}_R$ vs v_ℓ curve of Ash, Barrer and Sharma (1976). The turning point in their curve supported the idea of non-blockage in the Henry Law region following the work of Aylmore and Barrer (1966). However upon recalculation it was found that one of the key points was plotted incorrectly and that in reality a fair fit curve could be drawn extrapolating back directly to $\tilde{K}_R = 1.0$ without the presence of a turning point (both curves are given in Figure 5.54). It is suggested that perhaps the authors were being influenced to a certain extent by what was expected at that time when constructing the $\tilde{K}_R$ vs v_ℓ curve of Ash, Barrer and Sharma (1976). However the evidence presented in the $\tilde{K}_R$ vs p_1/p_o curves does infer that initial blockage of key sites occurs for the carbons, Graphon, Black Pearls and Carbolac. The indications are that even at very low coverages in the Henry Law region of adsorption there is still substantial blockage of a non sorbed internal indicator gas by the strongly sorbed hydrocarbon for each type of carbon membrane.

It can be seen from Figure 5.53 that a graduation in the shape of the blockage curve exists. Total blockage occurs soonest in the carbon with the lowest ϵ/A. As the value of the hydraulic radius increases the appearance of a plateau emerges, a region where only a minimal increase in blockage takes place with a substantial increase in amount adsorbed. It is not possible to conclude a great deal from the change in the blockage curve with ϵ/A due to the apparent 'universality' of each curve to different hydrocarbons. The Carbolac data covered the

Figure 5.53. Variation of $\tilde{K}_R$ with p_1/p_o : He/hydrocarbon/Carbolac, Black Pearls, Graphon

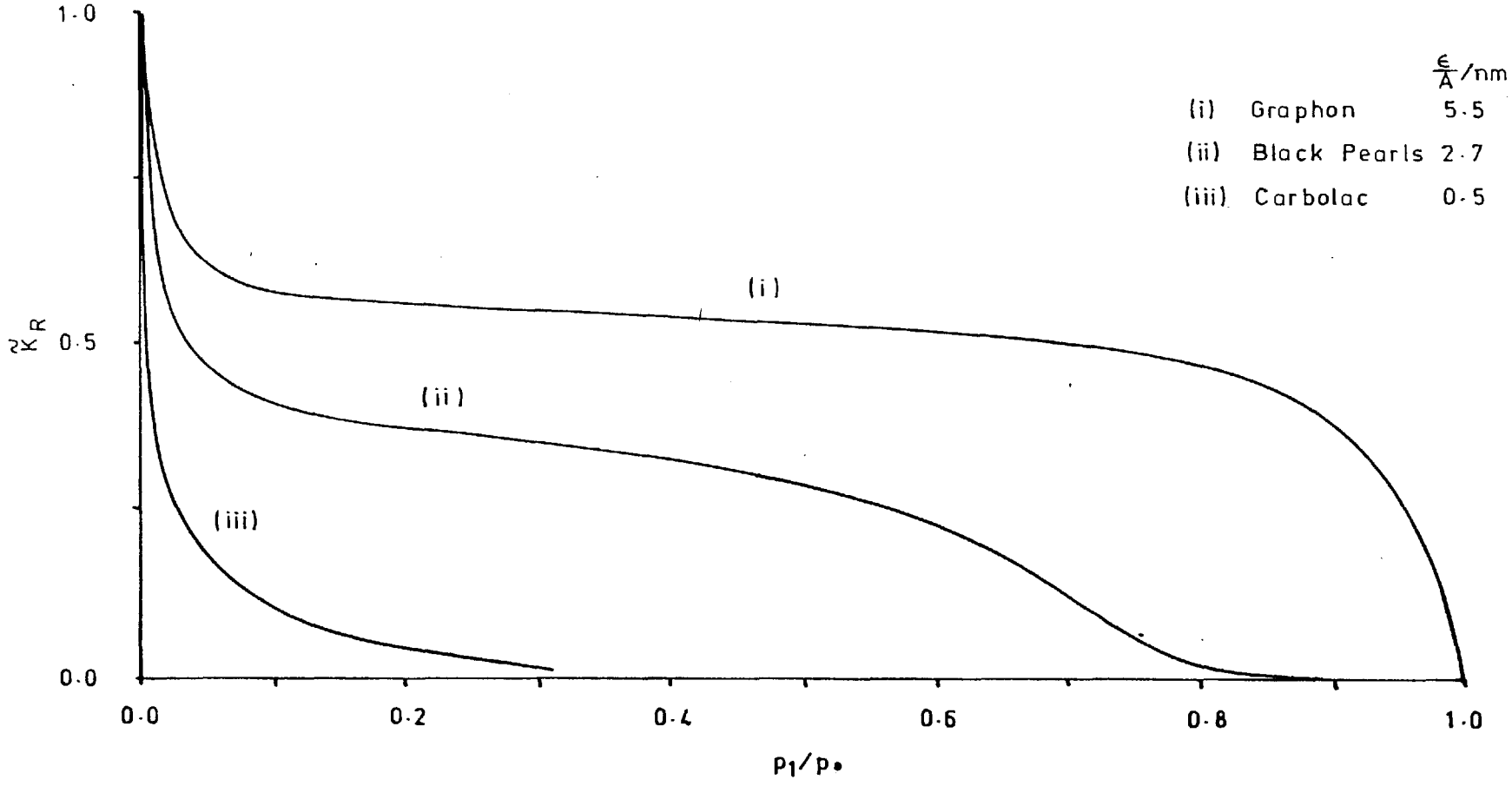

Figure 5.54. Concentration - Dependence of $\tilde{K}_R$: He/hydrocarbon/Carbolac

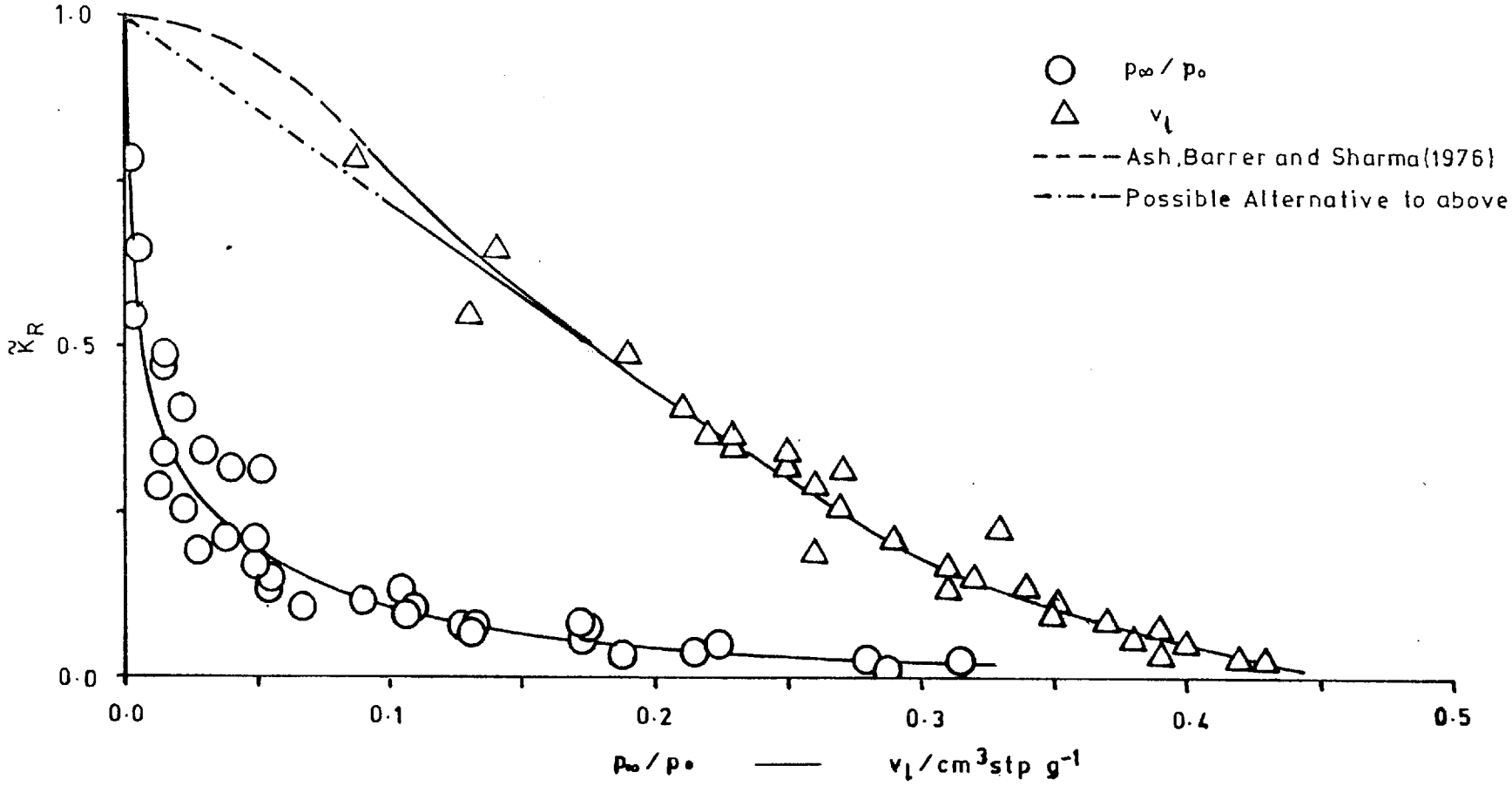

range C_2H_6 to near C_5H_{12}. It would be expected that if blockage was characteristic of a given ϵ/A different curves would result from different sized hydrocarbons, which is not the case.

Other work on the flow of mixtures through Carbolac also yield characteristic blockage curves. The flow of the mixtures, He/hydrocarbon (Sharma, 1970), He/NH_3 (Lowson, 1968) and H_2/SO_2 (Pope, 1961) has been treated to obtain the blockage curves shown in Figure 5.55.

Despite the fact that the experimental data of Lowson is somewhat scattered, each system can be seen to possess a characteristic blockage curve. The work of Pope employed the hydrogen component of the mixture as the non-sorbed indicator gas. The Carbolac membrane F (Ash, Baker and Barrer, 1968) used by Pope possessed a very low specific surface, A (m^2m^{-3}) compared to the other membranes. This is indicated by the enhqnced value of ϵ/A, each membrane possessing $\epsilon \simeq 0.5$.

It appears that the presence of key blockage sites, presumably situated at constrictions in the channels is common to all three carbon membranes but that at higher amounts adsorbed each membrane has its own characteristic behaviour for specific gas mixtures.

5.2.4. Formulation of 'Extra' Flow

(a) Introduction

When the adsorbed film is less than or equal to a monolayer in thickness the force promoting the extra flow may be called a two dimensional spreading pressure. This spreading pressure may be related to the rate of migration and can be described in two ways. It may be interpreted as a random-walk diffusive process or in hydrodynamic terms.

The random-walk idea treats the diffusion process in terms of an activated 'hopping' of adsorbed molecules from one site to another and results in the definition of diffusion coefficients. The hydrodynamic approach utilizes a relationship between the rate of movement of adsorbed molecules and the shear stress between them and the solids surface.

As the coverage increases beyond monolayer the diffusion concept does not have a great deal of physical significance, although formal

Figure 5.55. Blockage Curves for Carbolac : different mixtures

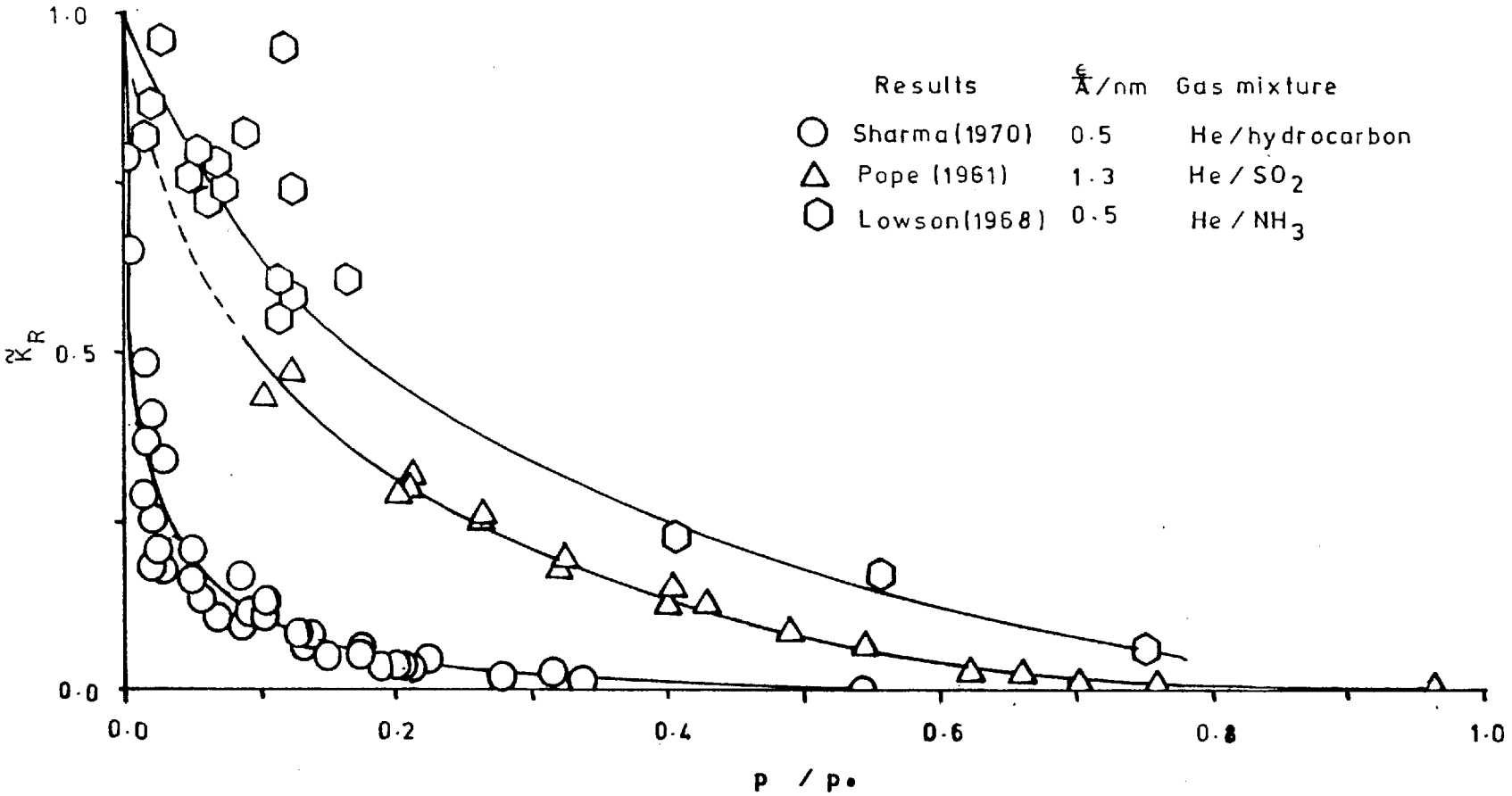

diffusion coefficients can still be derived. It is generally accepted that for thick films and capillary condensate the rate of migration of sorbed gas should be related to a capillary pressure gradient and treated in hydrodynamic terms.

(b) Activated Diffusion Process

1. Diffusion Coefficients

The classical work of Carman and Raal (1951) into the flow of SO_2, CF_2Cl_2 flow through membranes constructed of Linde Silica and Carbolac derived diffusion coefficients and considered their variation with both temperature and coverage. The variation with coverage fell into three distinct regions. An initial rapid increase with a sharp upper limit in the vicinity of $v/v_m = 1$ was found to be characteristic of a monolayer. The diffusion coefficient despite passing through a maximum followed by a minimum then remained relatively constant and this region marked multilayer formation. Rapid increase with poor reproducibility then occurred in the region approaching capillary condensation. The temperature dependence at constant coverage was found to be described by an Arrhenius type relationship and an activation energy for surface migration was obtained as a function of surface coverage. The energy remained constant until the coverage approached monolayer and then dropped sharply to another constant value.

In this study six diffusion coefficients have been defined (cf Chapter 2) by the application of Fick's diffusion equation. These are summarised in the following equations :

Integral Diffusion Coefficients:

$$\text{Overall Diffusion Coefficient : } \tilde{D}(C_1) = \frac{\ell}{A_c} \cdot \frac{J_\infty}{C_1} \qquad (2.26)$$

$$\text{Surface Diffusion Coefficient : } \tilde{D}_s(C'_{s_1}) = \frac{\ell}{A_c} \cdot \frac{J_s}{(AC'_{s_1})} \qquad (2.27)$$

$$\text{Gas phase Diffusion Coefficient: } D_g(C'_{g_1}) = \frac{\ell}{A_c} \cdot \frac{J_g}{(\epsilon C'_{g_1})} \qquad (2.28)$$

Differential Diffusion Coefficients:

Overall Diffusion Coefficient : $$D(C_1) = \frac{\ell}{A_c}\left(\frac{\partial J_\infty}{\partial C_1}\right) \quad (2.23)$$

Surface Diffusion Coefficient : $$D_s(C'_{s_1}) = \frac{\ell}{A_c}\cdot\left(\frac{\partial J_s}{\partial AC'_{s_1}}\right) \quad (2.24)$$

Gas phase Diffusion Coefficient: $$D_g(C'_{g_1}) = \frac{\ell}{A_c}\cdot\left(\frac{\partial J_g}{\partial \epsilon C'_{g_1}}\right) \quad (2.25)$$

The difference between the two types of coefficient (mathematically given in equation 2.30) is that the integral value is an average over the large concentration difference present in the membrane, whereas the differential coefficient is the value for an infinitesimally small concentration difference

$$\tilde{D}(C_1) = \frac{1}{C_1}\int_0^{C_1} D(C_1)\, dc \quad (2.29)$$

It is possible to evaluate the diffusion coefficients by equivalent routes involving the slopes of the isotherms and differential permeabilities. These routes require two graphical differentiations and are inherently less accurate. They were disregarded and the above definitions were used for the diffusion coefficient determinations.

The most detailed flow system investigated here was that of isobutane/Graphon and this is initially employed to consider the relevance of specific diffusion coefficients. Figures 5.56 and 5.57 illustrate the variation of the overall diffusion coefficients (both integral and differential) with temperature and coverage. The surface and gas phase diffusion coefficients arise from the division of the total flow into two components, J_s and J_g. J_s is the extra flow associated with the presence of a mobile adsorbed film (Barrer and Gabor, 1960). A value of J_s (where the extra flow is only partially on the surface) may be calculated from the total measured flux and a known value of J_g. The flow of helium at a given temperature and pressure is used to evaluate J_g for the sorbable gas at the same pressure by the relationship :

$$J_g^{He}\left(\frac{M^{He}}{T}\right)^{\frac{1}{2}} = J_g\left(\frac{M}{T}\right)^{\frac{1}{2}}$$

If the value taken for J_g^{He} is that from single species flow measurements the effect of blockage of the gas phase flow is not taken

Figure 5.56. Concentration - Dependence of D : i-C_4H_{10}/Graphon

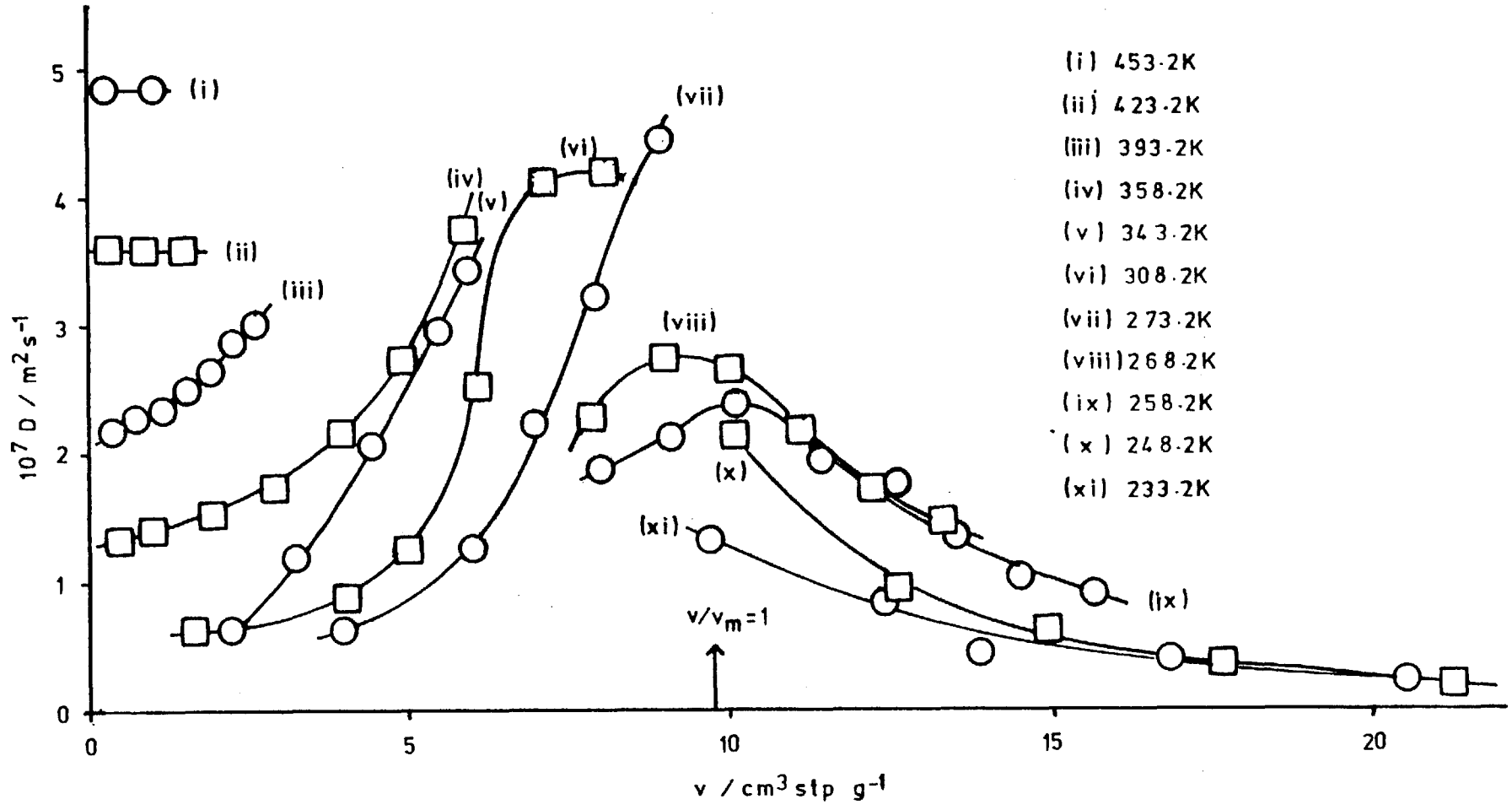

Figure 5.57. Concentration - Dependence of $\tilde{D}$: i-C_4H_{10}/Graphon

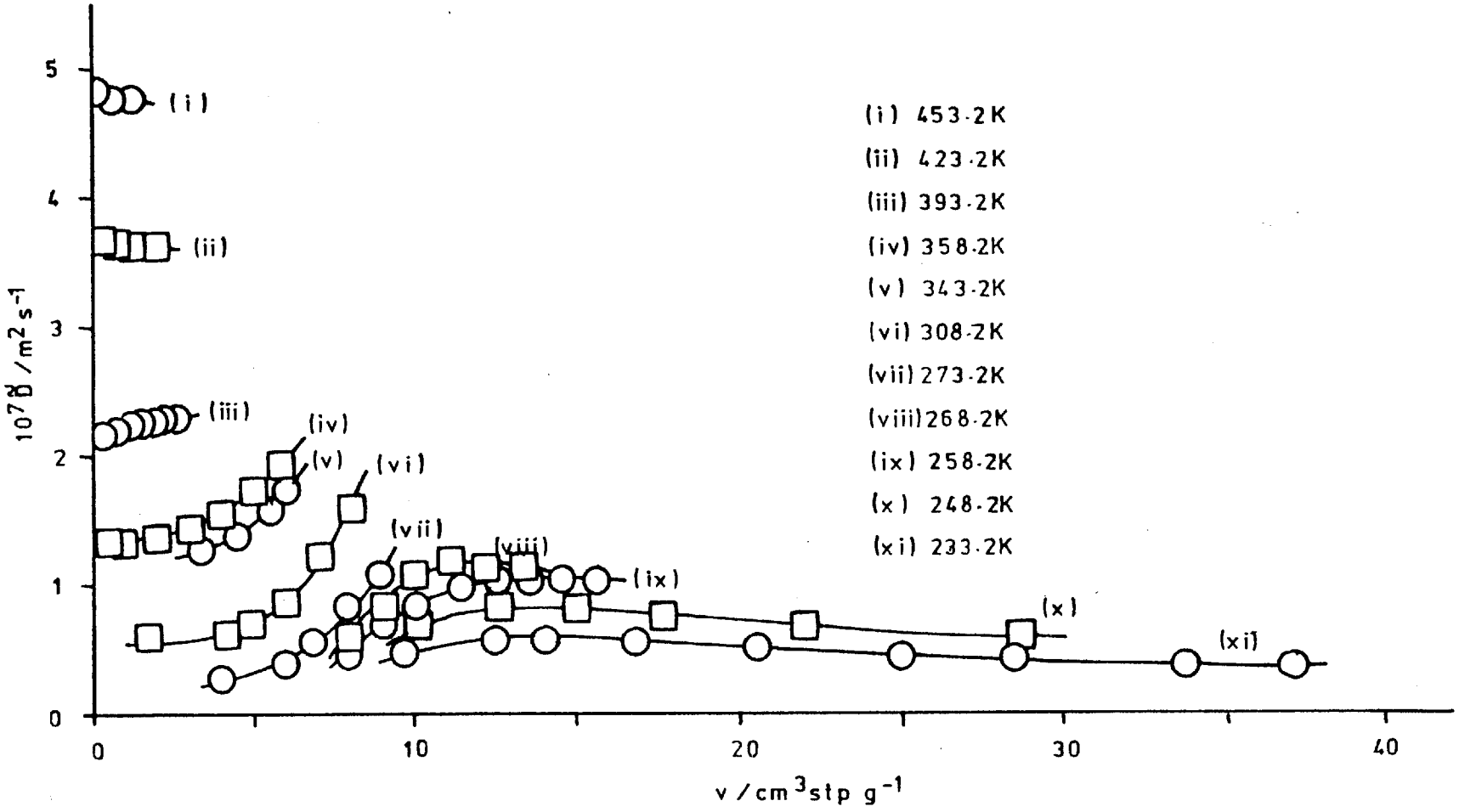

into account. This will tend to underestimate the extra flow component, especially at higher coverages. However at these coverages it has been seen that the extra flow is the dominant component (cf Figure 5.19). Using this approach the quantities designated J'_s, $\tilde{K}'_s$, $\tilde{D}'_s$ and D'_s are derived.

However if the gas phase flux is corrected to take into account the effect of blockage a different series of quantities, designated J''_s, $\tilde{K}''_s$, $\tilde{D}''_s$ and D''_s will be obtained. This approach, using the helium as a non-sorbed internal indicator has been used in previous studies [Ash, Barrer and Pope (1963b); Ash, Barrer and Lowson (1973); Ash, Barrer and Sharma (1976)] and should result in a slightly more refined division of the flux into two components.

The variation of the surface diffusion coefficients, $\tilde{D}'_s$, D'_s, $\tilde{D}''_s$ and D''_s with coverage are given in Figures 5.58 to 5.61 and the differences will be discussed later. The gas phase diffusion coefficient may be a constant value for a given temperature (as the pure helium flow is independent of pressure) or it may vary in the same manner as the helium flow in the mixture experiments (due to blockage of the gas phase flow by the adsorbed layer). The type of behaviour therefore depends upon which division of the flux is adopted. The gas phase diffusion coefficient for pure helium flow has previously been discussed in relation to structure factors (cf §5.2.1).

The general trends common to each set of diffusion coefficients agree with the results of Carman's original work: an increase up to a maximum in the vicinity of monolayer coverage for the differential coefficients, then a decrease to a relatively constant value. The presence of the rapid increase due to capillary condensation was not evident in the results presented here presumably due to the coverages not being high enough. A strong temperature dependence exists which can be described by an Arrhenius type relationship from which an activation energy may be obtained ($D = D_o \exp(-E/RT)$). The properties of this energy will be discussed later with those derived from different sources.

A more detailed examination of the diffusion coefficients may be made if Figures 5.62 to 5.71 are considered. Here the different diffusion coefficients are plotted together as a function of coverage

Figure 5.58. Concentration - Dependence of $\tilde{D}'_s$: i-C_4H_{10}/Graphon

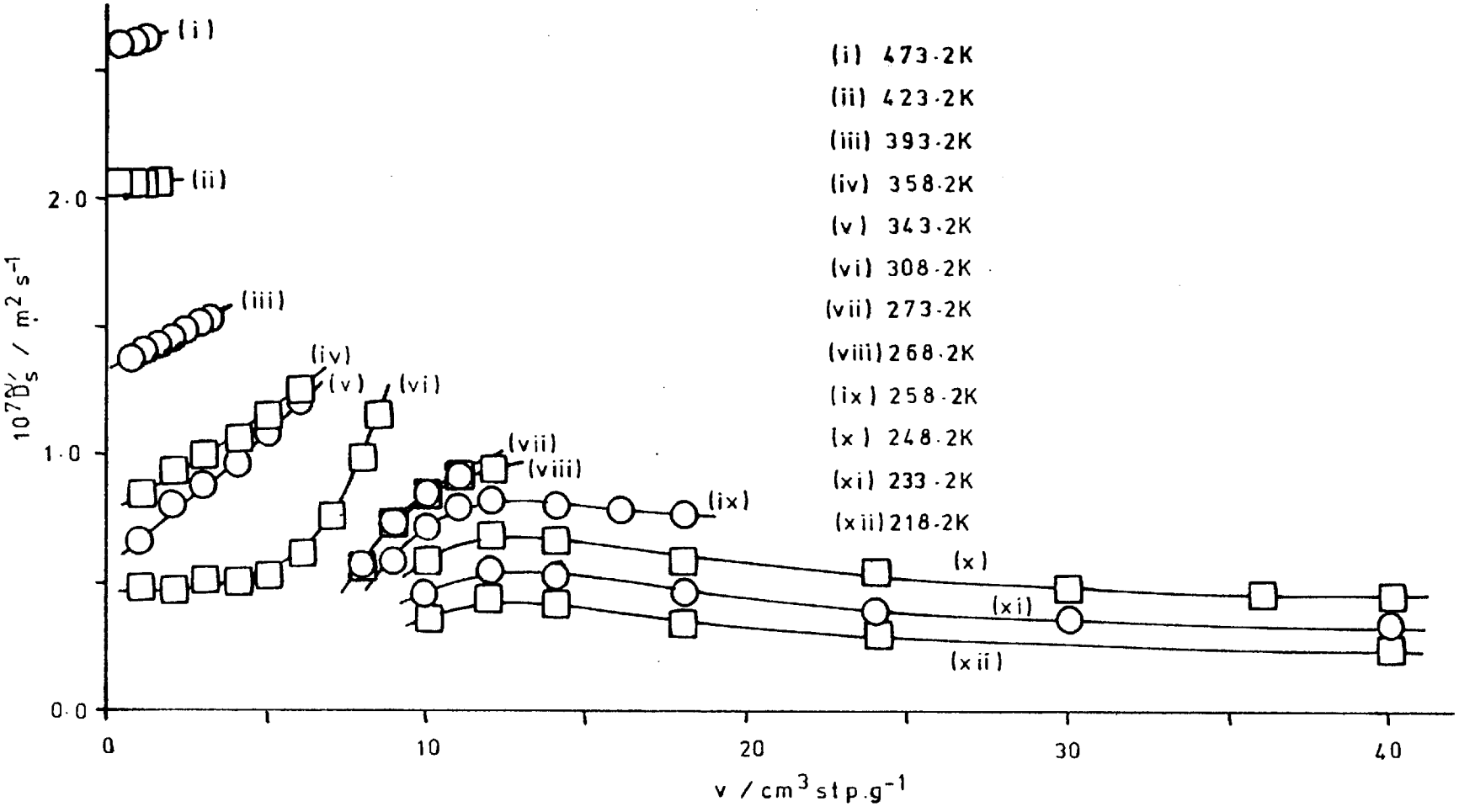

Figure 5.59. Concentration - Dependence of D_s' : i-C_4H_{10}/Graphon

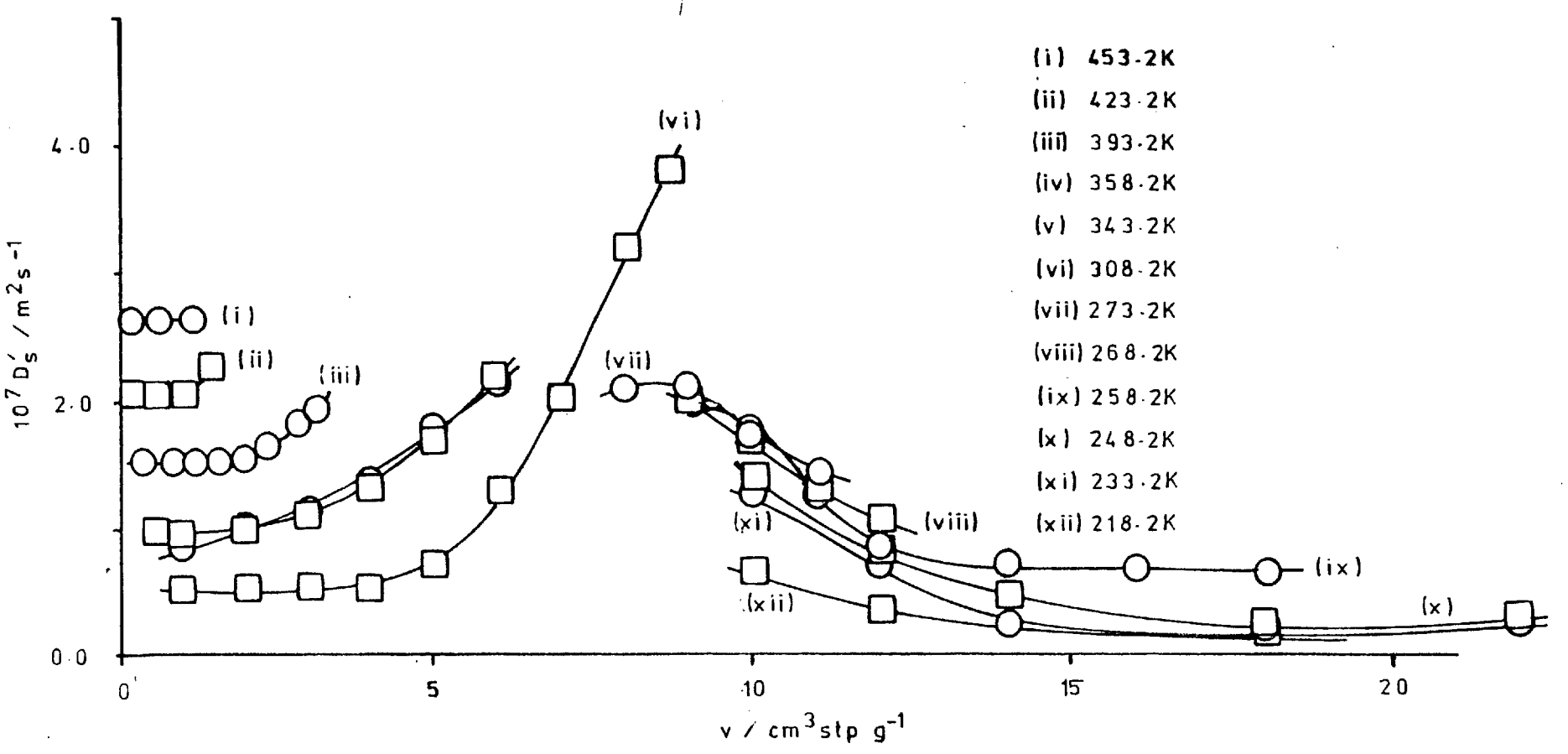

Figure 5.60. Concentration - Dependence of $\tilde{D}''_s$: i-C_4H_{10}/Graphon

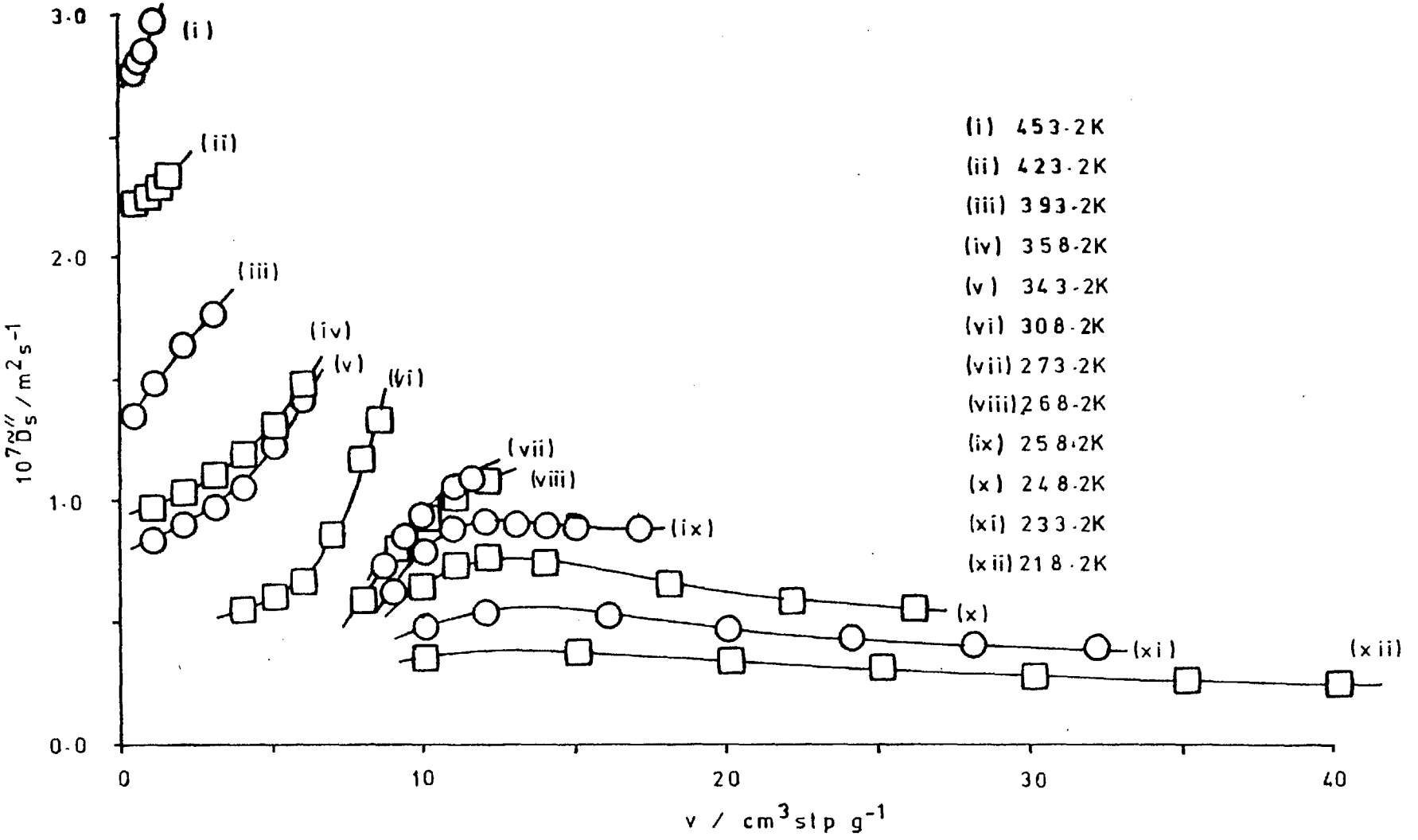

Figure 5.61. Concentration - Dependence of D_s'' : i-C_4H_{10}/Graphon

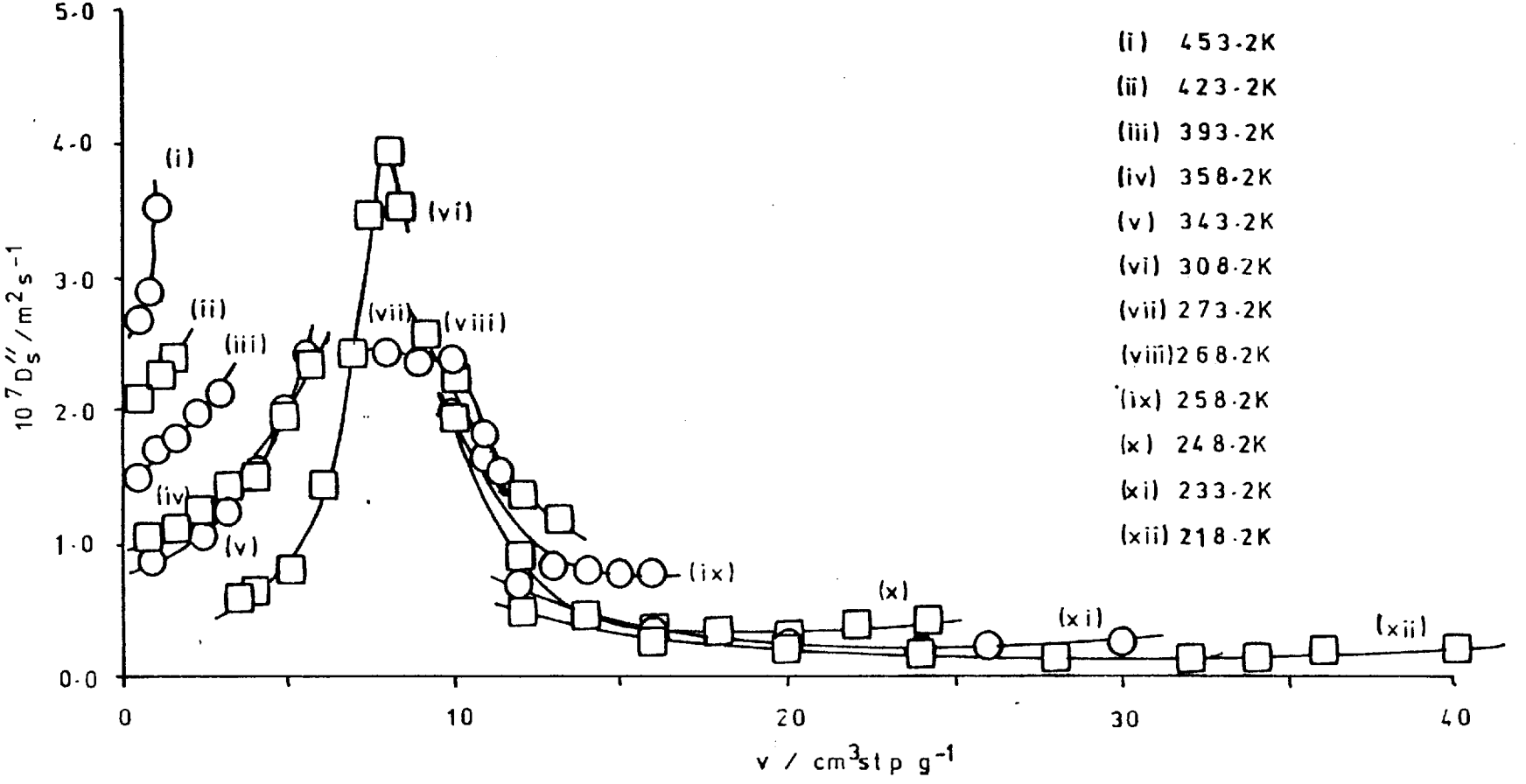

for each temperature. It can be seen that in all cases the differential coefficient $\geq$ integral coefficient, the difference between the two increasing as the coverage increases. Also the general trend (with one or two exceptions) in the magnitude of the coefficients is $D > D''_s > D'_s$ and $\tilde{D} > \tilde{D}''_s > \tilde{D}'_s$.

The low coverage behaviour of the overall diffusion coefficients may be explained as a direct consequence of the flux being directly proportional to the coverage and the constant permeabilities in the Henry Law region. Recalling the relationship between the integral and differential coefficients :-

$$\tilde{D} = \frac{1}{C_1} \int_0^{C_1} D(C)\, dc \qquad (2.29)$$

the behaviour of the two coefficients relative to each other can be predicted. The differential form of equation (2.29)

$$D(C_1) = \tilde{D}(C_1) + C_1\left(\frac{\partial D(C_1)}{\partial C_1}\right) \qquad (2.30)$$

indicates that if

$$D(C_1) \gtreqless \tilde{D}(C_1) \text{ then } \frac{\partial \tilde{D}(C_1)}{\partial C_1} \gtreqless 0 \qquad (5.9)$$

It may be seen (Figures 5.62 to 5.71) that generally all these conditions are adhered to but it must be noted that the differential coefficients were not obtained directly from the integral diffusion coefficients by means of equation (2.30), but from the flux curves and definitions given in equations (2.23) to (2.28). As $\tilde{D}$ is initially independent of concentration at low coverages, $\tilde{D} = D$. The differential coefficient then increases much more rapidly than $\tilde{D}$, goes through a maximum value and decreases becoming equal to the integral coefficient at the maximum in the $\tilde{D}$ vs C curve. The differential coefficient then remains less than the integral one.

A good comparison between the diffusion coefficients evaluated in this study and in other work is provided by the studies of Ash, Barrer and Edge (1976) and Ash, Barrer, Chio and Edge (1979). Propane and isobutane flow through Graphon membrane N resulted in the determination of overall diffusion coefficients. The isobutane results at T/K = 273.2 and 308.2 are compared with the coefficients obtained from this study in

Concentration - Dependence of Diffusion Coefficients

Figure 5.62 : i-C_4H_{10}/Graphon : T/K = 453.2.

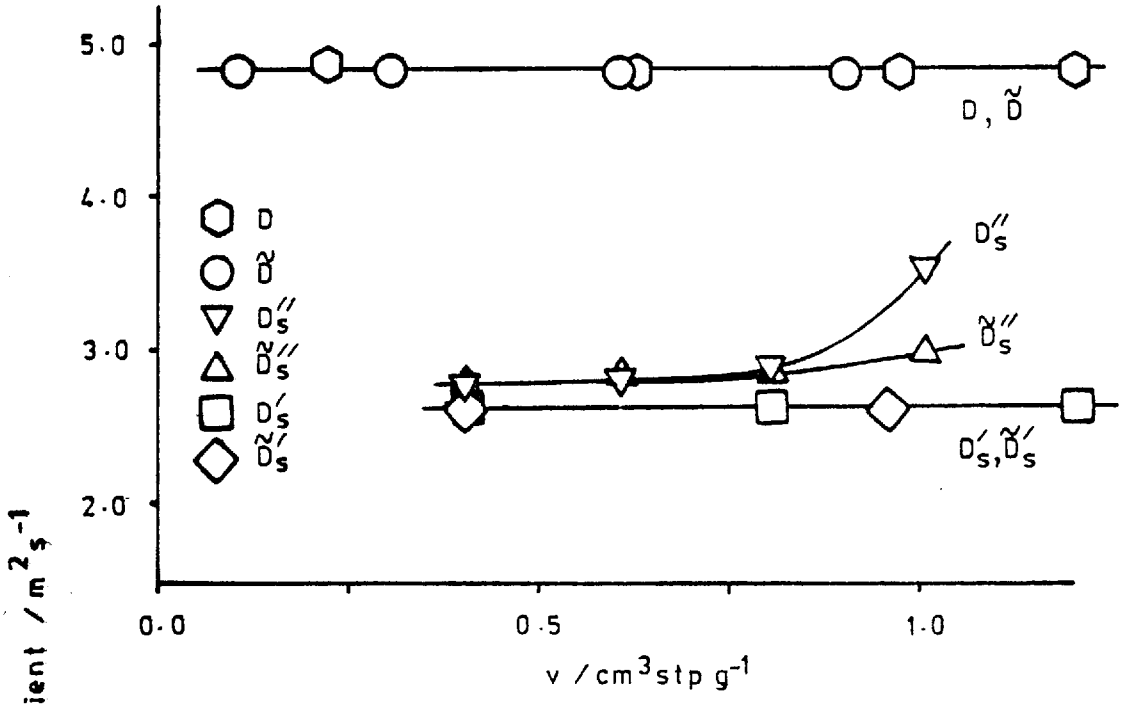

Figure 5.63. : i-C_4H_{10}/Graphon : T/K = 423.2

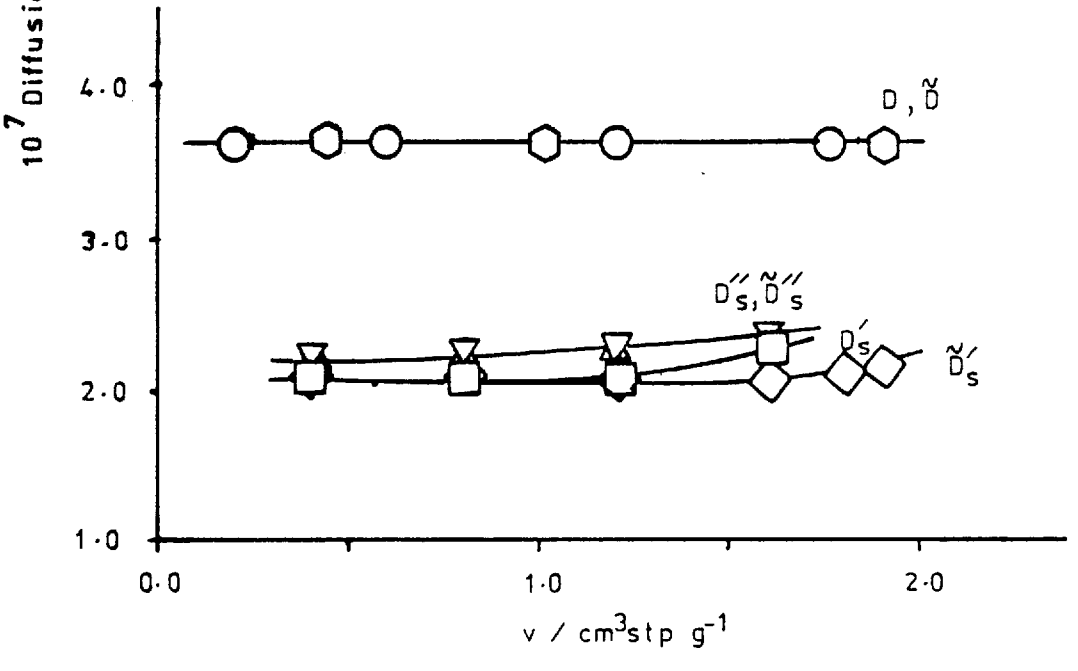

Concentration - Dependence of Diffusion Coefficients

Figure 5.64. : i-C_4H_{10}/Graphon : T/K = 393.2

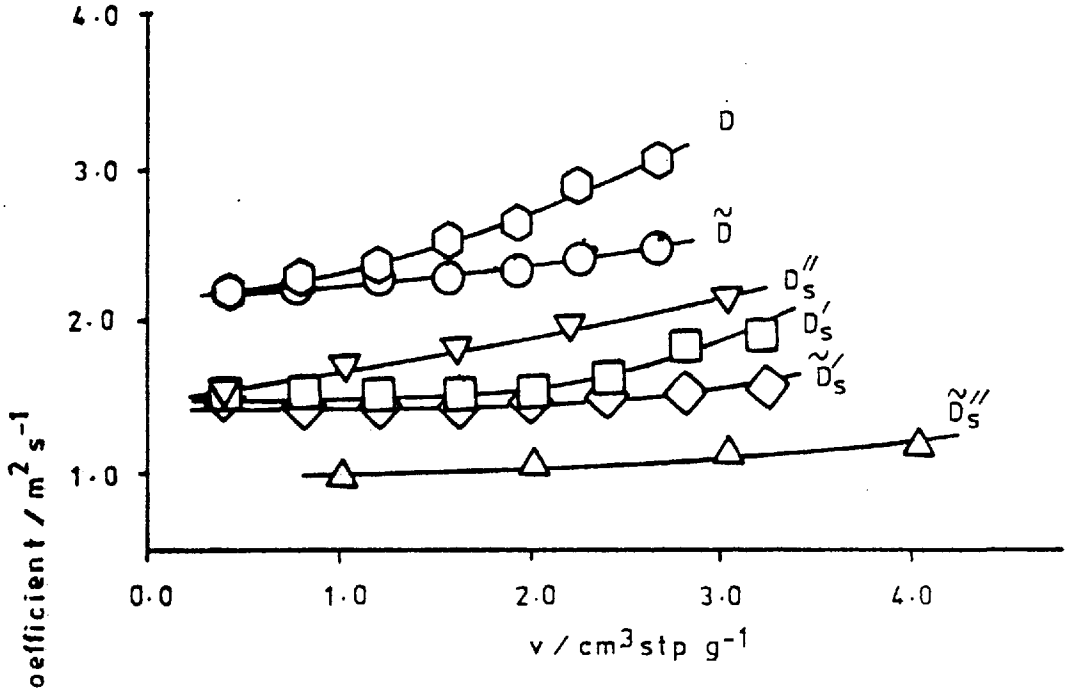

Figure 5.65. : i-C_4H_{10}/Graphon : T/K = 358.2

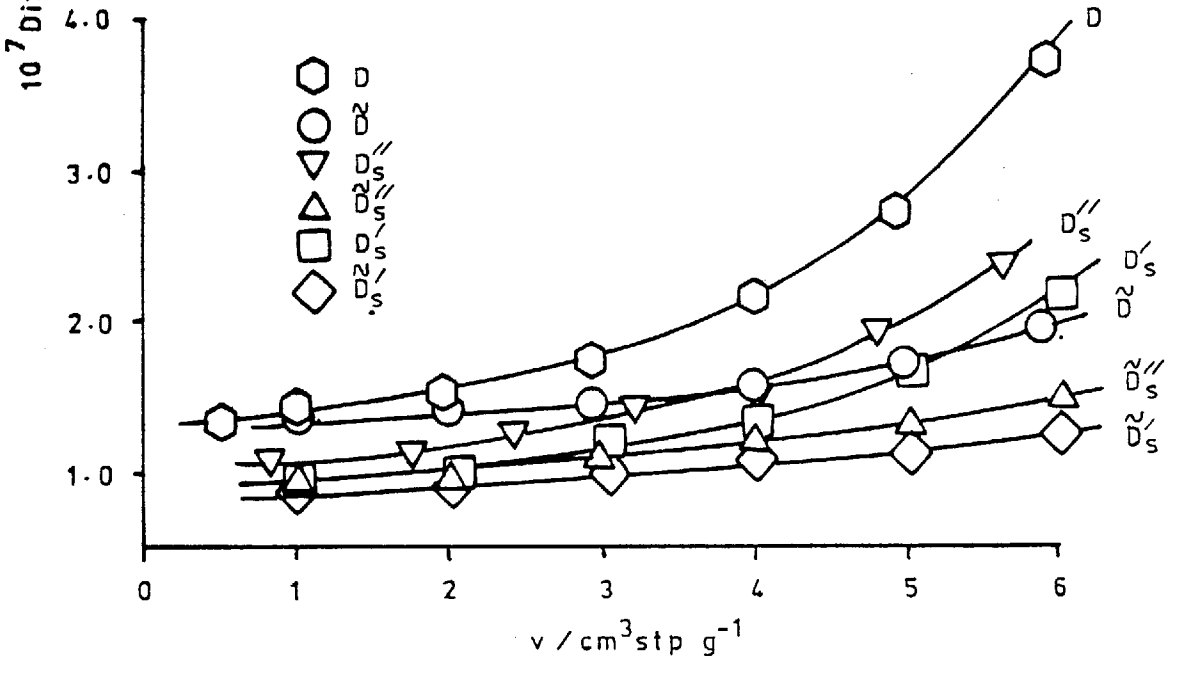

Concentration - Dependence of Diffusion Coefficients

Figure 5.66. : i-C_4H_{10}/Graphon : T/K = 343.2

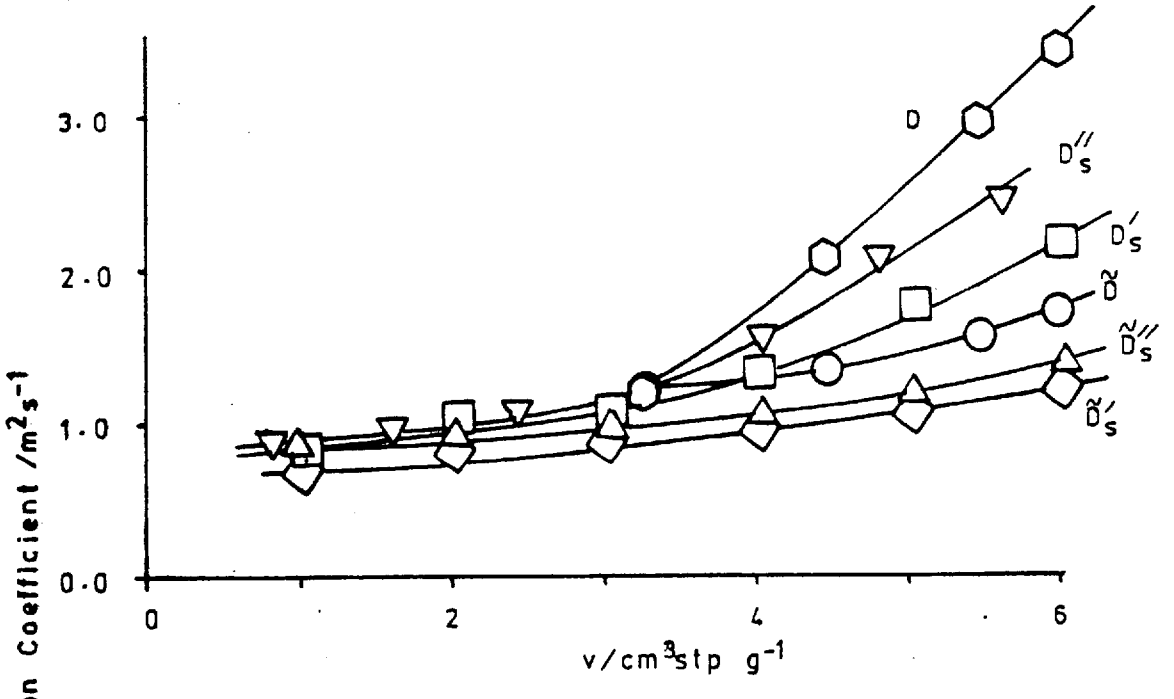

Figure 5.67. : i-C_4H_{10}/Graphon : T/K = 308.2

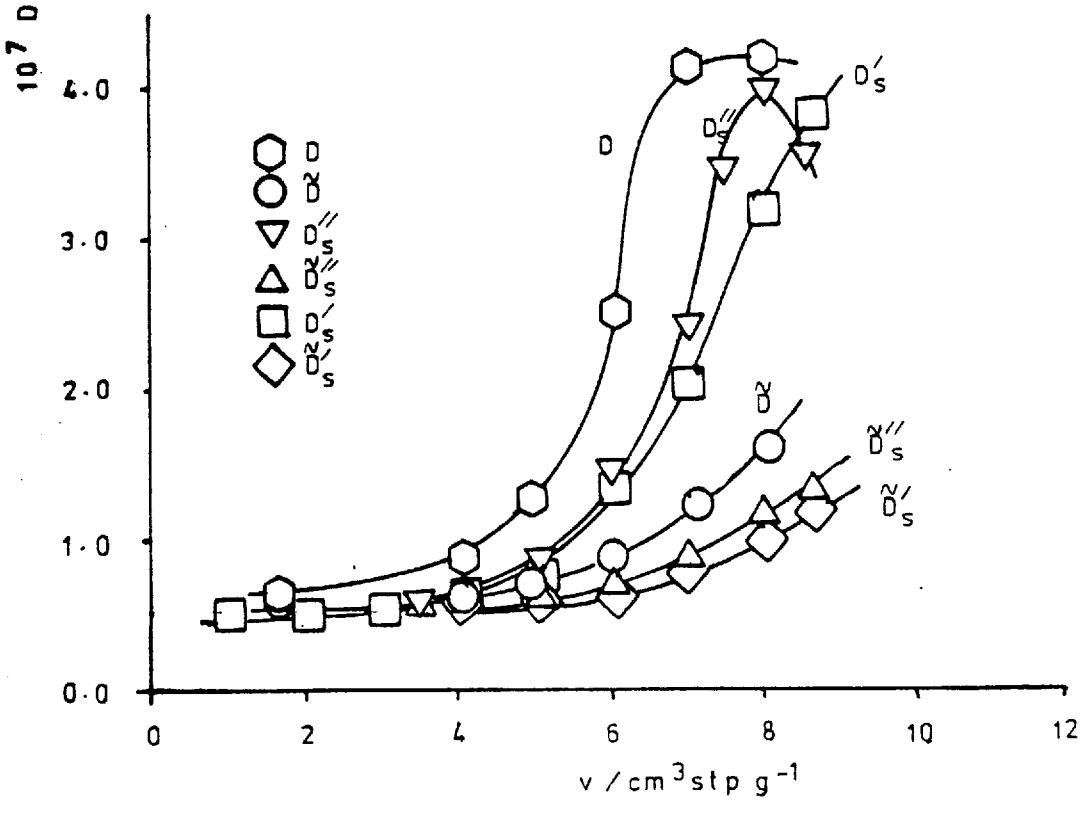

Concentration - Dependence of Diffusion Coefficients

Figure 5.68. : i-C_4H_{10}/Graphon : T/K = 273.2

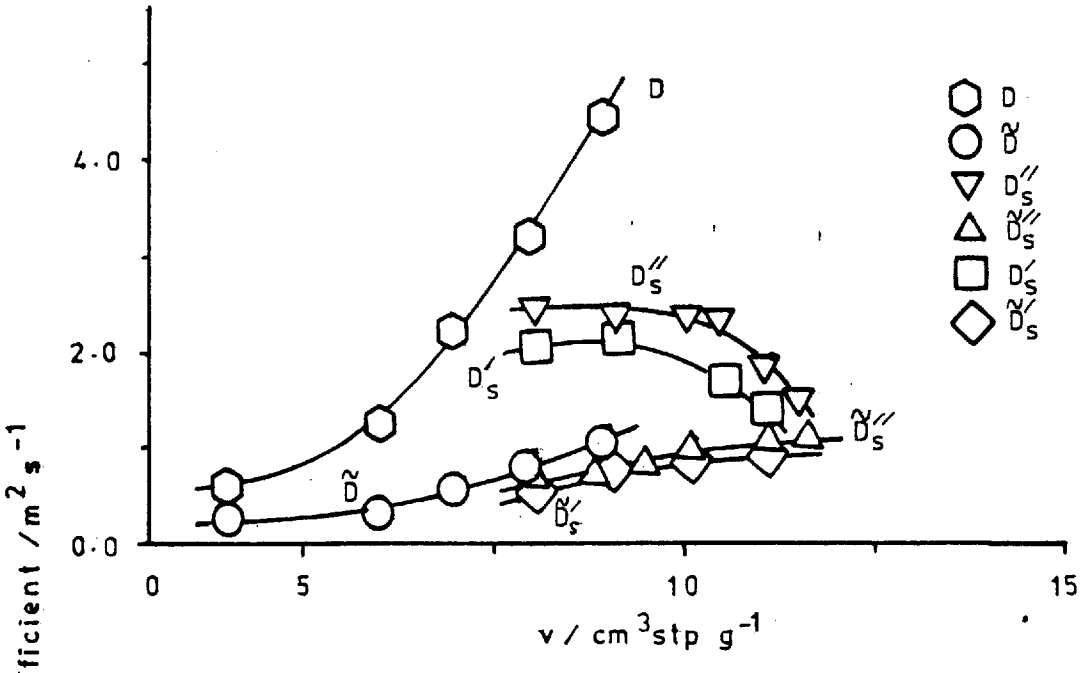

Figure 5.69. : i-C_4H_{10}/Graphon : T/K = 268.2

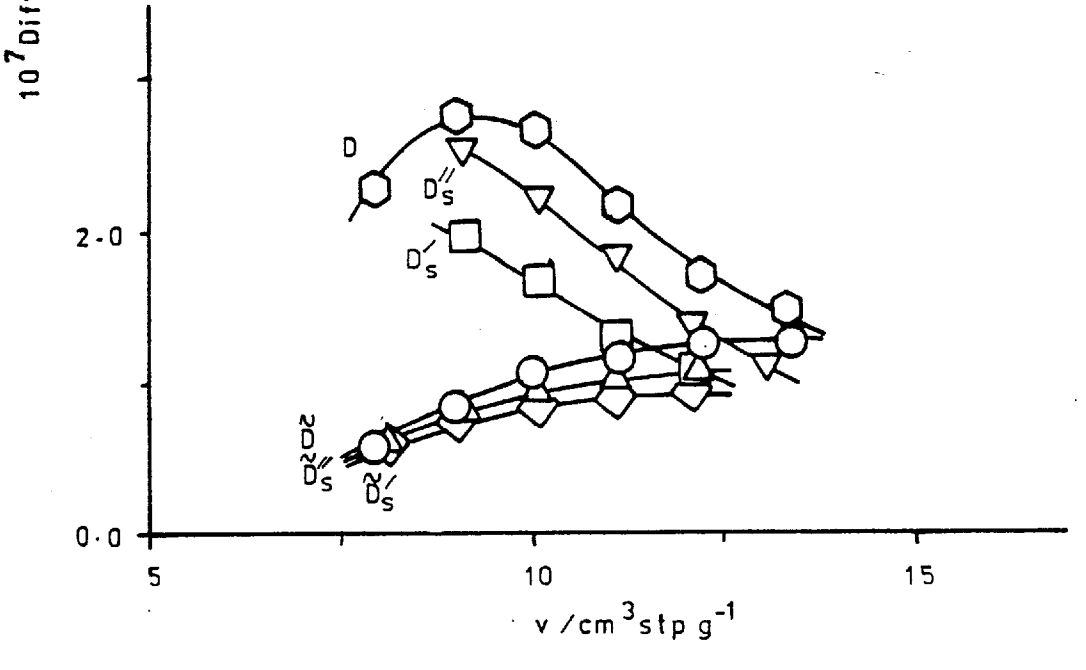

Concentration - Dependence of Diffusion Coefficients

Figure 5.70. : i-C_4H_{10}/Graphon : T/K = 258.2

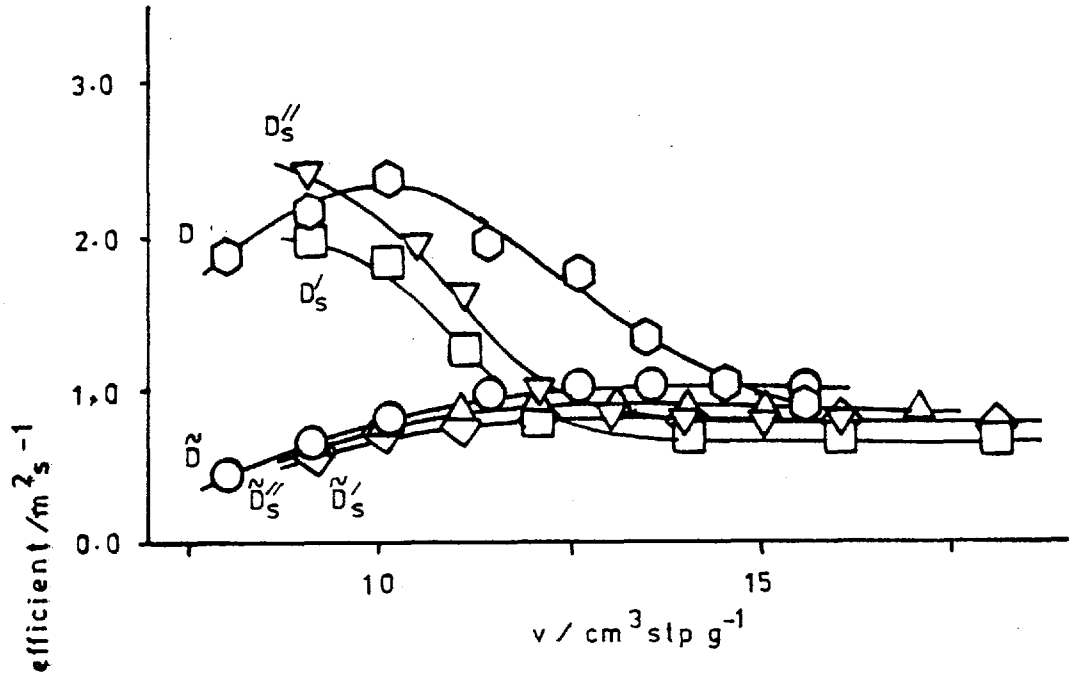

Figure 5.71. : i-C_4H_{10}/Graphon : T/K = 248.2

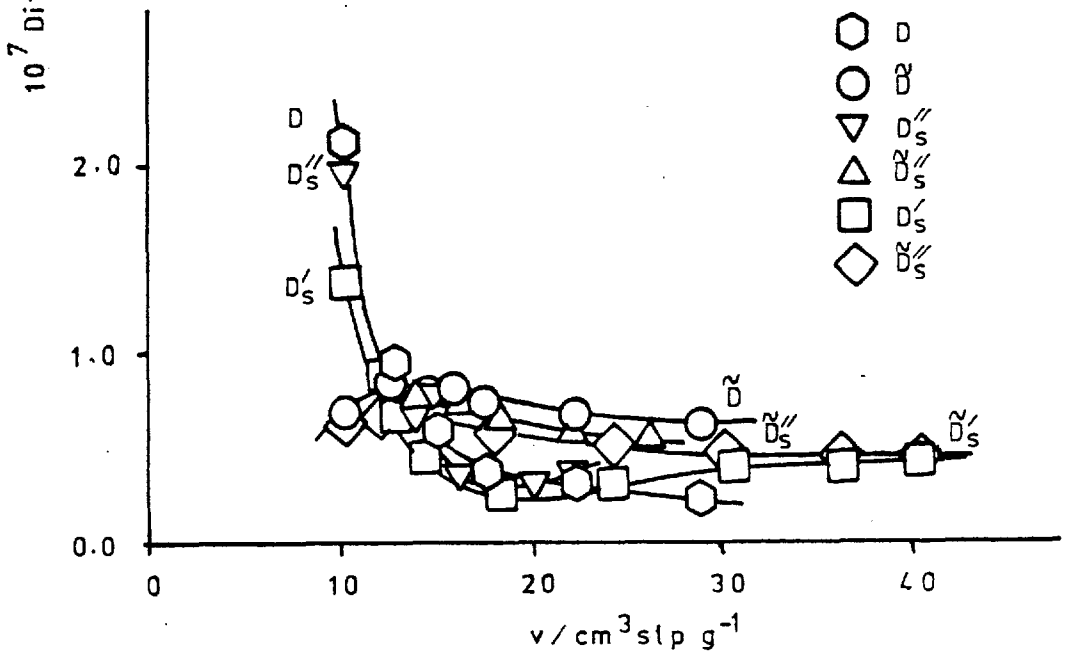

Figures 5.72 and 5.73. It can be seen that each set of results gives diffusion coefficients similar both in magnitude and in variation with coverage. A best-fit curve was drawn through the results at 273.2 K whilst those at 308.2 K are presented as independent studies. Perhaps the most obvious difference between the two studies is that the results of this investigation at 308.2 K provide evidence for the maximum whilst those of Ash, Barrer, Chio and Edge (1979) do not. Both membranes were constructed from the same sample of Graphon and both were compressed to the same mean porosity. However the lengths varied from 0.971 cm with 3 packing increments to 4.21 cm and 8 packing increments for membranes Q and N respectively. This marked similarity in the behaviour of the diffusion coefficient for two different membranes provides evidence in support of the work of Ash, Barrer, Chio and Edge (1979). They showed that the functional dependence of D was dominated by a dependence on concentration and not a positional coordinate (x-dependence) for the case of strongly sorbed gases.

Just as there was an observed similarity between the molar flux curves and the adsorption isotherms, Ash, Barrer and Nicholson (1963) derived a relationship between the diffusion coefficient and the isotherms. From the definition of J_s and J_g :

$$\frac{J_s}{J_g} = \frac{D_s.A.dC'_s}{D_g.\epsilon.dC'_g} = \frac{D_s.A.\sigma}{D_g.\epsilon} \qquad (5.10)$$

where

$$\sigma \left(= \left(\frac{dC'_s}{dC'_g} \right) \right)$$

is the slope of the isotherm. If J and J_g are constant for a given equilibrium coverage then J_s/J_g must be a constant and :

$$\frac{D_s}{D_g} = k. \frac{1}{\sigma} \qquad (5.11)$$

where k is a constant. Ash, Baker and Barrer (1967) compared the variations of $1/\sigma$ and D_s with coverage and found good qualitative agreement for the systems, SO_2/Carbolac, Ar/Black Pearls, SF_6/Graphon at specific temperatures. In Figures 5.74 and 5.75 similar plots are presented. It is assumed that D_g is not a function of coverage.

Figure 5.72. Concentration - Dependence of D, $\tilde{D}$: i-C_4H_{10}/Graphon : T/K = 273.2

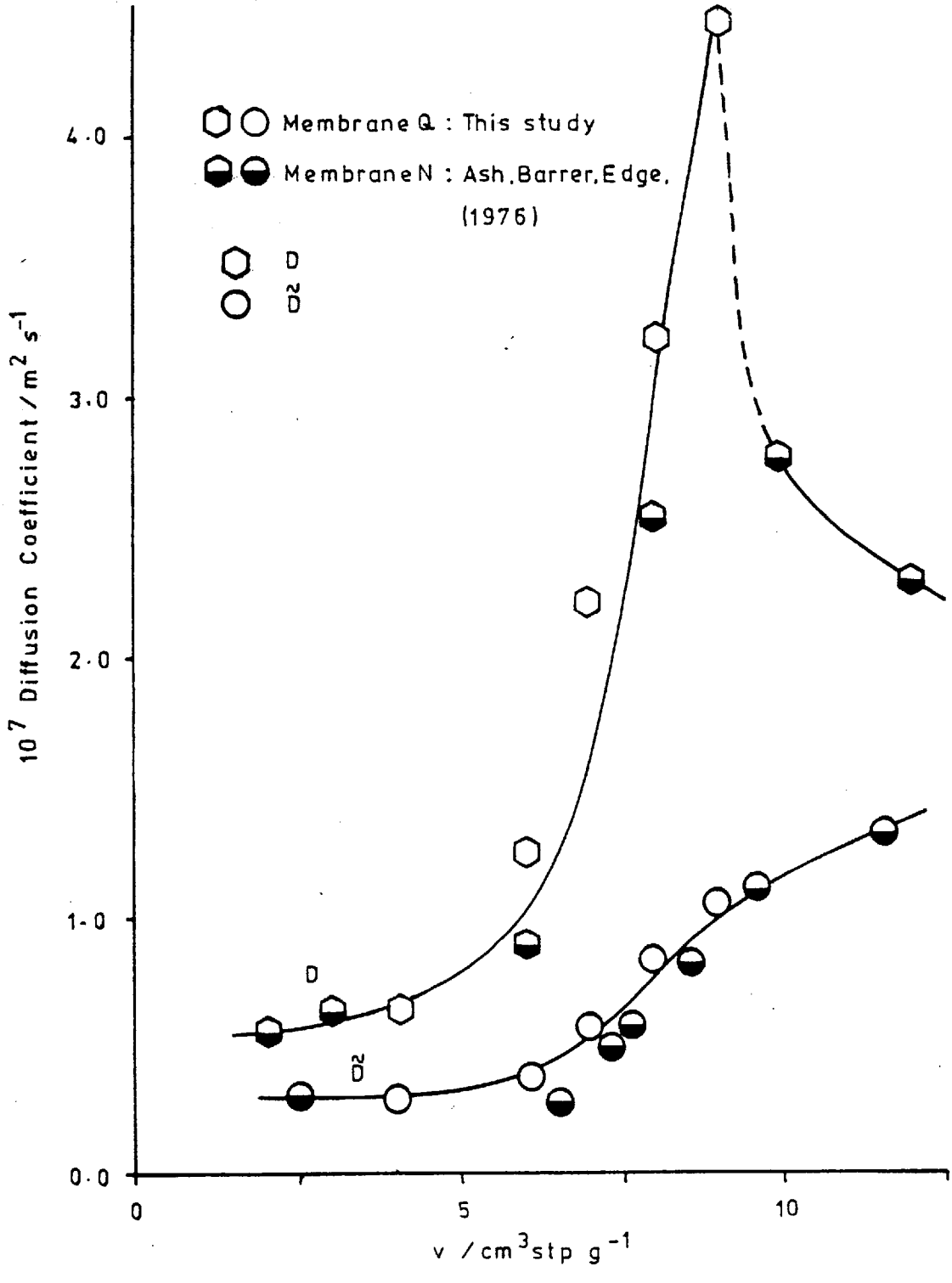

Figure 5.73. Concentration - Dependence of D, $\tilde{D}$: i-C_4H_{10}/Graphon : T/K = 308.2

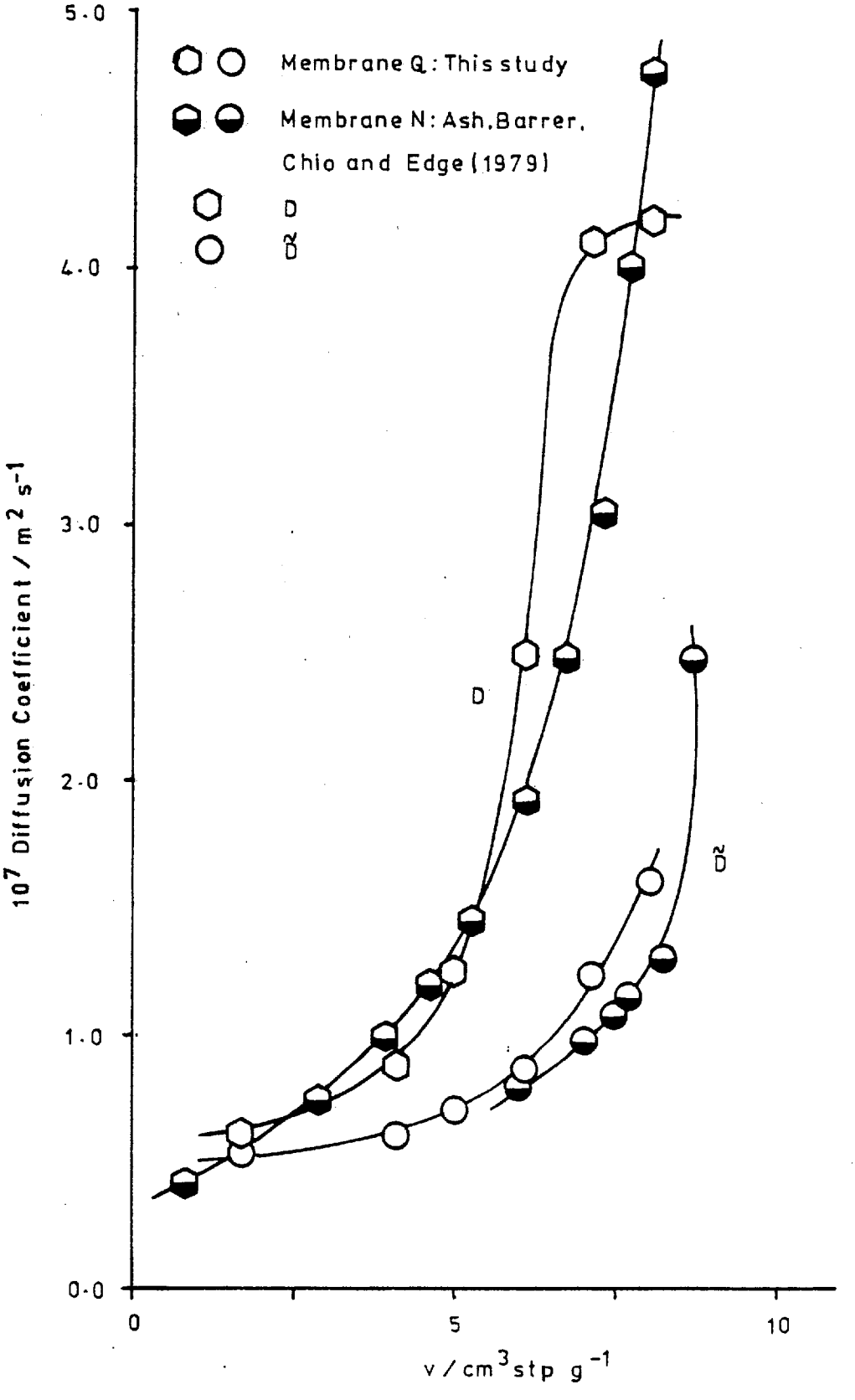

Figure 5.74. Concentration - Dependence of $1/\sigma$ and D'_s : i-C_4H_{10}/Graphon : T/K = 453.2, 358.2.

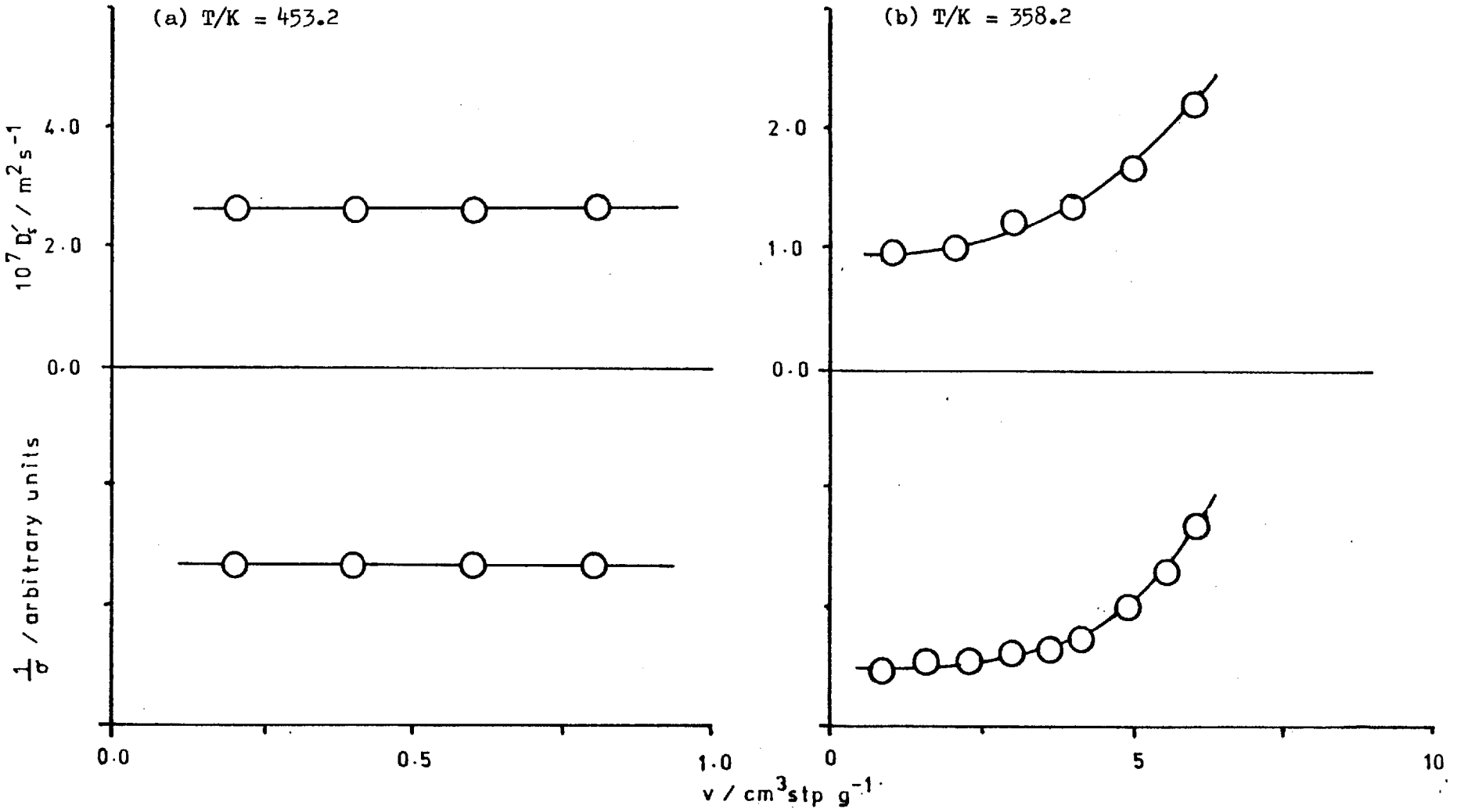

Figure 5.75. Concentration - Dependence of $1/\sigma$ and D'_s : i-C_4H_{10}/Graphon : T/K = 273.2, 233.2

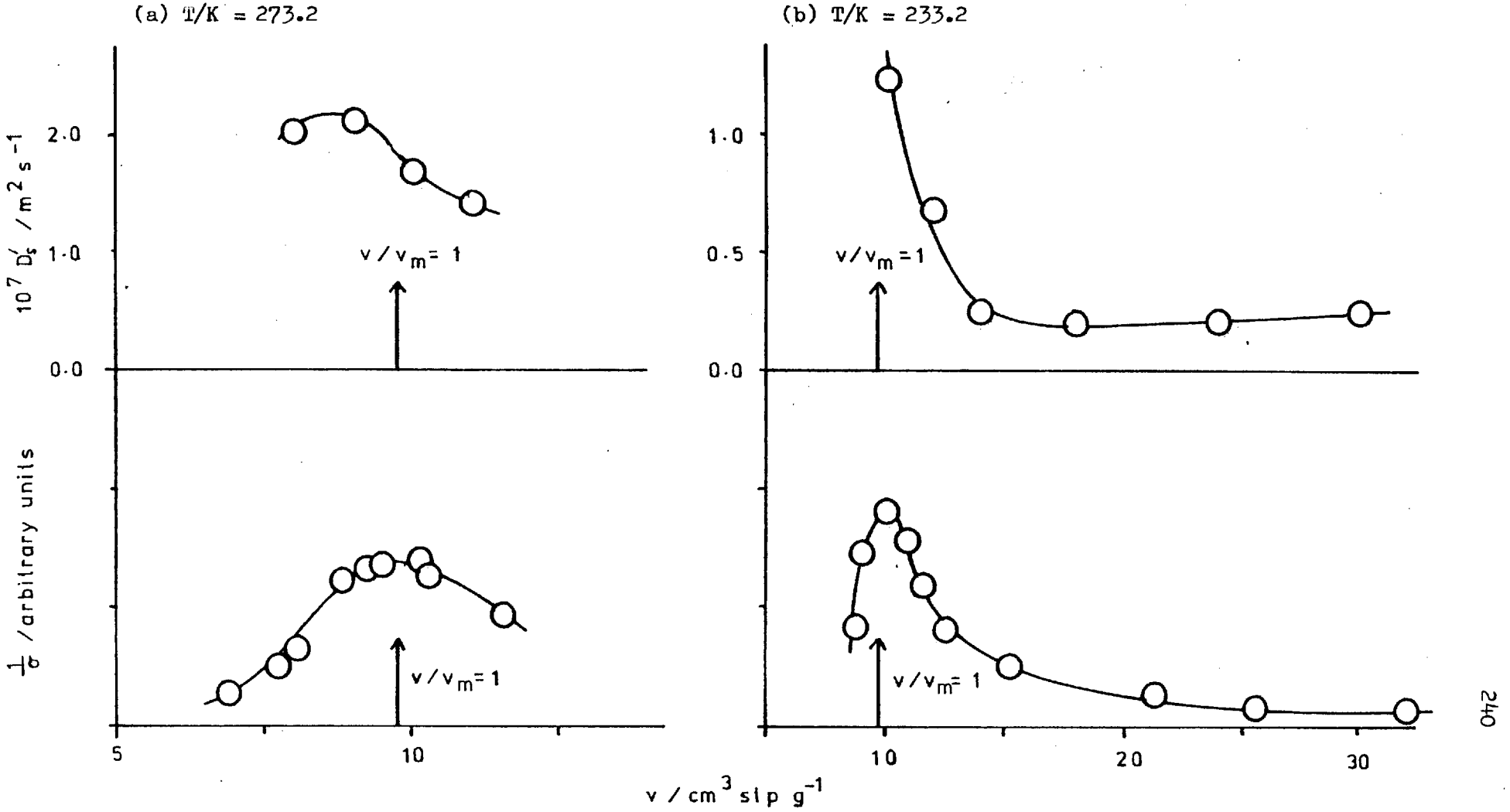

Hence values of D_s' (no blockage condition) are plotted as a function of coverage along with values of $1/\sigma$ (arbitrary units) for several temperatures. The similar course of $1/\sigma$ and D_s' as functions of amount sorbed is apparent supporting the derivation of equation (5.11).

It can be seen from Figures 5.56 to 5.61 that the internal consistency of the integral coefficients is much superior to that of the differential ones. This is to be expected as the integral values arise directly from measured quantities whereas the differential values require graphical differentiation of the flux curves. Consideration of the surface diffusion coefficients shows them to be somewhat inconsistent with the better division being that resulting in $\tilde{D}_s''$ and D_s''. As the isobutane/Graphon system was by far the most detailed examination made it was decided that the division of the total flow into two components with associated diffusion coefficients (D_g and D_s) was not merited for the remaining systems.

It is worth noting at this point that the treatment of Gilliland, Baddour, Perkinson and Sladek (1974) was applied to the data of this study. They relate the change in D_s with surface concentration to a change in the strength of adsorption as estimated from the heat of adsorption, q_{st}. This model has been found to fit the data of several other workers [CF_2Cl_2/silica (Carman and Raal, 1951), SO_2/Carbolac (Pope, 1961), CO_2, SO_2, NH_3/porous glass (Gilliland et al., 1974)]. However the results of the isobutane/Graphon system under study were not correlated by the plot of $\ln D_s$ vs q_{st}/RT.

The propane/Graphon results were treated in the same way to evaluate the overall diffusion coefficients, D and $\tilde{D}$. These are presented in Figures 5.76 and 5.77 as functions of coverage. The concentration dependence is similar to that observed for the isobutane system where a maximum in the differential coefficient occurred around the monolayer coverage (cf Figure 5.56). The magnitude of the coefficients is greater by approximately a factor of two for the propane results at a comparable temperature and coverage. The comparison between integral and differential diffusion coefficients is again made for specific temperatures (Figures 5.78 to 5.81). In the Henry Law region of adsorption (Figures 5.78 and 5.79) the two coefficients are constant and equal, as predicted by the relationship (5.9). However, presumably

Figure 5.76. Concentration - Dependence of D : C_3H_8/Graphon

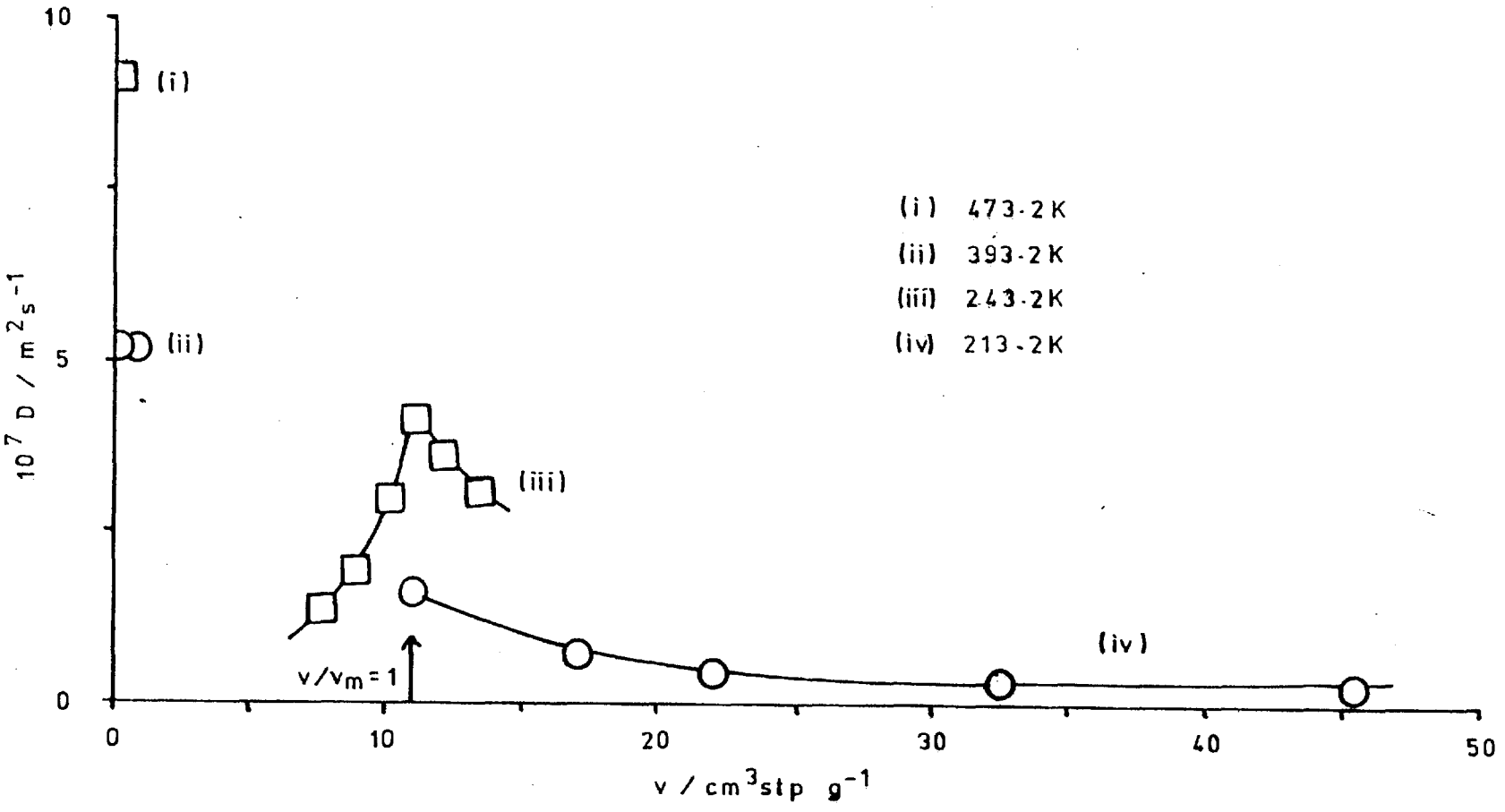

Figure 5.77. Concentration - Dependence of $\tilde{D}$: C_3H_8/Graphon

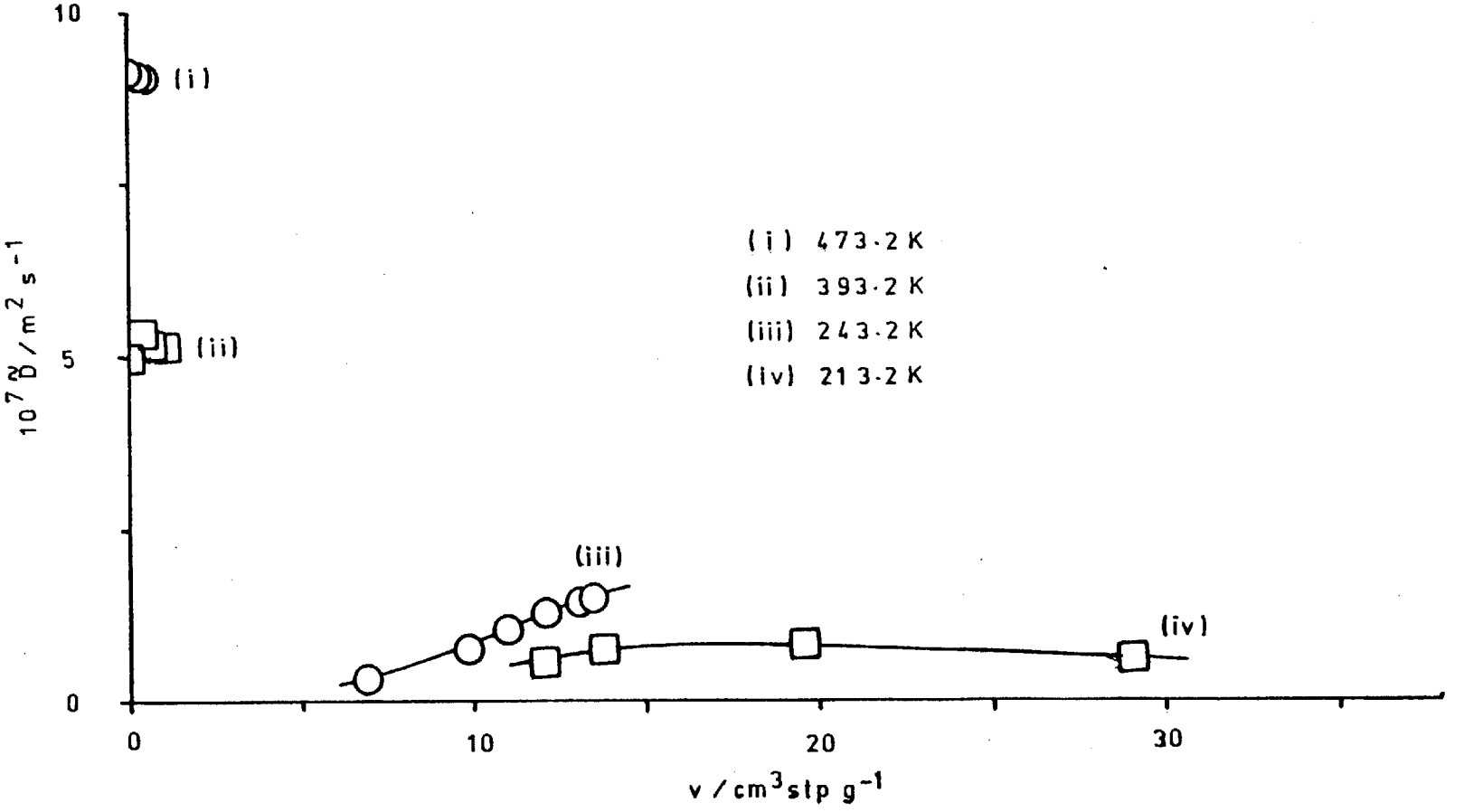

Concentration - Dependence of Diffusion Coefficients

Figure 5.78. : C_3H_8/Graphon : T/K = 473.2

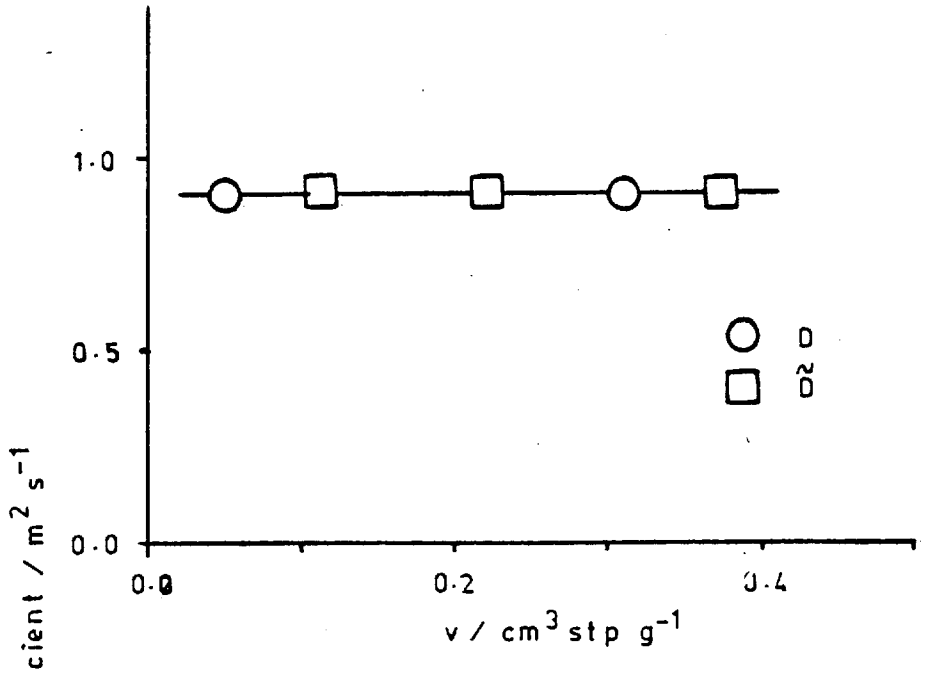

Figure 5.79. : C_3H_8/Graphon : T/K = 393.2

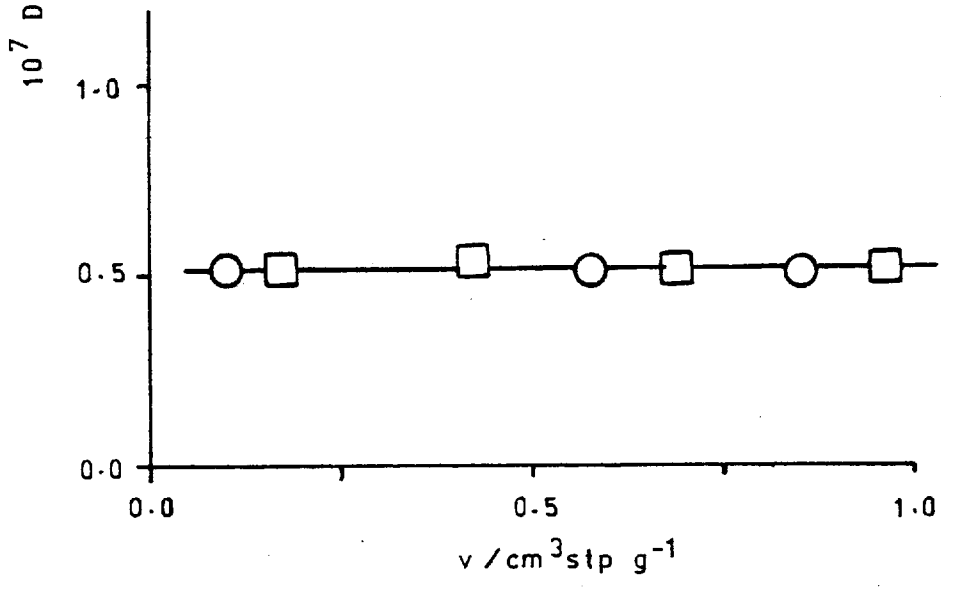

Concentration - Dependence of Diffusion Coefficients

Figure 5.80. : C_3H_8/Graphon : T/K = 243.2

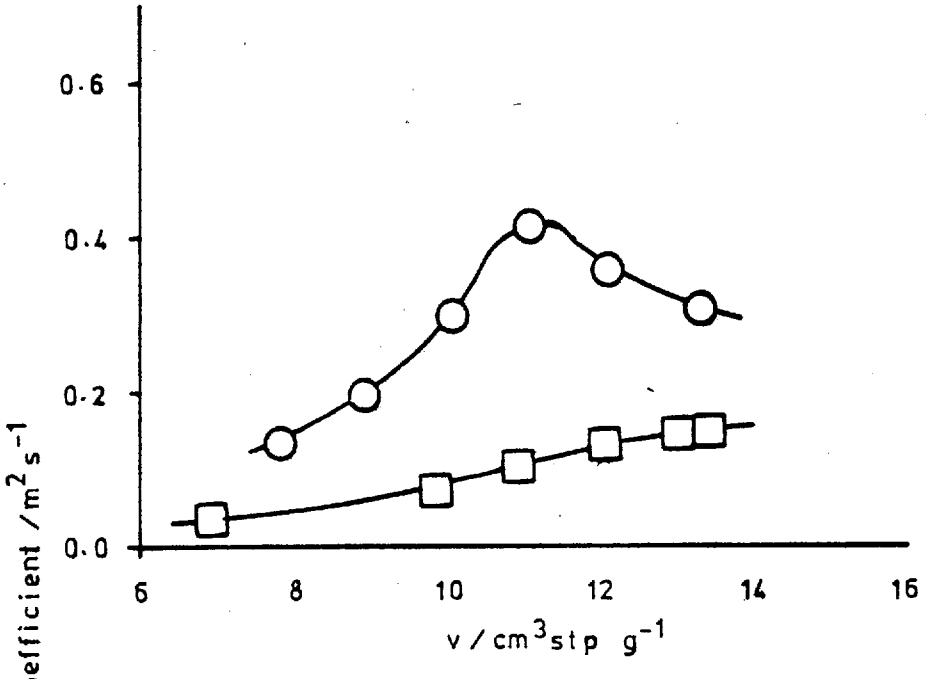

Figure 5.81. : C_3H_8/Graphon : T/K = 213.2

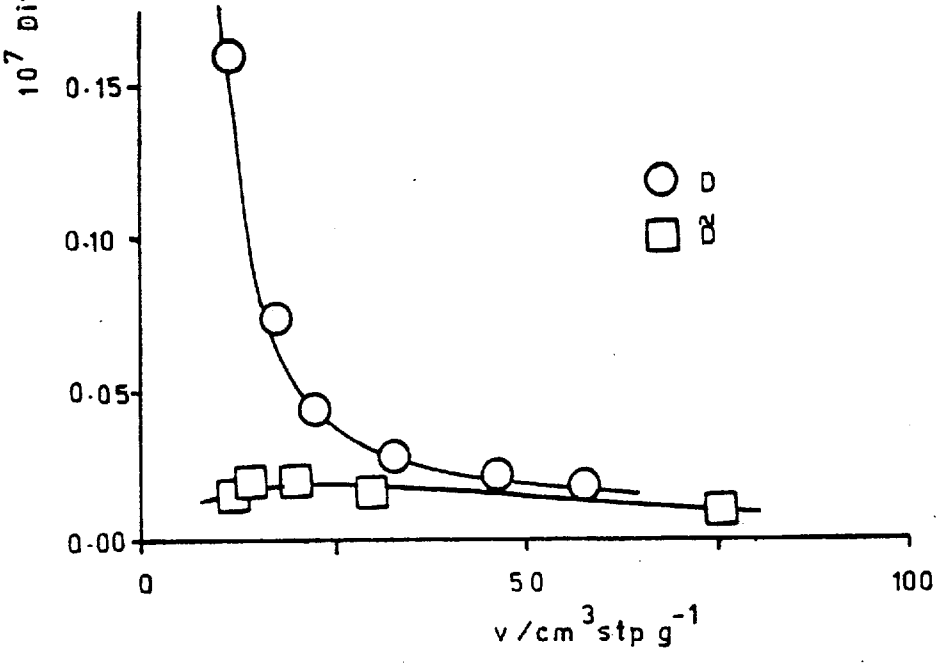

due to errors in the relevant flux curve the results at 213.2 K (Figure 5.81) to not exhibit a crossing point when the $\tilde{D}$ curve reaches its maximum. It must also be noted that Figure 5.81 does have a greatly expanded 'y' axis which tends to accentuate the difference between the two coefficients. Unfortunately a comparison with the results of Ash, Barrer and Edge (1976) was impossible due to the absence of a common temperature.

Diffusion coefficients were also evaluated for the flow of propane and isobutane through the graphitised Black Pearls membrane. The variation of the overall coefficients, D and $\tilde{D}$ with coverage is shown in Figures 5.82 to 5.85. Again the characteristic format is found. A monotonic increase in the differential coefficient, D, up to a maximum value in the region of monolayer coverage, followed by a sharp drop to a relatively constant value. The monolayer capacities, v_m, given in Figures 5.82 and 5.84 are taken from Table 4.2 and were determined, in the case of Black Pearls from sorption data measured on the free powder. A different value of v_m could have arisen from sorption measurements on the membrane and resulted in a better correlation between v_m and the position of the maximum.

In Figure 5.82 the propane results indicate the beginning of a rapid rise in the differential diffusion coefficient. This agrees with the initial findings of Carman and Raal (1951) in which a third region "marked by a rapid increase in D and a rather poor reproducibility" was obtained. This region corresponds to a narrow range of pressures in which filling of pore space by capillary condensation is approached. There is also the indication of a slight rise in the isobutane results (Figure 5.84).

Again the integral and differential quantities are compared for each temperature separately and the results given in Figures 5.86 to 5.91. The expected behaviour of D and $\tilde{D}$ as predicted from equation (2.30) is again apparent with the three mathematical criteria summarised by the relationship (5.9) being fulfilled. The condition that $\tilde{D} = D$ when $d\tilde{D}/dC_1 = 0$ infers that the D curve will cross the $\tilde{D}$ curve at a maximum or minimum in the integral curve. Both maxima and minima are observed in Figures 5.87 and 5.91 and it can be seen that the differential curve does indeed cross the integral curve at these points. From the propane

Figure 5.82. Concentration - Dependence of D : C_3H_8/Black Pearls.

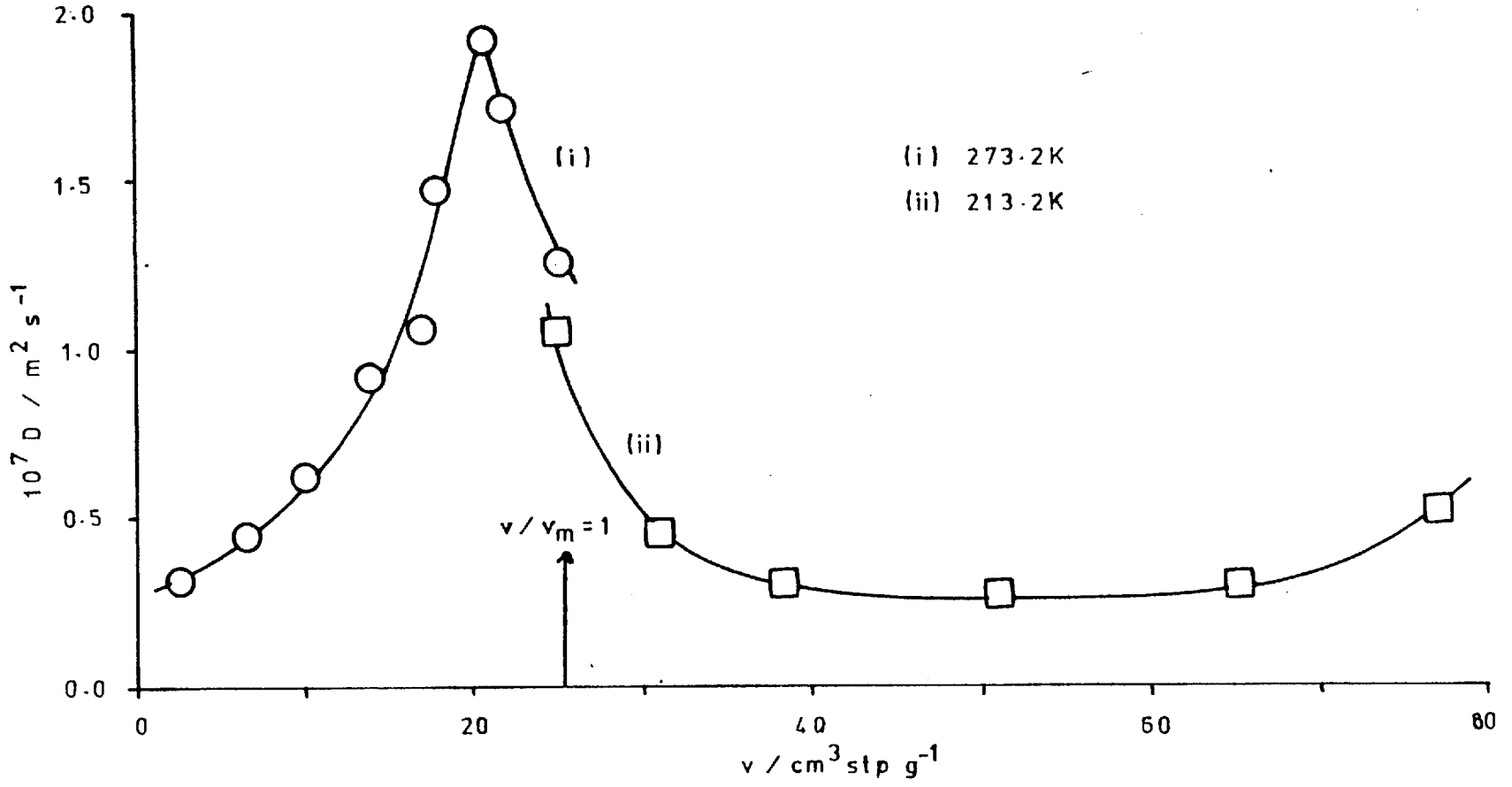

Figure 5.83. Concentration - Dependence of $\tilde{D}$: C_3H_8/Black Pearls

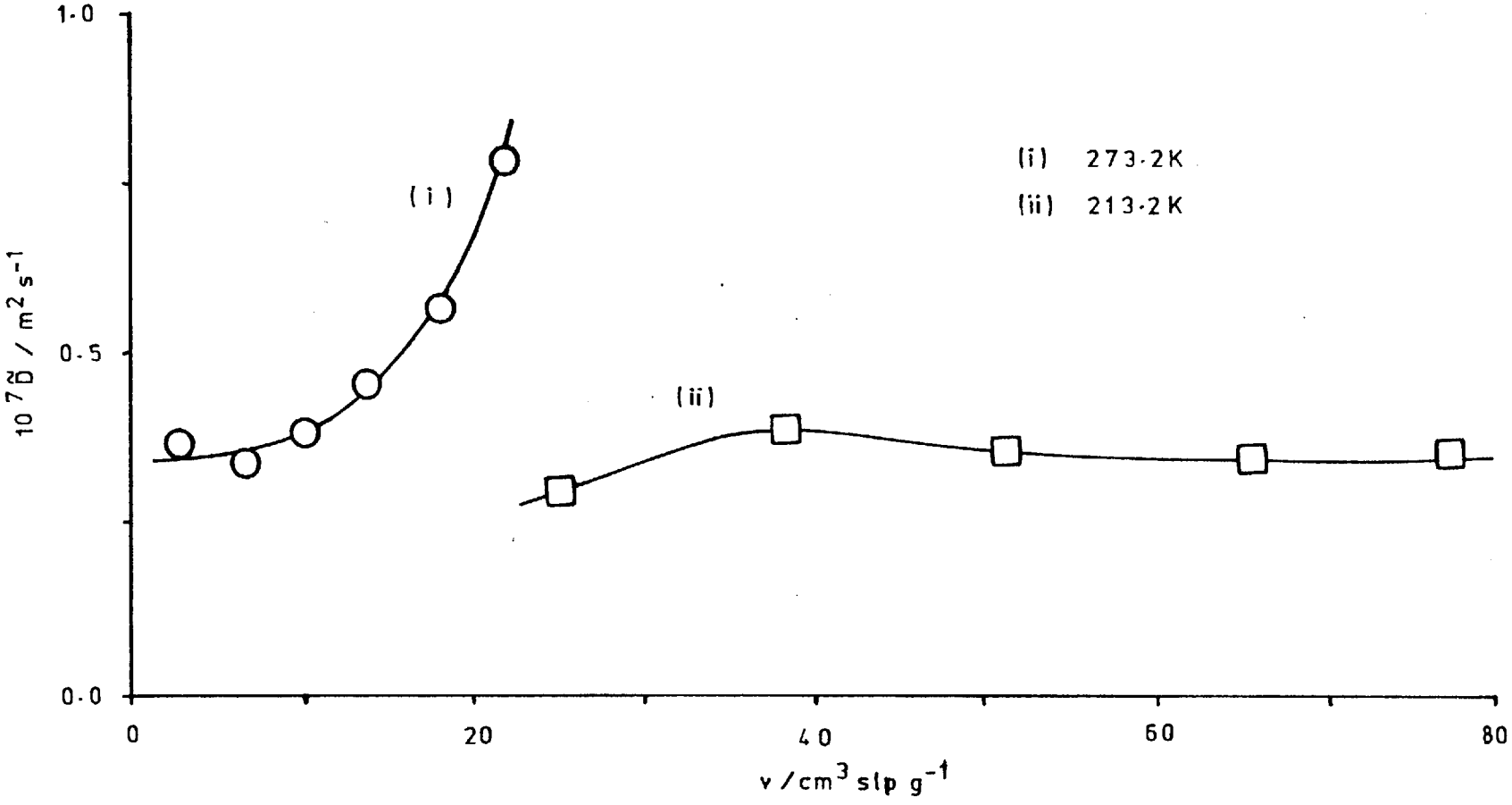

Figure 5.84. Concentration - Dependence of D : i-C_4H_{10}/Black Pearls

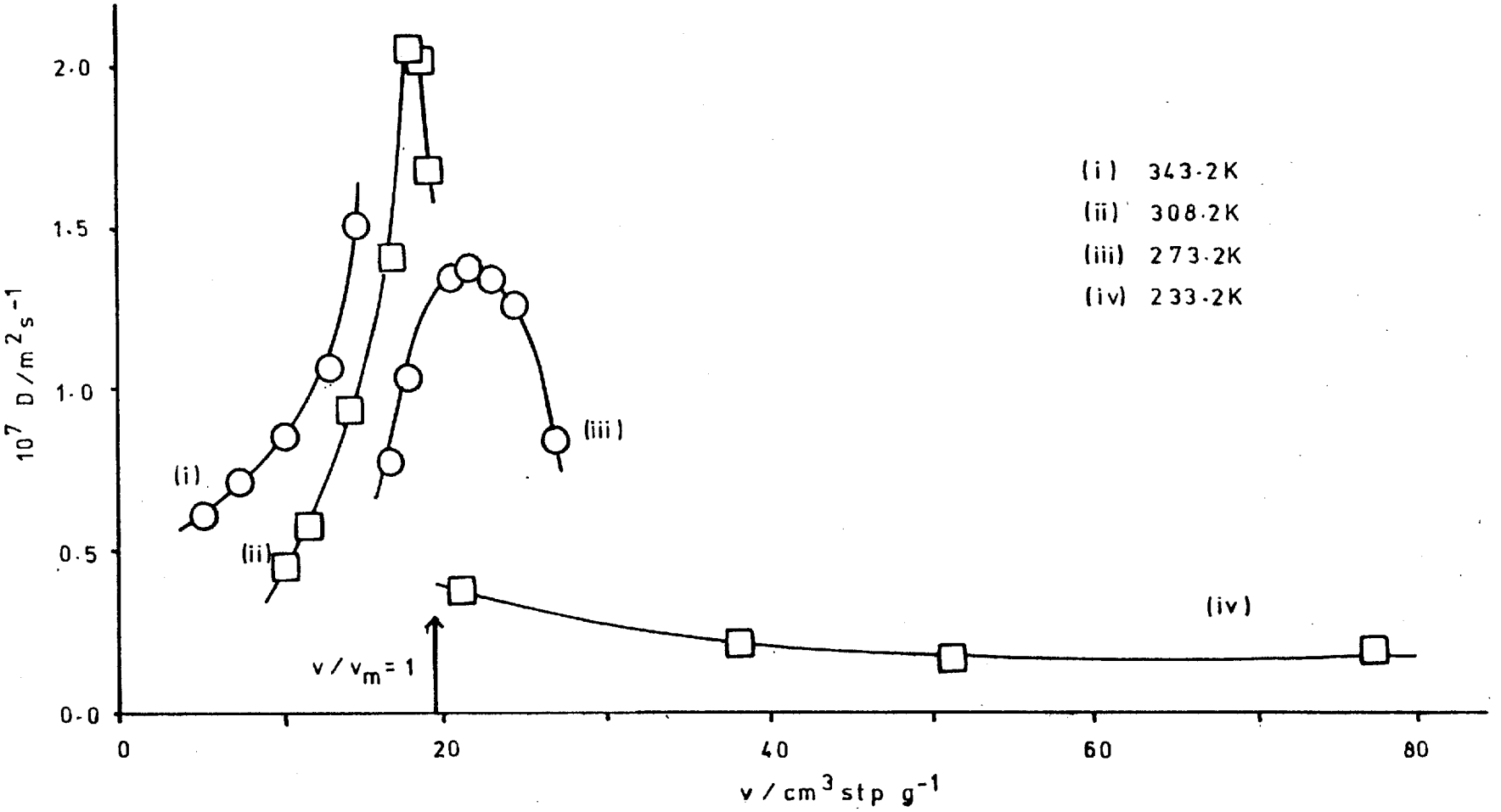

Figure 5.85. Concentration - Dependence of $\tilde{D}$: i-C_4H_{10}/Black Pearls

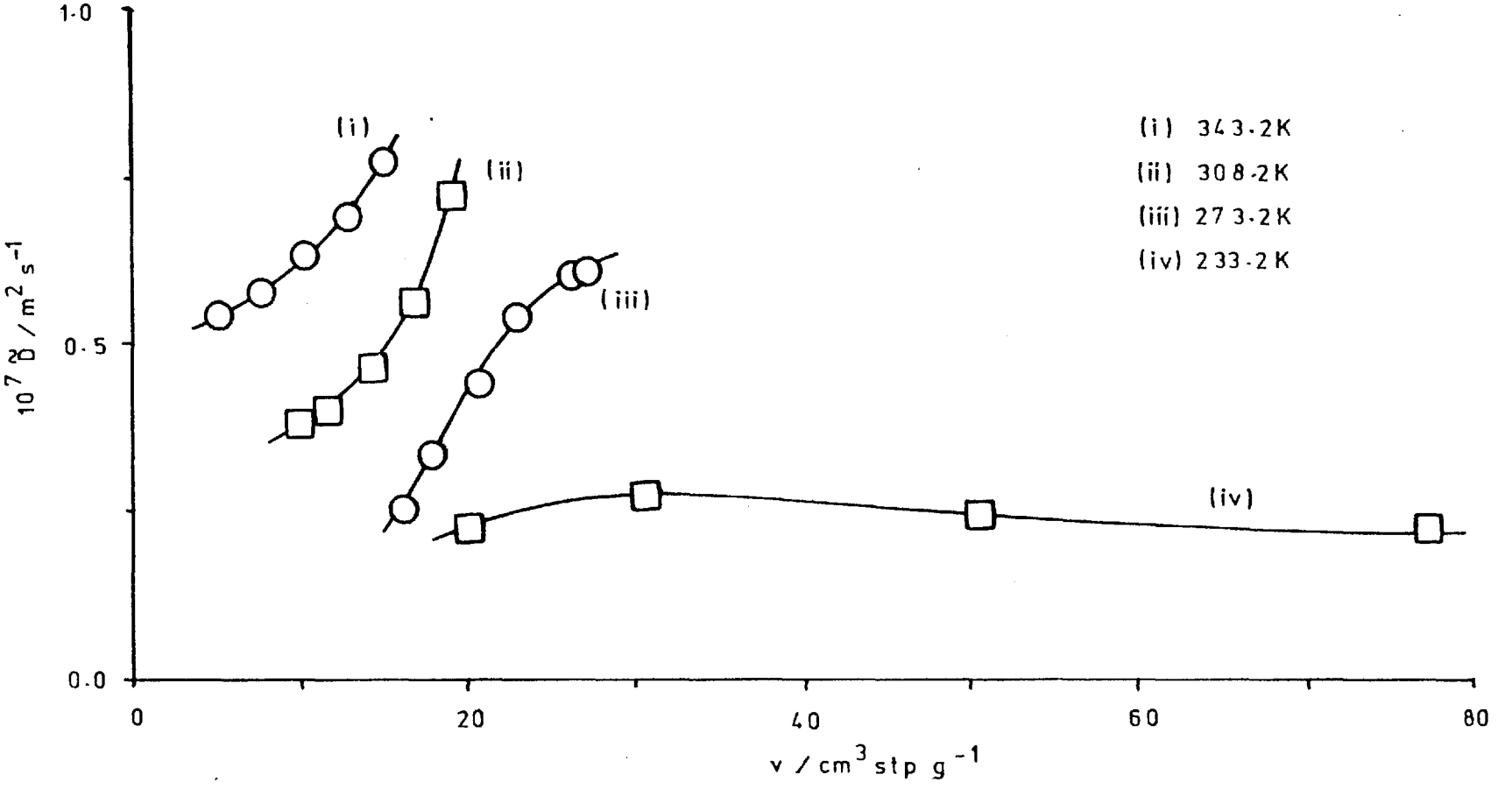

Concentration - Dependence of Diffusion Coefficients

Figure 5.86 : C_3H_8/Black Pearls : T/K = 273.2

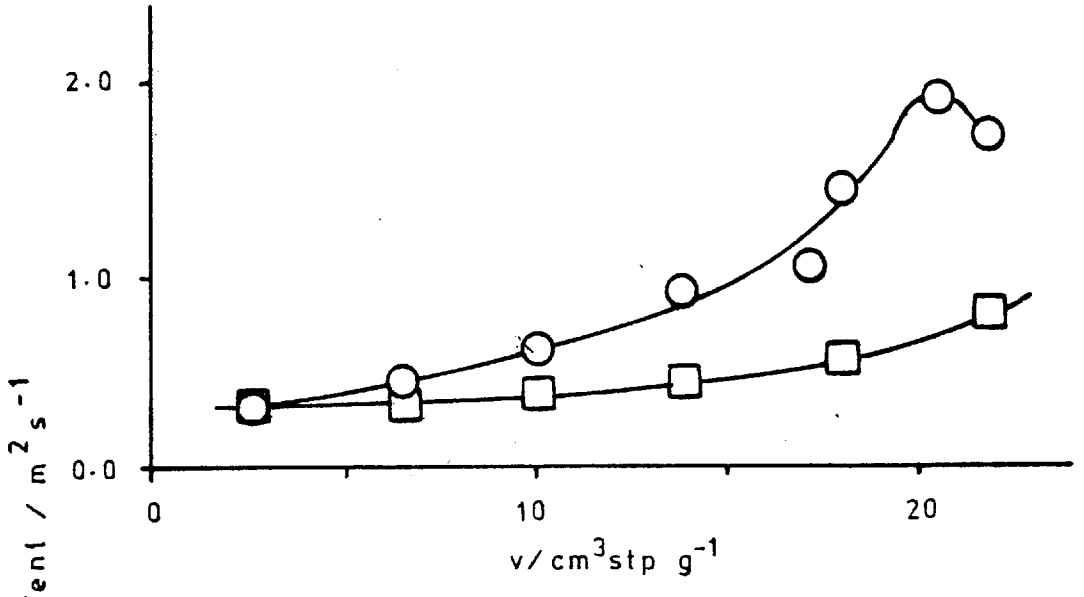

Figure 5.87 : C_3H_8/Black Pearls : T/K = 213.2

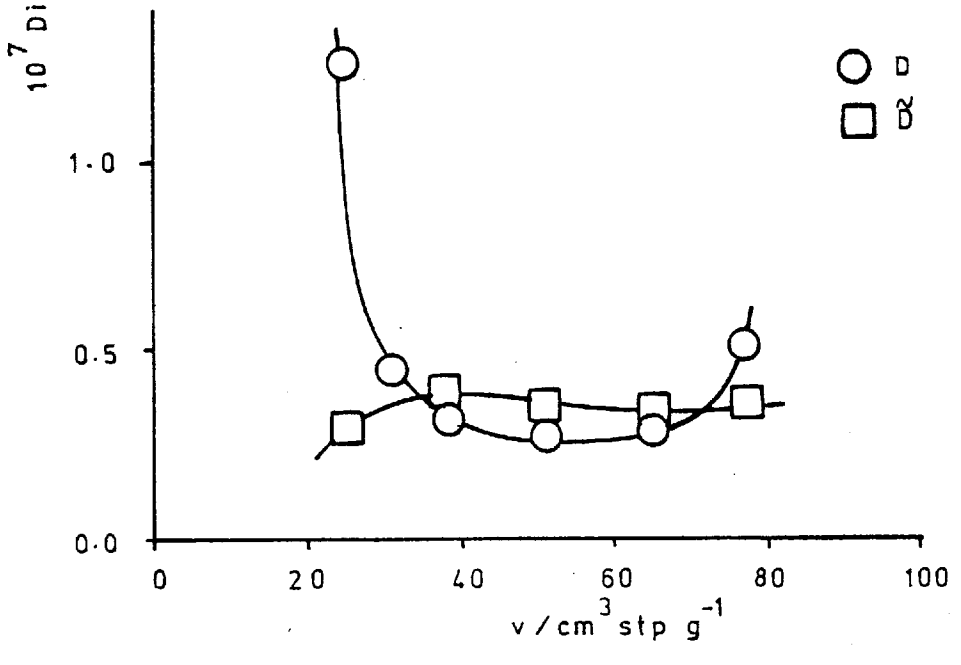

Concentration - Dependence of Diffusion Coefficients

Figure 5.88. : i-C_4H_{10}/Black Pearls : T/K = 343.2

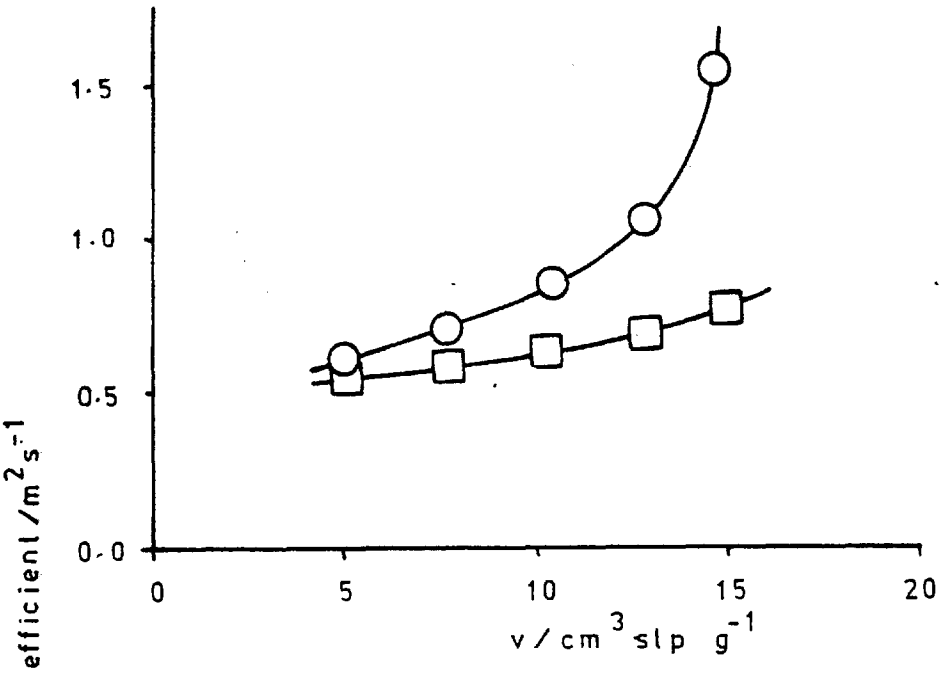

Figure 5.89. : i-C_4H_{10}/Black Pearls : T/K = 273.2

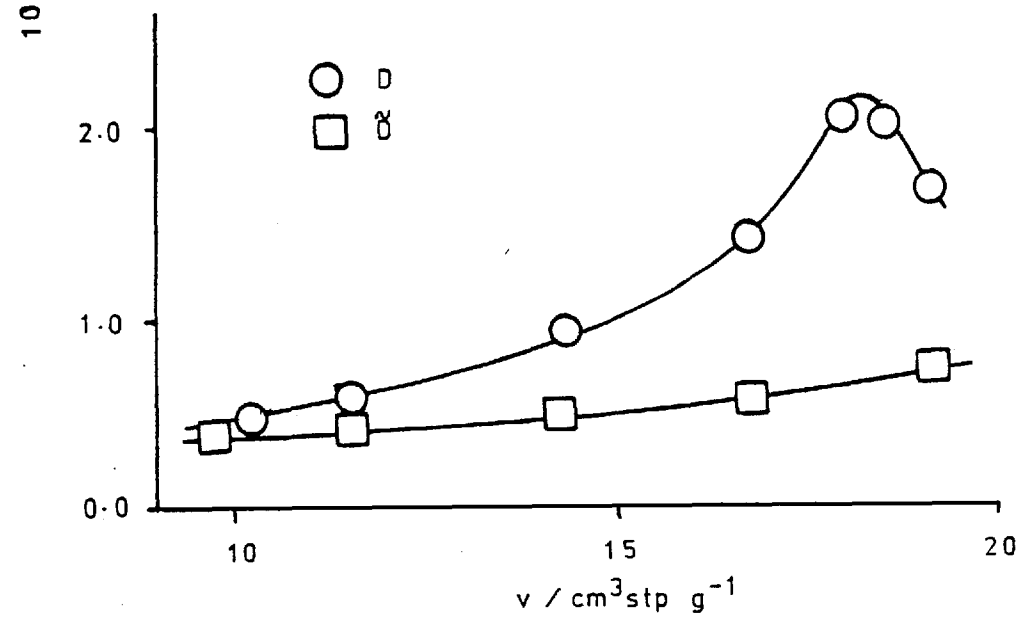

Concentration - Dependence of Diffusion Coefficients

Figure 5.90. : i-C_4H_{10}/Black Pearls : T/K = 273.2

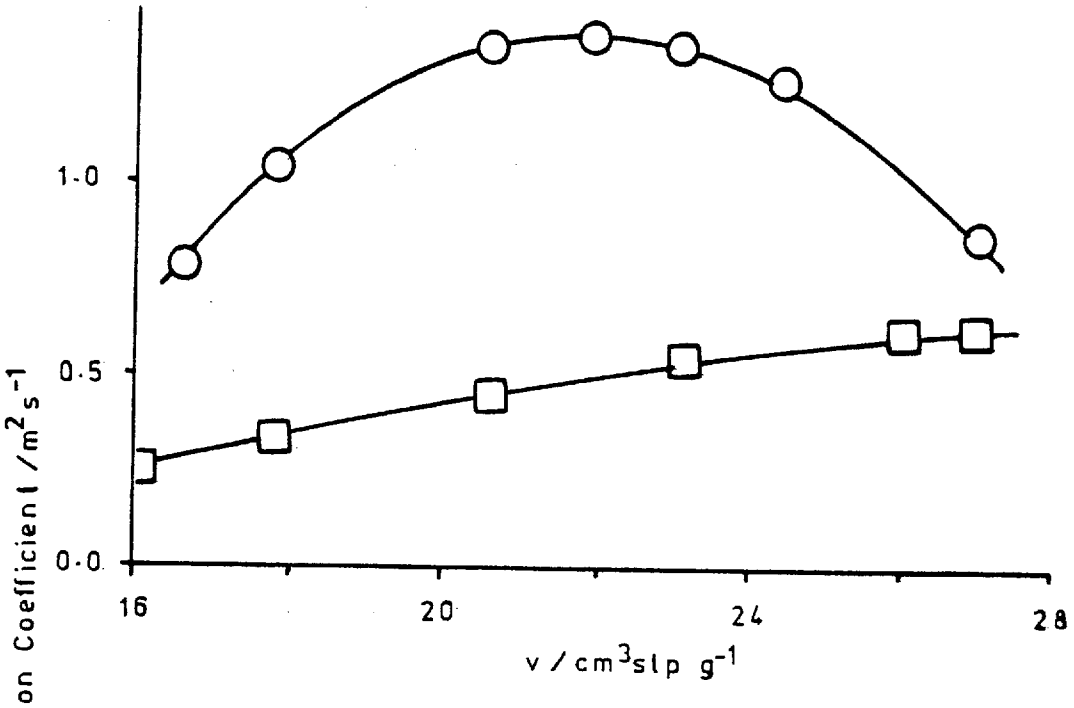

Figure 5.91. : i-C_4H_{10}/Black Pearls : T/K = 233.2

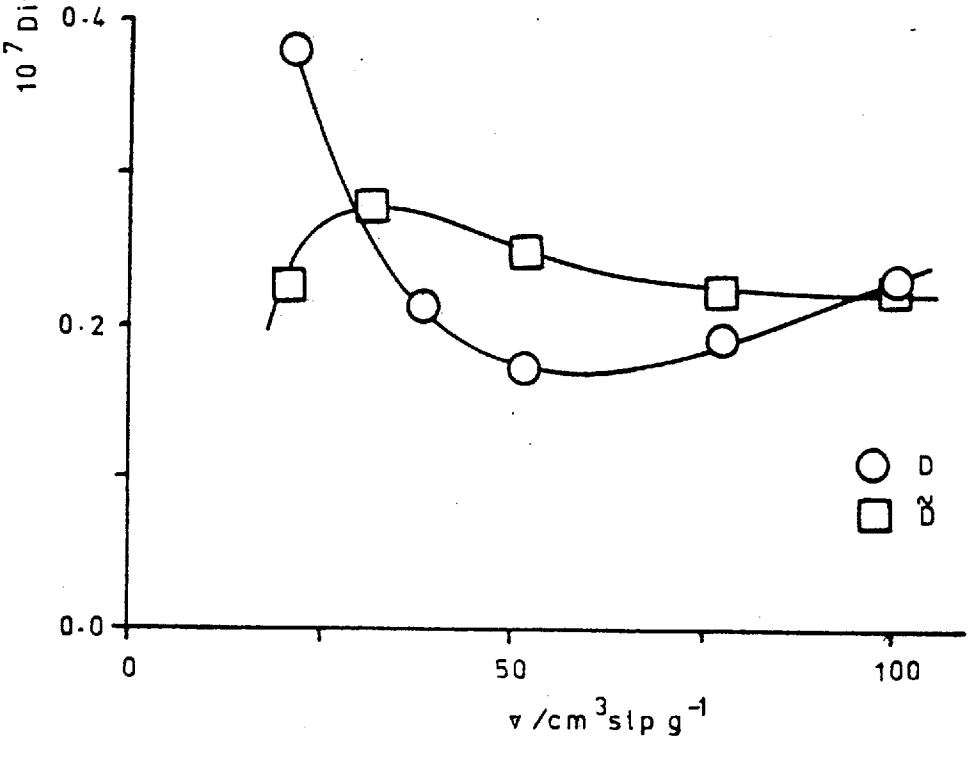

results at 273.2 K and the isobutane results at 343.2 K (Figures 5.86 and 5.88) it may be seen that the values of D and $\tilde{D}$ converge at low coverages and if the coverage was reduced further into Henry Law adsorption the two coefficients should reach a constant value as observed in the Graphon system (e.g. Figures 5.62 and 5.78).

(b) Activation Energy of Surface Migration

It has been shown previously that a marked temperature dependence of the diffusion coefficients exists (e.g. Figures 5.56 to 5.61). This dependence can be described by an Arrhenius type relationship of the general form

$$D = D_o \exp(-E/RT) \qquad (5.11)$$

where E (J mol^{-1}) is an activation energy for the diffusive process evaluated at constant coverage.

In their study of CF_2Cl_2 flow through a Carbolac membrane, Carman and Raal (1951) measured an extensive set of surface diffusion coefficients and determined activation energies. The concentration dependence of these energies was of the general form given in Figure 5.92. The activation energy for surface diffusion remained fairly constant as the coverage was increased. Then in the region of monolayer coverage a sharp drop occurred to another fairly constant value.

Figure 5.92 : General form of the Concentration-dependence of E

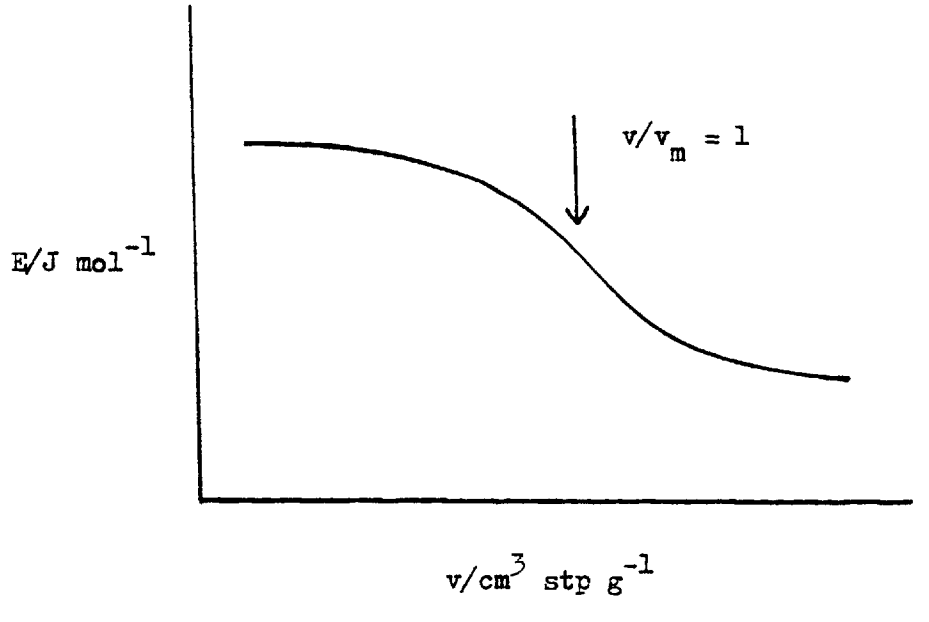

Barrer and Strachan (1955) investigated the flow of Ar, Kr and N_2 through Carbolac membranes where the adsorption was in the 'near Henry Law' region.

In this dilute film region the surface diffusion coefficients tended to increase and associated with this behaviour was a slow decrease in the activation energies. This was interpreted by the authors in terms of a heterogeneous adsorbing surface. The filling of the most energetically sorbing sites occurred first and diffusion of molecules from these sites requires the largest energy. Thus the activation energy tended to decrease as the coverage increased.

However Ross and Good (1956) in a study of n-butane flow through Graphon observed an increase in E up to a maximum value around monolayer coverage. This increase was explained in terms of lateral interactions between the adsorbed molecules. As the coverage increases these interactions become more important and the molecules require additional energy before being released for surface diffusion. It must be noted that their energies of activation were calculated from the dependence of the surface diffusion coefficient on coverage at only two temperatures and subsequently must be treated with some caution.

An investigation into the flow of argon and nitrogen through a porous ceramic (Lallemand and Eyraud, 1973) supports the original work of Carman with a concentration-dependence of E similar to the form shown in Figure 5.92.

It was possible to obtain activation energies from the isobutane/Graphon system and those calculated from the integral surface diffusion coefficients, $\tilde{D}_s'$ and $\tilde{D}_s''$ are shown in Figure 5.93(a) and (b). Due to the overlapping and general inconsistency of the differential diffusion coefficients, D_s' and D_s'' it was impossible to obtain activation energies from Figures 5.59 and 5.61. However activation energies were also calculated from the overall diffusion coefficients and these are presented in Figures 5.94 (a) and (b). It can be seen that the integral diffusion coefficient provides an activation energy with less scatter than the differential diffusion coefficient and that both result in an energy of activation of similar magnitude and concentration dependence. The concentration dependence is similar to that observed in the studies of

Figure 5.93. Concentration - Dependence of E : i-C_4H_{10}/Graphon

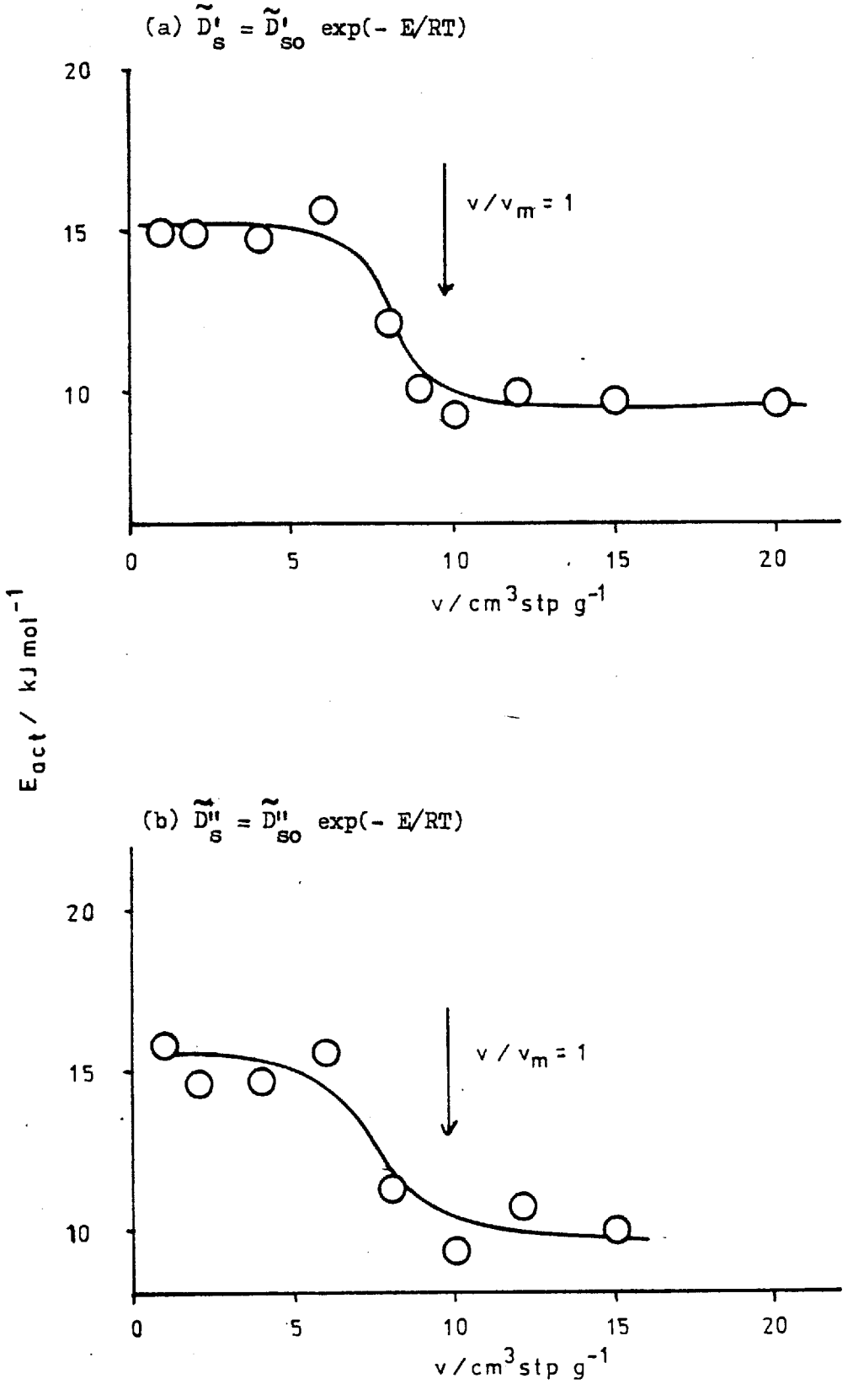

Figure 5.94. Concentration - Dependence of E : i-C_4H_{10}/Graphon

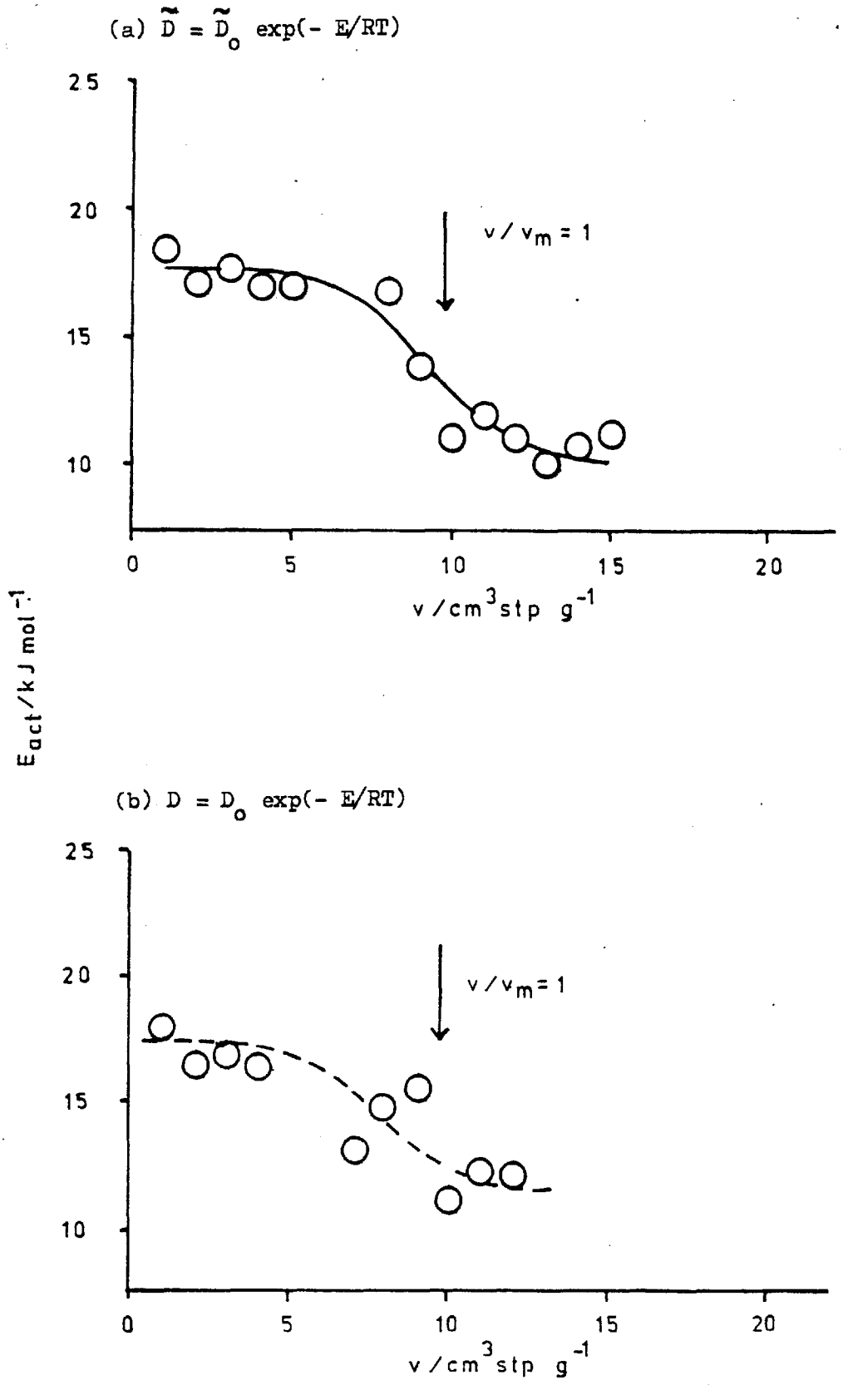

Figure 5.95. Concentration Dependence of E : i-C_4H_{10}/Black Pearls

(a) $\tilde{D} = \tilde{D}_o \exp(-E/RT)$

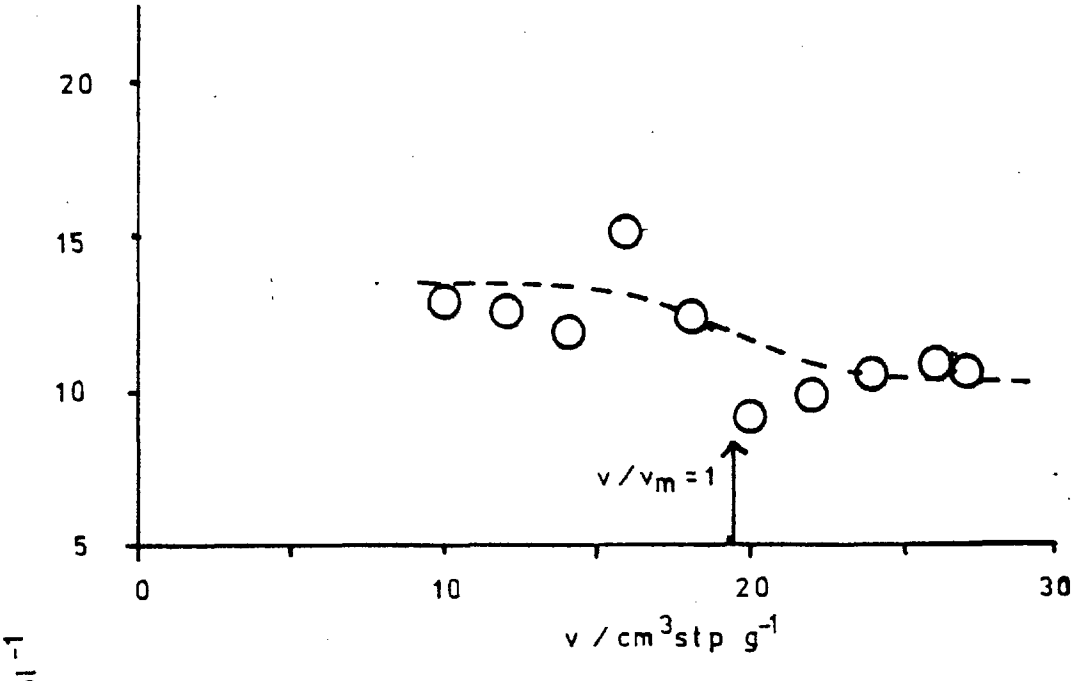

E_{act} / kJ mol^{-1}

(b) $D = D_o \exp(-E/RT)$

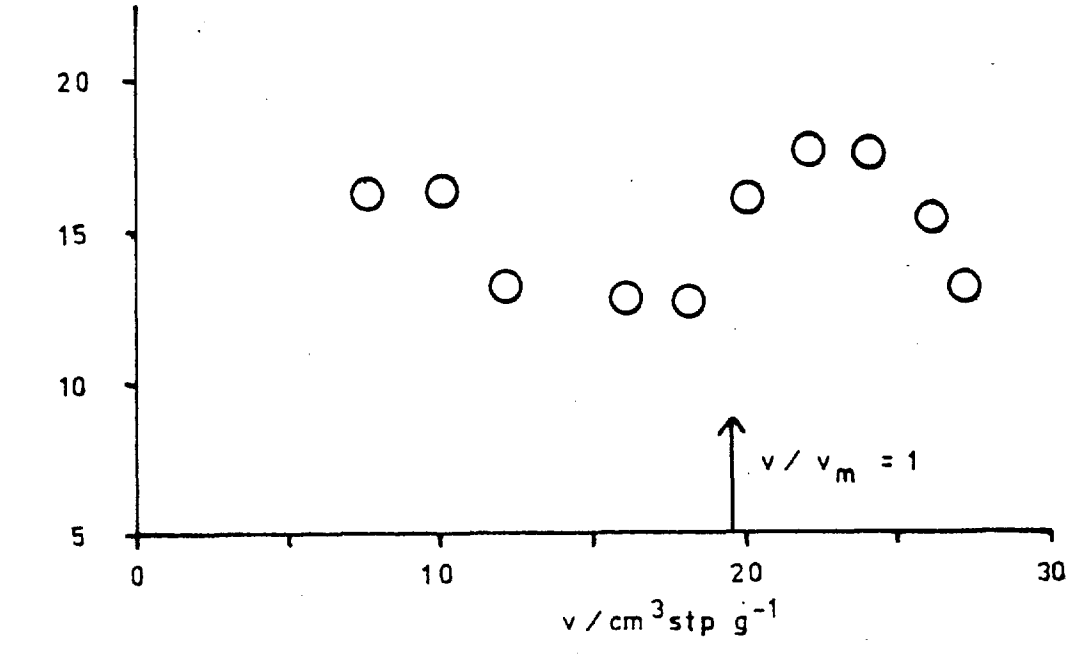

Carman and Raal (1951) and Lallemand and Eyraud (1973) and that schematically shown in Figure 5.92. Due to the reasons previously given only overall diffusion coefficients were calculated for the C_3H_8/Graphon, C_3H_8/Black Pearls and i-C_4H_{10}/Black Pearls systems. As can be seen it is impossible to calculate any meaningful activation energies from the C_3H_8 results on either Graphon or Black Pearls due to insufficient data.

The isobutane-Black Pearls system was more thoroughly examined and as a result the diffusion coefficients obtained were quite extensive. Despite this any evaluation of the activation energy involved a dependence on only two temperatures. As can be seen from Figure 5.95 this resulted in meaningless energies although the energy calculated from the integral diffusion coefficient does to a certain extent resemble the general format of Figure 5.92. The basic shape of the concentration dependence of the activation energy can only be used to signify that around a monolayer coverage something happens to drastically reduce the energy of activation enabling transport to occur. This phenomenon has generally been accepted to be indicative of a change in the mechanism from an 'activated hopping' process to a process more akin to hydrodynamic flow.

(c) Hydrodynamic Flow

It has been seen previously that the magnitude of the flux and permeability of a sorbed gas exhibits an extremely rapid increase in the vicinity of the saturated vapour pressure. This has been attributed (cf 5.2.2) to multilayer formation and capillary condensation. Various attempts have been made in the literature to correlate these large flows in terms of a hydrodynamic flow process. Carman (1952) described the flow in this region as being due to a capillary pressure difference. Gilliland, Baddour and Russel (1958) utilize the concept of a spreading pressure (Babbit, 1950) acting as the driving force governing flow. Rhim and Hwang (1974) consider the flow of capillary condensate based on a model of equivalent cylindrical capillaries. Each of these approaches has been found to describe the flow adequately for specific systems but none appears to be generally applicable.

The system examined in this study has not considered the flow near the saturated vapour pressure to any great extent with the result

that any description of the flow in this region must be purely qualitative, i.e. at high coverages a rapid increase in the transport of sorbed gas occurs. A further study of flow in this region has been instigated (Whiting, 1977) and is at present being pursued in these laboratories.

It is important to note that the boundary conditions employed in the 'conventional' technique result in a particularly complex situation in the vicinity of the saturated vapour pressure. The ingoing concentration may well be such that capillary condensation occurs at the ingoing face but due to the large concentration gradient across the membrane, achieved by maintaining the outgoing side pressure very small there may only be Henry Law adsorption at the outgoing face. This means that the idea of hydrodynamic flow of capillary condensate through a membrane maintained under such conditions is incorrect. The results from the 'pressure-decay' system should however be better suited to a hydrodynamic analysis as at large times only a very small concentration gradient exists across the membrane. This latter technique and its relationship to hydrodynamic flow is further discussed in Section 5.3.2 (b).

5.3. Discussion of 'Pressure Decay' Results and Comparison with 'Conventional' Results

5.3.1. General Features

The flow of helium and isobutane both as single species and as components in a binary mixture was studied for the Graphon membrane over a range of temperatures. This membrane system had previously been examined by 'conventional' flow techniques (cf §5.2) but it was considered of interest to investigate its behaviour under the different boundary conditions presented by the 'pressure-decay' technique. It is believed that this is the first comparison of this type to be made for membranes constructed from carbon powders. A previous study (Ash, Barrer and Sharma, 1976) has considered the flow of hydrocarbons and hydrocarbon mixtures through a Carbolac membrane using only 'pressure-decay' conditions.

This technique provides a situation where at very long times only a small concentration gradient exists between the two sides of the

membrane. Consequently, the measured quantities are differential permeabilities and differential diffusion coefficients. The theory behind the determination of the differential permeability predicts that for constant D at large times a plot of ln (Δp) vs t should be linear, where Δp is the pressure difference between the two sides of the membrane. However it was experimentally observed that these linear portions commenced at short times and were maintained without any appreciable change of slope until large times. A consequence is that differential quantities may be measured at short times when theoretically the measurement should only be possible at very long times. Long periods of linearity outside those predicted by theory have recently become increasingly common in diffusion studies. A sorption kinetics study (Barrer and Clarke, 1974) of the hydrocarbon/Zeolite A system observed an initial linear dependence of the amount adsorbed upon $\sqrt{t}$. This was predicted for small time by a solution of Fick's equation when the diffusion coefficient was independent of concentration. However this linearity persisted even when the conditions were such that the diffusion coefficient was a function of concentration. A technique known as 'the early time procedure' has also produced some surprise results (Ash, Barrer and Edge, 1976). The procedure is a method of calculating diffusion coefficients directly from unsteady-state flow data. Again the theory (for constant D) predicts a linear plot (in this case for ln $[t^{\frac{1}{2}} dp_2/dt]$ vs $1/t$) for sufficiently small t. However it was observed that this relationship was valid for hydrocarbon flow through a Graphon membrane under conditions where the diffusion coefficient was most definitely dependent on concentration.

The pressure decay study of Sharma (1970) which employed a Carbolac membrane produced plots of ln (Δp) vs t which exhibited an initial curved portion before becoming linear at longer times. For this study involving Graphon the single species results produced linear plots at short times. A selection of experimental plots are given in Figures 5.96 to 5.99 covering a range of temperatures.

5.3.2. Single Species Flow

(a) Helium

The helium flow measurements presented in Figures 4.58 and 4.59 are the permeabilities as functions of pressure and temperature. The

Figure 5.96. Plot of ln (Δp/cm Hg) vs t : Helium*Graphon : T/K = 308.2

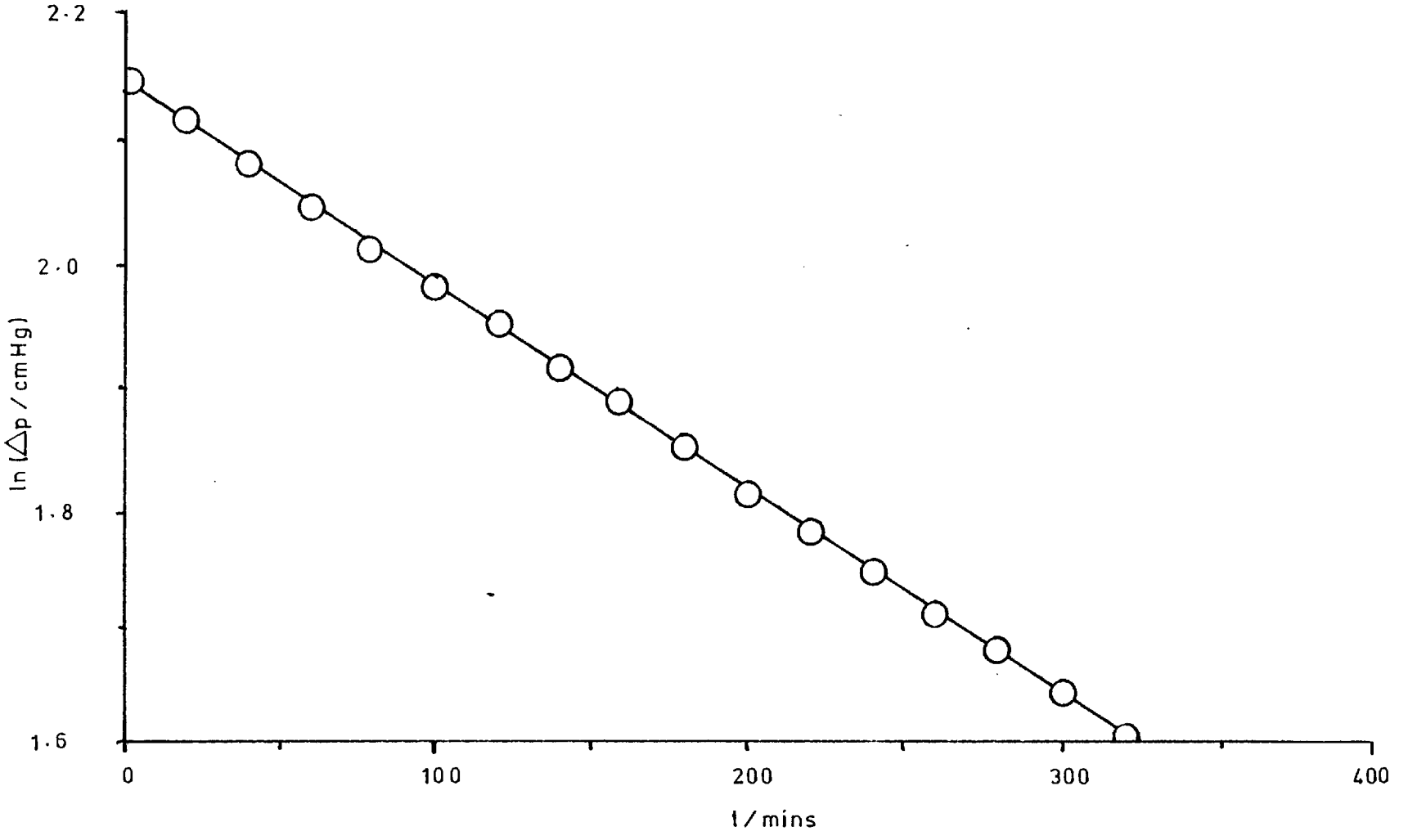

Figure 5.97. Plot of ln (Δp/cm Hg) vs t : i-C_4H_{10}/Graphon : T/K = 393.2

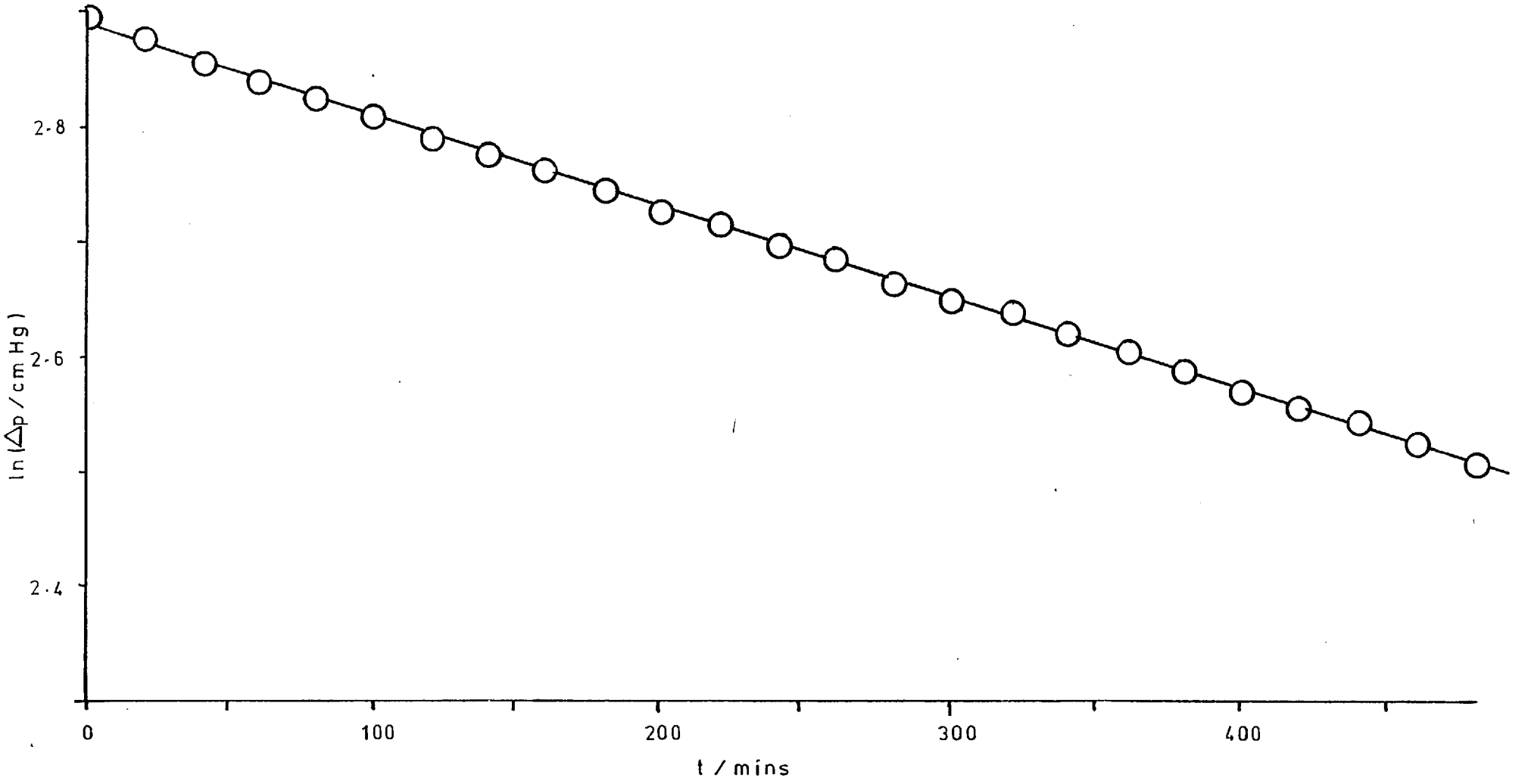

Figure 5.98. Plot of ln (Δp/cm Hg) vs t : i-C_4H_{10}/Graphon : T/K = 308.2

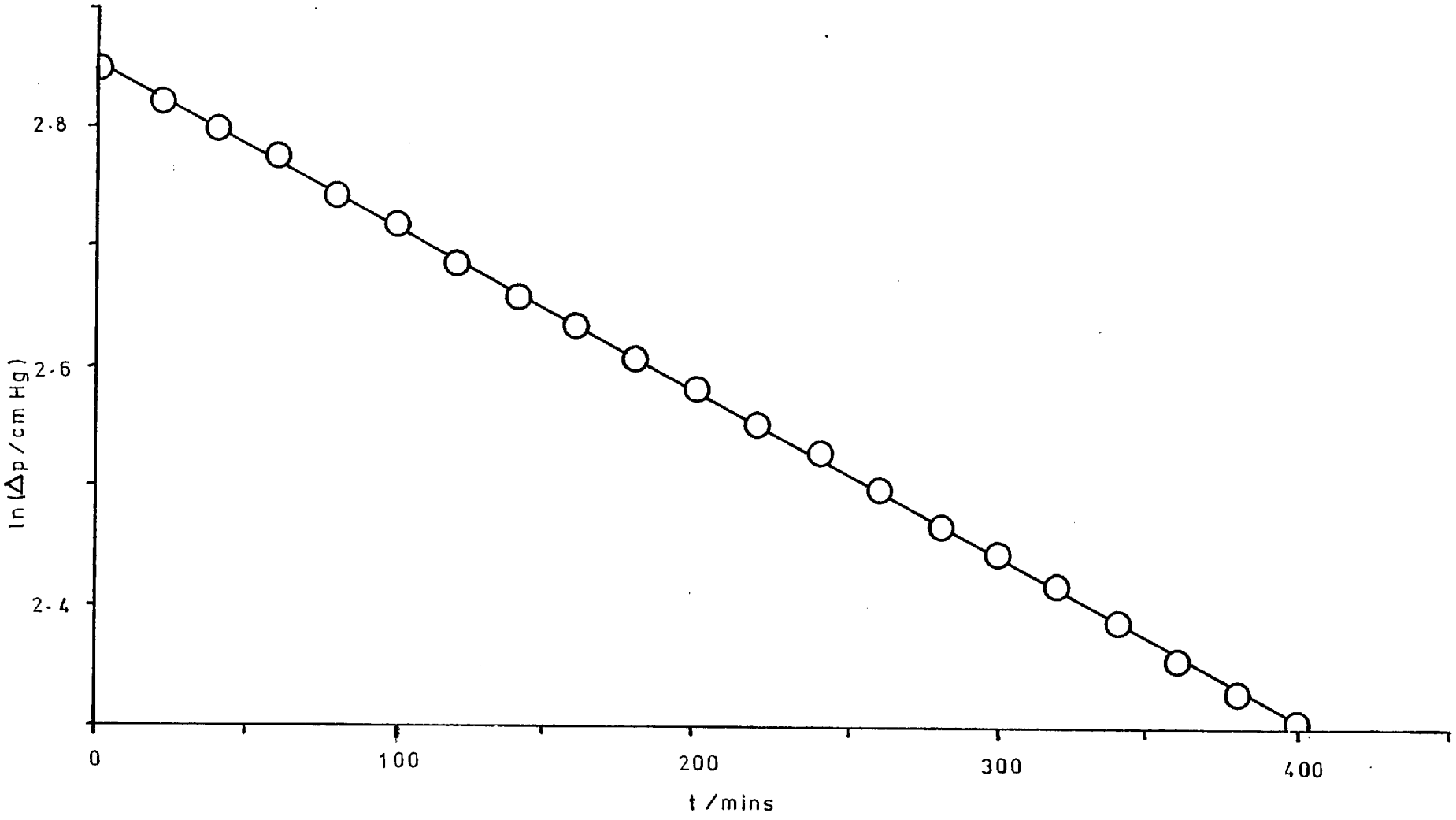

Figure 5.99. Plot of ln (Δp/cm Hg) vs t : i-C_4H_{10}/Graphon : T/K = 233.2

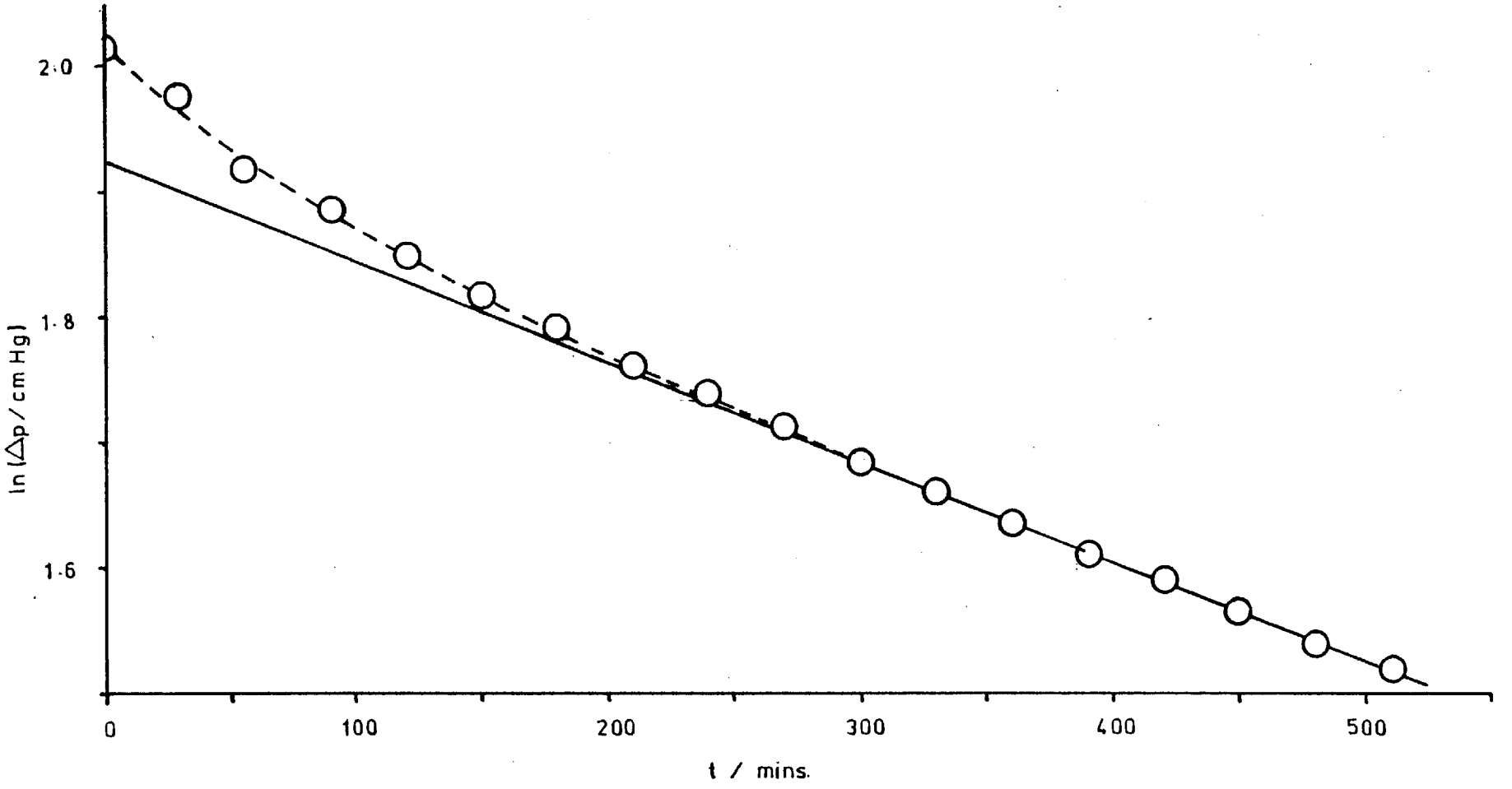

behaviour of the membrane was similar to that produced by the 'conventional procedure' and discussed in Section 5.2.1. There was however a slight difference in the constant $KT^{-\frac{1}{2}}$ as determined by the two procedures, $1.78 \times 10^{-7} m^2 s^{-1} K^{-\frac{1}{2}}$ and $1.66 \times 10^{-7} m^2 s^{-1} K^{-\frac{1}{2}}$ for the 'conventional' and 'pressure-decay' respectively. It is true that one method determines an integral permeability, $\tilde{K}$ whilst the other provides a differential one, K but these two are related by equation (2.48).

$$K(C_g') = \tilde{K} + \left(\frac{\partial \tilde{K}}{\partial C_g'}\right) C_g' \qquad (2.48)$$

For helium flow the integral permeability is independent of concentration and subsequently K should equal $\tilde{K}$. Thus the observed difference must be due to either experimental error, a calibration error or perhaps some alteration to the membrane characteristics in transferring it from one apparatus to another. It is pertinent to add at this point that although experimental runs were taken to long times (in the literal sense) it was impracticable to achieve the condition of $\Delta p \Rightarrow$ zero. This may have the effect that the measured permeabilities are not truly differential quantities. Further work is being undertaken on the Graphon system to clarify the situation but it is assumed, at present that differential permeabilities are measured.

(b) Isobutane

The isobutane differential permeabilities are shown in Figures 4.56 and 4.57 as functions of equilibrium pressure, p_∞ and relative pressure, p_∞/p_o. The general shapes of the plots are similar to those obtained for the 'conventional' arrangement. At high temperatures K^* does not exhibit a marked dependence on pressure. Then as the temperature is lowered the magnitude of K^* and the pressure dependence increases. This behaviour was observed for the pressure decay study of Ash, Barrer and Sharma (1976). The dependence increases until at very low temperatures a minimum is observed. If, however the integral and differential permeabilities are plotted on the same graph for a given temperature clear-cut differences emerge. These types of plot are given in Figures 5.100 to 5.103 with the integral values measured on the 'conventional' apparatus and the differential values experimentally obtained using the

Comparison of Integral and Differential Permeabilities : i-C_4H_{10}/Graphon

Figure 5.100. T/K = 393.2

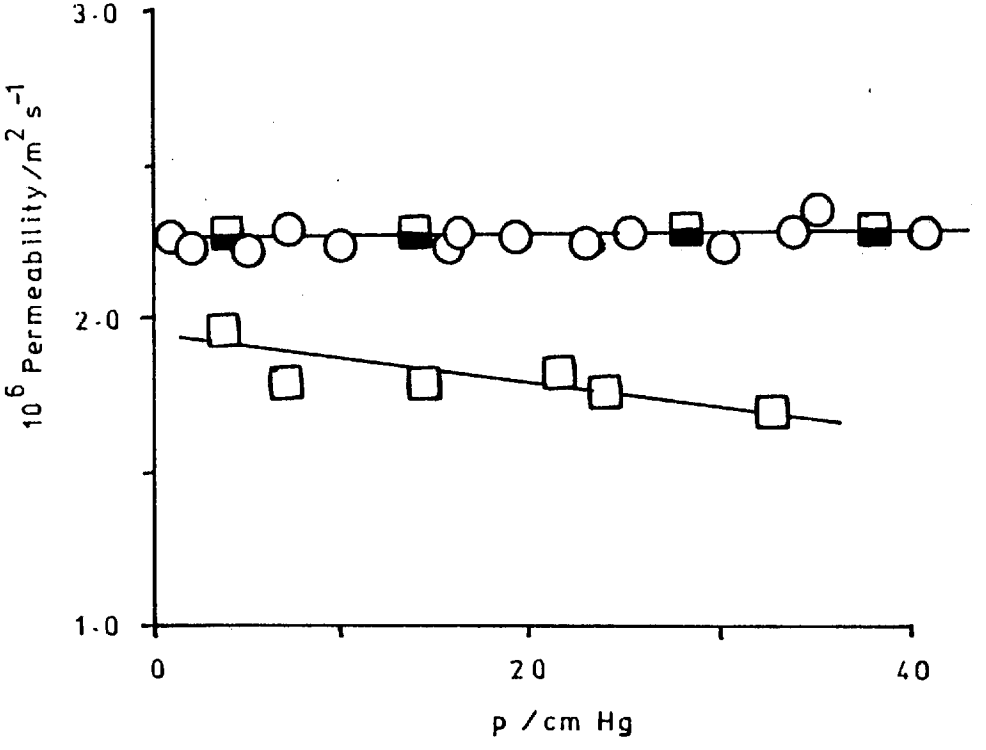

Figure 5.101. T/K = 308.2

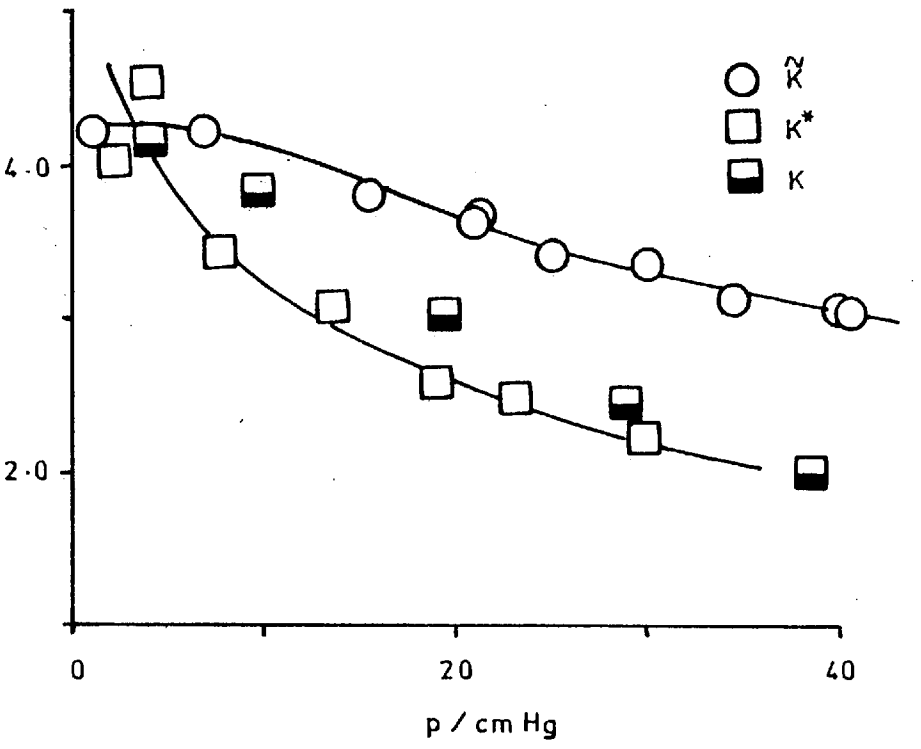

Comparison of Integral and Differential Permeabilities : $i\text{-}C_4H_{10}$/Graphon

Figure 5.102. T/K = 273.2

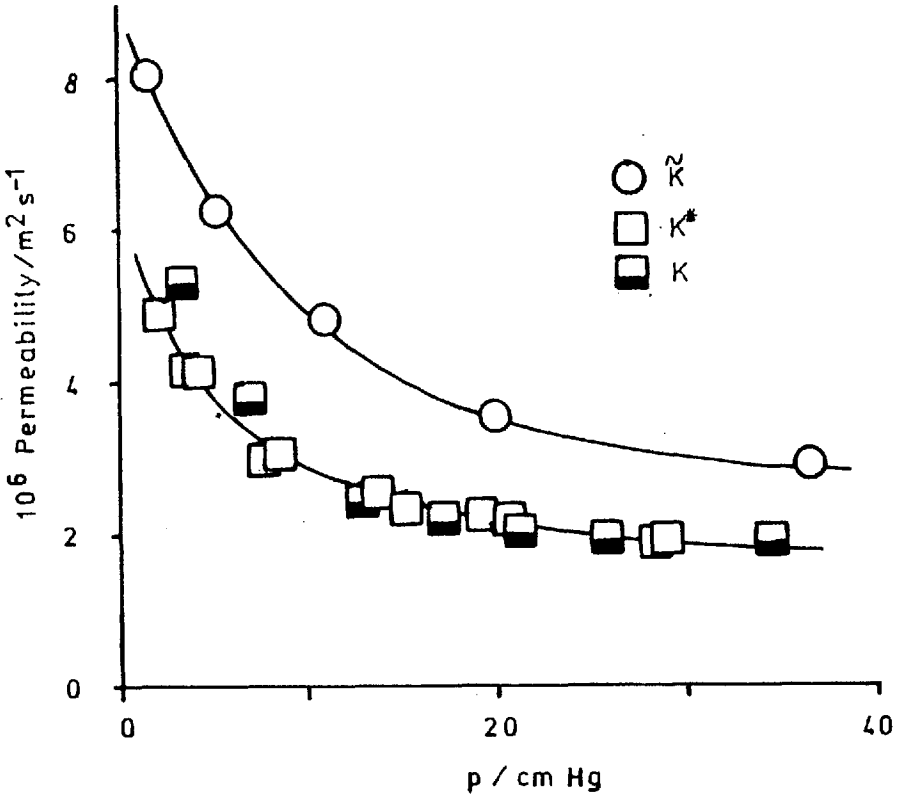

Figure 5.103. T/K = 233.2

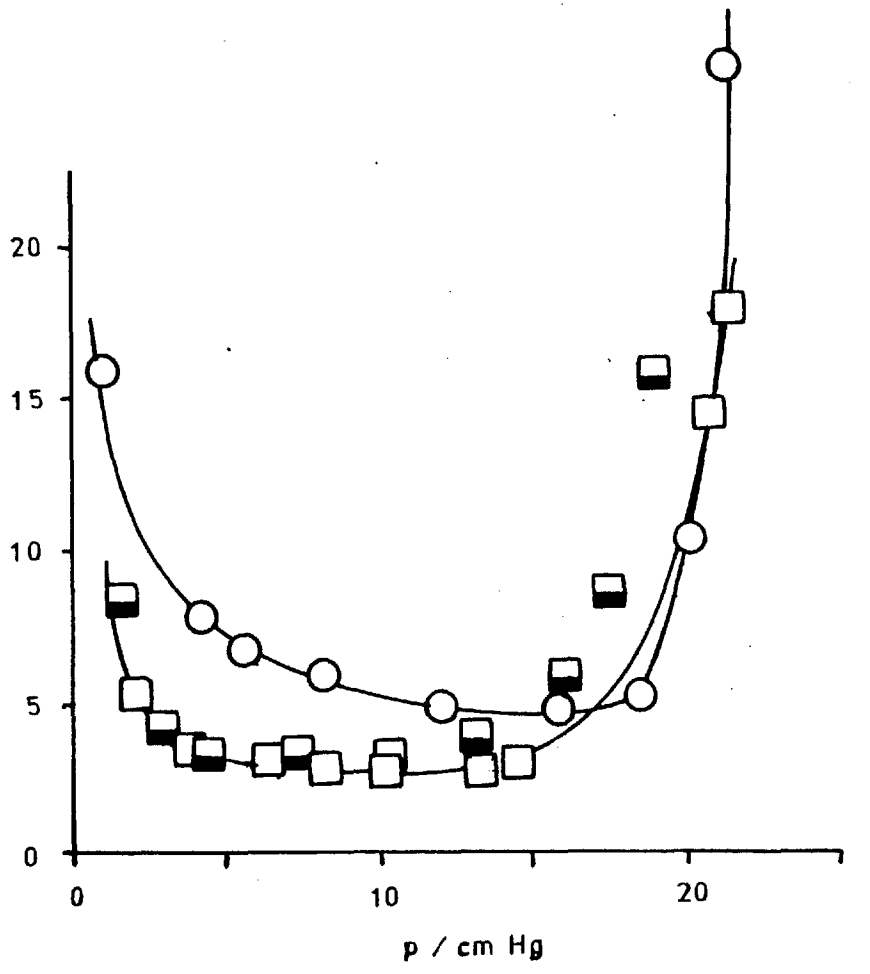

'pressure-decay' technique. Also included in the figures are differential values as calculated from the experimental measurements made on the 'conventional' apparatus by the relationship (5.12) (equation (2.46) after substitution for C'_{g1}):

$$K(p_1) = \ell RT \frac{\partial J_{oo(p_1)}}{\partial p_1} \qquad (5.12)$$

Considering initially the integral values, the calculated differential values and the relationship between the two (similar to equation (2.48)):

$$K(p_1) = \tilde{K}(p_1) + p_1 \frac{\partial \tilde{K}(p_1)}{\partial p_1} \qquad (5.13)$$

The behaviour of each coefficient relative to each other is rationalized, when $\tilde{K}$ is independent of p_1 then $K = \tilde{K}$ (cf Figure 5.100) and by the K curve crossing the $\tilde{K}$ curve at its minimum (when $\partial K/\partial p_1 = 0$) as in Figure 5.103. This type of relationship is similar to that exhibited by the integral and differential diffusion coefficients as discussed in Section (5.2.4). This complementary behaviour is however a mathematical requirement arising from equation (5.13). If a comparison is made between the actual measured differential permeabilities and the calculated ones several distinct differences are immediately apparent.

At high temperature (Figure 5.100) the calculated differential permeability, K is independent of increasing equilibrium pressure of isobutane but the measured differential permeability, designated K^* tends to decrease with increasing pressure. Also K and K^* do not appear to converge as p_{oo} tends to zero.

As the temperature is decreased both K and K^* exhibit similar though not identical behaviour, both tend to decrease as the pressure is increased. The absolute values at 308.2 K tend to converge and at 273.2 K the two are identical in the region $10 < p/\text{cm Hg} < 40$ (cf Figure 5.102).

For the flow at 233.2 K (Figure 5.103) the two permeabilities each exhibit a minimum in their pressure dependence. Also, as predicted by equation (5.13) both curves cross the integral permeability curve in the vicinity of its broad minimum. However they do not cross it at identical spots and while at high pressures the K curve agrees with the

equation in that $K > \tilde{K}$ when $d\tilde{K}/dp_1 > 0$ the K^* curve does not. It does cross near the minimum but then it tends to converge with the integral permeability, $\tilde{K}$ curve.

It is important not to have any preconceived ideas about the behaviour of the differential permeabilities based upon those obtained from the 'conventional' flow apparatus. The same membrane has been employed for both studies but the experimental conditions are quite different. At the present time it is only within the scope of this investigation to compare and contrast the results obtained by this, the first comparison of its type to be made. It was suggested (§5.2.4 (c)) that due to the existence of an infinitesimally small concentration gradient in the membrane the idea of hydrodynamic flow at high coverages may be more appropriate than in the case of the 'conventional' arrangement. To this end the following sections on diffusion coefficients and coefficients of resistance are included.

Diffusion Coefficients

An overall differential diffusion coefficient, D^* was evaluated as a function of coverage and temperature by the relationship (2.90) which is recalled here :

$$K^*(C'_{g_{\infty}}) = D^*(C'_{g_{\infty}})[\epsilon + A\sigma_{\infty}] \qquad (2.90)$$

where σ_{∞} $(= \partial C'_s/\partial C'_g)$ is the slope of the isotherm at $(C'_{g_{\infty}})$. The isotherms were those measured on the sample of Graphon pellets. The variation of D^* with coverage is illustrated in Figure 5.104. At high temperatures D^* is independent of coverage. As the coverage increases up to monolayer the diffusion coefficient also increases to a maximum value in the vicinity of $v/v_m = 1.0$. Then with multilayer adsorption the coefficient decreases to a constant value. These results agree with those measured on the 'conventional' apparatus and those initially measured by Carman and Raal (1951) which fell into three regions (previously discussed in Section 5.2.4 (b)). However also included in Figure 5.104 are the overall differential diffusion coefficients, D obtained from the 'conventional' arrangement and calculated by equation (2.23). It is obvious that although the basic trends are common to both D and D^* the absolute magnitudes are not. In fact

Figure 5.104. Concentration - Dependence of D, D* : i-C_4H_{10}/Graphon

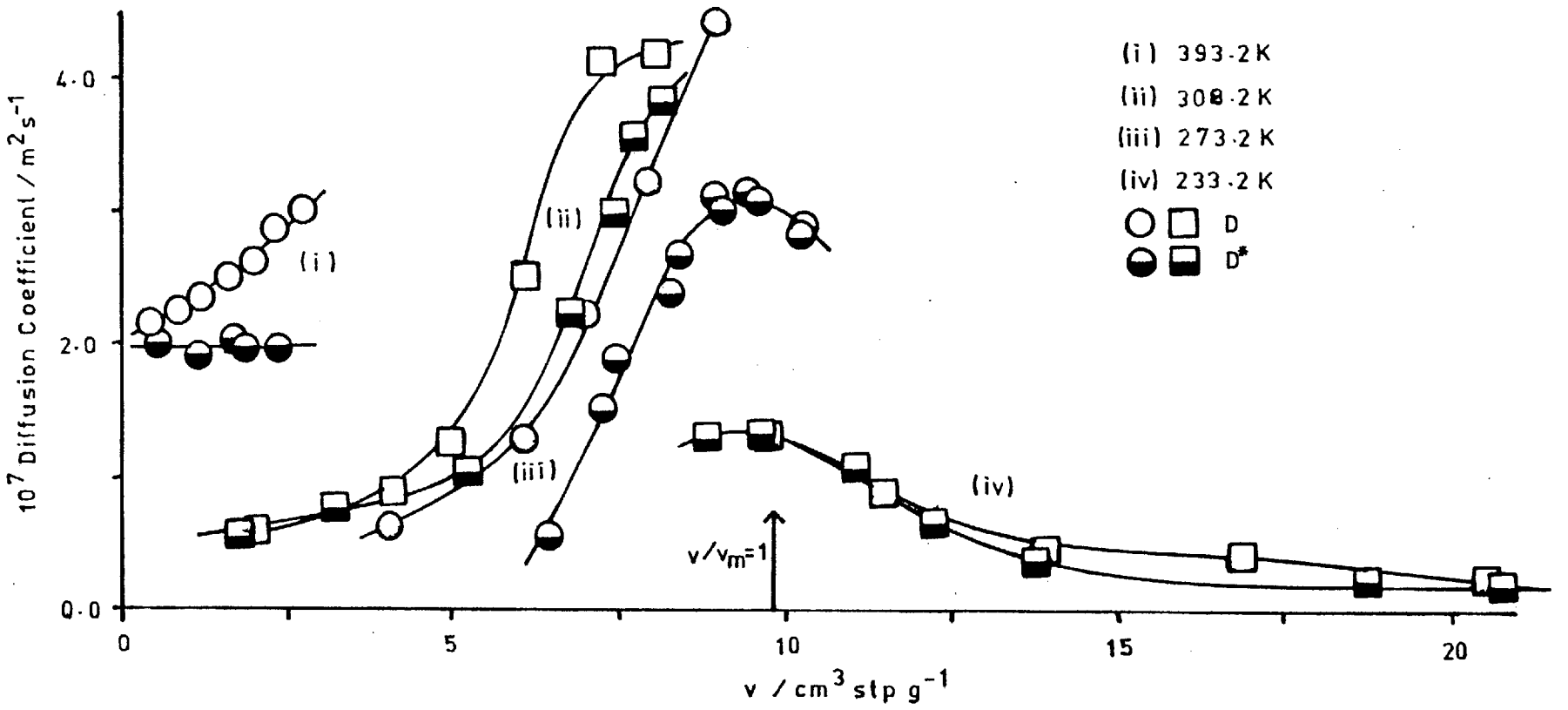

only the results at 233.2 K are in good agreement. Considering the marked difference between D and D^* at 393.2 K; D^* is independent of coverage whilst D shows a significant concentration dependence. These differences can be rationalized with the aid of the defining equations (2.50) and (2.90). The slope of the isotherm, σ, ϵ and A will be the same for both cases but the differential permeabilities differ as shown in Figures 5.100 to 5.103 and thus the diffusion coefficients must differ. The results at 308.2 K also correspond to the differences in K and K^*, each being fairly similar at either extreme of the range resulting in similarities between D and D^* the same regions.

It would be expected then that D and D^* should be identical for the results at 273.2 K due to the close similarity between K and K^* at this temperature (Figure 5.102). This is seen not to be the case in Figure 5.104. An explanation may lie in the fact that D was calculated from the flux curve by equation (2.23) and the isotherm slope did not enter into the calculation. However D^* made use of 'σ' in equation (2.90). It is conceivable that the graphical differentiation of the isotherm is inaccurate, especially in the vicinity of the monolayer coverage where only slight curvature exists. Similarly the graphical differentiation of the J vs C_1 curve (required to evaluate D) may be at fault for the same reason. Purely on the grounds that a maximum in the D curve is expected in the region of a monolayer coverage the differentiation of the flux curve may be assumed to be somewhat suspect. However again it must be emphasised that the differential D^* should be considered in its own right due to the totally different procedures employed in the evaluation of D and D^*.

Hydrodynamic Flow

The treatment of Gilliland, Baddour and Russel (1958) has been frequently employed to describe flow in hydrodynamic terms. Use is made of the fundamental equation proposed by Babbit (1950) where :

$$C_R u = - \frac{d\emptyset}{dx} \qquad (5.14)$$

C_R is the coefficient of resistance ($Nm^{-3}s$), u is the average rate of movement of adsorbed film (ms^{-1}) and $\emptyset$ is a spreading pressure (Nm^{-1}).

Assuming that the gas phase and adsorbed phase are in equilibrium, ideal gas behaviour, and that the Gibbs adsorption equation applies then the rate of movement can be expressed by

$$u = -\frac{1}{C_R} \cdot C'_s \cdot \frac{RT}{p} \cdot \frac{dp}{dx} \tag{5.15}$$

Then the extra flow, J_s/A_c for a porous media is given by

$$J_s/A_c = AC'_s u' \tag{5.16}$$

where $u' = u/\mathcal{K}$ with $\mathcal{K}$ being a dimensionless structure factor.

Combining equations (5.15) and (5.16) results in:

$$\frac{J_s}{A_c} = -\frac{ART}{\mathcal{K}C_R} \cdot \frac{(C'_s)^2}{p} \cdot \frac{dp}{dx} \tag{5.17}$$

The following extension to the treatment was provided by Mr D. Whiting of these laboratories. Recalling the definition of a permeability:

$$\frac{J_\infty}{A_c} \equiv -\frac{K}{RT} \cdot \frac{dp}{dx} \tag{5.18}$$

$$= \frac{J_g}{A_c} + \frac{J_s}{A_c} \tag{5.19}$$

where $\frac{J_g}{A_c} = -\frac{K_g}{RT} \cdot \frac{dp}{dx}$ and $\frac{J_s}{A_c} = -\frac{K_s}{RT} \cdot \frac{dp}{dx}$ (5.20)

thus :

$$\frac{J_s}{A_c} = -\frac{K_s}{\ell RT} \cdot \frac{dp}{dx} = -\frac{ART}{\mathcal{K}C_R} \cdot \frac{(C'_s)^2}{p} \cdot \frac{dp}{dx} \tag{5.21}$$

Equation (5.21) may be rearranged to allow the calculation of βC_R where $\beta = \mathcal{K}/A$:

$$\frac{\mathcal{K}}{A} C_R = \frac{(R\,T\,C'_s)^2}{K_s \cdot p} = \beta C_R \tag{5.21'}$$

The variation of βC_R with coverage is given in Figure 5.105. These values of βC_R have been evaluated using the measured differential permeability, K^* which has been divided into the extra flow permeability, K_s^* by means of the two methods discussed in Section 5.2.4 (b) (C'_s being evaluated for p_∞). As can be seen the coefficient of resistance

Figure 5.105. Concentration of C_R : i-C_4H_{10}/Graphon

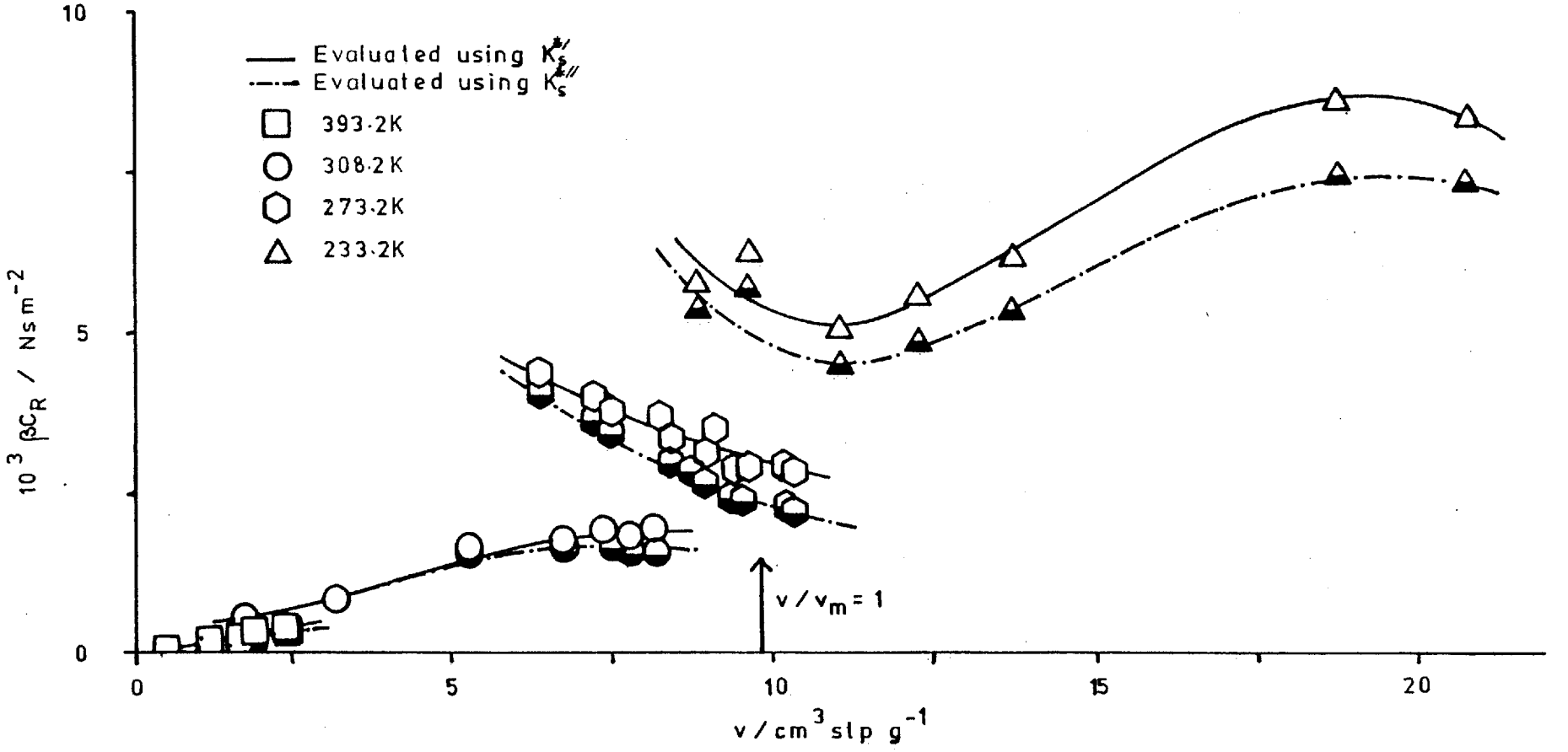

(represented by βC_R) is both a function of temperature and amount adsorbed. The coefficient is believed to be characteristic of only the nature of the solid surface and the adsorbed molecule. However the correlation between the surface flow rates and the hydrodynamic flow equation, employed by Gilliland, Baddour and Russel (1958) required that a plot of J_s vs $\int_{p_1}^{p_2} (C_s')/p^2 . dp$ should be linear. This correlation arises from the further treatment of equation (5.21) resulting in the relationship:

$$\frac{J_s}{A_c} = \frac{A\ RT}{\mathcal{K}\ \ell C_R} \int_{p_2}^{p_1} \frac{(C_s')^2}{p} \cdot dp \qquad (5.22)$$

if it is assumed that C_R is independent of pressure and subsequently coverage. The results of this pressure decay study show that for the isobutane/Graphon system at coverages up to twice the monolayer capacity this assumption is not true as C_R is obviously concentration dependent. Ash, Barrer and Pope (1963) and Lallemand and Eyraud (1973) also observed that C_R was dependent on coverage. Lallemand and Eyraud found that the behaviour was described by an empirical equation of the form:

$$C_R = A\ e^{-\beta\theta} + B \qquad (5.23)$$

where A, B and β are constants for a given system at a certain temperature and θ is the coverage (v/v_m). This relationship was applicable up to values of $p_\infty/p_o \simeq 0.7$ when the onset of capillary condensation was predicted. In this latter region approaching the saturated vapour pressure of the sorbable gas a flow relationship was derived based on the work of Carman (1952), who considered the driving force promoting the flow to be due to a large capillary pressure difference resulting from the difference in gas pressure between the two sides. Lallemand and Eyraud (1973) suggest that it is necessary to include an effect due to the temperature difference between the two ends of a slug of capillary condensate. This effect is produced by the release of the heat of condensation of the vapour and subsequent evaporation of condensate at the lower concentration side of the slug.

These latter stages of flow when relatively densely adsorbed films are present require a much more detailed investigation with the pressure decay technique than has been carried out in this exploratory work.

As has been previously mentioned (cf §5.2.4 (c)) it is not justifiable to apply the models of hydrodynamic flow to the one sided 'conventional' results.

The conditions present in the 'pressure-decay' arrangement provide an ideal opportunity for an in-depth study of flow in the higher coverage regions and the subsequent application of correlations such as those produced by the investigations mentioned above.

5.3.3. Helium/Isobutane Mixture Flow

The transport of helium/isobutane mixtures through the Graphon membrane was studied at T/K = 393.2, 308.2, 273.2 and 233.2. These temperatures were chosen specifically to enable the full range of $0.0 < p_{\infty}/p_o$ 1.0 to be examined. The results given in Figures 4.60 and 4.61 illustrate the variation in the relative permeability of the helium, K_R^* ($= K^*_{He\,mix}/K^*_{He\,pure}$) with the equilibrium pressure, p_{∞} (cm Hg) and relative pressure of isobutane, p_{∞}/p_o.

It can be seen that the general features are similar to those obtained with the 'conventional' apparatus. The existence of the plateau in the K_R^* vs p_{∞}/p_o curve is again indicated with its position and length virtually unaltered by the different technique (cf Figure 4.61). At the high coverage end of the plateau a certain degree of scatter enters the results. This effect does not appear to have been eliminated despite the boundary conditions being upheld. In the 'conventional' arrangement the problems concerning the maintenance of a constant ingoing composition (cf §4.2.3) were cited as possible reasons for the scatter. It is possible that temperature fluctuations in the thermostat baths or the problems involved in circulation of the mixtures past the outgoing face (cf §3.4.3 (a)) may be viable explanations.

The basic blockage characteristics have been previously discussed in detail in Section (5.2.3) and the same conclusions can be drawn from the 'pressure-decay' results.

In the 'conventional' arrangement the primary blocking of the gas phase will take place at the ingoing face due to the large surface concentration existing there. However from the similarity of the curves

in Figure 4.59 it would appear that the presence of a uniform layer of adsorbate in the membrane has no extra effect, supporting the idea that whatever blockage exists takes place primarily as the indicator gas enters the membrane.

Pursuing the postulate of key blockage sites in the membrane (such as constrictions) it might be expected that these, if occupied not just at the ingoing face may have an additional contribution to the blockage in the initial period of severe blockage for the 'pressure-decay' conditions. To this end the blockage curve in the region $0 < p_{\infty}/p_o < 0.1$ was expanded and compared to the best fit curve of the 'conventional' results in Figure 5.106. It can be seen that the 'pressure-decay' results do lie slightly below those of the 'conventional' arrangement although the two sets converge at $p_{\infty}/p_o \simeq 0.05$. This result provides yet more evidence, admittedly rather limited in support of adsorption sites, which are instrumental in governing the flow of a non-sorbed component being present throughout the length of this membrane formed from Graphon.

Figure 5.106. Variation of K_R^* with p_∞/p_0 : i-C_4H_{10}/i-C_4H_{10}/Graphon

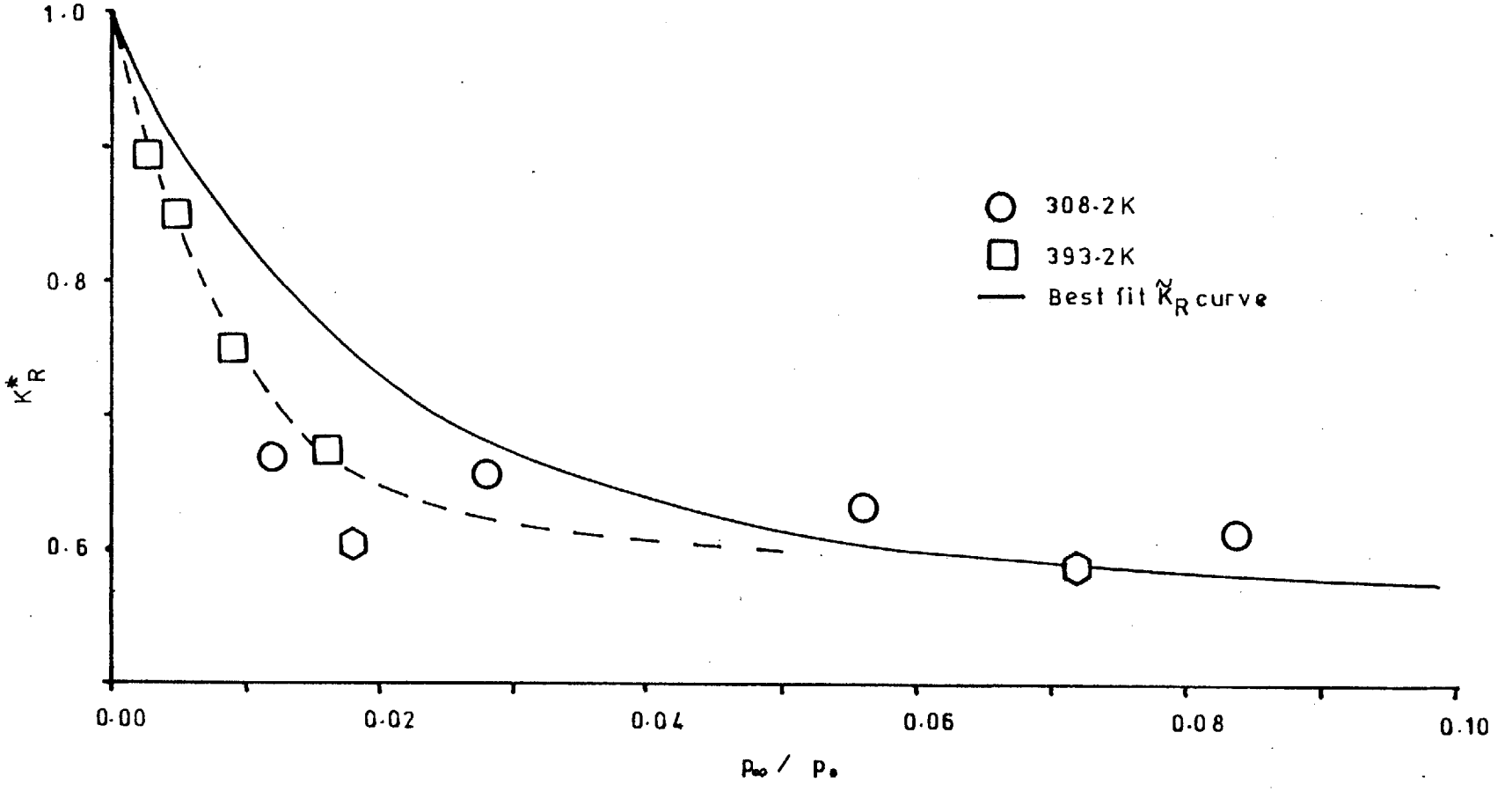

CHAPTER 6 : SUMMARY OF RESULTS AND RECOMMENDATIONS FOR FURTHER WORK

A: Adsorption studies were undertaken to assist the interpretation of the flow results. An investigation was made into the effect of compaction on the adsorption properties of Graphon. The presence of 'low coverage hysteresis' was indicated. Nitrogen isotherms were measured at low temperatures for B.E.T. and 't' plot analyses.

B: A flow study was made on the Graphon membrane Q under two completely different sets of boundary conditions as provided by the 'conventional' and 'pressure-decay' arrangements.

C: The blockage effect of an adsorbed film of gas (isobutane) in the Graphon membrane were unaffected by the choice of technique: conventional or pressure-decay. This was indicative of blockage primarily occurring at a specific plane in the membrane.

D: The presence of 'key sites' to the gas phase flow was indicated by the substantial blockage which took place with only small amounts of adsorbed gas. Evidence was obtained to support the idea of blockage in the Henry Law region for membranes constructed from both Graphon and graphitised Black Pearls.

E: A long plateau in the blockage curve has been found to exist for the Graphon membrane where minimal further blockage occurred despite substantial adsorption of hydrocarbon. A condition of total blockage prevailed in the vicinity of the saturated vapour pressure of hydrocarbon.

F: A comparison between the blockage effects of the carbons, Carbolac, graphitised Black Pearls and Graphon has been made.

G: Pure hydrocarbon (C_3H_8, i-C_4H_{10}) flow measured by the conventional technique resulted in the presence of broad minima in the integral permeabilities. The rapid rise near the saturated vapour pressure corresponded to the total blockage condition (cf E).

H: Differential hydrocarbon permeabilities, arising from the 'pressure-decay' technique were compared to those calculated from the integral permeabilities. The two were similar in the medium coverage region but marked differences were observed at the extremes of coverage.

I: Overall diffusion coefficients (both differential and integral) were calculated. These showed a marked concentration dependence and exhibited maxima in the vicinity of monolayer coverage. They were also described by an Arrhenius-type relationship resulting in the determination of an activation energy for diffusion.

J: The total permeability for the isobutane/Graphon system was split in two ways using the helium flow as an indicator of the gas phase hydrocarbon permeability. Surface diffusion coefficients were calculated but due to internal inconsistencies the division appeared unjustified.

K: It is felt that further work on the 'conventional' type of apparatus is of limited use, although it would be of interest to consider the flow of weakly adsorbed gas mixtures to extend the observations of the Ar/isobutane/Graphon study undertaken here.

The 'pressure-decay' technique merits further investigation in the following realms:

1. - In the Henry Law region of adsorption when the adsorption isotherm is linear, are the differential permeabilities concentration-dependent and do they become equivalent to those calculated from the integral permeabilities?

2. - Can the 'universality' of the blockage curve obtained for the Graphon and Black Pearls systems be extended to include a much larger range of hydrocarbon molecules?

3. - How would the behaviour alter if high pressures of gases were used and the necessity of low temperature work eliminated? This is a much broader question and would require a large amount of basic research with high pressure techniques.

APPENDIX A : ADSORPTION ISOTHERM DATA

1. Graphon/Nitrogen
2. Black Pearls/Nitrogen
3. Graphon pellets/Propane
4. Graphon membrane/Propane
5. Graphon pellets/Isobutane
6. Graphon membrane/Isobutane
7. Black Pearls Powder/Propane
8. Black Pearls Powder/Isobutane

1 : Nitrogen/Graphon Isotherm

T / K	p / cm Hg	v / cm^3 stp g^{-1}	p / cm Hg	v / cm^3 stp g^{-1}
77.4	0.036	13.23	27.28	31.13
	0.429	17.32	30.44	33.41
	1.009	18.19	32.61	34.95
	1.421	18.52	33.97	35.85
	2.358	19.01	35.34	36.47
	3.046	19.15	38.22	38.23
	4.380	19.53	39.48	39.37
	5.588	19.87	40.83	40.47
	7.016	20.29	44.02	42.53
	8.731	20.52	45.36	43.86
	10.39	21.06		
	12.06	21.74	43.99	42.52
	14.81	22.82	40.89	40.43
	16.92	23.88	36.23	37.67
	18.24	24.73	30.98	34.00
	19.95	25.22	23.14	28.31
	20.16	25.84	24.08	28.67
	22.51	27.49	24.95	29.37

2 : Nitrogen/Black Pearls Isotherm

T / K	p / cm Hg	v / cm^3 stp g^{-1}	p / cm Hg	v / cm^3 stp g^{-1}
77.4	0.023	28.31	26.59	77.49
	0.083	34.41	27.97	79.69
	0.187	38.21	29.24	81.86
	0.535	41.83	30.55	83.82
	1.354	44.73	32.88	87.71
	1.467	44.96	34.71	90.43
	2.472	46.77	36.52	93.14
	3.838	48.49	38.58	96.37
	5.583	50.79	40.57	99.61
	5.972	51.21	42.37	102.8
	7.784	53.04		
	8.959	54.25	41.78	101.7
	10.28	55.53	38.40	96.40
	12.21	57.59	35.56	91.81
	13.00	58.49	33.87	89.09
	14.60	60.31	31.20	84.81
	17.00	63.32	28.97	81.05
	17.98	64.61	27.68	79.03
	19.35	66.55	25.09	74.86
	21.12	69.01	19.61	66.61
	22.30	70.69	14.81	60.45
	23.40	72.44	10.79	55.99
	24.74	74.31	7.636	52.89

3 : Graphon Pellets/Propane Isotherms

T / K	p / cm Hg	v / cm^3 stg g^{-1}	10^7 C'_s / mol (m^2 membrane)$^{-1}$	C'_g / mol (m^3 gas phase)$^{-1}$
473.2	2.553	0.0290	0.1444	0.8652
	5.551	0.0587	0.2919	1.002
	9.201	0.1024	0.5098	3.117
	13.39	0.1435	0.7139	4.538
	19.33	0.2061	1.026	6.553
	26.13	0.2864	1.426	8.854
	32.05	0.3492	1.738	10.86
	35.74	0.3913	1.948	12.11
	48.46	0.5359	2.666	16.43
393.2	3.423	0.0931	0.4631	1.396
	7.148	0.2009	0.9998	2.915
	11.37	0.3213	1.598	4.638
	14.57	0.4074	2.028	5.945
	21.42	0.6186	3.078	8.737
	30.19	0.8886	4.423	12.31
	39.57	1.209	6.015	16.14
	47.70	1.436	7.146	19.46
	38.46	1.191	5.929	15.69
	24.25	0.7783	3.873	9.893
	17.17	0.5434	2.704	7.002
	11.67	0.3823	1.902	4.761
	5.671	0.2104	1.046	2.314
273.2	2.046	1.837	9.138	1.201
	2.606	2.366	11.78	1.529
	3.721	3.296	16.39	2.184
	4.704	4.073	20.26	2.761
	5.250	4.506	22.42	3.081
	8.441	6.205	30.88	4.953
	11.50	7.158	35.63	6.749
	15.25	7.903	39.33	8.951
	19.70	8.486	42.23	11.56
	24.18	8.937	44.48	14.19
	27.69	9.213	45.85	16.25
	31.61	9.480	47.17	18.55
	42.69	10.14	50.47	25.06
	54.19	10.72	53.35	31.80
	46.67	10.44	51.98	27.39
	40.14	10.11	50.30	23.56
	31.78	9.632	47.93	18.65
	23.81	9.028	44.92	13.97
	17.24	8.314	41.37	10.12
	12.48	7.513	37.40	7.328
	6.867	5.555	27.65	4.030
	3.921	3.516	17.46	2.302

continued

3 (continued) : Graphon Pellets/Propane Isotherms

T / K	p / cm Hg	v / cm^3 stp g^{-1}	10^7 C'_s / mol (m^2 membrane)$^{-1}$	C'_g / mol (m^3 gas phase)$^{-1}$
243.2	0.884	3.846	19.13	0.5829
	1.595	6.247	31.09	1.052
	3.239	8.333	41.48	2.136
	6.535	9.549	47.53	4.308
	11.02	10.34	51.47	7.265
	14.89	10.85	54.01	9.814
	19.32	11.39	56.62	13.99
	26.65	12.19	60.66	17.57
	34.79	13.06	65.00	22.93
	42.08	13.99	69.63	27.75
	46.66	14.73	73.29	30.77
	42.10	14.01	69.75	27.75
	26.85	12.11	60.26	17.70
	19.37	11.34	56.47	12.77
	11.43	10.34	51.46	7.536
	5.249	9.186	45.72	3.461
213.2	0.191	5.643	28.08	0.1437
	3.131	10.95	54.52	2.354
	5.607	11.84	58.94	4.217
	8.119	12.77	63.55	6.107
	11.48	14.39	71.63	8.638
	13.23	15.32	76.25	9.949
	15.81	17.32	86.21	11.89
	17.86	19.59	97.51	13.43
	20.82	23.21	115.4	15.66
	22.79	26.27	130.7	17.14
	24.67	29.99	149.3	18.55
	26.43	35.39	176.1	19.88
	27.64	42.40	211.0	20.79
	28.11	48.74	242.6	21.13
	29.03	60.68	301.9	21.82
	29.56	71.48	355.6	22.23
	30.11	81.05	403.4	22.65
	28.95	68.69	339.4	21.78
	28.05	52.99	263.8	21.09
	26.51	38.21	190.1	19.94
	22.50	25.83	127.8	16.92
	15.68	17.43	86.73	11.79
	8.688	12.96	64.21	6.534

4 : Graphon Membrane/Propane Isotherms

T / K	p / cm Hg	v / cm^3 stp g^{-1}	$10^7 c'_s$ / mol (m^2 membrane)$^{-1}$	c'_g / mol (m^3 gas phase)$^{-1}$
243.2	2.274	7.177	35.72	1.499
	4.136	8.832	43.95	2.727
	5.791	9.688	48.21	3.819
	8.893	9.837	48.95	5.664
	12.42	10.49	52.21	8.192
	16.44	11.38	56.66	10.84
	20.30	12.35	61.49	13.39
	23.12	13.21	65.75	15.25
	26.96	14.10	70.19	17.78
	37.62	17.60	87.61	24.82
	34.39	17.30	86.12	22.67
	30.17	15.82	78.76	19.90
	18.48	12.15	60.48	12.19
	13.23	11.22	55.86	8.727
	6.261	10.29	51.22	4.127
	1.362	5.512	27.43	0.8982
213.2	5.607	13.05	64.92	4.217
	7.791	13.80	68.70	5.860
	10.17	15.99	79.63	7.649
	12.35	18.61	91.59	9.293
	13.90	20.45	101.6	10.46
	17.28	23.09	114.9	13.00
	23.58	35.33	175.7	17.74
	28.81	77.69	386.6	21.68
	30.64	150.4	748.8	23.06
	31.45	195.4	972.5	23.66
	29.94	146.8	730.6	22.51
	29.43	101.1	502.9	22.15
	26.46	54.54	271.4	19.91
	21.16	28.50	141.8	15.92
	15.43	21.41	106.6	11.61
	13.56	19.41	96.62	10.20
	9.917	15.47	76.98	7.461
	5.496	12.75	63.46	4.136
	3.170	11.77	58.49	2.385
	1.297	9.828	48.91	0.9757

5 : Graphon Pellets/Isobutane Isotherms

T / K	p / cm Hg	v / cm^3 stp g^{-1}	$10^7 C'_s$ / mol $(m^2$ membrane$)^{-1}$	C'_g / mol $(m^3$ gas phase$)^{-1}$
453.2	9.009	0.2632	1.000	3.188
	13.93	0.4091	2.035	4.931
	21.48	0.6173	2.671	7.601
	31.42	0.8763	4.361	11.12
	45.27	1.205	5.802	16.02
	35.20	0.9936	4.944	12.46
	24.48	0.7334	3.649	8.664
	16.76	0.5315	2.645	5.931
	10.91	0.3634	1.808	3.862
423.2	3.872	0.1729	0.8605	1.467
	5.680	0.2411	1.200	2.152
	7.928	0.3431	1.707	3.006
	10.31	0.4544	2.261	3.907
	12.21	0.5478	2.725	4.627
	16.63	0.7294	3.630	6.302
	24.25	1.253	6.236	9.188
	33.95	1.482	7.374	12.87
	44.40	1.926	9.583	16.83
	37.89	1.703	8.475	14.36
	31.70	1.463	7.283	12.01
	24.31	1.149	5.718	9.212
	17.42	0.8488	4.224	6.601
	11.97	0.5950	2.961	4.536
	4.371	0.2841	1.414	1.656
	2.027	0.1769	0.8588	0.7682
*393.2	3.733	0.3090	1.705	1.523
	6.152	0.5020	2.769	2.508
	8.175	0.6570	3.685	3.334
	10.08	0.8000	3.978	4.111
	13.34	1.050	5.806	5.441
	16.84	1.307	7.237	6.868
	22.57	1.717	9.512	9.206
	30.48	2.274	12.59	12.43
	38.99	2.814	15.59	15.90
	46.98	3.262	18.08	19.16
	54.47	3.656	20.28	22.23
	30.34	2.274	12.59	12.37
	9.657	0.8300	4.591	3.939
	3.305	0.3240	1.793	1.348

* Determined by Dr A.V.J. Edge in these laboratories

continued

5 (continued) : Graphon Pellets/Isobutane Isotherms

T / K	p / cm Hg	v / cm^3 stp g^{-1}	$10^7 C'_s$ / mol (m^2 membrane)$^{-1}$	C'_g / mol (m^3 gas phase)$^{-1}$
*358.2	4.126	0.7570	4.148	1.847
	6.748	1.256	6.884	3.020
	9.418	1.620	8.881	4.217
	13.52	2.341	12.83	6.053
	16.45	2.753	15.09	7.364
	19.63	3.195	17.52	8.789
	24.61	3.856	21.09	11.02
	30.04	4.420	24.25	13.45
	34.93	4.845	26.58	15.64
	39.56	5.180	28.43	17.71
	48.08	5.770	31.68	21.52
	58.49	6.277	34.49	26.19
	28.75	4.343	23.82	12.87
	12.57	2.285	12.53	5.627
	6.285	1.223	6.700	2.814
	3.229	0.6750	3.701	1.446
343.2	6.386	1.723	8.577	2.984
	8.293	2.209	10.80	3.874
	10.29	2.701	13.43	4.809
	13.69	3.438	17.10	6.397
	15.34	3.769	18.75	7.168
	20.92	4.674	23.26	9.775
	28.49	5.521	27.48	13.31
	37.23	6.242	31.06	17.39
	48.93	6.875	34.21	22.85
	38.83	6.374	31.72	18.14
	30.54	5.778	28.75	14.27
	23.87	5.102	25.39	11.15
	17.96	4.285	21.32	8.393
	13.34	3.429	17.07	6.233
	10.10	2.721	13.55	4.719
	5.448	1.528	7.607	2.546
308.2	2.927	2.547	12.67	1.523
	4.062	3.451	17.18	2.113
	4.886	3.969	19.75	2.542
	6.551	4.897	24.37	3.409
	7.881	5.405	26.91	4.101
	8.884	5.735	28.54	4.623
	11.54	6.387	31.78	6.004
	14.95	6.952	34.60	7.779
	18.83	7.385	36.76	9.799
	23.45	7.761	38.63	12.20
	25.36	7.900	39.32	13.19
	37.71	8.584	42.72	19.62
	55.21	9.358	46.58	28.99

continued

* Determined by Dr A.V.J. Edge in these laboratories

5 (continued) : Graphon Pellets/Isobutane Isotherms

T / K	p / cm Hg	v / cm^3 stp g^{-1}	$10^7 C'_s$ / mol $(m^2$ membrane$)^{-1}$	C'_g / mol $(m^3$ gas phase$)^{-1}$
308.2 (cont.)	42.76	8.904	44.31	22.25
	32.13	8.435	41.97	16.72
	23.88	7.945	39.55	12.43
	17.20	7.354	36.60	8.951
	12.58	6.647	33.08	6.547
273.2	0.469	1.880	9.359	0.2751
	0.530	2.074	10.32	0.3111
	1.272	4.818	23.98	0.7468
	1.544	5.328	26.51	0.9065
	3.798	7.357	36.62	2.229
	6.050	7.970	39.66	3.553
	8.012	8.318	41.40	4.704
	11.26	8.685	43.23	6.609
	15.73	9.144	45.51	9.235
	21.07	9.628	47.92	12.37
	26.48	10.07	50.13	15.55
	30.46	10.43	51.94	17.88
	42.41	11.70	58.25	24.88
	36.27	11.09	55.19	21.29
	25.28	10.11	50.30	14.84
	13.38	9.055	45.06	7.854
268.2	0.405	2.216	11.03	0.2421
	0.938	4.659	23.18	0.5609
	1.059	5.045	25.11	0.6332
	4.085	7.791	38.77	2.443
	6.662	8.392	41.77	3.984
	8.993	8.738	43.48	5.378
	14.77	9.478	47.16	8.831
	20.91	9.968	49.60	12.50
	27.59	10.69	53.21	16.49
	34.03	11.38	56.66	20.34
	37.93	12.02	59.82	22.67
	47.54	13.74	68.38	28.42
	52.08	14.62	72.75	31.13
	47.24	13.62	67.79	28.24
	35.73	11.60	57.74	21.38
	27.31	10.58	52.63	16.33
	19.59	9.767	48.60	11.71
	13.22	9.167	45.63	7.907
	7.335	8.440	42.01	4.387
	5.464	8.104	40.33	3.267

continued

5 (continued) : Graphon Pellets/Isobutane Isotherms

T / K	p / cm Hg	v / cm^3 stp g^{-1}	$10^7 C'_s$ / mol (m^2 membrane)$^{-1}$	C'_g / mol (m^3 gas phase)$^{-1}$
258.2	0.246	2.360	11.74	0.1528
	0.843	6.144	30.58	0.5237
	4.756	8.709	43.34	2.953
	8.188	9.292	46.24	5.085
	11.09	9.708	48.31	6.895
	14.21	10.14	50.46	8.828
	19.32	10.92	54.36	12.00
	24.45	11.88	57.43	15.19
	28.41	12.84	61.95	17.65
	30.84	13.50	67.20	19.15
	32.98	14.10	70.22	20.44
	38.91	16.50	82.13	24.17
	42.83	18.51	92.14	26.59
	45.29	19.71	98.12	28.12
	45.88	20.10	100.0	28.48
	39.47	16.84	83.79	24.51
	33.40	14.42	71.76	20.75
	25.88	12.28	61.12	16.07
	22.23	11.55	57.49	13.81
	16.77	10.61	52.79	10.42
	12.96	10.07	50.11	8.051
	9.469	9.580	47.68	5.883
	5.681	8.980	44.70	3.528
	2.805	8.247	41.04	1.742
	1.511	7.423	36.94	0.9387
	1.072	6.824	33.96	0.6662
	0.805	6.373	31.72	0.5000
248.2	0.320	4.617	22.98	0.2069
	1.934	8.443	42.02	1.250
	6.036	9.588	47.72	3.903
	9.919	10.45	52.03	6.413
	13.00	11.15	55.52	8.407
	15.49	11.39	57.05	10.02
	20.09	13.26	66.01	12.99
	21.62	13.88	69.08	13.98
	25.83	16.89	84.07	16.69
	29.32	20.42	101.6	18.96
	32.74	23.77	118.2	21.17
	35.37	29.70	147.8	22.85
	38.58	42.59	212.0	24.94
	37.23	38.03	189.2	24.07
	35.21	29.75	148.2	22.77

continued

5 (continued) : Graphon Pellets/Isobutane Isotherms

T / K	p / cm Hg	v / cm^3 stp g^{-1}	$10^7 c'_s$ / mol $(m^2$ membrane$)^{-1}$	c'_g / mol $(m^3$ gas phase$)^{-1}$
233.2	0.122	2.774	13.81	0.0083
	0.422	7.419	36.93	0.2903
	4.579	10.40	51.78	3.149
	6.402	11.24	55.93	4.403
	7.352	11.76	58.54	5.057
	8.347	12.51	62.25	5.741
	10.10	14.29	71.12	6.947
	11.07	15.16	75.44	7.613
	12.71	17.75	88.34	8.741
	13.67	19.59	97.51	9.403
	14.96	22.68	112.8	10.29
	16.24	25.43	126.5	11.17
	17.06	32.81	163.3	11.73
	18.45	39.18	195.0	12.69
	18.07	37.06	184.4	12.43
	17.27	32.90	163.7	11.88
	16.03	26.83	133.4	11.02
	14.49	21.47	106.9	9.966
	12.41	16.81	83.68	8.534
	9.850	13.14	65.40	6.775
	5.928	11.01	54.78	4.077
	3.344	9.814	48.76	2.299
	1.950	8.733	43.46	1.341
218.2	0.177	8.381	41.70	0.1302
	3.054	11.68	58.13	2.245
	3.765	12.87	64.06	2.767
	4.223	14.05	69.92	3.103
	4.805	15.77	78.49	3.530
	5.588	18.35	91.35	4.107
	5.640	19.66	97.81	4.146
	6.155	22.00	109.5	4.524
	6.805	24.75	123.0	5.000
	7.213	28.70	142.8	5.302
	7.571	36.19	180.0	5.565
	8.031	46.12	229.5	5.901
	8.261	63.61	316.6	6.071
	8.336	85.03	433.3	6.125
	8.713	111.7	555.8	6.403
	8.828	138.5	689.3	6.488
	8.648	130.1	647.4	6.354
	8.577	125.3	623.4	6.304
	8.446	120.5	599.6	6.206
	8.264	111.3	553.4	6.073
	8.045	97.68	491.7	5.913
	8.020	93.15	463.6	5.895
	7.965	88.65	441.2	5.854

6 : Graphon Membrane/Isobutane Isotherms

T / K	p / cm Hg	v / cm^3 stp g^{-1}	$10^7 C'_s$ / mol $(m^2$ membrane$)^{-1}$	C'_g / mol$(m^3$ gas phase$)^{-1}$
248.2	3.427	0.892	49.23	1.000
	6.364	10.85	53.98	4.111
	8.983	12.01	59.80	5.806
	11.79	13.08	65.09	7.619
	16.43	16.35	81.37	10.62
	21.69	21.01	104.6	14.02
	26.62	26.77	133.1	17.20
	29.94	32.29	160.6	19.35
	32.34	35.84	178.3	20.89
	39.62	97.98	487.5	25.61
	43.67	177.5	883.3	28.22
	40.35	130.8	651.3	26.07
	39.10	76.45	380.4	25.26
	33.29	44.38	220.8	21.52
	18.49	22.22	110.6	11.95
	11.79	12.94	64.39	7.619
233.2	1.743	9.810	48.83	1.199
	3.183	10.45	52.02	2.190
	4.393	11.62	57.84	3.022
	6.322	12.22	60.83	4.350
	8.736	14.31	71.22	6.010
	11.38	17.78	88.49	7.832
	13.73	22.78	113.3	9.449
	15.31	27.09	134.8	10.54
	18.36	47.17	234.7	12.64
	20.29	118.6	590.1	13.96
	21.78	166.5	828.6	14.99
	20.74	132.3	658.5	14.27
	19.72	110.0	547.6	13.57
	15.35	31.28	155.7	10.56
	11.29	20.79	103.5	7.769
	6.451	13.09	65.18	4.439
218.2	1.382	10.55	52.53	1.016
	2.478	11.66	58.04	1.821
	3.307	13.83	68.86	2.431
	4.863	17.03	84.75	3.575
	5.995	24.73	122.9	4.407
	6.980	30.75	152.9	5.131
	7.336	38.60	192.0	5.393
	8.165	59.73	297.	6.002
	8.330	85.40	424.9	6.123
	8.429	99.02	492.9	6.196
	9.125	170.8	850.1	6.708
	9.524	216.5	1078	7.000

continued

6 (continued) : Graphon Membrane/Isobutane Isotherms

T / K	p / cm Hg	v / cm^3 stp g^{-1}	$10^7 C'_s$ / mol $(m^2$ membrane$)^{-1}$	C'_g / mol $(m^3$ gas phase$)^{-1}$
218.2 (contd)	9.456	203.0	1010	6.951
	9.142	159.6	794.2	6.719
	8.341	125.7	625.7	6.132
	7.649	70.58	351.2	5.623
	7.181	40.32	200.6	5.279
	5.226	20.94	104.2	3.840
	3.922	15.33	76.29	2.883
	2.128	10.81	53.78	1.564
	0.991	9.113	45.35	0.7285

7 : Black Pearls Powder/Propane Isotherms

T / K	p / cm Hg	v / cm^3 stp g^{-1}	$10^7 C'_s$ / mol (m^2 membrane)$^{-1}$	C'_g / mol (m^3 gas phase)$^{-1}$
273.2	2.103	5.446	11.49	1.235
	3.660	8.144	17.18	2.148
	4.842	10.03	21.17	2.842
	6.440	12.29	25.92	3.781
	8.410	14.25	30.07	4.937
	10.47	15.88	33.54	6.148
	14.01	17.78	37.52	8.225
	16.08	18.73	39.52	9.440
	19.64	19.85	41.89	11.53
	25.23	21.15	44.63	14.81
	31.28	22.25	46.94	18.36
	36.93	23.09	48.71	21.68
	40.82	23.64	49.87	23.95
	45.35	24.22	51.11	26.61
	40.68	23.65	49.89	23.87
	27.33	21.65	45.68	16.04
	21.60	20.15	42.49	12.68
	14.91	18.24	38.49	8.757
	11.01	16.31	34.41	6.464
	7.328	13.20	27.84	4.302
	5.430	10.86	22.90	3.191
248.2	1.013	8.753	18.47	0.6546
	2.081	12.27	25.89	1.345
	2.399	15.51	32.72	1.550
	4.317	19.49	41.12	2.789
	7.824	22.68	47.85	5.057
	11.09	23.92	50.47	7.168
	12.62	24.67	52.05	8.152
	16.79	25.96	54.78	10.85
	20.63	27.34	57.67	13.33
	24.40	28.47	60.02	15.77
	27.48	29.33	61.87	17.76
	29.16	29.91	63.12	18.84
	30.41	30.47	64.27	19.65
	35.67	32.21	67.97	23.04
	40.86	33.36	70.37	26.41
	43.34	34.22	72.17	28.01
	36.59	32.02	67.56	23.63
	30.93	30.33	63.94	19.98
	24.67	28.52	60.18	15.94
	18.98	26.88	56.69	12.26
	10.92	26.02	54.84	7.053

7 (continued) : Black Pearls Powder/Propane Isotherms

T / K	p / cm Hg	v / cm^3 stp g^{-1}	$10^7 C'_s$ / mol $(m^2$ membrane$)^{-1}$	C'_g / mol $(m^3$ gas phase$)^{-1}$
213.2	0.172	12.14	25.61	0.1294
	0.324	17.69	37.33	0.2442
	1.041	23.31	49.17	0.7848
	2.411	25.99	54.83	1.814
	4.396	28.29	59.63	3.307
	7.489	31.47	66.39	5.635
	9.258	33.56	70.81	6.965
	12.54	38.11	80.35	9.436
	15.60	43.78	92.34	11.74
	16.65	46.16	97.41	12.53
	18.46	51.14	107.9	13.89
	20.34	57.14	120.5	15.30
	21.28	60.81	128.3	16.01
	21.96	64.08	135.2	16.52
	23.67	72.46	152.8	17.80
	24.88	80.47	169.7	18.72
	25.47	85.09	179.5	19.16
	26.87	98.53	207.8	20.21
	27.40	109.7	231.5	20.61
	26.63	107.5	226.7	20.03
	26.37	104.8	221.1	19.84
	25.53	96.09	202.2	19.21
	25.19	93.56	197.4	18.95
	24.51	85.17	179.7	18.44
	23.25	74.83	157.9	17.48
	21.60	65.26	137.7	16.24
	19.73	56.54	119.3	14.84
	17.35	48.91	103.2	13.05
	14.82	41.62	87.76	11.15
	11.92	36.43	76.86	8.969
	9.237	32.43	68.41	6.947

8 : Black Pearls/Isobutane

T / K	p / cm Hg	v / cm^3 stp g^{-1}	$10^7 c_s'$ / mol $(m^2$ membrane$)^{-1}$	c_g' / mol $(m^3$ gas phase$)^{-1}$
343.2	3.180	2.992	6.312	1.486
	4.900	4.026	8.493	2.290
	6.776	5.066	10.68	3.166
	10.01	6.696	14.14	4.675
	11.04	7.145	15.08	5.158
	14.89	8.818	18.43	6.959
	17.17	9.607	20.27	8.022
	19.28	10.32	21.79	9.008
	21.03	10.85	22.88	9.828
	25.32	11.98	25.28	11.83
	30.30	13.02	27.47	14.16
	35.53	13.95	29.43	16.60
	38.25	14.50	30.60	17.87
	47.40	15.63	32.98	22.15
	38.19	14.49	30.57	17.84
	30.84	13.25	27.96	14.41
	25.41	12.11	25.55	11.88
	17.61	9.872	20.83	8.229
308.2	1.852	4.716	9.785	0.9637
	4.452	8.572	18.09	2.316
	5.650	9.958	21.01	2.939
	9.189	12.95	27.31	4.781
	12.32	14.66	30.94	6.412
	14.63	15.44	32.56	7.610
	17.33	16.30	34.39	9.016
	22.57	17.39	36.06	11.74
	28.23	18.32	38.65	14.69
	33.38	19.06	40.22	17.37
	37.15	19.54	41.23	19.33
	44.36	20.24	42.70	23.08
	34.42	19.15	40.41	17.91
	25.62	17.97	37.92	13.33
	21.73	17.29	36.47	11.30
	12.02	14.50	30.59	6.253
	7.650	11.68	24.63	3.979
273.2	1.106	9.873	20.83	0.6493
	3.106	16.14	34.04	1.823
	7.632	19.39	40.92	4.479
	11.02	20.59	43.44	6.471
	13.39	21.23	44.79	7.862
	17.35	22.23	46.91	10.18
	22.32	23.37	49.30	13.10
	27.13	24.46	51.60	15.93

continued

8 (continued) : Black Pearls/Isobutane

T / K	p / cm Hg	v / cm^3 stp g^{-1}	$10^7 C'_s$ / mol $(m^2$ membrane$)^{-1}$	C'_g / mol $(m^3$ gas phase$)^{-1}$
273.2 (contd)	30.93	25.38	53.54	18.16
	33.39	25.96	54.73	19.61
	38.05	27.20	57.29	22.33
	42.81	28.57	60.29	25.13
	44.02	29.64	62.52	25.84
	41.19	28.78	60.72	24.18
	30.19	25.95	54.73	17.72
	23.55	24.37	51.42	13.83
	19.02	23.37	49.31	11.17
	10.24	21.07	44.45	6.014
	6.237	19.43	40.99	3.661
248.2	0.180	9.921	20.93	0.1164
	0.947	17.95	37.87	0.6495
	6.199	23.64	49.87	4.013
	8.750	25.44	53.67	5.665
	11.72	27.71	58.86	7.586
	15.64	31.24	65.92	10.12
	19.16	36.78	77.61	12.41
	21.43	40.13	84.68	13.87
	24.14	46.12	97.29	15.63
	25.54	50.53	100.7	16.54
	27.74	59.13	124.7	17.96
	28.50	64.30	135.7	18.45
	30.51	79.28	167.3	19.75
	32.66	94.50	199.4	21.14
	34.69	115.4	243.6	22.46
	32.17	104.6	220.6	20.82
	30.44	91.83	193.7	19.71
	29.52	78.54	165.7	19.11
	28.08	65.89	139.0	18.18
	25.81	54.34	114.6	16.71
	22.85	44.17	93.19	14.79
	18.70	35.91	75.62	12.11
	13.95	29.81	62.89	9.031
233.2	0.149	12.79	27.01	0.1024
	4.176	25.38	53.54	2.872
	7.762	31.08	65.58	5.339
	8.872	33.59	70.86	6.101
	10.23	37.71	79.53	7.034
	11.54	39.40	83.13	7.939
	11.83	44.46	93.81	8.138
	12.53	46.56	98.23	8.617

continued

8 (continued) : Black Pearls/Isobutane

T / K	p / cm Hg	v / cm^3 stp g^{-1}	$10^7 C'_s$ / mol $(m^2$ membrane$)^{-1}$	C'_g / mol $(m^3$ gas phase$)^{-1}$
233.2	13.55	51.70	109.1	9.322
(contd)	13.95	54.16	114.2	9.594
	14.83	61.02	128.7	10.19
	15.44	66.79	140.9	10.62
	15.74	70.02	147.7	10.82
	16.45	79.59	167.9	11.32
	17.32	90.71	191.4	11.91
	18.03	101.9	215.1	12.39
	19.09	113.9	240.3	13.13
	19.37	117.6	248.1	13.32
	19.95	130.6	275.6	13.72
	20.71	141.7	299.0	14.24
	20.88	151.2	318.9	14.36
	18.94	149.3	315.1	13.02
	18.45	143.0	301.8	12.69
	18.05	134.9	284.7	12.42
	17.77	127.0	267.9	12.22
	17.17	119.4	251.8	11.81
	17.05	111.8	235.8	11.73
	16.69	104.3	220.0	11.48
	16.40	96.89	204.1	11.28
	16.02	89.71	189.3	11.02
	15.63	82.74	174.6	10.75
	15.14	75.99	160.4	10.41
	14.62	69.48	146.6	10.06
	13.92	63.25	133.4	9.576
	13.16	57.36	120.9	9.049
	12.16	51.92	109.1	8.361

APPENDIX B : 'CONVENTIONAL' FLOW DATA

1. Helium/Graphon
2. Helium/Black Pearls
3. Propane/Graphon
4. Isobutane/Graphon
5. Propane/Black Pearls
6. Isobutane/Black Pearls
7. Helium/Propane Mixtures/Graphon
8. Helium/Isobutane Mixtures/Graphon
9. Helium/Propane Mixtures/Black Pearls
10. Helium/Isobutane Mixtures/Black Pearls
11. Argon/Isobutane Mixtures/Graphon

1 : Helium/Graphon

$\frac{T}{K}$	$\frac{p_1}{cm\ Hg}$	$\frac{10^6\ \tilde{K}}{m^2 s^{-1}}$
308.2	0.708	3.140
	1.046	3.107
	1.422	3.133
	1.648	3.181
	2.255	3.165
	3.224	3.149
	3.568	3.126
	4.329	3.124
	6.406	3.104
	7.102	3.075
	8.430	3.142
	10.20	3.133
	15.06	3.098
	17.34	3.141
	20.02	3.137
	21.93	3.150
248.2	4.149	2.873
	6.075	2.797
	7.880	2.790
	5.168	2.828
	2.753	2.822
273.2	4.446	2.972
	3.520	2.8799
	5.121	2.8951
	5.129	2.901

2 : Helium/Black Pearls

$\frac{T}{K}$	$\frac{p_1}{cm\ Hg}$	$\frac{10^6\ \tilde{K}}{m^2 s^{-1}}$
308.2	2.270	0.7506
	5.846	0.7526
	9.478	0.7423
	15.63	0.7525
	20.17	0.7477
273.2	5.123	0.6917
	10.15	0.6952
	3.749	0.6799
233.2	4.569	0.6463
343.2	4.410	0.7623
	5.620	0.7681
213.2	4.717	0.6024

3 : Propane/Graphon

$\frac{T}{K}$	$\frac{p_1}{cm\ Hg}$	$\frac{p_1}{p_o}$	$\frac{10^8\ J}{mol\ s^{-1}}$	$\frac{10^6\ \tilde{K}}{m^2 s^{-1}}$
473.2	10.18	-	0.4377	1.724
	20.42	-	0.8795	1.727
	33.55	-	1.464	1.749
393.2	5.409	0.0013	0.3132	1.929
	13.93	0.0034	0.8312	1.988
	22.72	0.0054	1.349	1.979
	32.03	0.0078	1.857	1.932
	1.685	0.0004	0.1005	1.987
243.2	7.538	0.0600	2.307	6.308
	15.59	0.1241	3.732	4.933
	25.89	0.2062	5.212	4.148
	33.67	0.2681	6.276	3.678
	37.11	0.2955	6.624	3.678
	1.797	0.0349	0.721	8.272
213.2	4.919	0.1538	2.259	8.301
	10.25	0.3206	3.331	5.872
	17.66	0.5524	4.793	4.904
	24.71	0.7726	6.094	4.456
	29.90	0.9357	8.806	5.321
	30.76	0.9619	32.47	19.07
	30.29	0.9473	29.76	17.75
	30.11	0.9414	9.446	5.668
	2.001	0.0626	1.306	11.79

4 : Isobutane/Graphon

T / K	p_1 / cm Hg	p_1/p_o	$10^8 J$ / mol s^{-1}	$10^6 \tilde{K}$ / $m^2 s^{-1}$
453.2	5.326	0.0010	0.2557	1.844
	15.68	0.0029	0.7503	1.862
	25.72	0.0049	1.253	1.871
	35.46	0.0068	1.731	1.875
	43.36	0.0083	2.126	1.883
	56.05	0.0107	2.726	1.868
	50.20	0.0096	2.463	1.884
423.2	5.136	0.0015	0.2930	2.046
	14.99	0.0044	0.8470	2.026
	25.18	0.0074	1.422	2.026
	35.24	0.0104	1.991	2.026
	44.58	0.0130	2.483	1.998
	56.12	0.0164	3.128	1.999
	9.409	0.0028	0.5375	2.049
393.2	0.898	0.0004	0.0612	2.271
	2.196	0.0010	0.1469	2.229
	5.099	0.0024	0.3405	2.225
	10.08	0.0048	0.6861	2.268
	19.35	0.0091	1.292	2.225
	14.98	0.0071	0.9998	2.224
	22.84	0.0108	1.5483	2.259
	9.996	0.0050	0.6731	2.244
	35.01	0.0165	2.475	2.356
	30.04	0.0142	2.014	2.234
	42.59	0.0201	2.901	2.270
	40.68	0.0192	2.785	2.281
	16.08	0.9976	1.101	2.281
	7.366	0.0035	0.5071	2.294
	25.13	0.0119	1.713	2.271
	33.78	0.0158	2.329	2.298
358.2	4.994	0.0045	0.4554	2.768
	15.02	0.0134	1.363	2.755
	25.78	0.0231	2.302	2.711
	35.24	0.0315	3.111	2.680
	45.30	0.0405	3.941	2.641
	55.93	0.0501	4.752	2.579
	51.04	0.0457	4.319	2.569
	40.66	0.0364	3.541	2.644
	2.040	0.0018	1.893	2.817

continued

4 (continued) : Isobutane/Graphon

T / K	p_1 / cm Hg	p_1/p_o	$10^8 J$ / mol s^{-1}	$10^6 \tilde{K}$ / $m^2 s^{-1}$
343.2	5.077	0.0062	0.5509	3.156
	15.51	0.0190	1.628	3.053
	25.81	0.0317	2.679	3.020
	39.35	0.0485	3.871	2.861
	10.39	0.0128	1.106	3.097
308.2	1.225	0.0035	0.1983	4.228
	20.83	0.0594	2.881	3.613
	15.40	0.0439	2.246	3.810
	6.759	0.0193	1.096	4.235
	29.82	0.0850	3.831	3.356
	24.99	0.0712	3.289	3.438
	39.91	0.1138	4.666	3.054
	50.62	0.1443	5.335	2.753
	21.02	0.0599	2.946	3.661
	40.46	0.1153	4.717	3.045
	46.72	0.1332	5.132	2.869
	34.68	0.0988	4.163	3.135
273.2	10.78	0.0907	2.273	4.882
	5.147	0.0433	1.386	6.235
	1.439	0.0121	0.4974	8.003
	19.73	0.1659	3.046	3.575
	36.17	0.3042	4.605	2.948
	50.11	0.4215	5.679	2.624
	56.95	0.4789	6.907	2.808
	66.19	0.5567	7.029	2.459
268.2	2.016	0.0203	0.7806	8.801
	6.643	0.0670	1.835	6.280
	13.39	0.1351	2.812	4.774
	22.72	0.2293	3.706	3.708
	34.19	0.3451	4.642	3.086
	53.31	0.5381	6.244	2.662
258.2	1.566	0.0233	0.7593	10.61
	20.40	0.3032	3.545	3.802
	41.99	0.6240	6.022	3.138
	10.14	0.1507	2.419	5.222
	28.53	0.4239	4.346	3.333

continued

4 (continued) : Isobutane/Graphon

T / K	p_1 / cm Hg	p_1/p_o	$10^8 J$ / mol s^{-1}	$10^6 \tilde{K}$ / $m^2 s^{-1}$
248.2	1.946	0.0441	0.9890	10.69
	12.43	0.2815	2.822	4.775
	22.56	0.5108	3.959	3.692
	33.07	0.7488	5.427	3.452
	40.53	0.9178	10.54	5.468
	37.30	0.8447	6.468	3.648
	28.11	0.6365	4.461	3.339
	40.01	0.9061	9.484	4.986
	39.33	0.8906	8.885	4.752
	6.247	0.1415	1.903	6.407
	42.15	0.9544	22.24	11.10
	3.069	0.0695	1.043	7.569
233.2	0.904	0.0412	0.7314	15.99
	4.030	0.1838	1.587	7.781
	8.120	0.3703	2.427	5.906
	12.17	0.5500	3.071	4.987
	15.83	0.7217	3.774	4.712
	20.14	0.9186	10.69	10.49
	18.55	0.8460	4.941	5.264
	21.29	0.9708	27.97	25.96
218.2*	0.456	0.0466	0.6017	24.40
	1.039	0.1062	0.9159	16.30
	1.519	0.1553	1.099	13.39
	3.042	0.3110	1.556	9.460
	5.318	0.5438	2.148	7.470
	7.042	0.7200	2.803	7.360
	8.205	0.8389	3.896	8.780
	8.382	0.8570	4.519	9.970
	8.680	0.8875	9.562	20.37
	8.832	0.9031	10.61	22.22
	9.004	0.9206	15.05	30.90
	9.274	0.9483	21.54	42.95
	9.587	0.9803	24.71	47.66

* Measurements determined by Mr D. Whiting in these laboratories.

5 : Propane/Black Pearls

$\frac{T}{K}$	$\frac{p_1}{cm\ Hg}$	$\frac{p_1}{p_o}$	$\frac{10^8\ J}{mol\ s^{-1}}$	$\frac{10^6\ \tilde{K}}{m^2\ s^{-1}}$
273.2	0.757	0.0021	0.1817	6.157
	5.278	0.0149	1.145	5.564
	10.65	0.0300	2.049	4.934
	14.84	0.0418	2.701	4.668
	19.81	0.0558	3.491	4.520
	30.54	0.0861	4.616	3.877
	39.10	0.1102	5.124	3.361
213.2	1.781	0.0556	1.506	16.93
	4.755	0.1487	2.729	11.49
	11.24	0.3515	3.609	6.428
	17.45	0.5456	4.539	5.207
	22.88	0.7154	6.047	5.291
	24.63	0.7702	7.165	5.824
	27.85	0.8709	10.21	7.341

6 : Isobutane/Black Pearls

$\frac{T}{K}$	$\frac{p_1}{cm\ Hg}$	$\frac{p_1}{p_o}$	$\frac{10^8\ J}{mol\ s^{-1}}$	$\frac{10^6\ \tilde{K}}{m^2\ s^{-1}}$
343.2	4.382	0.0054	0.4575	3.364
	10.08	0.0124	0.9828	3.141
	9.628	0.0118	0.9369	3.135
	15.17	0.0186	1.395	2.964
	20.96	0.0257	1.815	2.791
	24.49	0.0301	2.079	2.736
	31.44	0.0386	2.486	2.548
	41.56	0.0510	3.080	2.388
308.2	5.211	0.0148	0.9448	5.247
	15.32	0.0437	2.112	3.990
	23.43	0.0668	2.772	3.424
	29.89	0.0852	3.321	3.215
	40.08	0.1143	3.882	2.803
	2.503	0.0071	0.5017	5.801
	8.486	0.0242	1.374	4.684
273.2	2.908	0.0245	1.048	9.243
	12.04	0.1012	2.524	5.378
	21.31	0.1792	3.242	3.903
	32.04	0.2694	4.059	3.250
	36.59	0.3077	4.260	2.987
233.2	4.792	0.2183	1.7410	7.955
	10.24	0.4667	2.599	5.557
	14.96	0.6817	3.655	5.350
	20.84	0.9496	8.401	8.827
	18.25	0.8313	5.995	7.193
	16.89	0.7694	4.692	6.083
	2.049	0.0933	1.212	12.95
	7.158	0.3261	2.213	6.771
	12.57	0.5727	3.172	5.526

7 : Helium/Propane Mixtures/Graphon

T / K	$p_1(C_3H_8)$ / cm Hg	p_1/p_o	$10^6 \tilde{K}_{He\ mix}$ / $m^2 s^{-1}$	$\tilde{K}_R$
473.2	10.18	-	3.721	0.9588
	20.21	-	3.677	0.9477
	33.59	-	3.528	0.9093
393.2	5.357	0.0013	3.306	0.9347
	13.99	0.0034	3.281	0.9275
	22.86	0.0056	3.130	0.8849
	32.03	0.0078	2.994	0.8465
	1.676	0.0004	3.392	0.9589
243.2	4.954	0.0394	1.665	0.5985
	2.303	0.0183	1.753	0.6303
	10.40	0.0828	1.672	0.6010
	20.49	0.1631	1.593	0.5727
	17.12	0.1363	1.659	0.5962
	26.03	0.2076	1.673	0.6014
	36.04	0.2869	1.619	0.5819
	29.51	0.2349	1.567	0.5634
213.2	4.892	0.1529	1.514	0.5814
	10.00	0.3128	1.469	0.5640
	17.34	0.5424	1.386	0.5322
	24.36	0.7618	1.299	0.4988
	29.19	0.9126	1.255	0.4817
	30.52	0.9542	0.2618	0.1005
	30.00	0.9382	0.7094	0.2724
	30.97	0.9684	0.3932	0.1509
	1.950	0.0609	1.524	0.5853

8 : Helium/Isobutane Mixtures/Graphon

T / K	$p_1(i\text{-}C_4H_{10})$ / cm Hg	p_1/p_o	$10^6 \tilde{K}_{He\ mix}$ / $m^2 s^{-1}$	$\tilde{K}_R$
453.2	5.356	0.0010	3.685	0.9703
	15.86	0.0030	3.551	0.9350
	25.85	0.0049	3.505	0.9228
	34.63	0.0066	3.365	0.8861
	43.54	0.0083	3.373	0.8881
	56.02	0.0107	3.209	0.8452
	50.11	0.0095	3.170	0.8347
	20.44	0.0039	3.604	0.9489
	29.79	0.0057	3.517	0.9262
	10.50	0.0020	3.670	0.9665
	40.12	0.0076	3.301	0.8693
423.2	5.174	0.0015	3.554	0.9686
	15.19	0.0045	3.317	0.9039
	25.19	0.0074	3.199	0.8719
	35.39	0.0104	3.175	0.8651
	44.62	0.0130	3.184	0.8676
	55.91	0.0164	3.002	0.8175
393.2	40.89	0.0193	2.685	0.7589
	45.49	0.0215	2.635	0.7448
	51.69	0.0244	2.639	0.7491
	29.64	0.0139	2.830	0.8001
	35.19	0.0166	2.733	0.7726
	20.22	0.0095	2.994	0.8464
	25.43	0.0120	2.868	0.8107
	16.40	0.0077	3.039	0.8590
	8.599	0.0041	3.191	0.9021
	12.65	0.0059	3.096	0.8753
	2.063	0.0009	3.356	0.9487
	5.510	0.0026	3.259	0.9215
358.2	4.998	0.0045	2.993	0.8865
	15.01	0.0134	2.647	0.7839
	25.80	0.0231	2.381	0.7053
	35.17	0.0315	2.310	0.6842
	45.51	0.0407	2.222	0.6583
	55.84	0.0499	2.115	0.6264
	51.06	0.0457	2.189	0.6483
	40.53	0.0363	2.258	0.6689
	2.093	0.0019	3.171	0.9391

continued

8 (continued) : Helium/Isobutane Mixtures/Graphon

T / K	$p_1(i\text{-}C_4H_{10})$ / cm Hg	p_1/p_o	$10^6 \tilde{K}_{He\ mix}$ / $m^2 s^{-1}$	$\tilde{K}_R$
343.2	4.001	0.0049	2.816	0.8522
	7.923	0.0097	2.580	0.7807
	12.32	0.0151	2.484	0.7515
	20.69	0.0254	2.311	0.6994
	25.66	0.0315	2.219	0.6715
	31.31	0.0384	2.199	0.6655
	37.61	0.0462	2.121	0.6418
	44.59	0.0547	2.141	0.6479
308.2	1.233	0.0035	2.697	0.8612
	0.538	0.0015	2.879	0.9195
	15.56	0.0438	1.832	0.5851
	6.806	0.0194	2.028	0.6475
	25.34	0.0722	1.703	0.5438
	39.41	0.1123	1.738	0.5551
	21.58	0.0615	2.008	0.6411
	40.47	0.1154	1.801	0.5752
	47.31	0.1349	1.839	0.5872
	50.41	0.1437	1.842	0.5883
	43.86	0.1250	1.825	0.5826
	34.59	0.0986	1.864	0.5952
273.2	10.65	0.0895	1.670	0.5665
	5.215	0.0439	1.733	0.5877
	1.278	0.0107	1.859	0.6304
	19.81	0.1666	1.709	0.5749
	26.16	0.2200	1.756	0.5956
	36.09	0.3036	1.728	0.5859
	49.26	0.4143	1.574	0.5339
	43.25	0.3638	1.635	0.5546
	58.21	0.4895	1.667	0.5655
	65.56	0.5514	1.634	0.5543
	16.06	0.1351	1.722	0.5840
	24.59	0.2068	1.716	0.5821
	46.18	0.3884	1.723	0.5845
268.2	1.998	0.0199	1.798	0.6154
	6.532	0.0659	1.707	0.5842
	13.24	0.1336	1.716	0.5875
	19.99	0.2018	1.665	0.5699
	31.02	0.3131	1.658	0.5674
	26.44	0.2669	1.653	0.5658
	53.14	0.5363	1.537	0.5262
	38.49	0.3885	1.646	0.5635
	46.12	0.4654	1.638	0.5608

continued

8 (continued) : Helium/Isobutane Mixtures/Graphon

$\frac{T}{K}$	$\frac{P_1(i\text{-}C_4H_{10})}{cm\ Hg}$	p_1/p_o	$\frac{10^6 \tilde{K}_{He\ mix}}{m^2 s^{-1}}$	$\tilde{K}_R$
258.2	1.520	0.0226	1.679	0.5858
	10.33	0.1535	1.648	0.5748
	20.37	0.3026	1.617	0.5643
	35.43	0.5265	1.587	0.5536
	47.19	0.7011	1.485	0.5782
	41.95	0.6234	1.561	0.5447
	28.26	0.4199	1.602	0.5591
248.2	1.843	0.0417	1.623	0.5775
	12.19	0.2762	1.586	0.5642
	22.17	0.5019	1.598	0.5687
	28.00	0.6341	1.455	0.5177
	33.42	0.7568	1.417	0.5041
	38.94	0.8819	1.340	0.4768
233.2	0.815	0.0372	1.517	0.5568
	3.776	0.1722	1.485	0.5450
	8.488	0.3870	1.439	0.5285
	12.10	0.5519	1.482	0.5439
	16.18	0.7376	1.334	0.4898
	19.77	0.9014	0.7742	0.2842
	18.65	0.8504	1.281	0.4704
	21.96	1.000	0.0011	0.0004
	19.44	0.8857	0.9788	0.3593
	20.48	0.9328	0.7112	0.2611
	21.52	0.9806	0.2128	0.0781
	21.27	0.9689	0.5469	0.2008
218.2	5.345	0.5465	1.326	0.5034
	7.841	0.8017	1.221	0.4633
	8.467	0.8657	1.001	0.3800
	8.863	0.9062	1.171	0.4446
	9.397	0.9608	0.6729	0.2554
	9.524	0.9738	0.4177	0.1585
	9.138	0.9343	1.029	0.3909
	6.845	0.6999	1.274	0.4836

9 : Helium/Propane Mixtures/Black Pearls

T / K	$p_1(i\text{-}C_4H_{10})$ / cm Hg	p_1/p_o	$10^6 \tilde{K}_{He\ mix}$ / $m^2 s^{-1}$	$\tilde{K}_R$
273.2	1.064	0.0029	0.5032	0.7134
	5.302	0.0149	0.4359	0.6180
	10.06	0.0283	0.3602	0.5107
	15.62	0.0440	0.3347	0.4745
	24.62	0.0694	0.3392	0.4809
	30.45	0.0858	0.3323	0.4711
	38.62	0.1088	0.3307	0.4689
213.2	4.565	0.1427	0.2315	0.3716
	10.93	0.3417	0.2249	0.3609
	17.12	0.5352	0.2018	0.3240
	2.032	0.0635	0.2236	0.3589
	19.63	0.6138	0.1803	0.2893
	24.49	0.7658	0.0615	0.0987
	27.71	0.8664	0.0143	0.0230
	22.62	0.7073	0.1246	0.2001

10 : Helium/Isobutane Mixtures/Black Pearls

T / K	$p_1(i\text{-}C_4H_{10})$ / cm Hg	p_1/p_o	$10^6 \tilde{K}_{He\ mix}$ / $m^2 s^{-1}$	$\tilde{K}_R$
343.2	4.934	0.0060	0.5691	0.7199
	10.09	0.0123	0.5138	0.6499
	14.70	0.0180	0.4708	0.5956
	1.944	0.0024	0.5873	0.7429
	3.061	0.0037	0.5165	0.6534
	2.390	0.0029	0.5448	0.6892
	4.859	0.0059	0.5250	0.6641
	31.15	0.0382	0.3947	0.4993
	41.87	0.0513	0.3693	0.4672
	22.52	0.0276	0.4246	0.5371
	1.884	0.0023	0.5222	0.6606
	0.622	0.0008	0.5257	0.6650
308.2	5.202	0.0148	0.3901	0.5208
	15.28	0.0435	0.3613	0.4823
	23.18	0.0661	0.3388	0.4523
	29.44	0.0839	0.3287	0.4388
	39.51	0.1126	0.3144	0.4197
273.2	2.856	0.0240	0.3268	0.4633
	11.32	0.0952	0.2699	0.3827
	21.17	0.1780	0.2638	0.3740
	31.71	0.2667	0.2802	0.3973
	36.28	0.3051	0.2655	0.3764
233.2	4.612	0.2101	0.2229	0.3421
	9.915	0.4517	0.1967	0.3019
	14.47	0.6593	0.1335	0.2049
	20.57	0.9372	0.0001	0.0002
	17.99	0.8199	0.0053	0.0081
	16.48	0.7509	0.0379	0.0582
	15.12	0.6888	0.0972	0.1492

11 : Argon/Isobutane Mixtures/Graphon

$\frac{T}{K}$	$\frac{p_1(i\text{-}C_4H_{10})}{cm\ Hg}$	p_1/p_o	$\frac{10^6\ \tilde{K}_{Ar\ mix}}{m^2 s^{-1}}$	$\frac{\tilde{K}_{Ar\ mix} M_{Ar}^{\frac{1}{2}}}{\tilde{K}_{He\ pure} M_{He}^{\frac{1}{2}}}$
453.2	0.00	0.0000	1.480	1.231
	10.38	0.0019	1.415	1.177
	22.11	0.0042	1.317	1.095
	33.99	0.0065	1.296	1.078
	47.78	0.0091	1.245	1.035
	28.24	0.0054	1.353	1.126
393.2	0.00	0.0000	1.399	1.250
	10.47	0.0049	1.175	1.049
	20.27	0.0096	1.095	0.978
	26.93	0.0127	1.032	0.951
	36.69	0.0173	1.006	0.898
	47.76	0.0225	0.9848	0.879
308.2	0.000	0.0000	1.332	1.344
	9.884	0.0282	0.6832	0.6892
	21.28	0.0607	0.6468	0.6525
	3.919	0.0112	0.7849	0.7918
	16.31	0.0465	0.6443	0.6499
	30.93	0.0818	0.6239	0.6294
	2.101	0.0059	0.8955	0.9034
	1.080	0.0031	1.000	1.009
	40.641	0.1158	0.6499	0.6556
	52.180	0.1487	0.6661	0.6719
273.2	0.000	0.0000	1.375	1.473
	0.515	0.0043	0.8769	0.9396
	0.942	0.0079	0.7511	0.8048
	2.165	0.0183	0.6171	0.6612
	3.926	0.0330	0.5715	0.6123
	7.896	0.0664	0.5541	0.5937
	16.19	0.1362	0.5214	0.5587
	34.80	0.2927	0.5497	0.5889
	28.12	0.2365	0.5520	0.5914
	41.92	0.3525	0.5503	0.5896
	18.25	0.1535	0.5533	0.5928
233.2	2.069	0.0942	0.4580	0.5315
	4.853	0.2211	0.4649	0.5391
	10.31	0.4696	0.4418	0.5124
	14.92	0.6798	0.4222	0.4896
	12.76	0.5812	0.4411	0.5115
	17.44	0.7947	0.4226	0.4901
	19.41	0.8843	0.3635	0.4216
	20.91	0.9525	0.1974	0.2289

APPENDIX C : 'PRESSURE-DECAY' FLOW DATA

1. Helium/Graphon
2. Isobutane/Graphon
3. Helium/Isobutane Mixtures/Graphon

1 : Helium/Graphon

$\frac{T}{K}$	$\frac{p_\infty}{cm\ Hg}$	$\frac{10^6\ K^*}{m^2 s^{-1}}$
393.2	3.904	3.260
	8.252	3.265
308.2	3.861	2.876
	4.519	2.951
	5.914	2.917
	8.867	2.9119
	8.954	2.936
	17.59	2.943
273.2	3.681	2.748
	3.918	2.732
	5.303	2.714
	12.199	2.722

2 : Isobutane/Graphon

T / K	p_∞ / cm Hg	p_∞ / p_o	$10^6 K^*$ / $m^2 s^{-1}$
393.2	3.657	0.0017	1.967
	6.890	0.0032	1.787
	14.45	0.0068	1.781
	21.55	0.0102	1.815
	23.90	0.0113	1.760
	31.46	0.0148	1.690
308.2	2.167	0.0062	4.028
	3.881	0.0111	4.537
	7.533	0.0215	3.404
	13.48	0.0384	3.062
	18.99	0.0542	2.555
	22.98	0.0655	2.470
	29.52	0.0841	2.209
273.2	2.128	0.0179	4.946
	3.668	0.031	4.180
	4.166	0.0350	4.103
	7.681	0.0646	3.012
	8.526	0.0717	3.082
	13.58	0.1142	2.544
	15.01	0.1262	2.328
	19.06	0.1603	2.275
	20.58	0.1731	2.174
	28.09	0.2363	1.917
	28.57	0.2403	1.942
233.2	2.059	0.0938	5.238
	3.433	0.1564	3.632
	6.274	0.2858	3.343
	8.037	0.3661	2.993
	10.02	0.4563	2.786
	13.20	0.6016	2.813
	14.31	0.6518	3.171
	20.84	0.9494	14.46
	21.34	0.9720	17.79

3 : Helium/Isobutane Mixtures/Graphon

T / K	$p_{\infty}(i\text{-}C_4H_{10})$ / cm Hg	p_{∞}/p_o	$10^6 K^*_{He\ mix}$ / $m^2 s^{-1}$	K^*_R
393.2	4.995	0.0024	2.999	0.9128
	9.761	0.0046	2.845	0.8659
	19.13	0.0090	2.517	0.7661
	33.99	0.0160	2.262	0.6885
308.2	4.205	0.0019	1.982	0.6813
	9.829	0.0280	1.947	0.6693
	19.54	0.0557	1.870	0.6428
	29.31	0.0836	1.821	0.6260
273.2	2.128	0.0179	1.683	0.6145
	8.522	0.0717	1.645	0.6006
	14.46	0.1216	1.499	0.5473
	28.57	0.2403	1.436	0.5243
	52.53	0.4418	1.469	0.5364
233.2	9.836	0.4481	1.3550	0.5355
	14.35	0.6537	1.2611	0.4984
	17.65	0.8041	0.9798	0.3872
	20.29	0.9244	0.5451	0.2154
	21.40	0.9750	0.5148	0.2034
	21.50	0.9795	0.7660	0.3027

REFERENCES

Abram, J.C. and Morris, A.C., 1971 3rd Conf. on Industrial Carbons and Graphite, Soc. Chemical Industry.

Allen, T. and Burewski, D., 1977 Powd. Tech., 18, 139.

Ash, R., Baker, R.W. and Barrer, R.M., 1967, Proc. Roy. Soc. A 299, 434.

Ash, R., Baker, R.W. and Barrer, R.M., 1968, Proc. Roy. Soc. A 304, 407.

Ash, R., Barrer, R.M., Chio, H.T. and Edge, A.V.J., 1979 Proc. Roy. Soc. A 365, 267.

Ash, R., Barrer, R.M., Clint, J.H., Dolphin, R.J. and Murray, C.L., 1973 Phil. Trans. Roy. Soc. A 275, 255.

Ash, R., Barrer, R.M. and Coughlan, B., 1972 J. Colloid Interface Sci., 38, 61.

Ash, R., Barrer, R.M. and Edge, A.V.J., 1976 J. Chem. Soc. Faraday I, 72, 2777.

Ash, R., Barrer, R.M. and Foley, T., 1976 J. Membrane Sci., 1, 355.

Ash, R., Barrer, R.M. and Lowson, R.T., 1970 Surf. Sci., 21, 265.

Ash, R., Barrer, R.M. and Lowson, R.T., 1973 J. Chem. Soc. Faraday I, 69, 2166.

Ash, R., Barrer, R.M. and Nicholson, D., 1963 Z. Phys. Chem., 37, 257.

Ash, R., Barrer, R.M. and Pope, C.G., 1963a Proc. Roy. Soc. A 271, 1.

Ash, R., Barrer, R.M. and Pope, C.G., 1963b Proc. Roy. Soc. A 271, 19.

Ash, R., Barrer, R.M. and Sharma, P., 1976 J. Membrane Sci., 1, 17.

Ash, R. and Grove, D.M., 1960 Trans. Farad. Soc., 56, 1357.

Aylmore, L.A.G. and Barrer, R.M., 1966 Proc. Roy. Soc. A 290, 477.

Babbit, J.D., 1950 Can. J. Res. A 28, 449.

Baker, R.W., 1966 Ph.D. Thesis, University of London.

Barnes, C., 1934 Physics 5, 4.

Barrer, R.M., 1963 Appl. Mat. Res., 2, 129.

Barrer, R.M. and Clarke, D.J., 1974 J. Chem. Soc. Faraday I, 70, 535.

Barrer, R.M. and Gabor, T., 1959 Proc. Roy. Soc. A 251, 353.

Barrer, R.M. and Gabor, T., 1960 Proc. Roy. Soc. A 256, 267.

Barrer, R.M. and Grove, D.M., 1951 Trans. Farad. Soc., 47, 826.

Barrer, R.M. and Robins, A.B., 1953 Trans. Farad. Soc., 49, 807.

Barrer, R.M. and Strachan, E., 1955 Proc. Roy. Soc., A 231, 52.

Beebe, R.A., Biscoe, J., Smith, W.R. and Wendell, C.B., 1947 J. Am. Chem. Soc., 69, 95.

Beebe, R.A., Millard, B. and Cynarski, J., 1953 J. Am. Chem. Soc., 75, 839.

Biscoe, J. and Warren, B.E., 1942 J. App. Phys., 13, 364.

Blaine, R., 1943 Bull. Am. Chem. Soc., Test Mat., 123, 51.

Breton, E.A. and Massignon, D., 1963 J. Chim. Physique, 60, 294.

Brubaker, D.W. and Kammermeyer, K., 1953 Ind. Eng. Chem., 45, 1148.

Brunauer, S. and Emett, P.H., 1937 J. Am. Chem. Soc., 59, 1553.

Brunauer, S., Emett, P.H. and Teller, E., 1938 J. Am. Chem. Soc., 60, 309.

Carman, P.C., 1950 Proc. Roy. Soc. A 203, 55.

Carman, P.C., 1952 Proc. Roy. Soc. A 211, 526.

Carman, P.C. and Marlherbe, P. le R., 1950 Proc. Roy. Soc. A 203, 165.

Carman, P.C. and Raal, F.A., 1951 Proc. Roy. Soc. A 209, 38.

Carman, P.C. and Raal, F.A., 1951 Proc. Roy. Soc. A 209, 59.

Chirnside, G.C. and Pope, C.G., 1964 J. Phys. Chem., 68, 2377.

Clausing, P., 1930 Ann. Phys. Lpz, 7, 489.

Clint, J.H., 1966 Ph.D. Thesis, University of London.

Clint, J.H., 1972 J. Chem. Soc. Faraday I, 68, 2239.

Cranston, R.W. and Inkley, F.A., 1957 Adv. Catalysis 9, 143.

Craven, R.J., 1976 Ph.D. Thesis, University of London.

Damköhler, G.Z., 1935 Z. Phys. Chem. A174, 222.

de Boer, J.H., Linsen, B.G. and Osinga, Th.J., 1965 J. Catalysis, 4, 643.

de Boer, J.H. Linsen, B.G., van de Plas, Th. and Zondervan, G.J., 1965 J. Catalysis, 4, 649.

de Boer, J.H. and Lippens, B.C., 1965 J. Catalysis, 4, 319.

Di Corcia, A. and Samperia, R., 1973 J. Phys. Chem., 77, 1301.

Dollimore, D. and Heal, G.R., 1970 J. Colloid Interface Sci., 33, 508.

Dollimore, D., Spooner, P. and Turner, A., 1976 Surf. Tech., 4, 121.

Elkington, P.A. and Cuthreys, G. 1969 J. Phys. Chem., 73, 2321.

Fick, A., 1855 Ann. Physick 170, 59.

Field, G.J., Watts, H. and Weller, K.R., 1963 Rev. Pure Applied Chem., 2.

Gilliland, E.R., Baddour, R.F., Perkinson, G.P. and Sladek, K.J., 1974 Ind. Eng. Chem., Fundam., 13, 95.

Gilliland, E.R., Baddour, R.F. and Russel, J.L., 1958 J. Amer. Inst. Chem. Engrs., 4, 90.

Graham, T., 1846 Phil. Trans. Roy. Soc., 136, 573.

Gregg, S.J. and Sing, K.S.W., 1967 Adsorption, Surface Area and Porosity (Academic Press, London and New York).

Hall, C.E., 1948 J. Appl. Phys., 19, 271.

Heckman, F.A. and Harling, D.F., 1966 Rubber Chem. Tech., 39, 1.

Hess, W.M., Ban, L.L., Eckert, F.J. and Chirico, V., 1968 Rubber Chem. Tech., 41, 356.

Hill, T.L., 1947 J. Chem. Phys., 15, 767.

Hirschfelder, J.O., Curtiss, C.F. and Bird, R.B., 1954 Molecular Theory of Gases and Liquids (J. Wiley, New York).

Horiguchi, Y., Hudgins, R.R. and Silveston, P.L., 1971 Can. J. Chem. Eng., 49, 76.

Houska, C.R. and Warren, B.E., 1954 J. Appl. Phys., 25, 1503.

Hwang, S.T. and Kammermeyer, K., 1966 Can. J. Chem. Eng., 44, 82.

Hwang, S.T. and Kammermeyer, K., 1967 Sept. Sci., 2, 555.

Isirikyan, A.A. and Kiselev, A.V., 1961 J. Phys. Chem., 65, 601.

Isirikyan, A.A. and Kiselev, A.V., 1962 J. Phys. Chem., 66. 205.

Joyner, L.G. and Emett, P.H., 1948 J. Am. Chem. Soc., 70, 2353.

Kammermeyer, K., 1958 Ind. Eng. Chem., 50, 697.

Kammermeyer, K. and Wyrick, D., 1958 Ind. Eng. Chem., 50, 1309.

Kiselev, A.V., 1957 Proc. Sec. Conf. on Surf. Act., 2, 100.

Kiselev, S.V., 1958 The Structure and Properties of Porous Solids, p.195 (Butterworths, London).

Knudsen, M., 1909 Ann. Phys. Lpz, 28, 75.

Lal, M. and Spencer, D., 1974 J. Chem. Soc. Faraday II, 70, 910.

Lallemand, A. and Eyraud, C., 1973 Bull. Soc. Fr. Ceram., 99, 25.

Lecloux, A., 1970 Proc. I.U.P.A.C. Int. Symp. Surface Area Determination, Bristol 1969 (Butterworths, London).

Lecloux, A. and Pirard, J.P., 1979 J. Colloid Interface Sci., 70, 265.

Livingston, H.K., 1949 J. Colloid Sci., 4, 447.

Lowson, R.T., 1968 Ph.D. Thesis, University of London.

Mason, E.A., Evans, R.B. and Watson, G.M., 1961 J. Chem. Phys., 35, 2076.

Mason, E.A., Evans, R.B. and Watson, G.M., 1962 J. Chem. Phys., 36, 1894.

McClellan, A.L. and Harnsberger, H.F., 1967 J. Colloid Interface Sci., 23, 577.

Mikhail, R.S., Bodor, E.E. and Brunauer, S., 1968 J. Colloid Interface Sci., 51, 260.

Moori, J., Pierce, C. and Nelson-Smith, R., 1953 J. Phys. Chem., 57, 657.

Murray, C.L., 1976 Ph.D. Thesis, University of London.

Nicholson, D. and Petropoulos, J.H., 1973 J. Colloid Interface Sci., 45, 459.

Nicholson, D. and Petropoulos, J.H., 1975 Ber. Bunsen-Gesellschaft, 79, 796.

Nicholson, D. and Sing, K.S.W., 1979 Colloid Sci., 3 (Spec. Period. Rep. Chem. Soc.).

Parfitt, G.D., Sing, K.S.W. and Urwin, D., 1975 J. Colloid Interface Sci., 53, 187.

Pierce, C., 1968 J. Phys. Chem., 72, 3673.

Pierce, C. and Ewing, B., 1964 J. Phys. Chem., 68, 2562.

Polley, M.H., Schaeffer, W.D. and Smith, W.R., 1953 J. Phys. Chem., 57, 469.

Pope, C.G., 1961 Ph.D. Thesis, University of London.

Pope, C.G., 1967 Trans. Farad. Soc., 63, 734.

Rhim, H. and Hwang, S.T., 1975 J. Colloid Interface Sci., 52, 174.

Rigden, P.J., 1943 J. Soc. Chem. Ind. (Trans.), 62, 1.

Roberts, G.T., 1973 J. Phys. A: Math., Nucl. Gen., 6, 570.

Ross, J.W. and Good, R.J., 1956 J. Phys. Chem., 60, 1167.

Ross, J.W., Olivier, P. and Saelens, J.K., 1962 J. Phys. Chem., 66, 696.

Sams, J.R. Constaharis, G. and Halsey, G.D., 1962 J. Phys. Chem., 66, 2154.

Sandler, S.I., 1972 Ind. Eng. Chem. Fundam., 11, 424.

Schmoluckowski, M. von, 1910 Ann. Phys. Lpz., 33, 1559.

Sharma, P., 1970 Ph.D. Thesis, University of London.

Shull, C.G., 1948 J. Am. Chem. Soc., 70, 1405.

Spacek, P. and Kubin, M., 1967 J. Polym. Sci., C 16, 705.

Terman, M., 1973 J. Colloid Interface Sci., 45, 270.

Tsimillis, K. and Petropoulos, J.H., 1977 J. Phys. Chem., 81, 2185.

Voet, A., Lamond, T.G. and Sweigart, D., 1968 Carbon, 6, 707.

Volmer, M. and Adhikari, G., 1925 Z. Physik, 35, 170.

Volmer, M. and Adhikari, G., 1926 Z. Phys. Chem., 119, 46.

Volmer, M. and Esterman, J., 1921 Z. Physik, 7, 13.

Wade, W.H., 1965 J. Phys. Chem., 69, 322.

Weber, S. 1954 Kgl. Danske Videnskab. Selskab. Mat. Fys. Medd., 28.

Weissberg, H.L., 1963 J. Appl. Phys., 34, 2636

Weisz, P.B., 1975 Ber. Bunsen-Gesellschaft, 79, 798.

Whiting, D.E.G., 1977 3rd Year, Res. Proj. Chem. Imperial College, University of London.

Young, D.M. and Crowell, A.D., 1962 Physical Adsorption of Gases, p.284 (Butterworths, London)

Zwietering, P., 1956 Proc. Int. Symp. React. Solids III.